Subsea Pipeline Design, Analysis, and Installation

Qiang Bai

Yong Bai

Notice
No responsibility is assumed by the publisher for any injury and/or damage to persons or property as a matter of products liability, negligence or otherwise, or from any use or operation of any methods, products, instructions or ideas contained in the material herein. Because of rapid advances in the medical sciences, in particular, independent verification of diagnoses and drug dosages should be made.

For information on all **Gulf Professional** publications
visit our web site at store.elsevier.com

Foreword

I am delighted to write a brief Foreword to this extensive handbook for subsea pipeline design and installation. It is often a challenge to find a single book that discusses all aspects of subsea pipeline design and installation in sufficient detail that the practicing engineer can have this book or volume of books as a desk reference for a large range of design topics, instead of the engineer having to search for specific subject matter in Conference Proceedings. And the authors have succeeded in accomplishing just that. The effort it took in writing well over a 750 pages of text and formulae and cross-checking was truly a labor of love and dedication to the profession of subsea pipeline engineers, and for those readers who wish to know more about a particular subject, the list of references at the end of each chapter is truly outstanding.

Frans Kopp
January 2014

Preface

It has been 8 years since our book "Subsea Pipelines and Risers" (SPR) was published by Elsevier. This new book "Subsea Pipeline Design, Analysis and Installation" reflects upon the new pipeline technologies developed by the oil and gas industry. It only concentrates on the first part of the book SPR - Subsea pipelines. All chapters in the book SPR are rewritten and updated. In addition, almost 20 new chapters are added in the new book. This new book is written for engineers who work in the field of subsea pipeline engineering.

With the rapid development of subsea pipeline engineering technology, researchers and engineers keep on exploring and advancing new design and analysis methods in this field. The limit state design technology was developed in 1990s when our first pipeline book was published based on our technical papers. All chapters have been completely revised based on our engineering practice in Houston this past decade.

The deep water pipeline technology is represented by the installation engineering required to lay the pipelines in water depth of 2000 m and deeper. Finite element analysis of pipeline dynamic nonlinear behavior becomes more and more important.

New materials are one of the new directions for pipeline technologies. The authors have been active in the qualification of composite pipelines, RTP pipelines and flexible pipelines. We have performed numerous laboratory tests for the use of new materials for subsea pipelines.

We hope that this book is a useful reference source of subsea pipeline design, analysis, and installation for subsea engineers.

Dr. Qiang Bai & Prof. Yong Bai
Houston, USA

1 Introduction

Chapter Outline

1.   Introduction

Subsea pipelines are used for a number of purposes in the development of subsea hydrocarbon resources, as shown in Figure 1.1. A pipeline system can be a single-pipe, pipe-in-pipe, or bundled system. Normally, the term of subsea flowlines is used to describe the subsea pipelines carrying oil and gas products from the wellhead to the riser base; the riser is connected to the processing facilities (e.g., a platform or a floating production storage and offloading vessel (FPSO)). The subsea pipelines from the processing facilities to shore are called *export pipelines*, while the subsea pipelines from the platform to subsea equipment used to transfer water or chemical inhibitors are called *water injection* or *chemical flowlines*.

The design process for each type of line in general terms is the same, and it is this general design approach that is discussed in this book.

Finally, in Chapter 23, a pipeline design project is used as an example to demonstrate how the technical development described in this book is used to save on costs and ensure quality and safety.
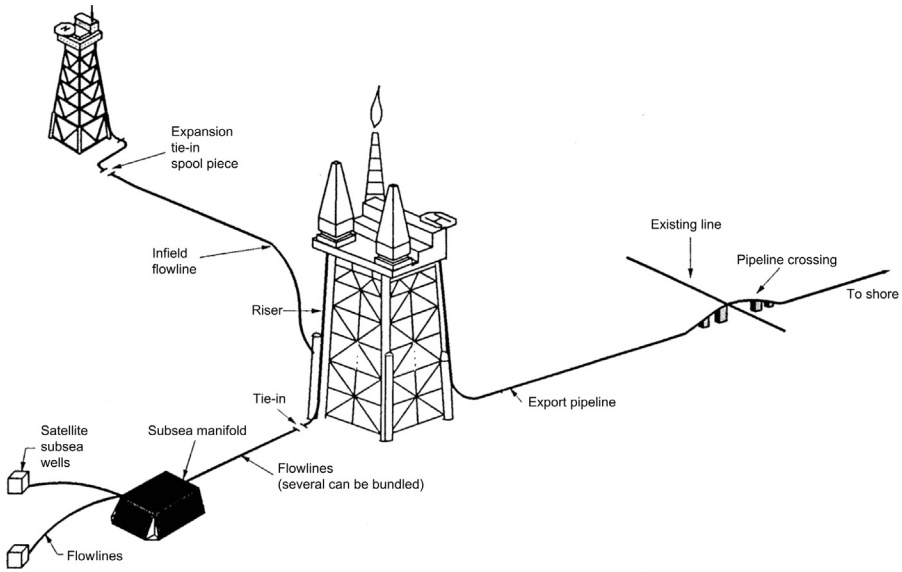
Figure 1.1 Subsea pipelines.
Source: Bai and Bai [1].

2. Design Stages and Process

Design Stages

The design of pipelines is usually performed in three stages:

- Conceptual design engineering.
- Front end engineering design (FEED) engineering.
- Detail design engineering.

The objective and scope of each of these design stages varires, depending on the operator and the size of the project. However, the primary process and purposes are generally summarized as follows [2]:

1. **Conceptual engineering.** The primary objectives of conceptual engineering normally are
   - To establish technical feasibility and constraints on the system design and construction.
   - To eliminate nonviable options.
   - To identify the required information for the forthcoming design and construction.
   - To allow basic cost and scheduling to be estimated.
   - To identify interfaces with other systems, planned or currently in existence.

   The value of this early engineering work is that it reveals potential difficulties and areas where more effort may be required in the data collection and design areas.
2. **Front end engineering design.** The primary objectives of FEED normally are
   - To perform pipeline design so that the system concept is fixed. This includes
     - To verify the sizing of the pipeline.
     - To determine the pipeline grade and wall thickness.

- To verify the pipeline against design and code requirements for installation, commissioning, and operation.
- To prepare authority applications.
- To perform a material takeoff sufficient to order the line pipe (should the pipe fabrication be a long lead item, hence requiring early startup).

The level of this engineering design is sometimes specified as being sufficient to detail the design for inclusion into an engineering, procurement, construction, and installation (EPCI) tender. The EPCI contractor should then be able to perform the detailed design with the minimum number of variations as detailed in their bids.

3. **Detail engineering.** The detailed engineering phase is, as the term suggests, the development of the design to a point where the technical input for all procurement and construction tendering can be defined in sufficient detail. The primary objectives can be summarized as

- Route optimization.
- Selection of wall thickness and coating.
- Confirmation of code requirements regarding strength, vortex-induced vibrations (VIV), on-bottom stability, global buckling, and installation.
- Confirmation of the design and additional design as defined in the preliminary engineering.
- Development of the design and drawings in sufficient detail for the subsea scope. This may include pipelines, tie-ins, crossings, span corrections, risers, shore approaches, and subsea structures.
- Preparation of detailed alignment sheets based on most recent survey data.
- Preparation of specifications, typically covering materials, cost applications, construction activities (i.e., pipe laying, survey, welding, riser installations, spoolpiece installation, subsea tie-ins, subsea structure installation), and pre-commissioning (i.e., flooding, pigging, hydrotesting, cleaning, drying).
- Preparation of material take off (MTO) and compilation of necessary requisition information for the procurement of materials.
- Preparation of design data and other information required for the certification authorities.

Design Process

The object of the design process for a pipeline is to determine, based on given operating parameters, the optimum pipeline size parameters. These parameters include

- Pipeline internal diameter.
- Pipeline wall thickness.
- Grade of pipeline material.
- Type of coating-corrosion and weight (if any).
- Coating wall thickness.

The design process required to optimize the pipeline size parameters is an iterative one, summarized in Figure 1.2. The design analysis is illustrated in Figure 1.3.

Each stage in the design process should be addressed whether it is a conceptual, preliminary, or detailed design. However, the level of analysis varies, depending on
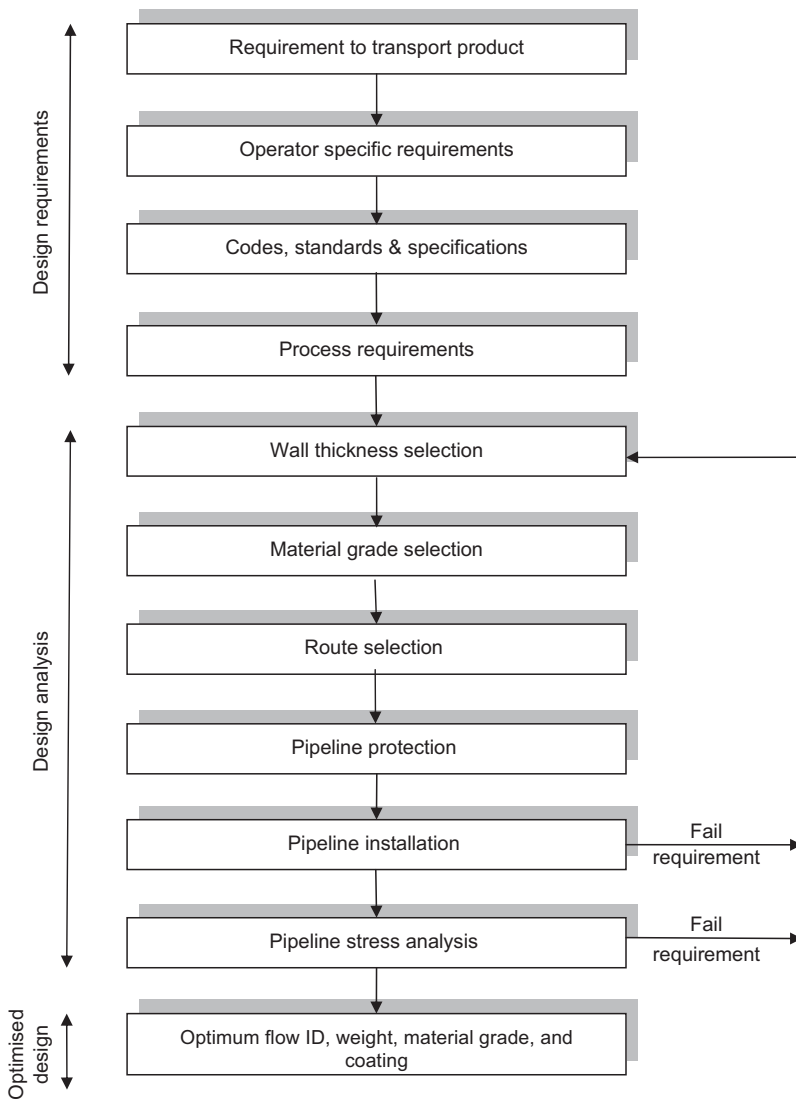
Figure 1.2 Subsea pipeline design process.
Source: Bai and Bai [1].

the requirements. For instance, when reviewing the objectives of the detailed design (Section 1.2.1), the design should be developed such that the following are determined:

- Pipeline wall thickness, grade, coating, and length are specified so that pipeline can be fabricated.
- Route is determined such that alignment sheets can be compiled.
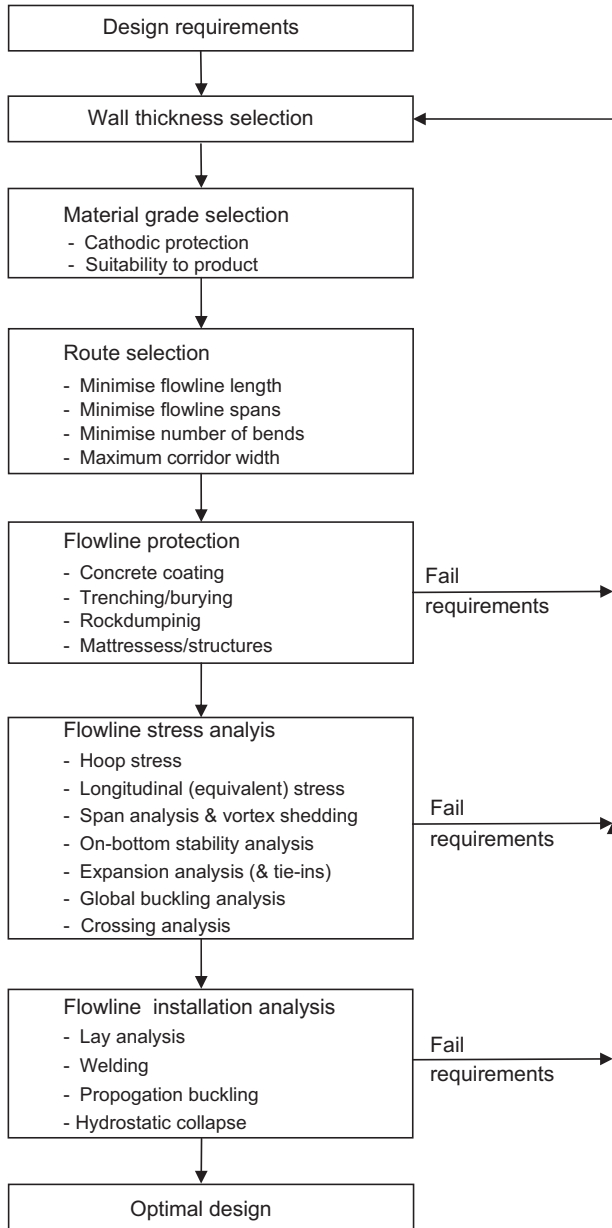
Figure 1.3 Flowline design analyses.
Source: Bai and Bai [1].

- Pipeline stress analysis is performed to verify that the pipeline is within the allowable stresses at all stages from installation, testing to operation. The results also include pipeline allowable spans, tie-in details (including expansion spool pieces), allowable testing pressures, and other input to the design drawings and specifications.
- Pipeline installation analysis is performed to verify that stresses in the pipeline at all stages of installation are within the allowable values. The analysis should specifically confirm that the proposed method of pipeline installation would not result in pipeline damage. The analysis has input into the installation specifications.
- Analysis of global response.
  - Expansion, effective force, and global buckling.
  - Hydrodynamic response.
  - Impact.
- Analysis of local strength.
  - Bursting, local buckling, ratcheting.
  - Corrosion defects, dents.

3.   Design through Analysis

The offshore and subsea industries recently experienced a technical revolution in the design process. Advanced methods and analysis tools allow a more sophisticated approach to design, which takes advantage of modern materials and revised design codes supporting the limit state design concepts and reliability methods. The new approach is called *design through analysis* (DTA), where the finite element method is used to simulate the global behavior of pipelines as well as the local structural strength [3]. The two-step process is used in a complementary way to determine the governing limit states and to optimize a particular design.

The advantage of using advanced engineering is a substantial reduction of project CAPEX (capital expenditure) and OPEX (operating expenditure) by minimizing unnecessary conservatism in the design through a more accurate determination of the effects of local loading conditions on the structure. Rules and design codes have to cover the general design context, where there are often many uncertainties in the input parameters and the application of analysis methods. Where the structure and loading conditions can be accurately modeled, realistic simulations reveal that aspects of the design codes may be overly conservative for a particular design situation. The FEM (finite element methods) model simulates the true structural behavior and allows specific mitigating measures to be applied and documented.

Better quality control in pipeline production allows more accurate modeling of material, while FEM analysis tools allow engineers to simulate the through-life behavior of the entire pipeline system and identify the most loaded sections or components. These are integrated into a detailed FEM model to determine the governing failure mode and limit criteria, which is compared to the design codes to determine where there is room for optimization. The uncertainties in the input data and responses can be modeled with the help of statistics to determine the probability distributions for a range of loads and effects. The reliability approach to design decisions can then be applied to optimize and document the fitness for purpose of the final product.

Engineers have long struggled with analytical methods, which consider only the parts of the structural systems they are designing. How the different parts affect each other and, above all, how the structural system will respond to loading near its limiting capacity requires a nonlinear model that accurately represents the loads, material and structure. The sophisticated nonlinear FEM programs and high-speed computers available today allow engineers to achieve numerical results, which agree well with observed behavior and laboratory tests.

The simulation of global response together with local strength is often necessary because design parameters and local environment are project-specific. A subsea pipeline is subject to loading conditions related to installation, seabed features, intervention works, testing, various operating conditions, and shutdowns, which prescribe a load path essential to the accurate modeling of nonlinear systems involving plastic deformation and hysteresis effects. For example, simulation can verify that a pipeline system undergoing cyclic loading and displacement is self-stabilizing in a satisfactory way or becomes unstable, needing further restraint. The simulation of pipeline behavior in a realistic environment obtained by measurement allows engineers to identify the strength and weaknesses of their design to obtain safe and cost-effective solutions. Traditionally, pipeline engineers compute loads and load effects in two dimensions and either ignore or combine results to account for three-dimensional (3D) effects. This approach could lead to an overly conservative or, unsafe design. DTA has demonstrated the importance of three-dimensional finite element analysis for highly loaded pipelines undergoing large thermal expansion.

Design through analysis involves the following activities:

- Performing the initial design according to guidelines and codes.
- Determining the global behavior by modeling the whole pipeline system.
- Simulating the through-life load conditions.
- Identifying potential problem areas.
- Checking the structural failure modes and capacity by detailed finite element modeling.
- Developing strategies for minimizing cost while maintaining a uniform safety level.
- Performing design optimization cycles.
- Documenting the validity and benefits of the design.
- Providing operation and maintenance support.

4. Pipeline Design Analysis

General

Pipeline stress analysis is performed to determine if the pipeline stresses are acceptable, in accordance with code requirements and client requirements during pipeline installation, testing, and operation. The analysis performed to verify that stresses experienced are acceptable includes

- Hoop stress.
- Longitudinal stress.

- Equivalent stress.
- Span analysis and vortex shedding.
- On-bottom stability analysis.
- Thermal expansion analysis, including tie-in design.
- Global buckling analysis.
- Crossing analysis.

The first of the three design stages is the initial wall thickness sizing. These initial sizing calculations should also be performed in conjunction with the hydrostatic collapse/propagation buckling calculations from the installation analysis.

The analysis methods for pipeline design are briefly discussed next, as an introduction to separate chapters.

Pipeline Stress Checks

Hoop Stress

Hoop stress (σ_h) for a thin wall pipe can be determined using the following equation, as shown in Figure 1.4:

$$\sigma_h = (p_i - p_o)\frac{D}{2t} \tag{1.1}$$

where:

p_i = internal pressure
p_o = external pressure
D = outside diameter of the pipeline
t = minimum wall thickness of the pipeline

Depending on the code or standard, the hoop stress should not exceed a certain fraction of the specified minimum yield stress (SMYS).
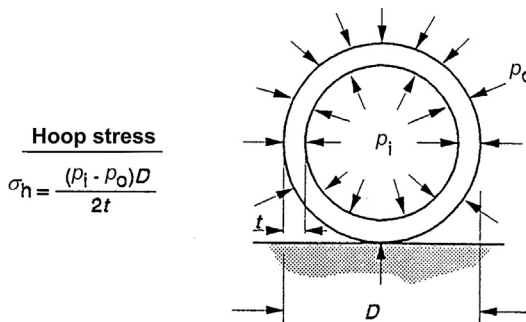
Figure 1.4 Pipe hoop stress.

Longitudinal Stress

The longitudinal stress (σ_l) of pipeline is the axial stress experienced by the pipe wall and consists of stresses due to

- End cap force induced stress (σ_{ec}).
- Bending stress (σ_b).
- Thermal stress (σ_t).
- Hoop stress (σ_h).

The longitudinal stress can be determined using the following equation:

$$\sigma_l = \sigma_{ec} + \sigma_b + \sigma_t + \nu\sigma_h \qquad [1.2]$$

The components of the longitudinal stress are illustrated in Figure 1.5. It should be ensured that sign conventions are utilized when employing this equation (i.e., tensile stress is positive).

Equivalent Stress

The combined stress is determined differently depending on the code/standards utilized. However, the equivalent stress (σ_e) can usually be expressed as:

$$\sigma_e = \sqrt{\sigma_h{}^2 + \sigma_l{}^2 - \sigma_h\sigma_l + 3\tau_{lh}{}^2} \qquad [1.3]$$

where

σ_h = hoop stress
σ_l = longitudinal stress
τ_{lh} = tangential shear stress

For high pressure pipes with D/t ratios less than 20 and ignorable shear stresses, the equivalent stress may be calculated as

$$\sigma_e = \sqrt{\frac{1}{2}\left[(\sigma_h - \sigma_l)^2 + (\sigma_l - \sigma_r)^2 + (\sigma_h - \sigma_r)^2\right]} \qquad [1.4]$$

Longitudinal stress

$\sigma_l = \sigma_{ec} + \sigma_t + \nu\sigma_h + \sigma_b$

σ_{ec} σ_t $\nu\sigma_h$ σ_b

P_i P_i σ_b

End cap stress Thermal stress Hoop stress Bending stress
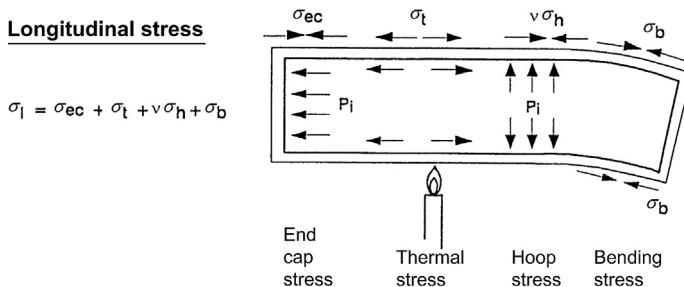
Figure 1.5 Longitudinal stress of pipeline.

where the radial stress, σ_r, varies across the pipe wall from a value equal to the internal pressure, p_i, on the inside of the pipe wall, to a value equal to the external pressure, p_o on the outside of the pipe. The magnitude of the radial stress is usually small when compared with the longitudinal and hoop stresses; consequently, it is not specifically limited by the design codes.

Span Analysis

Over a rough seabed or on a seabed subject to scour, pipeline spanning can occur when contact between the pipeline and seabed is lost over an appreciable distance, as shown in Figure 1.6. In such circumstances, it is normal code requirements that the line be investigated for

- Excessive yielding.
- Fatigue due to VIV.
- Interference with human activities (fishing).

Due consideration to these requirements will result in the evaluation of an allowable free-span length. Should the actual free-span lengths exceed the allowable length, then correction or remediation of the free span is necessary to reduce the span length. This can be a very expensive exercise, and consequently, it is important that free-span evaluation is as accurate as possible. In many cases, a multiple span analysis has to be conducted, accounting for the real seabed and in-situ structural behavior.

The flow of wave and current around a pipeline span, or any cylindrical shape, results in the generation of sheet vortices in the wake due to turbulent flow. These vortices are shed alternately from the top and bottom of the pipe, resulting in an
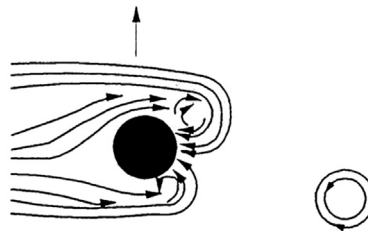
Figure 1.6 Pipeline span and vortex shedding.

oscillatory force being exerted on the span, as shown in Figure 1.6. If the frequency of shedding approaches the natural frequency of the spanning pipeline, then severe resonance can occur. This resonance can induce fatigue failure of the pipeline and cause the concrete coating to crack and possibly be lost.

The evaluation of the potential of a span to undergo resonance is based on the comparison of the shedding frequency and the natural frequency of the span. The calculation of shedding frequency is achieved by using traditional mechanics, although some consideration must be given to the effect of the closeness of the seabed. Simple models have, traditionally, been used to calculate the natural frequency of the span, but recent theories have shown these to be oversimplified and multiple-span analysis needs to be conducted for pipeline on a real seabed.

Another main consideration with regard to spanning is the possible interference with fishing. This is a broad subject in itself and is discussed in Chapter 16.

On-Bottom Stability Analysis

Pipelines resting on a seabed are subject to fluid loading from both waves and steady currents. For regions of the seabed where damage may result from vertical or lateral movement of the pipeline, it is a design requirement that the pipe weight be sufficient to ensure stability under the worst possible environmental conditions. In most cases, this weight is provided by a concrete weight coating on the pipeline in shallow water. In some circumstances, the pipeline may be allowed to move laterally, provided stress (or strain) limits are not exceeded. The first case is discussed briefly in this section, since it is applied in the large majority of design situations. Limit-state based stability design is discussed in Chapter 13.

The analysis of on-bottom stability is based on the simple force balance or detailed finite element analysis. The loads acting on the pipeline due to wave and current action are fluctuating drag, lift, and inertia forces. The friction resulting from the effective submerged weight of the pipeline on the seabed to ensure stability must resist these forces. If the weight of the pipe steel and contents or the use of rock berms is insufficient, then the design for stability must establish the amount of concrete coating required. In a design situation, a factor of safety is required by most pipeline codes.

Figure 1.7 illustrates the component forces on subsea pipelines under current loads. For the pipeline to be stable on a seabed the following relationship must be satisfied:

$$\gamma(F_{\mathrm{D}} - F_{\mathrm{I}}) \leq \mu_{\mathrm{L}}(w_{\mathrm{sub}} - F_{\mathrm{L}}) \qquad\qquad [1.5]$$

where

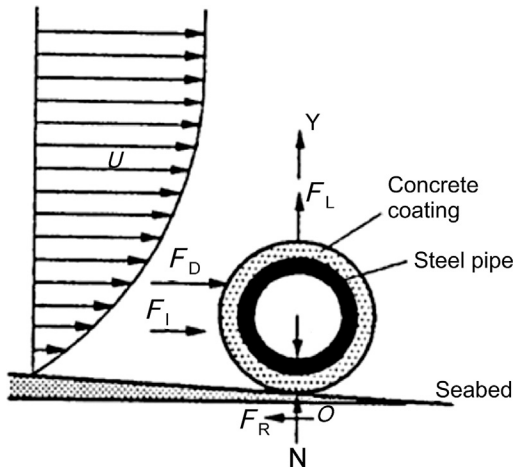γ = factor of safety, normally not to be taken as less than 1.1
F_{D} = hydrodynamic drag force per unit length
F_{I} = hydrodynamic inertia force per unit length
μ_{L} = lateral soil friction coefficient
w_{suib} = submerged pipe weight per unit length
F_{L} = hydrodynamic lift force per unit length

Figure 1.7 Subsea pipeline stability analysis.

The hydrodynamic forces are derived using traditional fluid mechanics with a suitable coefficient of drag, lift and diameter, roughness, and local current velocities and accelerations.

The effective flow to be used in the analysis consists of two components:

- The steady current, which is calculated at the position of the pipeline using boundary layer theory.
- The wave induced flow, which is calculated at the seabed using a suitable wave theory.

The selection of flow depends on the local wave characteristics and water depth. The wave and current data must be related to extreme conditions. For example, the wave with a probability of occurring only once in 100 years is often used for the operational lifetime of a pipeline. A less severe wave, say, 1 year or 5 years, is applied for the installation case where the pipeline is placed on the seabed in an empty condition with less submerged weight.

Friction, which depends on the seabed soils and submerged weight of the line, provides the equilibrium of the pipeline. It must be remembered that this weight is reduced by the fluid lift force. The coefficient of lateral friction can vary from 0.1 to 1.0, depending on the surface of the pipeline and on the soil. Soft clays and silts provide the least friction, whereas coarse sands offer higher resistance to pipeline lateral movement.

It can be seen that stability design is a complex procedure that relies heavily on empirical factors, such as force coefficient and soil friction factors. The appropriate selection of values depends strongly on the experience of the engineer and the specific design conditions.

The aim of the subsea pipeline stability analysis described is to determine the additional weight coating required. Should the weight of the concrete required for stability make the pipe too heavy to be installed safely, then additional means of stabilization are necessary. The two main techniques are

- To remove the pipeline from the current forces by trenching.
- To provide additional resistance to forces by use of anchors (rock berms) or additional weights on the pipeline.

In the latter case, the spacing of the anchors must be designed to eliminate the potential for sections of line between the fixed points to undergo large movements or suffer high stress levels. The safety of the line on the seabed is again the most important criterion in the stability design.

A finite element model for on-bottom stability analysis is discussed in Chapter 13.

Thermal Expansion Analysis

The thermal expansion analysis determines the maximum pipeline expansion at both termination ends and the maximum associated axial load in the pipeline. Both results have significant implications in the design as

- The axial load determines if the line may globally buckle during operation, and hence additional analysis or restraint is required.
- The end expansions dictate the expansion that the tie-in spools (or other) have to accommodate.

As shown in Figure 1.8, the expansion at the pipeline ends is a function of the operational parameters and the restraint on the pipeline. The line expands up to the "anchor point," and past this point, the line does not expand (hence, fully restrained). The distance between the pipeline end and this anchor point is determined based on the operational parameters and the pipeline restraints. The less the restraint, the greater the anchor length becomes and hence the longer the tie-in expansion becomes.

Global Buckling Analysis

Global buckling of a pipeline occurs when the effective axial compressive force within the line becomes so great that the line has to deflect laterally or vertically and so reduce these axial loads (i.e., takes a lower energy state). As more and more pipelines operate at higher temperatures (over $100°C$) the likelihood of global buckling becomes more pertinent.

Global buckling analysis is performed to identify whether buckling is likely to occur (see Figure 1.9). If it is, then further analysis is performed to either prevent buckling or accommodate it.

A method of preventing buckling is to rock dump the pipeline. This induces even higher loads in the line but prevents it from buckling. However, if the rock dump does

Expansion analysis
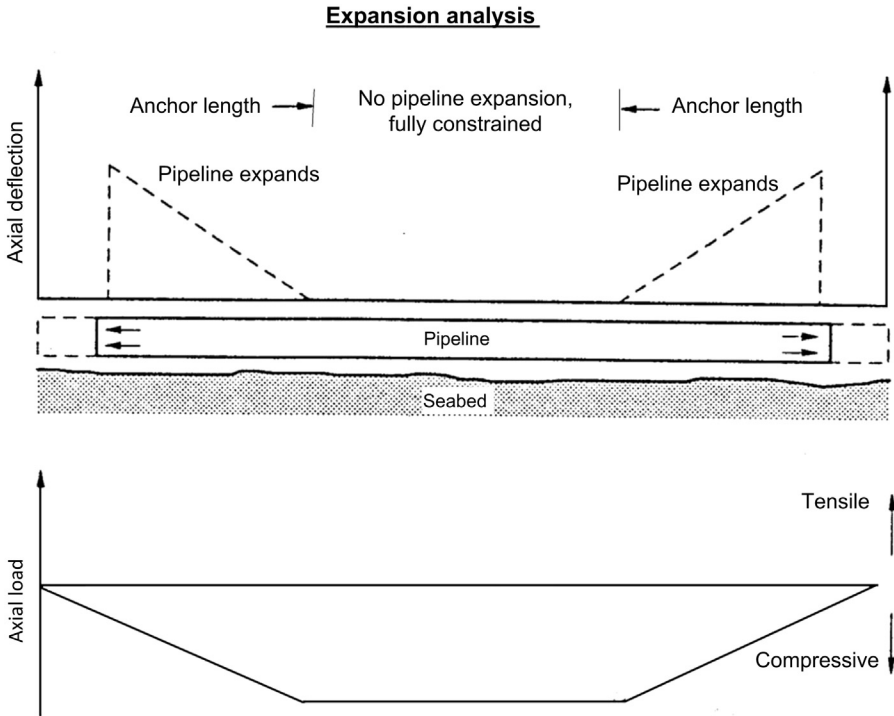
Figure 1.8 Thermal expansion of a pipeline.

not provide enough restraint, then global buckling may occur (i.e., upheaval buckling), which can cause failure of the line.

Another method is to accommodate the buckling problem by permitting the pipeline to deflect (for example, by snake lay, buckle mitigation methods such as sleepers, distributed buoyancies) on the seabed. This method is obviously cheaper than rock dumping and results in the pipeline experiencing lower loads. However, the analysis probably will have to be based on the limit-state design, as the pipe will have plastically deformed. This method is becoming more popular, and it can also be used with intermittent rock dumping, by permitting the pipeline to snake and then to rock dump, this reduces the likelihood of upheaval buckling.

The methods employed in calculating upheaval and lateral buckling are detailed in references [4] and [5] and in Chapters 10 and 11.

Pipeline Installation

There are various methods of installing pipelines and risers. For example,

- Pipe laying by lay vessel.
- Pipe laying by reel ship.
- Pipeline installation by the tow or pull method.
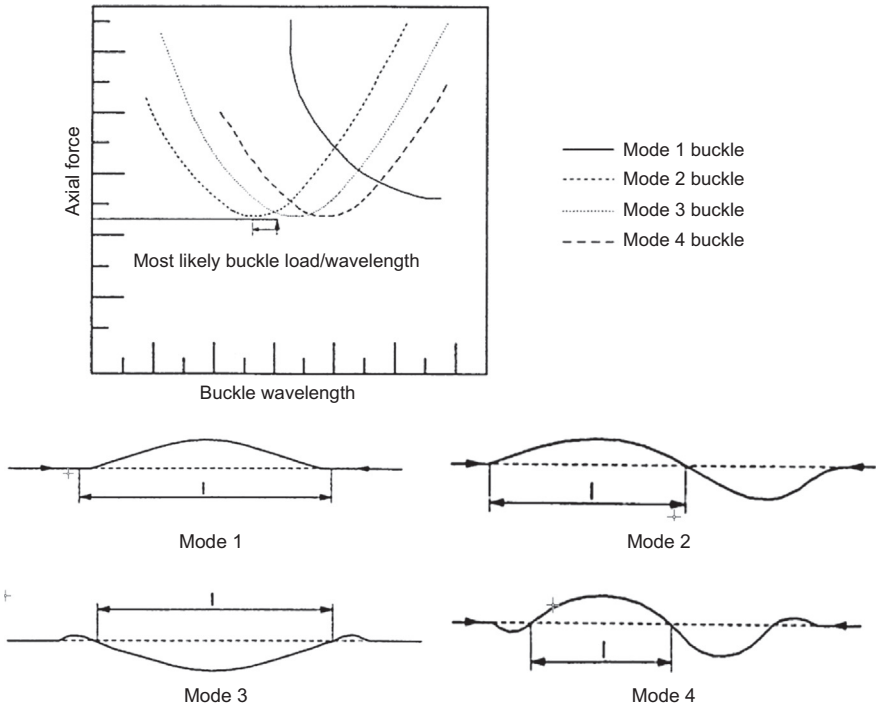
Figure 1.9 Global buckling of a pipeline.

The installation methods that determine the type of analysis performed are discussed as follows.

Pipe Laying by Lay Vessel

This method (including S-lay and J-lay) involves joining pipe joints on the lay vessel, where at a number of work stations, welding, inspection, and field joint coating take place (see S-lay in Figure 1.10). Pipe laying progresses with the lay vessel moving forward on its anchors. The pipe is placed on the seabed in a controlled S-bend shape. The curvature in the upper section, or overbended, is controlled by a supporting structure, called a *stinger*, fitted with rollers to minimize damage to the pipe.

The curvature in the lower portion is controlled by application of tension on the vessel using special machines. The pipeline designer must analyze the pipe lay configuration to establish that the correct tension capacity and barge geometry are set up and that the pipe will not be damaged or overstressed during the lay process.

The appropriate analysis can be performed by a range of methods from simple catenary analysis, to approximate solutions, to precise analysis using finite element analysis. The main objective of analysis is to identify stress levels in two main areas. The first is on the stinger (overbend), where the pipe can undergo high bending, especially at the last support. Since the curvature can now be controlled,
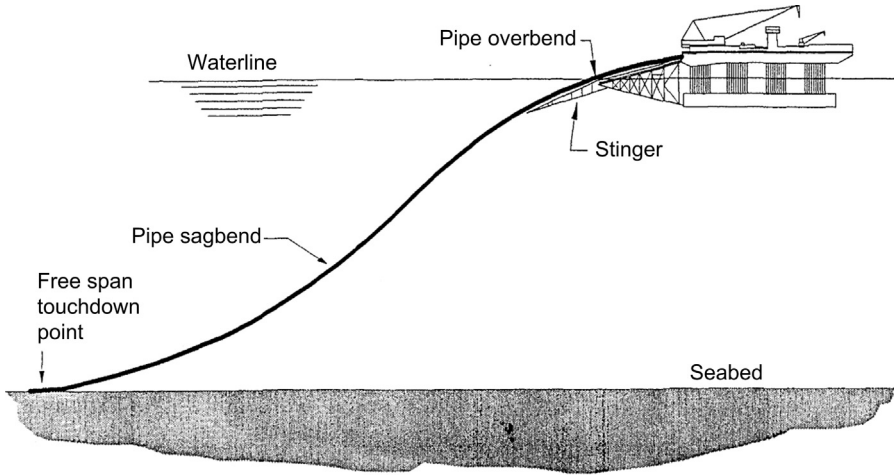
Figure 1.10 Typical pipe configuration during S-lay pipeline installation.
Source: Bai and Bai [1].

the pipeline codes generally allow a small safety factor for pipeline at the overbend section.

The second high stress area is in the sag bend, where the pipe is subject to bending under its own weight. The curvature at the sag bend varies with pipeline lay tension and consequently is less controllable than the overbend.

In all cases, the barge geometry and tension are optimized to produce stress levels in the pipe wall within specified limits.

Pipe Laying by Reel Ship

The pipe reeling method has been widely used in the North Sea and Gulf of Mexico for rigid pipeline sizes up to 18 inches in diameter. The pipeline is made up onshore and reeled onto a large drum on a purpose built vessel. During the reeling process, the pipe undergoes plastic deformation on the drum. During installation, the pipe is unreeled and straightened using a special straightened ramp. The pipe is then placed on the seabed in a similar configuration of J-lay to that used by the lay barge, although in most cases, a steeper ramp is used and overbend curvature is eliminated.

The analysis of pipe reeling lay can be carried out using the same techniques as for the lay barge. Special attention must be given to the compatibility of the reeling process with the pipeline steel grade, since the welding process can cause unacceptable work hardening in higher grade steels.

A major consideration in pipeline reeling is that the plastic deformation of the pipe must be kept within limits specified by the relevant codes, such as DNV-RP-F108. Existing reel ships reflect such code requirements.

Pipeline Installation by Tow or Pull

In certain circumstances, a pipeline may be installed by a towing technique, where long sections of line are made up onshore and towed either on the seabed or off the bottom by means of an appropriate vessel (tug or pull barge). The technique has its advantages for short lines and bundled lines, where several pipelines are collected together in a carrier. In this case, difficult fabrication procedures can be carried out onshore. The design procedures for towed or pulled lines depend greatly on the type of installation required. For example, it is important to control the bottom weight of a bottom towed line to minimize towing forces and at the same time give sufficient weight for stability. Therefore, a high degree of weight optimization may be needed, which can involve tighter control on pipeline wall thickness tolerances than for pipe laying, for example.

Detailed subsea pipeline installation is described in Chapter 33.

5. Finite Element Analysis

Since the mid-1980s, computer speed and software allow more accurate, detailed finite element analyses of pipeline behavior in order to optimize design and achieve cost reductions. The detailed finite element analyses of pipeline include in-place global response analysis, local strength analysis, and LCC (life cycle cost) design analysis.

The in-place global analyses simulate through-life behavior of pipelines, including the following design aspects:

- Installation.
- On-bottom stability.
- Expansion, upheaval, and lateral buckling.
- Free-span VIV.
- Trawl pullover and hooking response.

The in-place global analyses further incorporate reliability (probabilistic) design. Typical reliability design includes

- Calibration of safety factors used in the estimation of the appropriate cover height required to prevent upheaval buckling.
- Probabilistic analysis of hydrodynamic loads and soils friction for on-bottom stability design.

The local strength analyses provide tools for limit-state design to predict pipeline strength under the following failure modes [6]:

- Local buckling.
- Bursting.
- Ratcheting.
- Material nonhomogeneity.
- Fracture and fatigue based on damage mechanics.
- Trawl impacts and dropped objects.

The local strength analyses also incorporate probabilistic analysis. Typical probabilistic analyses are reliability-based strength criteria, in which safety factors are calibrated using structural reliability.

Advanced general-purpose finite element programs (ABAQUS and ANSYS) have been applied in the practical design of pipelines as described next:

1. **Advanced analysis for design** to simulate pipeline in-place behavior during the following through-life scenarios:
   - Installation [7].
   - Flooding, pressure test, dewatering, filling with product.
   - Pressure and temperature cycling due to operation and shutdowns.
   - Expansion, upheaval, and lateral buckling [4], [5].
   - Wave and current loads.
   - On-bottom stability [8].
   - Vortex-induced vibrations [9], [10].
   - Trawl board pullover and hooking [5].
   - Effects of changes in the seabed profile.
2. **Numerical tool as alternatives to** full-**scale tests** to develop design criteria with respect to allowable span height and energy absorption capacity requirement from consideration of protection of free-spanning pipeline against fishing gear impact loads and dropped objects loads [5]. Until some years ago, full-scale tests had been the only reliable method to determine strength. These tests require large amounts of resources and costs. Today, many full-scale tests may be performed numerically using the finite element approach.
3. **Numerical structural laboratory for limit-state design** to develop design criteria with respect to structural strength and material behavior as follows:
   - Local buckling and plastic collapse [11].
   - Bursting strength under load-controlled and displacement-controlled situations.
   - Ratcheting of ovalization due to cyclic loads [12].
   - Material nonhomogeneity and computational welding mechanics.
4. **Reliability-based design**, such as selecting wall thickness, especially corrosion allowance, based on reliability uncertainty analysis and LCC optimization [13, 14].
5. **Reliability-based calibration of safety factors** to select partial safety factors used in the LRFD (load resistance factored design) format by reliability-based calibrations [15], [16].

References

[1] Bai Y, Bai Q. Subsea pipelines and risers. Oxford, UK: Elsevier Science Ltd; 2005.
[2] Langford G, Kelly PG. Design, installation and tie-in of flowlines. JPK Report Job No. 4680.1 1990.
[3] Bai Y, Damsleth PA. Design through analysis applying limit-state concepts and reliability methods. Proc of ISOPE'98 1998.
[4] Nystrøm P, Tørnes K, Bai Y, Damsleth PY. Dynamic buckling and cyclic behavior of HP/HT pipelines. Proc of ISOPE'97 1997.
[5] Tørnes K, Nystrøm P, NØ Kristiansen, Bai Y, Damsleth PA. Pipeline structural response to fishing gear pullover loads. Proc of ISOPE'98 1998.
[6] Bai Y, Damsleth PA. Limit-state based design of offshore pipelines. Proc of OMAE'97 1997.

[7] Damsleth PA, Bai Y, Nystrømand PR, Gustafsson C. Deepwater pipeline installation with plastic strain. Proc of OMAE'99 1999.

[8] Ose BA, Bai Y, Nystrøm PR, Damsleth PA. A finite element model for in-situ behavior of offshore pipelines on uneven seabed and its application to on-bottom stability. Proc of ISOPE'99 1999.

[9] Kristiansen NØ, Tørnes K, Nystrøm PR, Damsleth PA. Structural modeling of multi-span pipe configurations subjected to vortex induced vibrations. Proc of ISOPE'98 1998.

[10] Reid A, Grytten TI, Nystrøm PR. Case studies in pipeline free span fatigue. Proc of ISOPE'2000 2000.

[11] Hauch S, Bai Y. Use of finite element methods for the determination of local buckling strength. Proc of OMAE'98 1998.

[12] Kristiansen NØ, Bai Y, Damsleth PA. Ratcheting of high pressure high temperature pipelines. Proc of OMAE'97 1997.

[13] Nødland S, Bai Y, Damsleth PA. Reliability approach to optimize corrosion allowance. Proc of Int Conf on Risk Based and Limit-State Design and Operation of Pipelines 1997.

[14] Nødland S, Hovdan H, Bai Y. Use of reliability methods to assess the benefit of corrosion allowance. Proc of EUROCORR'97 1997;2:47–54.

[15] Bai Y, Song R. Fracture assessment of dented pipes with cracks and reliability-based calibration of safety factors. Int J Pressure Vessels and Piping 1997;74:221–9.

[16] Bai Y, Xu T, Bea R. Reliability-based design and requalification criteria for longitu-dinally corroded pipelines. Proc of ISOPE'97 1997.

2 Wall Thickness and Material Grade Selection

Chapter Outline

1.   Introduction

General

In this chapter, the basis for the design of wall thickness is reviewed and compared with industry practice. The codes reviewed are ABS [1]; API [2]; ASME B31 [3, 4]; BS 8010 [5]; DNV [6]; and ISO [7]. The selection of wall thickness is one of the most important and fundamental tasks in the design of subsea pipelines. While this task involves many technical aspects related to different design scenarios, primary design loads relevant to the containment of the wall thickness are as follows:

- Internal pressure loads.
- External hydrostatic pressure loads.
- Longitudinal functional loads.

- Bending loads.
- External impact loads.

Different loads induce different failure mechanisms; therefore, the following failure criteria should be satisfied in the wall thickness design:

- Burst.
- Collapse.
- Buckle.

Pipeline bursting occurs when, due to the internal pressure (differential pressure), the tensile hoop stress in the pipe wall is higher than the yield stress and it reaches the ultimate tensile strength of the material; the tensile failure happens at the weakest location of the pipeline. The allowable stress design (ASD) principles ensure that the stress in the pipeline never exceeds the yield stress. The design practice of limiting the hoop stress for design against the differential pressure and limiting the equivalent stress for design against combined loads has proven to be very safe in general, except when external impact loads are critical to the integrity of the pipeline. Nevertheless, this practice has been used by the pipeline industry for decades with little change, despite significant improvements and developments in the pipeline technology, see Sotberg and Bruschi [8] and Verley et al. [9].

Considering the precise design and effective quality and operational control achieved by the modern industry and with the availability of new materials, the need to rationalize the wall thickness sizing practice for a safe and cost-effective design has been realized, see Jiao et al. [10]. Limit state design (LSD) specifies the failure conditions of the pipeline. The ultimate strength of the material with a safety factor is used for the design criteria. Limit state design enables the designer to account for the low probability of worst conditions and determine the pipe design required to achieve a satisfactory level of safety. These safety levels need to reflect a range of issues, including economic, public relations, and environmental costs. The limit state design for pipelines is detailed in Chapter 4.

New design codes also provide guidance on application of high strength and new materials, as well as design of high pressure and high temperature pipelines.

Pipeline Design Codes

ASME B31 Codes

The early history of pipeline design codes started in 1926 with the initiation of the B31 code for pressure piping [11, 12] followed by the well-known ASME codes B31.8 for gas transmission [4] and distribution piping systems and B31.4 [3] for oil transportation piping in the early 1950s. The main design principle in these two codes is that the pipeline is assessed as a pressure vessel, by limiting the hoop stress to a specific fraction of the yield stress.

A brief outline of the relative design codes is given next.

ISO 13623

A pipeline code for both offshore and onshore applications was developed by ISO (International Standards Organization) [7]. The guideline allows the use of structural reliability techniques by means of limit-state based design procedures, such as those proposed by SUPERB [10]. This code and guideline represent a valuable common basis for the industry for the application of design methods and philosophy.

API RP 1111

The recommended practice, API RP 1111 for offshore pipelines containing hydrocarbons has been updated based on the limit state design concept to provide a uniform safety level [2]. The failure mode for rupture and bursting is used as the primary design condition independent of pipe diameter, wall thickness, and material grade.

DNV Pipeline Rules

The first edition of DNV rules for the design, construction, and inspection of submarine pipelines and pipeline risers was issued in 1976, and the design section was based mainly on the ASME codes, although it was written for offshore applications only. The safety philosophy in the DNV'96 pipeline and DNV-OS-F101 [6] is based on that developed by the SUPERB Project. The pipeline is classified into safety classes based on location class, fluid category, and potential failure consequences. Further, a limit state methodology is adopted, and its basic requirement is that all relevant failure modes (limit states) are considered in the design.

ABS Guide for Building and Classing Subsea Pipeline Systems

A guide for building and classing subsea pipelines and risers was completed by ABS [1]. The guide uses working stress design (WSD) for the wall thickness design. The guide optionally allows use of limit state design and risk/reliability-based design. It does contain new criteria for defect assessment. Criteria for other failure modes relevant for the in-place condition, installation, and repair situations have been evaluated and developed based on design projects, relevant JIPs (Joint Industry Projects), and industry experience.

Pipeline Wall Thickness

The required pipeline wall thickness is made up of several components, which is expressed as

$$t_{\text{req}} = t_{\text{min}} + t_{\text{corr}} + t_{\text{fab}} \tag{2.1}$$

where

t_{min} = minimum wall thickness required for pressure containment, which is calculated based on the design code

t_{corr} = corrosion allowance; typically chosen between 0.12 and 0.24 in.
t_{fab} = manufacturing under tolerance on wall thickness

If the pipe is specified to API 5L, the negative manufacturing tolerance is –12.5% of t_{nom} for SMLS pipe with a wall thickness of 4 to 25 mm, –10% of t_{nom} for welded pipe with a thickness between 5 and 15 mm.

2.   Material Grade Selection

General

The steels applied in the offshore oil and gas industry vary from carbon steels (API standards Grade B to Grade X70 and higher) to exotic steels (i.e., duplex). The following factors are to be considered in the selection of material grades:

- Cost.
- Resistance to corrosion effects.
- Weight requirement.
- Weldability.

The higher the grade of steel (up to exotic steels), the more expensive it is per volume (weight). However, as the cost of producing high grade steels has reduced, the general trend in the industry is to use steel of higher grades. See Chapter 31, "Use of High Strength Steel." It is clear that the selection of steel grade forms a critical element of the design.

Fabrication, Installation, and Operating Cost Considerations

The choice of material grade used for the pipelines has cost implications on

- Fabrication of pipeline.
- Installation.
- Operation.

Fabrication

The cost of steels increases for the higher grades. However, the increase in grade may permit a reduction of pipeline wall thickness, resulting in the overall reduction of fabrication cost when using a high grade steel compared with a lower grade steel.

Installation

It is difficult to weld high grade steels; consequently, the lay rate is lower than laying lower grade steels. However, should the pipeline be laid in very deep water and a vessel is laying at its maximum lay tension, the use of high grade steel may be more suitable, as the reduction in pipe weight results in lower lay tension. In general, from an installation aspect, lower grade steel pipelines cost less to install.

Operation

Depending on the product being transported in the pipeline, the pipeline may be subjected to

- Corrosion (internal).
- Internal erosion.
- H_2S induced corrosion.

Designing for no corrosion defect may be performed by either material selection or modifying operation procedures (i.e., through use of chemical corrosion inhibitors).

To select a material for a pipeline, the effect of environmental parameters, such as temperature, pressure, water, CO_2, and H_2S, on the ability of material to resist corrosion should be known first. For sweet environments, carbon steel, low alloy martensitic steels, austenitic steels, lined pipe, and duplex stainless steels are more suitable, but for sour environments, the most suitable materials are carbon steel, duplex stainless steels, lined pipe, and nickel alloy-clad pipe.

Material Grade Optimization

Optimization of the material grade is rigorously applied today, based on experience gained from the past pipeline design and the technical advances in line pipe manufacturing and welding. The optimization is based on minimization of fabrication and installation cost while meeting operating requirements. As the selection of material grade has a significant impact on the operating life of the pipeline, the operator is normally involved in the final selection of material grade.

3. Pressure Containment Design

General

The hoop stress criterion limits the characteristic tensile hoop stress, σ_h, due to a pressure differential between internal and external pressures:

$$\sigma_h < \eta_h \text{ SMYS } k_t \tag{2.2}$$

where η_h is the design usage factor, SMYS is the specified minimum yield strength, and k_t is the material temperature derating factor, refer to Table 841.1.8-1 of ASME B31.8. The hoop stress equation is commonly expressed in the following simple form:

$$\sigma_h = (p_i - p_e)\frac{D}{2t} \tag{2.3}$$

where p_i and p_e are the internal and external pressures, respectively; D is the nominal outside diameter of pipe; and t is the wall thickness.

For subsea pipelines located in the off-platform zone, the design (usage) factor is specified as 0.72 by all major codes. For pipelines in the near-platform zone and risers

Table 2.1 Characteristic Thickness and Diameter Used in Various Pipeline Codes

Code	Thickness	Diameter
ABS (2006)	Minimum	Mean, $(D - t)$
ASME B31.1 (1951)	Minimum	External $- 0.8\ t_{min}$
ASME B31.3 (2002)	Minimum	External, mean or external $-0.8t_{min}$
ASME B31.4 (2006)	Nominal	External for $D/t > 20$
ASME B31.8 (2007)	Nominal	External for $D/t > 30$, otherwise mean
BS 8010 (2004)	Minimum	External, close to mean for $D/t \leq 20$
CEN 234WG3-103 (1993), [14]	Minimum	External
CSA-Z662-03 (2003), [15]	Minimum	External
Danish Guidelines	Minimum	Internal
DNV-OS-F101 (2010)	Minimum	Mean
NEN 3650 (1992), [16]	Minimum	Mean
NPD (1990)	Minimum	External

(safety zone), the usage factor is specified as 0.50 by ASME B31.8 or 0.60 by NPD [13]. The origin for a design factor 0.72 can be traced back to the (1935) B31 codes, where the working pressure was limited to 80% of the mill test pressure, which itself was calculated using Eq. [2.2] with a design factor up to 0.9. The effective design factor for the working pressure was therefore $0.8 \times 0.9 = 0.72$. Since the 1958 version of B31.8 codes, the factor 0.72 has been used directly to obtain the design pressure for land pipelines.

Furthermore, the definition of diameter and thickness used in Eq. [2.3] varies among the codes, see Table 2.1. In recent codes, such as NPD (1990) and BS 8010 (2004) [5], the minimum wall thickness is used rather than the nominal wall thickness, while the usage factor remains unchanged. This may result in a considerably higher steel cost, indicating such codes are relatively more conservative despite the significant improvements and developments in pipeline technology.

In most codes, the maximum SMYS used in Eq. [2.2] is limited to 490 MPa and the yield to tensile strength ratio to 0.85. This limits the use of high strength carbon steel, such as steel grade X80 or higher. The yielding check implicitly covers other failure modes as well. To extend the material grade beyond the current limit, explicit checks for other failure modes may be necessary; see Chapter 4.

DNV-OS-F101

The primary requirement of the pipe wall thickness selection is to sustain stresses for pressure containment. The tensile hoop stress is due to the difference between internal and external pressures and is not to exceed the permissible value, as given by the following hoop stress criterion:

$$\sigma_h = (p_i - p_e)\frac{D - t_1}{2t_1} \leq \eta\left(\text{SMYS} - f_{y,\text{temp}}\right) \tag{2.4}$$

Table 2.2 Design Factors η for Pipelines, Platform Piping, and Risers

	Hoop Stress	Longitudinal Stress	Equivalent Stress
Oil and gas pipelines, liquid hydrocarbon piping	0.72	0.80	0.90
Risers on nonproduction platforms	0.60	0.80	0.90
Gas piping, gas risers on production platforms	0.50	0.80	0.90

Source: Originally from ASME B31.4 and B31.8.

where

σ_h = hoop stress
p_i = internal pressure
p_e = external pressure
D = nominal outside diameter of pipe
t_1 = characteristic wall thickness, defined in Table 5.2 of DNV-OS-F101 [6]; for operation, equal to nominal wall thickness – fabrication tolerance – corrosion allowance
$f_{y,temp}$ = derating value due to temperature, (Figure 2 in Sec. 5 of DNV-OS-F101 [6])

The usage factor for pressure containment, as shown in Eq. (13.5) of DNV-OS-F101 [6], is expressed as

$$\eta = \frac{2 \cdot \alpha_U}{\sqrt{3} \cdot \gamma_m \cdot \gamma_{sc} \cdot \gamma_{inc}}$$

where

α_U = material strength factor
γ_m = material resistance factor
γ_{sc} = safety class factor
γ_{inc} = incidental to design pressure ratio.

ABS Guide for Building and Classing Subsea Pipeline Systems

As the requirement for pressure containment, the allowable hoop stress σ_h to be used in design calculations is to be determined by the following hoop stress criterion [1]:

$$\sigma_h = \eta_h \cdot \text{SMYS} \cdot k_T \qquad [2.5]$$

where

η_h = design factor (see Table 2.2, originally from B31.4 and B31.8)
k_T = temperature derating factor for gas when temperatures is above 121°C, see Table 841.1.8-1 of ASME B31.8 [4]; $k_T = 1$ for oil

The hoop stress σ_h in a pipe can be determined by the equation

$$\sigma_h = \frac{(p_i - p_e)(D - t)}{2t} \qquad [2.6]$$

where

  σ_h = hoop stress
  p_i = internal or external design pressure
  p_e = external design pressure
  D = nominal outside diameter of pipe
  t = minimum pipe wall thickness

For relatively thick-walled pipes, where the ratio D/t is equal to or less than 20, a more accurate hoop stress calculation method, such as BSI BS 8010-3, resulting in a lower stress, may be used.

U.S. Codes of Federal Regulations

In the United States, the production flowlines and risers are covered by 30 CFR 250 [17], Subpart J (MMS Department of the Interior), while export pipelines and risers are covered by 49 CFR 192 [18] (Gas) and 49 CFR 195 [19] (Oil) (Department of Transportation, DOT). CFR denotes the U.S. Code of Federal Regulations.

$$\sigma_h = \frac{p_i D_o}{2t} \leq \eta SET \ (49 \ CFR \ 195) \qquad [2.7]$$

$$\sigma_h = \frac{\Delta p_i D_o}{2t} \leq \eta SET \qquad (30 \ CFR \ 250, \ 49 \ CFR \ 192) \qquad [2.8]$$

The design factors defined in Table 2.2 are consistent with these regulations, as discussed next.

All three CFRs require hoop stress design factor of 0.72 for gas and oil pipelines and field flowlines. 30 CFR 250 and 49 CFR 195 require the design factor of 0.60 for flowline risers and oil export risers, while 49 CFR 192 requires the factor be 0.50 for gas export risers.

Both 30 CFR 250 and 49 CFR 195 require a test pressure of 1.25 times the maximum allowable operating pressure for pipelines and risers. 49 CFR 192 requires a test pressure of 1.25 times the maximum allowable operating pressure for pipelines and 1.5 for the risers.

30 CFR 250 requires that pipelines shall not be pressure tested at a pressure that produces a stress in the pipeline in excess of 95% of the specified minimum yield stress of the pipeline.

API-RP-1111

Maximum Design Burst Pressure

The hydrostatic test pressure, the pipeline design pressure, and the incidental over-pressure, including both internal and external pressures acting on the pipelines, shall not exceed that given by the following formulas [2]:

$$P_t \le f_d f_e f_t P_b \qquad\qquad [2.9]$$

$$P_d \le 0.80 P_t \qquad\qquad [2.10]$$

$$P_a \le 0.90 P_t \qquad\qquad [2.11]$$

where

f_d = internal pressure (burst) design factor; 0.90 for pipelines and 0.75 for pipeline risers
f_e = weld joint factor, longitudinal or spiral seam welds (see ASME B31.4 or ASME B31.8); only materials with a factor of 1.0 are acceptable
f_t = temperature derating factor, as specified in ASME B31.8; 1.0 for temperatures less than 121° C
P_a = incidental overpressure (internal minus external pressure)
P_b = specified minimum burst pressure of pipe
P_d = pipeline design pressure
P_t = hydrostatic test pressure (internal minus external pressure)

The specified minimum burst pressure P_b is determined by one of the following equations:

$$P_b = 0.90(\text{SMYS} + \text{SMTS})\left(\frac{t}{D - t}\right), \qquad\qquad [2.12]$$

or

$$P_b = 0.45(\text{SMYS} + \text{SMTS})\ln\left(\frac{D}{D_i}\right) \qquad\qquad [2.13]$$

where

D = outside diameter of pipe;
D_i = inside diameter of pipe;
$SMYS$ = specified minimum yield strength of pipe (see API Specification 5L, ASME B31.4, or ASME B31.8 as appropriate)
t = nominal wall thickness of pipe
SMTS = specified minimum tensile strength of pipe

Note: Equations [2.12] and [2.13] for the burst pressure are for $D/t > 15$. For low D/t, Eq. [2.13] is recommended.

Substituting the pressure test pressure into Eq. [2.9], the maximum design burst pressure is calculated:

$$P_d \leq 0.80 f_d f_e f_t P_b$$

Substituting the burst pressure P_h into Eq. [2.12], the maximum design burst pressure is calculated:

$$P_d \leq 0.80 f_d f_e f_t 0.90 (\text{SMYS} + \text{SMTS}) \left(\frac{t}{D - t} \right)$$

Longitudinal Load Design

The effective tension due to static primary longitudinal loads shall not exceed the value given by:

$$T_{eff} \leq 0.60 T_y \tag{2.14}$$

where

$$
\begin{aligned}
T_{eff} &= T_a - P_i A_i + P_o A_o \\
T_a &= \sigma_a A \\
T_y &= \text{SMYS} \cdot A \\
A &= A_o - A_i = \frac{\pi}{4} (D^2_o - D^2_i)
\end{aligned}
$$

A = cross-sectional area of pipe steel
A_i = internal cross-sectional area of the pipe
A_o = external cross-sectional area of the pipe
P_i = internal pressure in the pipe
P_o = external hydrostatic pressure
T_a = axial tension in pipe
T_{eff} = effective tension in pipe
T_y = yield tension of the pipe
σ_a = axial stress in the pipe wall

Rewriting the Eq. [2.14] yields, for external overpressure,

$$\sigma_{eff} = \sigma_a + \frac{\Delta P e \cdot A_o}{A} + P_i \leq 0.60 \text{SMYS}$$

where

σ_{eff} = effective stress
$\Delta P e$ = external overpressure, $P_o - P_i$

4. Equivalent Stress Criterion

The equivalent stress criterion based on von Mises' equivalent stress σ_{eq}, may be defined as

$$\sigma_{eq} = \sqrt{\sigma_l^2 + \sigma_h^2 - \sigma_l \sigma_h + 3 \tau_c^2} \leq \eta_e \cdot \text{SMYS} \tag{2.15}$$

in which η_e, is the usage factor, σ_l is the characteristic longitudinal stress, σ_h is the characteristic hoop stress, and τ_c is the characteristic tangential shear stress. The Tresca yielding criterion is used in some codes.

ASME B31.8 specifies a usage factor of 0.90 for both the safety zone and the midline zone. However, this criterion is not required in situations where the pipeline experiences a predictable noncyclic displacement of its support (e.g., fault movement or differential subsidence) or pipe sag leads to support contact as long as the consequences of yielding are not detrimental to the structural integrity of the pipeline.

BS 8010 (1993) requires a usage factor of 0.72 for risers and 0.96 for pipelines for functional and environmental (or accidental) loads, respectively, and a usage factor of 1.0 for construction or hydrotest loads. The SMYS is defined as a function of a temperature T in the equivalent stress equation.

The characteristic hoop stress is expressed as follows:

$$\sigma_h = \Delta p_d \frac{D - t_2}{2t_2} \qquad [2.16]$$

where

$t_2 = t - t_{corr}$
Δp_d = design differential overpressure

Variations in the code requirements for combined stress criterion are evident not only in terms of the usage factor, but also with respect to applicability of the criterion. While this design format may be suitable for predominantly longitudinal stresses, it becomes irrelevant when localized stress concentration, caused by, say, impact loads, is of concern. No explicit design criteria are currently available for design against impact loads.

For deepwater pipeline, the wall thickness should be designed such that sufficient bending moment or strain is reserved for free spans and external loads, as discussed in Chapter 4. In addition, it is necessary to design buckle arrests to stop possible buckle propagation.

5. Hydrostatic Collapse

The limit external pressure, p_l, is equal to the pipe collapse pressure and is to be calculated based on BS 8010, ABS, and DNV:

$$p_l^3 - p_{el} \cdot p_l^2 - \left(p_p^2 + p_{el} \cdot p_p \cdot f_0 \cdot \frac{D}{t} \right) \cdot p_l + p_{el} \cdot p_p^2 = 0 \qquad [2.17]$$

where

$$p_{el} = \frac{2 \cdot E}{(1 - v^2)} \cdot \left(\frac{t}{D} \right)^3 \qquad [2.18]$$

$$p_p = \eta_{fab} \cdot SMYS(T) \cdot \frac{2 \cdot t}{D} \qquad [2.19]$$

f_0 = initial out of roundness,[1] $(D_{\max} - D_{\min})/D$

D = average diameter

SMYS(T) = specified minimum yield strength in hoop direction

E = Young's modulus

ν = Poisson's ratio

η_{fab} = fabrication derating factor

The collapse equation, Eq. [2.17], is often expressed as follows:

$$(p_c - p_{el}) \cdot \left(p_c^2 - p_p^2\right) = p_c \cdot p_{el} \cdot p_p \cdot f_0 \cdot \frac{D_0}{t} \qquad [2.20]$$

The collapse equation can be solved by the following approach:

$$p_c = y - \frac{1}{3}b$$

where

$P_c = P_1$ in Eq. [2.17]

$b = -p_{el}$

$c = -\left(p_p^2 + p_p p_{el} f_0 \frac{D_o}{t}\right)$

$d = p_{el}p_p^2$

$u = \frac{1}{3}\left(-\frac{1}{3}b^2 + c\right)$

$v = \frac{1}{2}\left(\frac{2}{27}b^3 - \frac{1}{3}bc + d\right)$

$\phi = \arccos\left(\frac{-v}{\sqrt{(-u)^3}}\right)$

$y = -2\sqrt{-u} \cdot \cos\left(\frac{\phi}{3} + \frac{\pi}{3}\right)$

When calculating out of roundness, caution is required on its definition.

For installation and temporary conditions where the pipeline may be subject to a high external overpressure, cross-sectional instability in the form of collapse is to be checked. If for a pipe with D/t less than 50 and under combined bending strain and external pressure, the strain criteria may be as follows,

$$\frac{\varepsilon}{\varepsilon_b} + \frac{(p_e - p_i)}{f_c p_c} \leq g(\delta) \qquad [2.21]$$

where

ε = bending strain in the pipe

$\varepsilon_b = t/2D$; buckling strain under pure bending

---

[1] Out of roundness caused during the construction phase is to be included but not flattening due to external water pressure or bending in as-laid position. Increased out of roundness due to installation and cyclic operating loads may aggravate local buckling and is to be considered. Here it is recommended that out-of-roundness, due to through life loads, be simulated using finite element analysis.

$$\delta = \text{ovality} = \frac{D_{\max} - D_{\min}}{D_{\max} + D_{\min}}$$

$g(\delta) = $ collapse reduction factor $= (1 + 20\delta)^{-1}$

$f_c = $ collapse factor for using combined pressure and bending loads; 0.6 for cold expanded pipe, such as DSAW pipe, 0.7 for seamless pipe

$p_c = $ collapse pressure

$\varepsilon \geq f_1 \varepsilon_1$

$\varepsilon \geq f_2 \varepsilon_2$

The terms ε_1 and ε_2 are the maximum installation bending strain and maximum in-place bending strain, respectively. Safety factors, f_1 and f_2 should be determined by the designer with appropriate consideration of the magnitude of increases that may occur for installation bending strain or in-place bending strain. A value of 2.0 for the safety factor f_2 is recommended if no detailed information on the uncertainties of load effects is available. The safety factor f_1 may be larger than 2.0 for cases where installation bending strain could increase significantly due to off-nominal conditions or smaller than 2.0 for cases where bending strains are well defined (e.g., reeling) or in-place situation.

A lower safety factor may be allowed for installation phase provided that potential local buckling can be detected and repaired and buckling propagation can be stopped through use of buckle arrestors.

6. Buckle Arrestors

Wall Thickness and Length for Buckle Arrestors

During the installation, the risk of local buckling initiating a propagating buckle is considered to be high, hence, buckle arrestors are designed to limit the extent of the damage of a propagating buckle.

The equation used to determine whether a buckle arrestor is required may be taken as [2]

$$p_o - p_i \geq f_p P_{pr} \qquad [2.22]$$

where

$P_{pr} = $ propagating pressure for the pipeline, $P_{pr} = 24 \cdot \text{SMYS} \left(\frac{t}{D} \right)^{2.4}$;

$f_p = $ propagating buckle design factor, 0.80

$t = $ pipe wall thickness

$D = $ pipeline outer diameter

On solving the following equation, feasible buckle arrestor wall thickness and length combinations are obtained. This equation is valid for thick-walled cylindrical buckle arrestors (Sriskandarajah and Mahendran, 1987 [20]).

$$\left(P_x - P_{pr} \right) = \left(P_a - P_{pr} \right) \left[1 - \exp\left(-15 \frac{t_{BA} l_{BA}}{D_{BA}^2} \right) \right] \qquad [2.23]$$

where

$$P_x = \text{crossover pressure} = \text{SF } P_h \qquad\qquad [2.24]$$

l_{BA} = buckle arrestor length
SF = safety factor = 1.5

$$P_h = \rho_w g(h_{max} + h_t + h_s) \qquad\qquad [2.25]$$

where

P_h = hydrostatic pressure
ρ_w = seawater density
g = gravity
h_{max} = deepest depth with current pipeline thickness
h_t = tidal amplitude
h_s = storm surge

$$P_a = 34\text{SMYS}\left(\frac{t_{BA}}{D_{BA}}\right)^{2.5} \qquad\qquad [2.26]$$

where

P_a = propagating pressure for the buckle arrestor
t_{BA} = buckle arrestor wall thickness

$$D_{BA} = \text{buckle arrestor outer diameter} = D + 2t_{BA} \qquad\qquad [2.27]$$

For the design of a buckle arrestor, refer to the papers by Langner [21], and Kyriakides [22, 23].

Buckle Arrestor Spacing

The spacing of buckle arrestors is a trade-off between the cost of installing buckle arrestors at shorter spaces and the increased repair costs of longer intervals. The following equations have been compiled as an approach to optimizing the buckle arrestor spacing [24]:

$$C_{BA} = C_{Man} + C_{Matr} - C_{LP} \qquad\qquad [2.28]$$

where

C_{BA} = cost per buckle arrestor
C_{Man} = assumed manufacturing cost per buckle arrestor

$$C_{Matr} = \rho_s\, C_S\, V_{BA} \qquad\qquad [2.29]$$

C_{LP} = cost of pipeline pipe saved by inserting buckle arrestor

$$C_{LP} = L_{BA} \left[\frac{\pi}{4} \left[(D_i + 2t_P)^2 - D_i^2 \right] \rho_s C_s \right] \qquad [2.30]$$

where

t_P = pipeline thickness
ρ_s = steel density
C_s = cost of steel

$$V_{BA} = L_{BA} \left\{ \frac{\pi}{4} \left[(D_i + 2t_{BA})^2 - D_i^2 \right] \right\} \qquad [2.31]$$

where

V_{BA} = volume of buckle arrestor steel
C_P = cost of pipeline to be repaired, manufacturing assumed to be included in the day rate of a lay vessel

$$C_{P,Matr} = \rho_S \, C_S \, V_P \qquad [2.32]$$

$$V_P = (S + 3h) \left\{ \frac{\pi}{4} \left[(D_i + 2t)^2 - D_i^2 \right] \right\} \qquad [2.33]$$

where

V_P = volume of pipe to be repaired
S = spacing between buckle arrestors
h = greatest depth in the section considered

$$C_F = 30(C_{LV} + C_{DSV}) \qquad [2.34]$$

where

C_F = fixed cost if repair is needed
30 = assumed time [days] from when buckle occurs until repair is done and regular pipe laying is started
C_{LV} = daily rate of lay vessel
C_{DSV} = daily rate of diving support vessel

$$C_{TOTAL} = C_{BA}X + (C_F + C_P)M \qquad [2.35]$$

where

C_{TOTAL} = total cost of buckle arrestors, repair pipe, and repair

M = assumed probability of risk that a propagating buckle, during the laying, can be between 0 and 1. It is assumed to be 1 for the first 50 km of the first lay season, after which a probability of 0.05 is assumed until the end of the first lay season. For the second lay season, a probability of 1 is assumed, since the relative cost of delaying the installation of the riser is large

$$X = \frac{L}{S} \qquad\qquad\qquad [2.36]$$

where

X = number of buckle arrestors for the pipe length considered
L = pipe length considered

References

[1] ABS. Guide for building and classing subsea pipeline systems. American Bureau of Shipping; May 2006.

[2] API RP1111. Design, construction, operation, and maintenance of offshore hydrocarbon pipelines (limit state design). Washington, DC: American Petroleum Institute; 2009.

[3] ASME 31.4. Pipeline transportation systems for liquid hydrocarbons and other liquids. New York: American Society of Mechanical Engineers; 2006.

[4] ASME B31.8. Gas transmission and distribution piping systems. New York: American Society of Mechanical Engineers; 2007.

[5] BSI BS. 8010. Code of practice for pipeline —Part 2. Pipeline subsea. British Standards Institute; 2004.

[6] DNV. Offshore standard OS-F101, submarine pipeline systems. Det Norske Veritas; 2010.

[7] ISO. Petroleum and natural gas industries – pipeline transportation systems, ISO 13623. International Standards Organization; 2000.

[8] Sotberg T, Bruschi R. Future pipeline design philosophy—Framework. Int Conf on Offshore Mechanics and Arctic Engineering 1992.

[9] Verley R, Lund S, Moshagen H, et al. Wall thickness design for high pressure offshore gas pipelines. Int Conf on Offshore Mechanics and Arctic Engineering 1994.

[10] Jiao G, Sotberg T, Bruschi R, Verley R, et al. The SUPERB Project: Wall-thickness design guideline for pressure containment of offshore pipelines. Proc of OMAE'96 1996.

[11] ASME B31.1. ASME code for pressure piping, New York: American Society of Mechanical Engineers; 2001.

[12] ASME B31.3. Process piping. New York: American Society of Mechanical Engineers; 2002.

[13] NPD. Guidelines to regulations relating to pipeline systems in the petroleum activities; April 30, Norwegian Petroleum Directorate 1990.

[14] CEN 234WG3-103. Pipelines for gas transmission. European Committee for Standardization; 1993.

[15] CSA-Z662-03. Oil and gas pipeline systems. Canadian Standard Association; 2003.

[16] NEN 3650. Requirements for steel pipeline transportation systems. (Netherlands): Nederlands Normalisaatie Instituut; 1992.

[17] 30 CFR 250. Oil and gas and sulphur operations in the outer continental shelf. Code of Federal Regulations 2005.

[18] 49 CFR Part 192. Transportation of natural and other gas by pipeline: Minimum federal safety standards. Code of Federal Regulations 2005.

[19] 49 CFR Part 195. Transportation of hazardous liquids by pipeline. Code of Federal Regulations 2005.

[20] Sriskandarajah T, Mahendran IK. Parametric consideration of design and installation of deepwater pipelines. Presented at 1987 European Seminar Offshore Oil and Gas Pipeline Technology, 1987. Brown and Root U.K. Ltd; 1987.

[21] Langner CG. Buckle arrestor for deepwater pipelines. OTC 10711. Langner & Associates; 1999.

[22] Kyriakides S. Buckle propagation in pipe-in-pipe systems, Part I. Experiments. Int J Solids and Structures 2002;39:351–66.

[23] Kyriakides S, Vogler TJ. Buckle propagation in pipe-in-pipe systems, Part II. Analysis. Int J Solids and Structures 2002;39:367–92.

[24] Kenny A/S JP. Buckling arrestor design. Report No. D501-PK-P121-F-CE-003. J P Kenny A/S; 1997.

3 Buckling and Collapse of Metallic Pipes

1.   Introduction

The design of subsea pipelines and risers today is mainly based on a limit state design. In a limit state design, all foreseeable failure scenarios are considered and the system is designed against the failure modes that provide the lowest strength capacity. A pipe must sustain installation and operational loads. In addition, external loads, such as those induced by waves, current, uneven seabed, trawl-board impact, pullover, expansion due to pressure and temperature changes, need to be considered. Experience has shown that the main load effect on subsea pipes is bending combined with longitudinal force while subjected to external hydrostatic pressure during installation and internal pressure while in operation. A pipe subjected to bending may fail due to local buckling, collapse, or fracture, but it is the local buckling or collapse limit state that commonly dictates the design. The local buckling and collapse strength of metallic pipes have been the main subjects for many studies in

subsea and civil engineering, such as Murphey and Langner [1], Winter et al. [2], Ellinas et al. [3], Gresnigt [4], Mohareb et al. [5], and Bai et al. [6,7].

Bending Moment Capacity

The bending moment of pipe cross section is directly proportional to the pipe curvature, as shown in Figure 3.1.

The figure illustrates an initial straight pipe with low D/t (<60) subjected to a load scenario where pressure and longitudinal force are kept constant while an increasing curvature is applied. The moment-curvature relationship has several significant points. When applied load is increased, the pipe first is subjected to global deformation inside the material's elastic range without permanent deformation. The global deformation here means deformation that can be looked on as uniform over a range larger than 3–4 times the pipe diameter. After the linear limit of the pipe material has been reached, the pipe no longer returns to its initial shape after unloading, but the deformation still is characterized as global. If the curvature is increased further, material or geometrical imperfections initiate the onset of local buckling. Imperfections in geometry or material may influence where and at which curvature the onset of local buckling occurs but for all practical use, as long as it is small, does not influence the limit moment capacity. After the onset of local buckling, the global deformation continues, but more and more of the applied bending energy is accumulated in the local buckle, which continues until the limit point is reached. At this point, the maximum bending resistance of the pipe is reached and a geometrical collapse occurs on additional increase of the curvature. Until reaching the point of the start of catastrophic capacity reduction, the geometric collapse is "slow" and the changes in cross-sectional area negligible. After this point, material softening sets in and the pipe cross section collapses until the upper and lower pipe walls are in contact. For pipes subjected to longitudinal force or pressure close to the maximum capacity, the start of catastrophic capacity reduction occurs immediately
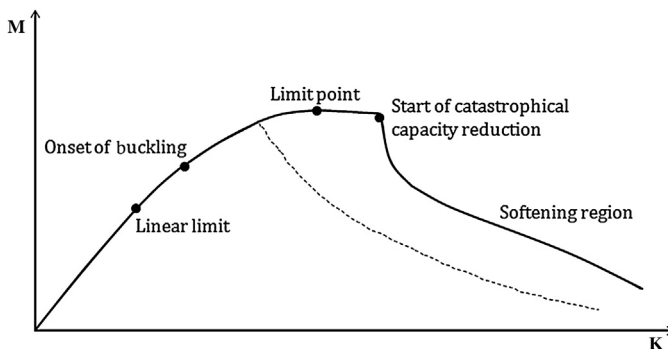
Figure 3.1 Relationship of bending moment vs. curvature.

after the limit point. The moment curvature relation for these load conditions are closer to that presented by the dashed line in Figure 3.1.

The moment curvature relationship provides information necessary for design against failure due to bending. Depending on the function of the pipe, any of the points just described can be used as the design limit. If the pipe is part of a carrying structure, the elastic limit may be an obvious choice as the design limit. However, for pipelines and risers where the global shape is less important, this criterion is overly conservative, due to the significant resources in the elastic-plastic range. Higher design strength can therefore be obtained by using design criteria based on the stress or strain levels reached at the point of onset for local buckling or at the limit point. For displacement-controlled configurations, it can even be acceptable to allow the deformation of the pipe to continue into the softening region (not in design). The rationale of this is the knowledge of the carrying capacity with high deformations combined with a precise prediction of the deformation pattern and its amplitude.

The limit bending moment for steel pipes is a function of many parameters. The main parameters are given here in arbitrary sequence:

- Diameter over wall thickness ratio.
- Material stress-strain relationship.
- Material imperfections.
- Welding (longitudinal as well as circumferential).
- Initial out-of-roundness.
- Reduction in wall thickness due to, say, corrosion
- Cracks (in pipe or welding).
- Local stress concentrations due to, say, coating.
- Additional loads and their amplitude.
- Temperature

The criteria focused on in this chapter are the bending moment capacity at the limit point shown in Figure 3.1. The limit bending moment (moment capacity) is a function of initial out-of-roundness, longitudinal force, and internal or external overpressure for materials with either isotropic or anisotropic characteristics in the longitudinal and hoop directions. Solutions obtained from both analytical expressions and finite element models are described, covering a diameter over wall thickness ratio from 10 to 60. The remaining parameters given in the list also are of importance in design of pipelines, but the main parameters generally are those studied in this chapter.

Failure Modes

As pointed out in the previous section, the limit moment depends highly on the amount of longitudinal force and pressure loads and, for cases with high external pressure, initial out of roundness. To clarify the approach used in the development of the analytical equations and give a better understanding of the obtained results, characteristics of the ultimate strength of pipes subjected to single loads and combined loads are discussed here. Figure 3.2 shows the cross-sectional deformations just before failure of pipes subjected to single load.
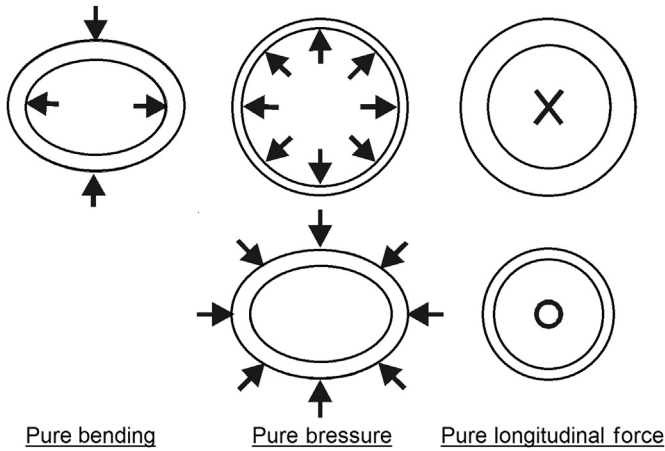
Figure 3.2 **Cross-sectional deformation of pipes subjected to single load.**

Pure Bending

A pipe subjected to increasing pure bending fails as a result of increased ovalization of the cross section and reduced slope in the stress-strain curve. Up to a certain level of ovalization, the decrease in moment of inertia is counterbalanced by increased pipe wall stress due to strain hardening. When the loss in moment of inertia can no longer be compensated for by the strain hardening, the moment capacity has been reached and catastrophic cross-sectional collapse occurs if additional bending is applied. For a low D/t ratios, the failure is initiated on the tensile side of the pipe, due to stresses at the outer fibers exceeding the limiting longitudinal stress. For D/t ratio is higher than approximately 30–35, the hoop strength of the pipe is so low compared to the tensile strength that the failure mode is an inward buckling on the compressive side of the pipe. The geometrical imperfections (excluding corrosion) normally allowed in pipeline design do not significantly influence the moment capacity for pure bending, and the capacity can be calculated as [8]

$$M_{C(F=0,P=0)} = \left(1.05 - 0.0015 \cdot \frac{D}{t}\right) \cdot \text{SMYS} \cdot D^2 \cdot t \qquad [3.1]$$

where D is the average pipe diameter, t is the wall thickness, and SMYS is the specified minimum yield strength. The term $(1.05 - 0.0015 \cdot D/t) \cdot \text{SMYS}$ represents the average longitudinal cross-sectional stress at failure as a function of the diameter over wall thickness ratio.

External Pressure

Theoretically, a circular pipe without imperfections should continue being circular when subjected to increasing uniform external pressure. However, due to material

and/o geometrical imperfections, there is always a flattening of the pipe, which with increased external pressure ends with the total collapse of the cross section. The change in out of roundness, caused by the external pressure, introduces circumferential bending stresses, where the highest stresses occur, respectively, at the top or bottom and two sides of the flattened cross section. For low D/t ratios, material softening occurs at these points, and the points behave as a kind of hinge at collapse. The average hoop stress at failure due to external pressure changes with the D/t ratio. For small D/t ratios, the failure is governed by the yielding of the cross section, while for larger D/t ratios, it is governed by elastic buckling. *Elastic buckling* means that the collapse occurs before the average hoop stress over the cross section has reached the yield stress. At D/t ratios in between, the failure is a combination of yielding and elastic buckling.

Several formulations have been proposed for estimating the external collapse pressure, but in this chapter, only Timoshenko and Gere's [9] and Haagsma and Schaap's [10] equations are described. Timoshenko and Gere's equation, which gives the pressure at which yielding in the extreme fibers begins, in general, represents a lower bound, while Haagsma and Schaap's equation, using a fully plastic yielding condition, represents an upper bound for the collapse pressure. The collapse pressure of pipes depends greatly on geometrical imperfections and, especially initial out-of-roundness. Both Timoshenko and Gere's and Haagsma and Schaap's collapse equations account for initial out of roundness.

Timoshenko and Gere's equation [9], giving the pressure causing yield at the outer pipe fiber, is

$$p_c^2 - \left[p_p + \left(1 + 1.5 \cdot \frac{f_0 \cdot D}{t} \right) \cdot p_{el} \right] \cdot p_c + p_p \cdot p_{el} = 0 \qquad [3.2]$$

where

p_c = characteristic collapse pressure

$p_{el} = \dfrac{2 \cdot E}{(1 - v^2)} \cdot \left(\dfrac{t}{D} \right)^3$

p_p = plastic buckling pressure, $2 \cdot \text{SMYS} \cdot (t/D)$

f_0 = initial out-of-roundness, $(D_{max} - D_{min})/D$

D = average diameter

t = wall thickness

E = Young's modulus

v = Poisson's ratio

It should be noted that the pressure, p_c, determined in accordance with Eq. [3.2] is lower than the actual collapse pressure of the pipe, and it becomes equal to the latter only in the case of a perfectly round pipe. Hence, by using p_c calculated from Eq. [3.2] as the ultimate value of pressure, the results normally are on the safe side [9].

Haagsma and Schaap's equation, giving the pressure at which fully plastic yielding over the wall thickness occurs, can be expressed as

$$p_c^3 - p_{el} \cdot p_c^2 - \left(p_p^2 + p_{el} \cdot p_p \cdot f_0 \cdot \frac{D}{t} \right) \cdot p_c + p_{el} \cdot p_p^2 = 0 \qquad [3.3]$$

This equation represents the theoretical upper bound for the collapse pressure. For low D/t ratios, the collapse pressure is closer to the collapse pressure calculated by Haagsma and Schaap's equation than that calculated by Timoshenko and Gere's equation [9].

The use of Timoshenko and Gere's and Haagsma and Schaap's equations relates specifically to a pipe that initially has linear elastic material properties and where the elastic buckling pressure is derived from classical analysis. This would be appropriate for seamless pipes or for pipes that have been subjected to an annealing process. However, for pipes fabricated using the UO or UOE method, there are significant nonlinearities in the material properties in the hoop direction, due to residual strains and the Bauschinger effect. These effects may be accounted for by introducing a strength reduction factor to the plastic buckling pressure term used in Eq. [3.2]. In this chapter, no attempt has been made to estimate the size of this reduction factor, but according to DNV-OS-F101 [11], the plastic buckling pressure shall be reduced by 7% and 15% for pipes fabricated by the UO and UOE processes, respectively.

Internal Pressure

For pure internal pressure, the failure mode is the bursting of the cross section. Due to the pressure, the pipe cross section expands and the pipe wall thickness decreases. The decrease in pipe wall thickness is compensated for by an increase in the hoop stress. At a certain pressure, the material strain hardening can no longer compensate for the pipe wall thinning and the maximum internal pressure has been reached. The bursting pressure can, in accordance with API -RP-1111 [12], be given as

$$P_b = 0.90(S + U)\frac{t}{D - t} \qquad [3.4]$$

where $0.45(\text{SMTS} + \text{SMYS})$ is the hoop stress at failure.

Tension

For pure tension, the failure of the pipe, as for bursting, results from pipe wall thinning. When the longitudinal tensile force is increased, the pipe cross section narrows down and the pipe wall thickness decreases. At a certain tensile force, the cross-sectional area of the pipe is reduced so much that the maximum tensile stress for the pipe material is reached. An additional increase in tensile force now causes the pipe to fail. The maximum tensile force can be calculated as

$$F_1 = \text{SMTS} \cdot A \qquad [3.5]$$

where A is the cross-sectional area and SMTS the longitudinal stress at failure.

Compression

A pipe subjected to increasing compressive force is subjected to Euler buckling. If the compressive force is further increased, the pipe finally fails due to local buckling. If

the pipe is restrained except for in the longitudinal direction, the maximum compressive force is close to the tensile failure force:

$$F_1 = \text{SMTS} \cdot A \qquad [3.6]$$

Combined Loads

For pipes subjected to single loads, the failure is, as described previously, dominated by either longitudinal or hoop stresses. For the combination of pressure, longitudinal force, and bending, the stress level at failure is an interaction between longitudinal and hoop stresses. In accordance with, among others, DNV (1995) [13] classification notes for buckling strength analysis of plates, this interaction can, neglecting the radial stress component and the shear stress components, be described as

$$\frac{\sigma_l^2}{\sigma_{ll}^2} - 2\alpha \frac{\sigma_l \sigma_h}{\sigma_{ll} \sigma_{hl}} + \frac{\sigma_h^2}{\sigma_{hl}^2} = 1 \qquad [3.7]$$

where

σ_l = applied longitudinal stress
σ_h = applied hoop stress
σ_{ll}/σ_{hl} = limit stress in their respective directions.

The limit stress may differ depending on whether the applied load is compressive or tensile. The α is a correction factor depending on the ratio between the limit stress in the longitudinal and hoop directions, respectively. Based on Eqs. [3.3], [3.4], [3.7], and finite element analyses, the following definition for the correction factor has been suggested for external and internal overpressure, respectively:

$$\alpha = 0.25 \frac{p_c}{F_1} \qquad [3.8]$$

$$\alpha = 0.25 \frac{p_h}{F_1} \qquad [3.9]$$

For pipes under combined pressure and longitudinal force, Eq. [3.7] may be used to find the pipe strength capacity. Alternatives to Eq. [3.7] are Von Mises, Tresca, Hill, and Tsai-Hill's yield condition [14]. Experimental tests have been reported [15–18]. For combined pressure and longitudinal force, the failure mode is very similar to those for single loads.

In general, the ultimate strength interaction between longitudinal force and bending may be expressed by the fully plastic interaction curve for tubular cross sections. However, if D/t is higher than 35, local buckling may occur at the compressive side, leading to a failure slightly inside the fully plastic interaction curve, Chen and Sohal [19]. When tension is dominating, the pipe capacity is higher than the fully plastic condition, due to tensile and strain-hardening effects. Based on finite

element results, the maximum compressive or tensile force related to bending has been found to be

$$F_1 = 0.5 \cdot (\text{SMYS} + \text{SMTS}) \cdot A \qquad\qquad [3.10]$$

where 0.5 (SMYS + SMTS) is longitudinal stress at failure.

As indicated in Figure 3.2, pressure and bending both lead to a cross-sectional failure. Bending always leads to ovalization and finally collapse, while the pipe fails in different modes for external and internal overpressure. When bending is combined with external overpressure, both loads tend to increase the ovalization, which leads to a rapid decrease in capacity. For bending combined with internal overpressure, the two failure modes work against each other and thereby "strengthen" the pipe. For high internal overpressure, the collapse always is initiated on the tensile side of the pipe, due to stresses at the outer fibers exceeding the material limit tensile stress. On the compressive side of the pipe, the high internal pressure tends to initiate an outward buckle, which increases the pipe diameter locally and thereby increases the moment of inertia and the bending moment capacity of the pipe. The moment capacity therefore is expected to be higher for internal overpressure than with a corresponding external pressure.

Additional Failure Modes

In addition to the failure modes just described, fracture is a possible failure mode for all the described load conditions. In particular for the combination of tension, high internal pressure, and bending, it is important to check against fracture because of the high stress level at the limit bending moment. The fracture criteria are not included in this chapter but are addressed in design.

2.   Analytical Solution of Limit Moment

In the following section, the limit moment for pipes subjected to combined loads is derived. To keep the complexity of the bending moment limit state equations on a reasonable level, the following assumptions have been made:

- Geometrically perfect pipe except for initial out-of-roundness.
- Elastic- perfectly plastic material.
- Entire cross section has reached the limit stress.
- No change in cross-section geometry before the limit stress is reached.
- The limit stress surface can be described in accordance with Eq. [3.7].

Limit Stress Surface

The pipe wall stress condition for the bending moment limit state can be considered as that of a material under biaxial loads. It is assumed that the pipe wall limit stress surface can be described in accordance with Eq. [3.11]. The limit stress surface is

described as a function of the longitudinal stress, σ_l; the hoop stress, σ_h; and the limit stress, σ_{ll} and σ_{hl} in their respective directions, neglecting the radial stress component and the shear stress components:

$$\frac{\sigma_l^2}{\sigma_{ll}^2} - 2\alpha \frac{\sigma_l \sigma_h}{\sigma_{ll} \sigma_{hl}} + \frac{\sigma_h^2}{\sigma_{hl}^2} = 1 \qquad [3.11]$$

where α is a correction factor depending on the σ_{ll}/σ_{hl} ratio. Solving the second-degree equation for the longitudinal stress, σ_l, gives

$$\sigma_l = \alpha \sigma_{ll} \frac{\sigma_h}{\sigma_{hl}} \pm \sigma_{ll} \sqrt{1 - (1 - \alpha^2)\left(\frac{\sigma_h}{\sigma_{hl}}\right)^2} \qquad [3.12]$$

The term σ_{comp} is now defined as the limit longitudinal compressive stress in the pipe wall and thereby equal to σ_l as just determined with the negative sign before the square root. The limit tensile stress, σ_{tens}, is accordingly equal to σ_l with the positive sign in front of the square root.

$$\sigma_{comp} = \alpha \sigma_{ll} \frac{\sigma_h}{\sigma_{hl}} - \sigma_{ll} \sqrt{1 - (1 - \alpha^2)\left(\frac{\sigma_h}{\sigma_{hl}}\right)^2} \qquad [3.13]$$

$$\sigma_{tens} = \alpha \sigma_{ll} \frac{\sigma_h}{\sigma_{hl}} + \sigma_{ll} \sqrt{1 - (1 - \alpha^2)\left(\frac{\sigma_h}{\sigma_{hl}}\right)^2} \qquad [3.14]$$

Bending Moment

The bending moment capacity of a pipe with an elastic-perfectly plastic material behavior can, assuming that the entire cross section has reached the limit stress, be calculated as

$$M_C(\sigma_l, \sigma_h) = -A_{comp}\bar{y}_{comp}\sigma_{comp} + A_{tens}\bar{y}_{tens}\sigma_{tens} \qquad [3.15]$$

where A_{comp} and A_{tens} are the cross sectional area in compression and tension, respectively; $\bar{y}$ their mass centers distance to the pipe center and stress level, see Figure 3.3.

For a geometrical perfect circular pipe, the area in compression and tension can approximately be calculated as

$$A_{comp} = 2\psi rt \qquad [3.16]$$

$$A_{tens} = 2(\pi - \psi)rt \qquad [3.17]$$
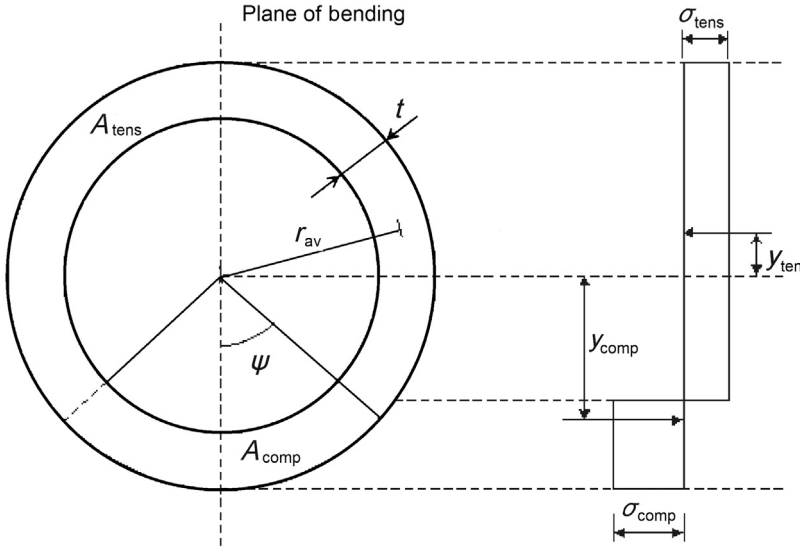
Figure 3.3 Cross section and idealized stress diagram for fully plastic pipe.

The distance from the mass center to the pipe cross section center is given by

$$\bar{y}_{\text{comp}} = r \frac{\sin(\psi)}{\psi} \tag{3.18}$$

$$\bar{y}_{\text{tens}} = r \frac{\sin(\psi)}{\pi - \psi} \tag{3.19}$$

where r is the average pipe wall radius and ψ is the angle from the bending plan to the plastic neutral axis. The plastic neutral axis is defined as the axis at which the longitudinal pipe wall stresses change from tensile to compressive.

Inserting Eqs. [3.16]–[3.19] into Eq. [3.15] gives the bending moment capacity as

$$M_C(\sigma_1, \sigma_h) = -2tr^2 \sin(\psi)\sigma_{\text{comp}} + 2tr^2 \sin(\psi)\sigma_{\text{tens}} \tag{3.20}$$

Location of Fully Plastic Neutral Axis

To calculate the angle to the fully plastic neutral axis from the plan of bending, it is necessary to start with looking at the true longitudinal pipe wall force, which approximately can be expressed as:

$$F = A_{\text{comp}}\sigma_{\text{comp}} + A_{\text{tens}}\sigma_{\text{tens}} \tag{3.21}$$

where the area in compression, A_{comp}, is calculated as

$$A_{\text{comp}} = 2\psi rt \qquad\qquad [3.22]$$

and the area in tension, A_{tens}, as

$$A_{\text{tens}} = 2(\pi - \psi)rt \qquad\qquad [3.23]$$

giving

$$F = 2rt\left[\psi\sigma_{\text{comp}} + (\pi - \psi)\sigma_{\text{tens}}\right] \qquad\qquad [3.24]$$

Solving Eq. [3.24] for ψ gives

$$\psi = \frac{F - 2\pi rt\sigma_{\text{tens}}}{2rt\left(\sigma_{\text{comp}} - \sigma_{\text{tens}}\right)} \qquad\qquad [3.25]$$

or

$$\psi = \frac{\pi\left(\sigma_{\text{comp}} - \sigma_{\text{tens}}\right)}{\sigma_{\text{comp}} - \sigma_{\text{tens}}}, \qquad F = 2\pi rt\sigma_{\text{l}} \qquad\qquad [3.26]$$

Moment Capacity

Substituting the expression for the plastic neutral axis, Eq. [3.26], into the equation for the moment capacity, Eq. [3.20], gives

$$M_{\text{C}}(\sigma_{\text{l}}, \sigma_{\text{h}}) = -2tr^2\,\sin\left[\frac{\pi(\sigma_l - \sigma_{\text{tens}})}{\sigma_{\text{comp}} - \sigma_{\text{tens}}}\right]\sigma_{\text{comp}} + 2tr^2\,\sin\left[\frac{\pi(\sigma_l - \sigma_{\text{tens}})}{\sigma_{\text{comp}} - \sigma_{\text{tens}}}\right]\sigma_{\text{tens}}$$

$$[3.27]$$

Substituting the expression for tensile and compressive stress, Eqs. [3.13] and [3.14], into Eq. [3.27] gives the final expression for the bending moment capacity:

$$M_{\text{C}}(\sigma_{\text{l}}, \sigma_{\text{h}}) = 4tr^2\sigma_{\text{ll}}\sqrt{1 - (1 - \alpha^2)\left(\frac{\sigma_{\text{h}}}{\sigma_{\text{hl}}}\right)^2}\,\cos\left[\frac{\pi}{2}\frac{\frac{\sigma_{\text{l}}}{\sigma_{\text{ll}}} - \alpha\frac{\sigma_{\text{h}}}{\sigma_{\text{hl}}}}{\sqrt{1 - (1 - \alpha^2)\left(\frac{\sigma_{\text{h}}}{\sigma_{\text{hl}}}\right)^2}}\right]$$

$$[3.28]$$

or, alternatively and more useful in design situations,

$$M_\mathrm{C}(F,p) = M_\mathrm{p}\sqrt{1 - (1-\alpha^2)\left(\frac{p}{p_l}\right)^2}\cos\left[\frac{\pi}{2}\frac{\frac{F}{F_1} - \alpha\frac{p}{p_l}}{\sqrt{1 - (1-\alpha^2)\left(\frac{p}{p_l}\right)^2}}\right] \qquad [3.29]$$

where

M_C = bending moment capacity
M_p = plastic moment
p = pressure acting on the pipe
p_l = limit pressure
F = true longitudinal force acting on the pipe
F_l = limit longitudinal force

Applicable Range for Moment Capacity Equation

To avoid complex solutions when solving Eq. [3.29], the expressions under the square root must be positive, which gives the theoretical range for the pressure to

$$-\frac{1}{\sqrt{1-\alpha^2}} \le \frac{p}{p_l} \le \frac{1}{\sqrt{1-\alpha^2}} \qquad [3.30]$$

where the limit load, p_l, depends on the load condition and α on the ratio between the limit force and the limit pressure. Since the wall thickness design is based on the operating pressure of the pipeline, this range should present no problems in the design. Given the physical limitation that the angle to the plastic neutral axis must be between 0 and 180 degrees, the equation is valid for the following range of longitudinal force:

$$\alpha\frac{p}{p_l} - \sqrt{1 - (1-\alpha^2)\left(\frac{p}{p_l}\right)^2} \le \frac{F}{F_1} \le \alpha\frac{p}{p_l} + \sqrt{1 - (1-\alpha^2)\left(\frac{p}{p_l}\right)^2} \qquad [3.31]$$

where the limit loads F_1 and p_l depend on the load condition and α on the ratio between the limit force F_1 and the limit pressure p_l. For the design of pipelines, this range is normally going to present no problems, but again, the range may be reduced due to the question of fracture.

3.   Finite Element Analysis

Introduction

To get a reliable finite element (FE) prediction of buckling/collapse deformation behavior, the following factors must be taken into account:

- A proper representation of the constitutive law of the pipe material.
- A proper representation of the boundary conditions.

- A proper application of the load sequence.
- The ability to address large deformations, large rotations, and finite strains.
- The ability to model or describe all relevant failure modes.

The material definition included in the finite element model is of high importance, since the model is subjected to deformation into the elasto-plastic range, for example, in the post buckling phase, strain levels between 10% and 20% are usual. A Ramberg-Osgood stress-strain relationship is commonly used in the finite element analysis (FEA), in which two points on the stress-strain curve are required along with the material Young's modulus. The two points can be anywhere along the curve, but the specified minimum yield strength (SMYS) associated with a strain of 0.5% and the specified minimum tensile strength (SMTS) corresponding to approximately 20% strain are normally used. The material yield limit has been defined as approximately 80% of the SMYS. The advantage in using the SMYS and SMTS instead of a stress-strain curve obtained from a specific test is that the statistical uncertainty in the material stress-strain relation is accounted for. It is thereby ensured that the stress-strain curve used in an FEA in general will be more conservative than that from a specific laboratory test.

To reduce computing time, the symmetry of the problem has been used to reduce the finite element model to one-quarter of a pipe section. The length of the model is two times the pipe diameter, which in general is sufficient to catch all buckling and collapse failure modes. The general purpose shell element used in the present model accounts for the finite membrane strains and allows for changes in shell thickness, which makes it suitable for large-strain analysis. The element definition allows for transverse shear deformation and uses thick shell theory when the shell thickness increases and discrete Kirchoff thin shell theory as the thickness decreases.

For a further discussion and verification of the used finite element model for buckling and collapse analysis, see Bai et al. [7], Mohareb et al. [5], Bruschi et al. [20], and Hauch and Bai [21].

Analytical Solution vs. Finite Element Analysis

In the following, the equations presented in the last section are compared with the results obtained from FEA. First are the capacity equations for pipes subjected to single loads compared with FE results for a D/t ratio from 10 to 60. Second, the moment capacity equations for combined longitudinal force, pressure, and bending are compared against FE results.

Strength Capacity under a Single Load

As a verification of the FE model, the strength capacities for single loads obtained from FEA are compared against the verified analytical expressions described in the previous sections of this chapter. The strength capacity has been compared for a large range of diameters over wall thicknesses to demonstrate the FE model's capability to catch the right failure mode independently of the D/t ratio. For all the analyses, the average diameter is 0.5088 [m], SMYS = 450 [MPa], and SMTS = 530 [MPa].
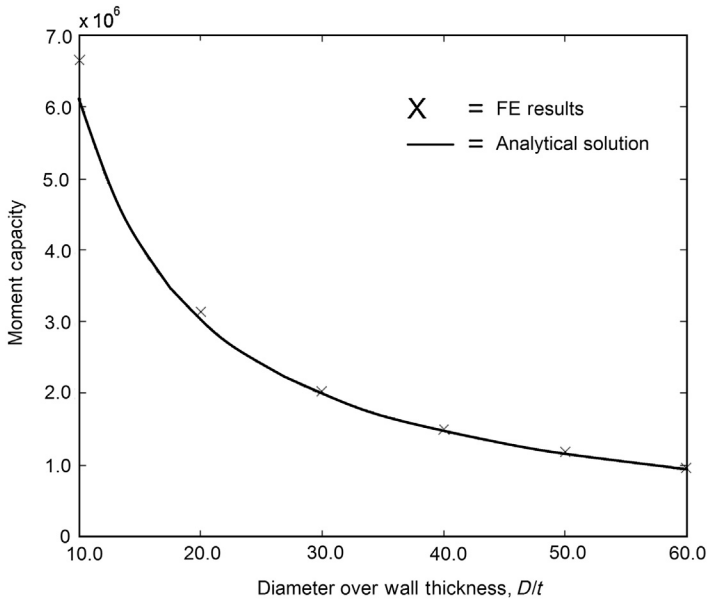
Figure 3.4 Moment capacity as a function of D/t for a pipe subjected to pure bending.

In Figure 3.4, the bending moment capacity found from FEA has been compared against the bending moment capacity equation, Eq. [3.1]. Figure 3.5 examines the limit tensile longitudinal force, Eq. [3.7]. In Figure 3.6, the collapse pressure Eqs. [3.2] and [3.5] and, in Figure 3.7, the bursting pressure Eq. [3.6] are compared with
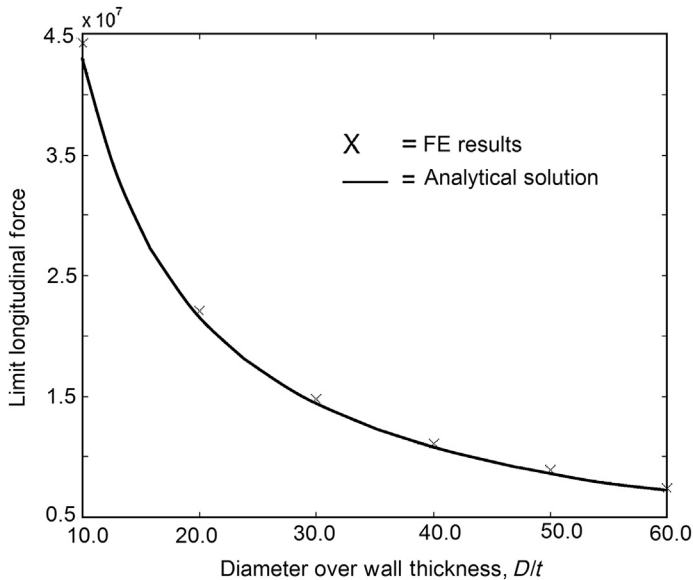
Figure 3.5 Limit long. force as a function of D/t for pipe under pure tensile force.
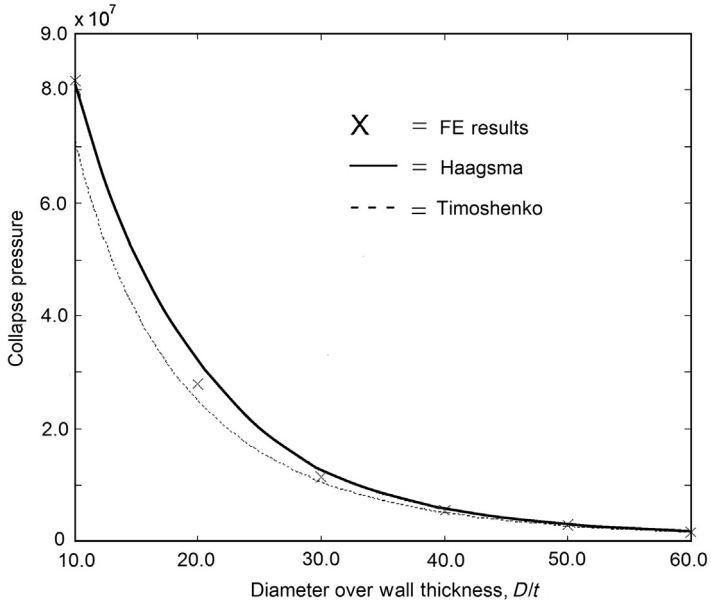
Figure 3.6 Limit long. force as a function of *D/t* for pipe under pure longitudinal force.
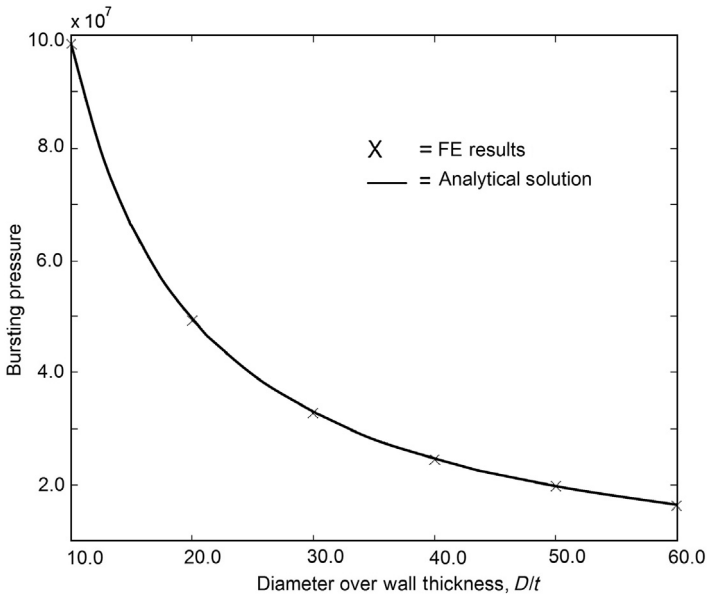
Figure 3.7 Bursting pressure as a function of *D/t* for pipe under pure internal pressure.

FE results. The good agreement between the FE results and analytical solutions presented in Figure 3.7 gives good reason to expect that the FE model also gives reliable predictions for combined loads.

Strength Capacity for Combined Loads

For the results presented in Figures 3.8 to 3.13, the pipe dimensions in Table 3.1 have been used.

Figures 3.8 and 3.9 show the moment capacity surface given by Eq. [3.29]. Figure 3.8 shows the moment capacity surface with a function of the external pressure and compressive longitudinal force side. Figure 3.9 shows the function from the top. Figures 3.4 to 3.7 demonstrate that the failure surface agrees well with FE analyses for a large D/t ratio range for single loads. Figure 3.9 demonstrates that Eq. [3.29] also agrees with FEA for combined loads. The failure surface is cut for different fixed values of longitudinal force and pressure, respectively, by the black lines. The cuts and respective FE results are shown in Figures 3.10 to 3.13.

In Figure 3.10, the moment capacity is plotted as a function of pressure. The limit pressure for external overpressure is given by Haagsma and Schaap's collapse equation, Eq. [3.3], and the limit pressure for internal overpressure by the bursting pressure, Eq. [3.4]. For the nonpressurized pipe, the moment capacity is given by Eq. [3.1]. In Figure 3.11, the moment capacity is plotted as a function of longitudinal force. The limit force has been given by Eq. [3.10] for both compression and tension. For a given water depth, the external pressure is approximately constant, while the axial force may vary. Figure 3.12 shows the moment capacity as a function of longitudinal force for an
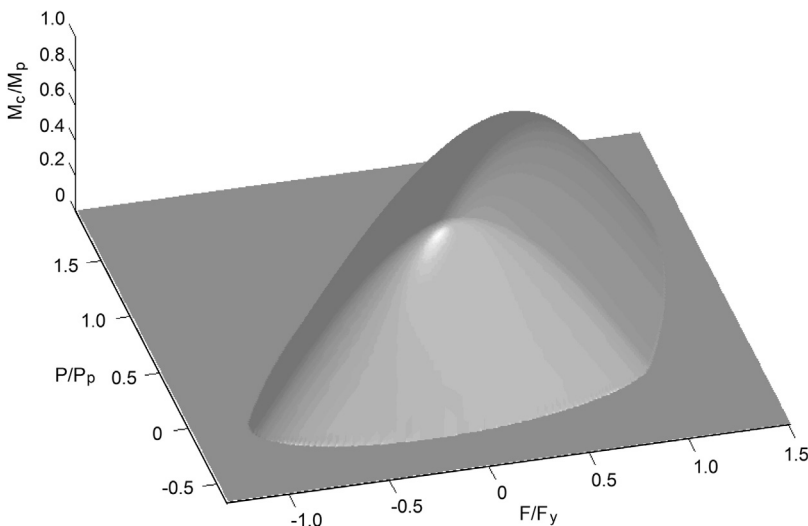
Figure 3.8 Limit bending moment surface as a function of pressure and longitudinal force.
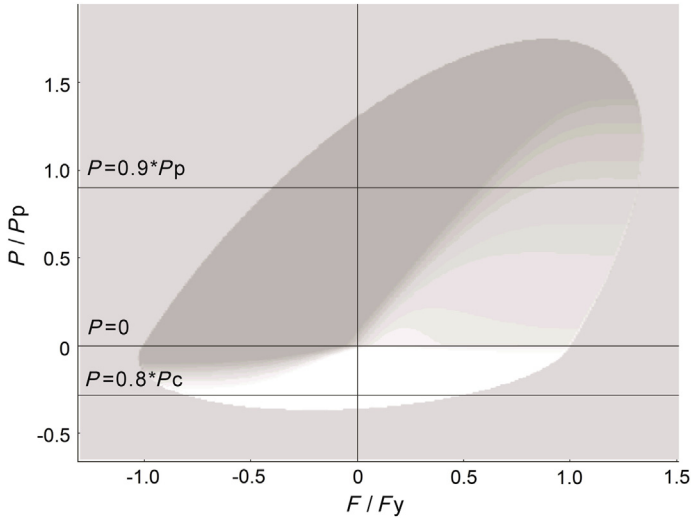
Figure 3.9 Limit bending moment surface as a function of pressure and longitudinal force.

external overpressure equal to 0.8 times the collapse pressure calculated by Haagsma and Schaap's collapse equation Eq. [3.3]. Figure 3.13 again shows the moment capacity as a function of longitudinal force, but this time for an internal overpressure equal to 0.9 times the plastic buckling pressure given by Eq. [3.2].
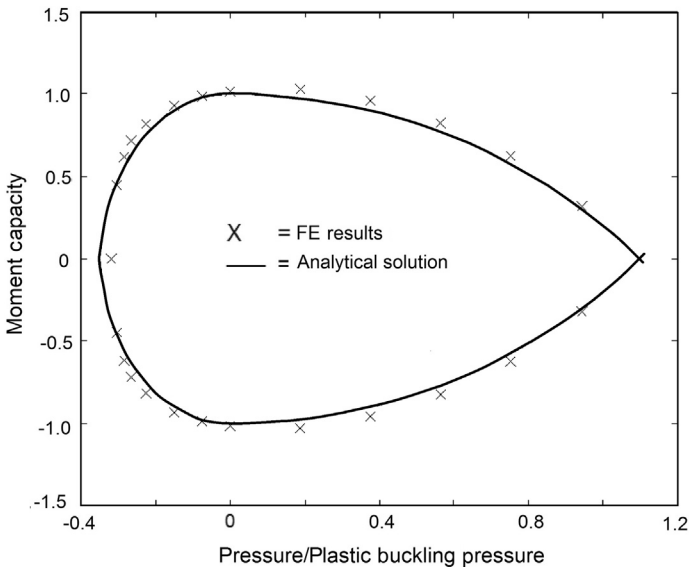
Figure 3.10 Normalized bending moment capacity as a function of pressure.
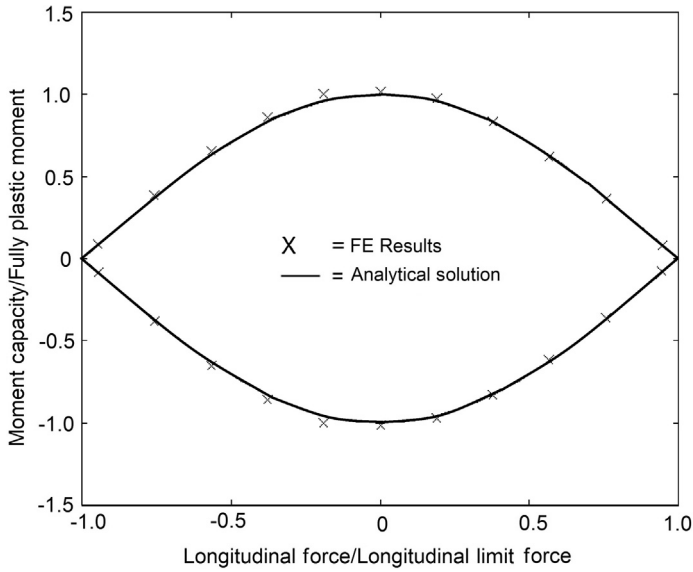
Figure 3.11 Normalized bending moment capacity as a function of longitudinal force. (Pressure equals zero.)
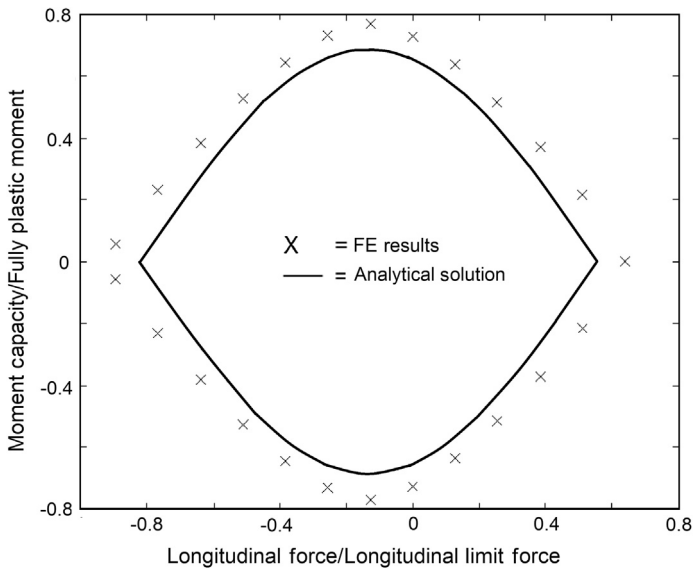
Figure 3.12 Normalized bending moment capacity as a function of longitudinal force.
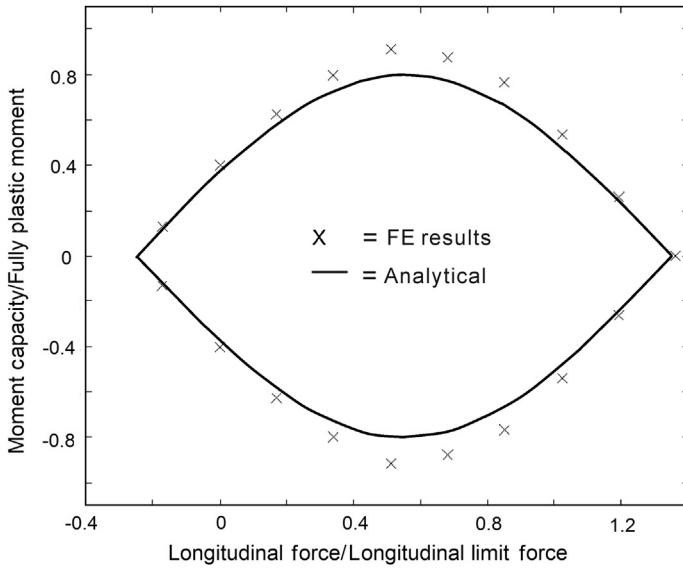
Figure 3.13 Normalized bending moment capacity as a function of longitudinal force.

Based on the results presented in Figures 3.10 to 3.13, it is concluded that the analytically deduced moment capacity and FE results are in good agreement for the entire range of longitudinal force and pressure. However, the equations tend to be a slightly nonconservative for external pressures very close to the collapse pressure. This is in agreement with the previous discussion about Timoshenko and Gere's [9] and Haagsma and Schaap's [10] collapse equations.

Usage and Safety Factors

The local buckling check can be separated into a check for load-controlled conditions due to bending moment and one for displacement-controlled conditions due to strain level. When no usage or safety factors are applied in the buckling check calculations, the two checks ought to result in the same bending capacity. In

Table 3.1 Parameters for Combined Load

Parameter	Value	Unit
D/t	35	[—]
f_0	1.5%	[—]
SMYS	450	MPa
SMTS	530	MPa
α	1/5 for external overpressure	[—]
	2/3 for internal overpressure	

pipeline design, the usage and safety factors are introduced to account for modeling and input uncertainties. The reduction in bending capacity introduced by the usage factors is not the same for load- and displacement-controlled conditions. Due to the pipe moment versus strain relationship, a higher allowable strength can be achieved for a given target safety level by using a strain-based criterion than by a moment criterion. In this chapter, only the allowable bending moment criterion is given. This criterion can be used for both load- and displacement-controlled conditions but, as mentioned, may be overly conservative for displacement-controlled conditions.

The usage factor approach presented in this chapter is based on shrinking the failure surface shown in Figures 3.8 and 3.9. Instead of representing the bending moment capacity, the surface is scaled to represent the maximum allowable bending moment associated with a given target safety level. The shape of the failure surface given Eq. [3.29] is dictated by four parameters: the plastic moment, M_p; the limit longitudinal force, F_l; the limit pressure, P_l; and the correction factor (shape parameter), α. To shrink the failure, the surface usage factors are applied to the plastic moment, longitudinal limit force, and the limit pressure, respectively. The usage factors are functions of modeling, geometrical, and material uncertainties and therefore vary for the three capacity parameters. In general, the variation is small, and for simplification purposes, the most conservative usage factor may be applied to all capacity loads. The correction factor α is a function of the longitudinal limit force and the limit pressure, and no usage factor is applied to this parameter. The modeling uncertainty is strtongly connected to the use of the equation. In the SUPERB (1996) [21] Project, the use of the moment criteria is divided into four unlike scenarios: (1) pipelines resting on uneven seabed, (2) pressure test conditions, (3) a continuous stiff supported pipe, and (4) all other scenarios. To account for the variation in modeling uncertainty, a condition load factor γ_C is applied to the plastic moment and the limit longitudinal force. The pressure, which is a function of internal pressure and water depth, is not subjected to the same model uncertainty, and the condition load factor is close to 1 and can be ignored. Based on this discussion, the maximum allowable bending moment may be expressed as [22]

$$M_{\text{Allowable}}(F, p) = \frac{\eta_{RM}}{\gamma_c} M_p \sqrt{1 - (1 - \alpha^2) \left(\frac{p}{\eta_{RP} p_l} \right)^2} \cos \left[\frac{\pi}{2} \frac{\frac{\gamma_c F}{\eta_{RF} F_l} - \alpha \frac{p}{\eta_{RP} p_l}}{\sqrt{1 - (1 - \alpha^2) \left(\frac{p}{\eta_{RP} p_l} \right)^2}} \right]$$

[3.32]

where

$M_{\text{Allowable}}$ = allowable bending moment
γ_c = condition load factor
η_R = strength usage factors

The usage and safety factor methodology used in Eq. [3.32] ensures that the safety levels are uniformly maintained for all load combinations.

4. Guidelines for Bending Strength Calculations

Introduction

In the following guidelines for bending strength calculations, the suggested condition load factor is in accordance with the results presented in the SUPERB (1996) report [7], later used in DNV (1996) and in DNV-OS-F101 [11], rules for submarine pipeline systems. The strength usage factors η_{RM}, η_{RF}, and η_{RP} are based on comparison with existing codes and the engineering experience of the authors, [11, 12, 22].

Bending Strength Calculation

Local Buckling

Local buckling may occur in pipelines subjected to combined pressure, longitudinal force and bending. The failure mode may be a yielding of the cross section or buckling on the compressive side of the pipe. The criteria given in these guidelines may be used to calculate the maximum allowable bending moment for a given scenario. Note that the maximum allowable bending moment given in these guidelines does not take fracture into account and that fracture criteria therefore may reduce the bending capacity of the pipe. This applies particularly for high-tension/high-pressure load conditions.

Load- versus Displacement-Controlled Situations

The local buckling check can be separated into a check for load-controlled situations (bending moment) and for displacement-controlled situations (strain level). Due to the relation between applied bending moment and maximum strain in a pipe, a higher allowable strength for a given target safety level can be achieved by using a strain-based criterion rather than a bending moment criterion. The bending moment criterion can, due to this, conservatively be used for both load- and displacement-controlled situations. In these guidelines, only the bending moment criterion is given.

Local Buckling and Accumulated Out-of-Roundness

Increased out-of-roundness due to installation and cyclic operating loads may aggravate local buckling and is to be considered. It is recommended that out of roundness, due to through life loads, be simulated using finite element analysis.

Maximum Allowable Bending Moment

The allowable bending moment for local buckling under load controlled conditions can be expressed as

$$M_{\text{Allowable}}(F,p) = \frac{\eta_{\text{RM}}}{\gamma_c} M_p \sqrt{1 - (1 - \alpha^2)\left(\frac{p}{\eta_{\text{RP}}p_l}\right)^2} \cos\left[\frac{\pi}{2} \frac{\frac{\gamma_c F}{\eta_{\text{RF}}F_l} - \alpha\frac{p}{\eta_{\text{RP}}p_l}}{\sqrt{1 - (1 - \alpha^2)\left(\frac{p}{\eta_{\text{RP}}p_l}\right)^2}}\right]$$

[3.33]

where

   $M_{\text{Allowable}}$ = allowable bending moment
   M_p = plastic moment
   p_l = limit pressure
   p = pressure acting on the pipe
   F_l = limit longitudinal force
   F = longitudinal force acting on the pipe
   α = correction factor
   γ_c = condition load factor
   η_R = strength usage factor

Correction Factor

The correction factor for local buckling under load controlled conditions can be expressed as

$$\alpha = 0.25 \frac{p_c}{F_l}, \qquad \text{for external overpressure}$$

$$\alpha = 0.25 \frac{p_b}{F_l}, \qquad \text{for internal overpressure}$$

If possible, the correction factor should be verified by finite element analyses.

Plastic (Limit) Moment

The limit moment may be given as

$$M_C(F = 0, P = 0) = \left(1.05 - 0.0015 \cdot \frac{D}{t}\right) \cdot \text{SMYS} \cdot D^2 \cdot t$$

[3.34]

where

   SMYS = specified minimum yield strength in longitudinal direction
   D = average diameter
   t = wall thickness

Limit Longitudinal Force for Compression and Tension

The limit longitudinal force may be estimated as

$$F_1 = 0.5 \cdot (\text{SMYS} + \text{SMTS}) \cdot A \qquad [3.35]$$

where

A = cross-sectional area, which may be calculated as $\pi\, D\, t$
SMYS = specified minimum yield strength in longitudinal direction
SMTS = specified minimum tensile strength in longitudinal direction

Limit Pressure for External Overpressure Condition

The limit external pressure, p_l, is to be calculated based on

$$p_1^3 - p_{el}p_1^2 - \left(p_p^2 + p_{el}p_p f_0 \frac{D}{t} \right)p_1 + p_{el}p_p^2 = 0 \qquad [3.36]$$

where

$p_{el} = \dfrac{2E}{(1 - \nu^2)}\left(\dfrac{t}{D}\right)^3$

$p_p = \eta_{fab}\text{SMYS}\frac{2t}{D}$, η_{fab} is 0.93 for UO pipes, 0.85 for UOE pipes, and 1 for seamless or annealed pipes

$f_0 = (D_{max} - D_{min})/D$, initial out-of-roundness caused during the construction phase is to be included but not flattening due to external water pressure or bending in as-laid position
SMYS = specified minimum yield strength in hoop direction
E = Young's modulus
ν = Poisson's ratio.

Limit Pressure for Internal Overpressure Condition

The limit pressure is equal to the bursting pressure given by

$$p_l = 0.5(\text{SMTS} + \text{SMYS})\frac{2t}{D} \qquad [3.37]$$

where

SMYS = specified minimum yield strength in hoop direction
SMTS = specified minimum tensile strength in hoop direction

Load and Usage Factors

Load factor γ_c and usage factor η_R are listed in Table 3.2.

Load condition factors may be combined; For example, the load condition factor for a pressure test of pipelines resting on an uneven seabed is $1.07 \times 0.93 = 1.0$.

Table 3.2 Load and Usage Factors

		Safety Classes		
	Safety Factors	Low	Normal	High
γ_c	Uneven seabed	1.07	1.07	1.07
	System pressure test	0.93	0.93	0.93
	Continuously stiff supported	0.82	0.82	0.82
	Otherwise	1.00	1.00	1.00
η_{RP}	Pressure	0.95	0.93	0.90
η_{RF}	Longitudinal force	0.90	0.85	0.80
η_{RM}	Moment	0.80	0.73	0.65

Summary

The moment capacity equations in the existing codes for some load conditions are overly conservative and for others nonconservative. This chapter presents a new set of design equations that are accurate and simple. The derived analytical equations have been based on the mechanism of failure modes and have been extensively compared with finite element results. The use of safety factors has been simplified compared with existing codes and the target safety levels are in accordance with DNV [10], ISO [11], and API [12]. The applied safety factor methodology ensures that the target safety levels are uniformly maintained for all load combinations.

References

[1] Murphey CE, Langner CG. Ultimate pipe strength under bending, collapse and fatigue. OMAE'85; 1985.

[2] Winter PE, Stark JWB, Witteveen J. Collapse behaviour of submarine pipelines/. In: Shell structures stability and strength. New York: Elsevier Publishers; 1985.

[3] Ellinas CP, Raven PWJ, Walker AC, Davies P. Limit state philosophy in pipeline design. J Energy Res Technol Jan. 1986.

[4] Gresnigt AM. Plastic design of buried steel pipelines in settlement areas. HERON, Delf University of Technology 1986;31(4).

[5] Mohareb ME, Elwi AE, Kulak GL, Murray DW. Deformational behaviour of line pipe. Structural Engineering Report No. 202. Edmonton: University of Alberta; 1994.

[6] Bai Y, Igland R, Moan T. Tube collapse under combined pressure, tension and bending. Int J Offshore and Polar Eng 1993;3(2):121–9.

[7] Bai Y, Igland R, Moan T. Tube collapse under combined external pressure, tension and bending. J Marine Struct 1997;10(5):389–410.

[8] SUPERB Project. Buckling and collapse limit state; December 1996.

[9] Timoshenko SP, Gere JM. Theory of elastic stability. 3rd ed., New York: McGraw-Hill; 1961.

[10] Haagsma SC, Schaap D. Collapse resistance of submarine lines studied. Oil Gas J February 1981.

[11] DNV. Submarine pipeline systems. DNV-OS-F101. Det Norske Veritas; October 2010.

[12] API. Design, construction, operation and maintenance of offshore hydrocarbon pipelines (limit state design). RP-1111. API; 2009.

[13] DNV. Buckling strength analysis. Classification Notes 30.1. Det Norske Veritas; July 1995.

[14] Hill R. The mathematical theory of plasticity. New York: Oxford University Press; 1950.

[15] Corona E, Kyriakides S. On the collapse of inelastic tubes under combined bending and pressure. Int J Solids Struct 1988;24(5):505–35.

[16] Kyriakides S, Yeh MK. Factors affecting pipe collapse. EMRL Report No 85/1. Austin: Engineering Mechanics Research Laboratory; 1985. University of Texas.

[17] Kyriakides S, Yeh MK. Plastic anisotropy in drawn metal tubes. J Eng Industry August 1988. 110/303.

[18] Kyriakides S, Ju GT. Bifurcation and localization instabilities in cylindrical shells under bending-I-Experiments. Int J Solids Struct 1992;29(9):1117–42.

[19] Chen WF, Sohal IS. Cylindrical members in offshore structures, thin-walled structure. Special issue on Offshore Structures. New York: Elsevier Applied Science; 1988.

[20] Bruschi R, Monti P, Bolzoni G, Tagliaferri R. Finite element method as numerical laboratory for analysing pipeline response under internal pressure, axial load, bending moment. OMAE'95; 1995.

[21] HauchS S, Bai Y. Use of finite element analysis for local buckling design of pipelines OMAE'98; 1998.

[22] ISO/DIS 13623. Petroleum and natural gas industries – Pipelines Transportation systems; 1998.

4 Limit-State Based Strength Design

Chapter Outline

1. Introduction

The subsea pipelines are increasingly being required to operate at high pressures and temperatures (HPHT) in recent years. Figure 4.1 indicates that this tendency is rising continually with oil and gas fields developed farther and farther from shore and into deeper and deeper waters. The higher pressure condition is the technical challenge of a higher material grade of pipe for the pipeline projects and causes sour service if the product includes H_2S, saltwater, and welding compatibility. The higher temperature operating condition causes the challenges of corrosion and the down-rated yield strength of pipe material and insulation coating. Pipelines subjected to high pressure and high temperature create a high effective axial compressive force due to high internal fluid temperatures and pressure in the operating condition, when the pipeline is restrained by soil on the seabed. Stress based traditional design codes are no longer applicable at the high temperatures, and the solution is to design such pipelines using limit state approaches.
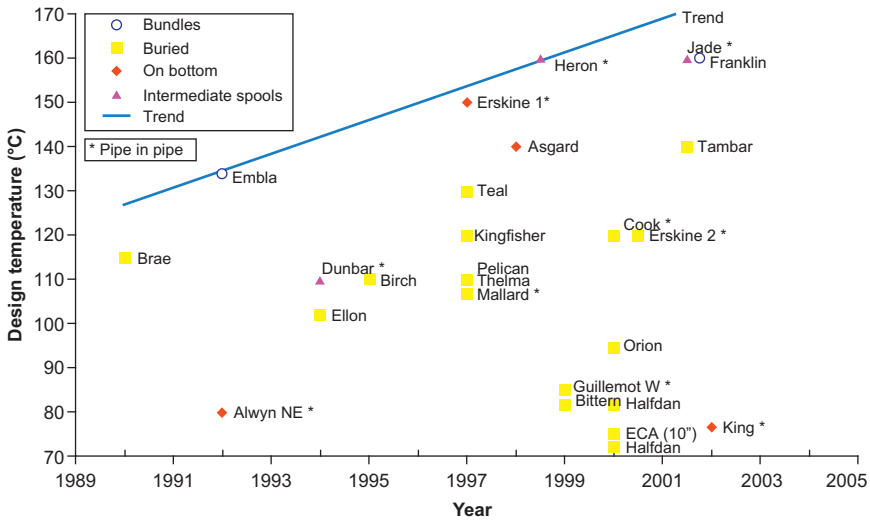
Figure 4.1 Tendency of pipeline inlet design temperature.
Source: Carr et al. [1]. (For color version of this figure, the reader is referred to the online version of this book.)

Currently, the HPHT pipeline design is based mainly on limit state principles, which are based on a set of limit states, or failure functions, covering all relevant failure modes. The limit state design checks against the failure modes independently, and several limit states are checked in the project design. A sufficient margin against failure is ensured by the application of partial safety factors, which reflect the uncertainties in loads and materials. The limit state strength design has become crucially important when the usage factors in wall thickness design are raised from those given by traditional design codes. In the past decades, a number of JIPs (joint industry projects) have been conducted with a focus on HPHT pipelines.

The HOTPIPE JIP [2] was sponsored by Statoil and Norsk Agip and performed by Statoil, DNV, and Snamprogetti. The HOTPIPE project established a design guideline that complies with DNV OS-F101 [3], which is based on the risk principles and limit state methodologies. It adopts load and resistance factors and formulates the criteria into a more general arrangement.

SAFEBUCK [4] was a JIP project sponsored by the major operators and focused on addressing issues associated with structural integrity under global lateral buckling. It outlined a basic design philosophy and recommended DNV OS-F101 and API RP 1111 [5] as the most suitable design codes. For global lateral buckling, the failure modes of local buckling, strain capacity, pipeline walking, and fatigue damages need to be checked.

Limit State Design

Most of the traditional design codes for pipelines and risers belong to the allowable stress design (ASD) method. However, structural design has been successfully

carried out using limit state design (LSD) with reliability based techniques that provide a consistent treatment of uncertainties for some days; the developments of the LSD step into the assessment of subsea pipeline design in recent years [3, 5]. The load resistance factored design (LRFD) method was introduced in DNV-OS-F101 as a design basis for the given structural limitations. This method incorporates uncertainties in the design into an approach of partial factors of safety. These uncertainties are grouped together as either partial load or material factors. The partial safety factors are associated with characteristic loads and resistance effects. The fundamental principle of the LRFD is to verify that characteristic factored design loads (L_d) do not exceed the factored design resistance effects (R_d) for any of the considered failure modes:

$$L_d \leq R_d \qquad\qquad\qquad [4.1]$$

where the factored design load, L_d, and factored design resistance, R_d, are expressed as follows:

$$L_d = L_F \gamma_F \gamma_C + L_E \gamma_E + L_I \gamma_F \gamma_C + L_A \gamma_A \gamma_C$$

$$R_d = \frac{R_k(f_k)}{\gamma_{sc} \gamma_m}$$

The load effect factors, γ_F, γ_E, γ_C, and γ_A are defined in Tables 4-4 and 4-5 of Section 4 in DNV-OS-F101 [3], which are determined using risk and reliability methods to provide a target reliability level. The terms γ_{sc} and γ_m defined in Tables 5-4 and 5-5 of Section 5 are the safety class resistance factor and material resistance factor, respectively.

Figure 4.2 illustrates the relationship of partial factors of characteristic loads and resistances in the limit state design. For example, the characteristic load and resistance may be stresses caused by the applied hoop stress, σ_h, and the pipeline yield strength, σ_y, represented by statistical distribution. The probability density function for the yield strength is found by a statistical analysis of measured test values from pipe mill certification records. The mean value and variability of the wall thickness and diameter are found from the pipe delivery records. If the load is larger than the resistance, the system fails.

The limit state design of pipeline is a rational design method based on the idea of a limit state, a condition that limits the continued safe operation of a pipeline. It is exceeded when the response of the pipeline to loading is unacceptable. Each limit state divides the pipeline into two states, the safe state and the failed state. The following four limit states are checked for the pipeline design [3]:

- **Ultimate limit state (ULS):** This state is associated with a single load application or overload situation. The pipeline may experience loss of structural integrity if the limit state is beyond
  - Bursting due to internal pressure, longitudinal force and bending.
  - Local buckling or collapse due to pressure, longitudinal force, and bending.
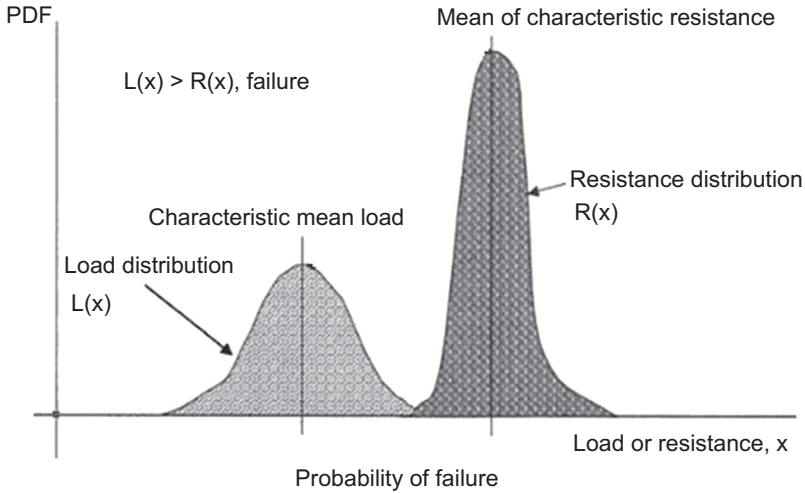
Figure 4.2 Partial factors in limit state design.

- **Serviceability limit state (SLS):** This state is not associated with catastrophic failure but reduces the operational capability or utility of a pipeline. If the limit state is beyond the following, the pipeline will not meet its functional requirement such as partially blocking the flow or preventing pigs from traveling along the pipeline due to the change of the local ovalization:
  - Global buckling, that is, upheaval buckling or lateral buckling.
  - Out of roundness for serviceability.
- **Fatigue limit state (FLS):** This is a ULS condition accounting for accumulated cyclic load effects:
  - Low-cycle fatigue due to cyclic lifetime thermal loading.
  - High-cycle fatigue of spanning pipeline due to VIV.
  - Fracture.
- **Accidental limit state (ALS):** This is a condition that, if exceeded, implies loss of structural integrity caused by accidental load:
  - Accumulated plastic strain due to abnormal action.

Definition of Failure

The purpose of mechanical engineering design is to ensure the safety and performance of a given pipeline over a given period of time and under a specified loading condition. However, absolute safety is an impractical objective because of the involved uncertainties. These uncertainties may be due to the randomness of loading, material properties, and dimensions. However, these uncertainties can be statistically expressed. As an alternative to the LRFD format, a reliability based design approach is used by DNV OS-F101 based on the risk limit of unacceptable consequences to provide the adequate safety margins. This involves selection of an appropriate target safety level based on a probabilistic design check. The check ensures that the

Table 4.1 Nominal Failure Probabilities Versus Safety Classes

Limit States	Probability Bases	Safety Classes			
		Low	Medium	High	Very high
SLS	Annual per pipeline	10^{-2}	10^{-3}	10^{-3}	10^{-4}
ULS	Annual per pipeline	10^{-3}	10^{-4}	10^{-5}	10^{-6}
FLS	Annual per pipeline	10^{-3}	10^{-4}	10^{-5}	10^{-6}
ALS	Annual per pipeline	10^{-3}	10^{-4}	10^{-5}	10^{-6}
—	Pressure containment	10^{-4}–10^{-5}	10^{-5}–10^{-6}	10^{-6}–10^{-7}	10^{-7}–10^{-8}

Source: DNV-OS-F101 [3].

calculated probability of failure, based on a recognized reliability method, is less than the target value. Table 4.1 lists the nominal target failure probability levels based on the failure type and safety class for different limit states. The target reliability levels are defined as a probability per kilometer per year. The definitions of the safety class for the partial safety factors are listed in Table 2-5 of Section 2, DNV OS-F101 [3], which vary with the transported fluid (water, oil, gas, etc.), location (in or out of the 500 m zone), and the time period (temporary or operational).

2. Stress Based Design and Strain Based Design

The limit-state based pipeline design includes stress based design and strain based design. Depending on the nature of the load event applied the system, it can be classified as displacement controlled or load controlled. DNV OS-F101 is utilized as key guidance for both load-controlled (stress-based) and displacement-controlled (strain-based) limit state checks.

Displacement and Load Control

Displacement Control

For a pipeline restrained by the surrounding medium, such as buried or reeled pipelines, the boundaries prevent the pipeline from additional bending other than that imposed by itself. The additional strains due to the bending are fully restrained by the fixed surrounding mediums or boundaries. A change of load, such as weight or internal pressure, does not change the shape of pipeline if the boundary conditions are fixed; therefore, the strain is limited. This condition is usually classified as strain or displacement control. In these cases, the strain based design criteria are used.

Load Control

For a pipeline free to bend under external loads, the development of pipeline bending depends strictly on the capacity of internal stress to balance the external

loads. The external loads do not change with the pipeline deformation. When the external bending actions due to the loads cause the material of pipe to exceed the elastic limit, uncontrollable failure of pipeline may occur. This condition is usually classified as stress or load control, for example, free spanning pipelines. The load in the spanning pipeline, such as hydrodynamic load or weight, is independent of the displacement of the pipeline. In these cases, the stress based design criteria are used.

Lateral buckling of pipelines is partially a displacement and partially a load control phenomenon because the restraint provided by the lateral friction on the seabed partially controls the deformation of pipeline in the lateral buckling. The effective compression load, however, decreases with lateral deflection of the pipeline when a lateral buckle occurs.

Stress Based Design

A stress based design, which is used in traditional pipeline design and the majority of pipelines installed to date around the world, limits the hoop stress and equivalent stress in the pipe under the worst loads by design factors on the specified minimum yield strength (SMYS) of the pipe material, depending on the considered design cases.

Hoop stress limit:

$$\sigma_h \leq \eta_1 \, \text{SMYS} \qquad\qquad\qquad [4.2]$$

Equivalent stress limit:

$$\sigma_e \leq \eta_2 \, \text{SMYS} \qquad\qquad\qquad [4.3]$$

The design factors, η_1 and η_2, are defined in the traditional pipeline design codes [3], [6], [7] , and [8]. Stress based design was widely used in traditional pipeline designs, which have a large experience basis. It is possible to be used up to 0.5% strain with ECA analysis when the limited welding qualification tests are satisfied [9, 10].

The hoop stress criterion for pipe may be used in combination with a material derating factor. The equivalent stress criterion limits the von Mises stress to a fraction of the SMYS. For D/t ratios larger than 20, the form of equivalent stress may be calculated and the criterion reads as

$$\sigma_e = \sqrt{\sigma_h^2 + \sigma_l^2 - \sigma_h \sigma_l + 3\tau^2} \leq \eta_2 \cdot \text{SMYS} \qquad\qquad [4.4]$$

where

σ_h = hoop stress
σ_l = longitudinal stress (axial stress)
τ = torsional shear stress
η_2 = usage factor (design factor)

For high-pressure pipes with D/t ratios less than 20, the shear stresses are ignorable; the form of equivalent stress may be calculated and the criterion reads as

$$\sigma_e = \sqrt{\frac{1}{2}\left[(\sigma_h - \sigma_l)^2 + (\sigma_l - \sigma_R)^2 + (\sigma_h - \sigma_R)^2\right]} \leq \eta_2 \cdot \text{SMYS} \qquad [4.5]$$

where σ_R is the radial stress. For the restrained pipeline such as buried on-land pipelines with no bending, the longitudinal stress due to internal pressure, external pressure, and increasing temperature is expressed as

$$\sigma_{L,R} = \frac{2\nu(p_i A_i - p_e A_e)}{A_s} - E\alpha(T_P - T_a) \qquad [4.6]$$

For the displacement-controlled buried pipeline, the temperature difference is also a control factor for the longitudinal stress and equivalent stress. The equivalent stress beyond the yield stress is also acceptable in cases in which the strain based design should be used.

For a stress based design of subsea pipeline, the bending moments, equivalent stresses, and allowable stresses are determined for the following scenarios:

- Empty condition.
- Flood condition.
- Hydrotest condition.
- Operational conditions.

The strength criteria are applicable for the following situations:

- Pipeline in-place behavior.
- Trawl pullover response.
- Free-spanning pipelines.

Strain Based Design

Strain based design is a methodology that sets strain limits in the design condition rather than the stress limits. It is applied to the cases where the displacement-controlled loads are the dominant design condition. In the displacement-controlled case, the magnitude of load depends on the displacement and deformation of the structure. Typical examples of pipeline systems in displacement-controlled cases are thermal expansion, ground movements, such as soil slope instability, seismic sideslip, pipeline reeling, and pipeline laying.

The traditional designs have been based on the yield state of the pipe material being the limit state, while the strain based designs use the state of ultimate tensile stress as the limit. Strain based designs take maximum advantage of the behavior characteristics of the pipe materials. This means allowing the pipeline to go beyond a yield state, the controlled plastic deformation of the pipe. It is normally applied to the controlled bending of a pipeline with no failures. Application of strain based design can achieve adequate pipeline safety and integrity, and reduce the cost of pipeline
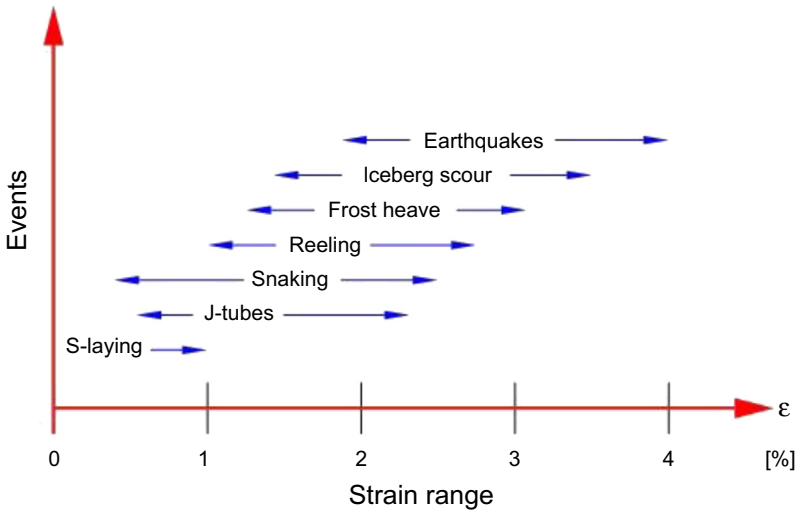
Figure 4.3 Available strain range of pipeline in displacement controlled events. (For color version of this figure, the reader is referred to the online version of this book.)

construction, operation, and maintenance. However, a limited strain based design cannot replace a stress based design. The resistance of the pipe wall to the hoop stress induced by the internal operating design pressure is usually the primary determinator of the required pipeline grade and wall thickness, even though strain based design is used in the project design.

The safe use of strain based design requires predominately displacement-controlled or displacement-restricted loading, such as offshore pipeline layed by reeling and S-lay, J-tubes, ground settlements and earthquakes, and temperature induced expansion and contraction. Recently, several projects adopted the strain based design approach. The pipelines are subjected to a large plastic deformation in both installation and operating conditions. In some cases, the maximum strain can reach 4% for a one-time loading. The possible strain ranges of pipeline in those cases are shown in Figure 4.3, which are

- Installation (reeling lay, etc.).
- Thermal loading (global buckling).
- Arctic loading (frost heave, thaw settlement, etc.).
- Seismic loading.

Extension of Stress Based Design Procedures

Design codes and standards for stress based design are much better developed than those for strain based design, while several standards also have some coverage of strain based design. There is a tendency to cover only limited types of loading, such as in API-RP-1111 for subsea pipeline [5]. DNV-OS-F101 [3] provides broad guidance
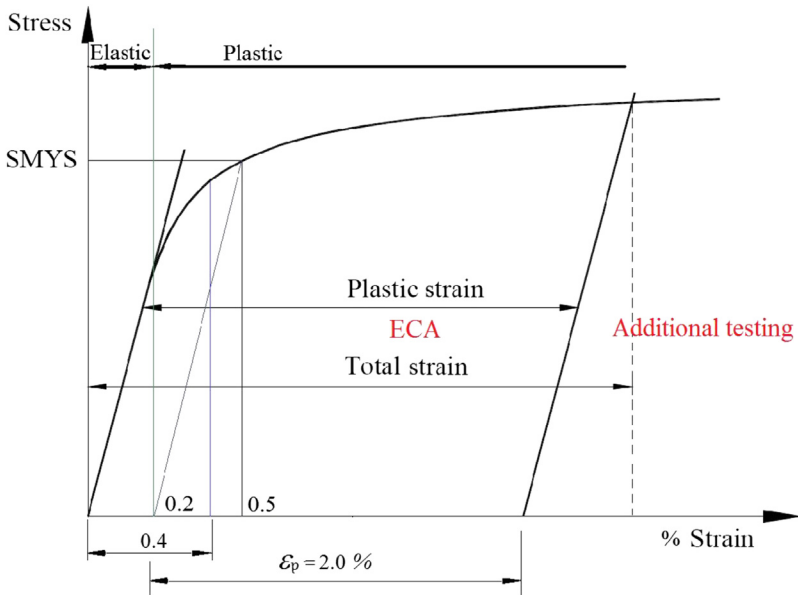
Figure 4.4 Girth weld defect acceptance criteria of pipelines. (For color version of this figure, the reader is referred to the online version of this book.)

on girth weld defect acceptance criteria for total longitudinal nominal strains ranging from elastic to plastic. As illustrated in Figure 4.4, some criteria follows:

$\varepsilon_{l,nom} \leq 0.4\%$, workmanship.

$\varepsilon_{l,nom} > 0.4\%$, ECA according to Appendix A.

$\varepsilon_{l,nom} > 1.0\%$ or $\varepsilon_p > 2.0\%$, additional testing according to supplementary requirement p.

The criteria and requirements for the cumulative plastic strain, ε_p, and the total longitudinal nominal strains, $\varepsilon_{l,nom}$, of the pipeline are illustrated in the figure. A supplementary requirement of the cumulative plastic strain, ε_p, which refers to line pipe, is higher than 2%. When the total longitudinal nominal strain is higher than 0.4%, engineering criticality assessments (ECAs) must be performed. ECAs are now commonly conducted during the design of offshore pipelines to calculate the allowable sizes for flaws in girth welds. The ECA is a method for assessing the acceptability of a flaw in a structure, that is, to demonstrate fitness for surface (FFS). The fracture control in pipelines under high plastic strains use an ECA during pipeline design to determine the tolerable sizes for girth weld flaws, which are detailed in Chapter 12, "Fatigue and Fracture."

Standards such as BS 7910 [9] and API 579 [10] are primarily stress based, and it is not straightforward to apply them to strain based situations. DNV-RP-F108 [11] addresses this gap by providing additional guidance derived from U.K. and Norwegian research programs. The standard stipulates that an ECA should be performed in accordance with the Level 3 procedure of BS 7910 for high–strain applications.

The Level 3 procedure of BS 7910 is a stress based approach in the form of a failure assessment diagram (FAD). The FAD relies on the existence of a limit load (or plastic collapse load). While the limit load is a good measure of a structure's load bearing capacity, it is a poor measure of the strain capacity. When the material response is in the plastic range, a small change in stress can result in a large change in strain. The FAD approach can work reasonably well if a material has a strong strain-hardening capacity, such as with certain lower-grade materials used in offshore applications. Modern high-strength line pipe materials, such as API-5L-X70 and above, typically exhibit low strain hardening. The strain-hardening capacity of the corresponding high-strength girth weld metal can be even lower. Consequently assessment results of the FAD approach can be quite insensitive to the strain level for these materials.

One of the limit states in the strain based design of pipelines is the tensile strain capacity. Girth welds tend to be the weakest link in the tensile strain capacity of the pipeline, due to the existence of weld defects and metallurgical or mechanical property changes from welding thermal cycles. *Girth weld* here refers to the entire weld region, including the deposited weld metal, fusion boundary, and the heat-affect zone (HAZ). Certain base metal (pipeline material here) properties are a critical part of the girth weld strain capacity, as they affect the metallurgical and mechanical properties of the weld region. For instance, the chemical composition of the base metal may play a critical role in the propensity of HAZ hydrogen cracking, particularly in older and high-carbon materials. In modern high-strength pipelines, HAZ softening and weld metal cracking may occur, both of which can have a significant effect on the tensile strain capacity of the pipeline.

3.   Ultimate Limit State

Bursting

Hoop Stress versus Equivalent Stress Criteria

Yielding is normally considered a serviceability limit state, since it does not result in an immediate ultimate failure, such as a rupture. The yielding of material needs to be limited because the excessive plastic strain may affect the long-term structural integrity of the pipeline. *Bursting* is defined as the point at which the uncontrolled tearing of the pipe wall occurs, and it leads to an ultimate rupture of the pipe. Therefore, bursting is an ultimate limit state.

An analytical study by Stewart et al. [12] and a finite element analysis have demonstrated that, for a pipe under combined internal pressure and bending,

- If a pipeline section is in a displacement-controlled condition, hoop stress criterion provides a good control of bursting.
- If a pipeline section is in a load-controlled condition, then equivalent stress criterion may be applied to ensure sufficient burst strength for pipes under combined internal pressure and axial loads.

For the load-controlled condition, an equivalent and longitudinal stress criterion should be used, according to the results from the analytical study and the finite element analysis. For pipelines in operation, it is generally conservative to apply the equivalent stress criteria to control bursting, since the dominating load is internal pressure combined with bending.

The bursting failure is governed by the tensile hoop stress. To ensure structural strength against bursting, the hoop stress should fulfill the following conditions:

- Yielding limit state $= \sigma_h \leq \eta_s \cdot$ SMYS, where η_s is a usage factor for SMYS.
- Bursting limit state $= \sigma_h \leq \eta_u \cdot$ SMTS, where η_u is a usage factor for SMTS.

Bursting Strength Criteria for Pipelines

Hoop Stress Criteria

The hoop stress criterion limits the characteristic tensile hoop stress, σ_h, due to a pressure differential between internal and external pressures:

$$\sigma_h \leq \eta_h \ k_t \ \text{SMYS} \qquad [4.7]$$

where η_h is the design usage factor and k_t is the material temperature derating factor. The hoop stress equation is commonly expressed in the following simple form:

$$\sigma_h = (p_i - p_e)\frac{D}{2t}, \quad \text{for thin walls} \qquad [4.8]$$

or

$$\sigma_h = (p_i - p_e)\frac{(D^2 + D_i^2)}{(D^2 - D_i^2)} - p_e, \quad \text{for thick walls} \qquad [4.9]$$

where p_i and p_e are the internal and external pressures, respectively; D is the outside diameter; D_i is the inside diameter; and t is the wall thickness.

For offshore pipelines located in the off-platform zone, the design (usage) factor is specified as 0.72 by all major codes. For pipelines in the near-platform zone (safety zone), the usage factor is specified as 0.50 by ASME B31.8 [8]. The origin for design factor 0.72 can be tracked back to the B31 (1935) codes, where the working pressure was limited to 80% of the mill test pressure, which itself was calculated using Eq. [4.7] with a design factor up to 0.9. The effective design factor for the working pressure was thus $0.8 \times 0.9 = 0.72$. Since the 1958 version of B31.8 codes, the factor 0.72 has been used directly to obtain the design pressure for land pipelines.

Equivalent Stress Criteria

For internal overpressure conditions, the allowable equivalent stress and allowable longitudinal stress are $\eta \cdot$ SMYS(T), and the usage factor η given in Table 4.2 is after Table 3 in Section 6.4 of ISO13623 [13].

Table 4.2 Equivalent Stress Design Factor

Load Combinations	Design Factor, η
Construction and environmental loads	1.0
Functional and environmental loads	0.9
Functional, environmental, and accidental loads	1.0

The equivalent stress design factor of 0.96 is used in BS 8010 and DNV OS-F101 under the functional and environmental loads during the operating condition. The design factor of 0.96 is used in DNV OS-F101 under construction and environmental loads.

Local Buckling and Collapse

Local Buckling, [14] and [15]

Local buckling may occur in pipelines subjected to combined pressure, longitudinal force, and bending. The failure mode may be a yielding of the cross section or buckling on the compressive side of the pipe. The criteria given in this section may be used to calculate the maximum allowable bending moment for a given scenario. Note that the maximum allowable bending moment given in these guidelines does not take fracture into account and that fracture criteria therefore may reduce the bending capacity of the pipe. This particularly applies to high-tension/high-pressure load conditions.

Load versus Displacement Controlled Conditions

The local buckling check can be separated into a check for load controlled conditions (bending moment) and that for displacement controlled conditions (strain level). Due to the relationship between applied bending moment and maximum strain in a pipe, a higher allowable strength for a given target safety level can be achieved by using a strain based criterion than the bending moment criterion. Consequently, the bending moment criterion can, conservatively, be used for both load and displacement controlled situations.

Local Buckling and Accumulated Out-of-Roundness

Increased out-of-roundness due to installation and cyclic operating loads may aggravate local buckling and should be considered. The dependence of the bending moment with curvature should be calculated, taking the elastoplastic material behavior into account, in which the ovality effects may be taken into consideration by using Brazier's formula. It is recommended that out-of-roundness due to through life loads be simulated using finite element analysis.

Maximum Allowable Bending Moment

The allowable bending moment for local buckling under load-controlled conditions can be expressed as

$$M_{\text{Allowable}}\,(F,\,p)$$

$$= \frac{\eta_{\text{RM}}}{\gamma_{\text{c}}} M_{\text{p}} \sqrt{1 - (1 - \alpha^2)\left(\frac{p}{\eta_{\text{RP}} p_{\text{l}}}\right)^2} \cos\left(\frac{\pi}{2} \frac{\frac{\gamma_{\text{c}} F}{\eta_{\text{RF}} F_l} - \alpha\frac{p}{\eta_{\text{RP}} p_l}}{\sqrt{1 - (1 - \alpha^2)\left(\frac{p}{\eta_{\text{RP}} p_l}\right)^2}}\right)$$

$$[4.10]$$

where

$M_{\text{Allowable}}$ = allowable bending moment
M_{p} = plastic moment
p_{l} = limit pressure
p = pressure acting on the pipe
F_{l} = limit longitudinal force
F = longitudinal force acting on the pipe
α = correction factor
γ_{c} = condition load factor
η_{R} = strength usage factor

- **Correction factor:**

$$\alpha = 0.25\frac{p_{\text{l}}}{F_{\text{l}}}, \quad \text{for external overpressure} \qquad [4.11]$$

$$\alpha = 0.25\frac{p_{\text{l}}}{F_{\text{l}}}, \quad \text{for internal overpressure} \qquad [4.12]$$

If possible, the correction factor should be verified by finite element analyses.
- **Plastic (limit) moment:** The limit moment may be given as

$$M_{\text{C}(F=0,\,P=0)} = \left(1.05 - 0.0015\cdot\frac{D}{t}\right)\cdot\text{SMYS}\cdot D^2\cdot t \qquad [4.13]$$

- **Limit longitudinal force for compression and tension:** The limit longitudinal force may be estimated as

$$F_{\text{l}} = 0.5\cdot(\text{SMYS} + \text{SMTS})\cdot A \qquad [4.14]$$

- **Limit pressure for external overpressure condition:** The limit external pressure, p_l, is to be calculated based on

$$p_l^3 - p_{el}p_l^2 - \left(p_p^2 + p_{el}p_pf_0\frac{D}{t}\right)p_l + p_{el}p_p^2 = 0 \qquad [4.15]$$

where
$p_{el} = \frac{2E}{(1-\nu^2)}\left(\frac{t}{D}\right)^3$

$p_p = \eta_{fab}SMYS\frac{2t}{D}$

f_0 = initial ovality, defined in Eq. [4.7]
E = Young's modulus
ν = Poisson's ratio

Note:
- The value of η_{fab} is 0.925 for pipes fabricated by the UO process, 0.85 for pipes fabricated by the UOE process, and 1 for seamless or annealed pipes.
- Ovality caused during the construction phase is to be included but not flattening due to external water pressure or bending in as-laid position.
- **Limit pressure for internal overpressure condition:** The limit pressure is equal to the bursting pressure, given by

$$p_l = 0.5(SMTS + SMYS)\frac{2t}{D} \qquad [4.16]$$

- **Load and usage factors:** Load factor γ_c and usage factor η_R are listed in Table 4.3.
  - Load condition factors may be combined, such as the load condition factor for a pressure test of pipelines resting on an uneven seabed, $1.07 \times 0.93 = 1.00$.
  - Safety class is low for temporary phases. For the operating phase, safety class is normal and high for areas classified as zone 1 and zone 2, respectively.

For displacement-controlled situations the following strain capacity check is given to ensure structural strength against local buckling:

$$\left(\frac{\gamma_F \cdot \gamma_c \cdot \gamma_{sncf} \cdot \gamma_D \cdot \varepsilon_{F,c} + \gamma_E \cdot \varepsilon_{E,c}}{\frac{\varepsilon_{M,c}}{\gamma_\varepsilon}}\right)^{0.8} + \frac{p_e}{\frac{p_c}{\gamma_R}} \leq 1 \qquad [4.17]$$

Table 4.3 Load and Usage Factors

		Safety Classes		
Safety Factors		**Low**	**Normal**	**High**
γ_c	Uneven seabed	1.07	1.07	1.07
	Pressure test	0.93	0.93	0.93
	Stiff supported	0.82	0.82	0.82
	Otherwise	1.00	1.00	1.00
η_{RP}	Pressure	0.95	0.93	0.90
η_{RF}	Longitudinal force	0.90	0.85	0.80
η_{RM}	Moment	0.80	0.73	0.65

where

$\varepsilon_{F,c}$ = characteristic functional longitudinal strain
$\varepsilon_{E,c}$ = characteristic environmental longitudinal strain
$\varepsilon_{M,c}$ = characteristic buckling strain capacity
γ_{sncf} = strain concentration factor accounting for increased strain in the field joints due to coating stiffness discontinuities
γ_F = functional load factor
γ_E = environmental load factor
γ_D = dynamic load factor
γ_c = condition load factor
γ_R = strength resistance factor
γ_ε = strain capacity resistance factor

Comparing to the equation established in DNV OS-F101, Section 5 D601 (Eq. 5.31), two additional safety factors (γ_{sncf} and γ_D) are included. These additional safety factors are

- γ_{sncf} for strain concentration factor.
- γ_D to take account for dynamic amplifications during a snap-through dynamic buckling (Nystrøm et al. [15]).

4. Serviceability Limit State

The out-of-roundness (OOR) for pipe ends is determined as the difference between the largest outside diameter and the smallest outside diameter, as measured in the same cross-sectional plane, and is defined according to the following equation:

$$OOR = D_{max} - D_{min} \qquad [4.18]$$

where

D_{max} = the largest measured inside or outside diameter
D_{min} = the smallest measured inside or outside diameter

The ovality of pipeline defined in DNV-OS-F101 is expressed in the following equation:

$$f_0 = \frac{D_{max} - D_{min}}{D_{nom}} \qquad [4.19]$$

It is different from the ovality defined in API RP-1111, which is defined as follows,

$$\delta = \frac{D_{max} - D_{min}}{D_{max} + D_{min}} \qquad [4.20]$$

The pipeline ovality, f_0, defined in DNV-OS-F101 is two times of that, δ, defined in API RP-1111 for the same pipe geometry. The maximum allowable ovality of line

pipe is limited by the pipeline specification, in which, in most cases, the pipeline ovality during the fabrication process is not to be more than 1.5% (f_0) or 0.75% (δ). The ovalilty of a reeled pipeline may be calculated by using Brazier formula, which was developed based on elastic tubes and a conservative estimate in the plastic region:

$$f_0 = 2(1 - v^2)\left(\frac{r_p^2}{R_{reel}t}\right)^2 \qquad [4.21]$$

where

   f_0 = ovality of pipeline defined in DNV-OS-F101
   R_{reel} = reel radius
   r_p = mean pipeline radius
   t = wall thickness of the pipe

The nominal bending strain in the reeled pipe on the reel or aligner is given by

$$\varepsilon_{nom} = \frac{d_p}{D_{reel} + d_p} \qquad [4.22]$$

where

   ε_{nom} = nominal bending strain
   D_{reel} = reel or aligner diameter
   d_p = outside diameter of pipeline

The ovality of the pipe may increase when the pipe is subject to reverse bending, and the effect of this on subsequent straining is to be considered. For a typical pipeline, the following scenarios influences the ovality:

- The ovality may increase during the installation process when the pipe is subject to reverse inelastic bending.
- Cyclic bending due to lateral buckling may occur as a consequence of shutdowns during operation, if global buckling is allowed to relieve temperature- and pressure-induced compressive forces.

The ovality due to point loads should be checked. Critical point loads may arise at free-span shoulders and artificial supports. The accumulative ovality, f_0, through the life cycle should not exceed 3%. This ovality requirement may be relaxed if the effect of ovality on moment capacity and strain criteria are included, the pigging requirements and repair systems are met, and cyclic-load-induced ovality have been considered.

   Finite element analysis may be performed to calculate the increase in ovality during the life cycle of a pipeline. The analysis is to include fabrication tolerances and all loads applied through the pipeline's life cycle, such as point loads, bending against a surface, axial load, and repeated pressure, temperature, and bending cycles.

5.   Fatigue Limit State

All stress fluctuations imposed on the pipelines and risers during the entire design life that have magnitudes and corresponding number of cycles large enough to cause fatigue effects should be taken into account when determining the long-term distribution of stress ranges. Typical reasons of stress fluctuations in pipelines and risers are

- Fluctuations in operating pressure and temperature.
- Direct wave action.
- Vibrations of the pipeline system due to VIV.
- Supporting structure movements.

The design criterion to be used depends on the analysis method, which may be categorized into methods based on fatigue tests (S-N curves) and methods based on fracture mechanics, which are detailed in the Chapter 12, "Fatigue and Fracture."

Ratcheting

Ratcheting is described in general terms as signifying incremental plastic deformation under cyclic loads in pipelines subject to high pressure and high temperatures. Pipe sections with plastic strain histories, including both tensile and compressive plastic strain but in unequal amounts, may be susceptible to ratcheting failure when the strain difference accumulates. The effects of ratcheting on out of roundness, local buckling, and fracture fatigue are to be considered. Pipe sections subjected to multiple cycles of plastic deformation should be designed to avoid a ratcheting failure. The pipe section should meet limits on accumulated strain during the initial cycles and be elastic on further cycles of loading.

Two types of ratcheting are evaluated and the acceptance criteria are as follows:

1. Ratcheting in hoop strain (the pipe expands radially) as a result of strain reversal for pipes operated at high internal pressure and high temperature. The cumulative hoop strain limit is 0.5%.
2. Ratcheting in curvature or ovalization due to cyclic bending and external pressure. The accumulative ovalization is not to exceed a critical value corresponding to local buckling under monotonic bending, or serviceability. The accumulative ovalization is to be accounted for in the check of local buckling and out-of-roundness.

A simplified code check of BS8010 for ratcheting is that the equivalent plastic strain is not to exceed 0.1%, based on elastic/perfectly plastic material and assuming that the reference for zero strain is the as-built state after hydrotesting. In case the simplified code check is violated, a finite element analysis may be applied to determine if ratcheting is a critical failure mode and quantify the amount of deformation induced by ratcheting.

A completely displacement-controlled cycle that causes tension and compression plastic strain in the longitudinal direction of the pipe can cause ratcheting when it is combined with internal or external pressure. Here, the ratcheting is on the circumferential strain, tending to expand the pipe under internal pressure and tending to

shrink it under external pressure. Increasing the longitudinal strain range or the pressure difference makes ratcheting strains larger.

Ratcheting need not only occur in the circumferential direction. The axial direction can undergo ratcheting extension or contraction when all or a significant fraction of the longitudinal loading is load –controlled, as tested by Hassan and Kyriakides and Xia and Ellyin, for example. Another means of accumulating cycle-by-cycle strain during cyclic plasticity is for the tension plasticity to combine with wrinkling or buckling during the compression portion of the cycles.

The wrinkling or buckling adds both stress concentrations to the subsequent longitudinal stresses and locally varying hoop direction strains. Critical locations for ratcheting analysis tend to be at locations of localized support, such as the ends of free spans, artificial supports, and adjacent to subsiding soil or seabed.

Global Buckling and Walking

When a pipeline section is subject to the loading that is between load control and displacement control in global axial compression, it should be designed to limit global buckling strains and account for global buckling in combination with other failure modes, which include local buckling, fracture, ductile failure, and cyclic failure modes, such as fatigue and pipeline walking. Pipeline walking is similar to ratcheting, a short pipeline may move axially under cyclic loads due to seabed slope, SCR load, or transient temperature profiles, but plastic deformation does not necessarily occur. The details on pipeline global buckling and walking are in Chapter 10, "Lateral Buckling and Pipeline Walking".

6.   Accidental Limit State

Accumulated Plastic Strain

If the yield limit is exceeded, the pipe steel will accumulate plastic strain. Accumulated plastic strain may reduce the ductility and toughness of the pipe material. Special strain aging and toughness testing must then be carried out. Accumulated plastic strain is defined as the sum of plastic strain increments irrespective of sign and direction. The plastic strain increments are calculated from the point where the material stress-strain curve deviates from a linear relationship, and the accumulated plastic strain is calculated from the time of fabrication to the end of life time. Accumulated plastic strain is limited to ensure that the material properties of the pipe do not become substandard. This is especially relevant for the fracture toughness. Accumulated plastic strain may also increase the hardness of the material and thus increase its susceptibility to stress corrosion cracking in the presence of H_2S. Stress corrosion cracking is also related to the stress level in the material. If the material yield limit is exceeded, the stress level necessarily is very high. Plastic deformation of the pipe also imposes high residual stress in the material, which may promote stress corrosion cracking.

The general requirement of the accumulated plastic strain is that it should be based on strain aging and toughness testing of the pipe material. It is stated that due to material considerations a permanent/plastic strain up to 2% is allowable without testing. In practice, this is valid also in the operational case. Accumulated plastic strain is commonly used in the determination of the effect of reeling, where cyclic bending plastic strain is counted for the multiple cycles within a reeling-unreeling cycle. If the pipeline is to be exposed to more than 2% accumulated plastic strain, as is often the case for a reeling installation method, the material should be strain aging tested. However, recent testing of modern pipeline steel has shown that plastic strains up to 5% can be acceptable.

To have an extra safety margin, a certain ratio between the yield stress and the ultimate tensile stress is also desirable. A requirement to this ratio is given in I300 of DNV-OS-F101, where the yield stress is determined not to exceed 90% of the ultimate stress for C-Mn steel, and 0.85 for 13 Cr steel. Accumulated plastic strain increases the yield stress of the material and also increases the yield/ultimate stress ratio.

Strain Concentration

Strain Concentration at Girth Weld Area

Pipes under longitudinal plastic strain can concentrate plastic strain in regions in or adjacent to the girth welds. This concentration can occur in the weld metal, for instance, due to choice of welding materials with lower strength than the base pipe or due to variability of pipe strength compared to the weld metal strength, which can leave a small proportion of the girth welds or even part of the girth welds with lower yield strength than adjacent pipe material. It can also occur in the adjacent regions of the heat-affected zone, which can soften relative to the base pipe for some materials. This section examines these strain concentrations and the available means to prevent or limit them.

Strain may be concentrated at the girth weld by [16]

- Shape of the cap.
- Shape of the root.
- Misalignment of the pipe wall centers across the weld.
- Differences in thickness across the weld.
- Pipe ovality.
- Differences in strength in and around the weld.

Strain concentration may be determined from elastic stress concentrations using the Neuber method [16]. In that method, the product of the plastic stress- and strain-concentration factors is set equal to the square of the elastic stress-concentration factor (SCF). If the stress increase is small, that is, there is little strain hardening; the plastic strain-concentration factor will be the square of the elastic SCF.

Ovality and differences in thickness can cause "high-low" across the weld, which is the primary geometrical strain concentrator for local elastic strain at girth welds. High-low is measured as an eccentricity of the mid-thickness position between the two sides of a weld. Strain concentrations at changes of section thickness, changes of

material grade, transitions to attachments, transitions in coating thickness, and localized areas of transverse loading also should be accounted for in assessments of allowable strains, both in tension and compression.

Concrete weight coating in offshore pipelines used for sea bottom service is not continued across field weld joints. This may cause bending loads to be concentrated around the field welds, as the stiffness of the pipe alone is lower than the weight-coated pipe composite. The span of this stiffness change may need to be considered to change with time if the load is in place more than a few minutes and the corrosion coating between the pipe and the weight coating can creep at the ambient temperature. It is necessary to evaluate the effects of the concrete coating on strain concentrations at field joints. It is found reasonable to assume that the SNCF is 1.2. This value is selected mainly due to an allowable strain as high as 0.4% from the fracture criterion [17].

DNV OS-F101 [3] requires that the pipe material meet additional quality requirements if it is to be used for accumulated plastic strains $\geq 2\%$. The quality requirements increase pipe inspection and restrict the maximum differences between the pipe end thicknesses and the local wall thickness variation.

Accidental Loads

Loads under abnormal and unplanned conditions and with an annual probability of occurrence less than 10^{-2} are classified as accidental loads, referring to DNV-OS-F101. Typical accidental loads can be caused by

- Extreme wave and current loads.
- Impact with a vessel or other drifting items (collision, grounding, sinking, iceberg).
- Dropped objects.
- Seabed movement or mud slides.
- Explosion.
- Fire and heat flux.
- Operational malfunction.
- Dragging anchors.

Table 4.4 Simplified Design Check Versus Accidental Loads

Prob. of Occurrence	Safety Class		
	Low	Medium	High
$>10^{-2}$	Accidental loads may be regarded similar to environmental loads and may be evaluated similar to ULS design check		
10^{-2}–10^{-3}	To be evaluated on a case by case basis		
10^{-3}–10^{-4}	$\gamma_c = 1.0$	$\gamma_c = 1.0$	$\gamma_c = 1.0$
10^{-4}–10^{-5}		$\gamma_c = 0.9$	$\gamma_c = 0.9$
10^{-5}–10^{-6}	Accidental loads or events may be disregarded		$\gamma_c = 0.8$
$<10^{-6}$			

Note: When the failure mode is bursting, the probability of occurrence should be on the order of 1–2 magnitudes lower.

The size and frequency of accidental loads may be defined through risk analyses. The design against accidental loads may be performed by direct calculation of the effects imposed by the loads on the structure or, indirectly, by design of the structure as tolerable to accidents.

DNV OS-F101 suggests a simplified design check with respect to accidental load, as shown in Table 4.4, with appropriate partial safety factors.

References

[1] Carr M, Bruton D, Leslie D. Lateral buckling and pipeline walking, a challenge for hot pipelines. OPT 2003, Amsterdam; 2003.

[2] Vitali L, Bruschi R, Mork K, Levold E, Verley R. HOTPIPE Project: Capacity of pipes subject to internal pressure, axial force and bending moment. ISOPE Conference 1999;2:22–33. France.

[3] DNV. Submarine pipeline systems. DNV-OS-F101. Det Norske Veritas; 2010.

[4] Carr M, Sinclair F, Bruton D. Pipeline walking—Understanding the field layout challenges, and analytical solutions developed for the SAFEBUCK JIP. OTC 17945; 2006.

[5] API. Design, construction, operation, and maintenance of offshore hydrocarbon pipelines (limit state design). API RP-1111. 4th ed. Washington, DC: American Petroleum Institute; 2009.

[6] ASME. Pipeline transportation systems for liquid hydrocarbons and other liquids. ASME B31.4. American Society of Mechanical Engineers; 2009.

[7] ASME. Gas Transmission and distribution piping systems, ASME B31.8. American Society of Mechanical Engineers; 2007.

[8] British Standard Institute. Code of practice for pipelines, Pipelines on land: design, construction and installation. BS8010; 1989.

[9] British Standard Institute. Guide on methods for assessing the acceptability of flaws in fusion welded structures. BS 7910; 2005.

[10] API. Fitness-for-service. API 579. 2nd ed. Washington, DC: American Petroleum Institute; 2007.

[11] DNV. Fracture control for pipeline installation methods introducing cyclic plastic strain. DNV-RP-F108. Det Norske Veritas; 2006.

[12] Stewart G, Klever FJ, Ritchie D. An analytical model to predict the burst capacity of pipelines. Proc. of OMAE; 1994.

[13] ISO. Pipeline transportation systems for petroleum and natural gas industries. ISO 13623; 2000.

[14] Hauch S, Bai Y. Bending moment capacity of Pipes. OMAE; 1999.

[15] Nystrøm P, Tørnes K, Bai Y, Damsleth P. Dynamic buckling and cyclic behavior of HP/HT pipelines. Proc. of ISOPE; 1997.

[16] Neuber H. Theory of stress concentration for shear-strained prismatic bodies with arbitrary nonlinear stress-strain law. ASME J. Appl. Mech. 1961;28:544–50.

[17] Ness OB, Verley R. Strain concentrations in pipeline with concrete coating. J. Offshore Mechanics Arctic. Eng. 1996:118.

5 Hydraulic and Thermal Analysis of Subsea Pipelines

Chapter Outline

1. Introduction

An important part of process design and analysis of subsea pipelines involves hydraulic engineering, a subdiscipline of fluid dynamics, which studies the flow and conveyance of fluids, such as oil, gas, and water, and deals with the collection,

storage, control, transport, regulation, and measurement of fluid flow. During the engineering design, it is essential to size a pipeline correctly and ensure the system deliverability of hydrocarbon fluids from one point in the pipeline to another. During the pipeline operation, it is critical to have accurate knowledge of pressure and temperature distributions along the pipeline for safe operations and troubleshooting. For subsea applications, the reservoir pressures, artificial lifts, and pumps and compressors provide the driving forces to move the fluids from the reservoirs to the topsides for processing and storage or to transport from the topsides of platforms to onshore facilities. To solve a hydraulic engineering problem with heat transfer and phase changes, a thorough understanding of fluid mechanics, heat transfer, thermodynamics, vapor/liquid equilibrium, and fluid physical properties for hydraulic systems is required. In general, single phase flows are relatively simple to analyze as compared to multiphase flows. In fact, multiphase flow is an active research area, and many publications address multiphase flow challenges every year.

In this chapter, hydraulic and thermal analysis for oil, oil-gas, gas, and water pipelines are delineated as follows:

- Hydraulic and thermal analysis of oil transportation pipelines includes steady state temperature and pressure drop along a pipeline, temperature and pressure drop after pipeline shutdown, and water hammer phenomena.
- Hydraulic analysis of gas transmission pipelines includes horizontal pipelines, undulated pipelines, hydraulic friction factor, and average pressure and temperature drop along pipelines.
- Hydraulic analysis of oil-gas two phase flow pipelines includes pressure drop along pipelines, liquid holdup, flow pattern criteria, hydraulic friction factor, slug flow, and erosion velocity.
- Hydraulic analysis of water pipelines includes sizing of pipelines, pressure drop, and water hammer issue.

2. Crude Oil Transportation Pipelines

General

Generally, heating is not necessary to transport crude oil with low viscosities and low freezing points in subsea pipelines, as the temperature difference between the crude oil in the pipe and the surrounding media is small. As the temperature drop along a pipeline is also insignificantly small, heat transfer analysis can be neglected. This kind of pipeline is called an *isothermal oil pipeline* in engineering design. The majority of energy consumed in transporting crude oil along a pipeline is pressure energy, and hydraulic analysis of isothermal oil pipelines is a critical component of the crude oil transportation pipeline engineering [1].

The energy consumption of an isothermal oil pipeline mainly includes two parts: one is used to overcome the terrain elevation difference, which is constant for a specific crude oil transportation pipeline and does not vary with the other parts of the oil transport process; another is the energy consumed to make crude oil flow in the

pipeline. This part of energy consumption, commonly referred to as *friction loss*, is related to the pipeline characteristics, the crude oil characteristics, flowing characteristics, and so on. In the isothermal transportation conditions, various frictional resistances in the pipeline can be calculated directly by using basic fluid dynamic principles.

However, in many cases, thermal analysis is required as part of pipeline engineering for crude oil transportation, especially for fluids that are viscous and have high freezing points or in cold weather conditions, where heating is necessary.

A crude oil transportation pipeline is a pipe system consisting of many straight sections, variety of valves, and fittings. Therefore, the friction loss of the long pipeline includes (1) the friction loss, h_f, due to fluid shear against the pipe wall, called the *pipe friction*; (2) the friction loss, h_i, caused by local disruptions of the fluid stream, such as valves, pipe bend, and other fittings, called *local friction*.

Friction Loss Along Pipelines

The fluid flow in a pipeline can be classified into three flow regimes: laminar flow, turbulent flow, and critical state (an unstable transition region between laminar and turbulent flow) based on the Reynolds number as expressed as the ratio of the inertial force and viscous force:

$$Re = \frac{VD}{\upsilon} \qquad [5.1]$$

where

> V = average velocity of the fluid, m/s
> D = inner diameter for pipelines, m
> υ = liquid kinematic viscosity, m²/s

Normally, the three flow regimes may be defined as the following:

1. $Re \leq 2000$, laminar flow.
2. $2000 < Re < 3000$, transitional flow.
3. $Re \geq 3000$, turbulent flow.

The Darcy-Weisbach equation for calculation of the friction loss along a pipeline, h_f, is one of the most versatile friction head loss equations for a pipe segment:

$$h_f = f \frac{L}{D} \frac{V^2}{2g} \qquad [5.2]$$

where

> L = length of the pipeline, m
> D = inner diameter for the pipeline, m
> V = average velocity of the fluid, m/s
> g = gravitational constant, m/s²
> f = the friction factor, [–]

Table 5.1 Friction Factor Correlations

Flow Region	Reynolds Range	Friction Factor, f
Laminar	$Re < 2000$	$f = 64/Re$
Smooth	$2000 < Re < Re_1 = \dfrac{59.5}{(\varepsilon/D)^{8/7}}$	$\dfrac{1}{\sqrt{f}} = 1.8\lg(Re) - 1.53$
		When $Re<10^5, f = \dfrac{0.3164}{Re^{0.25}}$
Transition zone	$Re_1 < Re < Re_2$	$\dfrac{1}{\sqrt{f}} = 1.8\lg\left[\dfrac{6.8}{Re} + \left(\dfrac{\varepsilon}{7.4D}\right)^{1.11}\right]$
Complete turbulence	$Re > Re_2 = \dfrac{665 - 765\lg(\varepsilon/D)}{\varepsilon/D}$	$f = \dfrac{1}{(1.74 - 2\lg(\varepsilon/D))^2}$

Source: Haaland [2].

The friction loss along a pipeline is directly related to the flow pattern, which may be determined by the Re number. According to "Simple and Explicit Formulas for the Friction Factor in Pipe Flow" [2], the fiction factor can be derived from the formulas in Table 5.1.

Temperature Drop Along Pipelines

The purpose of calculating the temperature drop along a pipeline is to ensure the maximum temperature drop to fall within a safe range, such that hydrate and wax deposition do not take place in the oil pipeline during the normal operation.

According to Eq. (19.36) of the chapter "Heat Transfer and Thermal Insulation" in the book, *Subsea Pipelines and Risers* [1], the temperature distribution along a pipeline is predicted using the following equation:

$$T(x) = T_a + (T_{in} - T_a)\exp\left(\dfrac{-U\pi Dx}{\dot{m}c_p}\right) \qquad [5.3]$$

where

T_{in} = inlet temperature of the crude fluid, °C
$T(x)$ = temperature of the crude fluid at the location x [m], °C
T_a = ambient temperature of the pipe surroundings, °C
D = total pipe outside diameter, m
x = pipeline length from inlet, m
$\dot{m}$ = mass flow rate of crude fluid, kg/s
c_p = specific heat capacity of crude fluid, J/(kg·°C)
U = overall heat transfer coefficient or U value based on pipe OD, W/(m²·°C)

Overall Heat Transfer Coefficient

The overall heat transfer coefficient, U, is defined in the following formula, Eq. (19.28) of the book, *Subsea Pipelines and Risers* [1]:

$$1/(UA) = \sum R_i = R_{film,in} + R_{pipe} + \sum R_{coating} + R_{film,out} \qquad [5.4]$$

where

$$R_{film,in} = \frac{1}{h_i A_i}$$

$$R_{pipe} = \frac{\ln(r_1/r_i)}{2\pi L k_{pipe}}$$

$$\sum R_{coating} = \frac{\ln(r_{n0}/r_{ni})}{2\pi L k_n}$$

$$R_{film,out} = \frac{1}{h_0 A_0}$$

A = area of heat transfer surface, A_i or A_0, m^2
A_i = internal area normal to the heat transfer direction, $A_i = 2\pi r_i L$, m^2
A_0 = outer area normal to the heat transfer direction, $A_0 = 2\pi r_0 L$, m^2
r_i = internal radius of pipeline, m
r_0 = outer radius of pipeline, m
r_1 = outer radius of steel pipeline, m
r_{n0} = outer radius of the coating layer n
r_{ni} = inner radius of the coating layer n
k_{pipe} = thermal conductivity of steel pipeline, W/(m·K)
k_n = thermal conductivity of coating layer n, W/(m·K)
h_i = internal convection coefficient, W/(m^2·K)
h_0 = outer convection coefficient, W/(m^2·K)

Internal Convection Coefficient

The internal convection coefficient, h_i, depends on the fluid properties, the flow velocity, and the pipe diameter. For the laminar flow (i.e., $Re_i < 2100$), h_i may be calculated using the Hausen equation (1943) [3] as follows:

$$Nu_i = 3.66 + \frac{0.0668 \left(\frac{D_i}{L_0}\right) Re_i \, Pr_i}{1 + 0.4 \left[\left(\frac{D_i}{L_0}\right) Re_i \, Pr_i\right]^{2/3}} \qquad [5.5]$$

where L_0 represents the distance from the pipe inlet to the point of interest. In most pipelines, $D_i/L_0 \approx 0$, and the preceding equation becomes

$$Nu_i = 3.66 \qquad [5.6]$$

For the transition region ($2100 < Re_i < 10^4$), the formula proposed by Gnielinski [4] can be used to calculate h_i:

$$Nu_i = \frac{\left(\frac{f}{8}\right)(Re_i - 1000)Pr_i}{1 + 1.27\left(\frac{f}{8}\right)^{1/2}\left(Pr_i^{2/3} - 1\right)}$$ [5.7]

For the fully turbulent flow, the formula proposed by Dittus and Boelter (1930) [5] can be used to calculate h_i:

$$Nu_i = 0.0255 \cdot Re_i^{0.8} \cdot Pr_i^{n}$$ [5.8]

where

f = friction factor, which can be obtained from the Moody diagram
Nu_i = Nusselt number, $Nu_i = h_i D_i / k_f$
Re_i = Reynolds number, $Re_i = V_i D_i \rho_f / \mu_f$
Pr_i = Prandtl number, $Pr_i = C_f \mu_f / k_f$
n = 0.4 if the fluid is being heated, and 0.3 if the fluid is being cooled
h_i = internal convection coefficient, W/(m²·°C)
D_i = pipeline inside diameter, m
k_f = thermal conductivity of the fluid, W/(m·°C)
V_f = velocity of the fluid, m/s
ρ_f = density of the fluid, kg/m³
μ_f = viscosity of the fluid, Pa·s
C_f = specific heat capacity of the fluid, J/(kg·°C)

Table 5.2 shows typical ranges of internal convection coefficients for turbulent flow.

External Convection Coefficient

Unburied Pipeline

The formula proposed by Hilpert (1933) [7] can be used to calculate the external convection coefficient ($h_{o,\ unburied}$) for the unburied pipeline:

$$Nu_0 = C\,Re_0^{m}Pr_0^{1/3}$$ [5.9]

Table 5.2 Typical Internal Convection Coefficients for Turbulent Flow

	Internal Convection Coefficient, h_i	
Fluid	**BTU/(ft² · hr · °F)**	**W/(m² · °C)**
Water	300–2000	1700–11350
Gases	3–50	17–285
Oils	10–120	55–680

Source: Gregory [6].

where

Nu_0 = Nusselt number, $Nu_i = h_{o, unburied} D_0/k_0$
Re_0 = Reynolds number, $Re_0 = V_0 D_0 \rho_0/k_0$
Pr_0 = Prandtl number, $Pr_0 = C_{p,0}\mu_0/k_0$
h_o = external convection coefficient, W/(m²·°C)
D_0 = pipeline outer diameter, m
k_0 = thermal conductivity of the surrounding fluid, W/(m·°C)
V_0 = velocity of the surrounding fluid, m/s
ρ_0 = density of the surrounding fluid, kg/m³
μ_0 = viscosity of the surrounding fluid, Pa·s
$C_{p,o}$ = specific heat capacity of surrounding fluid, J/(kg·°C);
C, m = constants, dependent on the Re number range and listed in Table 5.3

When the velocity of the surrounding fluid is less than approximately 0.05 m/s in water and 0.5 m/s in air, natural convection dominates and the following values may be used:

$$h_{o, unburied} = \begin{cases} 4 \ W/(m^2K), & \text{natural convection in air} \\ 200 \ W/(m^2K), & \text{natural convection in water} \end{cases}$$

Fully Buried Pipeline

By using a conduction shape factor for a horizontal cylinder buried in a semi-infinite medium, shown in Figure 5.1, the outer convection coefficient ($h_{o, buried}$) can be calculated by the following formula for the fully buried pipeline:

$$h_{o, buried} = \frac{k_{soil}}{\frac{D}{2}\cosh^{-1}\left(\frac{2Z}{D}\right)} \qquad [5.10]$$

where

h_{soil} = heat transfer coefficient of soil, W/(m²·°C)
k_{soil} = thermal conductivity of soil, W/(m·°C)
D = outside diameter of buried pipe, m
Z = distance between top of soil and center of pipe, m

Table 5.3 Constants of Correlation

Re_0	C	m
$4 \times 10^{-1} - 4 \times 10^{0}$	0.989	0.330
$4 \times 10^{0} - 4 \times 10^{1}$	0.911	0.385
$4 \times 10^{1} - 4 \times 10^{3}$	0.683	0.466
$4 \times 10^{3} - 4 \times 10^{4}$	0.193	0.618
$4 \times 10^{4} - 4 \times 10^{5}$	0.027	0.805
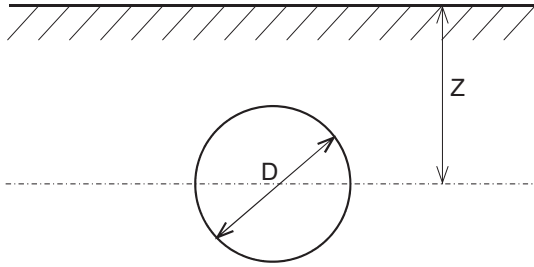
Figure 5.1 Cross section of a buried pipeline.

Partially Buried Pipeline

For partially buried pipeline, the external convection coefficient ($h_{o, partially}$) can be derived from the following formula:

$$h_{o, partially} = (1 - f)h_{o, buried} + f h_{o, exposed}$$ [5.11]

where

f = fraction of external surface of pipe exposed to the surrounding fluid
$h_{o, partially}$ = external heat transfer coefficient for partially buried pipeline, W/(m$^2 \cdot$°C).

Temperature Drop After Pipeline Shut Down

The purpose of this calculation is aimed at keeping the fluid temperature in the whole pipe higher than the freezing point temperature of the fluid. According to Eq. (19.40) of the chapter "Heat Transfer and Thermal Insulation" in the book, Subsea Pipelines and Risers [1], the following formula can be employed for this purpose:

$$T_t - T_e = (T_i - T_e) e^{-U\pi D L t / \Sigma m C_p}$$ [5.12]

where

T_t = temperature of the fluid at time t, °C
T_e = ambient temperature, °C
T_i = initial temperature at the beginning of shut down, °C
D = outer diameter of the insulation pipe, m
m = mass of internal fluid or coating layers, kg
C_p = specific heat capacity for the fluid pipe insulation layer, kJ/(kg·°C)
U = overall heat transfer coefficient, W/(m$^2 \cdot$°C)
t = time of the shutdown, s
L = length of the pipeline, m

Water Hammer

An important consideration in the design of single liquid phase pipelines is pressure surge, also known as *water hammer*. Normally, velocities and pressures of each point

in an oil pipeline vary with time, but their average values genearlly remain unchanged or change little, and the oil pipeline is considered to be at a steady state. During transient operations, such as startup, shutdown, and ramp-up, or turndown, the flow becomes unsteady, the fluid pressures and velocities in the pipeline change suddenly, and water hammer may take place that can lead to serious damages to the system integrity if no adequate procedure is followed.

For a short pipeline, the pressure surge due to water hammer can be calculated as follows:

$$\Delta H = \frac{a}{g} \Delta v = \frac{a}{g}(v_0 - v) \qquad [5.13]$$

with

$$a = \sqrt{\frac{K}{\rho\left(1 + \frac{Kd}{E\delta}\right)}} \qquad [5.14]$$

where,

ΔH = surge pressure due to the water hammer, m
a = propagation speed of the pressure wave, m/s
v_0 = speed of fluid before the pressure surge, m/s
v = speed of fluid after the pressure surge, m/s
ρ = density of the fluid, kg/m^3
K = fluid bulk modulus, pa
d = inside diameter of the pipe, m
δ = pipe wall thickness, m
E = pipe material modulus of elasticity, kg/m^2
g = gravitational constant, 9.8 m/s^2

Restart Pressure

The minimum restart pressure is evaluated to make sure the pipeline restarts without difficulty after it shutdowns for a given period of time. The following formula can be used for this purpose:

$$P = \frac{4\tau L}{D} + P_0 \qquad [5.15]$$

where

P = restart pressure, Pa
P_0 = outlet pressure of the pipe, Pa
τ = yield strength of the fluid, Pa
D = inner diameter of the pipe, m
L = length of the pipe, m

3.   Gas Transmission Pipelines

Composition and Properties of Gas Pipelines

The main composition of gas is hydrocarbons. In addition to hydrocarbons, water (H_2O), nitrogen (N_2), carbon dioxide (CO_2), and hydrogen sulfide (H_2S) are often found in a gas transmission pipeline. The main component of the hydrocarbons produced from the gas field is methane, which accounts for 90% by volume. Additional hydrocarbons, such as ethane and ethane plus, are contained in the gas produced from the oilfield [8].

Table 5.4 lists some typical physical properties of selected hydrocarbons. As the carbon number of a component increases, its boiling point rises. If the carbon number of a component is less than 5, the component is in the gas phase at atmospheric pressure. A typical composition of gas condensate is shown in Table 5.5.

Table 5.4 Physical Properties of Main Petroleum Components

Component	Formula	Boiling Temperature at 1 atm [°C]	Density at 1 atm and 15°C, [g/cm³]
Paraffins			
Methane	CH_4	−161.5	—
Ethane	C_2H_6	−88.3	—
Propane	C_3H_6	−42.2	—
i-Butane	C_4H_{10}	−10.2	—
n-Butane	C_4H_{10}	−0.6	—
n-Pentane	C_5H_{12}	36.2	0.626
n-Hexane	C_6H_{14}	69.0	0.659
i-Octane	C_8H_{18}	99.3	0.692
n-Decane	$C_{10}H_{22}$	174.0	0.730
Naphthenes			
Cyclopentane	C_2H_6	49.5	0.745
Methyl cyclo-pentane	C_2H_6	71.8	0.754
Cyclohexane	C_2H_6	81.4	0.779
Aromatics			
Benzene	C_6H_6	80.1	0.885
Toluene	C_7H_8	110.6	0.867
o-Xylene	C_8H_{10}	144.4	0.880
Naphthalene	$C_{10}H_8$	217.9	0.971
Others			
Nitrogen	N_2	−195.8	—
Carbon dioxide	CO_2	−78.4	—
Hydrogen sulfide	H_2S	−60.3	—

Source: Pedersen et al., 1989 [9].

Table 5.5 Typical Composition of Gas Condensate

Component		Composition (Mole %)
Hydrogen sulfide	H_2S	0.05
Carbon dioxide	CO_2	6.50
Nitrogen	N_2	11.71
Methane	C_1	79.06
Ethane	C_2	1.62
Propane	C_3	0.35
i-Butane	$i\text{-}C_4$	0.08
n-Butane	C_4	0.10
i-pentane	$i\text{-}C_5$	0.04
n-Pentane	C_5	0.04
Hexanes	C_6	0.06
Heptanes plus	C_7+	0.39

Source: Pedersen et al., 1989 [9].

In the usual composition list of hydrocarbons, the last hydrocarbon is marked with a "+", which indicates a pseudo- component that lumps together all the heavier components.

Hydraulic Analysis of Horizontal Pipelines

Horizontal pipelines here mean that the elevation difference is within 200 m along the pipeline. The following semi-empirical formula can be used to calculate the throughput under the engineering standard conditions ($P_0 = 0.101325$ MPa, $T_0 = 293.15$ K) [9]:

$$Q = 0.03848 \sqrt{\frac{(p_s^2 - p_t^2)d^5}{Z \cdot \lambda \cdot \gamma \cdot T \cdot L}} \qquad [5.16]$$

where

Q = pipeline throughput, m^3/d
d = pipeline inner diameter, m
p_s = pipeline input pressure, Pa
p_t = pipeline output pressure, Pa
λ = hydraulic friction factor
γ = gas relative density (to air)
T = average temperature of gas, K
L = pipeline length, m
Z = gas compressibility factor

For dry gas,

$$Z = \frac{100}{100 + 1.73 p_{cp}^{1.15}} \qquad [5.17]$$

For wet gas,

$$Z = \frac{100}{100 + 2.92p_{cp}^{1.25}}$$ [5.18]

where, p_{cp} is absolute pipeline average pressure, MPa.

Hydraulic Analysis of Undulating Pipelines

When the height difference of the gas pipeline is over 200 meter along a gas transmission pipeline, the following semi-empirical formula can be used to calculate the throughput under the engineering standard conditions

$$Q = 0.03845 \sqrt{\frac{\left[p_s^2 - p_t^2(1 + a\gamma h)\right]d^5}{Zf\gamma TL\left[1 + \frac{a}{2L}\sum_{i=1}^{n}(h_i + h_{i-1})L_i\right]}}$$ [5.19]

and

$$a = \frac{2g\gamma}{ZR_aT}$$ [5.20]

where

Q = pipeline throughput, m³/d
d = pipeline inner diameter, m
p_s = pipeline input pressure, Pa
p_t = pipeline output pressure, Pa
f = hydraulic friction factor
γ = gas relative density (to air)
T = average temperature of gas, K
L = pipeline length, m
Z = gas compressibility factor
h_i = the standard height of start point in each calculation section, m
h_{i-1} = the standard height of end point in each calculation section, m
g = gravity acceleration, m/s²
R_a = air constant, in the standard condition, R_a = 2887.1J/(kg·K)

Figure 5.2 shows the simple calculation graph of the undulating terrain pipeline.

Friction Factor

As mentioned in the previous section, the fluid flow can be divided into three regimes based on the Reynolds number: (1) laminar flow ($Re < 2000$), (2) critical flow
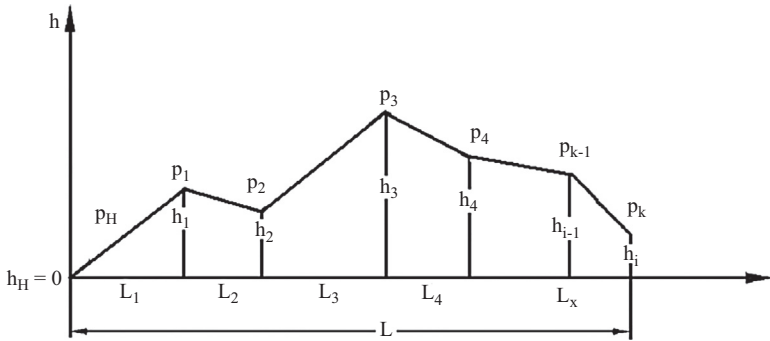
Figure 5.2 Undulating terrain pipeline.

(2000 < Re < 4000), (3) turbulent flow (Re > 4000). For a gas transmission system, the Reynolds number can be computed as follows [10]:

$$Re = 1.777 \times 10^{-5} \frac{Q\gamma}{d\mu}$$ [5.21]

where

Q = pipeline throughput, m³/d
d = pipeline inner diameter, m
γ = gas relative density (to air)
μ = gas kinetic viscosity, Pa·s

The hydraulic friction factors, f, can be calculated based on the following equations for different flow regimes. For Re < 2000,

$$\lambda = \frac{64}{Re}$$ [5.22]

For 2000 < Re < 3000,

$$\lambda = 0.0025\sqrt[3]{Re}$$ [5.23]

For Re > 3000,

$$\frac{1}{\sqrt{\lambda}} = -2.01 \cdot \lg\left(\frac{\varepsilon}{3.7065d} + \frac{2.52}{Re\sqrt{\lambda}}\right)$$ [5.24]

where ε is the equivalent roughness of the pipe wall, mm.

Generally, turbulent flows can be further divided into three subregions, as follows, and most long-distance gas transmission pipelines are in the quadratic resistance

region. Calculating the hydraulic friction factor according to the empirical formulas for the quadratic resistance region is recommended. Here, ε is the average value of pipeline absolute roughness, usually taken as 0.02–0.03 mm [2].

For the smooth region,

$$2000 < Re < \frac{59.7^{8/7}}{2\varepsilon/d} \qquad [5.25]$$

The empirical hydraulic friction factor is

$$f = \frac{0.1844}{Re^{0.2}} \qquad [5.26]$$

For the turbulent transition region,

$$\frac{59.7^{8/7}}{2\varepsilon/d} < Re < 11\left(\frac{2\varepsilon}{d}\right)^{-1.5} \qquad [5.27]$$

The empirical hydraulic friction factor formula is

$$f = 0.067\left(\frac{158}{Re} + \frac{2\varepsilon}{d}\right)^{0.2} \qquad [5.28]$$

For the quadratic resistance region,

$$Re > 11\left(\frac{2\varepsilon}{d}\right)^{-1.5} \qquad [5.29]$$

The empirical hydraulic friction factor formulas are

1. Weymouth equation (originally developed for small diameter, small throughput, high impurity gas pipelines with inner wall absolute roughness as large as 0.0508 mm),

$$f = \frac{0.009407}{\sqrt[3]{d}} \qquad [5.30]$$

2. Panhandle modified equation (smooth inner wall),

$$f = \frac{1}{68.1 Re^{0.0302}} \qquad [5.31]$$

Average Pressure of Gas Transmission Pipelines

When a gas transmission pipeline shuts down, the gas in the high-pressure section of the pipeline gradually flows to the low-pressure region. Pressure at the high-pressure

point (p_H) drops while pressure at the low-pressure point (p_k) rises, and eventually they come to equilibrium. The final average pressure (p_a) can be determined by the following equation:

$$p_a = \frac{2}{3}\left(p_H + \frac{P_K^2}{p_H + p_K}\right)$$ [5.32]

where

    p_a = absolutely average pressure, MPa
    p_H = absolute start point pressure, MPa
    p_K = absolute end point pressure, MPa

It is obvious that the average pressure is larger than the arithmetic mean pressure,

$$\left(p_a > \frac{p_H + p_K}{2}\right).$$

Thermal Analysis of Gas Transmission Pipelines

Temperature Profile Along a Gas Pipeline without the Chilly Choke Effect

If the chilly choke effect is not taken into account, the temperature at any point along a gas transmission pipeline can be described by Eq. [5.12]:

$$t_x = t_e + (t_s - t_e) \cdot e^{-ax}$$ [5.33]

where

    t_x = gas temperature at point x of the pipeline, °C
    t_e = environment temperature around pipeline, °C
    t_s = gas temperature at the start point, °C
    x = distance between the start point and any point along the pipeline, m

and

$$a = \frac{225.256 \cdot 10^6 \cdot K \cdot D}{Q \cdot c_p \cdot \gamma}$$ [5.34]

where

    K = total heat transfer coefficient of gas pipeline, W/(m·°C)
    D = pipeline outside diameter, m
    Q = pipeline throughput in the standard condition, m³/d
    γ = gas relative density (to air), dimensionless
    C_p = specific heat at constant pressure of gas, J/(kg·°C)

Temperature Profile Along a Gas Pipeline with the Chilly Choke Effect

As a real gas has chilly choke effect, the real temperatures in a gas pipeline is slightly lower than that given by the above equation. When chilly choke effect is taken into account, the temperature profile can be derived by the following equation:

$$t_x = t_e + (t_s - t_e) \cdot e^{-ax} - \frac{J \cdot \Delta P_x}{ax} \left(1 - e^{-ax}\right)$$ [5.35]

where

J = Joule-Thomson effect coefficient, °C/MPa
ΔP_x = pressure drop at x length along the pipeline, MPa

4. Hydraulic Analysis of Oil-Gas Production Pipelines

Pressure Drop Along Multiphase Flow Pipelines

The frictional pressure drop along a pipeline can be calculated with the following equation (Dukler's Model) [11]:

$$\Delta P_f = \frac{\lambda_m}{d} \frac{v_m^2}{2} \rho_f L$$

$$\rho_f = \rho_l \frac{R_L^2}{H_L} + \rho_g \frac{(1 - R_L)^2}{1 - H_L}$$ [5.36]

where

ΔP_f = frictional pressure drop along the pipeline, Pa
L = pipeline length (m)
ρ_L = liquid density, kg/m^3
ρ_g = gas density, kg/m^3
v_m = gas-liquid mixture velocity (m/s), $v_m = (Q_L + Q_g)/A$
d = pipeline inner diameter, m
λ_m = mixed transportation hydraulic friction factor, can be obtained from empirical regressions.
R_L = volume fluid rate, $R_L = Q_L/(Q_L + Q_g)$
H_L = section liquid holdup, which is expressed in the next section, the value is determined by the two-phase flow regime: separated flow regime, transitional flow regime, intermittent flow regime, and dispersion flow regime.

Section Liquid Holdup

The section liquid holdup of the separated flow, intermittent flow and dispersion flow in the horizontal pipeline, $H_L(0)$, may be obtained from the equations below:

$$H_L(0) = \frac{aR_L^b}{cFr}$$ [5.37]

where

$H_L(0)$ = section liquid holdup of the horizontal pipeline
R_L = flowing liquid volume fraction, $R_L = Q_L/Q_m$
Q_L = liquid volume flow, m³/s
Q_m = gas-liquid mixture volume flow, m³/s
Fr = Froude number, $Fr = v_m^2/gd$
v_m = gas-liquid mixture velocity, m/s
d = pipeline inner diameter, m
g = gravity acceleration, $g = 9.81\text{m/s}^2$
a, b, c = coefficients, the values for different flow pattern are shown in Table 5.6

The section liquid holdup of the transitional flow in the horizontal pipeline, $H_L(0)_T$ may be obtained from these equations:

$$H_L(0)_T = AH_L(0)_S + BH_L(0)_I \qquad [5.38]$$

where, the subscripts T, S, and I represent the transitional flow, the separated flow, and the intermittent flow, respectively. A and B are obtained from the following equations:

$$A = \frac{L_3 - Fr}{L_3 - L_2} \qquad [5.39]$$

$$B = 1 - A \qquad [5.40]$$

where L_2, L_3 are defined in Table 5.8. Fr is Froude number.

The section liquid holdup of the inclined pipeline, $H_L(\theta)$, can be obtained from these equations:

$$H_L(\theta) = \psi H_L(0) \qquad [5.41]$$

$$\psi = 1 + c\left[\sin(1.8\theta) - \frac{1}{3}\sin^3(1.8\theta)\right] \qquad [5.42]$$

$$c = (1 - R_L)\ln\left(dR_L^e N_{LW}^f Fr^h\right) \qquad [5.43]$$

Table 5.6 a, b, and c of Different Flow Patterns

Flow Pattern	a	b	c
Separated flow	0.980	0.4868	0.0868
Intermittent flow	0.845	0.5351	0.0173
Dispersion flow	1.065	0.5824	0.0609

Table 5.7 Coefficients Associated with Two-Phase Flow Patterns

Flow Pattern	d	e	f	h
Separated flow upward	0.011	−3.768	3.539	−1.614
Intermittent flow upward	2.96	0.305	−0.4473	0.0978
Dispersion flow upward	c = 0, ψ = 1			
Multitype flow downward	4.70	−0.3692	0.1244	−0.5056

$$N_{LW} = v_{sl} \left(\frac{\rho_L}{g\rho} \right)^{0.25}$$ [5.44]

where

$H_L(\theta)$ = the section liquid holdup where θ is the inclined angle
v_{sl} = liquid corrected velocity, m/s
σ = liquid surface tension, N/m
d, e, f, h = coefficients associated with the flow pattern are shown in Table 5.7

Flow Pattern Criteria of Two-Phase Flow

Table 5.8 lists the criteria of flow patterns for oil/gas two-phase flow.

Slugging of Oil-Gas Two Phase Flow

(a) *Slug Frequency*
The slug frequency can be more accurately calculated using the slug flow model of Hill & Wood [12]:

$$f_s = 0.275 \cdot \frac{w_m}{d} \cdot 10^{0.06807 h_l}$$ [5.45]

where
f_s = slug frequency, Hz
$w_m = w_l + w_g$, velocity of the gas-liquid mixture, m/s
h_l = depth of the stratified liquid layer, m
d = pipeline internal diameter, m

(b) *The Average Real Velocity of the Gas Bubbles*
The average real velocity of the gas bubbles can be calculated by the slug flow model of McQuillan & Whalley [13]:

$$w_{gs} = w_{ls} + 1.53 \cdot \left[\frac{\sigma g (\rho_l - \rho_g)}{\rho_l^2} \right]^{1/4}$$ [5.46]

Table 5.8 Criteria for Two-Phase Flow Pattern

Flow Pattern	Criteria		Equations of L
	R_L	Fr	
Separated flow	<0.01	<L_1	$L_1 = 316R_L^{0.302}$
	>0.01	<L_2	
Transitional flow	>0.01	>L_2 and <L_3	$L_2 = 9.252 \times 10^{-4}R_L^{-0.24684}$
Dispersion flow	>0.01 and <0.4	>L_3 and <L_1	$L_3 = 0.1R_L^{-1.4516}$
	>0.4	>L_3 and <L_4	
Dispersion flow	<0.4	>L_1	$L_4 = 0.5R_L^{-6.738}$
	>0.4	<L_4	

where

w_{gs} = average real velocity of the gas bubbles, m/s
ρ_1 = liquid density, kg/m^3
ρ_g = gas density, kg/m^3
σ = surface tension, N/m

The Liquid Holdup in the Slug

The liquid holdup in the slug can be calculated by the slug flow model of McQuillan and Whalley [13] as bfollows:

$$H_s = 1 - 0.058\left[D_{CD}\left(\frac{2f_sw_s^3}{D}\right)^{0.4} \times \left(\frac{\rho_1}{\sigma}\right)^{0.6} - 0.725\right] \qquad [5.47]$$

$$D_{CD} = 2\sqrt{0.4\sigma/\left[(\rho_l - \rho_g)g\right]} \qquad [5.48]$$

$$f_s = C_1Re_s^{-n} \qquad [5.49]$$

$$Re_s = \frac{w_sD}{\upsilon_1} \qquad [5.50]$$

where

υ_1 = liquid kinematic viscosity
f_s = fanning factor of gas-liquid mixture
Re_s = Reynolds number of gas-liquid mixture
C_1 and n : $C_1 = 16$, $n = 1$, when $Re_s < 2300$; $C_1 = 0.046$, $n = 0.2$, when $Re_s \geq 2300$.

The other parameters are the same as before.

The Velocity of Taylor Gas Bubbles and Dispersed Bubbles in the Film Layer

The velocity of Taylor gas bubble (w_t) and dispersed bubble (w_b) in the film layer of the slug may be obtained using the method proposed by Bendiksen [14]:

$$w_t = Cw_s + 0.35\sqrt{gD}\sin\alpha + 0.54\sqrt{gD}\cos\alpha \qquad [5.51]$$

where

C = constant related to the velocity distribution in the slug. For laminar flow, $C = 2$; for turbulent flow, $C = 1.2$.

$$w_b = 1.2w_s + 1.53\left[\frac{\sigma g(\rho_1 - \rho_g)}{\rho_l^2}\right]^{0.25} E_s^{0.1}\sin\alpha \qquad [5.52]$$

Slug Length

Slug length may be calculated by

$$L_u = \frac{w_t}{f_s} \qquad [5.53]$$

The Liquid Holdup of the Liquid Film

The liquid holdup of the liquid film, E_f, may be calculated by the slug flow models of Crawford and Weiberger [15] and McQuillan and Whalley [13], as follows:

$$E_f = 4D_{TD} - 4D_{TD}^2 \qquad [5.54]$$

$$w_f = \frac{w_s - (1 - E_f)w_t}{E_f} \qquad [5.55]$$

where

w_f = liquid film velocity, m/s

$$D_{TD} = 0.0682 \times \left[\frac{(\rho_1 \times \upsilon_1)^2}{D^3 g (\rho_1 - \rho_g) \rho_1} \right]^{\frac{1}{3}} \times \left[\frac{4\rho_1 |w_f| D_{TD} \times D}{\rho_1 \times \upsilon_1} \right]^{\frac{2}{3}} \qquad [5.56]$$

where

υ_1 = liquid kinematic viscosity, m^2/s

The liquid holdup of the liquid film, E_{lf}, may be obtained by solving the three equations, Eqs. [5.54] through [5.56], through iteration.

Gas Phase Velocity and Liquid Phase Velocity in the Liquid Film

Gas phase velocity, w_{gf}, and liquid phase velocity, w_{lf}, in the liquid film may be calculated by the slug flow model of Xiao and Brill [16], as follows:

$$w_s = w_{sl} + w_{sg} = w_1 E_s + w_b (1 - E_s) \qquad [5.57]$$

$$(w_t - w_1) E_s = (w_t - w_f) E_f \qquad [5.58]$$

$$w_s = w_f E_f + w_g (1 - E_f) \qquad [5.59]$$

The Average Liquid Holdup of a Slug Unit

The average liquid holdup (H_L) in the slug can be obtained by the slug flow model of McQuillan and Whalley [13], as follows:

$$H_L = 1 - \frac{w_{sg} - w_{gs}(1 - E_s) + w_t(1 - E_s)}{w_t} \qquad [5.60]$$

The Liquid Slug Length (L_s) and the Liquid Film Length (L_f) of the Slug Unit

$$L_s = L_u \times \frac{E - E_{lf}}{E_s - E_{lf}} \qquad [5.61]$$

$$L_f = L_u \times \frac{E_s - E_1}{E_s - E_f} \qquad [5.62]$$

Friction Factor of Two-Phase Flow

$$\frac{\lambda_m}{\lambda_o} = e^n \tag{5.63}$$

where

λ_m = hydraulic friction factor of two-phase flow pipeline
λ_o = hydraulic friction factor of two phases that are homogeneously mixed without slippage between the phases

$$n = \frac{-\ln m}{0.0523 - 3.182 \ln m + 0.8725(\ln m)^2 - 0.01853(\ln m)^4} \tag{5.64}$$

$$m = \frac{R_L}{[H_L(0)]^2} \tag{5.65}$$

$n = \ln(2.2m - 1.2)$, when $1 < m < 1.2$

For smooth pipes, the hydraulic friction factor without slippage (λ) can be found in the Moody diagram or obtained from the equation that follows:

$$\lambda_o = 2 \lg \left(\frac{Re_o}{4.5223 \lg Re_o - 3.8215} \right) \tag{5.66}$$

For no slippage, the Reynolds number, Re_o, is

$$Re_o = \frac{d v_m \left[\rho_L R_L + \rho_g (1 - R_L) \right]}{\mu_L R_L + \mu_g (1 - R_L)} \tag{5.67}$$

where

μ_L = liquid viscosity, Pa·s
μ_g = gas viscosity, Pa·s
v_m = gas-liquid mixture velocity, m/s

Erosional Velocity of Oil-Gas Two-Phase Flow

$$V_e = \frac{1.22C}{\sqrt{\rho_m}} \tag{5.68}$$

where

V_e = fluid erosion velocity, m/s
ρ_m = mixed density, kg/m^3
C = empirical constant

For continuous operation pipelines without solid particles, $C = 100$.

For intermittent operation pipelines without solid particles, $C = 125$.

For continuous operation pipelines aided by a corrosion inhibitor or made of corrosion-resistant materials, $C = 150 \sim 200$.

For intermittent operation pipelines aided by a corrosion inhibitor or made of corrosion-resistant materials, $C = 250$.

5. Water Transportation Pipelines

General

Subsea water pipelines are used for the delivery of injection water for water flooding. If several wellhead platforms in an oil field need water injection, the injected water is usually processed up to the specifications on the platform or on the FPSO (floating production storage and offloading), then the water is transported to each wellhead platform by a subsea water pipeline. When a wellhead platform is close to the center of the platform or FPSO, the water is transported to the injection well of the wellhead platform directly under the injection pressure. When the wellhead platform is far from the center of the platform or the FPSO, the size of the pipeline should be designed according to the required injection pressure and the friction loss of the subsea pipeline. The injection water is transported to the wellhead platform, filtered through the several stages to remove particles and microorganisms, and injected to the injection well by the injection pump of the wellhead platform to avoid the pressure in the pipeline being too high. Many variables need to be considered for a subsea water injection system during the engineering design phase.

Sizing of a Water Pipeline

The diameter of the pipeline can be calculated by the following formula:

$$d = \sqrt{\frac{4Q}{\pi v_e}} \qquad\qquad [5.69]$$

where

d = diameter of the water pipeline, m
Q = calculation flow of the water pipeline, m^3/s
v_e = economic velocity of water, m/s

Head Loss of Water Pipelines

Head Loss Along Water Pipelines

The equation for the head loss along a pipeline is as follows:

$$h_i = iL \tag{5.70}$$

where

h_i = head loss along the pipeline, m
L = calculated pipeline length, m
i = head loss of unit length (hydraulic gradient)

The head loss of unit length of an old pipeline can be calculated by the following formula:

$$v \geq 1.2 m/s, \quad i = 0.00107 \frac{v^2}{d^{1.3}} \tag{5.71}$$

$$v \geq 1.2 m/s, \quad i = 0.000912 \frac{v^2}{d^{1.3}} \left(1 + \frac{0.867}{v} \right)^{0.3} \tag{5.72}$$

where

v = average velocity in the pipeline, m/s
d = pipe inner diameter, m.

If a pipeline is new, the formula is also suitable, but the value of i is smaller.

Local Head Loss

In addition to pressure head losses due to pipe surface friction, the local losses are the pressure head loss occurring when the fluid flows through the appurtenances such as valves, bends, and other fittings. The local head losses in fittings may include

- Surface friction.
- Directional change of flow.
- Obstructions in flow path.
- Sudden or gradual changes in the cross section and shape of flow path.

The local losses are also termed *minor losses*. These descriptions are misleading for process piping systems where fitting losses are often much greater than the losses in straight piping sections. It is difficult to quantify theoretically the magnitudes of the local losses, so the representation of these losses is determined mainly using experimental data. Local losses are usually expressed in a form similar to that for the friction loss. Instead of f L/D in friction head loss, the loss coefficient K is defined for various fittings. The head loss due to fitting is given as follows:

$$h_2 = \sum K \frac{V^2}{2g} \tag{5.73}$$

Table 5.9 Loss Coefficients for Fittings

Fitting	K
Globe valve, fully open	10.0
Angle valve, fully open	5.0
Butterfly valve, fully open	0.4
Gate valve, full open	0.2
$^3/_4$ open	1.0
$^1/_2$ open	5.6
$^1/_4$ open	17.0
Check valve, swing type, fully open	2.3
Check valve, lift type, fully open	12.0
Check valve, ball type, fully open	70.0
Elbow, 45°	0.4
Long radius elbow, 90°	0.6

Source: Larock et al. [17].

where V is the downstream mean velocity. Two methods are used to determine the K value for different fittings, such as valve or elbow. One method is to choose a K value directly from a table that is invariant with respect to size and Reynolds number. Table 5.9 gives K values for several types of fittings. In this method the data scatter can be large and some inaccuracy is to be expected. The other approach is to specify the K for a given fitting in terms of the value of the complete turbulence friction factor, f_T, for the nominal pipe size. This method implicitly accounts for the pipe size. The Crane Company Technical Paper 410 details the calculation methods of K values for different fittings, which is commonly accepted by the piping industry.

Pressure Head of the Pipeline Start Point

The pressure head of the pipeline start point is the sum of the friction head loss (h_1), the local head loss (h_2), the altitude difference between the start point (h_3) and the end, and necessary residual head (h_4).

Water Hammer Issues

Causes of Water Hammer

1. Changes in the water pump rotation speed to start or stop the pumps and open or close the valves. Especially when operating rapidly, these actions drastically change the water flow speed and the water hammer happens.
2. Accidental pump suspension means that the pump power is suddenly interrupted in the operation.

Classification of Water Hammer

Water hammers can be divided into opening valve water hammer, closing valve water hammer, starting pump water hammer, and stopping pump water hammer.

Major Damages of Water Hammer

1. The pressure of the water hammer is so high as to destroy the water pumps, the valves, and pipeline. Or the pressure is too low, which makes the pipeline unstable and destroyed.
2. The motor rotor deforms or fractures, so that the reverse rotational speed of the pump is too high or near the critical speed, and the reverse rotation suddenly stops or the electromotor restarts.

Water Hammer Protection

1. **Closing or opening valve water hammer:** The most effective way is to extend the time of the closing or opening valve to avoid a direct water hammer. When the valve is closed with the pump running, the pressure before the valve is equal to the pump outlet pressure, whose maximum is usually equal to the pump's turnoff head and independent of the valve closing time but related to the type of the pump. The centrifugal pump should not be stopped when the valve is fully closed and should be stopped when the valve is closed about 15–30%. This can reduce the pump outlet pressure, prevent pump vibration, and extend the life of the valve.
2. **Starting pump water hammer:** The most effective way to prevent the starting pump water hammer is to exclude air in the pipeline, fill the pipeline with water, and start the pump when all the vales are opened except the valves at the outlet of the pump. Automatic exhaust valves or water filling facilities should be installed at the place where the pipeline uplifts. When the pump must be started with the pipeline empty, water hammer can be prevented if the pumps are started and the valves are opened stage by stage. The valve at the outlet of the water pump is opened about 15–30%, with others on the pipeline opened fully. After the pipeline is filled with water, all the valves are opened fully or adjusted to the required valve opening.
3. **Stopping pump water hammer:** According to the process calculation of the stopping water hammer, when the parameters of the water hammer are over the allowable value, the following measures can be taken:
   - Increase the diameter or the wall thickness of the pipeline.
   - Choose the motor whose GD^2 is bigger, GD^2 means the flywheel inertia of the water pump units.
   - Set the water hammer protection devices, such as air chamber, airbag-type water hammer eliminator, regulated pressure water hammer eliminator, and so on.

Water Hammer Pressure

The calculation of water hammer pressure needs both formulas and calculation charts, because the causes of water hammer are different and the formulas and charts for each cause are also different. In the calculation of subsea water pipelines, it is usually considered that water hammer pressure occurs only when the valve at the end of the calculated pipeline suddenly closes.

The calculation formulas of water hammer are shown as follows:

$$\Delta H = \frac{Rav_0}{g}$$ [5.74]

and

$$a = \frac{a'}{\sqrt{1 + (E_0/E)(d/\delta)C_1}}$$ [5.75]

where

ΔH = water hammer pressure, m
v_0 = the initial velocity of the liquid in the pipeline, m/s
a = propagation velocity of water hammer, m/s
a' = velocity of sound in water, 1435m/s
d = pipe inner diameter, m
δ = wall thickness, m
g = acceleration of gravity, m/s^2
E_0 = elasticity coefficient of water, 2.05939 Pa
E = wall material elastic coefficient, Pa
C_1 = parameter of different pipe wall thicknesses and supporting ways
R = dimensionless parameter found from Figure 5.3 according to the parameters ρ and θ
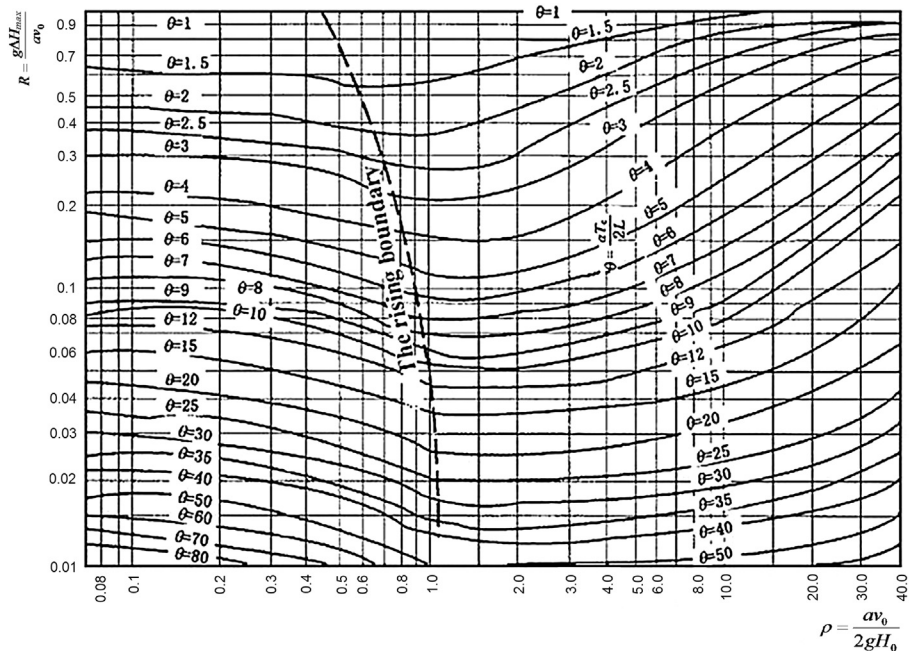
Figure 5.3 Water hammer calculation chart.
Source: Quick [18].

Table 5.10 Formulas of Different Pipeline Types Under Different Statues

Pipeline Types	Statues	Formula
Thin-wall pipeline ($d/\delta > 25$)	Pipe fixed only at upstream	$C_1 = 1 - \frac{\mu}{2}$
	All piping fixed, no axial movement	$C_1 = 1 - \mu^2$
	Piping adopts expansion joints connected	$C_1 = 1$
Thick wall elasticity pipeline ($d/\delta \leq 25$)	Pipe fixed only at upstream	$C_1 = \frac{2\delta}{d}(1+\mu) + \frac{d}{d+\delta}\left(1 - \frac{\mu}{2}\right)$
	All piping fixed, no axial movement	$C_1 = \frac{2\delta}{d}(1+\mu) + \frac{d(1-\mu^2)}{d+\delta}$
	Piping adopts expansion joints connected	$C_1 = \frac{2\delta}{d}(1+\mu) + \frac{d}{d+\delta}$

Note: μ is Poisson ratio of the wall material.
Source: Quick [18].

- The parameter C_1 can be calculated by the formulas in Table 5.10.
- The parameter ρ can be obtained from the equation that follows:

$$\rho = \frac{av_0}{2gH_0} \tag{5.76}$$

where
  ρ = a dimensionless parameter
  H_0 = initial head of pipeline, m

- The parameter θ can be obtained from the equation that follows:

$$\theta = \frac{at_c}{2L} \tag{5.77}$$

where θ is a dimensionless parameter and t_c is the closing valve time, s.

6.   Commercial Software for Design and Analysis

The engineering design and analysis of subsea pipelines, either for oil and gas pro-duction or transmission of processed fluids, such as natural gas and crude oil, can become really complex or, in most cases, require the aid of sophisticated software. For pipeline sizing, steady state modeling of coupled hydraulic and thermal perfor-mance with various insulation options is required to ensure deliverability and oper-ability. Most often used tools for this purpose in the oil and gas industry are PIPESIM from Schlumberger and HYSYS from Aspen or UNISIM from Honeywell. For transient operations, such as startup, shutdown, slugging, depressurization, and ramp up or turndown, OLGA from SPT Group is the standard tool for the design and analysis in the upstream oil and gas industry. LedaFlow, a newcomer developed by

SINTEF and commercialized by Kongsberg Oil and Gas Technologies, offers similar features to OLGA. While OLGA is a one-dimensional multiphase flow simulator, LedaFlow can model multidimensional two- and three-phase flows in large diameter pipelines.

References

[1] Bai Y, Bai Q. Subsea pipelines and Risers. Oxford, UK: Elsevier Science Ltd; 2005.

[2] Haaland SE. Simple and explicit formulas for the friction factor in pipe flow. J Fluids Eng 1983;105:89–90.

[3] Hausen H. Darstellung des Warmeuberganges in Rohren durch verallgemeinerte Potezbeziehungen. Z VDI Beih Verfahrenstechnik 1943;(4):91.

[4] Gnielinski V. New equations for heat and mass transfer in turbulent pipe and channel flow. Int Chem Eng 1976;16:359–69.

[5] Dittus FW, Boelter LMK, Heat transfer in automobile radiators of the tubular type, University of California, 2. Berkeley: Publications on Engineering; 1930. 443–461.

[6] Gregory GA. Estimation of overall heat transfer coefficient for the calculation of pipeline heat loss/gain, Technical Note No. 3. Calgary, Canada: Neotechnology Consultants Ltd; 1991.

[7] Hilpert R. Warmeabgabe von geheizen Drahten und Rohren. Forsch Gebiete Ingenieurw. 1933;4:220.

[8] GPSA. Engineering data book. 12th ed. Tulsa: Gas Processors Suppliers Association; 2004.

[9] Pedersen KS, A. Fredenslund A, Thomassen P. Properties of oils and natural gases. Houston: Gulf Publishing Company; 1989.

[10] Yang XH, Zhu WL. The influence of inner surface roughness on the fiction factor of gas transmission pipeline. Petro-Chem Equipment, Lanzhou, China 2005:34.

[11] Dukler AE. Gas-liquid flow in pipelines. New York: American Gas Association; 1969.

[12] Hill TJ, Wood DG. A new approach to the prediction of slug frequency, paper SPE-20629, the 1990 SPE Annual Technical Conference and Exhibition, New Orleans, 23-26 September.

[13] McQuillan KW, Whalley PB. Flow patterns in vertical. Int J Multiphase Flow 1985;11(2):161–75.

[14] Bendiksen KH. An experimental investigation of the motion of long bubbles in inclined tubes. Int J Multiphase Flow 1984;10(4):467–83.

[15] Crawford C, Weinberger C, Weisman J. Two-phase flow patterns and void fractions in downward flow Part I: steady-state flow patterns. Int. J. of Multiphase Flow 1985;11(6): 761–82.

[16] Xiao JJ, Shonham O, Brill JP. A comprehensive mechanistic model for two-phase flow in pipelines. Louisiana: SPE 20631, SPE annual technical conference and exhibition; 1990.

[17] Larock BE, Jeppson RW, Watters GZ. Hydraulics of pipeline systems, CRC Press.

[18] Quick RS. Comparison and limitations of various water-hammer theories. Mech Eng 1927;49(5a).

6 Soil and Pipe Interaction

Chapter Outline

1. Introduction

Seabed soil-pipe interaction affects various aspects of subsea pipelines and risers during installation and operation, which include

- The on-bottom lateral stability of pipelines under hydrodynamic forces during the periods of both installation and operation.
- Thermal expansion of pipelines and global buckling.
- Pipeline laying, bottom towing and pulling-in methods of installation.
- The touchdown point of the SCR design.
- Pipeline spanning.

In the calculations of these various design aspects, an interaction model of the contact between the pipeline and seabed are often referred as *pipe-soil interaction model*. The pipe-soil interaction model consists of seabed stiffness and equivalent friction resistances from the soil to the longitudinal or lateral movements of the

pipe. The equivalent friction resistance is based mainly on the Coulomb friction for noncohesive soil (sand), cohesive soil (clay), or a combination of both soils (silt-soil and sand-soil), related with the soil density and the contact pressure between the soil and pipe.

The scope of this chapter is to identify different implications of pipe-soil interaction on in-place stability, expansion, and structural integrity of the pipeline, which includes

- Predicting the pipe penetration during installation and service life of pipelines.
- Defining the axial and lateral resistance applicable to the calculations for in-place stability under environmental and operational loads.
- Defining the soil parameters required for lateral buckling and axial walking analysis.

Soil Types and Classification

Soil data along the pipeline route are needed for modeling pipe-soil interaction. These data can be obtained by carrying out geophysical and geotechnical surveys, which provide soil parameters characterizing the different soils along the pipeline route. Soil classification systems provide a systematic method of categorizing soils according to their probable engineering behavior.

Many soil classification systems have been proposed. An original system classifies soil by grain size. Soils with particles larger than about 0.05 mm are called *coarse grained* (sands and gravels), while soils finer than this size are called *fine grained* (silts and clays). Another way to classify the different soil types is according to their plasticity and cohesion. For example, sands are nonplastic and noncohesive, that is, they do not stick together, whereas clays are both plastic and cohesive. Silts fall between clays and sands—they are at the same time fine grained but generally nonplastic and noncohesive.

Generally, soil behavior is categorized as "drained" or "undrained" behavior [1]. Soil is a porous media material comprising solid particles with void spaces containing gas and water. In subsea environments, the water pressure is generally high enough that gas is forced into solution and the soils are saturated with water. Soil behavior depends on the rate at which load (force) is applied to the soil. If the rate of load is greater than the rate at which pore water in the interparticle voids is able to move in or out of soil interparticle voids, then the soil is said to behave in an undrained manner. If the rate of loading is slower than the rate at which pore water is able to move in or out of soil interparticle voids, the soil is said to behave in a drained manner.

Whether a soil (sand or clay) behaves in a drained or undrained style depends on the rate of loading with respect to the permeability of the soil. Clay behavior is commonly considered to be undrained, because the rate of loading is usually much greater than the rate at which pore water can move in or out of interparticle voids. The permeability of clay is very low, on the order of 10^{-9} m/s. The clay strength is given by "undrained shear strength," denoted by symbol S_u or C_u and measured in kilopascals. Sand behavior is commonly considered as drained, because pore water can move in or out of interparticle space at a greater rate than the rate of loading.

Table 6.1 Estimates of Undrained Shear Strength of Clays

Description of Clay	Undrained Shear Strength, S_u, (kPa)
Very soft	1–20
Soft	20–40
Firm	40–75
Stiff	75–150
Very stiff	150–300
Hard	300–600
Very hard	>600

The sand strength is given in terms of the friction angle using the symbol ϕ. However, if clay is sheared at a very slow rate, such that enough time is allowed for the pore water to move in or out of the interparticle voids, then it will not exhibit undrained shear strength. Instead, it behaves more like sand with an applicable clay friction angle. Similarly, if sand is sheared under load at a very fast rate, such that the pore water lacks enough time to move around, then sand can exhibit undrained behavior.

Estimates of the consistency of fine-grained soil can be reliable for high-quality undisturbed samples. Descriptive terms for consistency relative to undrained shear strength, S_u, according to BS 5930, are also listed, as in Table 6.1.

In noncohesive soils, the relative density is a good means of characterizing the soil. Relative density D_r is a measure of soil packing in relation to standardized loose and dense soil states, defined as

$$D_r = \frac{e_{max} - e}{e_{max} - e_{min}} \qquad [6.1]$$

where

e_{max} = void ratio of soil in the loosest state
e = in situ void ratio
e_{min} = void ratio of soil in the densest state

Table 6.2 shows the general relationships between relative density, standard penetration resistance, and the angle of internal friction (by Peck and Meyerhof, cited in [2]) for noncohesive soils. These data can be used for preliminary design.

The ASTM Unified Soil Classification System (USCS) is a very convenient system for soil description in connection with pipeline projects. Offshore soils may be conveniently labeled as either sandy soils or clayey soils. The soils parameters requested from pipeline projects are listed in Table 6.3 for sand and clay, respectively. Recommended values of some key parameters are listed in Table 6.4. The recommended values of modulus of subgrade reaction, K_s, are listed in Table 6.5.

Table 6.2 Properties for Noncohesive Soils

| Type of Soil | Penetration Resistance, N | Relative Density, D_r | Angle of Internal Friction, ϕ | |
			Peck (1974)	Meyerhof (1956)
Very loose sand	<4	<0.2	<29	<30
Loose sand	4–10	0.2–0.4	29–30	30–35
Medium sand	10–30	0.4–0.6	30–36	35–40
Dense sand	30–50	0.6–0.8	36–41	40–45
Very dense sand	>50	>0.8	>41	>45

Table 6.3 Design Parameters for Sandy and Clayey Soils

	Sandy Soil	Clayey Soil
Material parameters	Gradient, specific gravity	Liquid and plastic limits
	Void ratios in loosest and densest state	Specific gravity
		Remolded shear strength
In-situ parameters	Void ratio and density index	Water content and liquidity index
	Bulk and dry densities	Bulk and dry densities
	Peak friction angle	Undrained shear strength
	Modulus of subgrade reaction	Drained shear strength
	Permeability	Sensitivity, consolidation parameters
		Modulus of subgrade reaction

Coefficients of Friction

The Coulomb friction model is the classic and simplest method to describe the pipe-soil interaction along the soil surface. In the model, the friction force is proportional to the normal pressure of the pipeline onto the soil. The ratio of the friction force to the contact pressure is a material constant related with soil properties and pipe penetration, named the *coefficient of friction*. The lateral friction coefficient is applicable to the lateral movement of unburied pipe on the seabed, while the axial friction coefficient is applicable to longitudinal (axial) movement of unburied pipe on the seabed. An anisotropic friction model, as shown in Figure 6.1, defines different coefficients of friction in the lateral and longitudinal directions of the pipeline.

It is not easy to quantify the friction model as it depends on both pipe and soil characteristics. In the North Sea, tests have been conducted in order to define a range

Table 6.4 Recommended Values of Key Parameters for Typical Subsea Soils

USCS Symbol	Soil Description	Submerged Density (kN/m^3)	Plane Angle of Friction ϕ, (deg.)	S_u (kN/m^2)
SW	Well-graded sands	8.5–11.5	34–41	
SP	Poorly graded sands	7.5–10.5	34–39	
	—Very loose	8.1	28	
	—Medium loose	9.3	34	
	—Very dense	10.6	40	
SM	Silty sands, poorly graded	8.0–11.5	31–37	
	—Very loose	8.9	27	
	—Medium loose	10.1	32	
	—Very dense	11.4	38	
SC	Clayey sands, poorly graded	8.0–11.0	29–35	
ML	Silts and clayed silts	8.0–11.0	26–33	
CL	Clays of low to medium plasticity	8.0–11.0	N/A	
CH	Clays of high plasticity	3.0–9.0	N/A	10–100
	—Very loose			10
	—Medium loose			50
	—Very dense			100

Table 6.5 Estimates of Modulus of Subgrade Reaction for Different Types of Soils

Soil Type	Subgrade Reaction K_s (MPa)
Very soft clay	1–10
Soft clay	3–33
Medium clay	9–33
Hard clay	30–67
Sandy clay/ moraine clay	13–140
Loose sand	5–13
Dense sand	25–48
Silt	1–11
Rock	550–52,000
Rock with marine growth	550–52,000

of coefficient of friction. The minimum and maximum values for the Coulumb friction model have been estimated. Table 6.6 represents the results obtained and used for North Sea applications based on BS PD 8010 [3]. These numbers could be good references when soil data are not possible.
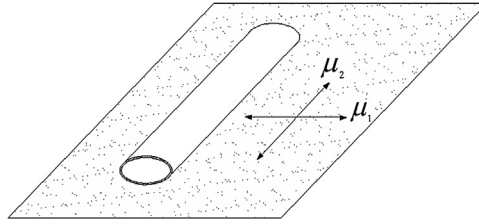
Figure 6.1 Anisotropic frictions between pipe and soil.

Effects of Lateral Friction

The selection of an appropriate lateral coefficient of friction depends on the soil characteristics and the type of analysis under consideration. A range of coefficients of friction should be considered due to its uncertainty. For instance, in the analysis of loop expansion, a high coefficient of lateral friction leads to high frictional restraint and hence high bending moments and stresses at the bend connecting the expansion loop to the pipeline, which requires higher effective compressive force to initiate buckling. If a low coefficient value is used, the lateral restraint is significantly reduced and, making the pipe at the bend easier to initiate, buckles. The selection of an appropriate value is therefore important and cannot be considered in isolation from the type of analysis to be performed.

Effects of Axial Friction

The choice of an axial coefficient of friction depends on the analysis to be performed, too. For instance, the maximum expected pull loads should be calculated assuming high friction forces, whereas the expansion movement for the same pipeline should be calculated using the lower value in the range, because lower axial friction increases pipeline end expansion. Low axial friction also allows longer pipe to create enough effective compressive axial force to initiate a lateral buckle.

Pipeline embedment, or burial, has a little effect on the axial coefficient of friction. However, the embedment of pipeline into the seabed significantly affects the forces required to move the pipeline laterally. Pipe-soil interaction for clay soil is investigated widely because it is the key factor for controlling pipeline global buckling in

Table 6.6 Coefficients of Friction Coefficients Used in the North Sea

Soil Type	Lateral Coefficient of Friction		Axial Coefficient of Friction	
	Minimum	Maximum	Minimum	Maximum
Noncohesive soils (sand)	0.5	0.9	0.55	1.2
Cohesive soils (clay)	0.3	0.75	0.3	1.0

deep water. The research results about the pipe-soil interaction are detailed in the next several sections.

Pipe-Soil Models

The interaction between pipe and seabed is one of the most important factors in the thermal-mechanical analysis of pipeline, which is usually incorporated into the finite element model, to represent the axial and lateral resistance loads applied by soil to the pipe. The most basic pipe-soil elements are spring sliders, which provide a bilinear elastic/perfectly plastic response in the axial and lateral directions. A suitable basic pipe-soil model of axial and lateral friction coefficients can be used for some pipeline design functions (such as on-bottom stability calculations or thermal expansion analysis) and in conceptual evaluation of lateral buckling. However, the Coulomb friction model is not appropriate in the detailed design for lateral buckling, as shown in Figure 6.2, particularly for large-amplitude lateral movement between berms due to lateral buckling, where the Coulomb friction model represents an oversimplification of the behavior. Nonlinear force-displacement responses for axial and lateral directions, as shown in Figure 6.3, are required, separately. It is necessary to introduce a subroutine in the Abaqus analysis, in which the nonlinear load-displacement response is modified to account for (1) brittle breakout behavior, (2) suction release, (3) residual resistance at large displacements, and (4) cyclic berm growth.

In the Coulomb friction model, the elastic slip is assumed to be the same in both the axial and lateral directions. However, the elastic slip in the lateral direction is normally many times that in the axial direction. The elastic slip in the axial direction is one of the control factors of pipeline walking under cyclic thermal loads. A decoupled friction model is required for the thermal-mechanical analysis related with lateral buckling to accurately simulate the nonlinear pipe-soil interactions, such as in Figure 6.3.

Lateral movement under cyclic thermal load
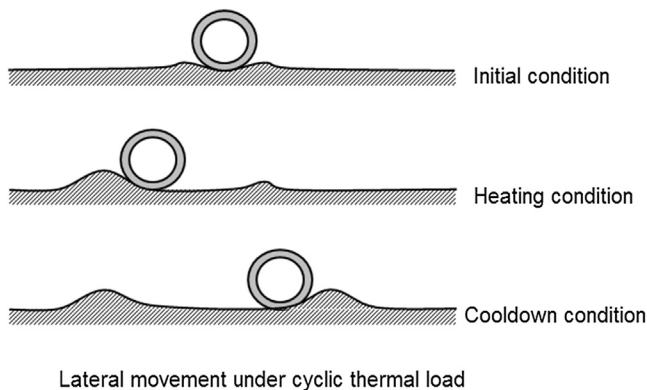
Figure 6.2 Pipeline lateral movement between soil berms.
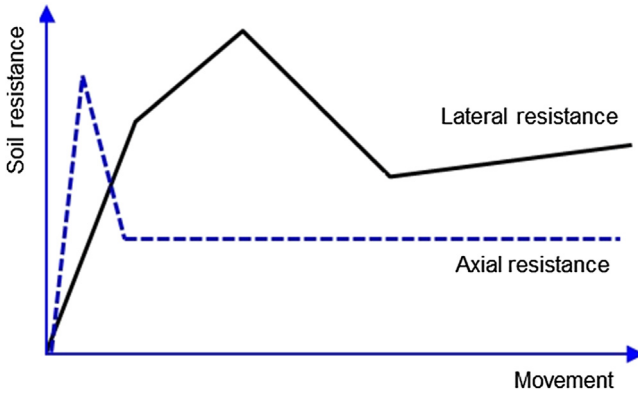
Figure 6.3 Axial-lateral soil resistance of a pipeline. (For color version of this figure, the reader is referred to the online version of this book.)

2. Pipe Penetration in Cohesive Soil

Introduction

Pipe penetration in a seabed is affected by the following fundamental issues:

- Geotechnical embedment, which is related to the ultimate bearing capacity of soil.
- Contribution due to SCR or pipeline laying operations in which dynamics and added load effects are considered.
- A potential effect due to scouring from the actions of waves and current or the soil lique-faction phenomena.

Initial Penetration

The assessment of the initial penetration of the pipeline into a seabed is an important step for other subsequent evaluations in subsea engineering; it affects the pipe-soil interaction in the lateral and axial directions. The initial penetration determines both the pipe-soil contact area and the interface shear strength for soil breakout. Figure 6.4 illustrates the definitions of parameters used in the model of pipe penetration. Pipe embedment is defined as the depth of penetration of the invert (the bottom of pipe) relative to the undisturbed seabed, denoted by symbol z.

The heave of soil during penetration increases the "local" embedment of the pipe, by raising the soil surface against the shoulders of the pipe. The pipe-soil contact arc length is the relevant parameter for pipe-soil interaction, which is related to the local embedment. The height of a typical heave created during monotonic vertical embedment is about 50% of the nominal embedment.

The mechanism of the initial settlement is that the pipeline sinks until the ultimate soil bearing capacity is adequately increased to support the pipeline loads. The pipeline initially imposes a line load once contacting with the seabed due to its circular cross section, and the effective bearing pressure is infinite at this first pipe-soil
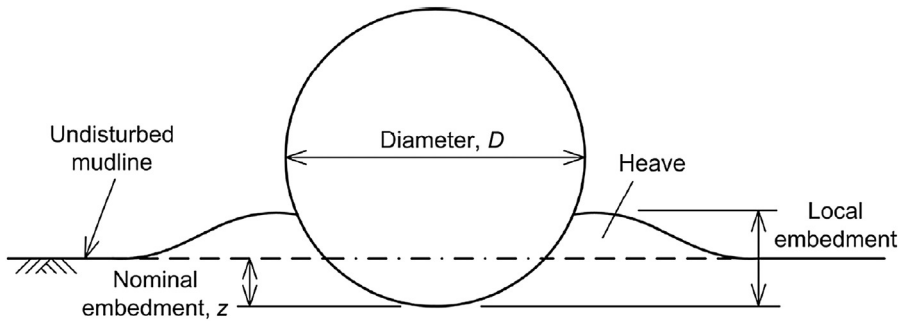
Figure 6.4 Pipe penetration in soil.
Source: Burton et al. [4].

contact. With the sinking of the pipeline, the bearing area gradually increases and the effective bearing pressure decreases until a settlement of half the pipe diameter is reached.

The approaches for calculating initial penetration define the pipe penetration as a function of the static ground pressure from pipeline based on different methods. These approaches are an approximation because cyclic soil effects are ignored. The approaches often used within the industry are addressed in the following sections.

Classical Bearing Capacity Method

Geotechnical embedment can be assessed using standard soil mechanics formulas. These formulas calculate the soil bearing capacity, which is compared with pressure due to pipe loads. The case of a pipeline resting on the seabed can be treated as a surficial strip footing referring to the Brinch Hansen formula [5]:

$$F_u = \alpha \cdot N_C + \gamma \cdot z \cdot N_q + \frac{1}{2} \cdot \gamma \cdot B \cdot N_\gamma \qquad [6.2]$$

where

F_u = ultimate bearing capacity, expressed as a stress
γ = soil submerged unit weight or submerged density
α = soil cohesion, undrained shear strength, S_u, for clay
z = pipe embedment depth
D = pipe outside diameter including coating
B = bearing width of pipe calculated as follows:
$B = 2 \cdot \sqrt{z \cdot (D - z)}$ for $z < D/2$
$B = D$ for $z > D/2$
N_C, N_q, N_γ = dimensionless bearing capacity factors, which are functions of the angle of friction, ϕ, as shown in Figure 6.5.

For saturated clay, it is generally accepted that undrained conditions (soil friction angle, $\phi = 0$) govern the soil condition, and the soil cohesion is equal to the undrained
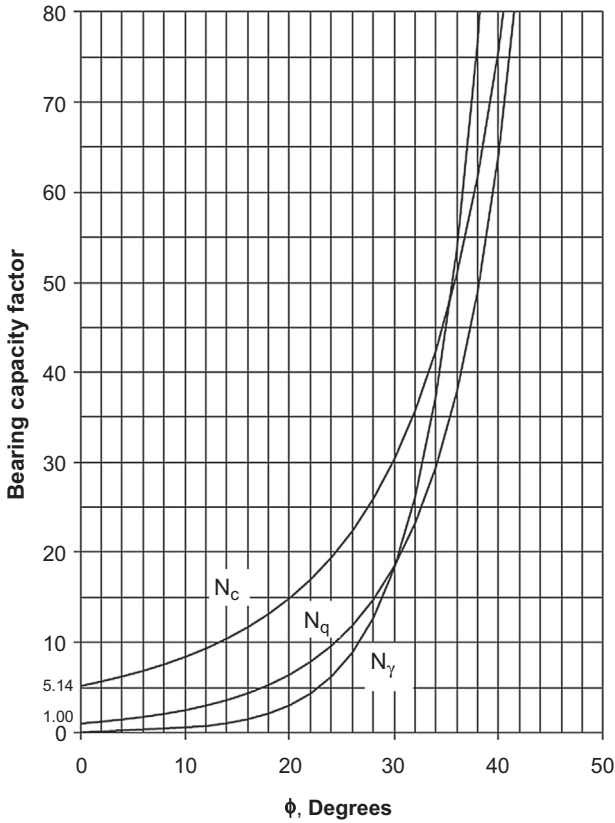
Figure 6.5 Bearing capacity factors, N_q, N_C, and N_γ.
Source: ALA-ASCE [6].

shear strength of the soil. Based on the preceding assumptions, the bearing capacity factors become $N_q = 1$ and $N_\gamma = 0$, Eq. [6.2] then reduces to

$$F_u = S_u N_C + \gamma z \tag{6.3}$$

This equation corresponds to the equations in the section on penetration and soil stiffness, as reviewed by DNV RP-F105 [7].

For very soft clays ($S_u < 10$ kPa), Terzaghi and Peck recommend the following reduced bearing capacity factor [2]:

$$N_C = \frac{2}{3}(\pi + 2) \approx 3.43 \tag{6.4}$$

Langford et al. suggest the several expressions of bearing capacity for the assessment of pipeline settlement in clays [8]. For the pipe embedment of $z < D/2$, the

contribution of pipe embedment to bearing capacity can be neglected, it leads to an upper bound of settlement,

$$F_u = S_u N_C \qquad\qquad [6.5]$$

and for the pipe embedment of $z > D/2$, the embedment contribution is taken into account,

$$F_u = S_u N_C + \gamma\left(z - \frac{D}{2}\right) \qquad\qquad [6.6]$$

with N_C is expressed as

$$N_C = 3.0 + \frac{z - \frac{D}{2}}{D} \qquad\qquad [6.7]$$

To account for the laying induced effects, the settlement calculations derived from this equations is recommended to be multiplied by a factor of 2.

Verley and Lund Method

Verley and Lund [9] fitted data from a variety of industry studies, expressing the normalized static pipeline penetration, z/D, in terms of two dimensionless groups. The equation estimates the embedment due to the pipe self weight as a function of vertical load, pipe diameter, undrained shear strength, and soil density:

$$\frac{z}{D} = 0.0071 \cdot \left(S \cdot G^{0.3}\right)^{3.2} + 0.062 \cdot \left(S \cdot G^{0.3}\right)^{0.7} \qquad\qquad [6.8]$$

where

   z = seabed penetration or embedment, m
   S = dimensionless group, $F_c/(D \cdot S_u)$
   G = dimensionless group, $S_u/(D \cdot \gamma')$
   F_c = vertical contact force per unit length, unit pipe submerged weight, kN/m
   D = pipeline external diameter, m
   S_u = undrained shear strength of soil at the depth of pipeline embedment, kPa
   γ' = submerged soil density, kN/m^3

Equation [6.8] is valid in the parameter ranges shown in Table 6.7.
   The Verley and Lund formula is based on a curve fitting to data with $S \cdot D^{0.3} < 2.5$. For larger values, the method overestimates the penetration. An alternative formula (linear), being valid for all values of $S \cdot D^{0.3}$, is given by

$$\frac{z}{D} = 0.09 \cdot \left(S \cdot G^{0.3}\right) \qquad\qquad [6.9]$$

Buoyancy Method

This method is intended for use with pipelines resting on very soft clays only [10]. The buoyancy method assumes that the soil has no strength and behaves like a heavy

Table 6.7 Parameter Ranges for Equation [6.8]

Parameters	Symbol	Value
Undrained shear strength	S_u	0.8–70 kPa
Pipe outside diameter	D	0.2–1.0 m
Pipe specific gravity	SG	1.06–2.5
Normalized pipe penetration	z/D	0.0–0.35
Soil resistance parameter	G	0.02–5.0

liquid. The penetration z is estimated by demanding that the soil-induced buoyancy of the pipeline is equal to the vertical contact force:

$$B = 2 \cdot \sqrt{D \cdot z - z^2}$$

$$A_s = (z/6B) \cdot \left(3 \cdot z^2 + 4 \cdot B^2\right) \qquad [6.10]$$

$$O = A_s \cdot L \cdot \gamma'$$

where B is the width of pipeline in contact with soil, A_s is the penetrated cross-sectional area of pipe, and O is the buoyancy.

Murff et al. Method (1989) [11]

$$\frac{F_z}{R \cdot S_u} = 4 \cdot (1 + \Theta) \cdot \cos(\Theta) + 4 \cdot \left(\frac{z}{R}\right) \qquad [6.11]$$

where

F_z = applied vertical contact force per unit length;
R = pipe radius;
S_u = soil undrained shear strength;
$\Theta = \sin^{-1}(1 - z/R)$
z = pipe penetration

Bruton et al. (2006)

The Bruton et al. method [12], developed in the SAFEBUCK JIP and based on both historical and recent model test data, determines the penetration from the load:

$$\frac{z}{D} = \frac{S_t}{45} \left(\frac{F_z}{D \cdot S_u}\right)^2 \qquad [6.12]$$

where

    F_z = applied vertical force (or effective submerged weight) per unit length
    D = pipeline total outside diameter, including coatings
    S_u = soil undrained shear strength at pipe invert
    S_t = soil sensitivity
    z = pipe penetration

Figure 6.6 presents a comparison of the Verley and Lund method, the Murff et al. method, and the Bruton et al. method for a soft clay seabed. The model test data given in Murff et al. [11] are also included for a reference. The input parameters used in each method are also given in the figure. It can be seen that the values used for the Murff et al. [11] and Verley and Lund [9] methods produce curves that correspond to those given by Cathie et al. [13]. The resulting curve using the Bruton et al. model lies within a similar range.

Lay Effects

It is well understood that the static submerged pipe weight during pipe laying is not a suitable parameter for penetration calculations. Observations have shown that the as-laid pipeline embedment is typically much higher than what would be expected by the equations based on bearing capacity theory from the static weight. The higher pipe penetration into the soil is due to the load condition during pipe laying because of pipe contact force and pipe movements.
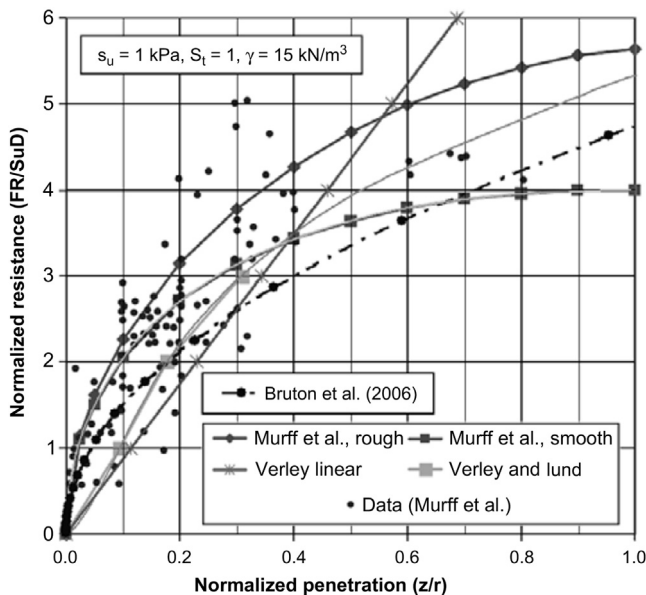
Figure 6.6 Comparison of penetration models.
Source: Langford et al. [8].

Mechanisms of Pipeline Embedment

The additional embedment of pipeline during pipe laying comes from two factors: stress concentration at the touchdown point and cyclic embedment due to dynamic effects. During pipe laying, whether by J-lay, reel-lay, or S-lay, the contact stresses between the pipe and the soil in the vicinity of the touchdown point usually exceeds the static submerged weight of the pipe. The degree of "overstress" of the contact is affected by the water depth, the stiffness of the soil, the bending rigidity of the pipeline, and the effective tension in the pipeline in the touchdown zone. The second reason for the additional pipe embedment is the dynamic movement of pipe within the touchdown zone, driven by the vessel motion and hydrodynamic loading of the hanging pipe. These loads induce a combination of vertical and horizontal motions of the pipeline at the seabed. Any cyclic movement of the pipeline during pipe laying leads to local softening of the seabed sediments. In addition, any lateral motion pushes soil away to either side of the pipe, creating a narrow trench in which the pipe becomes embedded.

Analysis and Simulation

Examples of actual pipe-lay penetration have been sporadically reported, for instance, in Lund's paper [14]. It is common to assess the separate effects of the touchdown stress concentration and the dynamic touchdown motion by applying multiplicative adjustments to the static embedment approach as follows:

- The as-laid pipe weight, p, as shown in Figure 6.7, is multiplied by a concentration factor due to the catenary shape, f_{lay}, to yield the maximum anticipated vertical force between the pipe and the soil, $F_{lay,p}$. The load concentration factor, f_{lay}, is typically around 2 to 3 for soft clay.
- The maximum touchdown load, $F_{lay,p}$, is used to assess the pipe embedment, z_{static}, based on the anticipated maximum static touchdown load.
- Dynamic lay effects are then accounted for by multiplying z_{static} by a dynamic touchdown factor, f_{dyn}, to finally reach the predicted as-laid embedment [12].

This approach is common practice but necessarily empirical, because typical values of f_{dyn} lie in the range 2–10, based on the comparisons between as-laid surveys and static embedment calculations, for pipes laid in relatively shallow water (<500 m depth) [14]. The additional lay-induced embedment in exceedance of z_{static} depends on the details of the lay process and the response of the seabed to the imposed cyclic loading.

Nondimensional Solutions for Load Concentration in Static Conditions [15]

Figure 6.7 shows a schematic of the pipeline configuration during pipeline laying. The standard catenary solution relates these geometry parameters to the tension, T_0, by

$$\frac{T_0}{z_w p} = \frac{\cos(\phi)}{1 - \cos(\phi)} \qquad\qquad [6.13]$$

(a) Complete pipeline

(b) Expanded view of touchdown region
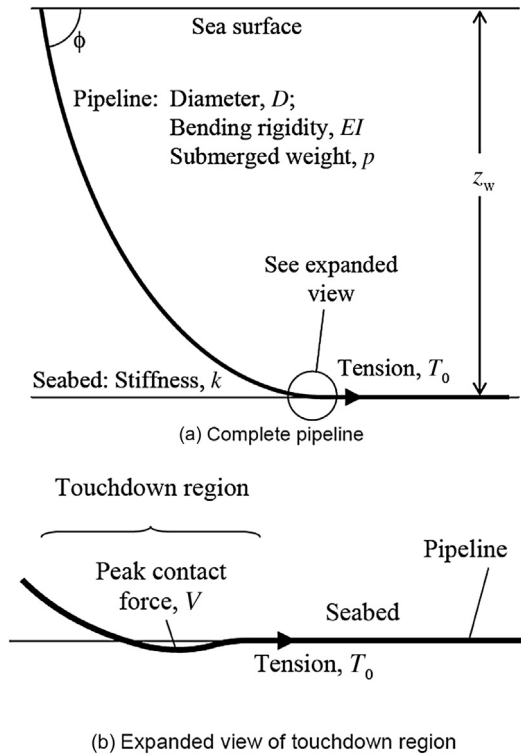
Figure 6.7 Static pipeline configuration during laying.
Source: Randolph and White [15].

After the touchdown boundary condition is included, a dimensionless tension is expressed in terms of the water depth and lay angle as

$$\frac{T_0}{\lambda p} = \left(\frac{\cos(\phi)}{1 - \cos(\phi)} z_w \right)^{3/2} \left(\frac{p}{EI} \right)^{1/2} \tag{6.14}$$

where λ is a characteristic length, expressed as

$$\lambda = \sqrt{\frac{EI}{T_0}} \tag{6.15}$$

For typical pipelines, with diameters from 0.2–0.7 m, values of $T_0/(\lambda p)$ rarely fall below 3 except in shallow water less than 500 m or very steep angles, such as greater than 85°.

The normalized maximum contact force expressed as a function of dimensionless stiffness is

$$\frac{V_{max}}{p} = 0.6 + 0.4 \cdot \left(\frac{\lambda^2 k}{T_0} \right)^{0.25} \tag{6.16}$$
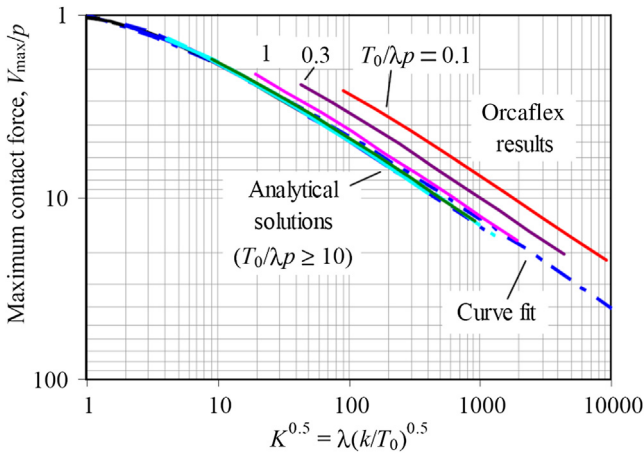
Figure 6.8 Maximum contact force in touchdown zone.
Source: Randolph and White [15]. (For color version of this figure, the reader is referred to the online version of this book.)

The analytical solution, Eq. [6.16], is plotted in Figure 6.8, which presents the relationship between the maximum normalized contact force, V_{max}/p with the dimensionless stiffness. The OrcaFlex solutions are plotted for reference.

Figure 6.9 shows the contact force distributions along seabed in touchdown region for the following condition:

• Water depths: 500–2000 m.
• Submerged pipe weights: 1.0–1.5 kN/m.
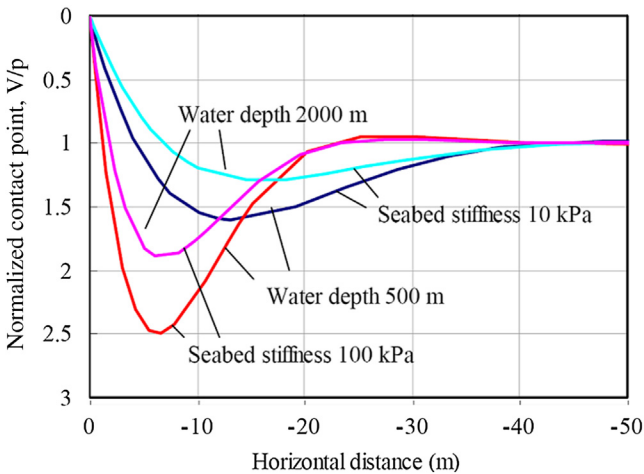
Figure 6.9 Contact force distributions along seabed in touchdown region.
Source: Randolph and White [15]. (For color version of this figure, the reader is referred to the online version of this book.)

- Lay angle: 83°.
- $T_0/\lambda p = 3\text{--}20$.
- Normalized stiffness: 6–450.

3. Pipe Penetration in Noncohesive Soils

Initial Penetration

Verley and Sotberg Method [16]

In noncohesive soils or sands, the initial embedment depth is defined as a function of contact force, pipe outside diameter, and submerged unit weight of the soil. The dimensionless initial embedment is determined by the following equation:

$$\frac{z_{init}}{D} = 0.037 \cdot K_e^{-0.67} \tag{6.17}$$

where

K_e = applied vertical force, $K_e = \gamma' D^2 / W'$
D = pipeline total outside diameter, including coatings
γ' = submerged soil density; for sand normally in range of 7,000 N/m^3 (very loose) to 13,500 N/m^3 (very dense)
W' = submerged pipe weight per unit length
z_{init} = pipe initial penetration (embedment)

Classical Bearing Capacity Method [6]

The bearing capacity procedures can be used to assess the preliminary settlement of pipeline in sands. Settlement of pipelines in sands are usually very low. For sands, the cohesion α is usually zero. Therefore, Equation [6.2] for the maximum bearing capacity reduces to

$$F_u = \gamma z N_q + \frac{1}{2} \gamma B N_\gamma \tag{6.18}$$

The dimensionless bearing capacity factors N_q and N_γ are given as a function of the angle of friction, ϕ, and shown in Figure 6.5.

Vertical Stability in Liquefied Soil

Subsea pipelines in shallow waters are often buried to protect them against damage by fishing equipment or drag anchors and to improve their on-bottom stability under different ocean conditions. In the design of buried pipelines, the assessment of pipeline flotation and sink potential due to the soil liquefaction under the design conditions of ocean or seismic events should be included, since these issues may

govern the pipe specific gravity, the burial depth, and the selection of engineered backfilling materials.

Soil liquefaction is the loss of strength of a soil from excess pore pressure caused by rapid and normally cyclic loading. Both cohesionless soils and cohesive soils may lose shear resistance during the repeated cyclic loadings. Cohesive soils may undergo remolding and become softer. The reasons for soil liquefaction include

- Wave action on the seabed in a shore approach section.
- Pressure waves in a seismic activity;.
- Rapid impulse loading in installation activities, such as trenching and plowing.
- Oscillatory motion of a pipeline.
- Gas venting from seabed of underlying strata.

The potential wave-induced liquefaction is of greatest concern in the design of shore approaches, where the shear stresses in the soil from wave passage are highest and it is difficult to rebury or protect the pipeline from mechanical damage due to continued exposure. The liquefaction due to seismic activity is different from the wave-induced liquefaction. The earthquake cycles and durations are much shorter than the ocean wave periods, but its load is more rapid and intense. In addition, earthquake loading may cause subsea slopes to fail, displacing buried pipelines.

Soil liquefaction is hazardous to pipeline instability. If a pipeline is buried and has a specific gravity lower than that of the liquefied soil, it will tend to rise to the surface, where it is subjected to wave-induced forces and possible mechanical damage. If the pipeline is denser than the liquefied soil, it will tend to sink, which may overstress the pipeline. Pipelines operating at high temperatures and pressures may bow when pipeline imperfections are formed and the restraint by the soil is reduced, which may result in upheaval buckling.

The pipe buoyancy increased at the embedment depth is highly dependent on the soil shear strength. As the pipe sinks into the soft clay, up to depths of about its diameter, the pipe specific gravity, with respect to the surrounding medium, decreases and the pipe becomes lighter. To prevent the movement of a pipeline in liquefied soil, the pipeline should be neither heavy enough to sink nor light enough to float. The pipelines to be buried should be checked for possible sinking or floatation. Sinking should be considered with maximum content density, such as water filled, and floatation should be considered with minimum content density, such as air filled.

A general global force balance equation for a buried pipeline flotation can be defined as

$$B = W' + R$$

where

$B =$ uplift force acting on the pipeline due to the accumulated excess pore pressures in the soil
$W' =$ submerged weight of pipeline
$R =$ soil resistance

Many researchers studied the flotation potential of a buried pipeline in soil, [17], [18], and [19]. The following relationships give an idealized range of pipe-specific gravity for a simplification:

$$SG_{\text{pipe,max}} = SG_{\text{soil}} + 0.24\frac{S_{\text{ur}}}{D} \qquad\qquad [6.19]$$

$$SG_{\text{pipe,min}} = SG_{\text{soil}} - 0.24\frac{S_{\text{ur}}}{D} \qquad\qquad [6.20]$$

Where:

$SG_{\text{pipe,max}}$ = the largest specific gravity of pipe that will not sink
$SG_{\text{pipe,min}}$ = the largest specific gravity of pipe that will not float
SG_{soil} = bulk specific gravity of the liquefied soil
S_{ur} = remolded shear strength of the soil
D = overall pipe diameter

If the actual specific gravity of pipe is within the range given by these equations, the pipe will remain stable in liquefied soil. The equations are good for preliminary engineering design.

4.   Axial Load–Displacement Response of Pipelines

Pipeline walking and lateral buckling of unburied pipelines in the design of deepwater developments have become increasingly important issues. The axial load due to cyclic thermal load combined with seabed gradient and SCR axial tension plays a critical role in the potential development of pipeline walking and lateral buckles. The soil lateral resistance to the pipeline determines the lateral buckling amplitude, where the pipe may move from its as-installed position and displace several diameters before coming to rest. Both peak and residual resistance in the axial and lateral directions are important for the design. A range of lower and upper bound values are required for the pipeline walking and lateral buckling analysis, due to the uncertainty of soil properties. The axial load–displacement response of pipelines is typically evaluated according to either "drained" or "undrained" models, depending on the soil type and loading conditions. Both models onsider the peak and residual resistances, respectively.

Figure 6.10 illustrates the variations of axial friction resistances with pipeline axial displacement in different conditions. The "brittle" axial resistance response, which is normally observed in the undrained soil condition, is usually defined by "breakout" and "residual" axial friction. Breakout axial resistance describes the mobilization of the maximum friction at quite small displacements with a linear relationship. A significant peak breakout resistance can occur when the pipe moves axially for the first time or after some time at rest, at a rate fast enough to generate excess pore pressure to keep soil with the undrained behavior. However, normally, during subsequent loading with limited setup time, the peak is not observed, leading to a
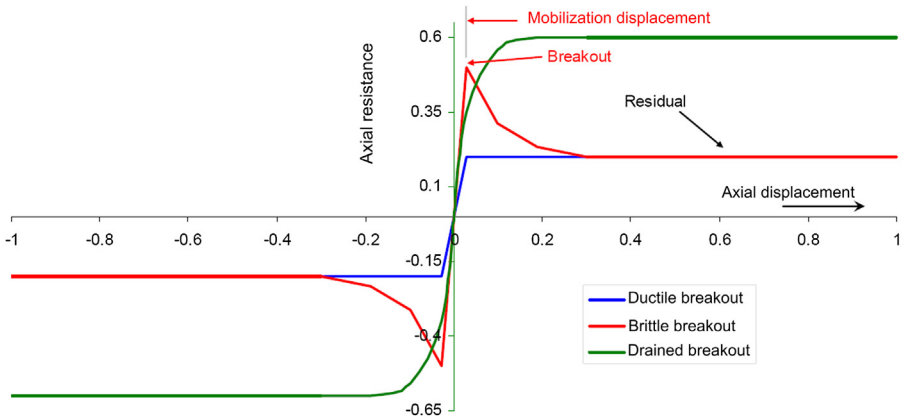
Figure 6.10 Axial friction resistance with pipeline axial displacement.
Source: Bruton et al. [4]. (For color version of this figure, the reader is referred to the online version of this book.)

ductile breakout response as shown in the figure. Once the pipe has started to move, the friction response remains the same as the residual friction resistance to larger displacements. The residual axial friction dominates the pipe-end expansion-contraction response and axial feed-in/feed-out to each lateral buckle. If the pipe displacement occurs very slowly, such that no excess pore pressure is generated, the axial soil response is "drained behavior," with a gradual increase to a significantly higher level of residual friction, as shown by the force displacement curve in dark gray in the figure. Normally, the axial friction coefficient of soil in the drained behavior is 0.6 according DNV guideline [20].

Cohesive Soil

An alpha method is based on the undrained model, assuming that a shear stress of αS_u acts on the pipe-soil contact surface, where S_u is the soil undrained shear strength; and α is the overall friction coefficient, assumed to be 1.0 for the peak friction at breakout. Once the pipe embedment has been determined, the axial soil resistance force per unit length of pipeline may be defined using the following equation:

$$F_{axial} = \alpha S_u A \qquad\qquad\qquad [6.21]$$

where

F_{axial} = axial resistance force
A = pipe-soil contact area per unit length around the perimeter of the pipeline, which is expressed as $2R \times \arccos[1 - (z/R)]$, with R being the pipe radius; that is, $R = D/2$.
α = also called the *adhesion factor*, reflects any changes in S_u and pipe-soil shearing due to the laying and the roughness of pipe surface. The experimental results [21] show that most of the peak axial resistance values following a pause period correspond to a shear stress close to the remolded shear strength. Therefore, the residual axial resistance initially

corresponds to $\alpha \sim 0.5$. Many authors [13] provide recommendations for values of α. For a simplification, it may be defined as [6]

$$\alpha = 0.608 - 0.123 S_u - \frac{0.274}{S_u^2 + 1} + \frac{0.695}{S_u^3 + 1} \qquad [6.22]$$

where S_u is in ksf.

It can be seen that these equations appear relatively simple, but the undrained model is difficult to be determined accurately, since it depends mainly on an evaluation of the interface shear strength and contact area, and the coating also plays a role [4]. The shear strength is controlled by the following several factors:

1. The shear strength at the contact surface.
2. The variation in shear strength with depth.
3. Remolding due to installation.
4. Consolidation and thixotropy effects.
- The contact area is affected by the displacement of the pipeline and the penetration history, which may include the development of a heave resulting in the soil berm. According to Cathie et al. [13], the heave may lead to a 35% increase in contact area at a depth of around $z/D = 0.25$.

Noncohesive Soil

The axial resistance for noncohesive soil can be defined using a "beta" frictional model. The 'beta" model relates the horizontal axial resistance to the applied vertical force using an overall friction factor:

$$F_{axial} = \mu \cdot W' \qquad [6.23]$$

where

F_{axial} = axial resistance force
μ = overall friction coefficient
W' = acting vertical force (pipeline submerged weight)

The value of overall friction coefficient, μ, may be calculated according to the following relationship:

$$\mu = f_r \mu_a \qquad [6.24]$$

where

f_r = wedging factor:

$$f_r = \frac{2 \sin \theta}{\theta + \sin \theta \cos \theta}$$

$\theta = \cos^{-1}(1 - 2z/D)$;
μ_a = axial friction coefficient; $\mu_a = \tan\phi$, and ϕ is the pipe-soil interface angle of friction (soil friction angle)

Equation [6.24] is also used for the drained response of soft deepwater clays. Drained friction coefficients as high as 0.75 (corresponding to a friction angle of 37°) have been measured for soft deepwater clays at low stress levels [4]. The pipe-clay interaction generally provides an undrained response for a quick moving pipe, while it shows a drained response for a slow moving pipe. The undrained and drained responses provide very different values of axial resistance. However, the transition from undrained to drained conditions is not well understood yet.

5. Lateral Load–Displacement Response of Pipelines

Pipeline on-bottom stability design is conventionally based on the static balance between hydrodynamic forces and the soil lateral resistance forces. In this approach, the soil lateral resistance is usually estimated with a Coulomb friction model by multiplying the acting vertical force (the submerged weight of the pipeline), with the soil coefficient of friction. However, the measured soil lateral resistance indicates that the soil resistance values are much higher than the analytical values obtained based on the soil friction factors alone. This discrepancy indicates that other parameters are involved in the soil resistance against the pipe's lateral movements. Especially, the initial pipe embedment due to the pipe submerged weight and induced dynamic pipeline laying force, together with the further pipe settlement due to the clay consolidation and pipe oscillatory motions, are shown to have a significant influence on the soil resistance to the pipe's lateral movement.

Traditionally, the evaluation of lateral pipe-soil resistance in clays has used equations including two-components: the first component is similar with the drained model used for the axial pipe-soil interaction, whereas the second component contains a passive soil resistance term in their formulation to account for the additional lateral stability gained by the pipe penetration into the soil, such as resistance of the soil berm. In general, the lateral soil resistance, F_L, is made up of F_F and F_R, in which F_F is a linear function of the pipe submerged weight and the pipe-soil lateral friction factor, and F_R depends on the pipe embedment caused by the pipe load history, as follows:

$$F_L = F_F + F_R \qquad\qquad [6.25]$$

where

F_L = total lateral soil resistance force
F_F = lateral frictional force due to the sliding resistance, given by $\mu_L W'$
μ_L = lateral coefficient of friction, assumed to take a value of 0.2 for clayey soil
F_R = lateral passive soil resistance

Brennodden and Stokkeland [22] and Verley and Lund [9] suggest equations for lateral soil resistance force based on this model, in which the second term, F_R, is evaluated with different equations. These models were developed mainly for the assessment of pipeline stability where lower-bound values are used for a conservative reason. Most recently, as part of SAFEBUCK, Bruton et al [12] provide a refined

version of this model based on the test results. The following sections describe methods applied to the lateral soil resistance assessment.

Cohesive Soil

Classic Geotechnical Theories

For soft cohesive soils with low undrained shear strength, the pipe embedment is relatively larger and therefore contributes highly to the lateral soil resistance. The pipeline laying process can cause remolding of the soft soil, due to the dynamic effects and the pipe movement at the touchdown location. The remolded strength of 50% original soil strength is often used in the analysis for soft clay, and it is utilized to evaluate the lateral soil resistance for the as-laid pipeline condition. The soil sensitivity is defined by the ratio of the shear strength to the remolded shear strength of the soil.

With the calculated pipe settlement relevant to the as-laid condition, the lateral resistance of the pipe per unit length can be expressed as [6]

$$F_{\mathrm{L}} = \begin{cases} N_{\mathrm{CH}} \cdot S_{\mathrm{u,reg}} \cdot D & \text{if} \quad z \geq \mathrm{D} \\ N_{\mathrm{CH}} \cdot S_{\mathrm{u,reg}} \cdot z & \text{if} \quad z < D \end{cases} \qquad [6.26]$$

where

N_{CH} = lateral bearing capacity factor [2]
$S_{\mathrm{u,reg}}$ = undrained shear strength of the remoulded soil

The lateral bearing capacity factor can be determined using Figure 6.11, which illustrates the relationship between N_{CH} and the embedment ratio (z/D).

Verley and Lund Method

Verley and Lund [9] developed a soil resistance model applicable for pipelines laying on clay soils. Data were collected from a number of large- and small-scale laboratory tests as well as some numerical analyses. Following the Verley and Lund model, the sliding force is obtained by considering the lateral coefficient of friction of 0.2 in clayey soil. For all clay, the maximum value of the lateral soil resistance for a given pipe penetration can be expressed as

$$F_{\mathrm{R}} = 4.13 D S_{\mathrm{u}} G^{-0.392} \left(\frac{z}{D}\right)^{1.31} \qquad [6.27]$$

where the dimensionless group

$$G = \frac{S_{\mathrm{u}}}{D \cdot \gamma_{\mathrm{s}}}$$
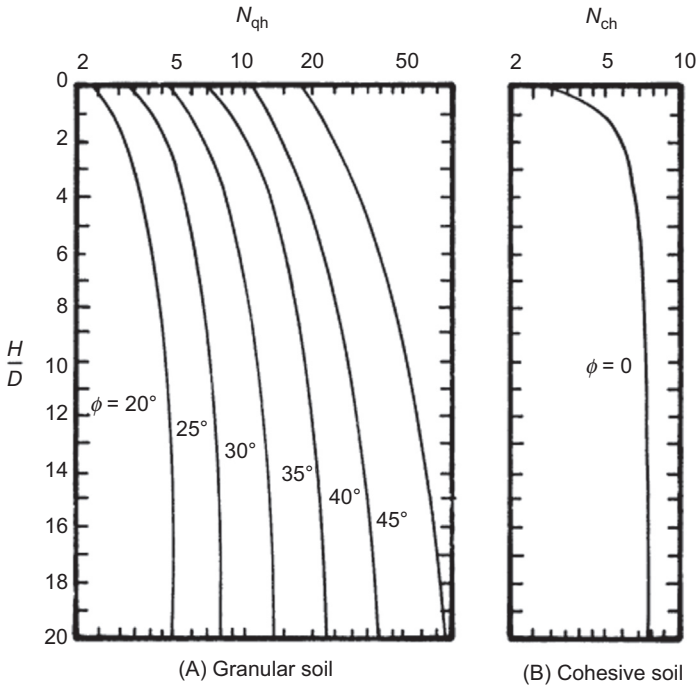
Figure 6.11 Hansen bearing capacity factors for various soil, N_{QH} and N_{CH}.

This soil resistance model was developed based on a given penetration, which should be calculated from Eq. [6.8] and its parameter ranges.

Time-Dependent Resistance Method

Brennoddenn and Stokkeland [22] performed some full-scale model tests for the Troll Phase 1 development. The results of these model tests revealed a significant increase in peak soil resistance, both axially and laterally, with increasing time of soil consolidation. The following methodology was proposed for calculating the soil maximum lateral resistance:

$$F_{1,\max} = k_{\max} \cdot \left(\mu \cdot q_s + \beta_{\max} \cdot S_u \cdot \frac{A_c}{D} \right) \qquad [6.28]$$

$$F_{1,\text{residual}} = k_{\text{residual}} \cdot q_s \cdot (\mu + \beta_{\text{residual}} \cdot \lambda) \qquad [6.29]$$

where

μ = coefficient of friction (= 0.2 for soft clay)
$k_{\max}/k_{\text{residual}}$ = empirical nondimensional coefficients depending on breakout velocity and pipe diameter; for the Troll condition, the coefficients are 0.8 and 0.6, respectively

$\beta_{max}/\beta_{residual}$ = empirical nondimensional coefficients depending on undrained shear strength; for the Troll condition, the coefficients are 1.47 and 1.09, respectively
λ = nondimensional weight parameter = $\rho_w \cdot D^2/q_s$
ρ_w = seawater density
q_s = unit submerged weight of the pipe
A_c = pipe-soil contact area, $2R \cdot a \cos(1 - z/R)$

These equations can also be simplified as follows.
Axial soil resistance (kN/m),

$$F_{a,max} = 1.05 \cdot A_c \cdot S_u \tag{6.30}$$

Lateral soil resistance (kN/m),

$$F_{l,max} = 0.8 \cdot (0.2 \cdot F_c + 1.47 \cdot S_u \cdot A_c/D) \tag{6.31}$$

where

F_c = vertical contact force, kN/m
$A_c = 2R \cdot a \cos(1 - z/R)$, m^2
z = seabed penetration, m
S_u = undrained shear strength, kPa

Bruton et al. Method

Bruton et al. [12] provide an equation that is essentially the same relationship of two components presented in Eq. [6.12], but the terms have been developed and adapted empirically. The updated model relates horizontal and vertical forces normalized against $S_u \cdot D$. The peak breakout resistance is calculated according to

$$h_{brk} = 0.2\nu + \frac{3}{\sqrt{\frac{S_u}{\gamma' D}}} \frac{z_{start}}{D} \tag{6.32}$$

where

h_{brk} = normalized peak breakout resistance, = $H_{brk}/(S_u \cdot D)$
H_{brk} = peak breakout force, kN/m
S_u = undrained shear strength at the pipe inversion, kN/m^2
D = pipe diameter, m
ν = normalized effective vertical load, = $F_z/(S_u \cdot D)$
F_z = vertical load, kN/m
γ' = effective soil unit weight, kN/m^3
z_{start} = pipe penetration into soil at startup

The residual resistance may be calculated using

$$\frac{h_{res}}{\nu_{res}} = 1.0 - 0.65 \cdot \left[1 - \exp\left(-0.5 \cdot \frac{S_{u,1D}}{\gamma' \cdot D} \right) \right] \tag{6.33}$$

where

h_{res} = normalised residual breakout resistance, = $H_{res}/(S_u \cdot D)$
H_{res} = residual breakout force
$S_{u,1D}$ = undrained shear strength at one diameter depth
D = pipe diameter
v_{res} = residual normalized effective vertical load, = $F_{z,res}/(S_u \cdot D)$
F_z = vertical load
γ' = effective soil unit weight

Equations [6.32] and [6.33] are simple derivations of the peak and residual lateral resistances. However, the suction on the rear side of the pipe can govern the peak resistance, although the corresponding relationship is not presented in Bruton et al. [12]. In addition, it is necessary to predict the displacements required to mobilize these respective resistances.

Noncohesive Soil

Lateral soil resistance for noncohesive soil in general consists of two parts: a pure Coulomb friction part, F_F, and a passive resistance, F_R, due to the buildup of soil penetration as the pipe moves laterally. The pure Coulomb friction part is also called *sliding resistance*, which is given by $\mu_L W'$. A typical model for passive soil resistance consists of four distinct regions [20]:

1. An elastic region where the lateral displacement is less than typically 2% of the pipe diameter.
2. A region where significant displacement may be experienced, up to half the pipe diameter for sand and clay soils in which the pipe-soil interaction causes an increase in the penetration and thus in the passive soil resistance.
3. After breakout, where the resistance and penetration decrease.
4. When the displacement exceeds typically one pipe diameter, the passive resistance and penetration may be assumed constant.

Figure 6.12 shows the passive resistances in the four regions. In the elastic region, $Y \le Y_1$, the stiffness k can be taken as 50–100 N/m for sand. The stiffness increases
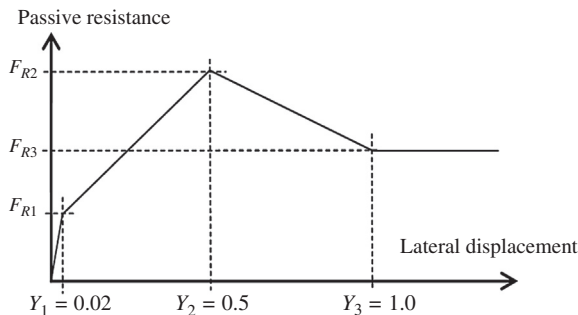
Figure 6.12 Passive resistance of pipeline on soil.
Source: DNV-RP-F109 [20].

with sand density. No work is done, and penetration is constant and equal to the initial penetration. In the second region, $Y_1 < Y \leq Y_2$, the penetration increases and therefore the passive resistance increases. If the displacement exceeds Y_2, the pipe is assumed to break out. The value of the breakout resistance, F_{R2}, cannot be computed a priori, as it depends on the accumulated pipe displacement in the region between Y_1 and Y_2. Penetration is reduced linearly from the breakout value at Y_2 to half this value at $Y = Y_3$, and passive resistance is reduced accordingly. For the fourth region, the lateral displacement is larger than Y_3, penetration and passive resistance can be assumed to be constant.

Passive resistance F_R on sand can be expressed as following equations:

$$\frac{F_R}{F_C} = \begin{cases} \left(5.0 \cdot k_s - 0.15 \cdot k_s^2\right) \cdot \left(\dfrac{z_p}{D}\right)^{1.25} & \text{if} \quad k_s \leq 26.7 \\[4mm] k_s \cdot \left(\dfrac{z_p}{D}\right)^{1.25} & \text{if} \quad k_s > 26.7 \end{cases} \qquad [6.34]$$

where

$k_s = \gamma' D^2 / (W' - F_z)$
F_c = vertical contact force between pipe and soil, $F_c = W' - F_z$
F_z = vertical hydrodynamic lift load, which may be ignored in global buckling analysis

"Light" and "Heavy" Pipes of Lateral Buckles

Pipelines in lateral buckles can be classified as "light," "neutral," and "heavy" pipes, based on the lateral response, as shown in Figure 6.13. After soil breakout, three types of large-amplitude lateral response are observed in the development of soil berms ahead of the laterally sweeping pipe; the figure schematically illustrates the lateral responses depending on the ratio of the pipeline weight to the seabed strength,
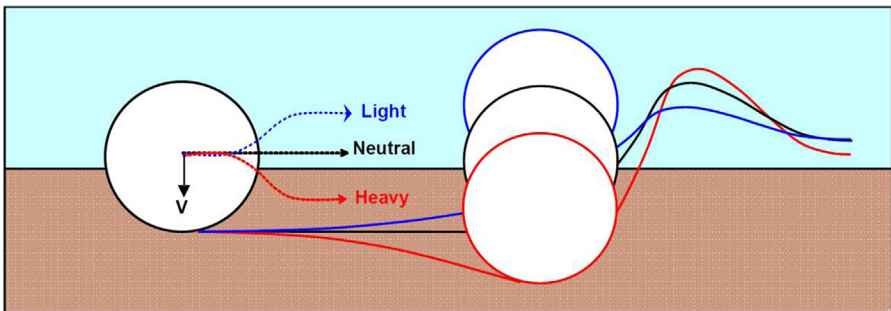
Figure 6.13 Pipeline lateral response.
Source: Hill and Jacob [23]. (For color version of this figure, the reader is referred to the online version of this book.)

$V/(S_u D)$, where V is the applied vertical force or effective submerged weight per unit length, which is F_z in Eq. [6.12].

For values of $V/(S_u D) < 1.5$, the pipelines are classified as "light" pipe. The experimental results show that the pipeline rises to the seabed surface after breaking out during the first lateral sweep, as shown in Figure 6.14(a). As the pipe rises and contact is lost with soil behind the pipe, eliminating tensile restraint, the lateral resistance reduces from the breakout value to a steady residual resistance.

For values of $V/S_u D > 2.5$, the pipelines are classified as "heavy" pipes, the pipeline generally moves downward after the initial breakout resistance is mobilized. This downward movement, coupled with the growth of a soil berm ahead of the pipe, leads to a steady increase in the lateral resistance, as shown in Figure 6.14(b).

(a) Light pipes
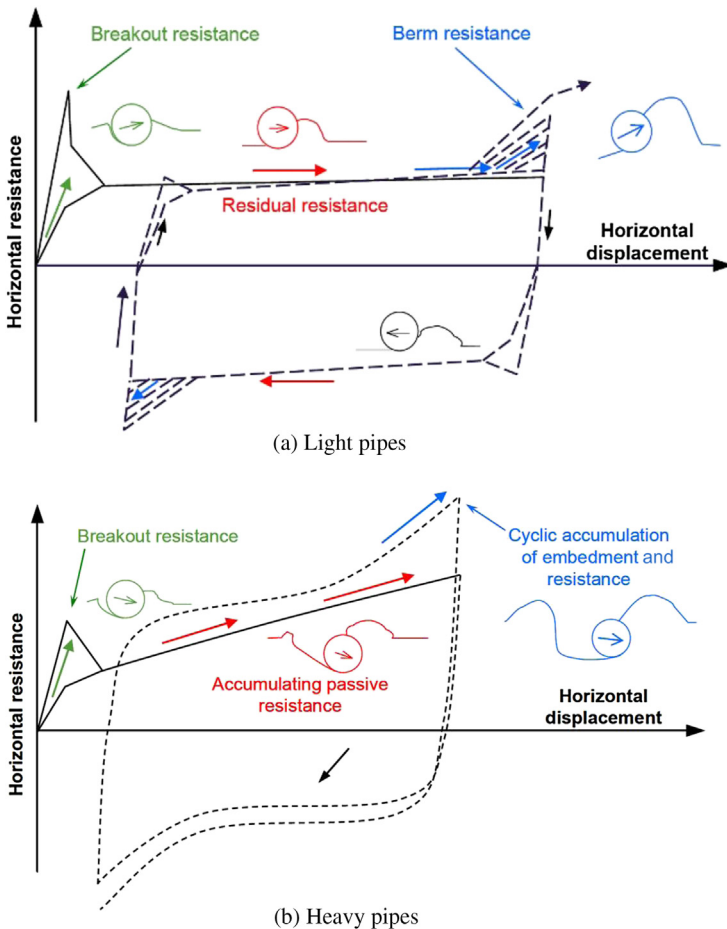
(b) Heavy pipes

Figure 6.14 Lateral pipe-soil responses for "light" and "heavy" pipes.
Source: Bruton et al. [24]. (For color version of this figure, the reader is referred to the online version of this book.)

Soil Berms of Lateral Buckles

The pipe cycles back and forth across the same patch of seabed due to thermal expansion and contraction of pipeline under cyclic thermal loads. Surface soil builds up into berms at the extremes of the pipe displacement range. Figure 6.15 shows the effect of soil berms by an example of numerical analysis for pipeline lateral buckling under cyclic thermal loads. The pipe buckle configuration without soil berm (a) in the model is compared with the case that soil berms are included (b). If soil berms are ignored, the lateral resistance can be assumed to remain constant with continuing lateral displacement. Numerical modeling based on this lateral response shows that buckles grow in amplitude with each cycle. If soil berms are included, the soil berms restrict the growth of the buckle so that cyclic displacements remain almost constant over a number of cycles, as shown in Figure 6.15(b). The berms lock in the stress range at a level close to the first cycle value; in contrast, neglecting the influence of
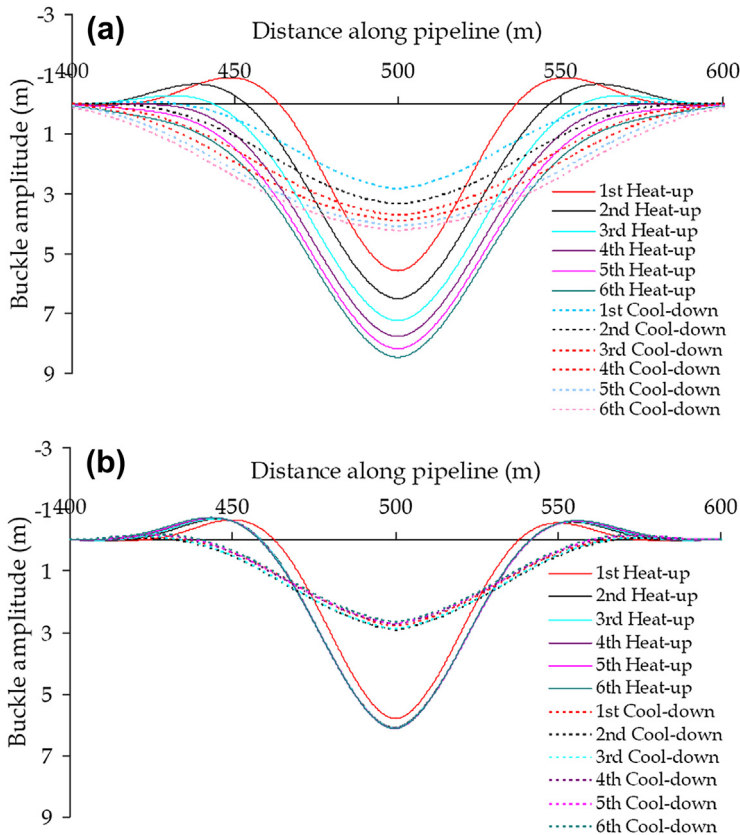
Figure 6.15 Pipe buckle configurations: (a) without berms and (b) with berms.
Source: Bruton et al. [4]. (For color version of this figure, the reader is referred to the online version of this book.)

berms allows the stress range to reduce as a result of growth in the buckle wavelength. A design calculation that neglects berms would underestimate the fatigue damage induced in the pipeline.

References

[1] Thusyanthan NI. Seabed soil classification, soil behaviour and pipeline design. OTC 23297; Offshore Technology Conference, Houston, 2012.

[2] Terzaghi K, Peck RB. Soil mechanics in engineering practice. 2nd ed. New York: John Wiley and Sons; 1967.

[3] BS. Code of practice for pipelines. Part 2. Subsea pipelines. BS PD 8010–2, British Standard Code; 2004.

[4] Bruton DAS, White DJ, Carr MC, Cheuk CY. Pipe-soil interaction during lateral buckling and pipeline walking—The SAFEBUCK JIP. OTC 19589; Offshore Technology Conference, Houston, 2008.

[5] Brown & Root. AGA submarine pipeline on-bottom stability—Analysis and design guidelines. vol. 1. Brown & Root, Houston; 1993.

[6] ALA-ASCE. Guidelines for the design of buried steel pipe; American Lifelines Alliance 2001.

[7] DNV. Free spanning pipelines. DNV-RP-F105; Det Norske Veritas 2006.

[8] Langford T, Dyvik R, Cleave R. Offshore pipeline and riser geotechnical model testing: Practice and interpretation. OMAE2007–29458, San Diego, 2007.

[9] Verley R R, Lund KM. A soil resistance model for pipelines placed on clay soils. In Proceedings of OMAE '95, vol. 5. Pipeline Technology, Copenhagen; 1995.

[10] Bai Y, Bai Q. Subsea pipelines and risers. Oxford, UK: Elsevier Ltd; 2005.

[11] Murff JD, Wagner DA, Randolph MF. Pipe penetration in cohesive soil. Géotechnique 1989;39(2):213–29.

[12] Bruton DAS, White DJ, Cheuk CY, Bolton MD, Carr MC. Pipe-soil interaction behavior during lateral buckling including large amplitude cyclic displacement tests by the SAFEBUCK JIP. OTC17944; Offshore Technology Conference, Houston, 2006.

[13] Cathie DN, Jaeck JC, Wintgens JF. Pipeline geotechnics—State of the art. International Symposium on Frontiers in Offshore Geotechnics, Perth; 2005.

[14] Lund KM. Effect of increase in pipeline penetration from installation. Proc Conf Offshore Mech Arctic Eng. OMAE2000-PIPE5047, New Orleans; 2000.

[15] Randolph MF, White DJ. Pipeline embedment in deep water: Processes and quantitative assessment. OTC 19128; Offshore Technology Conference, Houston, 2008.

[16] Verley R R, Sotberg T. A soil resistance model for pipelines placed on sandy soils. Proceedings of OMAE'92, Calgary; 1992.

[17] Gravesen H, Fredsoe J. Modelling of liquefaction, scour and natural backfilling in relation to marine pipelines, offshore oil and gas pipeline technology. Copenhagen: European Seminar; February 1983.

[18] Bonjean D, Erbrich C, Zhang J. Pipeline flotation in liquefiable soil. OTC 19668; Offshore Technology Conference, Houston, 2008.

[19] Endley SN, Potturi AK, Rao PM. An experimental study of pipeline flotation. OTC 19918; Offshore Technology Conference, Houston, 2009.

[20]   DNV. On-bottom stability design of submarine pipeline. DNV-RP-F109; Det Norske
       Veritas 2007.
[21]   White DJ, Ganesan SA, Bolton MD, et al. SAFEBUCK JIP—Observations of axial
       pipe-soil interaction from testing on soft natural clays. OTC 21249; Offshore Tech-
       nology Conference, Houston, 2011.
[22]   Brennodden H, Stokkeland A. Time-dependent pipe-soil resistance for soft clay. OTC
       6486; Offshore Technology Conference, Houston, 1992.
[23]   Hill AJ, Jacob H. In-situ measurement of pipe-soil interaction in deep water. OTC
       19528; Offshore Technology Conference, Houston, 2008.
[24]   Bruton DAS, White DJ, Langford T, Hill AJ. Techniques for the assessment of pipe-soil
       interaction forces for future deepwater developments. OTC 20096; Offshore Technology
       Conference, Houston, 2009.

7 Hydrodynamics around Pipes

1.   Introduction

General

Subsea environmental conditions play a predominant role in the design of almost all subsea structures, including subsea pipelines and risers. Environmental data relevant to subsea pipelines and risers include (1) wave heights, time periods and directions, as waves generate hydrodynamic forces on subsea structures; (2) wind speeds and direction, which drive sea currents; (3) currents and directions, which also cause hydrodynamic loads on pipelines and risers. These environmental data are used in the following analysis for subsea pipelines and risers:

- Pipeline stability analysis.
- Pipeline free span analysis.
- Pipeline installation analysis.
- Riser analysis and design.
- Seabed soil stability and liquefaction analysis.

Normally, two wave analysis methods are used in the design of subsea pipelines and risers: time domain analysis and frequency domain analysis. The time domain analysis is used most frequently for subsea pipelines and risers design. The wave loads are generated by a representative irregular wave, which can be described by its

wave heights and its associated time periods. The time domain analysis has the advantages of ease of data process and application. The time domain analyses for the installation scenario of subsea pipeline design are based on the significant wave height with an associated range of period in the wave conditions of a 1 year return period, and for the lifetime scenario such as on-bottom stability with the wave conditions of a 100 year return period.

Wave Data Processing

In time domain analysis, the wave data are typically characterized by significant wave height and a mean zero-crossing wave period. The significant wave height is a parameter used particularly throughout coastal engineering, both to define and model sea states.

Significant wave height, H_s, *is* defined as the mean of one third highest waves: If the process is Gaussian and narrow banded, then the significant peak-to-peak wave height can be calculated as four times of the zeroth moment of the process, m_0,

$$H_s = 4.0\sqrt{m_0} \tag{7.1}$$

where, m_0 is the zeroth moment of the wave power spectrum; H_s is one of the most commonly provided measures of wave height in subsea pipeline engineering. It is a fundamental parameter of sea state, which is indicative of the wave energy for a given sea state.

The maximum wave height, H_{max}, the probability of exceedance for a single wave out of a group is given by the Rayleigh density distribution, as shown in Figure 7.1.
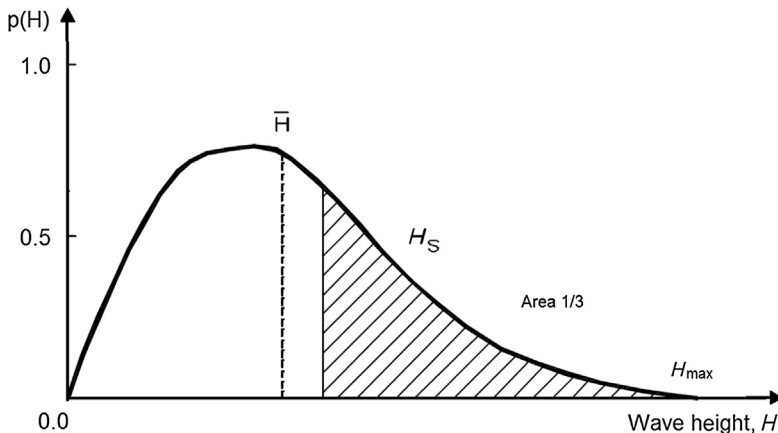
Figure 7.1 Rayleigh density function.
Source: Kellogg Brown & Root [1].

The significant wave height is determined from the statistical data of wave height, which is the mean of the shaded area.

From the Rayleigh distribution, the following wave heights are calculated:

$$H_s \cong 1.6 H_{mean} \qquad\qquad\qquad\qquad\qquad\qquad\qquad\qquad\qquad\qquad [7.2]$$

$$H_{max} \cong 1.86 H_s \cong 3 H_{mean} \qquad\qquad\qquad\qquad\qquad\qquad\qquad\qquad [7.3]$$

where H_{max} is the most probable largest wave height given by H_s. The factor of 1.86 is based on the assumption that the typical wave period is 10 [s], which means that about 1000 waves will pass the design location in 3 hours of sea states. However, the maximum wave height is limited by 0.78 water depth, where the breaking wave limit is reached. The significant wave period, T_s, is another commonly used parameter. It is the average period of the highest one third of all recorded wave periods.

Waves are well described as a narrowbanded, slightly non-Gaussian process, which is due to the crest amplitudes tending to be larger than the trough amplitudes. Although the wave height distribution is reasonably modeled as a Rayleigh distribution, crest amplitudes are underestimated by the Rayleigh distribution. The Rayleigh distribution wave height characteristics can be referred to Table 7.1.

While the significant wave height and the wave period are widely used parameters, it should be noted that several definitions are commonly used to describe the period of waves. In particular, the peak period and zero-up-crossing period are often used as alternatives to the significant wave period to characterize a sea elevation process. The peak period, T_p, the period of the wave containing the most power, is of particular interest when using the wave spectrum to define a wave model and is commonly used when describing irregular random sea states. The zero-up-crossing period, T_z, is the average time between successive movements of the water surface through the mean position in the upward direction.

Table 7.1 Characteristic Wave Heights Based on the Rayleigh Distribution

Characteristic Height	H/H_{rms}	$H/\sqrt{m_0}$	H/H_s
Standard deviation	0.354	1	0.25
Root mean square wave height	1	2.828	0.707
Mean height	0.866	2.507	0.626
Significant height $H_{1/3}$	1.416	4	1
Average of tenth highest waves $H_{1/10}$	1.8	5.091	1.271
Average of hundredth highest waves $H_{1/100}$	2.359	6.672	1.667

2.   Wave Theory

General

Most of the theory and formulas presented in this section are available from Faltinsen (1990) [2], Gran (1992) [3], and Langen et al. (1997) [4].

Figure 7.2 shows the parameters used when defining a two-dimensional (2D), regular, long-crested wave propagating in the positive *x*-direction. In the figure,

L = wave length
H = wave height
d = water depth, calculated by $Z_s - Z_b$
a = wave amplitude, $H/2$
T = wave period
g = acceleration of gravity
t = time
x = direction of wave propagation

Wave frequency is defined as follows:

$$\omega = \frac{2\pi}{T} \qquad\qquad [7.4]$$

and wave number is expressed as

$$k = \frac{2\pi}{L} \qquad\qquad [7.5]$$

According to potential wave theory, the dispersion relation expresses the relation between the wave period and wavelength and is given by

$$\frac{\omega^2}{gk} = \tanh(kd) \qquad\qquad [7.6]$$
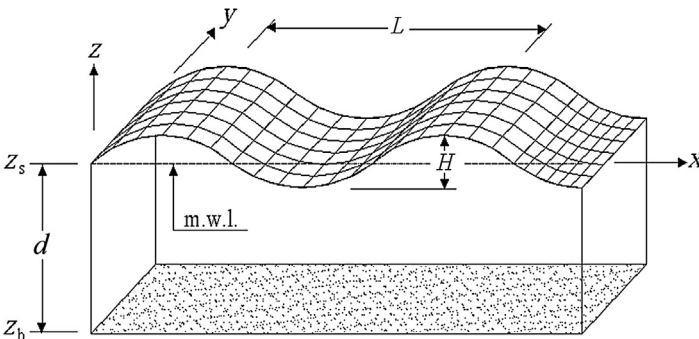
Figure 7.2 Parameters for defining 2D regular waves.

The validity of a wave theory can generally be quantified by the graph shown in Figure 7.3. It is a widely accepted presentation of the applicability of wave theories and is commonly used in coastal engineering codes. It is possible to select a wave theory based on three parameters: the wave height, H; the wave period, T; and the water depth, d, based on this figure.

Water depth classification as "shallow," "intermediate," and "deep" is a relative measure and depends on the wave period. The ordinate $H/(gT^2)$ is a measure of wave steepness, which is related to the angle of wave surface. The different wave theories shown in Figure 7.3 can generally be classified into two groups: linear wave theories (Airy) and nonlinear wave theories (Cnoidal and Stokes). Figure 7.3 shows that, in deep waters, linear wave theory can be used up to a wave steepness of 0.02 ft/s^2, while its application becomes increasingly limited as the water depth decreases.

Both the Airy and Stokes wave theories are the simplest theories, describing the shape of the water-air interface as a function of time. The Airy wave theory uses a sine function to represent the surface of the sea, while Stokes extended the description of the sea surface by a fifth order sine series. It is the simplest wave theory, but it is applicable to a wide range of circumstances.

The Stokes wave theory can provide a better approximation to the steeper waves typically encountered in shallower water. The Cnoidal wave theory is a better approximation in shallow water.
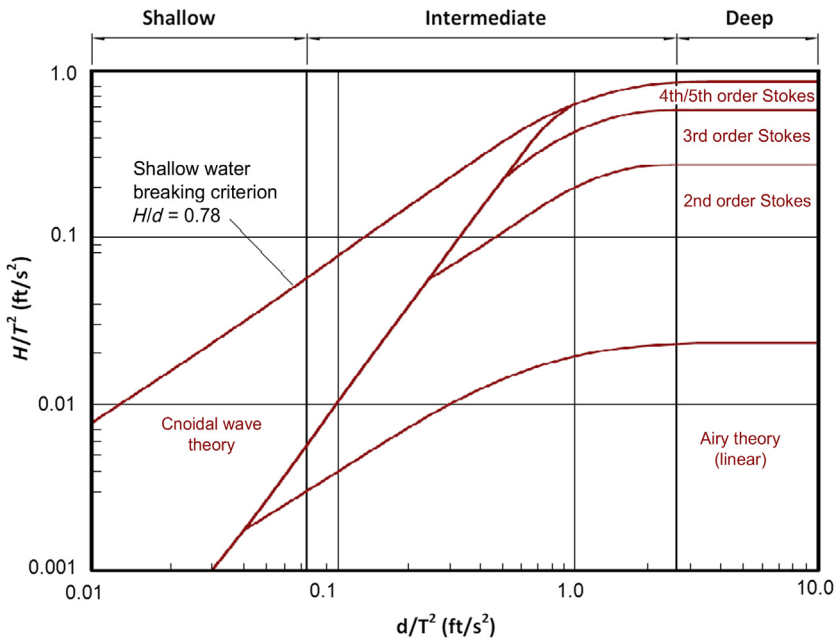
Figure 7.3 Validity ranges for wave theories.
Source: U.S. Army Corps of Engineers [5]. (For color version of this figure, the reader is referred to the online version of this book.)

In the fatigue limit state analysis for offshore structures, the average wave environment on a daily basis is of particular interest. Such a wave environment is generally characterized by relatively small waves with a small wave steepness, making it reasonable to use linear wave theory.

Comprehensive studies have been conducted to identify the most suitable wave theories for representing the near-bottom kinematics due to wave action. In Dean et al. (1986) [6], it was concluded that linear wave theory provides a good prediction of near-bottom kinematics for a wide range of relative water depth and wave steepness. One reason for this relatively good agreement is that the influence of nonlinearities considered in higher order wave theories is reduced with depth below the free surface. In Kirkgoz (1986) [7], it was also found that linear wave theory gave acceptable predictions of near seabed water particle velocities in waves close to the breaking point. It therefore seems appropriate to apply linear wave theory to near seabed objects for a wide range of wave heights, periods, and water depths. The calculated fluid velocities and accelerations of the surface waves are transferred to seabed level using linear wave theory.

Linear Wave Theory

Airy's linear wave theory was first published in 1845 and is also named the *Airy wave theory*. The linear wave theory assumes that the waves consist of small amplitudes in comparison to the wavelengths. It is for this reason that it is often referred to as *small amplitude wave theory*. Other assumptions made in developing linear wave theory include

- Incompressible, homogeneous fluid.
- Neglect surface tension and the Coriolis effect.
- Uniform and constant pressure at the surface.
- Ideal fluid without viscosity.
- Horizontal, impermeable seabed.
- Long-crested waves (2D approach).
- The fluid motion is irrotational.

Regular Long-Crested Waves

Figure 7.4 shows 2D, regular, long-crested wave defined by their wave amplitude and frequency, giving the following expressions for the wave kinematics:

$$\eta = a \cdot \sin(\omega t - kx + \alpha) \tag{7.7}$$

Fluid velocity component in the x-direction,

$$v_x = \frac{agk}{\omega} \cdot \frac{\cosh[k(d+z)]}{\cosh(kd)} \cdot \sin(\omega t - kx + \alpha) \tag{7.8}$$

Fluid velocity component in the z-direction,

$$v_z = \frac{agk}{\omega} \cdot \frac{\sinh[k(d+z)]}{\cosh(kd)} \cdot \cos(\omega t - kx + \alpha) \tag{7.9}$$
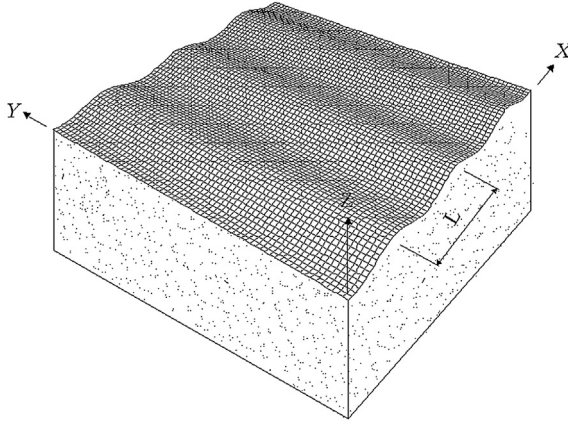
Figure 7.4 Regular, long-crested waves.

Fluid acceleration component in the x-direction,

$$a_x = agk \cdot \frac{\cosh[k(d+z)]}{\cosh(kd)} \cdot \cos(\omega t - kx + \alpha) \qquad [7.10]$$

Fluid acceleration component in the z-direction,

$$a_z = -agk \cdot \frac{\sinh[k(d+z)]}{\cosh(kd)} \cdot \sin(\omega t - kx + \alpha) \qquad [7.11]$$

Dynamic pressure,

$$p_{\text{dyn}} = \rho ag \cdot \frac{\cosh[k(d+z)]}{\cosh(kd)} \cdot \sin(\omega t - kx + \alpha) \qquad [7.12]$$

Random Long-Crested Waves

Figure 7.5 shows 2D, random, long-crested waves defined by significant wave height, peak frequency, and so forth. The formulation in this section is based on the use of a wave spectrum, as shown in Figure 7.6, to define the characteristics of the sea state.

As an example, the Joint North Sea Wave Project (JONWAP) proposed the JONS-WAP spectrum based on measurements in the North Sea, which can be defined as [1]

$$S(f) = \frac{\alpha g^2}{(2\pi)^4 f^5} \exp\left[-\frac{5}{4}\left(\frac{f}{f_p}\right)^{-4} \right] \gamma^{a_p} \qquad [7.13]$$
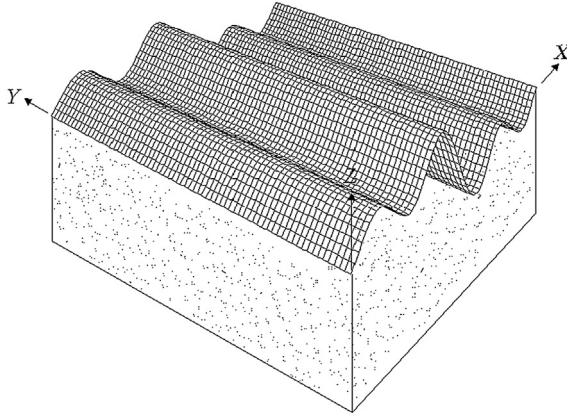
Figure 7.5 Random, long-crested waves.
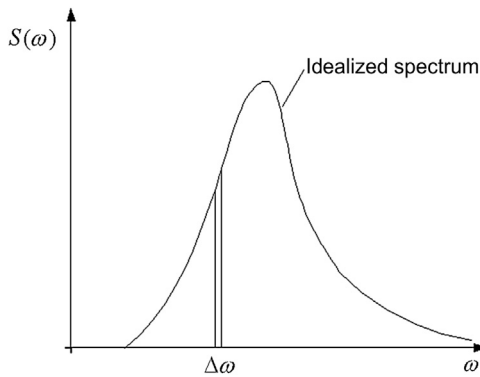
Figure 7.6 Wave spectrum.

where

$$
a_{\mathrm{p}} = \exp\left\{-\frac{\left(f - f_{\mathrm{p}}\right)^2}{2\sigma^2 f_{\mathrm{p}}^2}\right\}
$$

$$
\sigma = \begin{cases} 0.07 & \text{for} \quad f \le f_{\mathrm{p}} \\ 0.09 & \text{for} \quad f > f_{\mathrm{p}} \end{cases}
$$

f = frequency
f_{p} = spectral peak frequency
g = acceleration of gravity

a_p = Phillips' constant

σ = spectral width parameter

α = a constant that relates to the wind speed and fetch length. Typical values in the northern north sea are in the range of 0.0081 to 0.01

γ = the peakedness parameter of JONSWAP spectrum, determined from,

$$\gamma = \begin{cases} 1, & \gamma < 1 \\ \exp\left(5.75 - 0.367 T_{\text{peak}}\sqrt{\dfrac{g}{H_s}}\right), & 1 < \gamma < 5 \\ 5, & \gamma > 5 \end{cases} \qquad [7.14]$$

Nowadays, it is more common to use Goda's form, which specifies the spectrum in terms of H_s, T_p, and γ,

$$S(f) = \beta_J H_{1/3}{}^2 T_P{}^{-4} f^{-5} \exp\left[-\frac{5}{4}(T_P f)^{-4}\right] \gamma^{a_p}$$

where

$$\beta_J = \frac{0.06238}{0.230 + 0.0336\gamma - 0.185(1.9 + \gamma)^{-1}} [1.094 - 0.01915 \ln \gamma]$$

$$f_p = \frac{1}{T_p}, \quad \gamma(\text{shape factor}) = 1 \sim 7 \text{ (mean 3.3)}$$

From the wave spectrum, we can find several properties. The term λ_n denotes the nth (stress) spectral moment, defined by

$$\lambda_n = \int_0^\infty f^n S(f) df \qquad [7.15]$$

The term $H_{1/3}$ is the significant wave height and can be calculated by

$$H_{1/3} = 4\sqrt{\lambda_0} \qquad [7.16]$$

The average period, $\overline{T_0}$, measured at zero crossings is

$$\overline{T_0} = \frac{1}{f_0} = \sqrt{\frac{\lambda_0}{\lambda_2}} \qquad [7.17]$$

and the spectral band width parameter ε as

$$\varepsilon = \sqrt{1 - \frac{\lambda_2^2}{\lambda_0 \lambda_4}} \qquad \qquad [7.18]$$

By performing an inverse transformation, the wave amplitudes (a_i) and frequencies (ω_i) of each wave component is extracted from the wave spectrum.

Extraction of amplitudes and frequencies from the wave spectrum is for each wave component done according to

$$a_i = \sqrt{2 \cdot \Delta f \cdot S(f_i)} \qquad \qquad [7.19]$$

where

$$f_i = i \cdot \Delta f \qquad \qquad [7.20]$$

Δf = the constant difference between successive frequencies

$$k_i = \frac{(\omega_i)^2}{g} = \text{the deep water dispersion relation}, \omega_i = 2\pi \cdot f_i \qquad [7.21]$$

An example of wave amplitude time realization using the JONSWAP spectrum analysis is shown in Figure7.7.
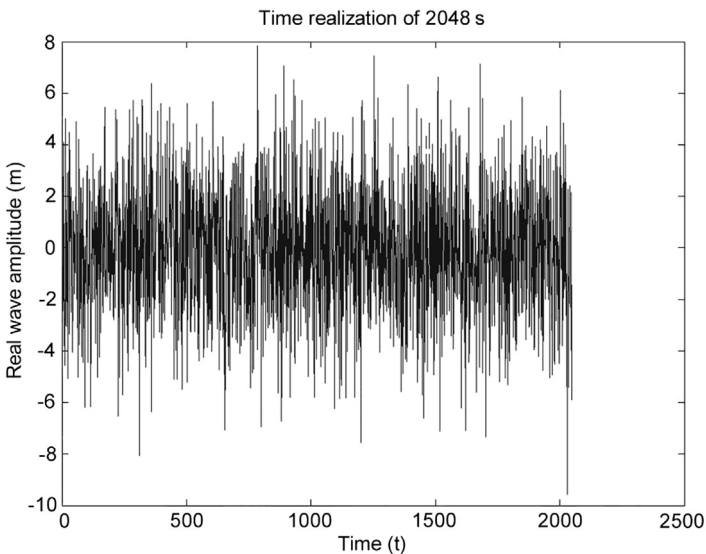
Figure 7.7 2048s zero mean wave amplitude time realization.

If a random phase angle α_i, uniformly distributed between 0 and 2π, is assigned to each wave component, the wave kinematics are represented as a sum of linear components as shown in Figure 7.8. If N is the number of wave components, typically a number power of 2, the sea state at a particular time and location can be represented by the following.

For surface elevation,

$$\eta = \sum_{i=1}^{N} a_i \cdot \sin(\omega_i t - k_i x + \alpha_i) \qquad [7.22]$$

For velocity component in the x-direction,

$$v_x = g \cdot \sum_{i=1}^{N} \frac{a_i k_i}{\omega_i} \cdot \frac{\cosh[k_i(d+z)]}{\cosh(k_i d)} \cdot \sin(-\omega_i t - k_i x + \alpha_i) \qquad [7.23]$$

For velocity component in the z-direction,

$$v_z = g \cdot \sum_{i=1}^{N} \frac{a_i k_i}{\omega_i} \cdot \frac{\sinh[k_i(d+z)]}{\cosh(k_i d)} \cdot \cos(\omega_i t - k_i x + \alpha_i) \qquad [7.24]$$
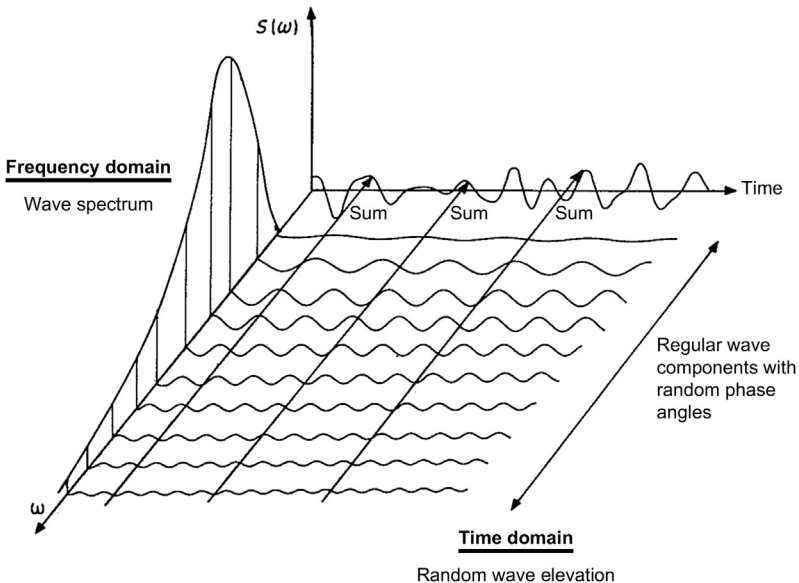
Figure 7.8 Frequency domain and time domain representation of long-crested waves.

For acceleration component in the x-direction,

$$a_x = g \cdot \sum_{i=1}^{N} a_i k_i \cdot \frac{\cosh[k_i(d+z)]}{\cosh(k_i d)} \cdot \cos(\omega_i t - k_i x + \alpha_i)$$ [7.25]

For acceleration component in the z-direction,

$$a_z = -g \cdot \sum_{i=1}^{N} a_i k_i \cdot \frac{\sinh[k_i(d+z)]}{\cosh(k_i d)} \cdot \sin(\omega_i t - k_i x + \alpha_i)$$ [7.26]

For dynamical pressure,

$$p_{dyn} = \rho g \cdot \sum_{i=1}^{N} a_i \frac{\cosh[k_i(d+z)]}{\cosh(k_i d)} \cdot \sin(\omega_i t - k_i x + \alpha_i)$$ [7.27]

Abaqus/Aqua is equipped with algorithms that allow for linear calculations according to the Airy wave theory. A single wave can be modeled by providing the program with the amplitude, wave period, phase angle, and propagation direction [8]. An irregular sea state may be modeled by repeating this input line as many times as desired, providing Abaqus with data on the individual waves, which are then superimposed within the program. However, at least 1000 sets of wave data are required to accurately simulate an actual sea state. Therefore, the UWAVE subroutine in ABAQUS is suggested to be used for modeling a complete sea state [9].

Nonlinear Wave Theory

For extreme load conditions, the height of the wave reaches values that do not allow for an accurate model under the assumption of linear wave theory. In storm conditions, waves are high and long crested and therefore do not satisfy the linear assumptions of a symmetrical, low amplitude wave profile.

One of the most fundamental nonlinear wave theories was developed by Stokes in 1847. It is based on a perturbation solution, which is developed as a power series. The Stokes wave theory uses the Airy wave as initial exact solution to develop the power series. Additional harmonic waves are then added to the basic harmonic of the linear wave theory using a perturbation parameter of $\varepsilon = kA$, a product of the wave number k and amplitude A.

$$\eta(x,t) = \varepsilon^1 \cdot \eta_1(x,t) + \varepsilon^2 \cdot \eta_2(x,t) + \cdots + \varepsilon^n \cdot \eta_n(x,t)$$ [7.28]

with this initial linear solution:

$$\eta_1(x,t) = \frac{1}{k} \cdot \cos(\omega t - kx + \alpha)$$ [7.29]

It was found that even fifth order Stokes theory is not accurate for steeper waves, which are common in shallow waters. The applicability of Stokes wave theory to offshore structures is thus limited. However, the fifth order Stokes theory is the only nonlinear wave theory included in the Abaqus/Aqua environment, it is recommended to use this function when it is appropriate.

3. Steady Currents

For the situation where a steady current exists, the effects of the bottom boundary layer may be accounted for. Seabed currents in design data are normally given at a reference height above the seabed. The location of the pipeline in the velocity boundary layer lowers the effective velocity at the pipeline height, and the mean current velocity over the pipe diameter may be applied in the analysis. According to DNV (2007) [10], this has been used in the subsea pipeline analysis assuming a logarithmic mean velocity profile:

$$v_c = \frac{v_c(z_r)\left(\frac{z_0}{D}+1\right)}{\ln\left(\frac{z_r}{z_0}+1\right)}\left\{\ln\left(\frac{D}{z_0}+1\right)-1\right\} \qquad [7.30]$$

where

$v_c(z_r)$ = current velocity at reference measurement height
z_r = reference measurement height (usually 3 m)
z_0 = bottom roughness parameter
D = total external diameter of pipe (including any coating)

The effect of the seabed roughness, z_0, is taken into account in this equation. The rougher the seabed, the thicker is the boundary layer and the lower the average velocity over the pipe height.

The total water particle velocity is obtained by adding the velocities from waves and currents together:

$$v_{total} = v_w + v_c \qquad [7.31]$$

4. Hydrodynamic Forces

Hydrodynamic Drag and Inertia Forces

A pipeline section exposed to a flow experiences hydrodynamic forces, due to the combined effect of increased flow velocity above the pipe and flow separation from the pipe surface. Figure 7.9 shows the water particle velocity distribution around the pipe. This section explains the different components of the force vector and the expressions used to calculate these components.
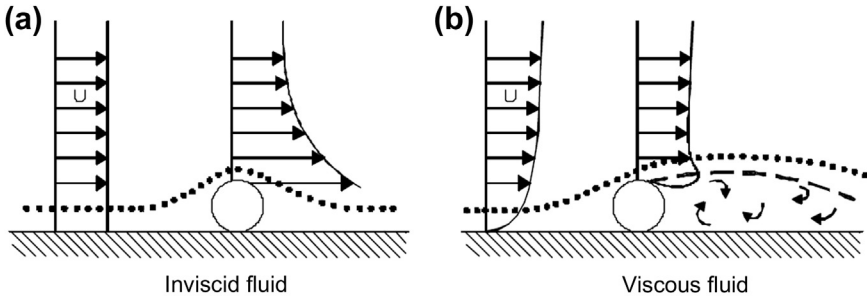
Figure 7.9 Flow field around the pipe.

Pipeline Exposed to Steady Fluid Flow

Fluid drag is associated with velocities due to steady currents superposed by any waves that may be present, as shown in Figure 7.10. The drag is mainly the result of the high pressure in front of the pipe and the low pressure region in the wake behind the pipe. The drag is influenced by the width of the wake, the following expression gives the transverse drag force component per unit length of the pipeline:

$$F_\text{D} = \frac{1}{2}\,\rho C_\text{D} D\, v_\text{n}|v_\text{n}| \qquad\qquad [7.32]$$

where

    C_D = transverse drag coefficient
    v_n = transverse water particle velocity
    ρ = density of seawater
    D = total external diameter of pipe
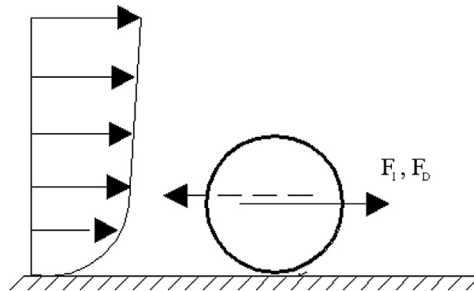
Figure 7.10 Fluid drag and inertia forces acting on a pipe section.

Pipeline Exposed to Accelerated Fluid Flow

Waves produce cyclic loadings on the water particles in the water column. These cyclic loads accelerate and decelerate the water particles in both the horizontal and vertical directions. A pipeline exposed to an accelerated fluid experiences a force proportional to the acceleration, this force is called the *inertia force*. The following expression gives the transverse inertia force component per unit length of a pipeline:

$$F_{\mathrm{I}} = \frac{\pi}{4}\, \rho D^2 C_{\mathrm{M}} a_{\mathrm{n}} \qquad [7.33]$$

where

$C_{\mathrm{M}} = (C_{\mathrm{a}} + 1)$, transverse inertia coefficient
a_{n} = transverse water particle acceleration
ρ = density of seawater
D = total external diameter of pipe

The Complete Morison's Equation

The formula just given does not take into account that the pipe itself may have velocity and acceleration. The inline force per unit length of a pipe is determined using the complete Morison's equation:

$$F_{\mathrm{IL}}(t) = \frac{1}{2}\rho C_{\mathrm{D}}\left(U - \frac{\partial y}{\partial t}\right)\left|U - \frac{\partial y}{\partial t}\right| + C_{\mathrm{M}}\frac{\pi}{4}\rho D^2 \frac{\partial U}{\partial t} - (C_{\mathrm{M}} - 1)\frac{\pi}{4}\rho D^2 \frac{\partial^2 y}{\partial t^2}$$

$$[7.34]$$

where

ρ = sea water density
D = outer diameter of the pipe
U = instantaneous (time-dependent) flow velocity
y = inline displacement of the pipe
C_{D} = drag coefficient
C_{M} = inertia coefficient
$\quad = (C_{\mathrm{a}} + 1)$, where C_{a} is the added mass coefficient
$\delta/\delta t$ = differentiation with respect to time

Drag and Inertia Coefficient Parameter Dependency

In general, the drag and inertia coefficient is given by

$$C_{\mathrm{D}} = C_{\mathrm{D}}[Re, \mathrm{KC}, \alpha, (e/D), (k/D), (A_{\mathrm{Z}}/D)] \qquad [7.35]$$

$$C_{\mathrm{M}} = C_{\mathrm{M}}[Re, \mathrm{KC}, \alpha, (e/D), (A_{\mathrm{Z}}/D)] \qquad [7.36]$$

The Reynolds number indicates the present flow regime, (i.e., laminar or turbulent) and is given as

$$Re = \frac{UL}{\nu}$$ [7.37]

where

U = flow velocity
L = characteristic length (diameter for pipelines)
ν = fluid kinematic viscosity.

The Keulegan-Carpenter number gives information on how the flow separation around cylinders will be for ambient oscillatory planar flow, $U = U_M \sin[(2\pi/T)t + \alpha)]$ and is given as:

$$KC = \frac{U_M T}{D}$$ [7.38]

where:

U_M = flow velocity amplitude
T = period
D = diameter
α = phase angle
t = time

The current flow ratio may be applied to classify the flow regimes:

$$\alpha = \frac{U_c}{U_c + U_w}$$ [7.39]

where

U_c = typical current velocity normal to the pipe
U_w = significant wave velocity normal to the pipe given for each sea state (H_s, T_p, θ_w)

Note that $\alpha = 0$ corresponds to pure oscillatory flow due to waves and $\alpha = 1$ corresponds to pure (steady) current flow.

The presence of a fixed boundary near the pipe (proximity effect) has a pronounced effect on the mass coefficient. The added mass increases as the pipe approaches a solid boundary, as shown in the following equation:

$$C_a = 1 + \frac{1}{\left[10 \cdot \left(\frac{e}{D}\right) + 1\right]}$$ [7.40]

where

e/D = gap ratio

The natural period of pipe oscillation increases as the added mass increases.

The roughness number (k/D) has a large influence on the flow separation and therefore also on the drag and mass coefficient (k = characteristic cross-sectional dimension of the roughness on the body surface).

There is a connection between the VIVs (vortex-induced vibrations) and the drag force. A crude approximation can be given as

$$C_D/C_{DO} = 1 + 2(A_Z/D) \qquad\qquad [7.41]$$

where

C_D = drag coefficient with VIV
C_{D0} = drag coefficient with no VIV
A_Z = cross-flow vibration amplitude

This formula can be interpreted as saying that there is an apparent projected area $D + 2A_Z$ due to the oscillating cylinder.

Hydrodynamic Lift Forces

Lift Force Using Constant Lift Coefficients

Lift force is produced in the same way as flow over an airplane. The presence of the seabed introduces an asymmetry between the flow over the top of the pipe and the flow underneath. This causes slower flow or no flow underneath the pipeline with high pressure and higher velocities over the top with low pressure, resulting in lift force.

The lift force per unit length of a pipeline (vertical lift force) can be calculated according to

$$F_L = \frac{1}{2}\, \rho D\, C_L\, v_n^2 \qquad\qquad [7.42]$$

where

C_L = lift coefficient for pipe on a surface
v_n = transverse water particle velocity (perpendicular to the direction of the lift force)
ρ = density of seawater
D = total external diameter of pipe

Typically, drag, inertia, and lift coefficients of hydrodynamic forces for a pipeline on seabed are empirically chosen as $C_D = 0.7$, $C_M = 3.29$, and $C_L = 0.9$.

Lift Force Using Variable Lift Coefficients

As can be imagined, the hydrodynamic lift coefficient (C_L) varies as a function of the gap that might exist between the pipeline and the seabed. The lift coefficients according to Fredsøe and Sumer (1997) [11] are given in Figure 7.11. It can be seen from the figure that a significant drop in the lift coefficient is present, even for very small ratios of e/D. This is true both for the shear and the shear-free flow.
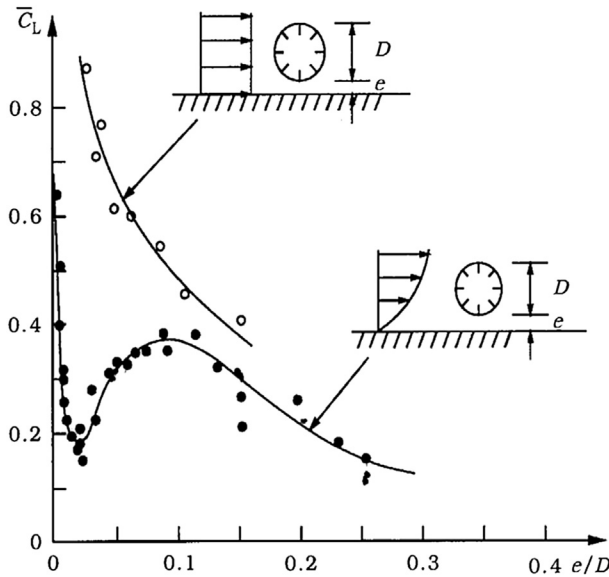
Figure 7.11 C_L **in shear and shear-free flow for** $10^3 < Re < 30 \times 10^4$.
Source: Fredsøe and Sumer [11].

References

[1]   Kellogg Brown & Root. Submarine pipeline on-bottom stability. Vol. 1. Analysis and
      design guidelines. PRCI Project PR-178–01132. Kellogg Brown & Root, Houston;
      December 2002.
[2]   Faltinsen OM. Sea loads on ships and offshore structures. Cambridge, UK: Cambridge
      University Press; 1990.
[3]   Gran S. A course in ocean engineering. New York: Elsevier; 1992.
[4]   Langen I, Gudmestad OT, Haver S, Gilje W, Tjelta TI. Forelesninger i Marin Teknologi.
      Høgskolen i Stavanger; 1997.
[5]   U.S. Army Corps of Engineers. Coastal engineering manual, Engineer Manual 1110-2-
      1100. Books Express Publishing, 2002.
[6]   Dean RG, Perlin M. Inter-comparison of near-bottom kinematics by several wave
      theories and field and laboratory data. Coastal Engineering 1986; 9.
[7]   Kirkgoz MS. Particle velocity prediction of the transformation point of plunging
      breakers. Coastal Engineering 1986; 10.
[8]   Simulia. ABAQUS user manuals, Version 6.12. Simulia; 2012. Providence, RI, USA.
[9]   Markus D. A code based methodology to account for wave loading in the design of
      offshore structures, Diploma Thesis. Germany: Universität Stuttgart; 2009.
[10] DNV. On-bottom stability design of submarine pipelines. DNV-RP-F109. Det Norske
      Veritas; 2007.
[11] Fredsøe B B, Sumer BMB. Hydrodynamics around cylindrical structures. Singapore:
      World Scientific Publishing Co; 1997.

8 Finite Element Analysis of In Situ Behavior

1.   Introduction

The design of high-pressure/high-temperature (HP/HT) pipelines on an uneven seabed has become an important issue in the recent years. The need to gain further insight into how expansion, seabed friction, and free spans influence on the pipeline behavior through selected load cases is the background of this chapter. The behavior of such pipelines is largely characterized by the tendency to undergo global buckling, either vertically if trenched or covered or laterally if the pipeline is exposed on the seabed. The main concern in the design of slender pipelines operating under HP/HT conditions is to control global buckling at planned locations. The large horizontal or vertical displacements induced by global buckling may result in high stresses and strains in the pipe wall that exceed code limits.

The simulation of the designed pipeline in a realistic three-dimensional environment obtained by measurements of the seabed topography, allows the engineers to

exploit any opportunities that the pipeline behavior may offer to develop both safe and cost-effective solutions. For example, the designer can first analyze the pipeline behavior on the original seabed. If some of the load cases result in unacceptably high stress or strain, seabed modification can be simulated in the finite element (FE) model and the analysis rerun to confirm that the modifications lead to the desired decrease in stress or strain.

The finite element model may be a tool for analyzing the in situ behavior of a pipeline. The pipeline in situ behavior means the pipeline behavior over its through-life load history. The pipeline load history can consist of several sequential load cases; for example,

- Installation.
- Hydrotesting (water filling and hydrotest pressure).
- Pipeline operation (content filling, design pressure, and temperature).
- Shutdown or cooldown cycles of pipeline.
- Upheaval and lateral buckling.
- Dynamic wave and current loading.
- Impact loads.

This chapter is based on a master's thesis by Ose [1], supervised by the author and the work has been influenced by papers presented in conferences: Nystrøm et al. [2], Tørnes et al. [3], and Kristiansen et al. [4].

2.   Finite Element Modeling of the Pipeline System

Static Analysis Problems

Installation

Modeling a pipeline in the installation condition is the first step of the in situ behavior analysis of pipeline system, to find the pipeline configuration when placed on the three-dimensional seabed. This configuration serves as an initial configuration for the subsequent parts of the analysis.

Primarily, it was not the behavior of the pipeline during the installation process that may be investigated, the important thing was to make sure that the lay tension and lay angle from the installation process was represented in such a way as to account for the buildup of residual forces in the pipeline, due to friction when the pipeline lands on the seabed.

The model may include the possibility of applying lay tension and specify the lay angel between the pipeline and the seabed to ensure good modeling of the contact forces in the touchdown zone as the pipeline lands on the seabed. Figure 8.1 shows the finite element model of seabed and pipeline before and under the installation process. As the pipeline stretches out, a stable equilibrium between the pipeline and the seabed must be ensured. This requires a representative pipe-soil interaction model. The pipe-soil interaction model typically consists of a definition of friction and seabed stiffness. It was realized that the seabed stiffness formulation must be able to describe several
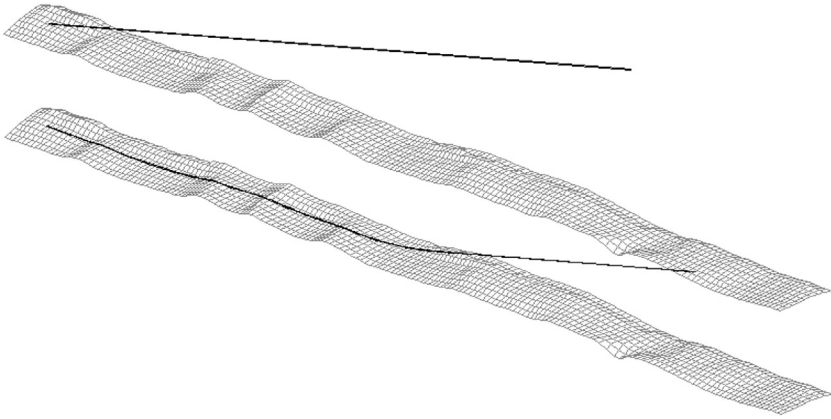
Figure 8.1 Finite element model during installation.

pressure and penetration relationships and that a subroutine for anisotropic friction model in the ABAQUS software [5] may be used to represent the difference in frictional resistance in the longitudinal and lateral directions of the pipe.

Flooding and Dewatering of the Pipeline

The flooding and dewatering of the pipeline result in changes in the pipe submerged weight and thus changes in the pipeline configuration. The friction force between the pipeline and the seabed is a function of the contact pressure and so increases when the pipeline is filled.

The flooding and dewatering of the pipeline could easily be modeled by a variation in the vertical load acting on the pipeline. But, a pipeline subjected to such load variations can in the filled condition experiences large axial strains due to the change in geometry when the pipe deforms and sinks into the free spans along the pipeline route, as shown in Figure 8.2. Due to this fact, the model to be established may use a large-displacement analysis procedure, and the effect of changes in the pipe section area due to high axial straining may be accounted for. Further, the material model may be able to represent the plastic behavior of the pipe section.

Effects of High Pressure and High Temperature

High temperatures from the contents of the pipeline cause material expansion of the pipe steel; this leads to an extension in the pipe length, and the pipeline may buckle and seek new deformation paths to maintain in equilibrium, as shown in Figure 8.3. The influence of material expansion due to variation of temperature may therefore be included in the model.

Material properties, such as yield stress, tensile strength, and Young's modulus, change with material temperature and, if necessary, may be accounted for.
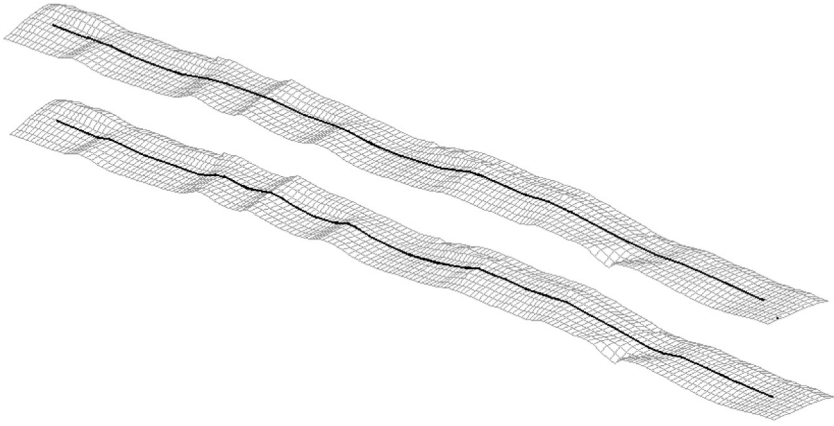
Figure 8.2 FE modeling of empty pipe versus water filled pipe.
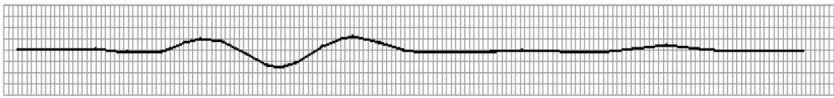
Figure 8.3 Pipeline configuration of lateral buckling due to temperature (scaled displacements).

External hydrostatic pressure is an important factor regarding the strength capacity of deepwater pipelines. Since the model may include a fully three-dimensional seabed, the external pressure may be a function of the water depth. Internal pressure can be modeled as constant, but the possibility to account for the static head of the contents may be included.

Dynamic Analysis Problems

Wave and Current Loading

Hydrodynamic forces arise from water particle velocity and acceleration. These forces can be fluctuating (caused by waves) or constant (caused by steady currents) and result in a dynamic load pattern on the pipeline, as shown in Figure 8.4. Drag, inertia, and lift forces are of interest when analyzing the behavior of a submerged pipeline subjected to wave and current loading.
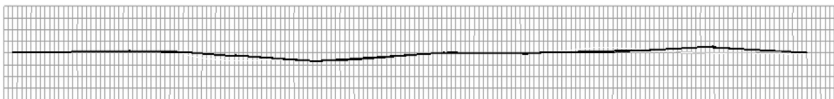
Figure 8.4 Horizontal displacement of pipeline subjected to wave and current loading.

Because of the dynamic nature of waves, the pipeline response when subjected to this type of loading may be investigated in a dynamic analysis. Further, several wave formulations are desirable. Two-dimensional regular or random long-crested waves and the three-dimensional (3D) regular or random short-crested waves may be included in the finite-element model to supply the wave kinematics in a dynamic analysis.

Trawl Gear Pullover Response

The trawl gear pullover loads may result in a dynamic plastic response. The calculation of loads and strength criteria are discussed in Chapter 16.

In a finite element analysis, implicit dynamic solutions, such as that described in Section 3, are used to simulate the time history of displacements, stresses, and strain. Details are given in Tørnes et al. [3].

3. Procedure and Load Steps in Finite Element Analysis

A basic concept in ABAQUS is the division of the load history into load steps. For each step, the user chooses an analysis procedure. This means that any sequence of load history and desired type of analysis can be performed. For example, in one static step the pipeline can be filled with gas, in the next static step emptied, and in the third step a dynamic analysis of the empty pipeline can be performed.

A typical load history from the established model is given as an example in Table 8.1.

The Static Analysis Procedure

The static analysis available from ABAQUS that is used in the model handles nonlinear responses from large-displacements effects, material nonlinearity, and boundary nonlinearities, such as contact, sliding, and friction (pipe-seabed interaction). ABAQUS uses Newton's method to solve the nonlinear equilibrium equations. Therefore, the solution is obtained as a series of increments with iterations to obtain equilibrium within each increment. For more information about static finite element analysis, please refer to Cooker et al. [6].

The Dynamic Analysis Procedure

A general dynamic analysis (dynamic analysis using direct integration) must be used to study the nonlinear dynamic response of the pipeline. General nonlinear dynamic analysis uses implicit integration of the entire model to calculate the transient dynamic response of the system. The direct integration method provided in ABAQUS, called the *Hilbert-Hughes-Taylor operator* (which is an extension of the trapezoidal rule), is therefore used in the model. The Hilbert-Hughes-Taylor operator is implicit, the integration operator matrix must be inverted, and a set of simultaneous nonlinear dynamic equilibrium equations must be solved at each time increment. This solution is done iteratively using Newton's method.

Table 8.1 Typical Load History of Pipeline in an ABAQUS Analysis

Load Step	Action	Analysis Procedure
1	Applying pipe self-weight and buoyancy	Static
2	Applying hydrostatic external pressure	Static
3	Applying lay tension	Static
4	Lowering pipeline down at the seabed (see Figure 8.1)	Static
5	Removing GAPSPHERE elements (winch)	Static
6	Modifying boundary conditions for installation condition	Static
7	Water filling (see Figure 8.2) for flooding condition	Static
8	Applying hydrotest pressure for hydrotesting condition.	Static
9	Removing hydrotest pressure and dewater	Static
10	Gas filling	Static
11	Applying operation pressure	Static
12	Applying operation temperature for operating condition (see Figure 8.3)	Static
13	Removing pressure and temperature for cooldown condition	Static
14	Applying wave and current loading (see Figure 8.4)	Dynamic

4. Element Types Used in the Model

Three types of elements are used in the established finite-element model of pipeline system, as shown in Figure 8.5:

- The rigid elements of type R3D4 used to model the seabed.
- The PIPE31H pipe elements used to model the pipeline.
- The GAPSPHER elements used as a winch when lowering the pipeline from its initial position and down at the seabed, as shown in Figure 8.1. These elements are removed from the model when the pipeline has landed and gained equilibrium at the seabed.

PIPE31H elements

R3D4 elements
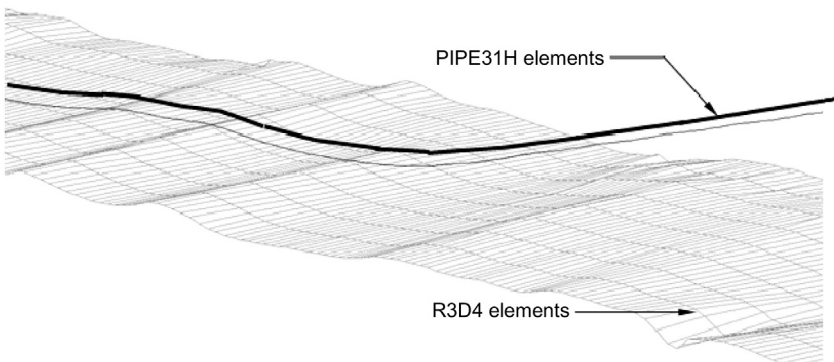
Figure 8.5 Element types used in the model.

PIPE31H Element

Figure 8.6 shows the 3D finite pipe element used in the established model, which is the two node, 12 degrees of freedom PIPE31H element. The element uses linear interpolation and therefore has a lumped mass distribution. The hybrid formulation makes the element well suited for cases with slender structures and contact problems, such as a pipe lying on the seabed.

The hybrid elements are provided by ABAQUS for use in cases where it is numerically difficult to compute the axial and shear forces in the beam by the usual finite element displacement method. The problem in such cases is that slight differences in nodal positions can cause very large forces in some parts of the model, which in turn, cause large motions in other directions. The hybrid elements overcome this difficulty by using a more general formulation, in which the axial and transverse shear forces in the elements are included, along with the nodal displacements and rotations, as primary variables. Although this formulation makes these elements more calculation intensive, they generally converge much faster when the pipe rotations are large and are more efficient overall in such cases.

The PIPE31H element is available with a hollow, thin-walled circular section and supports the possibility for the user to specify external or internal pressure. From ABAQUS version 6.12, thick-walled elements are also included in the software. The element can also account for changes in the pipe section area due to high axial straining of the pipe.

R3D4 Element

The four-node R3D4 rigid element, as shown in Figure 8.7, makes it possible to model complex surfaces with arbitrary geometry and has been chosen when modeling the seabed topography. A very important feature of ABAQUS when modeling the seabed has been the possibility to smooth surfaces generated with the rigid elements, this leads to a much better representation of the seabed than the initial faceted surface.

The smoothing is done by ABAQUS creating Bèzier surfaces based on the faceted surface of the seabed formed by the rigid elements. The resulting Bèzier surfaces, unlike the faceted element surface, are smooth and have a continuous outward surface
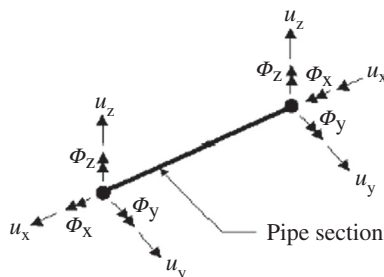
Figure 8.6 Two nodes, 12 degrees of freedom of 3D beam element.
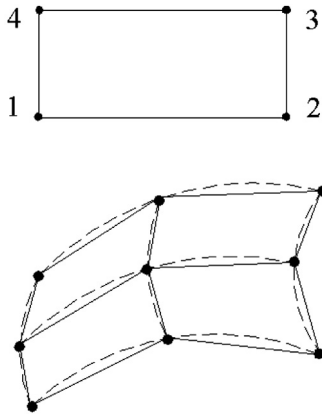
Figure 8.7 R3D4 rigid element and smoothing of surface of rigid elements.

normal. The Bèzier surfaces do not match the faceted geometry of the rigid surface exactly, but the nodes of the rigid elements defining the seabed always lie on the Bèzier surface. In addition, the user can specify the degree of smoothing to control the geometry of the smoothed surface.

In the established model, the set of R3D4 elements defining the seabed is used as a so-called master surface for contact applications with the pipe elements. This means that a contact pair (pipe-seabed) is defined and an interaction model is specified. This interaction model typically consists of a seabed stiffness and friction definition.

5.   Nonlinearity and the Seabed Model

The nonlinear stress analysis used in the model contains up to three sources of nonlinearity depending on the strain level, change in geometry, and load conditions:

- Material nonlinearity.
- Geometric nonlinearity.
- Boundary nonlinearity (friction, sliding, etc.).

Material Nonlinearity

The material model used is capable of representing the complete stress-strain relationship for the pipeline material, including nonlinear plastic behavior, as shown in Figure 8.8.

In the elastic area, the stress-strain relationship is governed by supplying the Young's modulus of the material. For the steel types commonly used as the material of structural pipe, the Young's modulus is temperature dependent. This can easily be accounted for in the model by numerically specifying the Young's modulus as a function of temperature.
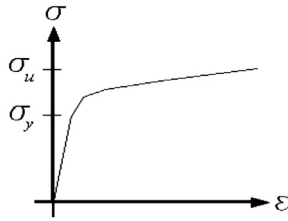
Figure 8.8 Stress-strain relationship.

The plastic behavior of the material is defined by specifying numerically the complete plastic stress-strain curve for the steel (e.g., from test data) in the material definition part of the input file. The true stress/true strain relationship is used in the ABAQUS model. The thermal expansion coefficient of the material can also be defined as a function of temperature if necessary.

Geometrical Nonlinearity

Geometrical nonlinearity is accounted for in the model. This means that strains due to change in the model geometry are calculated and this stiffness contribution (stress stiffness) is added to the structure stiffness matrix. In addition, the instantaneous (deformed) state of the structure is always used in the next increment and updated through the calculation.

The latter feature is especially important when performing the dynamic analysis of a pipeline subjected to wave loading. By including geometrical nonlinearity in the calculation, ABAQUS uses the instantaneous (instead of the initial) coordinates of the load integration points on the pipe elements when calculating water particle velocity and acceleration. This ensures that, even if some parts of the pipeline undergo very large lateral displacements (15–20 m), the correct drag and inertia forces are calculated on each of the individual pipe elements that make up the pipeline.

Boundary Conditions

Arbitrarily boundary conditions along the pipeline can be specified. If only a section of the total length of the pipeline is to be analyzed (e.g., between two successive rock dumpings), the user can simulate the stiffness of the rest of the pipeline with springs in each of the two pipe ends. If other constraints lie along the pipeline, these can be modeled by either fixing nodes or assigning springs to a number of nodes along the pipeline.

Seabed Model

The basis for constructing the 3D seabed model is data from measurements of the seabed topography from bathymetric surveys in the area where the pipeline is to be

installed. From this information, a corridor of width up to 40 m and lengths up to several kilometers is generated in the FE model to ensure a realistic environment when performing analysis of the pipeline behavior.

The seabed topography is represented with four node rigid elements that make it possible to model flat or complex surfaces with arbitrary geometries. An advantage when modeling the three-dimensional seabed is the smoothing algorithm used by ABAQUS. The resulting smoothed surfaces, unlike the flat rigid element surfaces, have a continuous outward surface normal across element boundaries and model the seabed better. The smoothed surfaces do not match the faceted geometry of the rigid surface exactly, but the nodes of the rigid elements defining the seabed always lie on the surface.

6. Validation of the Finite Element Model

A 1300 meter long pipeline section between two consecutive rock berms was analyzed, to compare with the results of similar finite element models [2, 7]. In Figure 8.9, the results from the water filled condition are given for the first 100 meters only, to get the details in the plots clearly.

Figure 8.9 shows the comparison of analyzed results between the ABAQUS software and the ANSYS software [8]. It can be seen that the two in-place models based on ABAQUS and ANSYS, respectively, give close prediction of axial stress, strain, bending moment, and configuration of pipeline on the seabed [9].

7. Dynamic Buckling Analysis

For a pipeline resting on a very uneven seabed, the vertical imperfections induce a more abrupt curvature than the horizontal imperfections created during laying. As a result, the critical buckling load required to lift the pipeline vertically is lower than the corresponding force needed to buckle horizontally. Although the initial movement occurs in the vertical plane, it was expected that, as the pipe's contact force with the seabed diminishes, the critical lateral buckling force would decrease and a lateral buckle could be initiated.

To investigate the pipeline behavior on an irregular seabed as realistically as possible, a 3D pipeline-seabed FE model was developed, where the 3D seabed bathymetry is imported as X,Y,Z data directly from a digital terrain model (DTM) program. The 3D pipe-seabed model can then be presented, as shown in Figure 8.10.

The lateral buckle is a sudden loss of axial stability, which results in a dynamic "snap" movement.Nystrøm et al. [2] investigated what actually happens with the pipe as it buckles in terms of stresses-strains, displacements, effective axial force, and the like. During the snap-through process, the pipeline experiences acceleration and velocity leading to dynamic effects that may be significant. The transient

Axial stress

Axial strain

Bending moment

Pipe configuration on seabed
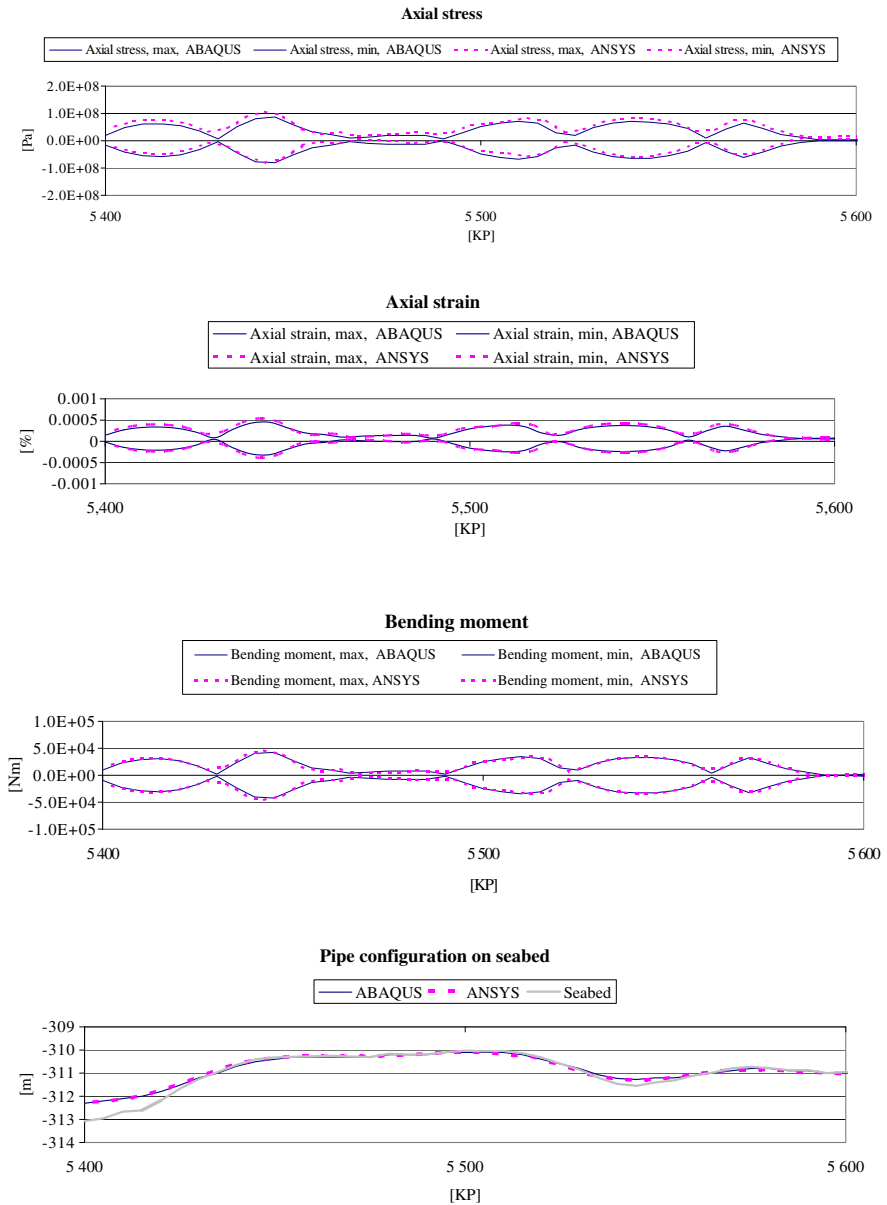
Figure 8.9 Comparison of ANSYS and ABAQUS for the water filled condition. (For color version of this figure, the reader is referred to the online version of this book.)
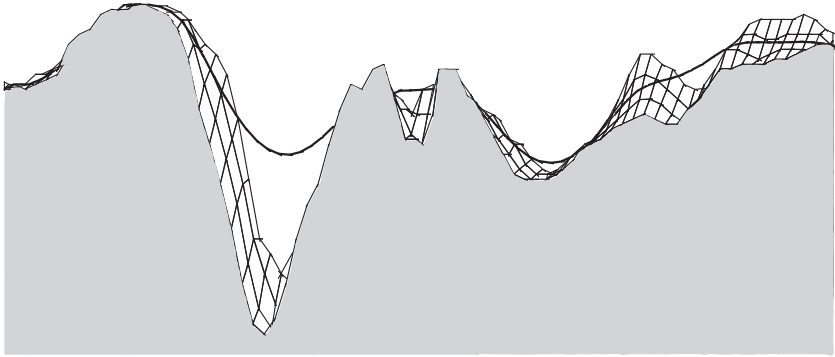
Figure 8.10 3D FEM in-place analysis; typical details from as-laid pipeline simulation.
Source: Nystrøm et al. [2].

pipeline buckling behavior was simulated using the general equilibrium equation for
a dynamic system:

$$[M]\{\ddot{u}\} + [C]\{\dot{u}\} + [K]\{u\} = \{F(t)\} \tag{8.1}$$

where

[M] = structure mass matrix
[C] = structure damping matrix
[K] = structure stiffness matrix
{u} = nodal displacement vector
{\dot{u}} = nodal velocity vector
{\ddot{u}} = nodal acceleration vector
{F(t)} = time-dependent nodal force vector

The dynamic response is caused by a change from potential energy to kinetic energy.
To account for the inertia effects of displacing the surrounding water, mass elements
were coupled to each pipe node.

In nonlinear finite element analysis, stress-strain results can be obtained from eight
positions around the pipe circumference, as presented in Figure 8.11.
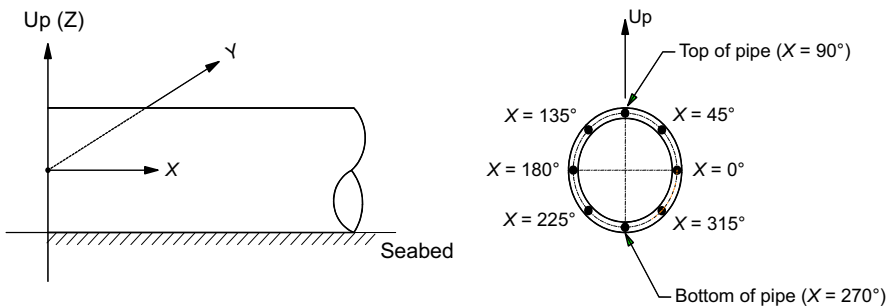
Figure 8.11 Definition of data position at pipe circumference.
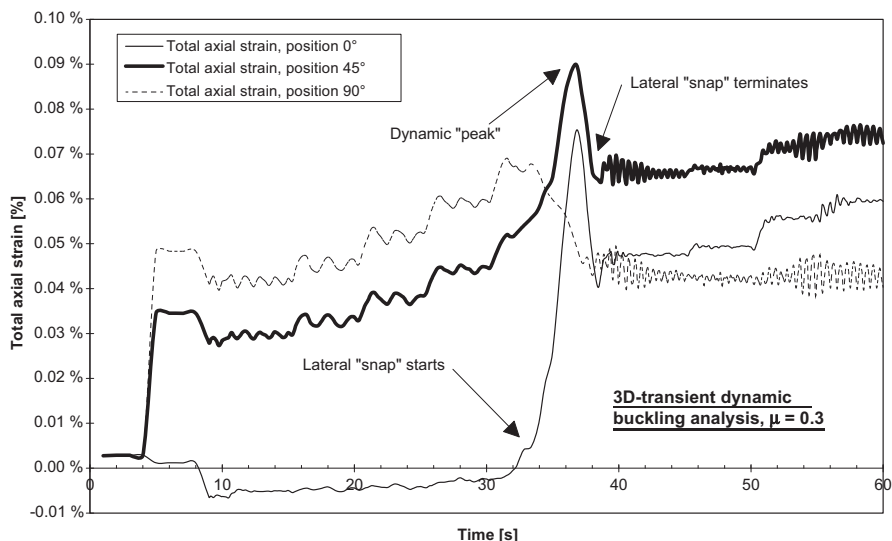
Figure 8.12 Total axial strain versus time.
Source: Nystrøm et al. [2].

Figure 8.12 shows the total axial strain from the 3D transient dynamic analysis at the buckle point plotted vs. time. At first, during heat up, the highest strains occur at the top of the pipe (Position 90°). However, as the pipeline lifted off the seabed for a certain distance, the horizontal plane interacts and a lateral "snap" buckle is initiated. The strain at Position 0° shows that, at time 32 s, a gradual change in the curvature is started, which peaks at 37 s. The maximum total axial strain of 0.09 % occurs at Position 45°, as a resultant of bending at Positions 0°and 90°.

As the snap movement continues, the strains decrease and eventually as the snap movement terminates at approximately 39 s, the maximum strain at Position 45° stabilizes at around 0.065% strain. Hence, the flowline has experienced a 35% higher total axial strain during the snap movement than in the postbuckled configuration.

The strain experienced during the dynamic snap is significantly higher than the postbuckled static result. As the previous dynamic analysis results show, the pipe buckles laterally in a continuous smooth manner, which is due to the inertia effects. When the buckled pipe reaches its maximum curvature, the kinetic energy continues to displace the pipe laterally away from the buckle point in a wave form. Although this energy wave dissipates relatively quickly, it causes some relaxation of the curvature at the buckle center. As a result, the strains reduce as the pipe approaches a stationary condition again.

8.   Cyclic In-Place Behavior During Shutdown Operations

Let us consider a pipeline subjected to cyclic temperature and internal pressure due to shutdown events, as described by Nystrøm et al. [2]. The cyclic capacity is defined as

the maximum differential loads of temperature and pressure between startup and shutdown at which the structure "shakes down" to an elastic state. Some concepts can be mentioned:

• Cyclic load leads to ductility exhaustion, causing fatigue and fracture.
• The pipeline remains intact, but the strains increase in each cycle until they are no longer acceptable.
• The strains in each cycle decrease until, eventually, the structure behavior is purely elastic. This is called *shakedown*.

The investigated flowline is assumed to be subjected to the following cyclic loads:

• 1 cyclic load during reeling on and off the lay vessel's drum.
• 1 cycle load during bending over the stinger and bending in the sag bend during installation phase.
• 100 cycles of planned and unplanned shutdowns in the lifetime.

It is assumed that the shutdown cycles are constant; that is, the same load range is used for the all load cycles. These shutdowns are conservatively assumed to occur when the content temperature goes from $130°C$ to ambient condition of $5°C$, that is, $\Delta T = 125°C$, and internal pressure goes from 370 bar to 0 bar. A pipeline on a 3D seabed surface is analyzed having both vertical and horizontal out of straightness. Internal pressure and temperature loads are applied up to full operational load. Thereafter, the internal pressure is reduced to 0 and the pipe wall temperature is gradually reduced to the ambient temperature. The corresponding total axial strains are shown in Figure 8.13 as a function of lateral displacement. The maximum tensile
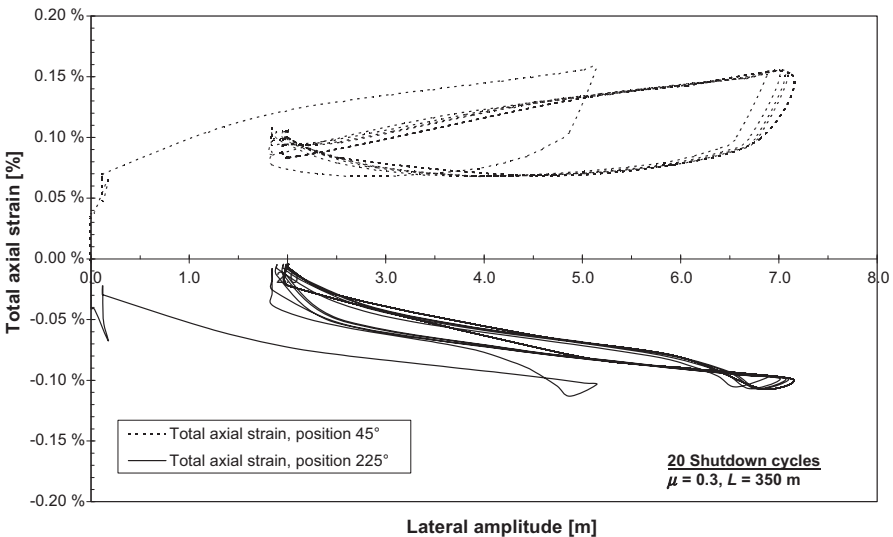
Figure 8.13 Total axial strain versus lateral displacement.
Source: Nystrøm et al. [2].

and compressive strains occur during the first cycle and shake down to +0.14% and –0.11%, respectively.

For more details about thermal expansion, global buckling, fatigue ,and facture of subsea pipelines, please refer to Chapters 9 to 12.

References

[1] Ose BA. A finite element model for in-situ behavior simulation of offshore pipelines on uneven seabed focusing on-bottom stability. Master's thesis, Stavanger University, Stavanger, Norway; 1998.

[2] Nystrøm P, Tørnes K, Bai Y, Damsleth P. Dynamic buckling and cyclic behavior of HP/ HT pipelines. Proc. of ISOPE'97, Honolulu; 1997.

[3] Tørnes K, Nystrøm P, NØ Kristiansen, Bai Y, Damsleth PA. Pipeline structural response to fishing gear pullover loads. Proc. of ISOPE'98, Montreal; 1998.

[4] Kristiansen NØ, Tørnes K, Nystrøm PR, Damsleth PA. Structural modeling of multi-span pipe configurations subjected to vortex induced vibrations. Proc. of ISOPE'98, Montreal; 1998.

[5] Simulia, ABAQUS. Version 6.12; 2012.

[6] Cook RD, Malkus DS, Plesha ME, Witt RJ. Concepts and applications of finite element analysis. John Wiley & Sons; 1989.

[7] Tørnes K, Nystrøm PR, Damlseth PA, Sortland H. The behavior of high pressure, high temperature flowlines on very uneven seabed. Proc. of ISOPE'97, Honolulu; 1997.

[8] ANSYS Inc. ANSYS, Version 5.5; 1998.

[9] Ose BA, Bai Y, Nystrøm PR, Damsleth PA. A finite element model for in-situ behavior of offshore pipelines on uneven seabed and its application to on-bottom stability. Proc. of ISOPE'99, Brest, France; 1999.

9 Thermal Expansion Design

Chapter Outline

1.   Introduction

High-Pressure and High-Temperature Pipelines

In recent years, more and more high-pressure and high-temperature oil-gas fields have been developed by using pipelines and risers to transmit oil/gas products. The term *high pressure and high temperature* (HPHT) was first introduced by the Department of

Table 9.1 Typical HPHT Projects Developed in the Gulf of Mexico

Project	Reservoir Pressure	Reservoir Temperature
Thunder Horse	15 ksi (1034 bar)	300°F (150°C)
Tubular Bells	20 ksi (1380 bar)	300°F (150°C)
Tahiti	15 ksi (1034 bar)	250°F (120°C)
Thunder Hawk	15 ksi (1034 bar)	250°F (120°C)

Trade Industry as "Where the undisturbed bottom hole temperature at the prospective reservoir depth is greater than 300°F (150°C) and the maximum anticipated pore pressure of any porous formation to be drilled through exceeds 10 ksi (689 bar)" [1]. Now the HPHT applications of 300°F and 10 ksi are common. The HPHT operation may be divided into three levels. Level I refers to wells with reservoir pressures up to 15 ksi (1034 bar) and temperatures up to 350°F (177°C). Some typical HPHT projects developed in the Gulf of Mexico in recent years are listed in Table 9.1. HPHT operating conditions to date have taken place under Level I conditions, as shown in Figure 9.1. Level II is the "extreme" HPHT operating conditions, which are characterized by the reservoir pressures of up to 20 ksi (1380 bar) or temperatures of up to 400°F (204°C). Level III is defined as the "ultra" HPHT operating conditions with temperatures of up to 500°F (260°C) or reservoir pressures of up to 30 ksi (2068 bar).

HPHT pipelines are increasing in deepwater areas such as West Africa and the Gulf of Mexico. In deep water, installation, flow assurance, thermal buckling, and management are critical issues for the HPHT pipeline design due to the severe conditions, such as higher water depth, high pressure, high temperature of product,
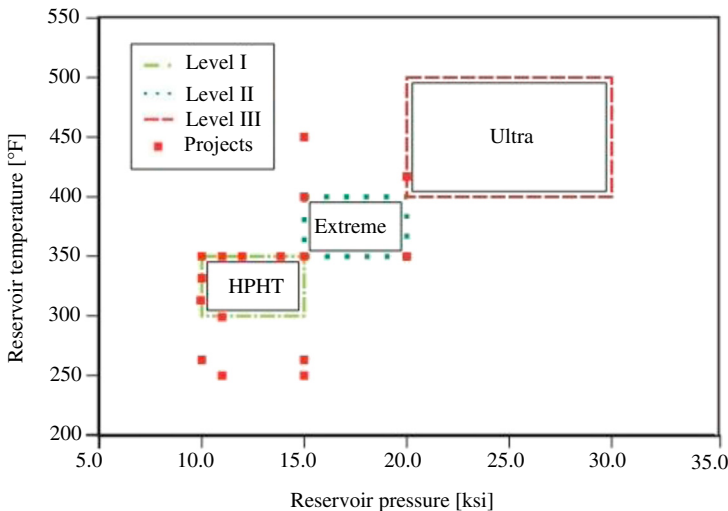
Figure 9.1 Operating temperature and pressure in HPHT projects.
Source: Maldonado et al. [1]. (For color version of this figure, the reader is referred to the online version of this book.)

and colder ambient condition [2]. HPHT pipelines laid on the seabed are susceptible to lateral buckling, resulting in lateral deflections that can lead to the pipeline failures due to an excessive strain at the apex of the buckles, local buckling, and fatigue damage. The lateral buckling is caused by a high compressive axial force building up as the pipeline tries to expand thermally but is restrained by axial soil resistance between the pipeline and the seabed.

Thermal Expansion

A pipeline system can be a single-pipe pipeline system, pipe in pipe (PIP), or a bundle system. Normally, the term *subsea flowline* is used to describe the subsea pipeline carrying oil and gas products from a wellhead to a riser base connected to the processing facilities (for example, a platform or a FPSO) with a riser. The subsea pipeline from processing facilities to shore is called *export pipeline*. The temperature and pressure of production in flowlines are normally higher than those of the ambient condition, so thermal expansion of flowline may be induced. Flowline axial walking, upheaval buckling, and lateral buckling due to thermal expansion and cyclic thermal loads may take place in these flowlines. Therefore, the thermal expansion of pipeline is an important issue in the design and operation of the subsea system. The thermal expansion of the pipeline depends on the temperature and pressure profiles along the pipeline, the pipeline submerged weight, and the axial friction force. In general, the maximum pipeline end expansion is calculated for the lower bound axial pipeline-soil friction coefficient; the highest pipeline axial stresses are derived from the upper bound axial pipeline-soil friction coefficient when there are global buckles. The increase in axial resistance from backfill along the route should also be accounted for in the calculation of thermal expansion. Thermal expansion analyses usually involve the following issues:

- Pipe-soil interactions.
- Tie-in design.
- Lateral and upheaval buckling (or global buckling) assessments.
- Axial walking and fatigue analysis.
- Free-span assessments.
- Pipeline crossing design and the others.

In this chapter, the basis of thermal expansion analysis is outlined first, then the calculation of pipeline displacements and expansion forces for several typical pipeline situations are summarized. Pipeline axial walking, lateral buckling, and upheaval buckling are discussed in Chapters 10 and 11.

2.   Pipeline Strains

Introduction

When a pipeline is subjected to a high internal pressure and temperature in hydrotest and operating conditions, it has a tendency to expand longitudinally due to the

pressure and temperature. However, the pipeline is restrained by the seabed friction when any expansion movement takes place. For a pipeline with free ends, the effective axial force is zero at the ends and gradually increases due to the frictional restraint of the seabed. The expansion stops when the force equilibrium is reached between the expansion forces and the seabed soil resistance. The point where pipe expansion stops is known as the *virtual anchor point* (VAP), and the expansion of pipeline takes place between the VAP and the pipeline end.

The axial strains of pipeline may be created by the pipe expansion. The pipeline equilibrium is achieved at the VAP, where the sum of all strain contributions is equal to the strain of fully restrained pipe section, which is zero when the pipeline is installed without residual lay tension and the internal pressure is the same as the external pressure of pipeline, for example, the case in which the land pipeline installation is approximately this condition.

The effects of pressure, temperature, and seabed soil friction on pipeline expansion are addressed in terms of their associated strain contributions in the following sections, in which the elastic behavior of the pipe material and the axial forces being proportional to the axial stress developed in the material are assumed.

$$F_{\text{w}} = \sigma_{\text{l}} A_{\text{s}} \quad\quad\quad [9.1]$$

where

F_{w} = true axial wall force at the pipe wall cross section
σ_{l} = longitudinal (axial) stress at the pipe wall
A_{s} = pipe cross-sectional area

Pressure Strain

The longitudinal strain derived from the pressure load comprises two components: the capped-end effect strain caused by the longitudinal pressure difference in the capped end and the Poisson's ratio effect strain due to the contributions of the hoop and radial stresses.

The longitudinal strain due to the capped-end effect is a constant along the entire length of a single pipeline, which is a reform of Eq. [9.1]:

$$\varepsilon_{\text{end}} = \frac{p_{\text{i}} A_{\text{i}} - p_{\text{e}} A_{\text{e}}}{EA_{\text{s}}} \quad\quad\quad [9.2]$$

where

ε_{end} = longitudinal strain due to the capped-end effect
p_{i} = internal pressure of the pipe
p_{e} = external pressure of the pipe
A_{i} = internal bore area of the pipe; $A_{\text{i}} = \pi(D - 2t)^2/4$
A_{e} = external area of the pipe; $A_{\text{e}} = \pi(D^2/4)$
A_{s} = cross-sectional area of the pipe; $A_{\text{s}} = A_{\text{e}} - A_{\text{i}}$
D = outer diameter (OD) of the pipe
t = wall thickness of the pipe

The sum of hoop and radial stresses is always constant at different radial locations of the pipe section, according to the Lame equation, shown later in Eq. [9.12], whether the pipeline has a thin or thick wall. The longitudinal strain due to the Poisson's ratio effects can be expressed as follows:

$$\varepsilon_{\text{Poisson}} = -\frac{v}{E}(\sigma_{\text{h}} + \sigma_{\text{r}}) = -\frac{2v}{E}\left(\frac{p_{\text{i}}A_{\text{i}} - p_{\text{e}}A_{\text{e}}}{A_{\text{s}}}\right) \tag{9.3}$$

where

$\varepsilon_{\text{Poisson}}$ = Poisson's ratio effect strain;
v = Poisson's ratio.

The longitudinal strain due to the capped-end effect is opposite to the longitudinal strain resulting from the Poisson's ratio effects of hoop and radial strains. The total longitudinal strain derived from the pressure load, including the capped-end and Poisson's ratio effects, is expressed as

$$\varepsilon_{\text{P}} = \varepsilon_{\text{end}} + \varepsilon_{\text{Poisson}} = \frac{1 - 2v}{E}\left(\frac{p_{\text{i}}A_{\text{i}} - p_{\text{e}}A_{\text{e}}}{A_{\text{s}}}\right) \tag{9.4}$$

Thermal Strain

The variation of temperature in an unstrained pipeline from its initial condition causes a longitudinal strain, which can be expressed as

$$\varepsilon_{\text{T}} = \alpha \Delta T \tag{9.5}$$

where

ε_{T} = longitudinal thermal strain
α = thermal expansion coefficient of pipe material
ΔT = temperature difference between the considered condition and the initial condition

Frictional Strain

When a pipe moves, a frictional resistance is developed between the pipe and seabed, tending to oppose the movement. This resistance is a passive effect and activated only as a result of the pipe movement relative to the seabed. The effect of frictional resistance is to build up a negative strain in the pipe opposing the effects of the pressure and temperature strain components. The friction strain is expressed in different equations for unburied pipeline and buried pipeline.

For Unburied Pipeline

For a long unburied pipeline with a free end (when a pipeline end is connected with an expansion loop, the pipeline end resistance can be ignored and assumed to be zero),

the frictional strain linearly increases with the distance from the free end, as expressed by the following relationship:

$$\varepsilon_f = -\frac{\mu_a w x}{A_s E} \qquad [9.6]$$

where

ε_f = friction strain
μ_a = longitudinal (axial) friction coefficient between pipe and seabed
w = weight per unit length of pipe (submerged weight for a subsea pipeline)
x = distance from the free end to the evaluated point

For Buried Pipeline

A buried pipe, surrounded by soil, is subjected to an increased friction resistance due to soil pressure effects acting around the circumference of pipeline. This tends to reduce the overall expansion movement. The axial soil force per unit length of buried pipeline can be expressed as [3],[4]:

$$F_b = \pi D_o \alpha_a C + \pi D_o H \gamma_s (1 + K_o) \tan(\delta)/2 \qquad [9.7]$$

where

F_b = axial soil resistance per unit length of buried pipeline
α_a = adhesion factor [1]
C = soil cohesion representative of the soil backfill
H = depth of pipeline centerline
γ_s = submerged weight of soil per unit volume
K_o = coefficient of pressure at rest
δ = internal angle of friction between pipe and soil

According to Eq. [9.1], the friction strain for a buried pipeline can be expressed as follows:

$$\varepsilon_f = -\frac{F_b x}{A_s E} = -\frac{\mu_a' w x}{A_s E} \qquad [9.8]$$

where μ_a' is the equivalent axial Coulomb friction factor for a buried pipeline, a ratio of axial soil resistance to the pipeline weight.

Total Pipeline Strain

The resultant total strain of pipeline, ε, is given by the following expression:

$$\varepsilon = \varepsilon_P + \varepsilon_T + \varepsilon_f \qquad [9.9]$$
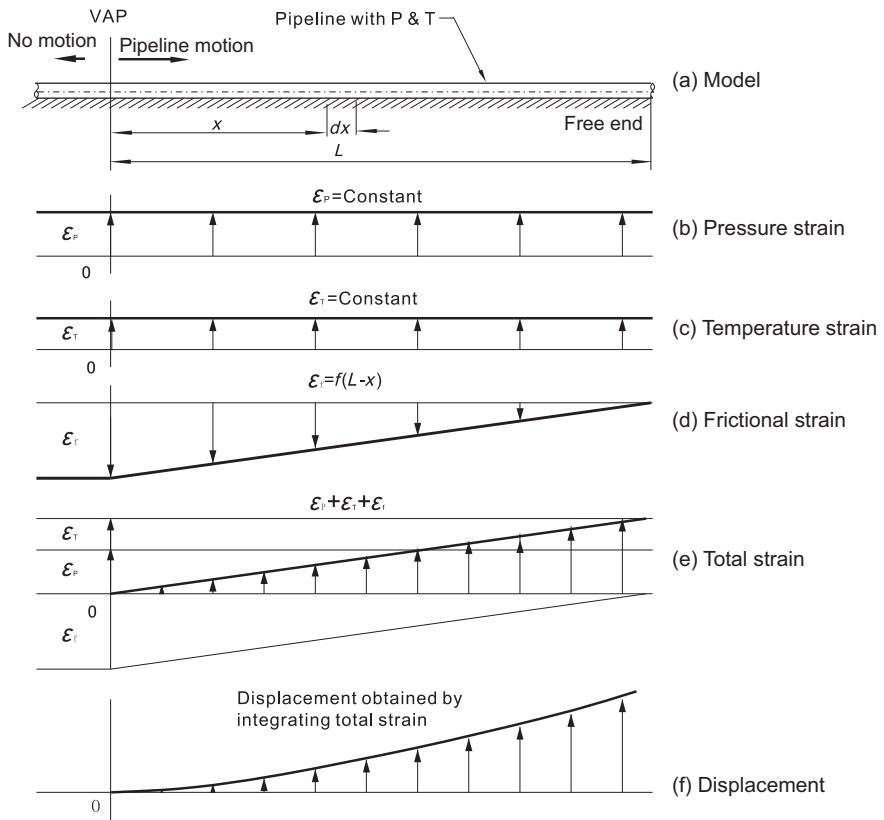
Figure 9.2 Distributions of strains and displacements along a long pipeline.

The diagrammatic representation of the individual strain components for a pipeline with zero initial strain along the pipe is shown in Figure 9.2. Constant internal and external pressures and constant temperature are applied along the pipeline with a constant cross section. The pressure strain and thermal strain are constant positive values along the pipeline, while the friction strain decreases linearly from zero at the free end of pipeline. The total strain is zero at the virtual anchor point, where the pipe expansion does not occur.

3. Pipeline Stresses

Pressure Effect

Pressures at internal and external surfaces of a pipe produce stresses in the wall of the pipe. Figure 9.3 illustrates the definitions for stress components of longitudinal stress, σ_l; hoop stress, σ_h; and radial stress, σ_r, of a pipe.

Longitudinal stress, σ_L
Hoop stress, σ_H
Radial stress, σ_R
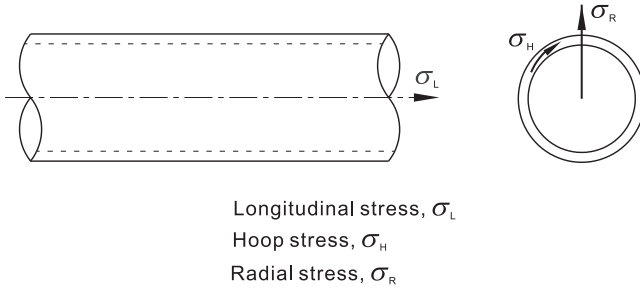
Figure 9.3 Definitions of pipe wall stress components.

Stress Components of Thin-Walled Pipe

There are three principal stresses at any point in the three mutually perpendicular directions along which there is no shear stress. The axial/longitudinal stress, circumferential/hoop's stress, and radial stress for a thin-walled pipe are a set of principal stresses if there is no shear stress.

The hoop stress for a thin-walled pipe can be obtained from the force balance, assuming the hoop stress to be constant in the radial direction:

$$\sigma_{h,thin} = \frac{p_i D_i - p_e D_e}{2t} \tag{9.10}$$

The radial stress, σ_r, is a compressive stress, varying across the pipe wall from a value equal to the internal pressure, p_i, on the inside of the pipe wall to a value equal to the external pressure, p_e, on the outside of the pipe. The magnitude of the radial stress, σ_r, is usually very small compared with the longitudinal, σ_l, and hoop stresses, σ_h; and the radial stress is negligible.

When there is shear stress, the principal stresses may be calculated approximately from these three stresses (σ_r, σ_h, and σ_l) of the pipeline. If the principal stresses are designated as σ_1 (maximum), σ_2, and σ_3 (minimum), then, using Mohr's circle, the two principal stresses are expressed as follows:

$$\sigma_1 = \frac{\sigma_h + \sigma_l}{2} + \sqrt{\frac{(\sigma_h - \sigma_l)^2}{4} + \tau^2}$$

$$\sigma_2 = \frac{\sigma_h + \sigma_l}{2} - \sqrt{\frac{(\sigma_h - \sigma_l)^2}{4} + \tau^2} \tag{9.11}$$

The third principal stress (minimum, i.e., σ_3) is zero.

Stress Components of Thick-Walled Pipe

Figure 9.4 illustrates a model of thick-walled pipe with a capped end. The stress components of the thick-walled pipe are expressed by the following equations:

$$\sigma_r = \frac{p_i D_i^2 - p_e D_e^2}{D_e^2 - D_i^2} - \frac{D_i^2 D_e^2}{D^2 \left(D_e^2 - D_i^2\right)} (p_i - p_e)$$

$$\sigma_h = \frac{p_i D_i^2 - p_e D_e^2}{D_e^2 - D_i^2} + \frac{D_i^2 D_e^2}{D^2 \left(D_e^2 - D_i^2\right)} (p_i - p_e)$$

$$\sigma_l = \frac{p_i D_i^2 - p_e D_e^2}{D_e^2 - D_i^2} + \frac{4 F_{ext}}{\pi \left(D_e^2 - D_i^2\right)} \qquad [9.12]$$

where

D = diameter in which hoop stress or radial stress is calculated
D_e = external pipe diameter
D_i = internal pipe diameter
F_{ext} = external force on the capped end
p_e = external pressure of the pipe
p_i = internal pressure of the pipe

The hoop stress, σ_h, varies across the pipe wall from a maximum value at the inner surface to a minimum value at the outer surface of the pipe when the internal pressure
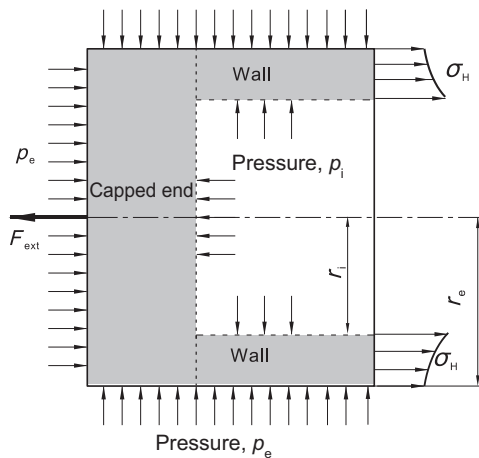
Figure 9.4 Capped end of a thick-walled pipeline.

is higher than the external pressure, as expressed in the hoop stress of Eq. [9.12]. The equation for the hoop stress is also called the *Lame equation*:

$$\sigma_r + \sigma_h = 2\frac{p_i D_i^2 - p_e D_e^2}{D_e^2 - D_i^2} = \text{constant} \qquad [9.13]$$

This means that a sum of hoop and radial stresses is a constant without changing with diameter, D, throughout the whole pipe cross section.

Figure 9.4 also illustrates the force balances in axial direction of the pipe with end cap. F_{ext} can be an interaction force between the pipe and other structures. Based on the definition of longitudinal stress of Eq. [9.12], the interaction force from external structures is expressed as

$$F_{ext} = \sigma_l A_s - p_i A_i + p_e A_e \qquad [9.14]$$

This external force, from such as PLET, anchor, stress joint, or chain, in subsea engineering, is also designated *effective axial force* at the end cap, because the pipeline external pressure of subsea pipeline may not be ignored, compared to that of land pipeline. If the effective axial force is expressed with S, then,

$$S = F_w - p_i A_i + p_e A_e$$

where the first term, F_w, is the true axial wall force, which is defined in Eq. [9.1]. The longitudinal stress, σ_h, is also expressed in the following equation:

$$\sigma_l = F_w / A_s = (S + p_i A_i - p_e A_e) / A_s \qquad [9.15]$$

Von Mises Stress (Equivalent Tensile Stress)

Von Mises found that, even though none of the principal stresses exceeds the material yield stress, yielding is still possible because of the combination of the stresses. The Von Mises criteria is a formula for combining the three principal stresses into an equivalent stress, and the equivalent stress is then compared to the yield stress of the material to judge the failure condition of the material. The equivalent stress is often called the *Von Mises Stress*, as a shorthand description. It is not really a stress but a number used as an index.

Von Mises criteria are among the most commonly used criteria for checking yield condition in the pipeline engineering:

$$\sigma_e = \sqrt{\frac{1}{2}\left[(\sigma_1 - \sigma_2)^2 + (\sigma_2 - \sigma_3)^2 + (\sigma_3 - \sigma_1)^2\right]} \qquad [9.16]$$

where σ_1, σ_2, and σ_3 are the principal stresses. In terms of the stress components in the rectangular coordinate system, the von Mises stress of a pipe can be written as

$$\sigma_e = \sqrt{\frac{1}{2}\left[(\sigma_1 - \sigma_h)^2 + (\sigma_h - \sigma_r)^2 + (\sigma_r - \sigma_1)^2\right] + 3\left(\tau_{lh}^2 + \tau_{lr}^2 + \tau_{hr}^2\right)} \qquad [9.17]$$

where, τ_{lh}, τ_{lr}, and τ_{hr} are the shear stresses. For a thin-walled pipe, neglecting small shear and radial stresses, the von Mises stress is given by

$$\sigma_e = \sqrt{\sigma_h^2 + \sigma_l^2 - \sigma_1\sigma_h + 3\tau^2} \qquad [9.18]$$

The shear stress τ is τ_{hr} due to the torsion in the pipe cross section.

Temperature Effect

A change of temperature produces a change of strain in the pipeline. When a pipeline moves in the axial direction, the pipeline is considered unrestrained. If the unrestrained pipeline is fully mobilized, the thermal stress, $\sigma_{T,U}$, of the unrestrained pipeline is zero:

$$\sigma_{T,U} = 0 \qquad [9.19]$$

However, when a pipeline is longitudinally fully restrained, the resultant longitudinal strain is zero, and the temperature expansion produces a compressive longitudinal stress in the pipe wall instead of strain:

$$\sigma_{T,R} = -E\alpha\Delta T \qquad [9.20]$$

where $\sigma_{T,R}$ is the thermal stress of a fully restrained pipe.

Stresses of the Pipeline

When the pipeline is on the seabed, the soil frictional resistance restrains the pipeline movement due to pressure and temperature, the pipeline is called restrained pipeline. The virtual anchored pipeline section is a fully restrained pipeline. In some pipeline routines, mechanical restraint may be designed to prevent the expansion of the pipeline. The restraint may be provided by a specially designed anchor, or by an adjacent structure to which the pipeline is attached. Because the pipeline is restrained by the anchor without movement, it is unable to activate the soil frictional resistance. The restraining structure or anchor therefore is subjected to the full expansion force generated by the pressure and temperature effects created within the pipeline.

Unrestrained Pipeline

Figure 9.5 shows a constant cross section of unrestrained pipeline fitted with blind flanges at the end under constant internal pressure, p_i; external pressure, p_e; and constant temperature, T, along the pipeline. The restraint force, F_{ext}, in the blind flange (capped end) is a function of wall force and fluid force, as expressed in Eq. [9.14]:

$$F_{ext} = F_w - F_f \qquad [9.21]$$

The fluid force is due to the fluid pressure acting on the end caps and can be expressed as follows:

$$F_f = p_i A_i - p_e A_e$$

The restraint force (anchor force) is zero for unrestrained pipeline:

$$F_{ext} = 0$$

The wall force at the capped end is due to the internal and external pressures:

$$F_w = p_i A_i - p_e A_e$$

When an unrestrained pipeline expands due to a temperature increase, there is a strain change due to the temperature effect but with no stress change due to the temperature effect. The wall force along the pipeline is constant because no restraint force is acting along the pipe and the longitudinal stress of unrestrained pipeline is

$$\sigma_{l,U} = \frac{p_i A_i - p_e A_e}{A_s} \qquad [9.22]$$

The hoop stress and radial stress are calculated from Eq. [9.12].
  The end expansion movement at the free end is

$$\Delta = (\varepsilon_P + \varepsilon_T)L \qquad [9.23]$$
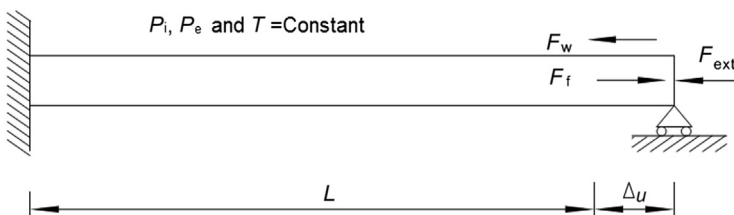
Figure 9.5 Unrestrained pipeline with constant pressure and temperature.

Fully Restrained Pipeline

Figure 9.6 shows a constant cross section of restrained pipeline with a blind flange at the end. The restraint force at the pipeline end for the restrained pipeline is,

$$F_{\text{ext}} = -E\alpha(T - T_{\text{a}})A_{\text{s}} - (1 - 2\nu)(p_{\text{i}}A_{\text{i}} - p_{\text{e}}A_{\text{e}})$$

The true wall force at the pipeline end is

$$F_{\text{w}} = \left[\frac{2\nu(p_{\text{i}}A_{\text{i}} - p_{\text{e}}A_{\text{e}})}{A_{\text{s}}} - E\alpha(T - T_{\text{a}})\right]A_{\text{s}}$$

The hoop and radial stresses of a restrained pipeline due to internal pressure remain the same as those of the unrestrained pipeline, which are calculated from Eq. [9.12], because the restraint condition in the radial and tangential directions remain unchanged.

The longitudinal stress changes as a result of the end restraint. The longitudinal forces are the result of fluid pressure acting on the end cap, which takes a load path directly into the end restraint. Therefore, the end cap effect of internal and external pressures does not give the pipeline longitudinal stresses for a fully restrained pipeline. The longitudinal stress due to the end cap is zero. The longitudinal pressure stress in the pipe wall of the restrained pipe is due to only the Poisson's ratio effect of hoop and radial stresses, which is expressed in the following equation:

$$\sigma_{\text{l,Poisson}} = \frac{2\nu(p_{\text{i}}A_{\text{i}} - p_{\text{e}}A_{\text{e}})}{A_{\text{s}}} \qquad [9.24]$$

Therefore, the combined longitudinal stress of the pipe wall in a fully restrained or virtual anchored pipe section, $\sigma_{\text{l,R}}$, is the sum of the temperature and Poisson's ratio pressure stress components as follows:

$$\sigma_{\text{l,R}} = \frac{2\nu(p_{\text{i}}A_{\text{i}} - p_{\text{e}}A_{\text{e}})}{A_{\text{s}}} - E\alpha\Delta T \qquad [9.25]$$
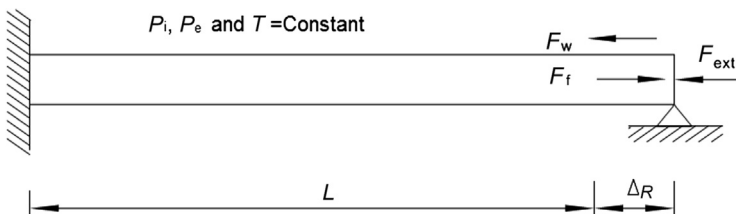
Figure 9.6 Restrained pipeline with constant pressure and temperature.

For a case of a friction restrained pipeline with a free end, the longitudinal stress of the pipe wall over the transition length is expressed as

$$\sigma_{l,R}(x) = \frac{p_i A_i - p_e A_e}{A_s} - \frac{\mu_a w x}{A_s} \tag{9.26}$$

In this case, the longitudinal stress at the free end is the same as that of unrestrained pipeline defined in Eq. [9.22]. With the increase of x, the distance from the free end, the longitudinal stress decreases, and it becomes the longitudinal stress defined in Eq. [9.25] when x is the distance from the free end to the virtual anchor point.

4. Effective Axial Force of the Pipeline

Sparks [5] introduced the term *effective axial force* to account for the effect of the internal and external pressures, and its definition is expressed in Eq. [9.14]. The background of the effective axial force and its applications in subsea engineering are summarized by Fyrileiv and Collberg [6]. The effective axial force governs the structural response of the pipeline in an overall perspective, influencing lateral buckling, upheaval buckling, anchor forces, end terminations, and natural frequencies of free spans. However, when it comes to local effects like local buckling, steel stresses, and yielding, the true axial force governs. The submerged weight of a subsea pipeline should be applied when the effective axial force in the pipeline is used.

Figure 9.7 illustrates a pipeline configuration and horizontal loads during a conventional S-lay installation. The equilibrium of horizontal forces requires that the installation residual lay tension, $F_{residual}$, at the pipeline end on the seabed after installation is equal to the barge horizontal tension, F_{pull}. When the pipeline is just
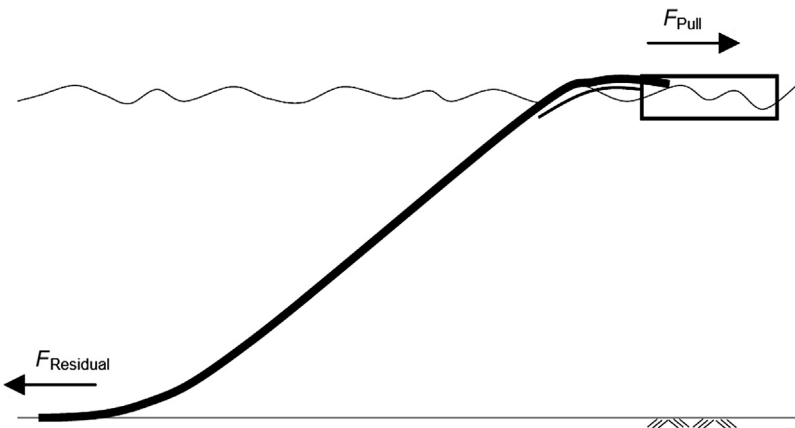
Figure 9.7 Pipeline horizontal loads in S-lay installation.

laid down on the seabed, the residual tension is the effective tension of pipeline at the end. Following the definition, the residual tension can be expressed as follows:

$$F_{\text{residual}} = F_{\text{w}} - p_{\text{i,install}}A_{\text{i}} + p_{\text{e}}A_{\text{e}} \qquad [9.27]$$

where F_{w} is the true axial wall force of pipeline on the seabed during installation, p_{e} is the external pressure of pipe, and $p_{\text{i,install}}$ is the internal pressure of pipe during installation. The true axial wall force in the installation condition becomes

$$F_{\text{w}} = F_{\text{residual}} + p_{\text{i,install}}A_{\text{i}} - p_{\text{e}}A_{\text{e}}$$

After the pipeline is installed and restrained on the seabed, the active loads causing effective axial force change are the internal pressure and temperature of the pipe in the operating condition. For the restrained pipeline, there is no axial movement when the internal pressure or temperature is increased, therefore, the axial strain does not change. The true axial wall force becomes compressive due to the thermal expansion and tension from the hoop stress and the Poisson's ratio effect if the pipeline is fully restrained:

$$F_{\text{w}} = F_{\text{residual}} + p_{\text{i,install}}\, A_{\text{i}} - p_{\text{e}}\, A_{\text{e}} + 2v\big(p_{\text{i}} - p_{\text{i,install}}\big)A_{\text{i}} - EA_{\text{s}}\alpha(T_{\text{i}} - T_{\text{install}})$$
$$[9.28]$$

From the definition, the following equation of the effective axial force is deducted for a fully restrained pipeline:

$$\begin{aligned}
S_0 &= F_{\text{w}} - p_{\text{i}}\, A_{\text{i}} + p_{\text{e}}A_{\text{e}} \\
&= F_{\text{residual}} - (1 - 2v)\big(p_{\text{i}} - p_{\text{i,install}}\big)A_{\text{i}} - EA_{\text{s}}\alpha(T_{\text{i}} - T_{\text{install}}) \qquad [9.29] \\
&= F_{\text{residual}} - (1 - 2v)(\Delta p_{\text{i}})A_{\text{i}} - EA_{\text{s}}\alpha(\Delta T_{\text{i}})
\end{aligned}$$

where

S_0 = effective axial force of a fully restrained pipeline
F_{residual} = residual lay tension or effective lay tension
Δp_{i} = internal pressure difference relative to laying condition
ΔT_{i} = temperature difference of pipeline relative to laying condition

Figure 9.8 illustrates the effective axial force distributions along a long subsea pipeline in the installation, hydrotest, and operating conditions, which depend on axial friction, submerged weight, length of the pipeline, end condition, lay tension, and pressure and temperature distributions along the pipeline in different conditions. The tension is expressed as a positive value, and the compression is expressed as a negative value in the figure.

When the pipeline is laid down on the seabed, no force is transferred between the soil and pipe, the effective axial force is equal to the residual lay tension in the pipeline. As shown in Figure 9.8, the whole pipeline includes the fully restrained
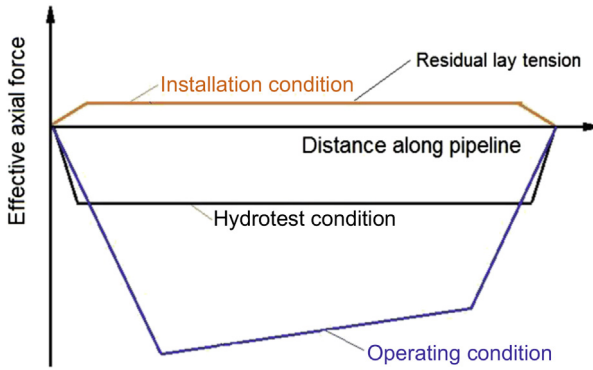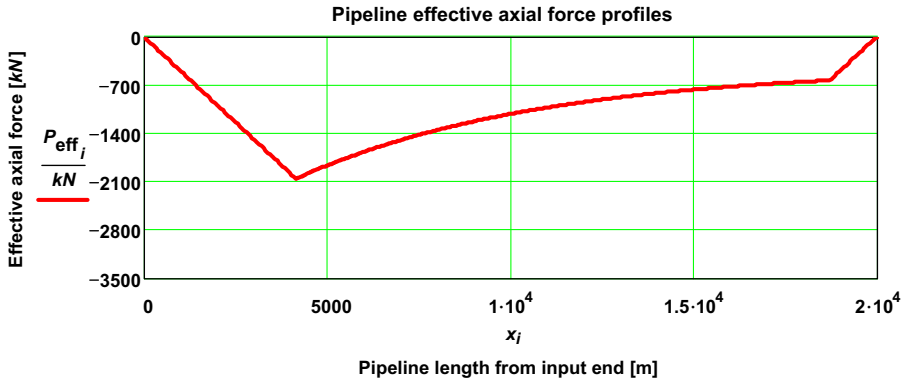
Figure 9.8 Effective axial force distributions along pipeline with no buckles. (For color version of this figure, the reader is referred to the online version of this book.)

pipeline section in the middle of pipeline and the unrestrained pipeline sections at both pipeline ends. The equations of effective axial force in the installation condition are expressed as follows:

$$S_{in,install} = \begin{cases} \mu_a w_{sub,install} x + F_{ext,in} & \text{for spool or riser connection} \\ F_{residual} & \text{for a fixed end} \end{cases}$$

$$S_{out,install} = \begin{cases} \mu_a w_{sub,install}(L - x) + F_{ext,out} & \text{for spool or riser connection} \\ F_{residual} & \text{for a fixed end} \end{cases}$$

$$S_{install} = \min\left(S_{in,install}, \ F_{residual}, \ S_{out,install}\right) \qquad [9.30]$$

where, $S_{in,stall}$, $S_{out,install}$, and $S_{install}$ are the effective axial forces of the inlet unrestrained pipe section, the outlet unrestrained pipe section, and the whole pipeline section, respectively, and x is the pipeline length from the inlet end.

The equations of effective axial force in the hydrotest or operating condition are expressed as follows:

$$S_{in,ope} = \begin{cases} -\mu_a w_{sub,ope} x + F_{ext,in} & \text{for spool or riser connection} \\ S_0 & \text{for a fixed end} \end{cases}$$

$$S_{out,ope} = \begin{cases} -\mu_a w_{sub,ope}(L - x) + F_{ext,out} & \text{for spool or riser connection} \\ S_0 & \text{for a fixed end} \end{cases}$$

$$S_{ope} = \max\left(S_{in,ope}, \ S_0, \ S_{out,ope}\right) \qquad [9.31]$$

5. Expansion of a Single-Pipe Pipeline

Introduction

The relative displacement of the pipeline can be calculated by integrating the total strain along the pipeline if the strain state of a pipeline is determined [7, 8, 9]. The calculations of the pipe end expansion for different pipeline problems are detailed in the following sections.

The expansion behavior of a pipeline can be determined in the following procedure:

• Determine the strain state of the pipeline.
• Determine the transition length of pipeline from the end to the anchor point.
• Integrate the strain over the transition length to obtain the total end expansion.

Axial Strain and End Expansion

Installation Condition

The axial strain of a fully restrained section in the installation condition can be expressed as follows:

$$\varepsilon_{l,install,R} = \frac{1}{E}\left[\sigma_{l,install} - \nu\left(\sigma_{h,install} + \sigma_{r,install}\right)\right]$$

The stresses are expressed in the following equations:

$$\sigma_{l,install} = \frac{F_{w,install}}{A_s} = \frac{F_{residual} + p_{i,install}A_i - p_eA_e}{A_s}$$

and

$$\sigma_{h,install} + \sigma_{r,install} = 2\left(\frac{p_{i,install}A_i - p_eA_e}{A_s}\right)$$

Therefore, the equation of axial strain for the fully restrained pipe section is rewritten as,

$$\varepsilon_{l,install,R} = \frac{1}{EA_s}\left[F_{residual} + (1 - 2\nu)\left(p_{i,install}A_i - p_eA_e\right)\right] \qquad [9.32]$$

The pipeline is disconnected from the installation pile after it is laid on the seabed, only a small external tension from PLET or spool, F_{ext}, acts at the pipeline end. The axial strain of the non-fully-restrained pipe section becomes

$$\varepsilon_{l,install,U} = \frac{1}{EA_s}\left[F_{ext} + (1 - 2\nu)\left(p_{i,install}A_i - p_eA_e\right)\right] + \frac{\mu_a w_{s,install}x}{EA_s} \qquad [9.33]$$

where x is the length from the pipeline end to the evaluated location. The second term of this equation, the friction strain, is positive if the first term is negative (the pipeline is contracted) for a subsea pipeline. The axial strain of the non-fully-restrained pipe section at the virtual anchor point, in which the fully restrained section connects the non-fully-restrained section, is equal to the axial strain of the fully restrained section, where no movement of pipeline occurs. The length of the non-fully-restrained pipe section in the installation condition is expressed as

$$L_{install} = \frac{F_{residual} - F_{ext}}{\mu_a w_{s,install}} \qquad [9.34]$$

The pipe expansion of the middle fully restrained pipeline section, Δ_R, is given as follows:

$$\Delta_R = \int_0^{L_R} \varepsilon_{l,install,R} dx = \varepsilon_{l,install,R} L_R$$

where L_R is the length of the restrained pipeline section. For a subsea pipeline, the first term of Eq. [9.32] is positive and the second term is negative. The pipeline is contracted when the external pressure is high enough that Δ_R has a negative value; otherwise, the pipeline is expanded when the pipeline is installed on the seabed.

The expansion of non-fully-restrained pipeline at the pipeline end, Δ_{end}, is given as

$$\Delta_{end} = \int_0^{L_{install}} \varepsilon_{l,install,U} dx = \left[\varepsilon_{l,install,R} - \frac{\mu_a w_{s,install} L_{install}}{2EA_s} \right] L_{install} \qquad [9.35]$$

The first term of the equation is the length change of the non-fully-restrained pipeline under the residual tension, which is caused by external hydrostatic pressure and lay tension just prior to the pipeline reaching the seabed. If the expansion of the pipeline is calculated based on the condition that the pipeline is just prior to reaching the seabed, the first term is erased and of no interest afterward. Therefore, in performing the expansion calculation in the hydrotest and operating conditions, the effect of hydrostatic pressure and lay tension on the expansion of the pipeline is not included:

$$\Delta'_{end} = \int_0^{L_{install}} \left(\varepsilon_{l,install,U} - \varepsilon_{l,install,R} \right) dx$$

$$= \int_0^{L_{install}} \left(\frac{1}{EA_s} [F_{ext} - F_{residual}] + \frac{\mu_a w_{s,install} x}{EA_s} \right) dx \qquad [9.36]$$

$$= -\frac{\mu_a w_{s,install} L_{install}^2}{2EA_s} = -\frac{(F_{residual} - F_{ext})^2}{2EA_s \mu_a w_{s,install}}$$

Operating Condition

The axial strain of the fully restrained pipeline section in hydrotest or operating conditions is the same as that in the installation condition due to no pipe movement in the fully restrained section after the pipeline is installed. It is expressed as follows:

$$\varepsilon_{\text{l,ope,R}} = \frac{1}{EA_s}\left[F_{\text{residual}} + (1 - 2v)\left(p_{\text{i,install}}A_i - p_e A_e\right)\right] \qquad [9.37]$$

The axial strain of the unrestrained pipeline section is expressed as follows:

$$\varepsilon_{\text{l,ope,U}} = \frac{1}{EA_s}\left[F_{\text{ext}} + (1 - 2v)\left(p_{\text{i,ope}}A_i - p_e A_e\right)\right]$$

$$+ \alpha(T_i - T_{\text{install}}) - \frac{\mu_a w_{\text{s,ope}}x}{EA_s} \qquad [9.38]$$

The third term of this equation, the friction strain, is negative because the first two terms are positive and the pipeline is expanded in the operating condition. The axial strain of the unrestrained pipe section at the virtual anchor point is equal to that of the fully restrained section:

$$F_{\text{ext}} + (1 - 2v)\left(p_{\text{i,ope}}A_i - p_e A_e\right) + EA_s\alpha(T_i - T_{\text{install}}) - \mu_A w_{\text{s,ope}}L_{\text{ope}}$$

$$= F_{\text{residual}} + (1 - 2v)\left(p_{\text{i,install}}A_i - p_e A_e\right)$$

The length of the unrestrained pipe section in the hydrotest or operating condition is expressed as

$$L_{\text{ope}} = \frac{F_{\text{ext}} - F_{\text{residual}} + (1 - 2v)\left(p_{\text{i,ope}} - p_{\text{i,install}}\right)A_i + EA_s\alpha(T_i - T_{\text{install}})}{\mu_a w_{\text{s,ope}}}$$

$$= \frac{F_{\text{ext}} - S_0}{\mu_a w_{\text{s,ope}}} \qquad [9.39]$$

or

$$S_0 = F_{\text{ext}} - \mu_a w_{\text{s,ope}}L_{\text{ope}}$$

The expansion of unrestrained pipeline at the pipeline end in the operating condition, $\Delta_{\text{end,ope}}$, is given as follows:

$$\Delta_{\text{end,ope}} = \int_0^{L_{\text{ope}}} \varepsilon_{\text{l,ope,U}}dx = \left[\varepsilon_{\text{l,install,R}} + \frac{\mu_a w_{\text{s,ope}}L_{\text{ope}}}{2EA_s}\right]L_{\text{ope}} \qquad [9.40]$$

The end expansion of the unrestrained pipeline section in the operating condition based on the pipeline with a residual tension in the installation condition is expressed as

$$\Delta'_{\text{end,ope}} = \frac{\mu_a w_{s,\text{ope}} L^2_{\text{ope}}}{2EA_s} = \frac{(F_{\text{ext}} - S_0)^2}{2EA_s \mu_a w_{s,\text{ope}}} \qquad [9.41]$$

Equation [9.40] for the end expansion of unrestrained pipeline section is used for both subsea pipeline and land pipelines. The difference of $\varepsilon_{1,\text{install,R}}$ between the subsea pipeline and the land pipeline cannot be ignored, because the residual tension and external pressure are completely different between these two type pipelines. However, if the end expansion of the subsea pipeline is calculated based on the condition that the pipeline is just about to reach the seabed, the unrestrained pipeline length and end expansion of pipeline are not the function of external pressure and residual tension, the same expansion is calculated from Eq. [9.41], applying to both the subsea pipeline and land pipeline. Therefore, in the following sections, the end expansion of the unrestrained pipeline section is calculated ignoring the contributions of external pressure and installation tension. In this case, the longitudinal strain derived from the pressure load is rewritten as

$$\varepsilon_P = \frac{(1 - 2\nu)\left(p_{i,\text{ope}} - p_{i,\text{install}}\right)A_i}{EA_s} \qquad [9.42]$$

The longitudinal strain due to the temperature variation is expressed as

$$\varepsilon_T = \alpha(T_i - T_{\text{install}}) \qquad [9.43]$$

Expansion of a Long Pipeline with an Unrestrained Boundary

Figure 9.2(a) shows a model of a long, land pipeline with unrestrained free ends, in which the residual lay tension, F_{residual}, and the external tension, F_{ext}, shown in Eq. [9.37] are very small and the axial strain in the installation condition is ignored. The free ends of the pipeline are sufficiently far from one end to another to allow the virtual anchor section forming in the middle of the pipeline; therefore, each of the ends behaves independently. The pipeline is also assumed to be of uniform cross section, with a uniform net internal pressure, P, and a uniform content temperature, T, in the operating condition. The pressure and temperature strain components, ε_P and ε_T, expressed in Eqs. [9.42] and [9.43], are uniformly distributed along the pipe, as shown in Figures 9.2(b) and 9.2(c). The frictional strain, ε_f, expressed in Eq. [9.6], increases linearly along the pipe, in proportion to the distance from the free end, as shown in Figure 9.2(d). The sum of the pressure, temperature, and friction strains at the VAP is zero. The length of pipeline between the VAP and the free end of pipeline is called as the *transition length*, L, which is determined from the following equation:

$$\varepsilon_P + \varepsilon_T - \frac{\mu w_s L}{A_s E} = 0 \qquad [9.44]$$

Solving for the transition length L gives

$$L = \frac{(\varepsilon_P + \varepsilon_T)A_s E}{\mu w_s}$$ [9.45]

The total expansion, Δ, at the free end, is given as follows:

$$\Delta = \int_0^L \left(\varepsilon_P + \varepsilon_T - \frac{\mu w_s (L - x)}{A_s E} \right) dx = \frac{(\varepsilon_P + \varepsilon_T)L}{2}$$ [9.46]

The distribution of the displacement along the pipeline is shown graphically in Figure 9.2(f).

Expansion of a Long Pipeline with Different Pipe Cross Sections

The pipeline section adjacent to an offshore platform sometimes is constructed with thicker wall pipes than the rest of the pipeline, to meet the design safety and cost requirements. The expansion analysis for this case is much more complicated, because the total expansion movement comprises the composite effect of two adjacent lengths of the pipe with different cross sections.

Figure 9.9(a) shows an expansion case of a pipeline with different cross sections. In the first pipeline section, from the free end to the point where the pipeline section change takes place, the pipeline length is a with a cross-sectional area of A_{s1} and a submerged weight of w_1. Beyond the change point of the cross section, the pipeline has a cross-sectional area of A_{s2} and a submerged weight of w_2. The subscripts 1 and 2 denote sections 1 and 2 of the pipeline.

The strain at a distance $(L - x)$ from the free end is expressed as follows:
For $0 < (L - x) < a$,

$$\varepsilon = (\varepsilon_{P1} + \varepsilon_T) - \frac{\mu w_1 (L - x)}{A_{s1} E}$$ [9.47]

For $a < (L - x) < L$,

$$\varepsilon = (\varepsilon_{P2} + \varepsilon_T) - \frac{\mu w_1 a}{A_{s2} E} - \frac{\mu w_2 [(L - a) - x]}{A_{s2} E}$$ [9.48]

where

L = total transition length
a = distance from free end to section discontinuity
ε_P = strain due to pressure
ε_T = strain due to temperature
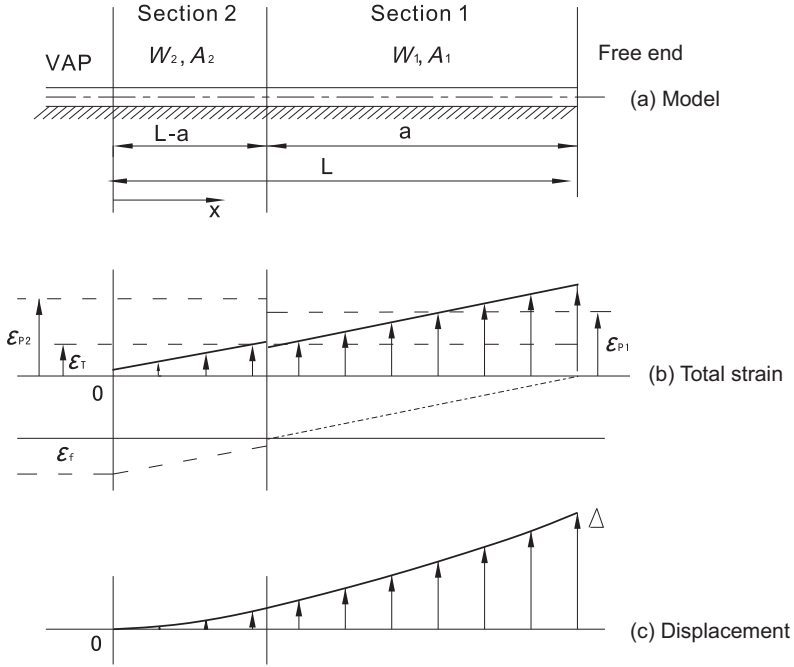
Figure 9.9 Strain and displacement distributions for different cross sections.

At the virtual anchor point, the total strain is zero, which can be expressed as follows:

$$\varepsilon_{P2} + \varepsilon_{T2} - \frac{\mu w_1 a}{A_{s2}E} - \frac{\mu w_2 (L - a)}{A_{s2}E} = 0$$

Therefore,

$$L - a = \left(\varepsilon_{P2} + \varepsilon_{T2} - \frac{\mu w_1 a}{A_{s2}E} \right) \frac{A_{s2}E}{\mu w_2} \qquad [9.49]$$

Figure 9.9(b) illustrates the distribution of the individual strain components and the total strain.

By integrating the total strain between the virtual anchor point and the free end, the displacement of the free end is obtained as follows:

$$\Delta = \left[2(\varepsilon_{P1} + \varepsilon_T) - \frac{\mu w_1 a}{A_{s1}E} \right] \frac{a}{2} + \left[(\varepsilon_{P2} + \varepsilon_T) - \frac{\mu w_1 a}{A_{s2}E} \right] \frac{L - a}{2} \qquad [9.50]$$

Figure 9.9(c) illustrates the displacement distribution along the pipeline for a long pipeline with different cross sections.

Expansion of a Pipeline with a Decaying Temperature Profile

The temperature of the pipeline contents decreases and tends to become the ambient seawater temperature due to the effect of heat loss through the pipeline walls to the ambient environment. If the inlet temperature of the pipeline content is higher than ambient, the content temperature therefore tends to decay with increasing distance along the pipeline. The temperature decay follows an exponential profile, as shown by the following expression:

$$T_P = T_a + (T_{in} - T_a)\, e^{-\beta y} \tag{9.51}$$

where

T_P = temperature of pipe content
T_a = ambient temperature
T_{in} = inlet temperature
y = distance from pipeline inlet
β = heat loss coefficient

Figure 9.10 shows an example of a long, free ended pipeline with an exponentially decaying temperature profile. The fluid flow of pipeline starts from the right free end. Substituting the temperature equation into the equation for thermal strain gives the following expression:

$$\varepsilon_T = \alpha(T_{in} - T_a)\, e^{-\beta(L-x)}$$

where

ε_T = temperature strain
x = distance from the virtual anchor point
α = coefficient of linear thermal expansion for pipe material

The total strain therefore becomes

$$\varepsilon = \varepsilon_P + \alpha(T_{in} - T_a)e^{-\beta(L-x)} - \frac{\mu w_s(L-x)}{A_s E} \tag{9.52}$$

Figure 9.10(b) shows the strain components and the total strain along the pipeline. At the virtual anchor point, $x=0$, and the total strain $\varepsilon=0$, giving the following equation:

$$0 = \varepsilon_P + \alpha(T_{in} - T_a)e^{-\beta L} - \frac{\mu w_s L}{A_s E}$$

Then, the transition length of the pipeline is

$$L = \left[\varepsilon_P + \alpha(T_{in} - T_a)e^{-\beta L}\right]\frac{A_s E}{\mu w_s} \tag{9.53}$$
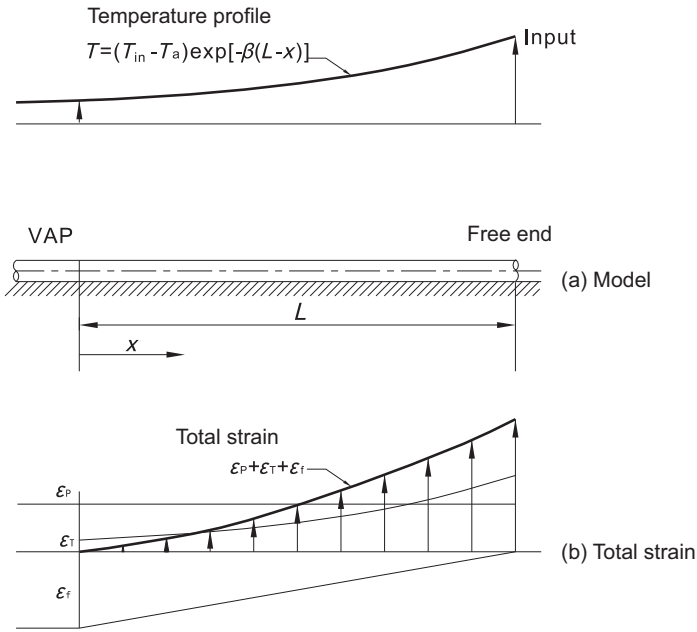
Figure 9.10 Strain distribution for a long pipeline with a temperature profile.

It can be seen from the equation that the unknown parameter, L, appears on both sides of the expression. Therefore, the equation needs to be solved by iteration. After the length is calculated, the total displacement of the free end can be obtained by integrating the strain over the transition length, L:

$$\Delta = \int_0^L \left[\varepsilon_P + \alpha(T_{in} - T_a)e^{-\beta(L-x)} - \frac{\mu w_s(L-x)}{A_s E} \right] dx$$

which gives

$$\Delta = \varepsilon_P L + \alpha(T_{in} - T_a)\frac{\left(1 - e^{-\beta L}\right)}{\beta} - \frac{\mu w_s L^2}{2A_s E} \qquad [9.54]$$

where Δ is the displacement of the free end of pipeline.

Expansion of a Short, Unrestrained Pipeline

A "short" pipeline is defined as one in which the sum of the transition lengths of both free ends is longer than the total length of the pipeline. For a short pipeline,
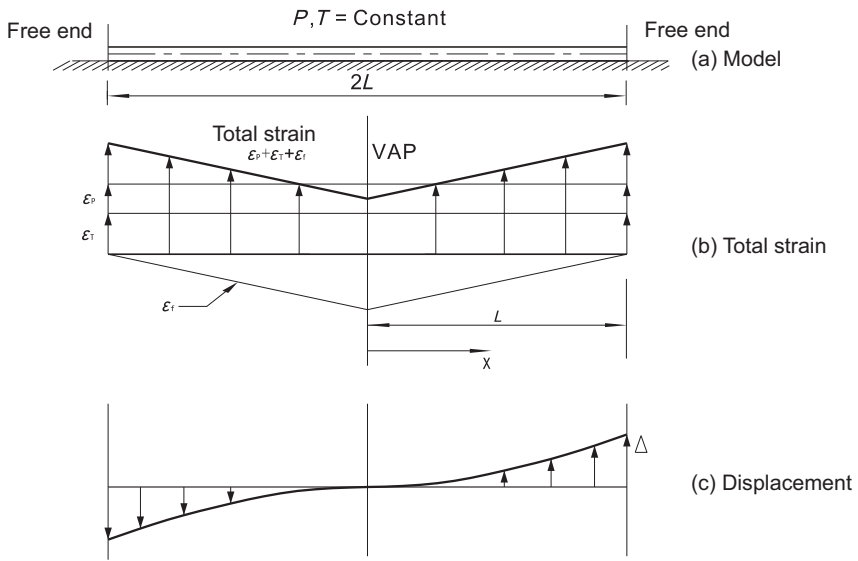
Figure 9.11 Strain distribution along a short pipeline.

it is necessary to consider the expansion of the pipeline as a whole, rather than treating the expansion of each end individually. This is because transition zones from each of the free ends meet and interfere in the central region of the pipeline.

Figure 9.11 shows a model of a short pipeline with constant temperature and pressure profiles along the pipeline with both free ends. The corresponding strain distributions are shown in Figure 9.11(b). The temperature and pressure strain components are both constant along the length of the pipe. The frictional component, however, increases linearly from each end of the pipeline, reaching a maximum value at the midpoint. At the midpoint, the axial forces acting on each half of the pipeline can be deduced to be equal in value and opposite in direction; therefore, they reach an equilibrium state at the midpoint, which also is a virtual anchor point. The transition length at each pipeline end is equal to half of the pipeline length if both pipeline ends are free ends.

The total strain at a distance x from the VAP is the sum of the temperature, pressure, and frictional components. The movement of the pipeline free end relative to the VAP is calculated by integrating the total strain over the entire transition length

$$\Delta = \int_0^L \left[\varepsilon_P + \varepsilon_T - \frac{\mu w_s (L - x)}{A_s E} \right] dx$$

gives

$$\Delta = \left(\varepsilon_P + \varepsilon_T - \frac{\mu w_s L}{2 A_s E} \right) L \qquad\qquad [9.55]$$

where

Δ = displacement of free end of pipeline
L = transition length (half of total pipeline length in this case)

Figure 9.11(c) shows the displacement distribution along the pipeline for this case.

6. Expansion of the Pipe-in-Pipe System

Introduction

Pipe bundles and pipe-in-pipe (PIP) configurations are widely used as part of subsea tiebacks to the existing platforms in many HPHT reservoirs to insulate the flowline to prevent the formation of wax and hydrate as the oil/gas cools along the pipeline. A PIP system is essentially made up of an insulated inner pipe (inner flowline pipe) and a protective outer pipe (outer carrier pipe). For detailed descriptions of PIP and bundle systems refer to Chapter 17.

The structural behavior of a PIP system depends on both the overall behavior of the system and the mechanism of load transfer between the inner and outer pipes. The overall effective axial force developed in the system depends on the operating conditions of temperature and pressure, and if the pipeline is in the end expansion zone (transition length), the friction resistance force is developed between the outer carrier pipe and the soil [10].

Virtual Anchor Point

A PIP pipeline lying on the seabed develops an effective axial force within the inner pipe when subjected to the operating temperature and pressure. As the pipeline expands under the operating conditions, soil friction forces between the outer pipe and the seabed oppose the free thermal expansion of the assembly and results in an overall effective axial force developing within the system. The magnitude of the maximum overall effective axial force depends on whether or not the pipeline develops full axial constraint. In the end expansion zone of the pipeline, the overall effective axial force is a function of soil friction, submerged weight of the pipe, and the distance from the pipe end, which can be given as

$$S = F_{ext} - w_S \cdot \mu_a \, x \qquad\qquad [9.56]$$

where S is the overall effective axial force, w_S is the submerged weight of the PIP, μ_a is the axial pipe-soil friction coefficient, x is the distance from the pipe end, and F_{ext} is

the resistance provided by the spool or PLET at the pipeline end (resistance is negative and pull is positive). The overall effective axial force increases from the pipe end up until the full axial constraints have developed, which is expressed as a single pipeline shown in Eq. [9.29]:

$$S_0 = F_{\text{residual}} - (1 - 2\nu)\left(\Delta p_{i,f}\right)A_{i,f} - EA_{s,f}\alpha_f\left(\Delta T_f\right) - EA_{s,c}\alpha_c(\Delta T_c) \qquad [9.57]$$

where

S_0 = overall effective axial force of a fully restrained PIP flowline
F_{residual} = residual lay tension or effective lay tension
$\Delta p_{i,f}$: = internal pressure difference of inner pipe relative to installation condition
ΔT_f = temperature difference of inner pipe relative to installation condition
ΔT_c = temperature difference of outer carrier relative to installation condition

End Expansion

The expansion of a pipeline is calculated based on the condition that the PIP flowline is just about to reach the seabed. The increases of strain for both inner pipe and outer carrier are expressed in the same way as a single pipeline, as shown in Eq. [9.41]. For the inner pipe,

$$\Delta \varepsilon_f = \frac{1}{EA_{s,f}}\left[T_f + (1 - 2\nu)\Delta p_{f,i}A_{f,i}\right] + \alpha_f \Delta T_f \qquad [9.58]$$

For the outer carrier,

$$\Delta \varepsilon_c = \frac{T_c}{EA_{s,c}} + \alpha_c \Delta T_c - \frac{\mu_a w_s x}{EA_{s,c}} \qquad [9.59]$$

where

T = effective tension at the pipeline end, which is sum of F_{ext}, F_{residual}, and the force between the inner pipe and outer carrier
$\Delta \varepsilon$ = increase of strain for the inner pipe or outer carrier
μ_a = coefficient of axial frictional resistance between the outer carrier and seabed
w_s = submerged weight per unit length for the PIP section
A_s = steel cross-sectional area
E = Young's modulus

For a PIP flowline with no intermediate bulkheads, both the inner pipe and outer carrier are tied together at both end bulkheads. The total elongations of both pipes are the same, which is expressed in the following equation, assuming no friction between the inner pipe and outer carrier:

$$\Delta \varepsilon_f = \Delta \varepsilon_{c,1} + \Delta \varepsilon_{c,2} \qquad [9.60]$$

$$\int_0^L \left(\frac{T1_f + (1 - 2v)\Delta p_{f,i} A_{f,i}}{EA_{s,f}} + \alpha_f \Delta T_f \right) dx$$

$$= \int_0^{L1_C} \left(\frac{T1_C - \mu_a w_s x}{EA_{s,c}} \right) dx + \int_{L-L2_C}^{L} \left(\frac{T2_C - \mu_a w_s (L - x)}{EA_{s,c}} \right) dx \qquad [9.61]$$

where

L = pipe length of PIP flowline
$L1_c, L2_c$ = transition length of carrier at the end 1(left) and the end 2 (right) respectively;
$T1, T2$ = effective tension of pipe at the end 1 and the end 2, respectively

The effective tensions of the inner pipe and outer carrier at both pipe ends have the following relationships:

$$T1_f + T1_C = F_{ext,1} + F_{residual,1} \qquad [9.62]$$

$$T2_f + T2_C = F_{ext,2} + F_{residual,2} \qquad [9.63]$$

$$T1_f + \alpha_f \Delta T(0)\left(A_{s,f} E\right) = T2_f + \alpha_f \Delta T(L)\left(A_{s,f} E\right) \qquad [9.64]$$

At the virtual anchor points of the outer carrier, the increase of strain is zero; therefore,

$$T1_C - \mu_a w_s L1_C = 0 \qquad [9.65]$$

$$T2_C - \mu_a w_s L2_C = 0 \qquad [9.66]$$

The transition lengths of the outer carrier at both ends, $L1_c$, $L2_c$, and the effective tensions at the ends for both inner pipe and outer carrier, $T1_f$, $T2_f$, $T1_C$, $T2_C$ can be solved from Eqs. [9.61] to [9.66]. Therefore, the end expansions of the outer carrier are calculated by the following equations:

$$\Delta 1 = \int_0^{L1_C} \left(\frac{T1_C - \mu_a w_s x}{EA_{s,c}} \right) dx \qquad [9.67]$$

$$\Delta 2 = \int_{L-L2_C}^{L} \left(\frac{T2_C - \mu_a w_s (L - x)}{EA_{s,c}} \right) dx \qquad [9.68]$$
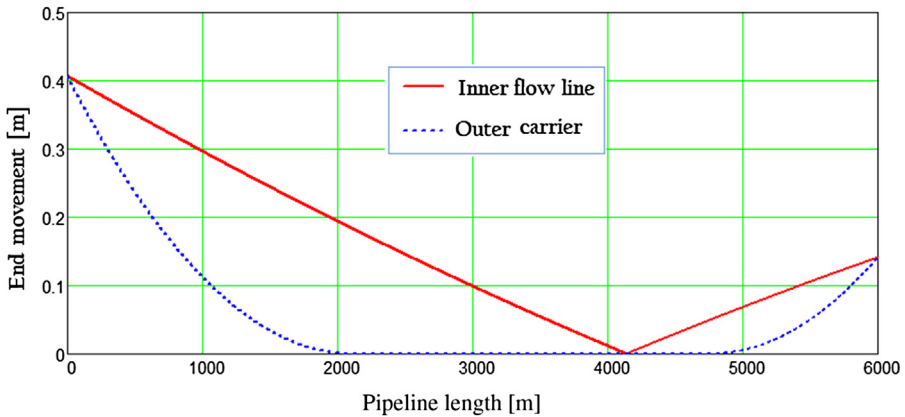
Figure 9.12 Displacement distributions along pipeline for a long PIP flowline. (For color version of this figure, the reader is referred to the online version of this book.)

If the PIP flowline length is shorter than the sum of virtual anchor lengths of both the ends of the outer carrier, the flowline is defined as a "short pipeline." The position of the virtual anchor point from the first flowline end is determined by the total effective tensions at both the flowline ends, given by the following equation:

$$L_1 = \frac{L}{2} + \frac{F_{ext,1} + F_{residual,1} - F_{ext,2} + F_{residual,2}}{w_S \cdot \mu_a}$$

Figure 9.12 shows calculation results of axial movements for both the inner pipe and outer carrier of a long PIP flowline.

7. Examples of Expansion Analysis

In this section, thermal expansion analyses for a single pipe with a temperature profile is carried out using a MATHCAD worksheet. The pipeline end expansions at both ends and the virtual anchor distance are calculated. Two temperature profiles along the pipeline are used as the examples:

1. Constant temperature profile along the pipeline.
2. Exponential decay temperature profile along the pipeline:

$$T_x = T_{amb} + (T_{in} - T_a)\exp\left(-\frac{\beta x}{L}\right)$$

The input parameters required for a thermal expansion analysis are summarized as follows,

- Pipeline and coatings properties.
- Pipeline contents weight.
- Temperature profile along the pipeline.
- Pressure profile (usually the design pressure applied along the whole route).
- Geotechnical data (friction coefficients, especially the axial friction factor).
- Burial depth of pipeline.

Detailed required input parameters are listed in Table 9.2.

Table 9.2 Input Data for Thermal Expansion Analysis

Pipeline Parameters	Symbol	Value	SI Units
Steel pipe outer diameter	D	323.9	mm
Pipeline length	L	20	km
Steel pipe wall thickness	t_w	14.3	mm
Steel density	ρ_s	7850	$kg \cdot m^{-3}$
Anticorrosion coating thickness	t_{c1}	0.5	mm
Anticorrosion coating density	ρ_{c1}	1300	$kg \cdot m^{-3}$
Insulation coating thickness	t_{c2}	30	mm
Insulation coating density	ρ_{c2}	800	$kg \cdot m^{-3}$
Contents density	ρ_c	800	$kg \cdot m^{-3}$
Elastic modulus of steel	E	2.1×10^{-5}	MPa
Poisson's ratio of steel	ν	0.3	
Coefficient of thermal expansion	α	1.17×10^{-5}	1/°C
Operating Data			
Pressure differential across pipe wall	ΔP	150.0	Bar
Inlet temperature	T_{in}	95	°C
Temperature decay constant	β	3.0	
Environmental Data			
Density of seawater	ρ_{sea}	1025	$kg \cdot m^{-3}$
Ambient temperature at installation	T_a	6.0	°C
Axial Coulomb friction coefficient	μ_a	0.7	
Submerged weight of soil	γ	9.0	$kN \cdot m^{-3}$
Coefficient of earth pressure at rest	k_0	0.5	
Burial depth	h	0.0	m

The analysis method of the MATHCAD worksheet is described as follows:

Step 1. Calculate the pipe submerged weight per unit length, W_{sub}.
Step 2. Determine the position of the VAP ($L_{VAP} = x$), where the soil friction force equals to the effective force, and the axial strain is equal to zero:

$$F_{f,VAP} = F_{E,VAP}$$

$$F_{f,VAP} = -\mu_a W_{sub} L_{VAP}$$

$$F_{E,VAP} = -A_b \Delta P(1 - 2v) - E\alpha(T_{VAP} - T_a)A_s$$

where A_b is the pipe bore area, A_s is the steel cross-sectional area, and W_{sub} is the pipeline submerged weight per unit length (N/m).
Step 3. Determine the end expansion, which is an integral of the axial strain from the VAP to the pipeline end:

$$\Delta = \int_0^{VAP} \left(\varepsilon_{pressure} + \varepsilon_{temp} - \varepsilon_{soil} \right) dx$$

Strain due to the difference between internal and external pressure:

$$\varepsilon_{pressure} = \frac{A_b \Delta P(1 - 2v)}{EA_s}$$

Strain due to the temperature increase from installation:

$$\varepsilon_{temp} = \alpha(T_x - T_a)$$

Strain due to soil friction resistance:

$$\varepsilon_{soil} = \frac{\mu W_{sub} x}{EA_s}$$

The analysis results of pipeline thermal expansion using the MATHCAD sheet include the end displacements, the effective axial force distribution, and the displacement distribution of the pipeline.

Expansion of a Pipeline with Constant Pressure and Temperature Profiles

The pressure and temperature profiles of this pipeline are illustrated in Figures 9.13 to 9.15.

Expansion of a Pipeline with a Decaying Temperature Profile

The decaying temperature profile of this pipeline are illustrated in Figures 9.16 to 9.18.

Temperature profiles

Temperature (C)

100

80

Tx_i ___

60

T_{amb} ----

40

20

0

0   5000 $1 \cdot 10^4$ $1.5 \cdot 10^4$ $2 \cdot 10^4$

x_i

Pipeline length from input end [m]
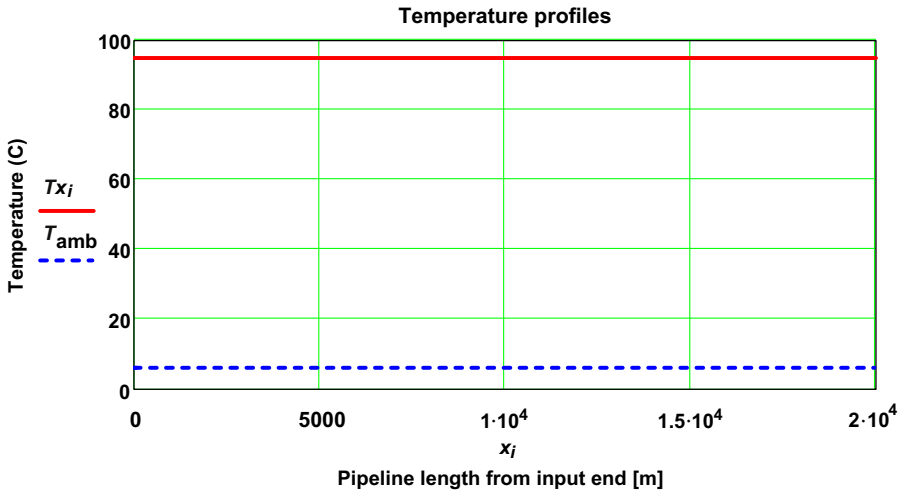
Figure 9.13 Temperature distribution along the pipeline. (For color version of this figure, the reader is referred to the online version of this book.)

Pipeline effective axial force profiles

Effective axial force [kN]]

0

$\dfrac{P_{eff_i}}{kN}$ ___ -2000

0   5000 $1 \cdot 10^4$ $1.5 \cdot 10^4$ $2 \cdot 10^4$

x_i

Pipeline length from input end [m]
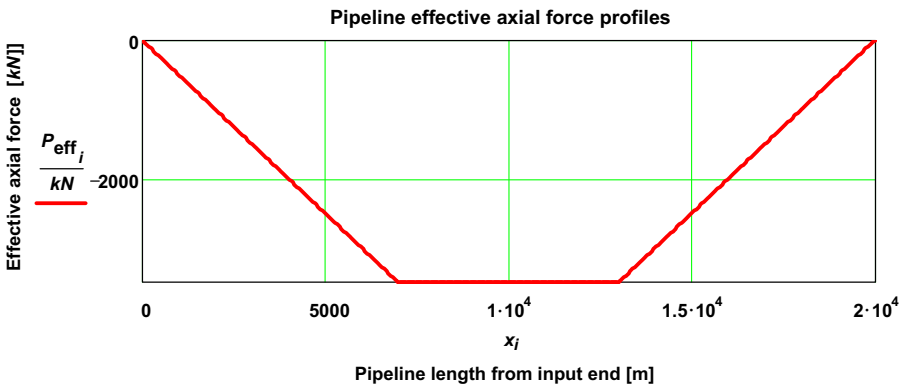
Figure 9.14 Effective axial force distribution for pipeline with a constant T profile. (For color version of this figure, the reader is referred to the online version of this book.)

Axial displacement distribution

Pipeline displacement [m]

6

4

2

Δ_i ___ 0

-2

-4

-6

0   5000 $1 \cdot 10^4$ $1.5 \cdot 10^4$ $2 \cdot 10^4$

x_i

Pipeline length from input end [m]
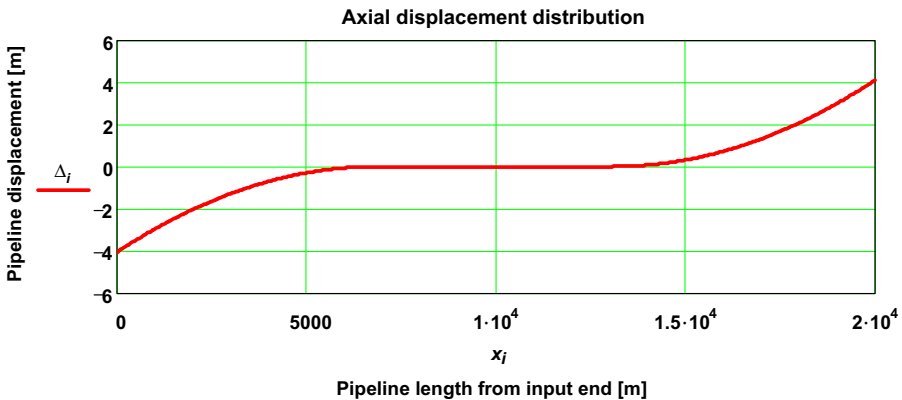
Figure 9.15 Axial displacement along pipeline with a constant T profile. (For color version of this figure, the reader is referred to the online version of this book.)

Temperature profiles

Temperature (C)

Tx_i ——
T_{amb} - - - -

x_i

Pipeline length from input end [m]
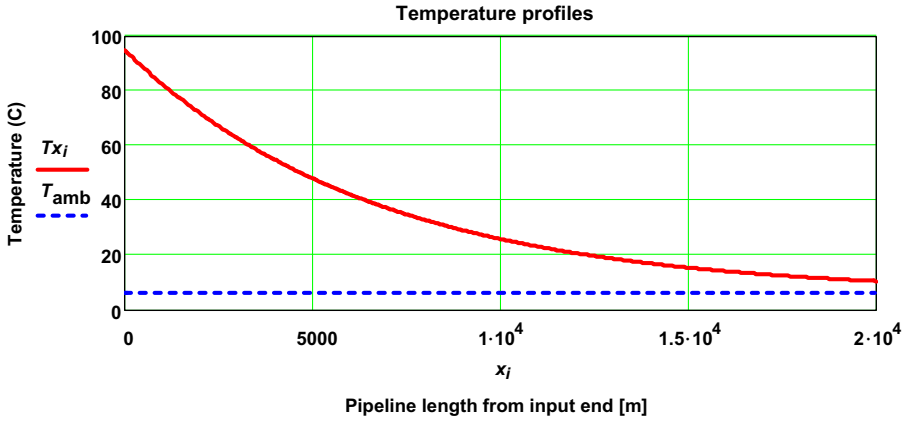
Figure 9.16 Temperature distribution along a pipeline in the operating condition. (For color version of this figure, the reader is referred to the online version of this book.)

Pipeline effective axial force profiles

Effective axial force [kN]

$\dfrac{P_{eff_i}}{kN}$ ——

x_i

Pipeline length from input end [m]

Figure 9.17 Effective axial force distribution for the pipeline with a decaying temperature profile. (For color version of this figure, the reader is referred to the online version of this book.)

Axial displacement distribution

Pipeline displacement [m]

Δ_i ——

x_i

Pipeline length from input end [m]
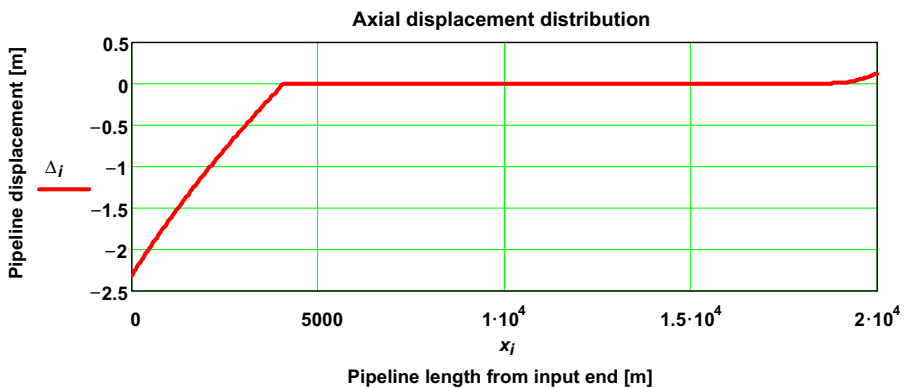
Figure 9.18 Axial displacement of the pipeline with a decaying temperature profile. (For color version of this figure, the reader is referred to the online version of this book.)

References

[1]   Maldonado B, Arrazola A, Morton B. Ultra-deep HP/HT completions: Classification, design methodologies, and technical challenges. Houston: OTC17927, Offshore Technology Conference; 2006.

[2]   Dixon M. HP/HT design issues in depth. E & P; 2005.

[3]   DNV. Global buckling of submarine pipelines. DNV-RP-F110, Det Norske Veritas, 2007.

[4]   ASCE. Guidelines for the design of buried steel pipe. American Lifelines Alliance 2001.

[5]   Sparks CP. The influence of tension, pressure and weight on pipe and riser deformations and stresses. J. Energy Res. Technol. 1984;106:46–55.

[6]   Fyrileiv O, Collberg L. Influence of pressure in pipeline design—Effective axial force. 24th International Conference on Offshore Mechanics and Arctic Engineering. Halkidiki, Greece: OMAE 2005-67502; 2005.

[7]   Palmer AC, Ling MTS. Movements of submarine pipelines close to platforms. Houston: OTC 4067 Offshore Technology Conference; 1981.

[8]   Choi HS HS. Expansion analysis of offshore pipelines close to restraints. 1995. ISOPE-1995, Hague, The Netherlands.

[9]   Suman JC, Karpathy SA. Design method addresses subsea pipeline thermal stresses. Oil Gas J. August 1993.

[10] Harrison GE, Kershenbaum NY, Choi HS. Expansion analysis of subsea pipe in pipe flowline. Proc. of 7th IOPEC, Honolulu; May 1997.

10 Lateral Buckling and Pipeline Walking

Chapter Outline

1. Introduction

Pipelines subjected to high pressure and high temperature (HPHT) may significantly expand and contract longitudinally during operational heating and cooling cycles, resulting in a global buckle formation occurring at pipeline locations with high out of straightness (OOS) or imperfection due to axial compressive loading, when the pipeline is restrained or semi-restrained by the pipe end devices and the soil. Lateral buckling occurs if the pipeline is exposed on the seabed, or upheaval buckling may occur if it is buried or constrained in a trench. Uncontrolled global buckling can

cause excessive plastic deformation of the pipeline, which could lead to localized buckling collapse or cyclic fatigue failure during operation due to multiple heat-up and cooldown cycles, if it is not properly managed. The lateral buckling does not always lead to a loss of containment failure. For a gas pipeline buckled in several places over a length of about 3 km, with lateral movements in few meters, there is no need for further action, because the stress range and fatigue are very low. However, it would be wrong to conclude that the lateral buckling cannot lead to a loss of containment failure. For example, in January 2000, a pipeline in Guanabara Bay, Brazil, suddenly buckled 4 m laterally and ruptured, leading to a damaging release of 7000 barrels of oil. The investigation showed that the pipeline displaced laterally due to the increase of pressure and temperature in the operating condition when the pipeline failure took place. Figure 10.1 illustrates pipeline failures due to fatigue and facture damage under cyclic thermal loads for a single pipe and a pipe in pipe (PIP).

The most relevant failure modes of pipeline lateral buckling may include [2]

- Local buckling; which is normally the governing failure mode resulting from excessive utilization.
- Loss of containment, as a result of
  - Fracture failure on the tensile side of the cross section, resulting from excessive utilization.
  - Low cycle fatigue under cyclic thermal loads.
  - Hydrogen induced stress cracking (HISC) in martensitic steels (13% Cr) and ferritic-austenitic steels (duplex and super-duplex).

When a pipeline on the seabed is heated, it tends to expand, and the expansion is resisted by the friction generated by the seabed. When the pipeline is cooled, it contracts, but the seabed friction resists the moving pipeline's return to the original position. If heat-up/cooldown cycles involve significant thermal gradients, then axial ratcheting of the pipeline can occur, with displacement toward the cold end. Over a number of cycles, this movement can lead to very large global axial movement with an associated overload of the spool piece or jumper at the pipeline end. This

Figure 10.1 Pipelines that failed due to fatigue damage.
Source: Perinet and Simon [1]. (For color version of this figure, the reader is referred to the online version of this book.)

cumulative axial movement is called *pipeline walking*. Pipeline walking can lead to the following problems:

- Overstressing of spool pieces or jumpers at pipeline ends.
- Loss of tension in an SCR (steel catenary riser) if the pipeline end is tied with the SCR.
- Increased loading within a lateral buckle due to lateral walking.
- Need for restraint using anchors to stop pipeline walking.
- Route curve pullout of restrained systems.

The phenomenon of lateral buckling and walking of pipelines has been widely investigated over the past decades. Many methods have been adopted over the years to mitigate the lateral buckling and pipeline walking. They include snake lay, sleepers, distributed buoyancy, trench and bury, and expansion spools. Planned buckle initiators such as distributed buoyancy sections or sleeper pipe upsets are often designed to manage the global buckling to ensure pipeline integrity and have been successfully used in many projects. The planned buckle initiators are spaced periodically along the pipeline to alleviate the axial load down to an acceptable level. In recent years, finite element analysis software has been widely used in the simulation and prediction of the pipeline response of global buckling.

Two joint industry projects (JIP), HOTPIPE and SAFEBUCK, were recently performed to develop industry knowledge of the design of HPHT pipelines susceptible to global buckling.

- HOTPIPE JIP [3] is strategy for the structural design of HPHT pipelines. The design criteria are based on the application of reliability methods to calibrate the partial safety factors in compliance with the safety philosophy established by DNV-OS-F101.
- The SAFEBUCK JIP–SAFEBUCK design guideline [4] proposes a methodology, based on in-place survey data of four operational pipelines donated by JIP members.

Lateral Buckling Response

If the compressive effective axial force is large enough, then slender structures, such as pipeline, undergo Euler buckling (global buckling). The global buckling includes lateral buckling and upheaval buckling. Typical lateral friction coefficients are less than unity; hence, the uniformly distributed lateral friction force generated by soil resistance is less than the submerged weight of a pipeline. A pipeline laid onto the seabed without trenching or cover tends to create lateral buckles rather than upheaval buckles. The problem of lateral buckling in pipelines was considered and theoretical analyze by Hobbs and Liang in early research [5]. Experiments performed as part of their work observed that the pipeline can deform into a number of buckle mode shapes; the most common of which are illustrated in Figure 10.2.

Modes 1 and 3 are symmetrical about an axis drawn through the center of the buckle and perpendicular to the original centerline of the pipeline, while Modes 2 and 4 are asymmetrical about this axis. Mode 1 is the mode normally observed in the pipeline upheaval buckle. This mode cannot occur in a lateral buckle because it requires concentrated lateral forces at each end of the buckle configuration for equilibrium. These lateral forces cannot be generated by lateral friction alone but by
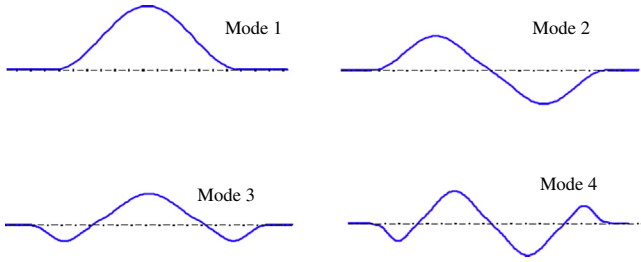
Figure 10.2 Euler buckling mode shapes. (For color version of this figure, the reader is referred to the online version of this book.)

soil in the vertical direction of the upheaval buckle. In the absence of these concentrated forces, the lateral deflection of the pipeline "overshoots" at each end of the central bow, and the pipeline adopts a Mode 3 rather than Mode 1 lateral buckles. Lateral buckle shapes are difficult to predict due to complicated soil-pipe interactions, random out-of-straightness features, and the inherent instability of buckling behavior. The Hobbs methodology is well established and compared with actual behavior of pipeline in a number of published papers from the mid-1980s.

Hobbs's Method

The parameters and equations used for the determination of lateral buckling are presented as follows [6]. The required effective axial force to buckle can be expressed as

$$P(z) = \frac{k_1 \cdot E \cdot I}{[L(z)]^2} + k_3 \cdot \mu_a \cdot \omega \cdot L(z) \cdot \left\{ \left[1 + \frac{k_2 \cdot E \cdot A \cdot \mu_1^2 \cdot \omega \cdot (L(z))^5}{\mu_a (E \cdot I)^2} \right]^{0.5} - 1 \right\}$$

[10.1]

The buckle amplitude is

$$y(z) = \frac{k_4 \cdot \mu_1 \cdot \omega \cdot [L(z)]^4}{E \cdot I}$$

[10.2]

The force left in the buckle is

$$P_{\text{buck}}(z) = \frac{k_1 \cdot E \cdot I}{[L(z)]^2}$$

[10.3]

The maximum moment induced in the buckle is

$$M = k_5 \cdot \mu_1 \cdot \omega \cdot [L(z)]^2$$

[10.4]

where

z = the location on the pipe
$L(z)$ = buckle length
μ_1 = the lateral pipe-seabed friction coefficient

Table 10.1 Buckling Constants k for Buckling Modes

Buckle Mode	k_1	k_2	k_3	k_4	k_5
1	80.76	6.391e-5	0.5	2.407e-3	0.0694
2	39.48	1.743e-4	1.0	5.532e-3	0.1088
3	34.06	1.668e-4	1.294	1.032e-2	0.1434
4	28.20	2.144e-4	1.608	1.047e-2	0.1483

μ_a = the axial pipe-seabed friction coefficient
ω = pipeline submerged unit weight
A = cross section area of pipe
E = Young's modulus
k_n = buckle constant

The values of buckling constants k_n in these equations are given in Table 10.1.

If a pipeline is subjected to buckle, the development of effective force is modified as the pipe feeds into the buckle. The force in the buckle drops as the buckle develops. The maximum amount of pipe that can feed into a buckle is equal to the unrestrained expansion of the line. However, the axial force in the buckled section (P) would not be zero. The increase in length of pipe Δl in the buckled section from the unbuckled state can be determined as

$$\Delta l = \frac{(P_{\text{buck}} - P) \cdot L}{A \cdot E} \tag{10.5}$$

Expansion of the adjacent slipping length (L_s) as force falls from P_0 to P at the start of the buckle can be expressed as

$$\Delta l_s = \frac{(P_{\text{buck}} - P) \cdot L_s}{A \cdot E} \tag{10.6}$$

where

$$L_s = \frac{P_{\text{buck}} - P}{\mu_a \omega} \tag{10.7}$$

The total expansion into the buckle is

$$\Delta L = \Delta l + \Delta l_s = \frac{(P_{\text{buck}} - P)}{A \cdot E} \cdot \left[L + \frac{(P_{\text{buck}} - P)}{\mu_a \cdot \omega} \right] \tag{10.8}$$

For buckling Modes 2 and 4, L is replaced by $2L$ in this equation, as they are double buckle modes. The Hobbs's assessment method is sufficient for the conceptual design to check if the pipeline is susceptible to global buckling.

Limit State Design for Lateral Buckling

Lateral (global) buckling of pipeline itself is not a failure mode; it may be allowed provided that the pipeline integrity is maintained in the postbuckling configuration. However, the possible failure modes of the postbuckled pipeline may include

- Local buckling.
- Ovality.
- Fatigue and fracture.
- Pipeline walking.

Essentially pipeline walking is not a true failure mode but is listed here because it may cause pipeline end connection, such as subsea jumpers, to fail.

Different design criteria of limit state design for the postbuckled pipeline are used by DNV-RP-F110 and Safebuck [7]. For the pipeline in the postbuckling condition, DNV-RP-F110 uses a load-controlled local buckling criterion, while Safebuck uses a displacement-controlled criterion. As the pipeline responses to the applied pressure and temperature primarily depend on the pipe-soil resistance used, the pipeline condition cannot be stated to be fully displacement controlled and use of the displacement-controlled condition needs to be supported by corresponding precautions. In the same way, as the load carrying capacity in the buckled condition is reduced, it cannot be considered being fully load controlled either. Pipeline buckle behaviors are difficult to predict, but the pipeline design must ensure the pipeline is safe without failures in various conditions, therefore, the following items should be solved for a global buckling control:

- The stress and strain are relative to the feed-in of pipe in the buckle locations, which depends on the buckle spacing, operation temperature, and pressure.
- The locations of global buckles depend on the local pipeline OOS.
- The soil resistance is difficult to predict accurately, and the soil resistance bounds in the lateral and axial directions should be used to solve the uncertainty of soil resistance.
- Reliability techniques are employed to understand the uncertainty of global buckles.

The possible failure of pipelines due to lateral buckling may be solved by (1) setting intermediate expansion spools to reduce axial force without buckling or (2) setting buckle "initiators" in straight pipelines to reduce the axial load by controlled buckles in given locations, in which suitably spaced buckle initiators ensure a limited thermal feed-in to the buckle site and hence acceptable loads in the buckle.

2. Buckle Initiation

Effective Axial Force

The global response of the pipeline is determined by the compressive effective axial force, which has been detailed in Chapter 9, Section 4, "Effective Axial Force of the Pipeline," of this book. For a fully restrained pipeline, the effective axial force is expressed as

$$S_0 = F_{\text{residual}} - (1 - 2\nu)(\Delta p_{\text{i}})A_{\text{i}} - EA_{\text{s}}\alpha(\Delta T_{\text{i}}) \qquad [9.29]$$

For a pipeline including a fully restrained pipeline section in the middle and unrestrained pipeline sections at both pipeline ends, the effective axial force in the operating condition is expressed as follows:

$$S_{\text{in,ope}} = \begin{cases} -\mu_a w_{\text{sub,ope}} x + F_{\text{ext,in}} & \text{for spool or riser connection} \\ S_0 & \text{for a fixed end} \end{cases}$$

$$S_{\text{out,ope}} = \begin{cases} -\mu_a w_{\text{sub,ope}} (L - x) + F_{\text{ext,out}} & \text{for spool or riser connection} \\ S_0 & \text{for a fixed end} \end{cases}$$

$$S_{\text{ope}} = \max \left(S_{\text{in,ope}}, S_0, S_{\text{out,ope}} \right) \tag{9.31}$$

Figure 10.3 illustrates the effective axial force distribution along a long pipeline in the operating condition with both free and fixed ends. The dot lines in the figure are for the pipeline with fixed both ends. For the pipeline with free ends, the effective axial force is zero at the ends and gradually increases due to the frictional restraint of the seabed, as shown with the solid line in the figure. The slope of the force profile in the slip zones is defined by the axial friction force, $\mu_a w_{\text{sub,ope}}$. At the virtual anchor point (VAP), where the frictional restraint is sufficient to suppress any expansion, the axial total strain in the pipe is zero. The figure shows that the system develops a fully constrained section in the middle section of the pipeline bounded by two VAPs. Expansions take place between the VAP and the pipeline end. If the pipeline is short, the overall length may be insufficient to fully restrain the pipeline, as illustrated in Figure 10.4. A free-ended short pipeline does not reach a position of
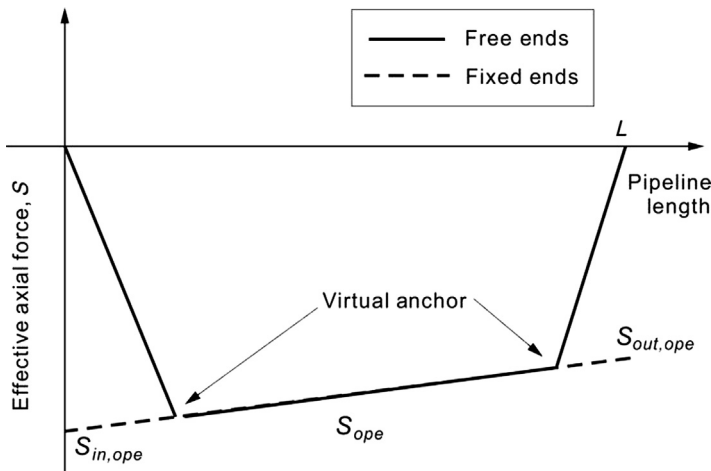
Figure 10.3 Effective axial force in a straight pipeline.
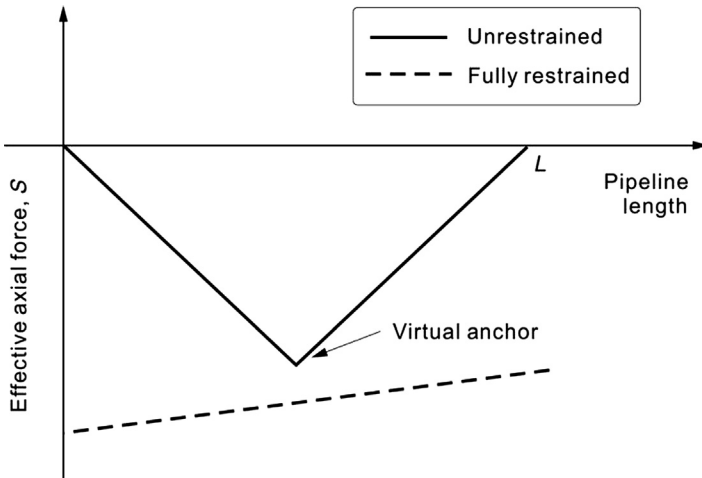
Figure 10.4 Effective axial force in a short, straight pipeline.

full constraint. Instead the pipeline forms a VAP close to the center and the pipeline expands outward two sides from this point. In this case, the displacement at the virtual anchor is zero, but the axial strain is not. The maximum axial force in the pipeline can be significantly below the fully constrained force.

Lateral Buckling

If the compressive effective axial force is large enough, lateral buckling may occur in the pipeline, the development of effective force is modified as the pipe feeds into the buckle in the postbuckling period. The effective axial force in the buckle drops as the buckle develops. Figure 10.5 shows the situation when a buckle forms at a location near the center of a pipeline. The drop in compressive effective force at the buckle causes the pipe to feed into the buckle from both sides. At the end of the feed-in section, the pipeline once again reaches a condition of full constraint.

If the pipeline is very long, it is possible that more than one buckle forms in the system. As illustrated in Figure 10.6, eight buckles formed in the pipeline. In all pipeline moving sections, the slope of the axial effective force profile is governed by the axial friction force. Between adjacent buckles, there must be a VAP at which the directions of pipe expansion changes.

Buckling Initiation Load

Lateral buckling is governed by three parameters: effective axial force, out-of-straightness, and boundary restraint. There are analytical solutions both for the pure elastic global buckling for different boundary conditions as well as for buckling on elastic foundation.
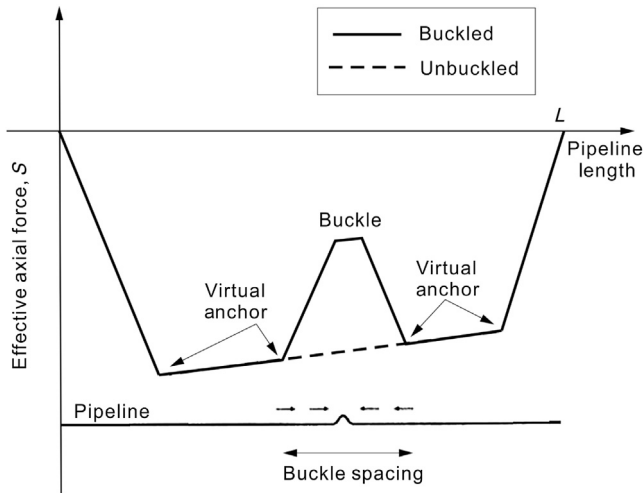
Figure 10.5 Axial force distribution in postbuckling configuration.
Source: Carr et al. [8].
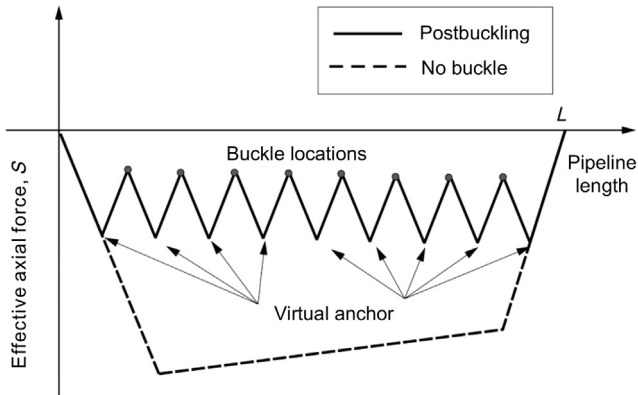
Figure 10.6 Effective axial force distributions under multiple buckles.

A typical effective axial force/buckle response curve is shown in Figure 10.7. The shape of the buckle response curve depends on the lateral resistance and the initial imperfection. The analytic equilibrium solution for a perfect pipe developed by Hobbs is plotted for a reference. When the imperfection is zero, the effective axial force for a buckle becomes infinite, which means a perfectly straight pipeline would not buckle. For very small imperfections, a large snap is obtained. As the initial out of straightness is increased, the snap occurs at lower effective axial loads and less dramatically. Eventually, for large enough imperfections, the snap is eliminated, to be replaced by a single-valued magnification of the initial bow.
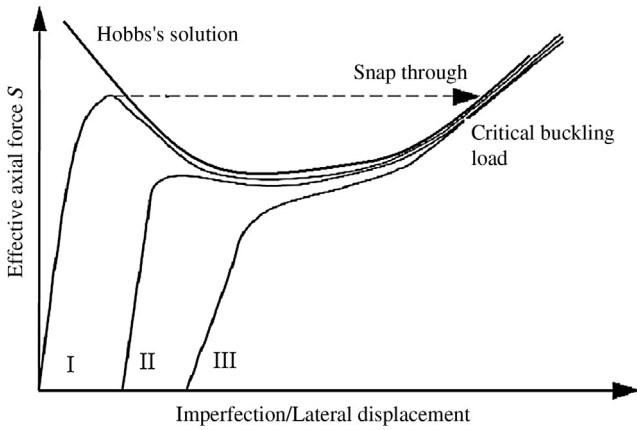
Figure 10.7 Global response curve of lateral buckling.
Source: Hobbs and Liang [5].

Although the Hobbs solution gives a buckle load, it is not widely used for pipeline buckle prediction because of uncertainties in the pipe-soil interaction. An FE analysis program combined with analytical solutions is normally used to ascertain the critical buckling load of a pipeline. FE analysis is used to evaluate the effects of lateral imperfections on the critical buckling load, which is difficult for the analytical buckling theory, but both methods get a reasonable agreement for the cases without lateral imperfections. Figure 10.8 shows an example of the critical buckling load of a pipeline on a single sleeper calculated with the general FE software ABAQUS. The
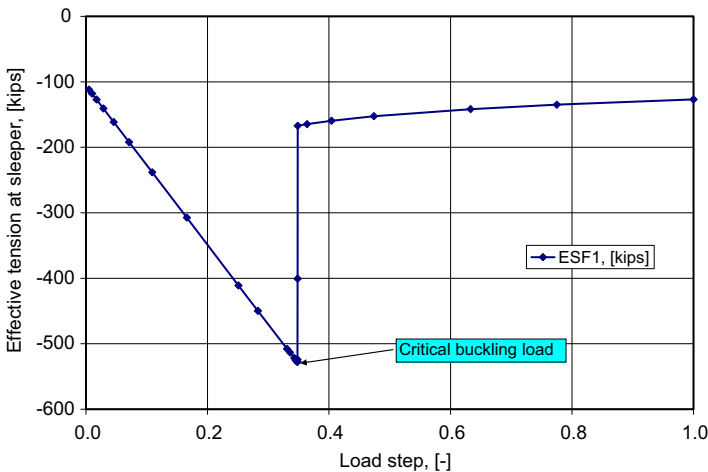
Figure 10.8 Critical buckling load based on FE analysis. (For color version of this figure, the reader is referred to the online version of this book.)

effective compression force increases first, as the increase in the temperature loading, and suddenly drops when it reaches the critical buckling load. In the figure, the temperature increases from the ambient temperature at the load step of 0.0 to the operating temperature at the load step of 1.0.

Parameter Effects of Sleepers on Critical Buckling Load

The critical buckling load of pipelines with the buckle initiator of a sleeper is a function of the following parameters: (1) pipeline stiffness, (2) curvature of lateral imperfection, (3) submerged weight and lateral contact resistances due to soil or sleeper surface, and (4) height of the sleeper.

   To evaluate the parameter effects of a buckle initiator device (a sleeper is set as the buckle initiator) on the critical buckling load, a series of FE and analytical analyses were carried out for a 18 inch OD, 1 inch WT, X65 pipeline with a 2 inch insulation layer. Figure 10.9 shows typical pipeline configurations with (a) a single sleeper and (b) a dual sleeper, in which the dimensions such as pipeline initial lateral offset L, vertical offset (sleeper height for both single and dual sleeper) H, and gap a are defined. The vertical offset height is referenced to where the pipeline crosses over the sleeper and may not be the maximum height of the pipeline imperfection for the dual sleeper case (in the middle of the gap between two sleepers). The effects of these parameters are discussed in the following sections.

Height of Sleeper, H

Figure 10.10 shows the effect of the vertical height, H, for both single sleeper and dual sleeper configurations on the critical buckling load of pipeline, assuming the pipeline is laid straight across the sleepers. The buckle initiation loads at sleepers decrease with increasing sleeper heights and increase with increasing pipeline wall thickness, due to an increase of pipeline stiffness. The critical buckling load of
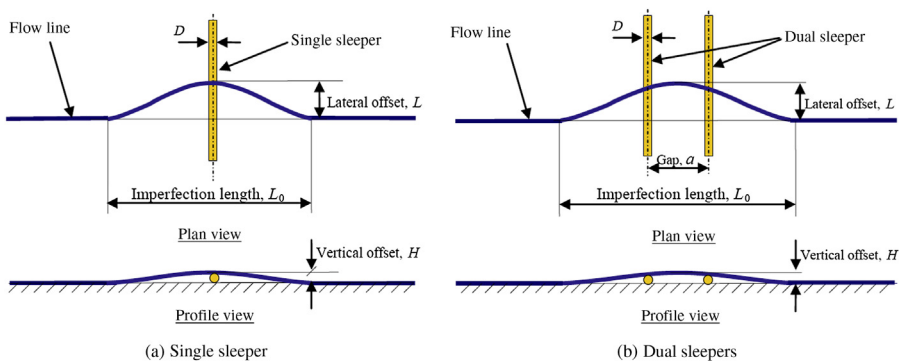
Figure 10.9 Pipeline crossing over sleepers.
Source: Bai et al. [9]. (For color version of this figure, the reader is referred to the online version of this book.)
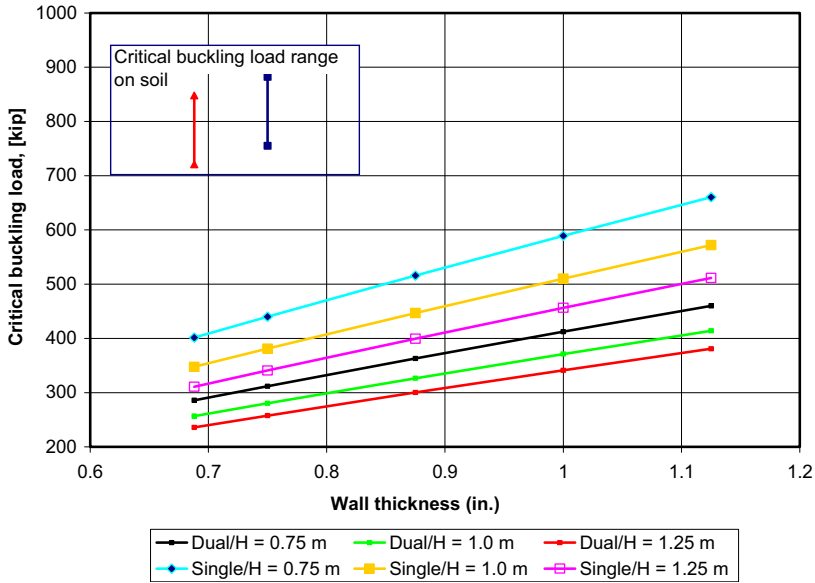
Figure 10.10 Sleeper buckle initiation load vs. pipe wall thickness. (For color version of this figure, the reader is referred to the online version of this book.)

pipeline on a seabed with a lateral imperfection radius of 1500 m is also plotted for reference. The lateral soil resistance is one of the key factors that determines the critical buckling loads of pipelines on the seabed. The range of critical buckling loads is shown in the figure, and the actual critical buckling load on the seabed should be within this range—but could be greater if the pipeline is straight in the plan view. The critical buckling loads of the pipeline at sleepers are much lower than this one directly on a seabed, which would ensure that the pipeline buckles on the sleepers first.

Lateral Offset, L

Figure 10.11 shows the critical buckle loads of dual sleepers with different pipeline lateral offsets from the pipeline centerline if laid straight. With an increase in the lateral offset, the critical buckle load decreases noticeably. Note that large lateral offsets may be difficult to implement during installation, only very small offsets are likely during normal installation.

The critical buckling loads of two buoyancy section lengths are also plotted for a reference. The critical buckling loads for both buckle initiators are at the same level if certain lateral imperfections on dual sleepers could be guaranteed. The length of buoyancy is a key parameter to control the critical buckling load. Longer buoyancy has a lower critical buckling load, but the buckle shape can become unstable if the buoyancy section is too long. The installation and materials costs for both methods should also be considered.
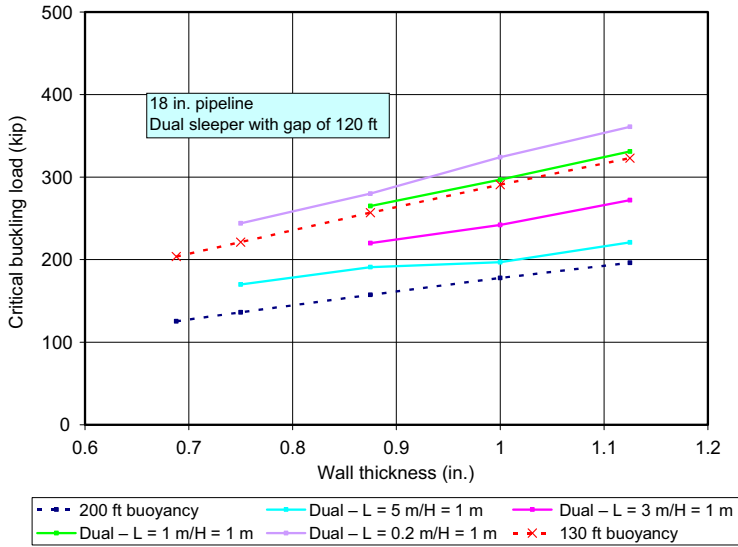
Figure 10.11 Comparison of the critical buckling loads between sleepers and buoyancy. (For color version of this figure, the reader is referred to the online version of this book.)

Gap between Sleepers, a

Figure 10.12 shows the effect of the gap between the two sleepers of the dual sleeper on the critical buckle load for different wall thicknesses. Increasing the gap leads to a decrease in the critical buckling load, but if the gap is too long, it can cause VIV and stress or strain problems.
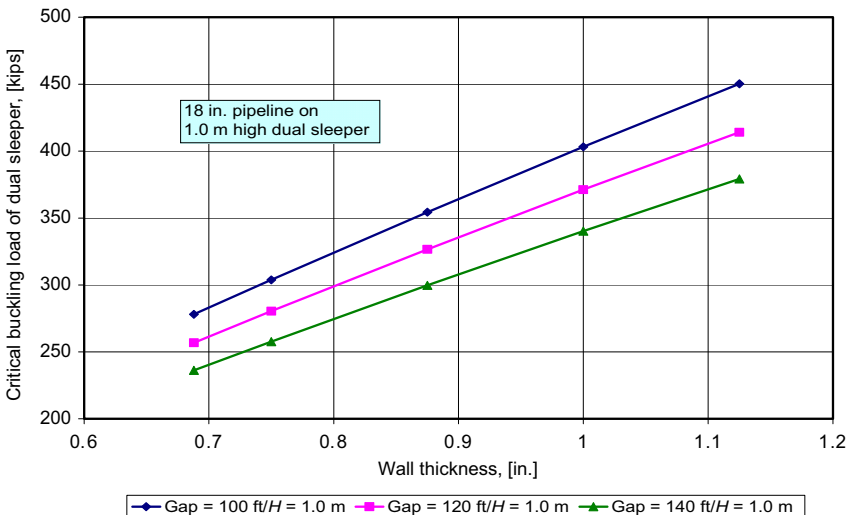
Figure 10.12 Effects of gap on the critical buckling load of dual-sleeper. (For color version of this figure, the reader is referred to the online version of this book.)

Buckle Initiator Spacing

Lateral buckling may naturally occur on the seabed at intervals along the pipeline when the effective compressive force is sufficiently high for the pipe to go through unplanned buckling at natural imperfections. Such imperfections come from the laying process, due to vessel motion, wave or current loading, and seabed variations. This "unplanned (rogue) buckle" relieves the effective axial compressive forces locally. The unplanned buckle can lead to an exceedance of the following design limit states: (1) excessive plastic deformation of the pipe, possibly leading to localized bending and collapse or (2) cyclic fatigue failure under cyclic thermal loads. However, lateral buckling can be controlled by setting buckle initiators (buckle mitigation devices), such as sleepers and buoyancy sections, at a planned interval. Figure 10.13 shows the single sleepers and dual sleepers used as buckle initiators.

If multiple buckle sites are adopted as a design solution of the lateral buckling of HPHT pipelines, it is needed to ensure that buckles will be triggered as intended at each buckle site. Appropriate spacing between the initiation sites is critical. There is a danger if the maximum distance between each buckle site is too short; it might cause interference between adjacent sites, that is, one buckle in effect suppresses the buckle at the adjacent site. If this is found to be an issue, further intervention may be necessary to increase the axial resistance between buckle sites, by increasing the pipe weight between buckle sites, introducing intermittent rock berm, and so forth.

The critical buckling load of pipeline on soil (naturally buckling on the seabed) should be higher than that at the planned buckling mitigation sites, to avoid pipeline buckling at uncontrolled locations before buckling at the planned locations.

The planned buckle spacing is determined by several factors. The sleeper spacing should be shorter than a "critical buckle spacing" (usually governed by the criteria
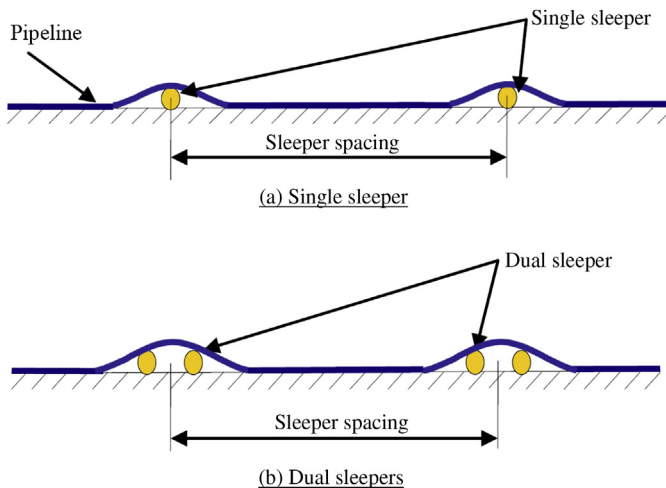
Figure 10.13 Pipeline configuration and sleeper spacing. (For color version of this figure, the reader is referred to the online version of this book.)
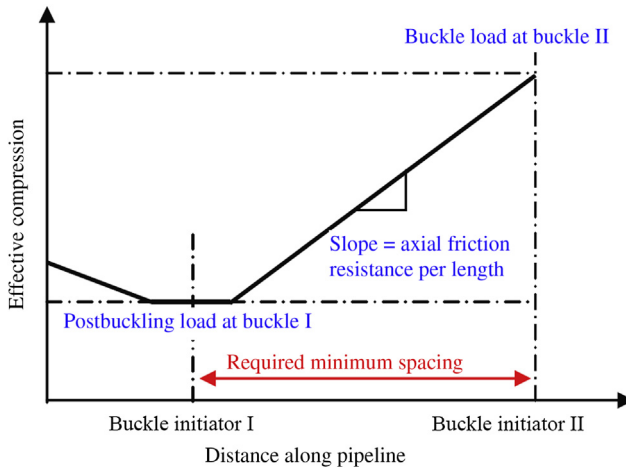
Figure 10.14 Minimum spacing between two buckle initiators.
Source: Bai et al. [9]. (For color version of this figure, the reader is referred to the online version of this book.)

that the maximum strain in each buckle is within the acceptable limit and the cyclic stress experienced during operation gives an acceptable fatigue life). If the sleeper spacing is longer than the critical spacing, the controlled buckling will exceed one or both limit states. The sleeper spacing should also be longer than a "minimum spacing" to ensure buckle independence at the adjacent buckle initiators. The critical buckling load at each planned initiator should always be less than the potential effective compression force at that initiator (i.e., the effective compression force buildup between two lateral buckles plus the lowest postbuckling force at the adjacent buckle locations), as shown in Figure 10.14. The lowest postbuckling force can be obtained from FEA in the worst soil and loading conditions.

Overall, the spacing between two adjacent buckle initiation sites is determined to satisfy the following three limit states:

- Lateral buckling must first occur at planned initiation sites, which means the spacing must be longer than the minimum spacing.
- Maximum stresses at planned and unplanned global buckles must satisfy the ultimate limit state requirements.
- Stress ranges and fatigue damage at planned and unplanned global buckles must satisfy the fatigue limit state requirement.

Buckling Reliability

The reliability of lateral buckling design schemes has been developed using structural reliability analysis (SRA) techniques reported in several papers, [10, 11, 12]. SRA methods are adopted to rationally treat the various sources of uncertainty involved in the buckling analysis. The probability of buckling initiation is calculated as

$$P_f = \text{Probability}[Z \leq 0] \qquad [10.9]$$

where P_f is the probability of failure and Z is the limit state function describing the buckle formation, which is obtained by recasting the buckling formation criteria. The following equation denotes the buckling limit state function:

$$Z = P_{cr} - P \qquad\qquad\qquad [10.10]$$

where

P_{cr} = the critical buckling load. For a pipeline with a lateral OOS, it can be expressed as $P_{cr} = \mu_{LS} \cdot W \cdot R$

μ_{LS} = the seabed static lateral friction coefficient

R = the effective radius of curvature over a sufficient length to induce buckling;

P = the driving force for the next buckling event $P = \mu_{LS} \cdot W \cdot x + \mu_{LD} \cdot P_1 + P_0$

The probability of buckling failure is determined by using first order reliability methods. Hence, all model uncertainties are modeled using normal distributions.

The SRA techniques can be used for the assessment of buckle initiation, buckle interaction, and the postbuckle state of the pipeline. The assessment considers sources of uncertainty in the design solution that may affect the success of the buckle initiator by investigating the pipeline global response for variations in the following design variables:

- Pipeline operating conditions.
- Pipeline mechanical design and pipe properties.
- Geotechnical properties.
- Planned and unplanned lateral buckle initiator properties.

Procedure of SRA Model

The method by which the pipeline response is modeled [10] is as follows:

1. Each buckle initiator—planned trigger/horizontal out of straightness/seabed feature—is associated with a nominal response, for the "best estimate" input data set.
2. A Monte Carlo simulation is used to give each buckle initiator a different input data set for each iteration. It is also used to locate the horizontal out of straightness features.
3. The nominal response is modified for each site to reflect the impact of the new input data set. This is achieved through numerical manipulation of a comprehensive database, which covers the entire range of each variable.
4. The pipeline postbuckle force profile is calculated based on the modified response, and the required information is extracted.
5. Steps 2 to 4 are repeated for enough iterations to provide statistical confidence in the results. For the ultimate limit state acceptance criteria of DNV-OS-F101, it is recommended that at least 10^6 iterations be completed.

The details of lateral buckling reliability of the pipeline design can be referred to in the papers [10–12]. SAFEBUCK developed a structural reliability model of the pipeline expansion process to calculate the probability of buckling and the likely spacing (probable VAS) between buckles, using probabilistic methods, as shown in Figure 10.15.
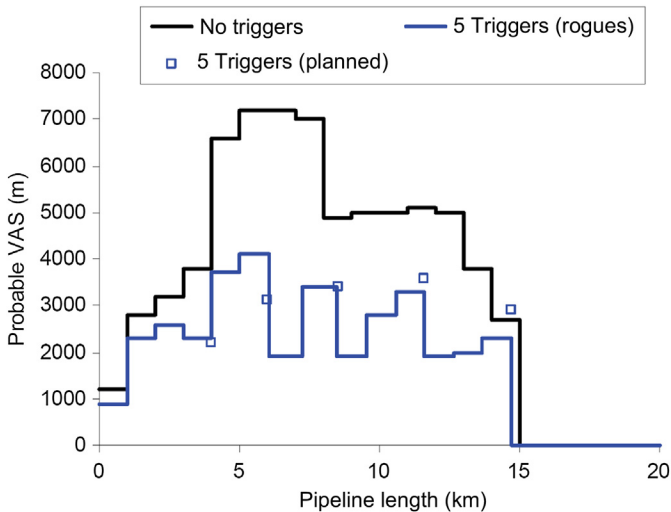
Figure 10.15 Minimum spacing between two buckle initiators.
Source: Bruton and Carr [13]. (For color version of this figure, the reader is referred to the online version of this book.)

3. Mitigation of Lateral Buckling

Introduction

Lateral buckle can be reduced or limited by reducing the buckle driving force and increasing buckle resistance. Using higher grade steel to decrease the wall thickness and lowering the operating pressure are methods to reduce the effective axial compressive force of pipeline, which is the main driving force behind buckling, but many engineering factors constrain the application of these methods. On the other hand, an increase of buckle resistance can be achieved by increasing soil resistance, axial restraint, bending resistance, or reducing OOS. Mechanical backfill, rock dump or mattresses for local restraint, and anchor flanges are the engineering practices to increase the buckle resistance. Lateral buckle mitigation can also be achieved by providing controlled lateral pipeline movements. Buckle mitigation devices are installed along the pipeline to provide planned buckle initiation sites, thereby forcing the pipeline to move laterally at these locations to relieve the axial load in the pipeline. The planned buckle initiation methods are described more fully with operational experience by Bai et al. [9]. The engineered buckle initiation methods that have been used on many deepwater projects to promote the reliable formation of lateral buckles and control the buckle spacing and operating loads include

- Snake lay pipeline sections to create lateral imperfections.
- Sleepers to create vertical upsets.
- Distributed buoyancy sections to create vertical imperfections with low submerged weights.

Snake-Lay Sections

For the snake lay method, the pipeline is laid in a snake configuration on the seabed. The zigzag pattern of the pipeline controls the lateral buckles so that they occur at the curved sections.

Figure 10.16 shows a typical snake lay with a zigzag pattern around a straight route centerline. The key dimensions of the "snake lay" are the buckle initiation/site pitch, site curve radius, and lateral amplitude as shown in the figure. The reliability of buckle formation can be increased by reducing the radius or increasing the lateral amplitude of curvature in each snake.

The buckle initiation/site pitch depends on the calculated minimum allowable distance, which limits the resulting thermal feed-in to acceptable levels and is dependent on the pipeline temperature profile in the section. Due to route considerations, the exact pitch and amplitude and the like vary along the route. To determine these key dimensions, finite element analysis is usually used, due to the complexity of the operation conditions and soil-pipe interactions. The typical pitch length is 1–2 km and the typical site bend radius is about 1 km. Snake lay may be a cost-effective buckle mitigation method when the pipeline is installed with planned curves on a relatively flat seabed at predetermined locations. The snake lay method is usually applicable to long pipelines at shallow and medium water depths. The advantage of the snake lay is simple execution for controlling the buckle initiation without expensive costs for subsea devices and installation. Usually a snaked curve achieves a lower critical buckling (buckle initiation) load at the pipe curved sections than in the straight pipe sections, due to the lateral imperfection. However, it is difficult to ensure enough lateral buckles in certain soil conditions and pipeline temperatures to reduce the maximum stress and fatigue damage down to an acceptable level.

Sleepers

A sleeper is typically a large diameter pipe section, with or without a simple support base, prelaid on the seabed perpendicular to the pipeline route to raise and support the pipeline above the seabed. Figure 10.9 illustrates two types of buckle mitigation devices using sleepers: single and dual sleepers. The sleepers create vertical out of
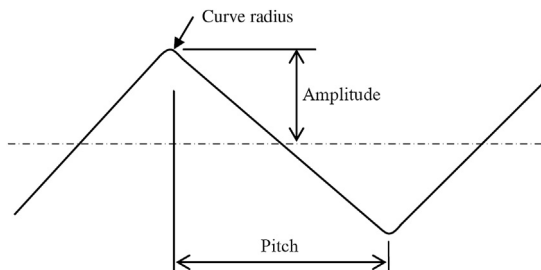
Figure 10.16 Typical snake-lay configuration.
Source: Bai et al. [9].

straightness features at discrete locations along the pipeline, which introduce initial vertical movements and subsequently develop global lateral buckles when the effective axial compressive force in the pipeline is high enough.

The advantages of vertical sleepers are that they create a definite out of straightness to lower the critical buckling force and reduce the uncertainties about the pipe-soil interaction. Pipe-sleeper contact reduces the lateral resistances to the pipeline at the designed buckle locations, although the soil berms at the pipeline touchdown points on both sides of the sleeper can offer some resistance to the pipeline's lateral movement. The reduction in lateral resistance for pipeline movement helps the pipeline initiate global buckles more easily and reduces the uncertainties associated with lateral soil resistance. However, the sleeper cannot be used in fishing areas and the created pipeline span length should be in the allowable range without a VIV problem.

Figure 10.17 shows the surveyed positions of a $12''$ pipeline and a single sleeper in the BP Greater Plutonio project, indicating the as-laid position (gray vertical line) and the postbuckling position (to the right) of the pipeline, where the light horizontal line represents the sleeper. The shadow to the left is where the pipe initially moved to during the hydrotest, before the full lateral buckle formed in operation.

Sleepers must be installed with a special emphasis on the accuracy of placement pipeline, prior to pipe laying. FE analysis is normally undertaken to determine the level of postbuckle displacement, bending moment, and strain and is addressed as a design issue of thermal expansion management. BP first adopted the single sleeper mitigation approach for in-field pipelines of the King project in the Gulf of Mexico [15], while Petrobras first adopted the dual sleeper mitigation approach in the pipeline of the PDET project off the coast of Brazil [10]. In the PDET project, the first approach was
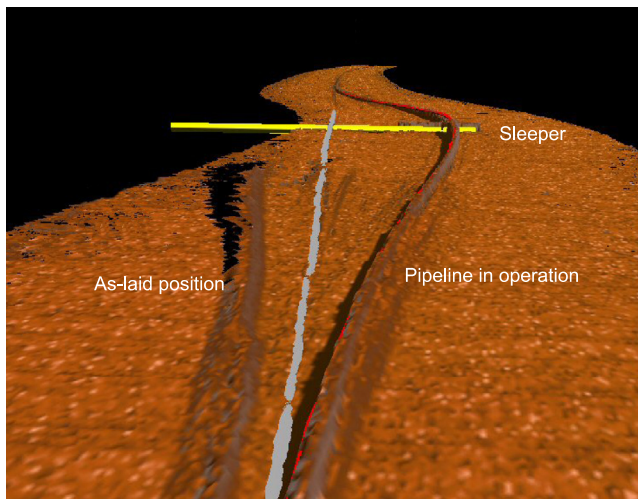
Figure 10.17 Lateral buckling of 12-inch pipeline on a single sleeper.
Source: Matheson et al. [14]. (For color version of this figure, the reader is referred to the online version of this book.)

to use the standard single sleeper, but the fatigue acceptance criterion was not fulfilled. The dual sleeper configuration was adequate to initiate lateral buckling at lower critical buckling load and meet the design criteria in the postbuckling configuration.

Distributed Buoyancy

The distributed buoyancy method distributes buoyancy modules at specific locations along the pipeline to act as buckle initiators and stress mitigation devices. Figure 10.18(a) shows a distributed buoyancy section on the pipeline, and Figure 10.18(b) shows a typical buckled configuration for a single buoyancy section with a length up to 100 m. The buoyancy force per unit length may be achieved either with increased insulation coating thickness or by attaching buoyancy modules with a calculated density to a number of pipe joints to ensure that the pipeline is near neutrally buoyant on a per unit length basis over the buoyancy section during normal operation. The amount of buoyancy varies from project to project, depending on the amount of stress mitigation needed. The length of each distributed buoyancy section, L_b is a key parameter to control the lateral buckling behavior. The localized buoyancy not only creates a small vertical OOS feature to encourage buckle initiation but also significantly reduces lateral soil resistance, although the locally high buoyancy/ seabed reactions occurring at the ends of the buoyancy section can increase lateral resistances locally.

Since BP first adopted the distributed buoyancy approach for the Thunder Horse Project pipelines in the Gulf of Mexico, the distributed buoyancy method has been used on a number of deepwater projects, including the Chevron Tahiti Project in the Gulf of Mexico [16]. With the distributed buoyancy method, discrete lengths of the pipeline (60–200 m) are installed with added buoyancy, facilitating sites for the initiation of controlled lateral buckle. A concern in employing this method is possible hydrodynamic instability.

Comparisons of Buckle Mitigation Devices

Figure 10.19 shows a comparison of buckled pipeline configurations using different buckle initiators. All these configurations are simulated using FEA, based on the same parameters. The bottom one is the case in which lateral buckling occurs without any buckle initiators. The configuration of pipeline buckle is Mode 3.

(a) Distributed buoyancy   (b) Typical buckle configuration
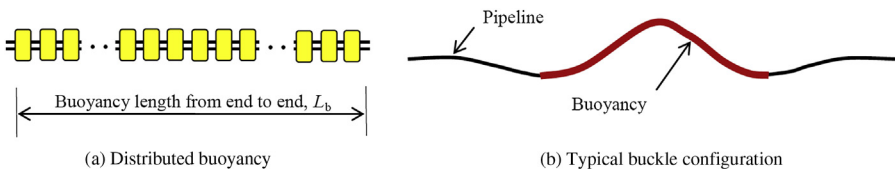
Figure 10.18 Distributed buoyancy and pipeline configuration.
Source: Bai et al. [9]. (For color version of this figure, the reader is referred to the online version of this book.)
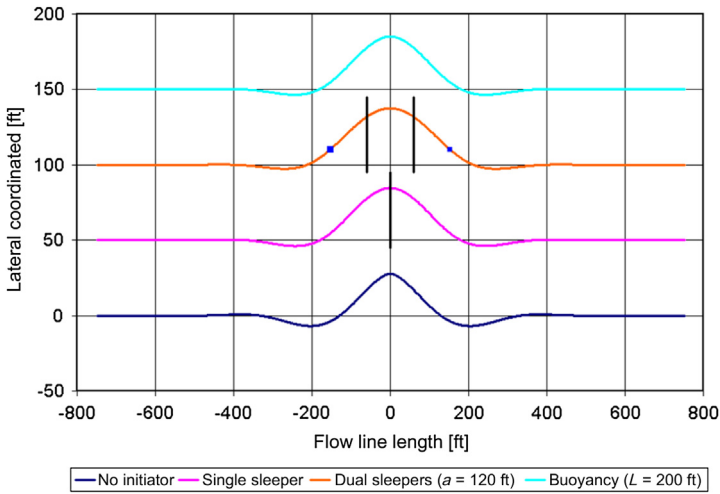
Figure 10.19 Comparison of buckle configurations for different buckle mitigation methods. (For color version of this figure, the reader is referred to the online version of this book.)

Above that is the case that a single sleeper is used. The second from the top is for a set of dual sleepers, while the top one is for a buoyancy section. The curvature of pipeline in the postbuckling configuration is the largest for the case without buckle initiators.

Figure 10.20 shows the cases that the gap of dual sleepers is 400 ft. In the buckled configuration, the middle section of pipeline touches the seabed due to a long sleeper
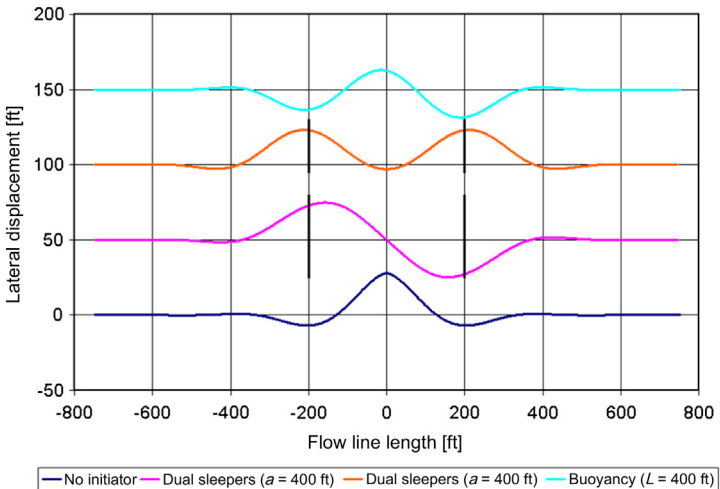
Figure 10.20 Comparison of buckle configurations for longer buckle initiators. (For color version of this figure, the reader is referred to the online version of this book.)

gap and the pipeline is buckled on the two sleepers separately. The top pipeline configuration is the case that 400 ft long distributed buoyancy is used. The pipeline buckling configurations become smoother after the buckle initiator is used. It means the stress and strain after buckling are lower than the case without buckle initiator.

Snake lay, sleepers, and distributed buoyancy are proven technologies as lateral buckle initiators and stress mitigation devices and have been employed in dozens of HPHT pipelines in the last several years. Snake lay is the simplest method, but its critical buckling load can be high. Distributed buoyancy typically has the lowest critical buckling load of the three methods. In general, dual sleepers have a lower critical buckling load than single sleepers, but it is still higher than that of long buoyancy section. Sleepers have the advantages of being easily procured and installed but may require a second installation vessel, and sleepers without supports may not be stable on large seabed slopes. For larger diameter pipelines, the dual sleeper may be a better option than the single sleeper, because the buckle initiation load is usually fairly high for a large diameter pipeline on a single sleeper. It is worth it to point out that multiple controlled buckle mitigation methods can be adopted in the same HPHT pipeline.

4. Pipeline Walking

Introduction

Pipeline walking normally occurs in short, high temperature pipelines. The term *short pipeline* means that the pipeline thermal expansion does not reach the constrained middle section of pipeline but to only a VAP located in the middle of the pipeline. "Short" pipelines can be a few kilometers long for a HPHT pipeline. The walking phenomenon can also occur in longer lines where lateral buckling has occurred.

Figure 10.21 illustrates the effective axial tension profiles of a short pipeline under operating and cooldown conditions. The slope of the effective axial tension profiles is defined by the axial friction force, $f = \mu \cdot w_{sub}$. The fully constrained effective axial force, S_0, as defined by Eq. [9.29] is also shown for a reference. For a pipeline to be fully mobilized on load and unload, the change in fully constrained force, ΔS, must exceed the height of the force envelope defined by axial friction, $f \cdot L$. The condition under which cyclic constraint occurs can be expressed in terms of a constraint friction, f^*:

$$f^* = \frac{|\Delta S|}{L} \qquad [10.11]$$

If the friction force f is less than f^* (i.e., $f/f^* < 1$), the pipeline is fully mobilized, and the pipeline is defined as "short," which is the most susceptible to pipe walking.

The effective axial force profiles change significantly when a pipeline is long enough for a pipeline section to become fully constrained, as illustrated in Figure 10.22. The fully constrained force is insufficient to mobilize the axial friction along the full length of the pipeline for a pipeline to reach full constraint on the first load, $f/f^* > 2$. A fully constrained section prevents walking unless the gradient of the thermal transient is extremely high.
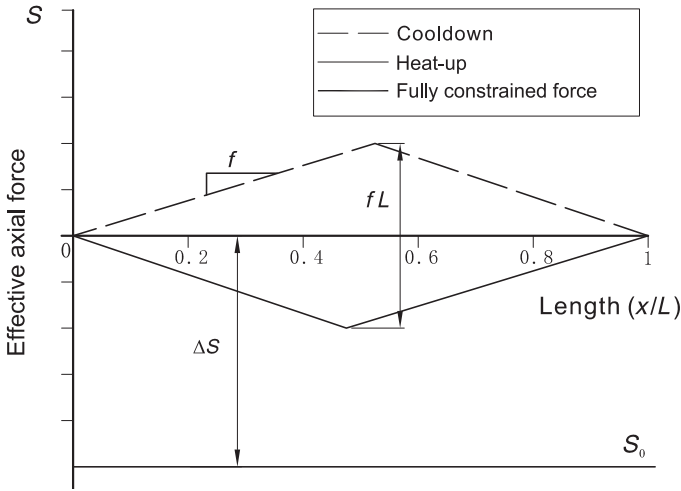
Figure 10.21 Effective axial force profiles for a "short" pipeline.
Source: Carr et al. [4].
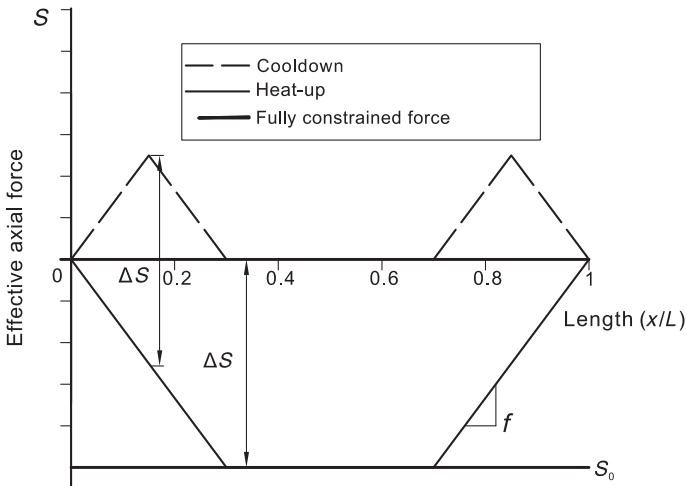
Figure 10.22 Effective axial tension profiles for a pipeline reaching full constraint.

Pipeline walking in short pipelines or long pipelines with formed lateral buckles may occur in the following conditions:

- The pipeline end is connected with a SCR, and pipe walking occurs in the same direction as tension from the SCR.
- A global seabed slope lies along the pipeline length, and pipe walking occurs from the high level to the low level of the seabed.

- Transient thermal gradients lie along the pipeline at the beginning of operating conditions, and pipe walking occurs from the "hot pipe end" to the "cool pipe end."
- Multiphase pipeline shutdown behavior increases the rate of walk downhill.

The mechanism of pipeline walking is the unbalance of effective axial force in the pipeline due to tension from the SCR, seabed slope, transient thermal gradients, or submerged weight change in the multiphase pipeline under cyclic thermal loads. Pipeline walking can be driven by each of these mechanisms; however, for most systems, the overall response is due to a combination of more than one. The phenomena and mechanism of pipe walking are detailed in the following sections.

SCRs

In deepwater field developments, it is common for pipelines to be tied with an SCR. Normally, an SCR is designed to pull the pipeline into tension at the SCR touchdown point (TDP). When the pipeline is short enough to become fully mobilized, the tension at the end of the pipeline can cause the short pipeline to walk during the heating and cooling cycles in the normal operating condition. It is assumed that the axial friction along the pipeline is sufficient to overcome the highest axial riser tension for axially stable pipelines. Figure 10.23 shows a typical floating production system with an SCR and flowline, and the flowline terminates at a subsea well or manifold.

Fully mobilized pipelines having a net effect force imbalance are subject to axial walking over a number of operating cycles, and the walking moves the pipeline incrementally toward the SCR TDP due to the tension. To control walking and prevent overstressing of the jumper connecting the PLET (pipeline end termination) to the well or manifold, an anchor is required at the PLET end. The slide PLET allows the flowline end to expand but limits its contraction by the anchor. After some walking,
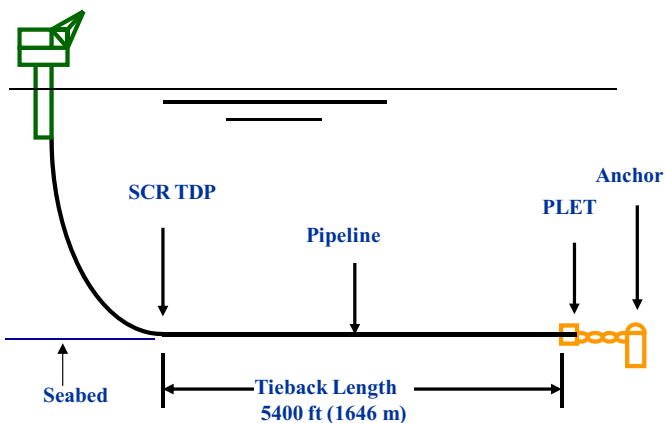
Figure 10.23 Typical subsea tieback with SCR flowline and PLET.
Source: Brunner et al. [17]. (For color version of this figure, the reader is referred to the online version of this book.)
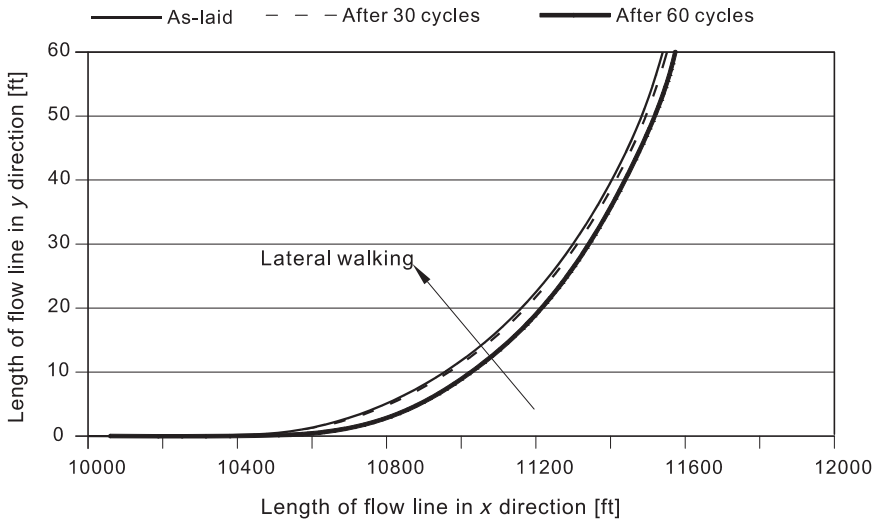
Figure 10.24 Typical pullout at route curve.
Source: Thompson et al. [18].

the flowline reacts against the anchor when the pipeline is contracted under cooldown conditions. The interaction between SCR dynamic loads and pipeline walking is very important in predicting flowline route curve pullout and anchor design. The maximum anchor loads due to pipeline walking are normally greater than the tension from riser dynamics alone and therefore govern the anchor pile design loads. However, the anchor can significantly increase tension in the pipeline during the cooldown procedure and the lateral instability at a route curve could occur, as shown in Figure 10.24, pulling out the route curve and allowing the pipe to walk farther axially, until the curvature is small enough to be laterally stable.

Figure 10.25 illustrates the effective axial force profiles of the pipeline in heat-up and cooldown conditions for a fully mobilized pipeline attached to an SCR at the cold end. The SCR applies a constant tension S_r, shown on the right of the figure. It is considered safe to assume that dynamic tension fluctuations can be ignored, as the duration of cooldown and heat-up procedures are expected to last several hours.

The tension from the SCR at the cold end of the pipeline causes asymmetry in the effect axial force profiles, with the operational virtual anchor, point A , located further from the SCR, and the shutdown anchor, B, closer to the SCR, as shown in the figure. Between the virtual anchors (A–B), the slope of the effective axial force profile remains the same on the heat-up and cooldown procedures, which is due to the friction force between soil and pipe. The slope of the force profile indicates the direction of movement, since it acts to resist movement. The pipeline section between points A and B expands toward the SCR on the heat-up procedure and contracts toward the SCR on the cooldown procedure. The pipeline section between A and B moves in the same direction during heat-up and cooldown cycles, and the expansion
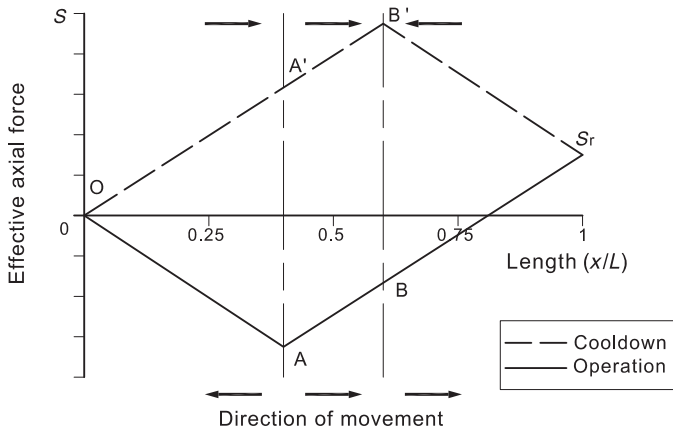
Figure 10.25 Effective axial force profiles for SCR at cold end of pipeline.
Source: Carr et al. [4].

and contraction are equal. The overall global displacement of the pipeline is therefore governed by the section between A and B, which causes the whole pipeline to displace toward the SCR in each heat-up and cooldown cycle.

The analytic analysis and FE validation [4] show that the pipeline walking per heat-up/cooldown cycle due to SCR tensions can be expressed as

$$\Delta_R = \frac{(|\Delta S| + S_r - f \cdot L)S_r}{EA \cdot f} \tag{10.12}$$

where

Δ_R = pipeline walk per cycle due to tension from the SCR
ΔS = change in fully constrained effective axial force between heat-up and cooldown
S_r = tension from the SCR
f = friction force, μW.

Seabed Slopes

The seabed slope along the route can cause pipeline walking under cyclic thermal loads. To analytically assess this phenomena, a pipeline is laid on a seabed with a slope ϕ. The weight component can be expressed as a modification of the friction force in the two directions, and it causes an asymmetry in the pipeline effective axial force profile. The weight component affects the shape of the effective axial force profile in a similar manner as the SCR tension, which is shown in Figure 10.26.

The analytic analysis and FE validation [4] show that the pipeline walking per heat-up/cooldown cycle due to a seabed slope can be expressed as

$$\Delta_\phi = \frac{(|\Delta S| + W \cdot L \cdot |\sin(\phi)| - W \cdot L \cdot \mu \cdot \cos(\phi)) \cdot L \cdot \tan(\phi)}{EA \cdot \mu} \tag{10.13}$$
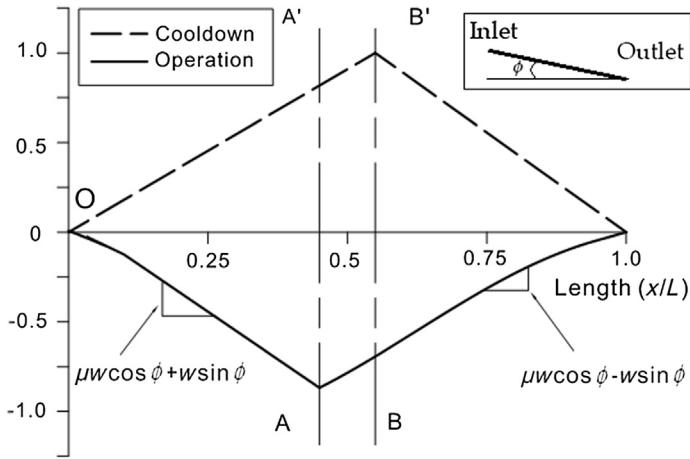
Figure 10.26 Effective axial force profiles for a sloping seabed.
Source: Carr et al. [4].

where

Δ_ϕ = pipeline walking per heat-up/cooldown cycle due to seabed slope
ΔS = change in fully constrained effective axial force between heat-up and cooldown
W = submerged weight of pipeline, N/m
μ = pipe-soil friction factor
L = pipeline length
ϕ = seabed slope

Thermal Transients

An important consideration in pipeline walking assessments is the direction of hydrocarbon flow and the resultant transients. Usually, the pipeline end closest to the wellhead or manifold is called the *hot end*, while the pipeline end at the reception facility or riser is the *cold end*. The direction of walking under thermal transient loading is generally toward the cold end of the pipeline.

Figure 10.27 illustrates a typical transient temperature profile of pipeline during the heat-up procedure. The temperature profile is nonlinear, because the pipeline is not heated uniformly along its length. The temperature rise of pipeline section goes forward along the pipeline over a period of time due to hot fluid moving forward. This leads to a nonlinear displacement response for all points along the pipeline. However, when a pipeline is in cooldown, fluid does not move and the fluid cools gradually along the whole pipeline. This leads to a linear load response during the cooldown process.

Figure 10.28 shows the distributions of effective axial force along pipeline during the steps of subsequent heat-up corresponding to the temperature profile as shown in
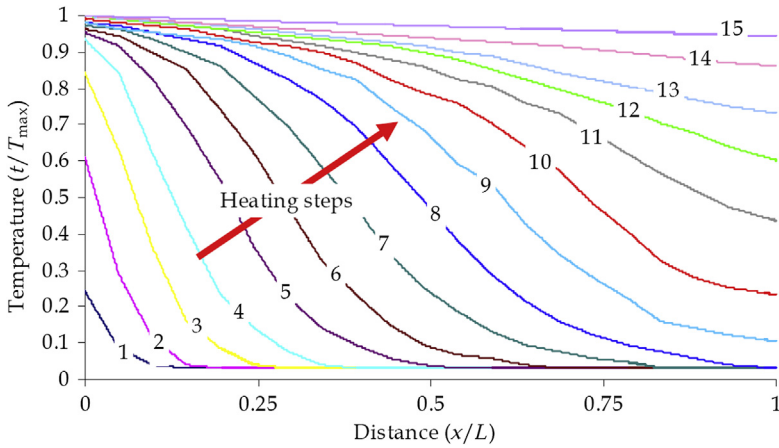
Figure 10.27 Typical temperature profiles along pipeline during heat-up procedure.
Source: Brutoin et al. [19]. (For color version of this figure, the reader is referred to the online version of this book.)
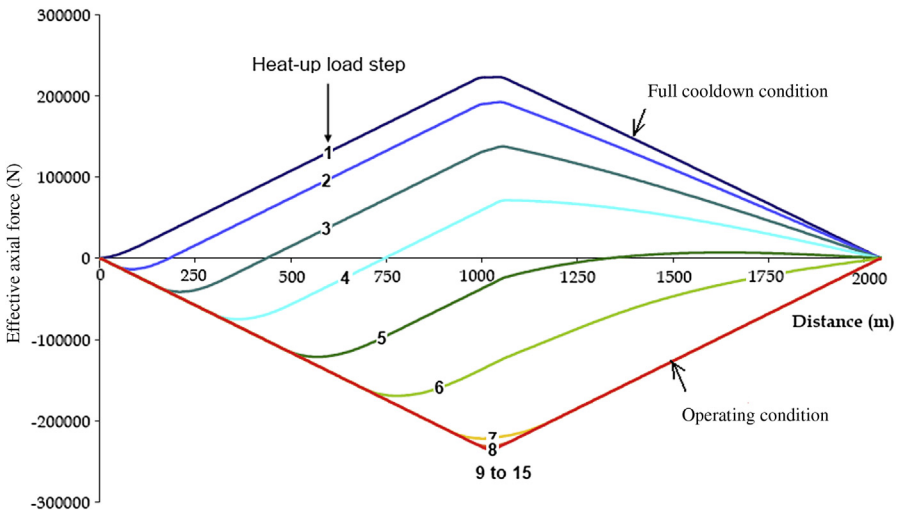
Figure 10.28 Effective axial force distributions along pipeline in heat-up procedure.
Source: Brutoin et al. [19]. (For color version of this figure, the reader is referred to the online version of this book.)

Figure 10.27. The distributions of effective axial force do not change after heat-up Step 8. As the pipeline heats up, the nonuniform expansion is obvious. Figure 10.29 shows a typical axial walking result at the mid-point and two ends of the pipeline due to the expansion and contraction under cyclic thermal loads. The pipeline walks from the hot end to the cold end.
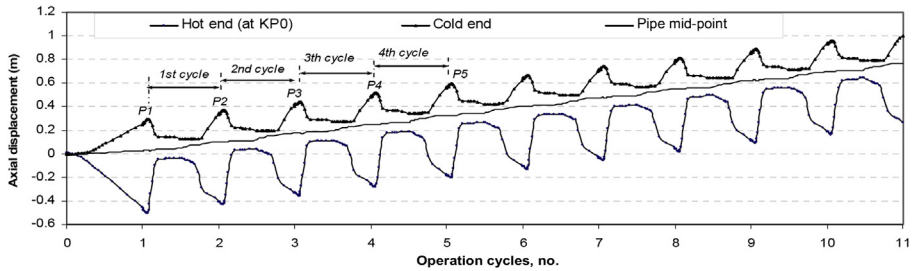
Figure 10.29 Axial walking under heat-up and cooldown operational cycles.
Source: Rathbone et al. [20].

Multiphase Flow Behavior

During the shutdown process in multiphase pipelines, the production flow stream can quickly separate into gas and liquid, which can result in significant variations in contents density and submerged weight along the pipeline. If the pipelines are laid on a slope, liquids typically settle at the bottom of the slope with gas accumulating at the top of the slope, as shown in Figure 10.30. This density variation can increase the propensity for pipeline walking down the slope.
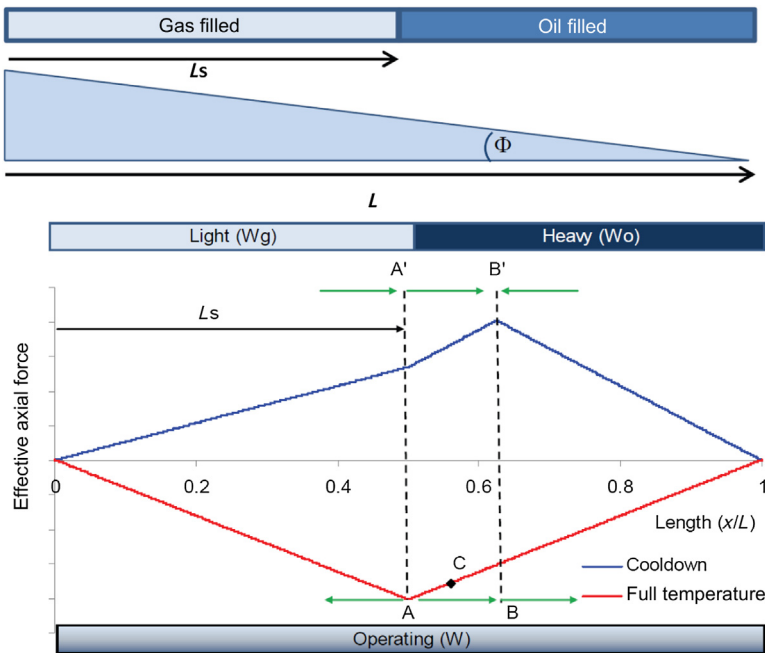
Figure 10.30 Pipeline walking due to liquid holdup in sloping seabed.
Source: Bruton et al. [21]. (For color version of this figure, the reader is referred to the online version of this book.)

The analytic analysis and FE validation [21] show that the pipeline walking per heat-up/cooldown cycle due to liquid holdup can be expressed as

$$\Delta_{\mathrm{L}} = \frac{(\Delta S_{\mathrm{c}} - \Delta S)X_{\mathrm{ab}}}{EA} \qquad\qquad [10.14]$$

where

Δ_{L} = pipeline walk per cycle due to liquid holdup
$\Delta L \Delta S$ = change in fully constrained effective axial force between heat-up and cooldown
ΔS_{c} = change in effective axial force over X_{ab} (multiphase)
X_{ab} = distance between virtual anchors
EA = axial stiffness of pipeline

Pipeline Walking Prevention

Axial walking itself does not cause the pipeline failure. However, as a result of the accumulated global displacement over a number of thermal cycles, axial walking may cause the failure of pipeline tie-in jumpers and spools. The walking occurred in a number of pipelines and led to at least one failure to date. To decrease the pipeline axial walking, increasing axial friction and pipeline anchoring are possible mitigation methods [10]. In shallower waters, rock dumping or burial is sometimes used; however, these techniques are often impractical and costly in deep water. Anchoring may be located anywhere along the pipeline; analysis has shown that midline anchors are subjected to lower loads than those located at the pipeline ends. Midline anchors are, however, often difficult to apply compared with anchors at the pipeline ends. Lower anchor load is required for the flowline system with more flexible anchor.

Anchoring

Axial anchoring is one method used to control and eliminate pipeline axial walking with a high probability of success. However, the anchors probably are large and heavy and require substantial vessels to install. The anchor location can be optimized to redistribute the end expansions. An anchor can be placed at VAP or at both pipeline ends to stop the walking. Anchoring at the pipeline ends is one of the most common methods for mitigation against pipeline walking. Figure 10.31 shows a pipeline expansion system schematic with an anchor applied at one end to control walking.

Anchoring at the first end of the pipeline is relatively easy, as the anchoring system can be included within the initiation system for the pipe laying operations. However, anchoring the pipeline at the second end or pipeline virtual anchor points requires a more complex solution. The suction anchor for the first end can be positioned accurately on the seabed prior to the start of pipe laying and either used to initiate the pipe laying or be connected to the pipeline after the laying operation. The connection to the pipeline can be made with a chain linking the suction anchor to the pipeline.

An alternative to the chain connection system at the pipeline's end is a system of direct mechanical connection of the pipeline to the suction anchor. Figure 10.32 shows two anchoring methods for the midsection of a pipeline. A preinstalled suction
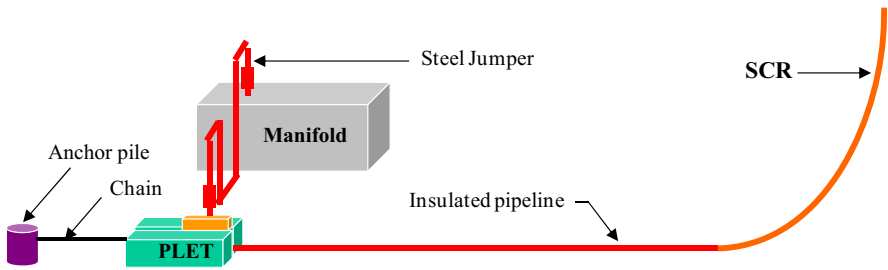
Figure 10.31 Flowline expansion system with an anchor to control walking.
Source: Brunner et al. [22]. (For color version of this figure, the reader is referred to the online version of this book.)
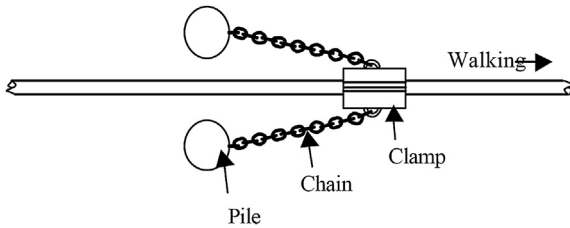
(a) Anchor and Chain Restraint for Pipeline
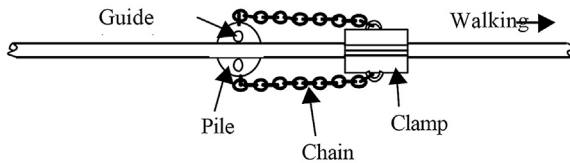
(b) Mid Line Axial Restraint System

Figure 10.32 Anchor system for middle section of pipeline.
Source: Perinet and Frazer [23].

pile can be used, fitted with a set of guides on the top. The pipeline is laid through the guides and a set of chains used to provide the connection to the suction anchor to provide the axial restraint to the pipeline.

Concrete Weight Coating

Axial and lateral friction resistances can be increased by applying a concrete weight coating, resulting in reduced end expansion and walking per cycle. The concrete coating can also help guarantee controlled buckles and reduce the axial feed-in to buckles. However, the likelihood of uncontrolled lateral buckling increases because of higher effective axial compressive force in the pipeline due to the higher axial

resistance. At the same time, the higher lateral friction may result in higher localized strains at the buckled locations, if the pipeline is buckled. It is often impractical to install concrete coated lines in deep water due to the heave weight of the pipeline, and they require an excessive top tension to install.

Trench-Bury

Trench-bury is another possible way to increase the axial friction resistance. However, the cost is high and equipment limited for deepwater trenching. Due to the insulating effects of the backfill, the operating temperature for a buried pipeline increases and the pipeline may be exposed to upheaval buckling. The determination of the trench depth is also challenging, due to the large uncertainty over backfill soil geotechnical properties.

Spot Rock Dump or Mattress

Spot rock dump or concrete mattresses can reduce the end expansion and walking per cycle. It can also help guarantee that controlled buckles occur, which reduces the corresponding axial feed-in to buckles. However, large quantities of rock dump or concrete mattresses are required to eliminate the walking problem. In addition, this method increases the installation time and cost, especially for mattresses. Specialist vessels are required for deepwater rock dumping.

References

[1] Perinet D, Simon J. Lateral buckling and pipeline walking mitigation in deep water. Houston: OTC 21803, Offshore Technology Conference; 2011.
[2] DNV. Integrity management of submarine pipeline systems. DNV-RP-F116, Det Norske Veritas; 2010.
[3] DNV. Global buckling of submarine pipelines. DNV-RP-F110, Det Norske Veritas; 2007.
[4] Carr M, Sinclair F, Bruton D. Pipeline walking—Understanding the field layout challenges, and analytical solutions developed for the SAFEBUCK JIP. Houston: OTC 17945, Offshore Technology Conference; 2006.
[5] Hobbs RE, Liang F. Thermal buckling of pipelines close to restraints. The Hague, The Netherlands: Offshore Mechanics and Arctic Engineering; 1989.
[6] Hobbs RE. In-service buckling of heated pipelines. J. Transportation Engineering March 1984;110(2):175–89.
[7] Collberg L, Carr M, Levold E. Safebuck design guideline and DNV RP F110. Houston: OTC 21575, Offshore Technology Conference; 2011.
[8] Carr M, Bruton D, Leslie D. Lateral buckling and pipeline walking, a challenge for hot pipelines. Amsterdam: OPT; 2003.
[9] Bai Q, Qi X, Brunner M. Global buckle control with dual sleepers in HP/HT pipelines. Houston: OTC 19888, Offshore Technology Conference; 2009.
[10] Rathbone A, Abdel-Hakim M, Cumming G, Tørnes K. Reliability of lateral buckling formation from planned and unplanned buckle sites. Estoril, Portugal: OMAE2008–57300, 27th International Conference on Offshore Mechanics and Arctic Engineering; 2008.

[11] Brown G, Brunner M, Qi X. Lateral buckling reliability calculation methodology accounting for buckle interaction. Houston: OTC 17795, Offshore Technology Conference; 2006.

[12] Carr M, Matheson IC, Peek R, Saunders P, George N. Load and resistance modeling of the Penguins flowline under lateral buckling. 23rd International Conference on Offshore Mechanics and Arctic Engineering. Canada: Vancouver; OMAE 2004–51192. Offshore Mechanics and Arctic Engineering; 2004.

[13] Bruton DAS, Carr M. Overview of the SAFEBUCK JIP. Houston: OTC 21671, Offshore Technology Conference; 2011.

[14] Matheson L, Carr M, Peek R, Saunders P, George N. Penguins flowline lateral buckle formation analysis and verification. 23rd International Conference on Offshore Mechanics and Arctic Engineering. Canada: Vancouver; 2004. OMAE2004–51202. Offshore Mechanics and Arctic Engineering.

[15] Harrison GE, Brunner M, Bruton DA. King flowlines—Thermal expansion design and implementation. Houston: OTC 15310, Offshore Technology Conference; 2003.

[16] Baker JHA, Bruton DAS, Matheson IC. Monitoring and effective integrity management of laterally buckled flowlines in deep water. Houston: OTC 17932, Offshore Technology Conference; 2006.

[17] Brunner M, Qi X, Zheng J, Chao J. Combined effect of flowline walking and riser dynamic loads on HP/HT flowline design. Houston: OTC 17806, Offshore Technology Conference; 2006.

[18] Thompson H, Zhang M, Brunner M, DeLack K, Qi X. Chevron Tahiti project flowline expansion control system. Houston: OTC 19858, Offshore Technology Conference; 2009.

[19] Bruton B, Carr M, Crawford M, Poiate H. The safe design of hot on-bottom pipelines with lateral buckling using the design guideline developed by the SAFEBUCK joint industry project. Brazil: Deep Offshore Technology; 2005.

[20] Rathbone A, Abdel-Hakim M, Cumming G, Tørnes K. Reliability of lateral buckling formation from planned and unplanned buckle sites. Estoril, Portugal: OMAE2008–57300, 27th International Conference on Offshore Mechanics and Arctic Engineering; 2008.

[21] Bruton DAS, Sinclair F, Carr M. Lessons learned from observing walking of pipelines with lateral buckles, including new driving mechanisms and updated analysis models. Houston: OTC 20750, Offshore Technology Conference; 2010.

[22] Brunner M, Qi X, Chao J. Challenges and solutions for deep water HP/HT flowlines. Marseille, France: Deep Offshore Technology; November 2003.

[23] Perinet D, Frazer I. Mitigation methods for deepwater pipeline instability induced by pressure and temperature variations. Houston: OTC 17815, Offshore Technology Conference; 2006.

11 Upheaval Buckling

Chapter Outline

1. Introduction

If a pipeline is not free to expand in the operating condition, restrained axial deformation results in an axial compressive force in the pipeline. The pipeline usually is not perfectly straight with some out of straightness (OOS), and the imperfections are typically due to the pipeline being laid over irregularities in the seabed profile. When the lateral restraint of a buried pipeline exceeds the vertical restraint force against uplift movement created by the pipeline submerged weight, the pipeline bending stiffness, and the covered soil resistance, the pipeline tends to move upward, and considerable vertical displacements may occur. This phenomenon is called *upheaval buckling*, which is a failure mode that has to be taken into account in the design of trenched and buried pipelines. The pipeline moves upward due to upheaval buckling, leading to possibly unacceptable local plastic deformations or collapse or vulnerability to fishing gear and other third-party activities.

The upheaval buckling of a pipeline has been known for a long time as a problem of land pipelines, and it has become one of the primary concerns in subsea pipeline design. The earliest documented upheaval buckling of a subsea pipeline is an 8-inch Rolf to Gorm pipeline in the Danish sector of the North Sea, as shown in Figure 11.1. The pipeline was insulated with a 2 inch thick PUF encased in a high density PE jacket. A 2 inch thick concrete weight coating was applied on top of the PE jacket, resulting in an overall pipe diameter of 0.45 m. The pipeline was buried to a depth of 1.15 m from the top of the concrete coating.

After this buckling failure, upheaval buckling becomes a subject of a major joint industry study, carried out by Shell International Petroleum Maatschappij (SIPM) in 1988–1990 with other major Europe oil companies. The analysis results were summarized and published in the 1990 OTC papers, [2]–[6]. Even though the failure did not lead to a loss of containment incident, the problem was recognized as potentially serious. Industry sensitivity to the upheaval buckling problem has been increased by a continuing trend toward higher operating pressures and temperature. With the increase of such high temperatures, almost all buried pipelines have a potential upheaval problem in the operating condition. In the North Sea, many pipelines are trenched to provide environmental stability and physical protection against fishing gear. The most commonly used method for upheaval buckling prevention is to increase the effective download of a trenched pipeline. Trenches can be done by natural or artificial backfill to provide restraint against upheaval buckling and increased thermal insulation of the pipeline.

The classical upheaval buckling analysis approach is to look for equilibrium states away from the initial state, under which the pipeline can be in a buckled configuration. The classical approach was developed in 1936 by Martinet, who was working on the upheaval problem of railway tracks, but the most accessible and complete description of this approach was by Hobbs [7]. The approach develops necessary conditions for a raised pipe to be in equilibrium but is not in itself an instability theory, since it does not explain how the pipeline jumps from the initial unbuckled configuration into the final buckled configuration. The upheaval buckling phenomena shows a very high degree of imperfection sensitivity, while the Euler column is not imperfection sensitive.
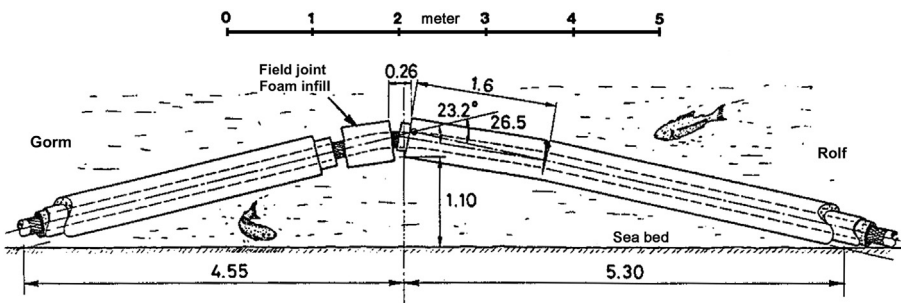
Figure 11.1 Example of subsea pipeline upheaval buckling.
Source: Nielsen et al. [1].

The progress of analysis approach was made and shown in the 1990 OTC papers, after realizing that imperfection is a key factor of the buckling problem. Figure 11.2 illustrates the relationship between the pipeline imperfection and the effective axial force for upheaval buckling. The imperfection with a larger curvature (smaller curve radius) has a lower compressive force than with a smaller curvature (larger radius) to initiate a buckle.

A joint industry project (JIP), HOTPIPE (1995–2002), was performed by Statoil, Norsk Agip, Snamprogetti, and DNV to develop industry knowledge of the design of HPHT pipelines susceptible to global buckling. The work of the JIP was summarized in several papers, [8] and [9], and comes up with a project guideline, DNV-RP-F110 (2007) [10] for the structural design of HPHT pipelines. The design criteria are based on the application of reliability methods to calibrate the partial safety factors in compliance with the safety philosophy established by DNV-OS- F101.

Figure 11.3 shows a configuration of trenched subsea pipeline under an initial imperfection. Two approaches to against the upheaval buckling are used in the engineering designs:

> Level I, an analytical model developed as a MATHCAD or Excel worksheet. It is usually used for preliminary design.
> Level II, a finite element model using general purpose FE software, such as ABAQUS. It is used for verification of analytical analysis of Level I or for some critical area in the detailed design.

Many analytical methods have been suggested in the last decades, some typical analytical models are described in the next section. The procedure of the Level I approach includes

1. Evaluate the initial configuration taken up by the pipeline when it is laid across an irregular seabed profile.
2. Calculate the external downward forces required to hold the pipeline in that initial configuration when it goes into operation.
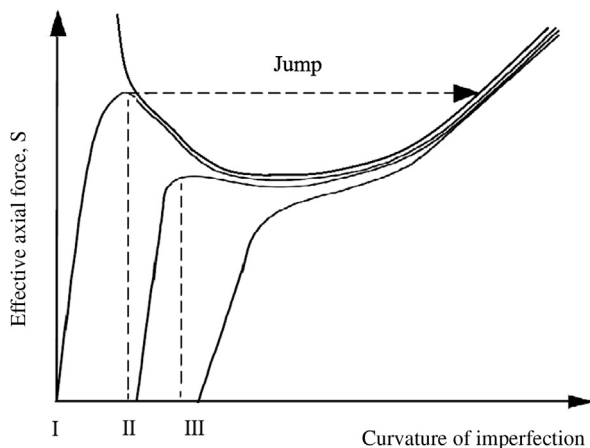
Figure 11.2 Response curve of upheaval buckling.
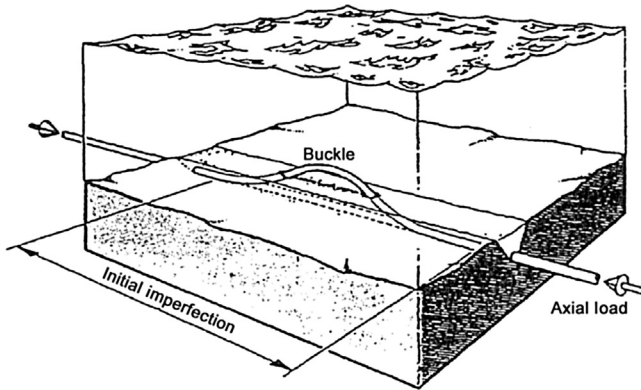
Figure 11.3 Upheaval buckling of a trenched pipeline.
Source: Pedersen and Mochelsen [11]

3. Determine the submerged weight of the pipeline and the uplift resistance of any soil cover or external anchoring.
4. Compare the required external force with the available force; if the available force is greater than the required force, the pipeline is stable, but if not, additional measures are needed to stabilize it.

Repeat these four steps for a range of imperfection heights, because the sizes and locations of the design foundation imperfections are unlikely to be available in the concept design phase. The typical range of heights is from 0.1 m to 0.7 m. Linear interpolation can be used to provide the cover requirements for intermediate cases. Analysis results can be summarized in a table for quick lookup in the concept design phase.

Level II analysis is a nonlinear numerical analysis using the FE method, taking account of elastic-plastic deformation of the pipe for the loading process of increasing operation temperature and pressure, based on the initial condition of the pipeline.

2. Analytical Solution of Upheaval Buckling

General

Upheaval buckling is caused by an increase in effective compressive axial force in trenched pipelines lying on an uneven seabed, due to temperature and pressure in the operating condition. The upheaval buckling phenomena is related to the following factors:

- The geometry, weight, and material properties of the pipeline.
- Operational pressure and temperature.
- Seabed profile and environmental characteristics.
- Cover and soil properties.

The vertical imperfections in pipeline are defined as as-trenched out of straightness, which are associated with upheaval buckling from the following sources:

- Imperfections of foundation (seabed), such as bounder, seabed profile, pipeline crossing locations, and the like. Depending on the shape of the foundation, the pipeline may follow the shape of the foundation.
- Pipeline imperfections introduced during the installation process by, for example, the reeling process or poor lineup during the welding process. The pipeline imperfection can be described in terms of its height and length, which may be determined by survey in the construction phase.
- Pipeline imperfections in the trench after the laying and trenching operation, such as variations in trencher performance or stop and start of the plough.

Figure 11.4(a) shows that, when the height to length ratio of the foundation imperfection is greater than the natural prop shape of the pipeline, there will be gaps under the pipeline. The foundation imperfection length, L_1, is smaller than the pipeline's natural wavelength. In this condition, the pipeline response to the imperfection under the compressive load follows the I curve in Figure 11.2. The pipeline deflection increases smoothly with the effective axial tension initially, and a large deflection is jumped at after a certain critical effective axial tension.

Figure 11.4(b) illustrates that the pipeline follows the foundation shape. The actual foundation wavelength, L_2, is greater than the pipeline's natural wavelength, and the pipeline response to the imperfection under thermal load is presented in the II curve of Figure 11.2. Partial separation between pipeline and foundation, and lifted crown is formed, and a large imperfection of pipeline may be created with the increase of the effective axial tension, as shown in Figure 11.5. Upheaval buckle may occur or not occur.

(a) Imperfection with gap between pipeline and foundation

(b) Imperfection with full contact soil foundation
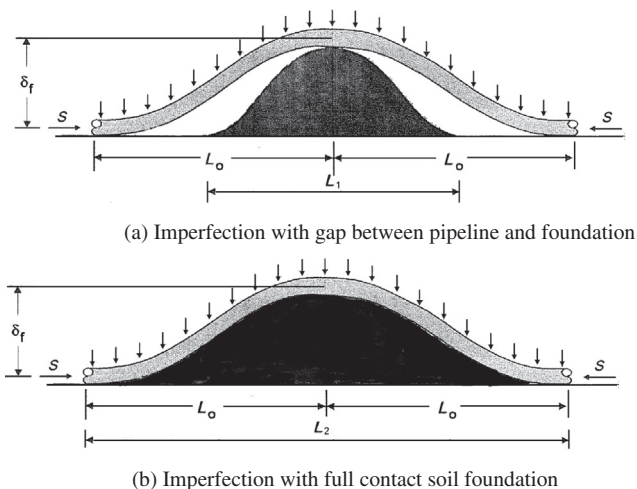
Figure 11.4 Imperfection pipeline and foundation.
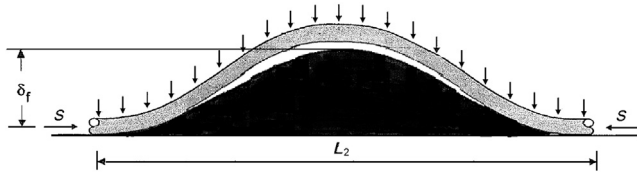
Figure 11.5 Lifted crown of pipeline with larger imperfection foundation.

Driving Force for Upheaval Buckling

Fully Constrained Pipelines

The driving force for triggering the pipeline upheaval buckling is the compressive axial force in the restrained pipeline due to the increase of temperature, the increase of internal pressure, and the residual tension left by laying pipe. Following the definition of the effective axial force in Chapter 9, the effective axial compressive force of fully constrained pipelines can be expressed as

$$S_0 = F_{\text{residual}} - (1 - 2\nu)(\Delta p_i)A_i - EA_s \alpha(\Delta T_i) \qquad [11.1]$$

where

S_0 = effective axial compressive force, (compressive, −; tension, +)
Δp_i = difference of internal pressure relative to laying condition. Since the internal pressure during installation normally is zero, this is identical to the operating internal pressure
ΔT_i = difference between operating temperature and installation temperature
A_i = internal bore area of the pipe
A_s = cross-sectional area of the pipe
E = Young's modulus
ν = Poisson's ratio
α = thermal expansion coefficient
F_{residual} = residual lay tension

Production profiles and reservoir analysis indicate that the maximum operating temperature and the maximum operating pressure may not occur at the same time. The design axial effective force should be calculated based on the worst combination that can occur, rather than on the two individual maximum values. The calculation of the driving force for the upheaval buckling at a particular point of the pipeline should take account of the predicted temperature and pressure profiles along the pipeline and not use the maximum values at the pipeline inlet.

Partial Longitudinal Constraint

If a pipeline end is connected with a riser or PLET, the effective axial compressive force from the virtual anchor point (VAP) to the pipeline end decreases with a slope of axial soil resistance from the fully restrained axial force at VAP.

Figure 11.6(a) illustrates an example of a pipeline end connected with a fixed riser. The pipeline end is able to expand toward the platform easily, because the riser is flexible by comparison with the pipeline end in the horizontal direction. Similarly, an expansion loop is incorporated to allow the pipeline to expand, and this expansion reduces the axial compressive force. Figure 11.6(b) shows the variation of effective axial compressive force along pipeline corresponding to the pipeline system shown in Figure 11.6(a).

The expansion movement of the pipeline toward the pipeline end is axially resisted by the seabed friction. If the axial frictional force between the pipeline and seabed is $\mu_a w_S$ per unit length, the effective axial force at a distance x from the platform is $R - \mu_a w_S x$, up to the VAP, at which the effective axial force becomes equal to the fully constrained force.

If the operating pressure and temperature are uniform along the length of the pipeline, the distance z at which the effective axial force reaches the fully constrained value is

$$z = \frac{R - S_0}{\mu_a w_S} \qquad\qquad [11.2]$$

Accordingly, the effective axial force in the flowline is

$$S_e = \begin{cases} R - \mu_a w_S\, x; & x < z \\ S_0; & x \geq z \end{cases} \qquad\qquad [11.3]$$
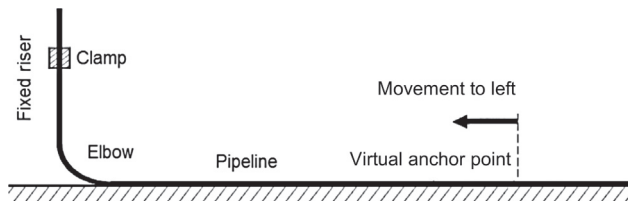
(a) Schematic
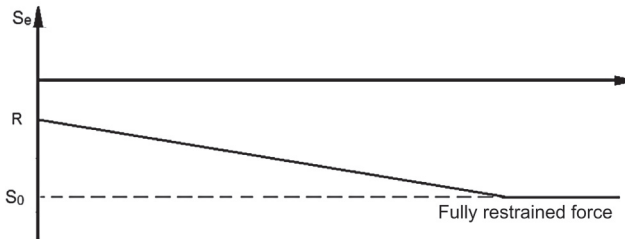
(b) Variation of effective axial compressive force

Figure 11.6 Effective axial compressive force of a pipeline connected with a riser.

where, μ_a is the axial friction coefficient and w_S is the submerged weight per unit length of pipeline. If a lateral or upheaval buckle occurs, the pipeline generally comes to rest with the axial force in the buckle less compressive than the force before the buckle occurred. The pipeline moves longitudinally towards the buckle from the both sides, but these movements are resisted by the frictional resistance from the seabed. The effect of buckling on the effective axial force in the pipeline is illustrated in Figure 11.7.

Residual Lay Tension

The residual lay tension of pipeline on the seabed, $F_{residual}$, can be calculated with installation software. If the pipeline is installed by pulling or towing, the residual tension is the pull force or the tow force. In general, it ranges from 10 kips to 60 kips, depending on water depth and pipe properties. If the pipeline is installed by S-lay or J-lay, the residual lay tension is a function of water depth and pipeline angle at the installation vessel.

The residual lay tension is difficult to accurately predict and in practice cannot be guaranteed. It may decrease with time due to axial creep or lateral movement. It is therefore generally assumed to be zero conservatively in the global buckling analysis.

Foundation Imperfection

An imperfection in the foundation is due to the variations in the vertical support conditions of the pipeline in the installed or buried condition when the seabed is not perfectly flat along the pipeline route. The imperfections may be caused by the presence of a boulder or some other isolated obstacle, varying soil properties along the pipeline length.

(a) Schematic

(b) Variation of longitudinal compressive force
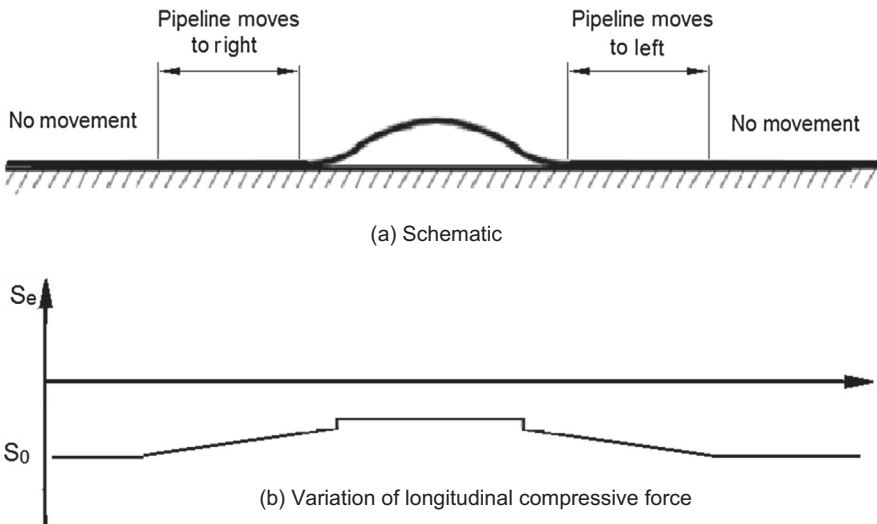
Figure 11.7 Effect of buckling on the effective axial force along a pipeline.

Stabilization of Pipeline

General

Different analytical models for against upheaval buckling are available in the literatures. However, analytical methods have the following limitations due to the assumptions on which they are based:

- linear elastic material behavior,
- simplified axial and lateral pipe-soil interaction,
- small deflection theory
- imposed shape of initial and post buckling configuration according to the assumed buckling mode.

Configuration of Spanning Pipeline

To make an initial assessment of the pipelines propensity for upheaval buckling and derive the driving force under the design and operational conditions, the spanning pipeline shown in Figure 11.4(a) is used for the analysis. The span configuration depends on the pipe properties, axial force, vertical load, and vertical deformation.

Figure 11.8 illustrates the profile of pipeline with a vertical imperfection under axial and vertical loads. This is a typical configuration for pipeline crossing. The horizontal distance is denoted by x, measured from the left pipeline touchdown point. The height of the pipeline is denoted by w, measured upward from seabed. The height of the vertical imperfection is denoted by δ, the total pipeline span length is $2L$. Only half of the system is considered, due to symmetry.

The pipeline is idealized as an elastic beam that carries an effective axial force S_0 and has flexural rigidity EI. It follows from elementary beam-column theory that the downward load $q(x)$ per unit length required to maintain the pipeline in equilibrium condition is

$$EI \frac{d^4w}{dx^4} - S_0 \frac{d^2w}{dx^2} = -q \qquad [11.4]$$
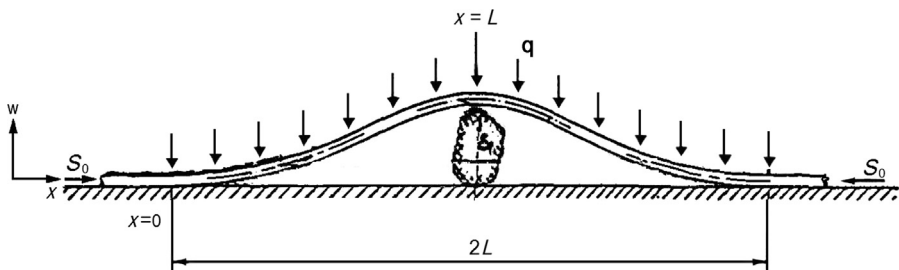
Figure 11.8 Pipeline with a vertical imperfection under axial and vertical loads.

with these boundary conditions:

$$w(0) = 0; \quad w'(0) = 0; \quad w''(0) = 0;$$
$$w(L) = \delta; \quad w'(L) = 0$$

[11.5]

The boundary conditions at $x = 0$ are simplified as a rigid pipe-soil contact. An more detailed assessment of spanning pipeline, including pipe-soil touchdown point and elastic pipe soil contact segment has been carried out and will be published in OMAE 2014. Equation [11.4] is applicable if the pipe is in an elastic condition. The pipeline spanning length, L, can be found using the equation with its boundary conditions, Eq. [11.5]. The solution of pipeline configuration is different when the effective axial force is tension or a compressive force.

The relationship between the span height and lengths are different for different axial force. For the case without effective axial force,

$$\frac{\delta}{\alpha} = \frac{L^4}{72}$$

[11.6]

For an effective axial tension,

$$\frac{\delta}{\alpha} = \frac{-\left[(kL)^2 + 4\right]\cosh(kL) + 4(kL)\sinh(kL) - (kL)^2 + 4}{2[1 - \cosh(kL)]k^4}$$

[11.7]

For an effective axial compressive force;

$$\frac{\delta}{\alpha} = \frac{\left[(kL)^2 - 4\right]\cos(kL) - 4(kL)\sin(kL) + (kL)^2 + 4}{2[1 - \cos(kL)]k^4}$$

[11.8]

where

$$k = \sqrt{\frac{|S_0|}{EI}} \text{ and } \alpha = \frac{q}{EI}.$$

The equation for the span length without axial force, Eq. [11.6], is rewritten as

$$L_0 = \sqrt[4]{\frac{72EI\delta}{q}}$$

[11.9]

After the pipeline profile is calculated, the profile can be differentiated to determine the curvature d^2w/dx^2 and its second derivative d^4w/dx^4, then the bending moment and bending stress along the pipeline can be calculated from the following equations:

$$M(x) = EI\frac{\partial^2 w}{\partial x^2}$$

[11.10]

$$\sigma_b(x) = \frac{M(x)D_0}{2I}$$

[11.11]

The shear force of pipeline cross section along the pipeline is expressed as

$$V(x) = EI \frac{\partial^3 w}{\partial x^3} - S_0 \frac{\partial w}{dx} \qquad [11.12]$$

Critical Buckling Load of Spanning Pipeline

Upheaval buckling occurs when the shear force of the pipeline, Eq. [11.12], at $x = L$ (the highest foundation imperfection in Figure 11.8) is zero for a pipeline under effective axial compressive force. Then,

$$\tan(kL) - (kL) = 0 \qquad [11.13]$$

The smallest solution of this equation is

$$kL = 4.493 \qquad [11.14]$$

Substituting this result to Eq. [11.8], we have the critical compressive axial force:

$$|S_{\text{critcal}}| = 3.962 \sqrt{\frac{qEI}{\delta}} \qquad [11.15]$$

and the corresponding critical span length is expressed as

$$L_{\text{critcal}} = 2.257 \sqrt[4]{\frac{\delta EI}{q}} \qquad [11.16]$$

The relationship between span length and effective axial force is presented in Figure 11.9, based on the calculation results from Eqs. [11.6]–[11.8]. The horizontal axis is a dimensionless axial force, $S_0 L_0^2 / EI$, and the vertical axis is a dimensionless span length, L/L_0. The term L_0 is the span length of pipeline when there is no axial force, which is expressed in Eq. [11.9]. The critical buckling point is shown in the figure with dashed lines. The polynomial correlation shown in the figure can be used in the quick engineering calculation.

Analysis of Upheaval Movements

The upheaval buckling of pipeline over a prop is analyzed in the last section. A brief description of a traditional upheaval buckling assessment for Level I analysis by Palmer et al. (1990) [4] is given in this section.

By using dimensionless terms, Eq. [11.4] can be written as follows:

$$\Phi_w = c\Phi_L^{-4} + d\Phi_L^{-2} \qquad [11.17]$$
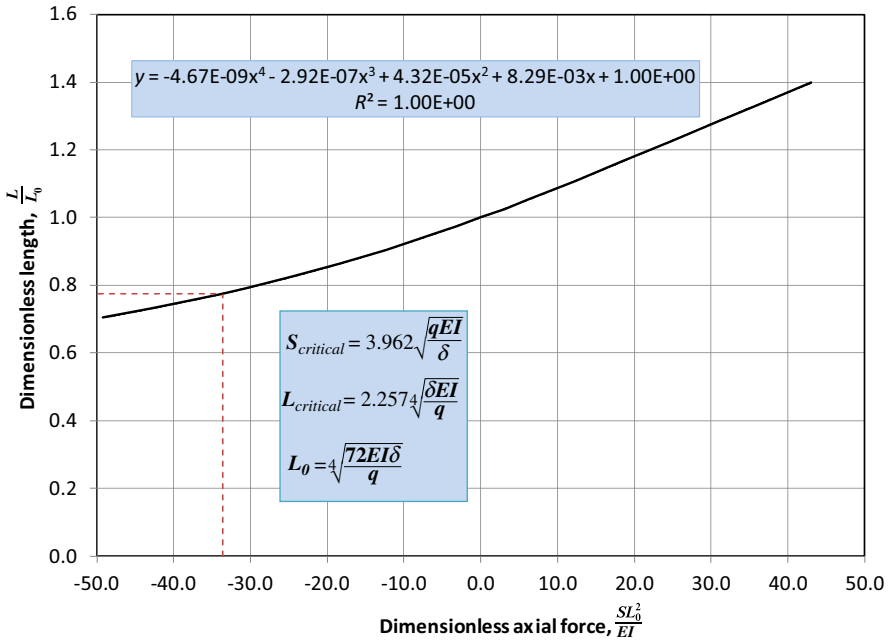
Figure 11.9 Dimensionless axial force and dimensionless span length.

where c and d are constants to be determined numerically. The dimensionless maximum download parameter is defined by

$$\Phi_{\mathrm{w}} = w_{\mathrm{req}} EI / \left(\delta_{\mathrm{f}}\, S_0^2\right) \qquad [11.18]$$

and the dimensionless imperfection length is defined by

$$\Phi_L = L_0 (S_0/EI)^{1/2} \qquad [11.19]$$

where

w_{req} = soil uplift resistance required to prevent upheaval buckling
δ_f = height of imperfection
L_0 = length of imperfection

Based on an extensive amount of analysis, the unknown values of c and d have been found, and Eq. [11.17] becomes

$$\Phi_w = \begin{cases} 0.0646, & \Phi_L < 4.49 \\ 5.68/\Phi_L^2 - 88.35/\Phi_L^4, & 4.49 < \Phi_L < 8.06 \\ 9.6/\Phi_L^2 - 343/\Phi_L^4, & \Phi_L > 8.06 \end{cases} \qquad [11.20]$$

The equation is plotted in Figure 11.10 with a solid line, and it provides a basis for estimating the required download when the imperfection height and wavelength are known. It has been shown [12] that the feature geometry being limited to prop-type and inability to account for the pipeline mobilization during operation are often seen as limitations to this formulation. The formulation does not always yield conservative results from the FEA numerical results shown in the figure, especially if there is a possibility of plastic deformation of pipe wall. To account for the pipeline mobilisation, the dimensionless maximum downloads parameter is redefined by

$$\Phi_{wm} = w_{req}EI/\left[(\delta_f + mob)S_0^2\right]$$

where mob is the pipeline mobilization displacement due to pressure and temperature in the operation.

For a lower imperfection length, the required download for pipeline stability is rewritten as

$$w_{req} = 0.0646\frac{\delta_f\,S_0^2}{EI} \qquad [11.21]$$

In most preliminary design case, the designer can determine the maximum height of a profile imperfection but not its length. An imperfection length can however be estimated from an assumption that the pipeline takes up a form dictated by the interaction of its flexural stiffness and its weight in the installed condition. A design formula for the required download for stability in the operating condition is

$$w_{req} = \left[1.16 - \frac{4.76(EIw_0/\delta)^{1/2}}{|S_0|}\right]|S_0|\left(\frac{\delta w_0}{EI}\right)^{1/2} \qquad [11.22]$$
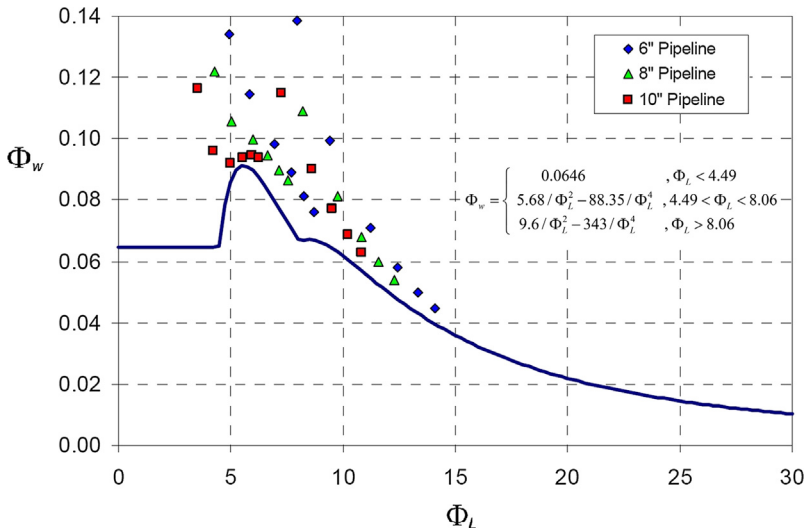
Figure 11.10 Universal design curve for required download. (For color version of this figure, the reader is referred to the online version of this book.)

where

w_{req} = total required download
w_0 = pipeline submerged weight in installation condition (empty)
S_0 = effective axial force
δ = prop (imperfection) height
EI = flowline bending stiffness

The initiation point at which buckling occurs is over an isolated base imperfection corresponding to a mound with the natural deflected form of the pipe as a prop imperfection with zero axial force present in the line and submerged weight equal to that of the pipe being flooded during trenching. When the flowline submerged weight is insufficient to provide an adequate upheaval resistance margin, soil or rock cover must be added. Upheaval resistance provided in this way consists of overburden weight acting directly on the outer surface of the pipe, together with shear resistance due to vertical movement of the associated soil wedge.

Snap Buckling and Upheaval Creep

Upheaval buckling during operation can take two basic forms, "snap" buckling and upheaval creep. Snap buckling generally occurs with a jump of vertical movement of pipeline because the driving force is sufficient to overcome all resistive forces when the pipeline is first put into operation. Upheaval creep is a phenomenon in which a buried pipeline progressively moves upward through backfill material due to driving forces by cyclic thermal loads of heat-up and cooldown. The pipeline expands and contracts cyclically due to this cyclic thermal loads in the lifetime of pipeline, which may cause the design criterion for upheaval buckling to not be conservative. Figure 11.11 illustrates an upheaval creep of an initially imperfection pipeline section after one year's operation.

A buried heated pipeline with an initial imperfection can lift itself upward, while in the operating condition, by slightly lifting the overburden without necessary being
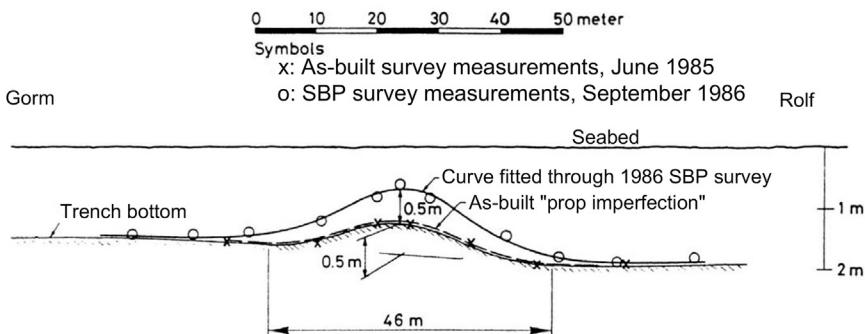
Figure 11.11 Observed upheaval creep of an initially "imperfect" pipeline section. *Source*: Nielsen et al. [1].

able to break out of the soil, that is, without upheaval snap buckling. The uplifted vertical deformations initially try to trace the same path back to the original imperfect configuration when the pipeline is unloaded. However, sand particles tend to fill the cavity below the pipeline created by the uplift and a small residual compression arises at the locations of pipeline deformation because of axial friction effects. These effects prevent a complete recovery to the original imperfect shape. On a subsequent reloading of the pipeline, these imperfections predispose the line to a vertical uplift at a lower temperature load than before, due to the magnification of the imperfection amplitudes. Therefore, if the size of the initial imperfection is above a certain limit, then a mechanism is created that may lead to upheaval buckling of the pipeline at a temperature lower than the design temperature after a number of heat-up and cool-down cycles. To avoid this upward creep of the pipeline, it is necessary to restrict the prebuckling deformations of the pipeline to very small values. As well as by a reduction of the allowable temperature rise, this can be done by imposing restrictions on the allowable imperfections of the pipeline and the trench.

The upheaval creep normally occurs only in clean sand and rock dumps with very limited component of silt or clay particles for pipeline displacements above a specified amount. Several studies have proposed various limits on the amount of allowable uplift to maintain the elastic recovery properties of the soil cover. It is recommended that the limiting of uplift movement to a value of 15–20 mm. Figure 11.12 illustrates the limiting permissible temperature, taken as the minimum temperature on the U-shaped curve.

A linear analysis of upheaval creep procedure was presented by Pedersen and Jensen [14] for a pipeline uplifting from the bottom of trench. It is assumed that the pipeline has an imperfection in the form of plastic deformations in combination with foundation imperfections. Figure 11.13 illustrates the model that has been derived from an elastic beam theory for the imperfect pipeline uplifted in the x-w coordinate system.
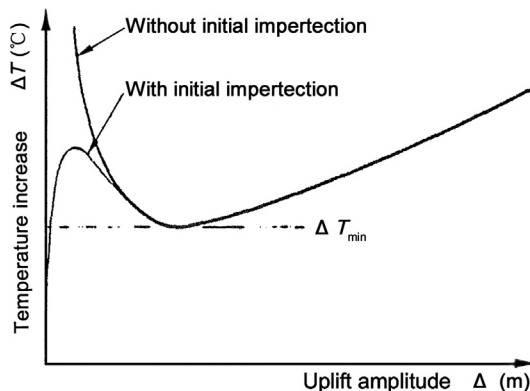
Figure 11.12 Uplifted pipe aptitude versus temperature rise.
Source: Ju and Kyriakides [13].
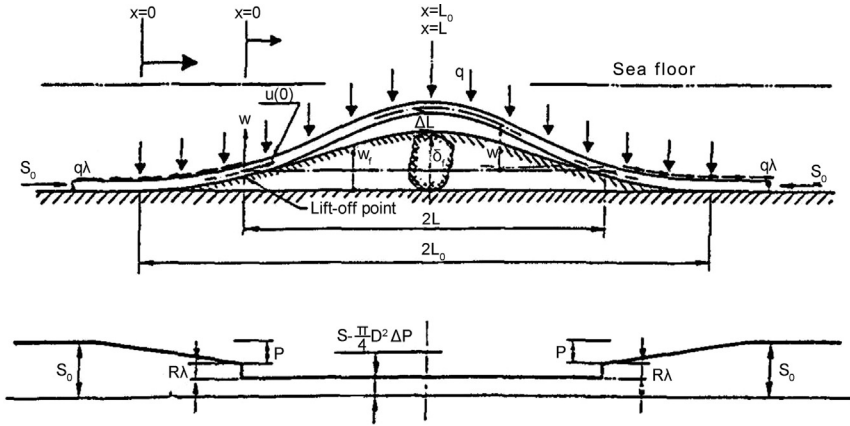
Figure 11.13 Uplifted pipelines (top) and variation in compressive axial force.
Source: Pedersen and Jensen [14].

The following is the numerical procedure for the calculation of uplift profile:

1. Calculate the k value associated with a given free span ($2L$) from Eq. [11.23]:

$$\left(\frac{\alpha}{k^3}+\frac{\gamma}{k}\right)\sin kL - \left(\frac{\beta}{k^2}-\kappa\right)\cos kL + \frac{1}{k^2}(-\alpha L+\beta) = 0 \qquad [11.23]$$

In this equation, the Greek letters are expressed in the following equations:

$$\alpha = \frac{q+q_p}{E\cdot I},$$

$$\beta = \frac{q_p\cdot(3L-2L_0)+3\cdot q\cdot L}{3\cdot E\cdot I},$$

$$\gamma = \begin{cases} \dfrac{q_f}{6EI}(L_0-L)(3L-L_0) & \text{for } L\le L_0 \\ 0 & \text{for } L > L_0 \end{cases}$$

$$\kappa = \begin{cases} \dfrac{q_f}{6EI}(L_0-L)^2 L & \text{for } L\le L_0 \\ 0 & \text{for } L > L_0 \end{cases}$$

where

q = total pipe weight per unit length, including weights of pipe and soil cover
q_p = weight due to pipe plastic deformation, calculated by $q_p = 72EI\delta_p/L_0^4$
q_f = pipe weight per unit length corresponding to δ_f, the height of a protruding stone or a pipe crossing

L_0 = half wave length of the foundation imperfection, given by, $L_0 = 2.913 \sqrt[4]{\delta_f \frac{EI}{q_f}}$
L = half uplift length as shown in Figure 11.12

then, the axial force of pipeline, S, is predicted using Eq. [11.24]:

$$S = EIk^2 \qquad\qquad [11.24]$$

2. Determine the deflection configuration from Eq. [11.25]:

$$w(x) = A\cos kx + B\sin kx + \frac{1}{k^2}\left(-\frac{1}{2}\alpha x^2 + \beta x + \frac{\alpha}{k^2} + \gamma\right) \qquad\qquad [11.25]$$

where

$$A = -\left(\frac{\alpha}{k^4} + \frac{\gamma}{k^2}\right), \quad B = -\frac{\beta}{k^3} + \frac{\kappa}{k}.$$

3. Calculate the associated pressure-temperature combination from Eqs. [11.26] and [11.27]:

$$S_0 = S - \frac{\pi}{4}D^2\Delta P + \sqrt{q\lambda EA_s \int_0^L \left\{(w')^2 - (w'_f)^2\right\}dx - (q\lambda L)^2} \qquad\qquad [11.26]$$

where S_0 is the effective axial compressive force away from the buckle, S is the compressive force in the uplift buckle, D is the steel pipe's outside diameter, ΔT is the temperature change, ΔP is the pressure difference between the product and environmental seabed, w' is the differential deflection, and w'_f is the differential initial deflection.

3. Finite Element Analysis of Upheaval Buckling

General

The buckling response of a pipeline should be analyzed using nonlinear finite element method, because FE analysis can describe this physical phenomena or behavior adequately by using large deflection theory. At the detailed design, FE analysis is normally used for marginal cases, where the simple analytical analysis shows the pipeline to be slightly unstable, or when the margin of safety has to be quantified in the conceptual design. The FE analysis of upheaval buckling has the following features:

- Possibility of using an arbitrary seabed profile.
- Consideration of the nonlinear material properties of the pipe.
- Allowance for mobilization distance for uplift resistance.

Finite Element Modeling

ABAQUS software [15] is a typical general FE program with 3D and nonlinear capacities to simulate the behavior of buried pipelines and pipelines laid on the seabed surface, under high temperature and high pressure loads.

Element Types

In general, a pipeline is simulated with pipe elements (PIPE31H, ELBOW31H) in the model to account for pressure and temperature effects in the analysis. The PIPE31H element is a 3D hybrid pipe element with six degrees of freedom at each node. The hybrid pipe elements have additional variables relating to the axial force and transverse shear force in the elements, which helps the computational convergence for nonlinear analysis. The length of element typically is on the order of one diameter where the buckle is expected to occur and may be longer in other straight segments.

Each of the pipeline elements interacts with the soil by mean of spring elements (SPRING2 or PSI34), and for each pipeline element, separate spring elements in the axial, lateral, and vertical directions are used to represent the pipe-soil interactions in all directions. The PSI34 elements are 3D pipe-soil interaction elements for modeling the interaction between a buried pipeline and the surrounding soil. These elements have only displacement degrees of freedom at their nodes. One side or edge of the element shares nodes with the underlying pipe element that models the pipeline, as shown in Figure 11.14. The nodes on the other edge represent a far-field surface, such as the ground surface, and are used to prescribe the far-field ground motion via boundary conditions.
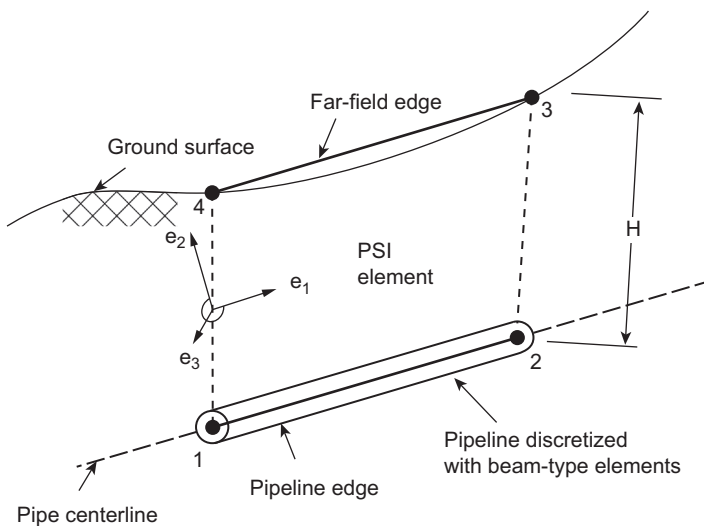
Figure 11.14 Pipe-soil interaction element (PSI).
Source: ABAQUS [15].

The PIPE-SOIL STIFFNESS command is the option for the element PSI34 to define the constitutive behavior for pipe-soil interaction elements in three directions. In the command, the constitutive model can be directly defined using the ASCE formulae for clay and sand [16].

Pipe-Soil Interaction

Pipe-soil interaction (PSI) is generally modeled using a series of independent nonlinear springs attached to the pipeline. These "springs" are characterized by nonlinear force-displacement relationships and represent an integration of the normal and tangential forces acting on the pipe surface when it interfaces with the surrounding soil, as shown in Figure 11.15.

Initial Pipeline Configuration

The development of the upheaval buckling mode is affected by the pipeline's initial as-laid configuration. The pipeline should be laid on the seabed or assumed imperfection under installation tension and environmental pressure from the initial straight and stress free pipe. The relevant buckling modes triggered by the pipeline on the seabed include stresses and strains in the pipeline with the initial configuration.

a) 3D soil restraint on pipeline   b) PSI with discrete springs

Transverse
horizontal   Axial   Transverse
vertical

c). Bi-linear soil springs used to represent soil force on pipe
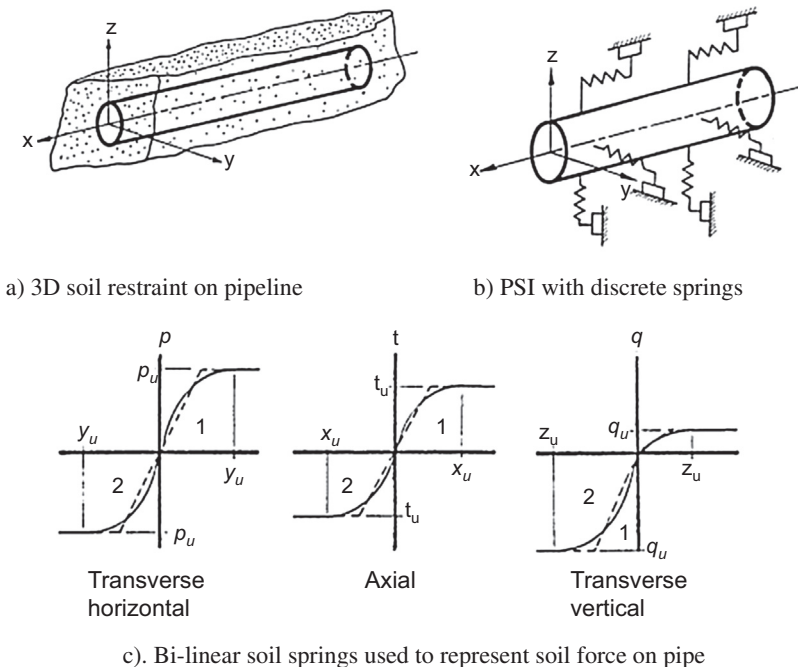
Figure 11.15 Pipeline-soil interaction modeling.
Source: ASCE [16].

However, in FE modeling, a lot of time normally is required to get the convergence in the contact between pipeline and seabed. For simplification, the imperfection profile of pipeline on a protruding object is predicted by Eqs. [11.6] to [11.8] and used as the initial pipeline profile for the FE modeling.

For the deflection shape of an elastic pipeline with no internal axial tension but with a bending stiffness of EI placed over an object with height of δ_f and loaded with a pipeline submerged weight per unit length, w_S, Eq. [11.6] gives the span length as

$$L_0 = \left[\frac{72 \cdot EI \cdot \delta_f}{w_S} \right]^{1/4} \qquad\qquad [11.27]$$

The analytical solution also gives the pipeline profile by following equation:

$$w(x) = \delta_f \cdot \left(\frac{x}{L_0} \right)^3 \cdot \left(4 - \frac{3x}{L_0} \right) \qquad\qquad [11.28]$$

Model and Analysis Steps

The FE model for simulating an upheaval buckling problem includes the following issues:

- Structure of the pipe system, including pipeline segment, spool pieces, pipeline crossings, in-line tie-ins, and PLETs.
- Installation effects, including the initial tensile loads due to lay installations.
- Seabed imperfection, seabed soil stiffness, and pipe-soil interactions.
- Trench resistance, cohesive and noncohesive soil cover, or combination of rock and natural backfill.

The upheaval buckling includes upheaval creep under cyclical thermal loadings. The load steps employed in the FE model should include installation, hydrostatic testing, normal operation, and heat-up/cooldown cycles. The following analysis procedure may be used to account for the loading cycles in the upheaval buckling and upheaval creep analysis:

- Lower the pipe onto the seabed profile to establish the contact between the pipeline and seabed.
- Apply the pipe weight and the buoyancy forces to simulate the installation condition.
- Apply pipe-soil interaction to keep pipeline configuration in the buried condition and remove contact.
- Flood and hydrotest the pipeline.
- Depressurize the pipeline.
- Heat-up with operation temperature and pressure.
- Cooldown to ambient temperature, including the change of prop imperfection during the cycles of loading.
- Heat-up and cooldown steps are repeated to check the upheaval creep of pipeline.

Design Criterion

Failure modes due to upheaval buckling for buried pipelines include

- Fracture and fatigue.
- Local buckling.
- Plastic deformations.

Several criterions must be satisfied for the pipeline to be safe against upheaval buckling:

1. **Upheaval creep/uplift:** Several studies have proposed various limits on the amount of allowable uplift to maintain the elastic recovery properties of the soil cover. For non-cohesive soil types, Pedersen and Michelsen [11] propose limiting the upheaval creep to a value equal to the uplift mobilization displacement, which is calculated from the following equation:

$$\frac{\delta_f}{D} = 0.02 + 0.08\frac{H}{D}$$

where δ_f is the uplift displacement corresponding to the peak uplift resistance (peak mobilization distance). Recently, Thusyanthan et al. [12, 17] proposed the following equation to predict the δ_f in loose sands in terms of H and D:

$$\frac{\delta_f}{D} = 0.02e^{\left[\frac{H}{2D}\right]}$$

2. **Strain criteria:** Follow DNV-RP-F110 [10].
3. **Local buckling:** Local buckling checks should be performed using the applicable code for the respective design.
4. **Fatigue and fatigue.**
5. **Ovalization.**

4. Stabilization Against Upheaval Buckling

General

Buried Pipeline

The subsea pipelines may be placed on the soil surface, but sometimes they are placed into trenches and subsequently backfilled. Burial of the pipeline has following advantages:

- The pipeline is protected against damage by marine vessel activities, for example, from dropped objects, laying of drag anchors, or fishing equipment such as trawl boards.
- Pipe movements due to currents and buoyancy are prevented when the pipelines with low submerged weight have challenges with stability.
- Heat loss along the length of the pipe is minimized. Temperature has a significant impact on the viscosity of the fluid, and low temperatures in the pipe may lead to hydrate formation.
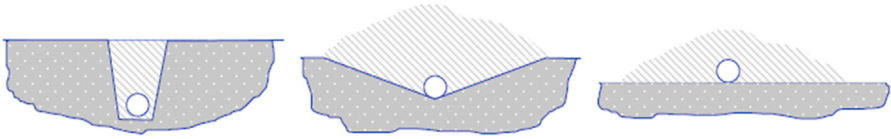
Figure 11.16 Possible scenarios for covered-restrained pipelines.
Source: DNV [10]. (For color version of this figure, the reader is referred to the online version of this book.)

Subsea pipeline trenching methods typically are categorized as

1. **Jetting:** The vehicle flushes the seabed through jets with a high-pressure fluid stream, eroding the seabed, and the soil (sand or soft clay) is fluidized, allowing the pipe to sink into the resulting "quicksand."
2. **Ploughing:** A trench is mechanically ploughed into the soil (sand or clay), the pipe is laid, and the soil is mechanically filled back over the pipe.

Figure 11.16 shows the possible scenarios for covered/restrained pipelines. The seabed soil, trenched soil, or additional soil is used for covering pipelines. At regions with hard seabed soil, rock dumping can be applied with rocks or gravel gathered from an onshore quarry. When rock dumping, cover material is dropped from a vessel through a steering pipe with acoustic profiling to minimize loss of rock. Trenching can also be performed without backfill to get a more even seabed. Normally the remolded strength of the soil above and around the pipe is significantly lower than that of the in-situ material.

Uplift Resistance of Soil Cover

Uplift resistance to upheaval buckling is provided by axial friction forces acting along the pipeline and by the uplift resistance loading of the backfill above the pipeline, due to the pipe weight and soil cover. Axial friction as well as the uplift resistance loading on the pipeline increase with the height of the soil cover. The prediction of upheaval buckling resistance for buried pipelines has been a challenge, as there are a huge uncertainty and randomness in the nature of soil cover created by various pipe burying techniques. The factors affecting the upheaval buckling resistance also include burial depth, time interval between burial and commissioning, rate of pipe pullout, and rock dump depth except for the soil properties.

Uplift Resistance versus Upheaval Buckling

Figure 11.17 illustrates a conventional pipe uplift resistance model. The resistance to pipe uplift occurs from (1) the submerged weight of pipe; (2) passive resistance from the dead weight of the column of soil bounded by vertical slip planes above the pipe ($W = \gamma'HD$); (3) active shear resistance mobilized along the line of the vertical slip planes, τ. In cohesionless soils, one popular hypothetical mechanism is the "vertical slip surface" model with linearly varying shear resistance with increased depth.
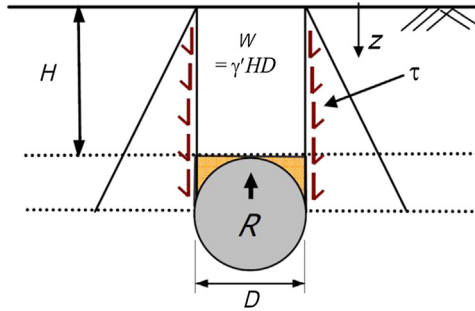
Figure 11.17 Uplift resistance model.
Source: Thusyanthan et al. [12]. (For color version of this figure, the reader is referred to the online version of this book.)

The uplift resistance per unit length can be derived from equilibrium in the vertical direction, (Schaminée et al., 1990) [5]:

$$\frac{R}{\gamma' H D} = 1.0 + \frac{f}{D}\frac{H}{} \qquad\qquad [11.29]$$

where

γ' = submerged weight of the soil and rocks dumped on the pipeline per length
D = pipeline overall diameter
H = the cover from the top of the pipe to the surface of the soil above the pipe centerline (backfill depth)
f = an uplift coefficient determined experimentally, generally about 0.7 for rock and 0.5 for sand, but occasionally much smaller in loose sand, as low as 0.1. This factor is also referred to as the *frictional resistance factor*, which can be expressed as follows:

$$f = K \tan(\phi)$$

where ϕ is the friction angle of cohesionless soil, and K is the coefficient of lateral earth pressure, $K = 1 - \sin^2(\phi)$. The values of these two parameters are suggested in DNV –RP-F110. For the lower bound of possible values,

$$f_{LB} = \begin{cases} 0.1 & \text{for} & \phi \le 30° \\ 0.1 + \dfrac{\phi - 30}{30} & \text{for} & 30° \le \phi \le 45° \\ 0.6 & \text{for} & \phi > 45° \end{cases}$$

DNV-RP-F110 recommends the use of the following uplift model for both cohesive (clay) and cohesionless (sand) soil, based on the Pederson and Jensen model [14]:

$$\frac{R}{\gamma' H D} = 1.0 + 0.1 \left(\frac{D}{H}\right) + \frac{f}{D}\frac{H}{}\left(1.0 + \frac{D}{2H}\right)^2 \qquad\qquad [11\text{-}30]$$

Table 11.1 Suggested f Values in the DNV Guideline

Backfill Type	ϕ_{peak} (°)	H/D Range	Mean of f	Range of f
Loose sand	30	[3.5, 7.5]	0.29	[0.1, 0.3]
Medium sand	35	[2.0, 8.0]	0.47	[0.4, 0.6]
Dense sand	40	[2.0, 8.0]	0.62	
Rock	N/A	[2.0, 8.0]	0.62	[0.5, 0.8]

Source: Wang et al. [17].

For cohesionless soils, suggested values of the uplift coefficient *f* and the applicable *H/D* range are summarized in Table 11.1.

Rocks are noncohesive materials and the relationship used to calculate the maximum resistance to uplift is similar to that of sand.

The current industry practice is to discount the shear contribution from uplift resistance for design scenarios with *H/D* ratios less than 1. However, recent research [12, 17] shows that the vertical slip surface model is a good representation of the true uplift deformation mechanism in loose sand at *H/D* ratios between 0.5 and 3.5. At very low *H/D* ratios (*H/D* < 0.5), the deformation mechanism is more wedgelike, but the increased contribution from soil weight is likely to be compensated by the reduced shear contributions. Hence, the design equation based on the vertical slip surface model still produces good estimates for the maximum available uplift resistance.

For cohesive soils, the uplift coefficient *f* can be expressed as

$$f = 2\overline{S}_u/\gamma'$$

where $\overline{S}_u$ is the average undrained shear strength at from center of the pipe to the top of trench.

5.   Design Against Upheaval Buckling

General

The most economical option is to do nothing to prevent upheaval buckling, to put the line into operation, then to stabilize any sections that show upheaval. The extent of deformation during upheaval buckling can be calculated using finite-element programs, if the plastic strains that develop in the pipe are acceptable, the pipeline has not suffered any loss of integrity, and it can remain in service. If the upheaval leaves a raised loop of pipeline above the seabed, the loop can be stabilized and protected by a careful rock dumping.

The most widely applied method of adding additional uplift resistance for mitigating upheaval buckling of buried pipelines is to cover the pipeline with dumped rock. The technology of rock dumping in deep water through pipes was developed in the late 1970s, initially for pipeline stabilization in the Danish sector of the North Sea, and has become an accepted routine operation [18]. However, continuous rock dumping is relatively expensive. This has prompted examination of ways of reducing

the quantity of rock needed for less cost. Many options are suggested, for example, reducing the driving force by reducing the wall thickness, using rock but in a more efficient way, using flexibles, and using bundles. Several of the options are detailed in the following section.

Reduction of Driving Force

The driving force for upheaval buckling is the effective axial compressive force due to temperature and pressure in the pipeline, which is expressed in Eq. [11.1]. The reduction of the driving force is able to be achieved in the following aspects.

Changes in Operating Parameters

It is possible to reduce operating pressure and temperature by omitting external insulation to reduce the temperature or by taking action to reduce the design pressure, if there are no flow assurance requirements in the operating pressure and temperature.

Reduction in Wall Thickness

The temperature term in the effective axial force equation is proportional to the wall thickness, t. This indicates that it is advantageous to reduce the wall thickness to the minimum possible. Reduction in wall thickness is a major topic in design because of cost. Increase in steel grade to X80 is one option with a little or no cost penalty, and X80 pipe can be welded without difficulty.

Increased Residual Tension

Another approach is to increase the residual tension. The as-laid tension is the horizontal component of the lay-barge tension applied at the surface. That tension can be increased, but some practical limitations include (1) possible external coating damage, (2) possible limitations of the mooring or DP system of the vessel, and (3) a long distance between the vessel and the touchdown point. However, the increases in the applied tension are significantly useful only for small-diameter pipelines. Because the relatively small-diameter pipeline would normally be laid with an applied tension about 0.5 MN (110 kips), which is only one fifth of the axial compressive force induced by the operating conditions, but for a large diameter pipeline, the effective axial compressive force in the operating conditions might be 10 MN, in comparison, a residual tension of 0.5 MN is only marginally useful.

Increased Flexibility

The effective axial compressive force can be reduced from its fully constrained value by allowing expansion movements to occur. This can be achieved by adopting expansion doglegs or expansion loops at the pipe ends, by laying the pipeline in a snaked or zigzag configuration, by laying the pipeline in a curve, or by even allowing the pipe to buckle laterally, if lateral buckling is easily mitigated.

Buried pipelines buckle upward because they can more easily move upward against their own weight and the uplift resistance of the cover than sideways or downward. On the other hand, for unburied, untrenched pipelines, buckling sideways is easier than upward.

Rock Dump or Mattress Stabilization

The pipeline buckling occurs at high locations in the pipeline profile. Therefore, the solution to hold down the pipeline at the high locations is placing extra weights, such as rocks, over it. If the critical imperfections cannot be identified confidently, a practicable but expensive option is to rock dump the whole length.

Cost analyses have shown that, if continuous rock dumping is selected, it can be more economical to lay the pipe, trench it, and dump rock over the trenched pipeline, rather than to rock dump over the pipeline on the natural seabed.

Pipe Bundle

Most bundles are constructed within a carrier pipe and connected to it at the ends by stiff bulkheads. If the internal lines and the carrier were all free to expand longitudinally under the operating condition, the internals would expand more than the carrier. Since the bulkheads prevent relative movements at the ends, the internal lines are put into compression while the carrier is in tension. The bundle as a whole expands longitudinally, but its expansion is resisted by the friction of seabed.

The resultant force across the bundle as a whole is compressive, but buckling does not generally occur because of the high flexural rigidity provided by the carrier. In addition, bundles in carriers are not generally trenched, so that they would buckle sideways rather than upward.

Route Selection and Profile Smoothing

A pipeline laid along an uneven seabed profile is much more subject to upheaval buckling than a pipeline laid along a smooth seabed profile. It may be possible to reduce this problem by careful route selection, both on the macro-scale and the micro-scale. A pipeline route can also be smoothed by "pre-sweeping" dredging. This is sometimes done to reduce spans but is an expensive option. An alternative is to smooth the pipeline profile during trenching. Most trenching operations leave the profile of the trench base smoother than the original seabed profile and eliminate short-wavelength irregularities.

References

[1] Nielsen NJR, Lyngberg B, Pedersen PT. Upheaval buckling failures of insulated flowlines: A case story. Houston: OTC6488, Offshore Technology Conference; 1990.

[2] Ellinas CP, Supple WJ, Vastenholt H. Prevention of upheaval buckling of hot submarine pipelines by means of intermittent rock dumping. Houston: OTC 6332, Offshore Technology Conference; 1990.

[3] Klever FJ, an Helvoirt LC. Dedicated finite-element model buckling response of submarine. Houston: OTC 6333, Offshore Technology Conference; 1990.

[4] Palmer AC, Ellinas CP, Richards DM, Guijt J. Design of submarine pipelines against upheaval buckling. Houston: OTC 6335, Offshore Technology Conference; 1990.

[5] Schamineé PEL, Zorn NF, Schotman GJM. Soil response for pipeline upheaval buckling analysis: Full scale laboratory tests and modeling. Houston: OTC 6486, Offshore Technology Conference; 1990.

[6] Guijt J. Upheaval buckling of offshore pipelines: Overview and introduction. Houston: OTC 6487, Offshore Technology Conference; 1990.

[7] Hobbs RE. In-service buckling of heated pipelines. ASCE J Transportation Engineering 1984;110:175–89.

[8] Collberg L, Mørk KJ, Levold E, Vitali L. HOTPIPE JIP: Design guidelines for HP/HT pipelines. OMAE2005-67523. Greece: Halkidiki; June 2005.

[9] Goplen S, Strøm P, Levold E, Hotpipe JIP. HP/HT buried pipelines. OMAE- 67524. Greece: Halkidiki; June 2005.

[10] DNV. Global buckling of submarine pipelines. DNV-RP-F110. Det Norske Veritas; 2007.

[11] Pedersen PT, Michelsen J. Large deflection upheaval buckling of marine pipelines, proceedings of behavior of offshore structures (BOSS). Norway: Trondheim; June 1988.

[12] Thusyanthan NI, Mesmar S, et al. Upheaval buckling assessment based on pipeline features. Houston: OTC 21802, Offshore Technology Conference; 2011.

[13] Ju GT, Kyriakides S. Thermal buckling of offshore pipelines. J Offshore Mechanics and Arctic Engineering 1988;110:355–64.

[14] Pedersen PT PT, Jensen JJ. Upheaval creep of buried heated pipelines with initial imperfections. J Marine Structures 1988;1:11–22.

[15] ABAQUS 6.10. ABAQUS analysis user's manual. Dassault Systemes; 2010.

[16] ASCE. Guidelines for the design of buried steel pipeline. Washington, DC: ASCE; July 2001.

[17] Wang J, Ahmed R, Haigh SK, Thusyanthan NL, Mesmar S. Uplift resistance of buried pipelines at low cover-diameter ratios. Houston: OTC 20912, Offshore Technology Conference; 2010.

[18] Palmer AC, Carr M, Maltby T, McShane B, Ingram J. Upheaval buckling: What do we know, and what don't we know? The International Seminar on Offshore Pipeline Technology; 1994.

12 Fatigue and Fracture

Chapter Outline

1. Introduction

This chapter provides an overview of fatigue and fracture relevant to the design and analysis of subsea pipelines and risers. The design and analysis procedures may be applied to other similar structures. The possibility of fatigue should be checked for any structural member that is subjected to cyclic loads. The fatigue life of the component is defined as the time it takes to develop a through-wall-thickness crack of the component.

Subsea pipeline and riser systems transmit production from a subsea drilling center to a hub facility, such as floating production storage and offloading system (FPSO), a

semisubmersible, or a tension-leg platform (TLP). Typically, the pipelines are several kilometers long and susceptible to fatigue loads in the installation and operation conditions, which include free span vortex-induced vibrations (VIVs) and cyclic thermal loads. VIVs may occur in both the risers and pipelines due to the spanning pipes in the transverse water current condition. Free spanning of the pipeline may occur depending on unfavorable seabed topography and soil properties. Once the free span is subjected to transverse water current, flow-induced vibration of the pipe due to vortex shedding can form a fatigue loading. This loading generates fluctuating axial stresses in the pipe, which act on the girth welds. VIVs and cyclic thermal loads are the primary concerns for subsea pipelines in the operating condition. The subsea risers are primarily affected by the host facility wave- and current-induced motions, which include first order wave-vessel motion, second order vessel motion, and vortex-induced motion. Both risers and spanning pipelines are subject to large number ($>10^3$) of relatively low range of stress cycles due to current and wave loads. The fatigue due to the high cycle loading is designated *high-cycle fatigue* (HCF). The stress range of HCF is low with deformation primarily elastic. The fatigue strength usually can be described by stress-based parameters.

On the other hand, the pipelines are subjected to cyclic thermal loads due to heat-ups and cooldowns of pipeline systems in the operating condition. Global buckling may occur in the pipeline as a result of high compressive effective force due to high temperature and high pressure. To control the global buckling, sleepers or buoyancies are placed at planned locations on the seabed to facilitate the lateral movement of the pipeline and control the curvatures or stresses and strains that are induced in the HPHT pipelines. Under these conditions, relatively large stress ranges may take place for a relatively low number of cycles (up to several hundred cycles of heat-ups and cooldowns in the service life) compared to HCF loads imposed on spanning pipelines and risers due to VIVs. This type of fatigue is called *low-cycle fatigue* (LCF). LCF is associated with plasticity in many cases; a strain-based parameter may be used for fatigue evaluation.

Fatigue Analysis Methodology

Fatigue is a progressive, localized structural damage, due to the initiation of a crack and its subsequent propagation, when a structure is subjected to the cyclic loading. Most structural failures are due to fatigue. Two engineering methods generally are used to assess and design against fatigue: (1) the stress versus number of cycles to failure (S-N) approach, which shows the relationship of the stress range and endurance time based on Miner's law; (2) the facture mechanics (FM) approach, which assess fatigue crack growth rate based on the Paris's law.

The S-N curve is based on S-N data, determined by fatigue testing of the considered welded detail, and the linear damage hypothesis. If the fatigue life estimated by S-N curves is shorter than the required service life for a component where a failure may lead to severe consequences, the fracture mechanics approach may be performed. However, this does not mean that the fracture mechanics method is better than the S-N approach. The fracture mechanics approach calculates the crack growth

using the Paris equation and the final fracture condition using recognized failure assessment diagram (FAD). The design fatigue life calculated by a fracture mechanics crack growth analysis should be at least 10 times the service life for all components for subsea pipelines. The initial flaw size for the fracture analysis should be the maximum acceptable flaw specified for the nondestructive testing during pipe welding.

S-N Approach versus FM Analysis

FM analyses for pipelines and risers normally give shorter fatigue lives than those obtained via the S-N approach, because the S-N data are obtained from the specimens with good quality welds, which have initial flaw depth on the order of 0.l–0.2 mm that is usually undetectable by ultrasonic testing (UT) from the outside of the pipe. With current technology, a practical limit of root flaw detection is estimated to be 0.5 mm, but it typically is taken as about 2 mm, which is the limit of detectability that should be used in FM calculations. In contrast to pipelines and risers, welds of most plates fail starting from a weld toe that can be detected via magnetic testing (MT), which has a better resolution than UT for the surface-breaking defects. Hence, the difference between S-N and FM calculations in plates is not as apparent. In addition, fabrication quality control in plates is much more consistent with S-N assumptions used in the fatigue analysis.

Unless the inspection resolution is improved to the level of detecting flaws presented in pipeline and riser welds, a significant discrepancy in fatigue lives obtained by S-N approach and FM analysis will remain.

2. Fatigue S-N Approach

Fatigue Assessment Based on S-N Curves

The S-N means stress range versus number of cyclic loading to failure. Figure 12.1 shows a typical S-N curve, in which the stress amplitude, S_a, is plotted on the vertical axis and the logarithm of the number of cycles to failure is plotted on the horizontal axis.

If the material is loaded below the limit stress, S_e, it will not fail, regardless of the number of loading cycles. The stress amplitude at which failure occurs for a given number of cycles is the fatigue strength. N is the number of cycles required for a material to fail at a certain stress range in fatigue life. The stress range, $\Delta S = S_{max} - S_{min}$, and number of cyclic loading are defined in Figure 12.2.

The design S-N curves are derived from fatigue tests based on the mean-minus-two-standard-deviation curves for relevant experimental data. Analysis of fatigue data requires techniques of statistics, especially survival analysis and linear regression. The S-N curves are associated with a 97.6% probability of survival. Generally, S-N curves can be accurately obtained only by tests, depending on joint details and welding procedure. Codes and standards, [1, 2], have historically provided such
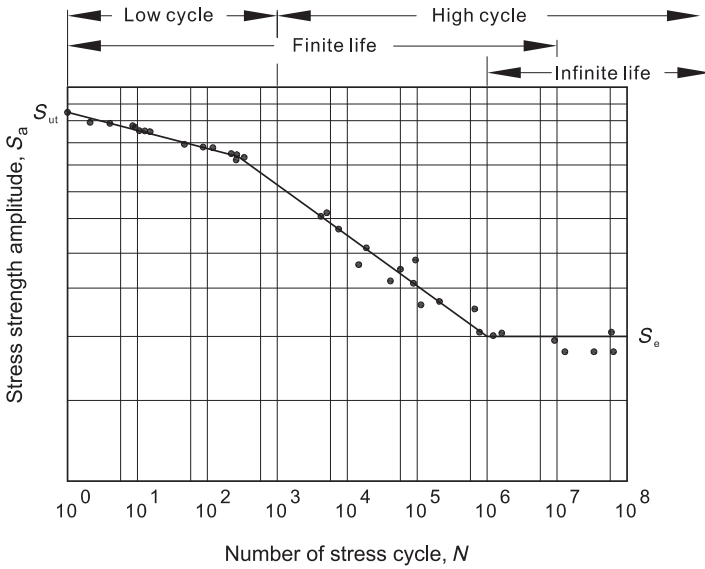
Figure 12.1 Typical S-N curve.

curves for generic welding procedures and types of joint detail but are primarily based on welded plate data.

Miner's Rule

In 1945, Miner developed a method called *Palmgren-Miner's rule*, which had first been proposed by Palmgren in 1924. Figure 12.3 shows the Palmgren-Miner's rule,
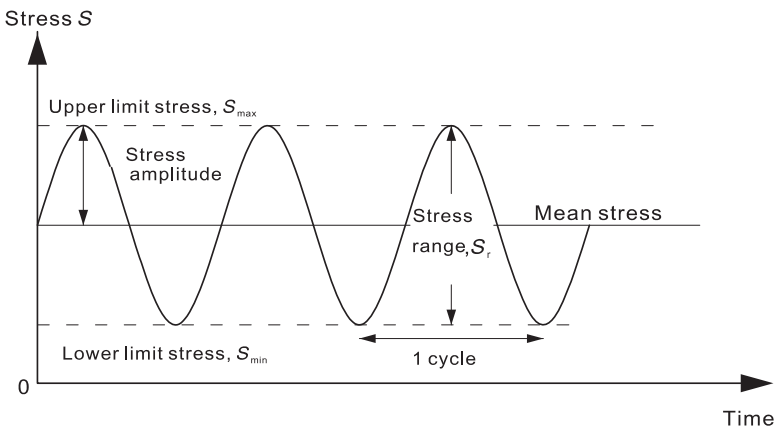
Figure 12.2 Fatigue load.
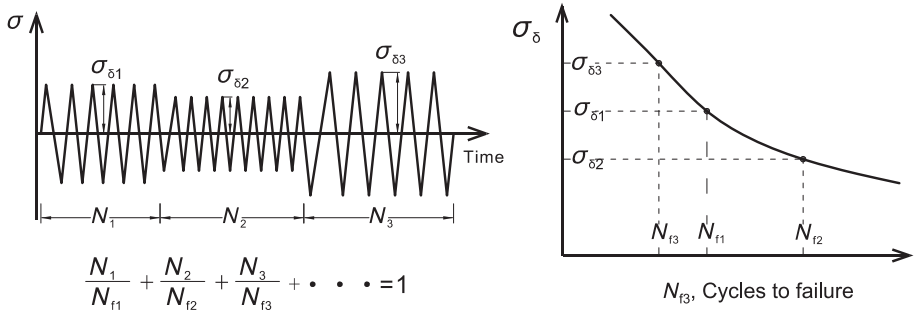
Figure 12.3 Palmgren-Miner rule.

which is also called the *Palmgren-Miner linear damage hypothesis*. It states that, when the long-term stress range distribution is expressed by a stress histogram, the fatigue damage may be calculated based on the accumulation law under the assumption that fatigue failure occurs when the Miner sum reaches one:

$$D_{\text{fat}} = \sum_{i=1}^{M_{\text{c}}} \frac{n_i}{N_i} \leq \eta \qquad\qquad [12.1]$$

where

D_{fat} = accumulated fatigue damage
η = allowable damage ratio/usage factor
N_i = number of cycles to failure at the *i*th stress range defined by S-N curve
n_i = number of stress cycles with stress range in block *i*
M_{c} = number of stress blocks.

Although Miner's rule is a useful approximation in many circumstances, it has two major limitations:

- It fails to recognize the probabilistic nature of fatigue, and there is no simple way to relate life predicted by the rule with the characteristics of a probability distribution.
- In some circumstances, cycles of low stress followed by high stress cause more damage than would be predicted by the rule. One drawback to the rule is that it does not consider the effect of overload or high stress that may result in a compressive residual stress. High stress followed by low stress may have less damage due to the presence of compressive residual stress.

The fatigue assessment can be carried out based on the following steps:

- Reduce the complex loading to a series of simple cyclic loading.
- Create an histogram of cyclic stress range.
- For each stress level, calculate the cumulative damage obtained from the S-N curve.
- Combine the individual contributions using an algorithm such as Miner's rule.

The procedure for fatigue analysis is based on the assumption that it is necessary to consider only the ranges of cyclic principal stresses in determining the fatigue

endurance; that is, mean stresses are neglected for fatigue assessment of welded connections.

The S-N curves to be used for calculation of the fatigue life of subsea pipelines and risers are defined by the following formula [1]:

$$\log N = \log a - m \cdot \log \Delta \sigma \qquad \qquad [12.2]$$

where N is the allowable stress cycle numbers; a and m are parameters defining the curves, which are dependent on the material and structural detail; $\Delta \sigma$ is the stress range (the difference between maximum stress and minimum stress in a stress cycle) including the effect of stress concentration. The key factors for the S-N approach include

- Selection of suitable S-N curves.
- Calculation of the stress-concentration factor (SCF) at the weld.
- Application of a correction factor to correct for the effect of thickness.

Fatigue Design Standards for Offshore Engineering

Two typical fatigue design standards for subsea pipelines and risers and subsea structures are BS7608:1993 [1] and DNV-RP-C203: 2008 [2]. ASME B31.4 and B31.8 design codes require the fatigue analysis as a design issue, but neither provides guidance on an appropriate analysis method. API 1111 refers to the design S-N curves recommended by BS7608. DNV-OS-F101 [3] references the fatigue recommended practice RP-C203. Basically, both BS7608 and DNV-RP-C203 are essentially a collection of fatigue design recommendations from a number of BSI sources and from the UK HSE guidance. DNV-RP-C203 specifically addresses girth welds in pipelines, while BS7608 refers to structural members.

HSE [4] and DNV [2,3,5] introduced the following classifications for the fatigue design of girth welds in tubes for the applications to North Sea structures:

- Class C for double-sided welds subsequently ground flushed and proven to be free from significant welding flaws.
- Class D for down-hand double-sided welds except those made by submerged arc welding (SAW).
- Class E for SAW and positional welds made by any process.
- Class F for single-side welds made on permanent backing.
- Class F2 for single-side welds made without backing, concerning over joint misalignment and poor weld root conditions.

Figure 12.4 shows the positions of fatigue design S-N curves labeled with letters (C, D, E, F, etc.) for girth welds based on BS7608. From Class C to F, the fatigue lives decrease monotonously for the same stress range. The girth weld is the primary concern of a pipeline subjecting to fatigue loading. Some pipe welding equipment allows some large diameter pipelines to be girth welded from both the outside and inside, as in the case of butt welded plate. The weld toes on both the inside and outside surfaces are the most likely sites for fatigue crack initiation. Mainly for economic and
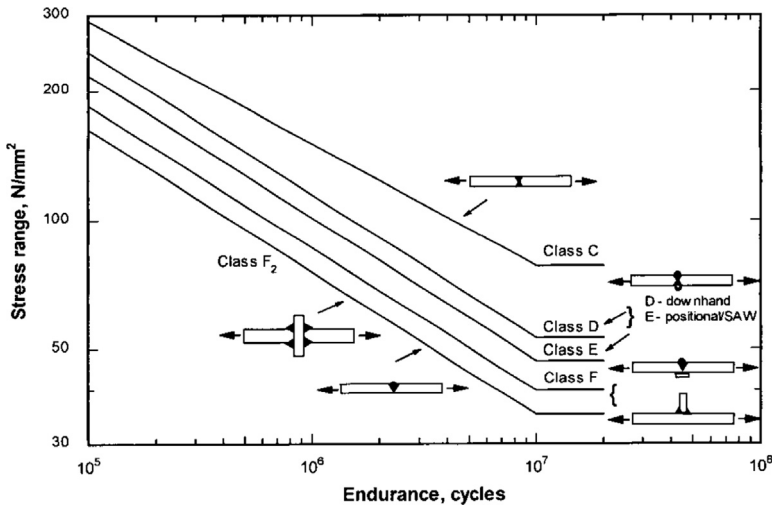
Figure 12.4 Fatigue design S-N curves for girth welds.
Source: BS7608 [1].

practical reasons, subsea pipelines are usually fabricated on the barge in the field using single-sided girth welds, and the fatigue is critical in the weld root for this kind of weld.
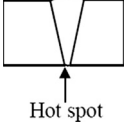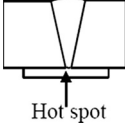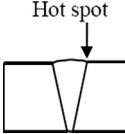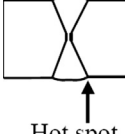
Table 12.1 shows the classification of welds in pipeline design and analysis, summarized in DNV-RP-C203. For the hot spot at the weld root of the pipeline internal surface, the F1 or F3 S-N curve without SCF is used, while for the hot spot at the weld top of the outer surface of a pipeline, the D S-N curve with SCF is used. S-N curves in both the air and seawater with cathodic protection are provided in DNV-RP-C203. An S-N curve in seawater usually is applied to the outer surface of the pipeline, while an S-N curve in air is applied to the pipeline ID, because the inner surface of the pipeline comes in full contact the internal production fluids. The S-N curves for free corrosion (without corrosion protection) are also provided in the design code. It is also common to use F2 S-N curves of BS-7068 in the pipeline design and analysis.

Subsea pipe-in-pipe (PIP) systems may be subjected to low-cycle fatigue damage due to lateral buckling under cyclic thermal loads and high-cycle fatigue damage due to VIVs. Typically, the weld joint for PIP systems comprise a butt weld on the internal pipe and either split shells or some form of sleeve arrangement for the external pipe connection. Special attention should be given to the fatigue assessment for the inner surface of internal pipe since it is subjected to the corrosive environment of production, and the outer face of the external pipe is subjected to a seawater environment.

The codes from which the S-N curves are chosen from usually give the equations to calculate the stress concentration factor due to pipe misalignment at the weld. The stress ranges should be multiplied by an appropriate stress concentration factor. For the condition of sour service, the stress ranges should be multiplied by both the stress

Table 12.1 Classification of Welds in Pipelines

Description					
Welding	**Geometry and Hot Spot**	**Tolerance Requirement**	**S-N Curve**	**Thickness Exponent k**	**SCF**
Single side	(figure) Hot spot	δ ≤ min (0.15t, 3 mm)	F1	0.00	1.0
		δ > min (0.15t, 3 mm)	F3	0.00	1.0
Single side on backing	(figure) Hot spot	δ ≤ min (0.1t, 2 mm)	F	0.00	1.0
		δ > min (0.1t, 2 mm)	F1	0.00	1.0
Single side	Hot spot (figure)		D	0.15	Eq. (2.9.1)
Double side	(figure) Hot spot		D	0.15	Eq. (2.9.1)

Source: Dowling and Townley [6].

concentration factor due to the pipe misalignment and the knockdown factor due to the sour service.

Control Factors for Fatigue Damage

Effect of Seawater

Figure 12.5 shows examples of Class E S-N curves for steel welded joints operating in seawater under various conditions, which is widely adopted for riser girth welds. For steels that are allowed to freely corrode in seawater, the fatigue life is reduced by a factor of about 3. Cathodic protection in seawater restores the steel performance in air, but only at low stresses and provides no benefit at high stresses. From the fatigue viewpoint, cathodic protection might be more harmful than free corrosion at high applied stresses due to hydrogen embrittlement, especially in high-strength steels.
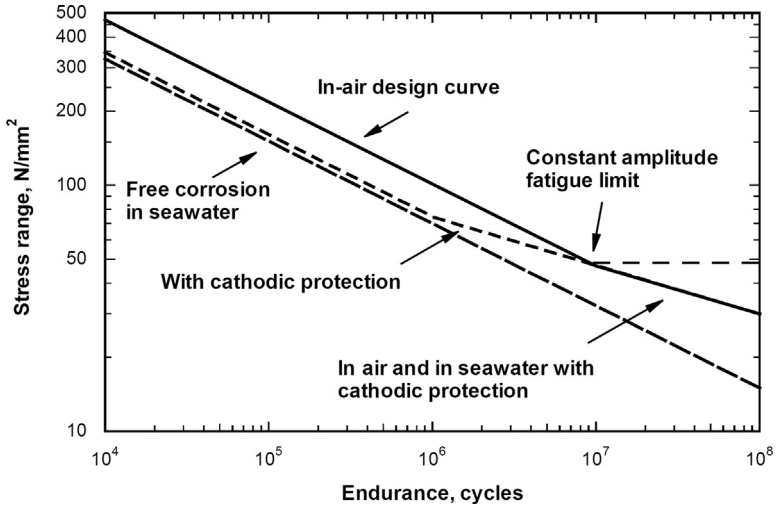
Figure 12.5 Examples of design S-N curves for steel welded joints.
Source: Maddox et al. [7].

Figure 12.6 compares the S-N curve in seawater with cathodic protection to that of the in-air S-N curve. When the fatigue limit is higher than 10^7, the curves are in the same line, but when the fatigue limit is lower than 10^7 for the same stress range, the S-N curves in seawater with cathodic protection gives a lower fatigue life.
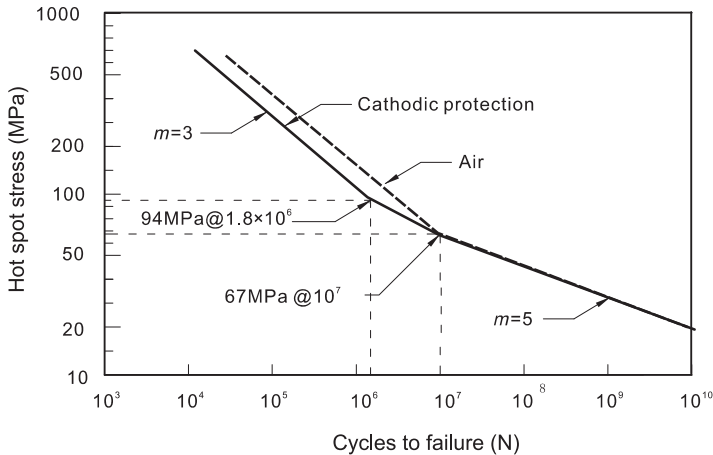
Figure 12.6 S-N curves for tubular joints in air and in seawater.
Source: Dowling and Townley [6].

Effect of Wall Thickness

For material thicknesses above the reference thickness, the following thickness effect should be applied for the S-N curve by a modification of stress range using a ratio of wall thickness with a reference thickness:

$$\log N = \log a - m \cdot \log \left[\Delta\sigma \cdot \left(\frac{t}{t_{\text{ref}}} \right)^k \right] \qquad\qquad [12.3]$$

where

m = negative inverse slope of the S-N curve
$\log a$ = intercept of $\log N$ axis
t_{ref} = reference thickness of 25 mm for welded connections other than tubular joints; for tubular joints, the reference thickness is 32 mm
t = nominal wall thickness of the pipe; $t = t_{\text{ref}}$ is used for thickness less than t_{ref};
k = thickness exponent on fatigue strength; $k = 0.10$ for tubular butt welds made from one side, $k = 0.25$ for threaded bolts subjected to stress variation in the axial direction

Stress Concentration Factors

Stress concentration factors (SCFs) at girth welds arise from geometrical misalignments when the pipes are fitted together. The combined effect of these misalignments induces a local secondary bending stress that augments the otherwise plain nominal stress in the pipe section, as the nominal bending moment and axial forces are transferred across the weld. Figure 12.7 shows the types of misalignment and distortion at girth welds of pipe. The SCFs can be obtained by direct FE analysis of the joint, by direct measurement with strain gauges, or by formulas obtained from parametric studies.

The SCF induced by the local axial misalignment, e, can be estimated by the method of Connelly and Zettlemoyer [8]:

$$\text{SCF} = 1.0 + 2.6 \frac{e}{t_{\min}} \left[\frac{1}{1 + 0.7 \left(\frac{t_{\text{thick}}}{t_{\text{thin}}} \right)^{1.4}} \right] \qquad\qquad [12.4]$$

(a) Offset misalignment   (b) Angular distortion   (c) Ovality
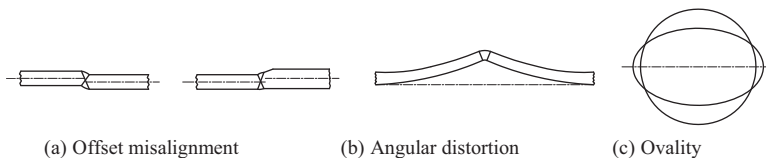
Figure 12.7 Types of misalignment and distortion.

In this formula, the SCF is the maximum surface stress of the thinner pipe divided by the cross-sectional area of the thinner pipe where the axial and local bending stresses are additive. The formula represents a mean fit to data points generated via FE analyses of mismatched pipes. The location where the maximum stress occurs is not necessarily the inner surface of the pipe. The SCF may be slightly conservative when fatigue failures initiate from the root pass of the weld. For design, the SCF needs to be adjusted to reflect the difference between the nominal thickness used in the pipeline or riser response analysis and the actual thin wall at which the SCF occurs.

The local misalignment that determines the SCF at a girth weld can be based on dimensional tolerances that vary with the size and manufacturing process of the pipe. Referring to Figure 12.8, the local misalignment, e, can generally be expressed as a function of the local out of roundness, OOR, and the wall thicknesses of the matching pipes, t_{thick} and t_{thin}, as follows:

$$e = \text{OOR} + \frac{t_{thick} - t_{thin}}{2} \qquad [12.5]$$

For the purpose of design, the maximum eccentricity, e_{max}, can be obtained by assuming the worst possible mismatch as determined from the thickness tolerances and OOR:

$$e_{max} = \text{OOR}_{max} + \frac{t_{thick} - t_{thin}}{2} \qquad [12.6]$$

in which

$$\text{OOR}_{max} = \text{OD}_{max} - \text{OD}_{min} \qquad [12.7]$$

and

$$t_{max} = t \cdot (1 + \alpha/100) \quad \text{and}$$

$$t_{min} = t \cdot (1 - \beta/100), \quad \text{with } t \text{ equal to the nominal pipe thickness}$$

and α and β to the percentages above and below the nominal thickness, respectively.
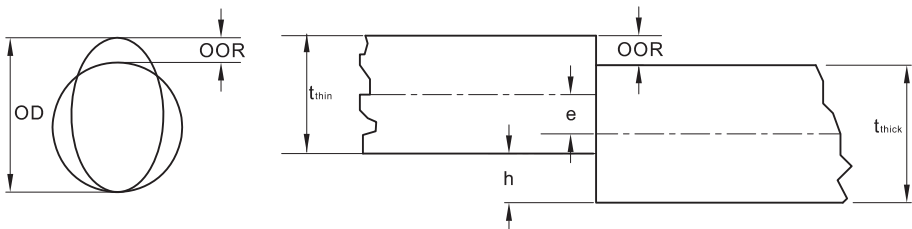
Figure 12.8 Local wall thickness mismatch conditions.
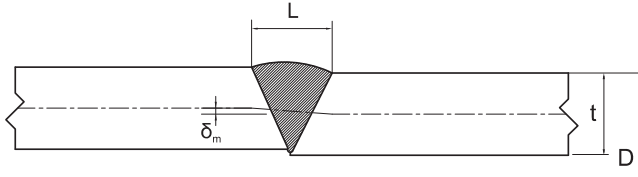
Figure 12.9 Dimensions of a welding cross section.

For weld grooves that are not symmetrical in shape, a stress concentration for the weld root due to maximum allowable eccentricity should be included. The stress concentration factor can be assessed based on the following expression [2]:

$$SCF = 1 + \frac{3\delta_m}{t} e^{-\sqrt{t/D}}$$ [12.8]

where the notations are shown in Figure 12.9. This stress concentration factor can also be used for fatigue assessments of the weld toes, refer also to Table 12.1. The nominal stress on the outside of the pipe should be used for fatigue assessment of the outside, and the nominal stress on the inside of the pipe should be used for fatigue assessment of the inside.

For welded pipes, ovality normally governs the resulting eccentricity. Therefore, the effect of tolerances can simply be added linearly. For seamless pipes, it is realized that the thickness tolerance contributes by a similar magnitude to the resulting eccentricity. A resulting tolerance to be used for calculation of the stress concentration factor using the preceding equation with $\delta_m = \delta_{Tot}$ can be obtained as

$$\delta_{Tot} = \sqrt{\delta_{thickness}^2 + \delta_{ovality}^2}$$ [12.9]

where

$\delta_{thickness} = (t_{max} - t_{min})/2$
$\delta_{ovality} = D_{max} - D_{min}$, if the pipes are supported such that they are flush outside at one point (no pipe centralizing)
$\delta_{ovality} = (D_{max} - D_{min})/2$, if the pipes are centralized during construction
$\delta_{ovality} = (D_{max} - D_{min})/4$, if the pipes are centralized during construction and rotated until a good fit around the circumference is achieved

Effect of H₂S

If the hydrocarbon fluids are not corrosive, fatigue test data generated in air are appropriate for girth weld roots in pipelines and SCRs. In such circumstances, standard fatigue design rules, and standard fatigue test techniques in air can be applied. The weld cap usually has to be dressed smooth to facilitate automatic ultrasonic testing (AUT), which also has benefits for fatigue strength, so this is of less
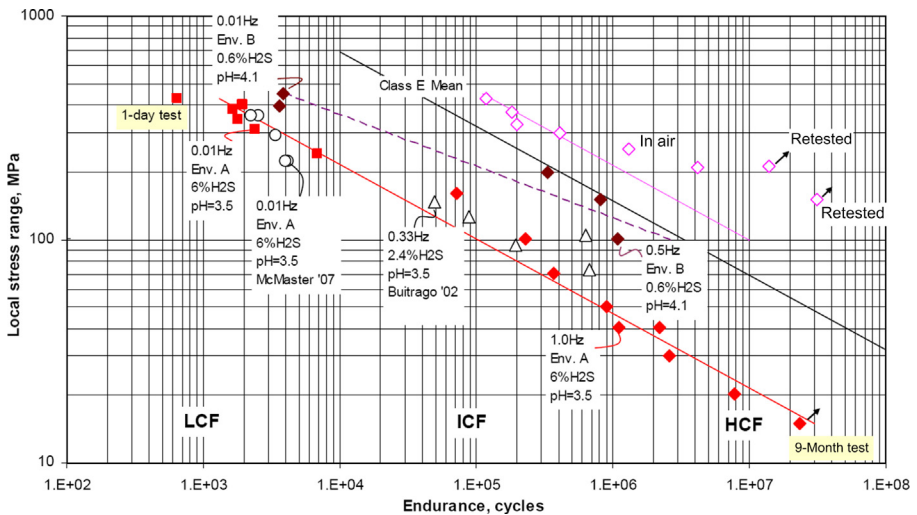
Figure 12.10 Sour endurance data for HCF and LCF.
Source: Buitrago et al. [9]. (For color version of this figure, the reader is referred to the online version of this book.)

concern in the weld cap than the root, even though it is operating in a seawater environment.

When production fluids contain H_2S, CO_2, and chlorides, fatigue data generated in air are no longer relevant. The pipeline or riser is under the "sour" conditions if the production includes H_2S and saltwater. Figure 12.10 presents endurance data plotted in a stress range versus a cycles to failure format or S-N curve, shown as open and solid diamonds. The sour fatigue performance in the intermediate-cycle fatigue (ICF) regime degrades, relative to in air, with the milder environment *B* degrading less than one order of magnitude on life and less than with the more sour environment *A*, which degraded between one and two orders of magnitude. The figure also shows that the effect on fatigue of sour environments even at relatively low H_2S concentrations remains very significant, when compared to that in-air degradation factor on life between 10 and 100 for the tests. The actual effect, being dictated primarily by the particular environment, material, and stress level, requires qualification tests.

In the LCF regime, the applicability of the S-N, expressed in terms of stress, appears to be limited by the yield stress of the material at about 1000 cycles. For shorter lives, new data under displacement control conditions is required because of high stress range. A fatigue "knockdown" factor is used to express the degradation of fatigue life with the ratio of fatigue cycles in sour or brine environments to that in laboratory air.

In the fatigue analysis and design for pipelines and risers in sour service, a knockdown factor should be imposed to the stress ranges in applying the S-N curve to the single-pipe flowline ID or the PIP flowline inner pipe ID. The magnitude of the knockdown factor depends on the severity of the H_2S content of the production. When

Figure 12.11 Fatigue endurance data in a sweet environment.
Source: Pargeter and Baxter [10]. (For color version of this figure, the reader is referred to the online version of this book.)

only the stress ranges at the mid wall are available, these stress ranges may be directly applied to the calculation for the pipe ID for conservative results. For the pipe OD, the stress ranges may be obtained from the stress ranges at the mid wall by multiplying them by the factor of 2OD/(OD + ID) for conservative results.

Effect of CO_2

Another potentially harmful environment arises in the product carried by some pipelines under so-called sweet conditions, from the presence of CO_2 and saltwater. Figure 12.11 shows a summary of the test data of fatigue endurance in air and a sweet environment. It can be seen that all the data except for one are to the right of the mean Class E curve taken from BS7608 [1]. Fatigue endurance at 0.2 Hz exceeds air data by a factor of about 8. Increasing the frequency by an order of magnitude changes the environmental effect at 300 MPa; therefore, the endurance becomes a factor of 2 lower than the in-air results.

The increases in fatigue endurance are believed to be due to a competition between material removal by general corrosion and the fatigue crack growth rate, such that the fatigue crack growth is hindered under highly corrosive conditions. The reductions in fatigue endurance are believed to have been due to crack tip dissolution.

Fatigue Life Improvement Techniques

For welded joints, improvement on fatigue performance can be obtained by a number of methods, including controlled burr grinding of the weld toe, hammer peening, or as-welded profile control to produce a smooth concave profile that blends smoothly

with the parent metal. The purpose of removing or reducing the size of the weld toe flaws is to extend the crack initiation part of fatigue life. Following are two typical methods to reduce the local stress at the weld area:

- Grinding.
- Remelting by TIG (tungsten inert gas) dressing.

Reduction of Stress Concentration

The primary aim of grinding is to remove or reduce the size of the weld toe flaws, in the mean time; it reduces the local stress concentration. The quality of grinding depends on the skill level of the operator.

Introduction of Beneficial Compressive Residual Stress

The aim of TIG dressing is to remove the weld toe flaws by remelting the material at the weld toe, to reduce the local stress concentration of the local weld toe profile. Clamping the weld toe in compression by

- Hammer and needle peening.
- UIT (ultrasonic impact treatment).
- LTT (low-temperature transform electrode).

Fatigue life improvement techniques also include

- Reducing axial misalignment caused by
  - High-low pipe joint wall mismatch at an internal surface, typically at a level of 0.5 mm with pipe end machining or sorting process.
  - Wall thickness variation in adjacent pipes.
- Weld cap grinding by removal of the weld cap.

Fatigue Assessment Based on Δε-N Curves

The number of strain cycles to failure may be assessed according to the American Welding Society (AWS) standards Δε-N curves, where N is a function of the range of cyclic bending strain Δε. The Δε-N curves are expressed as follows:

$$\Delta \varepsilon = 0.055 N^{-0.4} \quad \text{for } \Delta \varepsilon \geq 0.002 \qquad [12.10]$$

and

$$\Delta \varepsilon = 0.016 N^{-0.25} \quad \text{for } \Delta \varepsilon \leq 0.002 \qquad [12.11]$$

These two-part curves are based on strain ranges adjacent to the weld that include geometrical concentrations of strain but do not include concentrations of strain due to the weld cap, root profile, or welding imperfections. The strain range Δε is the total amplitude of strain variations, that is, the maximum less the minimum strains occurring in the pipe body near the weld during cyclic loads.

Local strain concentrations due to buckling need to be included in the $\Delta\varepsilon$ to account for cases where buckling occurs on the compression part of the cycle. Strain concentrations from buckling may be expected to be large enough to severely reduce the allowable number of fatigue cycles.

3. Fracture

General

Depending on the plastic deformation of the material, the two fracture modes are defined as either ductile or brittle. Ductile fracture has characteristics of extensive plastic deformation ahead of the crack and the crack is "stable" from further extension unless increased stress is applied. Brittle fracture on the other hand is characterized by relatively little plastic deformation and the crack is "unstable" and propagates rapidly without increase in the applied stress. Figure 12.12 shows typical tensile specimens and their stress-strain curves for both brittle and ductile materials. An obvious
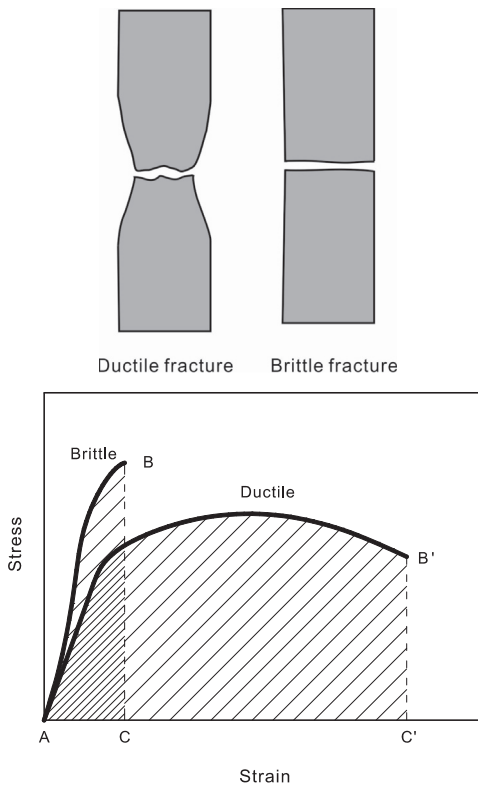
Figure 12.12 Stress and strain curves of brittle and ductile materials.

(a)	(b)	(c)	(d)	(e)
Necking,	Cavity formation,	Form a crack,	Crack propagation,	Fracture
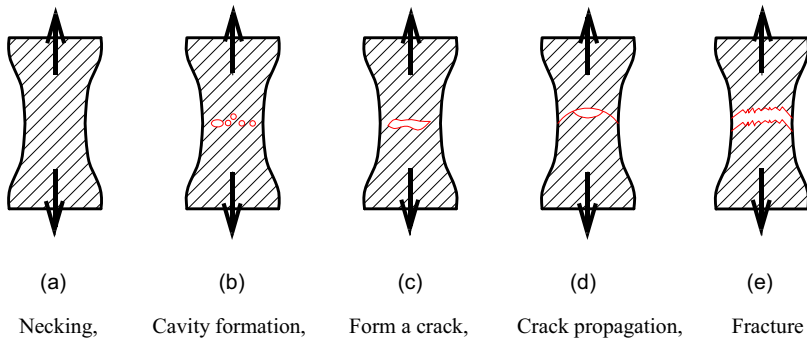
Figure 12.13 Failure procedure due to ductile fracture: (a) necking, (b) cavity formation, (c) formation of a crack, (d) crack propagation, (e) fracture. (For color version of this figure, the reader is referred to the online version of this book.)

necking prior to failure appears for ductile material but no necking for brittle failure surfaces.

Figure 12.13 shows a typical failure procedure of a tensile specimen due to ductile fracture. Ductile fracture occurs in most metals, while brittle fracture usually occurs in ceramics, ice, and cold metals. For pipeline steels, ductile behavior is preferable. Pipeline failure due to brittle or ductile fracture behavior increases with increasing fatigue damage. Fractures in the pipelines can be initiated at most service stress levels from defects, which may be introduced by outside forces, welds, corrosion, material defects, and environmental conditions. When the stresses acting on a defect of the pipeline overcome the fracture initiation tolerance and reach critical size beyond what the physical and material properties and operating conditions that the pipeline can handle, fractures occur.

Fracture mechanics analysis may be used to develop flaw acceptance criteria to limit the pipeline fatigue damage. The pipelines are assumed to be intrinsically flawed. Fracture mechanics is used to characterize the propagation of fatigue cracks. The fatigue life is based on propagation of an initial flaw to a critical size. The main steps for the fracture mechanics analysis include

- Assumption of an initial flaw size based on inspection capabilities.
- Development of crack-growth data specific to the material.
- Calibration of the crack propagation model to relevant component fatigue test results.
- Engineering criticality assessment (ECA) analysis:
  - Dynamic stress analysis.
  - Calculation of critical flaw size.
  - Defining allowable flaw size.
  - Calculation of fatigue crack growth.
  - Calculation of fatigue life.
- Segment testing.
- Comparison of segment test and ECA results.
- Determination of acceptance criteria.
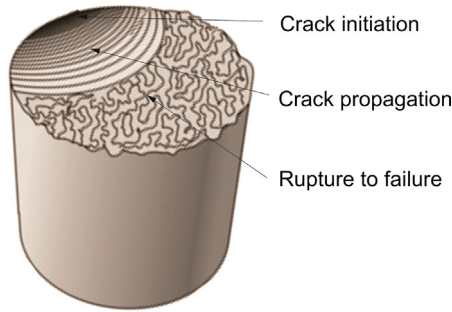
Figure 12.14 Fracture surface due to fatigue. (For color version of this figure, the reader is referred to the online version of this book.)

Fracture mechanics analysis is very useful not only in controlling fatigue limiting cracks but also in providing guidance for selecting appropriate weld inspection techniques and reducing the number of welds needing to be cut out and replaced.

Crack Initiation and Propagation

Figure 12.14 shows a fracture surface of ductile material due to fatigue. Failure of a material due to fracture may be divided into three steps:

- **Crack initiation:** The initial crack occurs in this stage. The crack may be caused by surface scratches caused by handling or tooling of the material, threads (as in a screw or bolt), slip bands or dislocations intersecting the surface as a result of previous cyclic loading or work hardening.
- **Crack propagation:** The crack continues to grow during this stage as a result of continuously applied stresses.
- **Rupture to failure:** Catastrophic rupture occurs when the material cannot withstand the applied stress. This stage happens very quickly.

The fatigue life of material due to fracture consists of the time periods of crack initiation and propagation and is expressed as follows:

$$N_f = N_i + N_p \tag{12.12}$$

where N_i is the number of cycles to initiate fracture and N_p the number of cycles to propagate to failure. For high-cycle fatigue or low stress range levels, most of the life is spent in crack initiation and N_i is high, while for the low-cycle fatigue or high stress range levels, the crack propagation step predominates.

Fracture Toughness

There are three basic modes of crack tip deformation due to load directions, as illustrated in Figure 12.15: opening (Mode I), in-plane shear (Mode II), and out-of-plane shear (Mode III). Mode I is the condition in which the crack plane is normal

Mode I   Mode II   Mode III
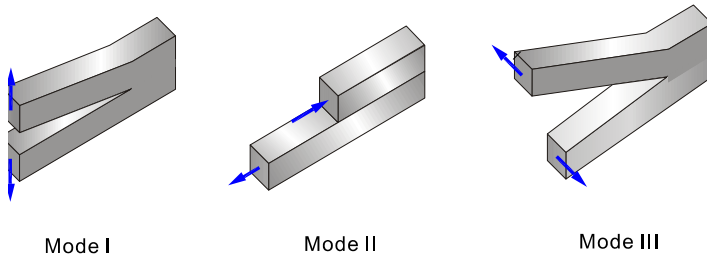
Figure 12.15 Loading modes for a crack. (For color version of this figure, the reader is referred to the online version of this book.)

to the direction of largest tensile loading. This is the most commonly encountered mode; therefore, the stress intensity factor for Mode I, K_I is used for the fracture evaluation.

The stress intensity factor can be considered as a stress-based estimate of fracture toughness. It is derived from a function that depends on the applied force at failure. The stress intensity factor, K, is a function of loading, crack size, and structural geometry. The stress intensity factor may be represented by the following equation:

$$K_I = \sigma\sqrt{\pi\alpha\beta} \qquad\qquad\qquad\qquad\qquad [12.13]$$

where

K_I = stress intensity factor in $\left[MPa\sqrt{m}\right]$ or $\left[Psi\sqrt{in}\right]$
σ = applied stress in MPa or psi
α = crack length in meters or inches
β = crack length and component geometry factor that is different for each specimen and is dimensionless.

The stress intensity factor is used to determine the fracture toughness of most materials. As the stress intensity factor reaches a critical value (K_C), unstable fracture occurs. This critical value of the stress intensity factor is called the *fracture toughness* of the material. The fracture toughness can be considered the limiting value of stress intensity, just as the yield stress might be considered the limiting value of applied stress.

Fracture toughness is a quantitative way of expressing a material resistance to brittle fracture when a crack is present. If a material has a large value of fracture toughness, it will probably undergo ductile fracture. Brittle fracture is very characteristic of materials with a low fracture toughness value. The fracture toughness K_{IC} of selected materials is listed in Table 12.2.

The fracture toughness depends on both temperature and specimen thickness, which is a variable until limiting conditions (maximum constraint) are reached. Fracture toughness is a parameter to express the stress required to propagate a preexisting flaw. It is a very important material property, since the occurrence of flaws is not completely avoidable in the processing, fabrication, or service of a material or component. Flaws may appear in a material as cracks, voids,

Table 12.2 Fracture Toughness K_{IC} of Selected Materials

| Material | Fracture Toughness | | |
	Charpy V-Notch Energy [ft.lbs]	CTOD [mm]	K_{IC} [ksi$\sqrt{\text{in}}$]
Glass	<1	<0.01	1 to 5
Aluminum	5 to 25	0.1 to 0.6	20 to 50
Titanium	10 to 50	0.1 to 0.7	60 to 100
Cast iron	10 to 30	0.1 to 0.5	30 to 90
Steel	40 to 250	0.05 to 2.0	100 to 250

Source: Cordes [11].

metallurgical inclusions, weld defects, and other problems. It is common practice to assume that a flaw of some chosen size is present in some number of components and use the linear elastic fracture mechanics (LEFM) approach to design critical components. This approach uses the flaw size and features, component geometry, loading conditions, and fracture toughness to evaluate the ability of a component containing a flaw to resist fracture.

CTOD

The crack tip opening displacement (CTOD) test measures the resistance of a material to the propagation of a crack. CTOD is used on materials that can show some plastic deformation before failure occurs that causes the tip to stretch open. Accurate measurement of this displacement is one of the essentials of the test.

The two common definitions of the CTOD, as shown in Figure 12.16, are

1. The opening displacement of the original crack tip, δ.
2. The displacement, δ, at the intersection of a 90° vertex with the crack flanks.

These two definitions are equivalent if the crack blunts in a semicircle.

The CTOD of a crack at the edge of a three-point bending specimen is shown in Figure 12.17. In the figure, $CTOD_m$ is the measured crack tip opening displacement,
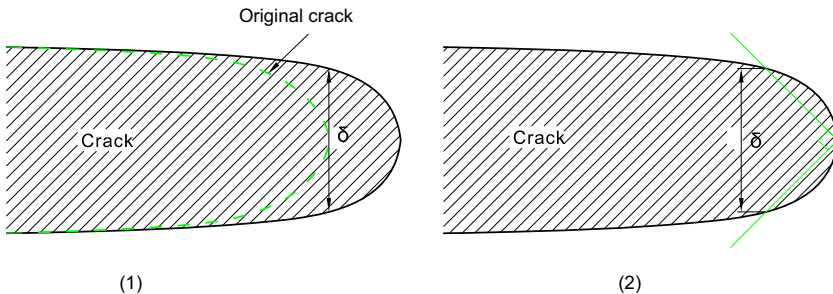
Figure 12.16 Definitions of CTOD. (For color version of this figure, the reader is referred to the online version of this book.)
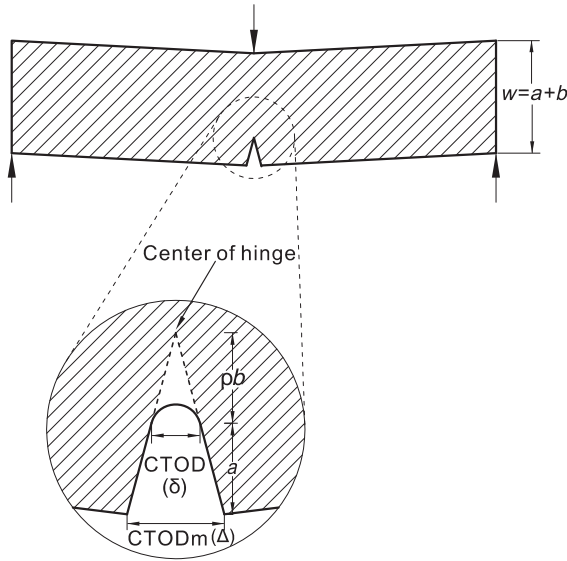
Figure 12.17 CTOD measured from three-point bending specimen.

usually near the edge of the specimen for ease of access, CTOD is the real crack tip opening displacement, a is the length of the crack, and b is the width of the rest of the specimen. The CTOD can be calculated from the simple geometry of two similar triangles:

$$\text{CTOD} = \frac{\rho b}{a + \rho b} \text{CTOD}_m \quad \text{or} \quad \delta = \frac{\rho b}{a + \rho b} \Delta \qquad [12.14]$$

where ρ is a dimensionless rotational factor used to locate the center of the hinge.

J-Integral

The J-integral represents a way to calculate the strain energy release rate, or work (energy) per unit fracture surface area in a material. The theoretical concept of the J-integral was developed by James R. Rice and G. P. Cherepanov independently in the mid-1960s. The total J-integral is calculated by considering the elastic and plastic parts separately and expressed in the following equations when the amount of the ductile crack growth is less than 10% of the initial remaining ligament:

$$J = J_e + J_p \cong J_e + J_{P0} \qquad [12.15]$$

where

J_e = elastic part of the J-integral
J_p = plastic part of the J-integral
J_{p0} = plastic part of the J-integral without crack growth correction

The elastic part of the J-integral is directly linked to the stress intensity factor, K, through the relation [5]

$$J_e = K^2/E' \qquad [12.16]$$

where, $E' = E$ for plane stress (E is Young's modulus), and $E' = E/(1 - v^2)$ for plane strain. The plastic part of the J-integral is calculated through the plastic work applied to the cracked specimen:

$$J_p = \frac{\eta_p U_p}{B(W - a_0)} \qquad [12.17]$$

where: η_p is a dimensionless function of the geometry, U_p is the plastic part of the area under the load versus the CMOD curve, B is the width of the specimen, $W - a_0$ is the remaining ligament, and a_0 is the initial crack length [5].

Comparison between J-Integral and CTOD

The CTOD parameter was applied extensively to fracture analysis of welded structures in the United Kingdom, beginning in the late 1960s, due to the development of oil resources in the North Sea, while fracture research with the J-integral in the United States was driven primarily by the nuclear power industry during the 1970s. Both the J-integral and CTOD are the parameters of fracture toughness and are related to each other through the following equation:

$$J = m \, \sigma_y \, \text{CTOD} \qquad [12.18]$$

where m is the plastic constraint factor and σ_y is the yield stress. The plastic constraint factor m is an empirical parameter and has been defined by ASTM based on crack depth, a, to thickness, W, ratio and the ratio of yield to ultimate strengths, σ_u, as follows:

$$m = -0.111 + 0.817 \frac{a}{W} + 1.36 \frac{\sigma_u}{\sigma_y} \qquad [12.19]$$

CTOD can be considered a strain-based estimate of fracture toughness. However, it can be separated into elastic and plastic components. The elastic part of CTOD is derived from the stress intensity factor, K. The plastic component is derived from the crack mouth opening displacement. As with CTOD, the elastic component of J is based on K, while the plastic component is derived from the plastic area under the force-displacement curve.

Fracture Toughness Testing [12]

Fracture toughness is a critical input parameter for fracture-mechanics based fitness for service assessments. It had become established practice to use pipe specimens tested under bending to derive a value of fracture toughness for use in the calculation of a critical defect size through the various levels of engineering criticality
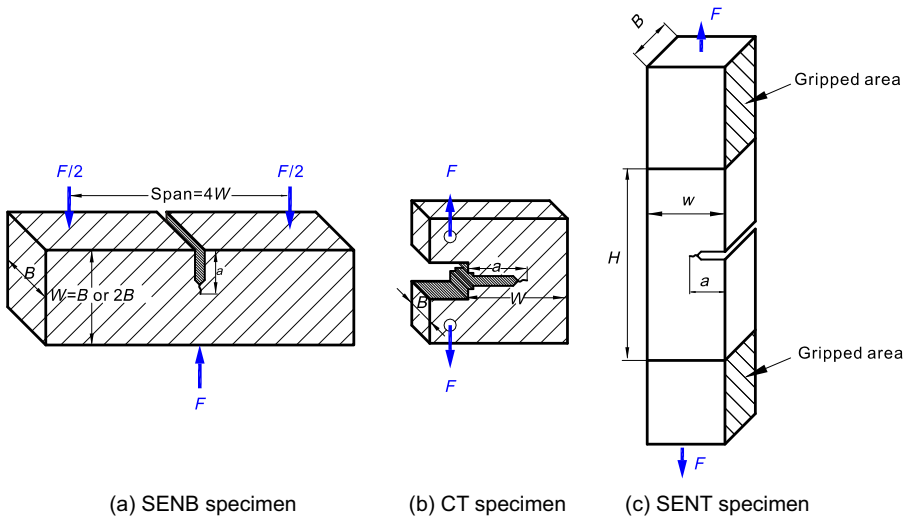
Figure 12.18 Examples of common fracture specimen types. (For color version of this figure, the reader is referred to the online version of this book.)

assessments. Although fracture toughness can sometimes be obtained from the literature or materials properties databases, it is preferable to determine this by experiments for the particular material and joints being assessed. Various measures of fracture toughness exist, and it is preferable to determine fracture toughness in a rigorous fashion, in terms of K, CTOD, or J.

The most widely used fracture toughness test configurations are (1) the single edge notch bend (SENB or three-point bend), (2) the compact (CT) specimens, and (3) the single edge notch tension (SENT) specimen, as shown in Figure 12.18. The compact specimen has the advantage that it requires less material, but is more expensive to machine and more complex to test compared to the SENB specimen. Also, special requirements are needed for temperature control. SENB specimens are typically immersed in a bath for low temperature tests. Although the compact specimen is loaded in tension, the crack tip conditions are predominantly bending. If limited material is available, it is possible to fabricate SENB specimens by welding extension pieces for the loading arms to the material sample.

Although the fracture toughness factor, such as K, CTOD, or J-integral, is usually used to describe the material's fracture resistance, the crack tip constraint, that is, the degree of crack tip stress triaxiality also influences the fracture resistance, as the stress and strain state at a crack tip is not fully characterized by the fracture toughness alone. Specimens with a high crack-tip constraint are often related to high stress triaxiality at the crack tip. The crack-tip constraint can be expressed by T stress for the expansion of symmetric isotropic linear elastic crack-tip fields or by the Q parameter for the elastic-plastic crack-tip fields.

Figure 12.19 shows the dependence of the material's fracture resistance on the specimen geometries. Fracture toughness is strongly dependent on geometry and
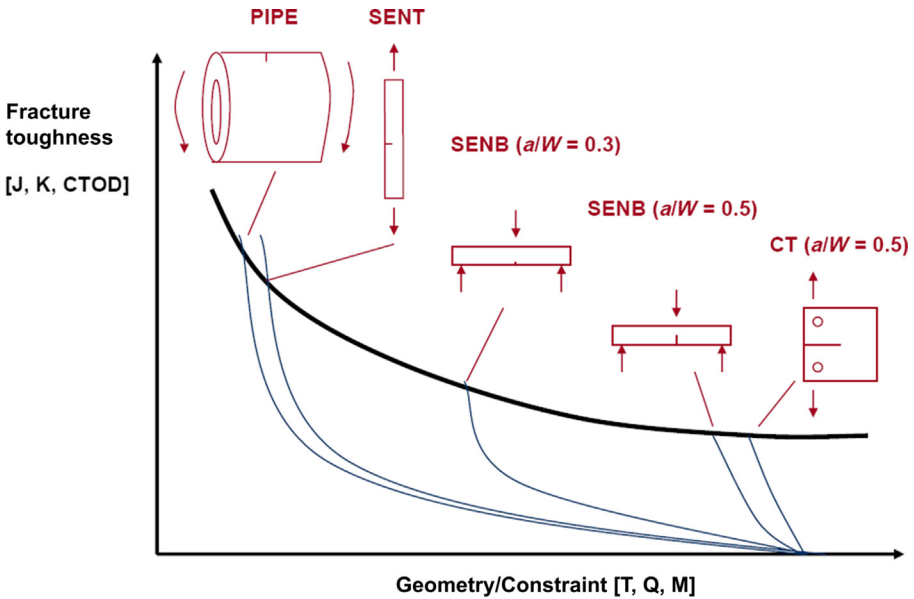
Figure 12.19 Materials resistance depends on specimen geometry.
Source: Thaulow et al. [13]. (For color version of this figure, the reader is referred to the online version of this book.)

loading conditions. The thick line represents the fracture toughness, such as the material property, while the thin lines represent the applied crack driving force. The structure is expected to fracture when the applied force exceeds the material resistance. A pipe subjected to bending load is also illustrated in the figure. The pipe geometry exhibits typically much lower constraint than the fracture mechanics SENB specimens.

Both SENB and CT specimens have deep cracks, and bending dominates the deformation at the uncracked ligament, which results in a high constraint on the crack tip. Fracture toughness testing on SENB and CT specimens can provide a reasonable assessment of fracture resistance for engineering structures having similar loading condition and crack-tip constraint but not for pipelines in the reeling process. In the reel-on/reel-off process of a pipeline, the girth welds are loaded predominantly in bending and tension. In addition, the typical crack size in girth welds is in general much smaller than the thickness of pipe wall. The crack-tip constraint caused by these condition is lower than that in deeply cracked specimens. Therefore, the test results obtained from SENB and CT specimens provide overconservative assessments for the pipeline reeling process. The SENT specimen can generate similar deformation features and crack-tip constraint conditions existing in a pipeline during installation and service. Figure 12.20 shows a comparison of fracture analysis results for the relevant test conditions. The deformation field and opening stress at the crack tip between the pipe and SENT are very similar. SENT specimens have not yet been qualified for operational conditions, due to limited information about the effect of internal pressure. But results from SINTEF shows that internal pressure has no influence on the fracture

(a) Pipe section

(b) SENT specimen

(c) SENB specimen
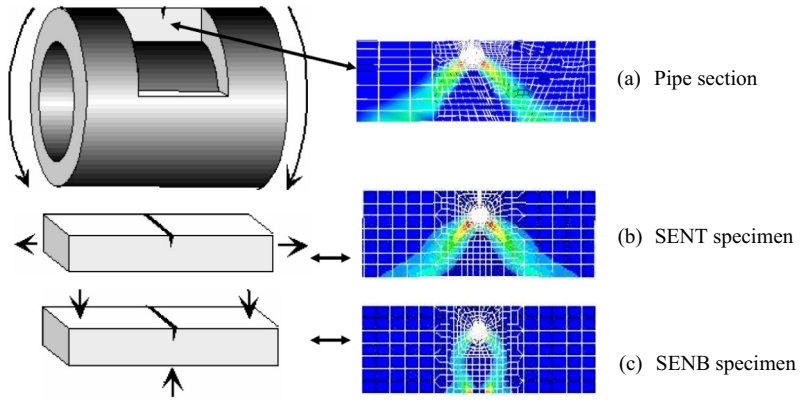
Figure 12.20 Comparison of analysis results for relevant test conditions.
Source: Thaulow et al. [13].

toughness for ductile materials, which means that SENT specimens can be used for establishing fracture properties also under the operating conditions [14].

The SENT specimens are loaded in tension, and the maximum net section stress can be measured directly from the specimens. This net section stress can be used as the plastic collapse limit in the ECA analysis.

Fatigue Crack Propagation

The rate at which a crack grows has considerable importance in determining the life of a material. Figure 12.21 shows a typical log-log plot of fatigue

Fast fracture
$K_{max}=K_c$

$da/dN=A(\Delta k)^m$
Paris regime

m
1

Threshoad

Δk_{th}

da/dN, [mm/cycle]

Δk, [MPa$\sqrt{m}$]

Final crack depth, a_f

Initial crack width, $2C_i$
Final crack width, $2C_f$

Initial crack depth, a_i
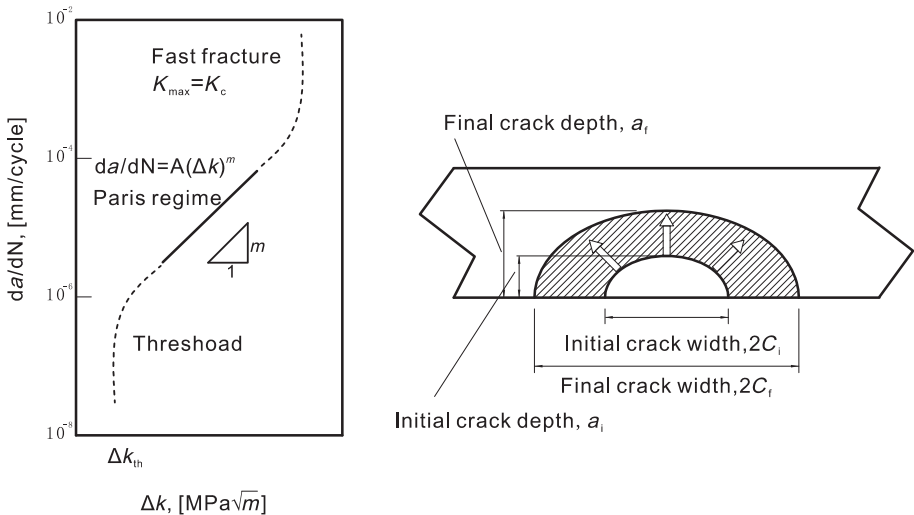
Figure 12.21 Fracture crack growth curve.

crack propagation, in which three stages of crack growth, I, II, and III, can be divided into,

- **Stage I (near threshold):** Transition to a finite crack growth rate from no propagation below a threshold value of ΔK. The threshold represents an endurance limit.
- **Stage II (Paris regime):** "Power law" dependence of crack growth rate on ΔK.
- **Stage III (fast fracture):** Acceleration of growth rate with ΔK.

The propagation of a crack occurs during the second step of fatigue failure. As a crack begins to propagate, the size of the crack also begins to grow. The rate at which the crack continues to grow depends on the stress level applied. The rate at which a crack grows can be expressed as the Paris law, which states that da/dN scales with ΔK through the power law as shown in the following equation:

$$da/dN = A \left(\Delta K\right)^{m} \qquad [12.20]$$

where A and m are properties of the material, da is the change in crack length, and dN is the change in the number of cycles; $m \approx 3$ for steel material; $m \approx 4$ for aluminum material; ΔK is the change in the stress intensity factor or, by equation,

$$\Delta K = K_{\max} - K_{\min} = Y\Delta\sigma\sqrt{\pi a} \qquad [12.21]$$

The stress intensity factor, K, is derived from linear elastic fracture mechanics. This parameter is used to describe the magnitude of the stresses, strains, and displacements ahead of the crack tip. The velocity of a moving fatigue crack, da/dN is found from experimentally generated curves of a versus N. BS7910 (1999) [15] provides recommended values for the Paris law, which should be suitable for the fatigue analysis. Material specific data obtained from tests are relatively inexpensive and may be used in lieu of codified data.

If idealized stress intensity factor solutions are utilized, such as smooth plate solutions, in lieu of the finite element fracture mechanics analysis of the actual geometry, then relevant stress concentration factors should be applied to the stress range to account for increased applied stress due to local weld geometry, pipe mismatch, and the like.

Engineering Criticality Assessment

General

An engineering criticality assessment is a procedure based on fracture mechanics that may be used to supplement the traditional fatigue S-N approach and determine the flaw acceptance and inspection criteria in fatigue and fracture design of pipelines and risers. It is an alternate acceptance criterion for the girth weld inspection compared to the traditional workmanship acceptance criteria. ECA requires advanced weld inspection techniques, higher strength and toughness weld metal, and stricter welding controls. ECA is a fracture mechanics based analysis whereby the flaws are accepted or rejected. The basic philosophy of the analysis is based on the relationships among flaw size, mechanical properties, material toughness, and applied stress. ECA analysis

ensures that the calculated flaw size limit is acceptable from both brittle fracture and plastic collapse viewpoints, using a failure assessment diagram that defines the boundaries into which failure by an unstable fracture will not occur for a given flaw, applied stress, material strength, and CTOD. The flaw size and position are tested and derived from nondestructive tests of the actual material to be welded. ECA is often less conservative in the flaw evaluation than the traditional criteria and can reduce the reject rate of welds considerably. Using ECA acceptance criteria for pipeline girth weld inspection can significantly reduce the cost of constructing a transmission pipeline by minimizing unnecessary repairs.

ECA is used primarily in strain-based design to set the acceptable flaw size for inspection. The methods are applied to both girth- and seam-welded areas based on the engineering understanding of brittle and ductile fracture and plastic collapse. ECA is also used for "fitness for service" and "structural integrity." The chief ambition of ECA is to determine if a piece of equipment or structure is sound enough to meet the service requirements for which it was intended. Assessment of cracks in pipelines is one of the important areas of an integrity management plan. For example, in the automated ultrasonic testing pipeline inspection industry, it is crucial that welds are analyzed to determine if there are any defects that can shorten a pipeline's service life.

ECA is typically performed using industry accepted practices such as Electric Power Research Institute (EPRI), CTOD method, or more rigorous analyses, such as the R-6 method. Pipelines and risers have typically been assessed using the BS7910 standard [15], which allows for material behavior ranging from brittle fracture to plastic collapse of the cross section. However, most modern materials with good ductility are often best characterized by nonlinear fracture mechanics and are well treated using the failure assessment diagram approach.

ECA Procedure

A number of industry codes provide guidance for carrying out ECA analysis. BS 7910, "Guide on Methods for Assessing the Acceptability of Flaws in Metallic Structures" [1], and API-RP-579, "Recommended Practice for Fitness for Service" [17], are typical codes used in oil and gas industry. The analysis procedure in accordance with BS 7910 is summarized as follows:

- Determine extreme and long-term loads.
- Conduct fracture analysis to determine maximum allowable flaw sizes.
- Select small initial flaw dimensions, conduct fatigue crack growth to determine life based on long-term load data.
- Iteratively vary initial flaw dimensions and repeat flaw growth analysis until target design life is achieved.
- Repeat for a range of flaw aspect ratios to determine distribution of maximum acceptable flaw dimensions.
- Repeat for internal and external surface flaws and embedded flaws.
- Develop or confirm acceptance criteria.

Figure 12.22 shows an example of the allowable flaw dimensions, which is a plot of allowable flaw size as a function of height and length. The allowable flaw dimensions
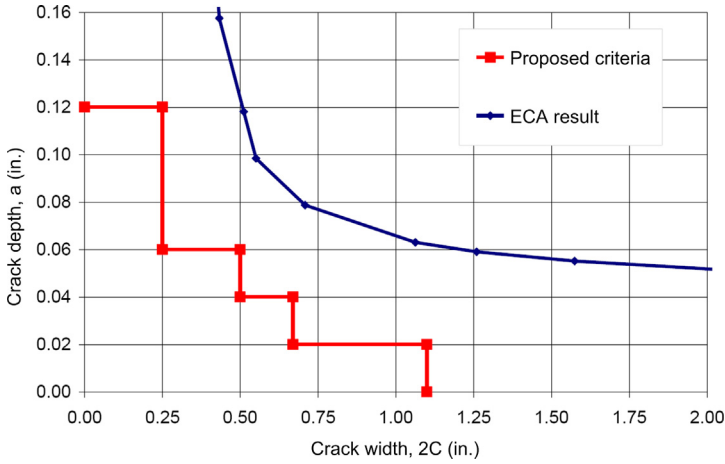
Figure 12.22 Allowable flaw dimensions and maximum allowable flaws from the ECA.
Source: Cordes [11].

are derived using the results of an ECA and the sensitivity of the nondestructive examination (NDE) equipment that is to be used for determining flaw dimensions. This may be used when defining or confirming the weld acceptance criteria. The allowable flaw dimensions shown in the figure are derived assuming ± 0.5 mm (0.02 in.) tolerance on flaw depth detection for the NDE with a safety factor of 2.0.

Flaw Types

The flaw types that may be considered in an ECA are categorized as surface, embedded, and through thickness flaws. Surface flaws may occur on either the inner or outer surface of a welded pipeline or riser joint and are defined as internal surface or external surface flaws, respectively. The flaw dimensions in accordance with BS 7910 are shown in Figure 12.23.

Circumferential cracks are driven by axial stress, while axial cracks are driven by hoop stress. Typically, surface flaws result in the maximum allowable flaw sizes with

(a) Through thickness flaw
Required dimensions: $2a, B$

(b) Embedded flaw
Required dimensions: $2c$, p, $2a, B$

(c) Surface flaw
Required dimensions: $a, 2c, B$
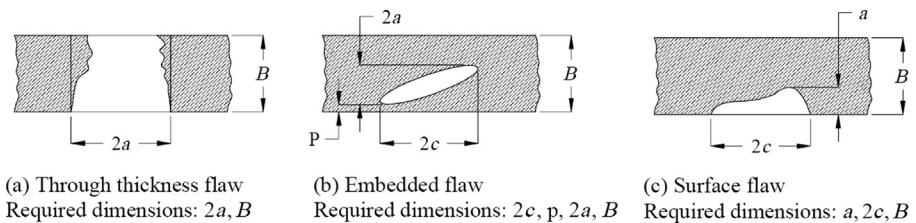
Figure 12.23 Flaw configurations.
Source: BS 7910 [15].

smaller dimensions than those of embedded flaws and internal surface flaws. This is predominantly due to the occurrence of higher stresses at the outer surface compared to the inner surface under bending loads.

Acceptance Criteria

The purpose of the ECA is to determine the critical nature of surface breaking and embedded flaws related to specific service loading histories. It establishes the allowed critical flaw sizes beyond which the pipelines or risers fail prematurely due to crack propagation or fracture.

The critical flaw sizes derived from ECA are to be incorporated into the project NDE acceptance criteria as a standard so that the NDE contractor can calibrate the specified NDE technique and maintain continuity of the system throughout the project. For each of the flaw types considered, different size limits are derived and the sensitivities associated with detection of each flaw type must then be considered to define the acceptable limiting flaw size.

The selected NDE technique must possess the ability to quantify the dimensions of the detectable flaws to compare them to the critical flaw size determined by the ECA. Flaws larger than the critical flaw size are an indication that the welded joint is not of the desired standard and needs to be repaired or cut out.

Failure Assessment Diagram

Structures made from materials with sufficient toughness may not be susceptible to brittle fracture, but they can fail in plastic collapse if they are overloaded. API RP 579 [16], BS7910 [15], and R6 procedure [17] give guidance for assessing the acceptability of defects in welded structures based on the failure assessment diagram method. The FAD method was originally derived from the two-criterion approach [6]. This approach states that structures can fail by either of two mechanisms, brittle fracture or plastic collapse; and these two mechanisms are connected by an interpolation curve based on the strip yield mode. The FAD is widely accepted and used for the assessment of defects found in metallic structures. The FAD defines the failure envelope for a crack subjected to interaction between brittle fracture and plastic collapse.

Figure 12.24 shows a typical FAD plotted in terms of L_r and K_r, in which L_r is the load ratio defined as the ratio of the applied load (P) to a reference load (P_0) and K_r is the fracture ratio defined as the ratio of the applied stress intensity factor (K_I) to the critical stress intensity factor of the material (K_{mat}). When the assessment point is below the FAD envelope, the crack is stable; otherwise, the crack growth is unstable.

The original shape of the FAD is valid for linear elastic deformation under small-scale yielding condition. In the strip yield model of the FAD, the reference load is the yield strength of the material. A more general formulation of a FAD was constructed by many authors using the J-integral. The J-based FADs have been constructed for Ramberg-Osgood materials numerically based on deformation plasticity or for other elastic-plastic materials based on incremental plasticity. For ductile materials, the
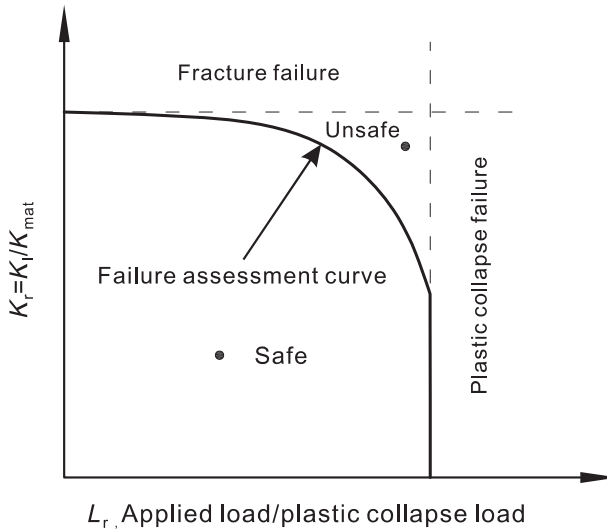
Figure 12.24 Failure assessment diagram for flawed structure.

fracture ratio on the FAD is defined as the ratio of the applied J_I to the value of the J-R curve. K-based FAD in a Level 2 ECA or J-based FAD in Level 3 ECA determines the critical flaw size of a fatigue crack.

BS 7910 includes three assessment levels, which differ with respect to an increasing complexity of the analysis in conjunction with less conservative results at the higher levels:

- **Level 1:** Simplified assessment.
- **Level 2:** Normal assessment, containing 2A-generalized FAD not requiring stress-strain data, and 2B- material-specific FAD.
- **Level 3:** Ductile tearing assessment.

Figure 12.25 shows a comparison of the BS7910 FAD curves of three levels. The ECA analysis is based on the location of a material- and component-specific assessment point relative to the FAD curve. In the simplest case, the component is regarded as safe when the assessment point lies inside the area circumscribed by the FAD, and it is assumed to be in a critical state when it lies outside. When applying a BS 7910 FAD analysis in a proof test context, as provided by the rerounding of the pipe, it is important to understand that the criteria of conservatism are quite different with respect to the initial crack size after the overload event and with respect to the final crack size at failure. For common fracture evaluations, the term *conservative* means underestimation of the critical crack size at failure. By contrast, in the context of a proof test, *conservative* means to overestimate the critical crack size that just survives the overload.
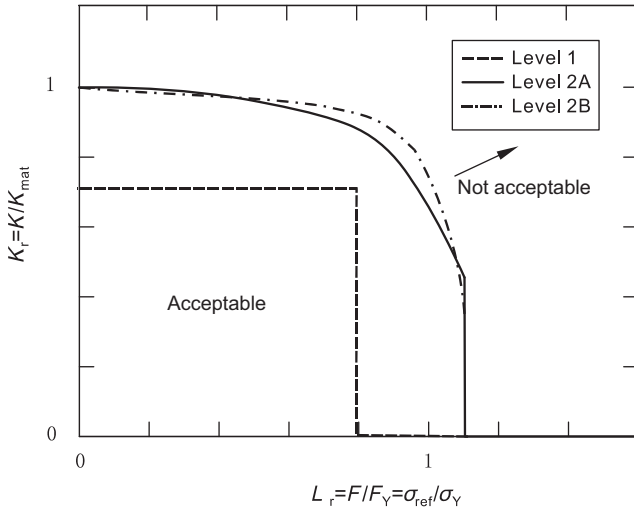
Figure 12.25 Comparison of BS 7910 assessment curves at different levels.

In the general failure assessment diagram of BS7910 Level 2A, the assessment curve is presented as

$$K_r = \left(1 - 0.14L_r^2\right)\left[0.3 + 0.7\exp\left(-0.65L_r^6\right)\right] \qquad [12.22]$$

where

$$K_r = \frac{K_I}{K_{mat}} + \rho$$

$$L_r = \frac{\text{total applied load}}{\text{plastic collapse load of the flawed structure}}$$

where K_I is the stress intensity factor, K_{mat} is the fracture toughness, and ρ is the plasticity correction factor. When secondary stresses, such as residual stresses are present, the factor ρ is necessary to account for interactions between the primary and secondary stress contributions. L_r is a load ratio defined as a reference stress over the lower yield strength of 0.2% proof stress. The reference stress characterizes the possibility of plastic collapse.

As L_r increases, plasticity also increases the effective crack tip driving force, but it is important to recognize that the K_r parameter uses the linear elastic stress intensity factor with no allowance for the effect of plasticity on the crack tip driving force. It is considered that, if fracture occurs, it will be when the total effective crack tip driving force, namely, the elastic-plastic value of crack tip driving force, reaches a critical value equivalent to the fracture toughness, at $\sqrt{EJ_{ep}} = K_{mat}$. The applied linear

elastic stress intensity factor is equivalent to $\sqrt{EJ_e}$, where J_e is the linear elastic J-integral:

$$K_r = \frac{K_I}{K_{mat}} + \rho = \sqrt{\frac{J_e}{J_{ep}} + \rho} \qquad [12.23]$$

In Level 2B, the assessment curve is given by

$$K_{2B}(L_r) = \begin{cases} \left(\dfrac{E\varepsilon_{ref}(L_r)}{L_r\sigma_Y} + \dfrac{L_r^3\sigma_Y}{2E\varepsilon_{ref}(L_r)} \right)^{-0.5} & \text{if} \quad L_r \leq L_r^{max} \\ \\ 0 & \text{if} \quad L_r > L_r^{max} \end{cases} \qquad [12.24]$$

It exhibits an offset at plastic collapse:

$$L_r^{max} = \frac{\sigma_Y + \sigma_U}{2 \cdot \sigma_Y} \qquad [12.25]$$

4. Recognized Industry Codes of ECA

General

Fracture mechanics deals with the behavior of cracked bodies subjected to stresses and strains. These fractures may be due to primary applied loads or secondary self-equilibrated stress fields (or residual stresses), where the local crack tip phenomena can be characterized by measured parameters, such as crack length and nominal stress calculated in the absence of the crack, together with finite geometry correction factors. Application of fracture mechanics in the engineering critical assessment of defects in wedding has been codified in documents like BS PD 6493: 1991 [18], currently under revision as BS 7910 [15], the CEGB R6 procedure [17], API-1104 Appendix A, DNV-OS-F101 [3], and DNV-RP-F108 [5]. Most of these procedures involve two-parameter assessment through a FAD that considers the independent possibility of plastic collapse and fast fracture. The industrial practices as BS 7910 and API 1104 use stress-based ECA, while DNV-OS-F101 and DNV-RP-F108 use strain-based ECA. The stress-based ECA may be as excessively conservative, particularly when strain-based design is needed and relevant strength parameters of the girth weld are from standard material testing.

In pipeline installation and operation such as reeling and lateral buckling, high strain may be formed. In recent years, the strain-based design for pipelines has been widely accepted by industry, but the definition of acceptable flaw criteria for girth welds subjected to axial strain within the context of existing codified fracture mechanics based assessment procedures is problematic, since these methods are essentially stress based. To extend the ECA standard method to large strain

conditions, several challenges have to be understood: weld strength mismatching, fracture toughness, and welding residual stresses. DNV-OS-F101 and DNV-RP-F108 with strain-based ECA were developed to satisfy these conditions.

Beyond the general knowledge presented in the previous sections, an overview of these codes establishes deeper understanding of the issues surrounding fractures and shows the nuances between the problems that various groups have had to encounter.

PD 6493

In the United Kingdom, the ECA of potential or actual defects in engineering structures is codified in two prime documents, PD 6493: 1991 [18] and the CEGB R6 procedure [17], both of which have been developed over 20 years. PD 6493 has now been replaced by the more extensive procedures in BS 7910: 1999 [15].

The original PD 6493: 1980 document paid limited attention to the possibility of plastic collapse, as it was concerned primarily with assessment of weld defects. The approach of the Central Electricity Generating Board (CEGB) was different, as much of its equipment operates at high temperatures, where plastic collapse might assume equal, even greater, importance to fracture. Based on its situation, CEGB proposed a two-parameter technique of assessing the possibility of plastic collapse and fracture separately, then plotted these possibilities as the axes on a FAD. This was the basis of the R6:1976 document.

Failure assessment diagrams immediately led to a need for fracture parameters that could deal with extensive plasticity. R6 essentially provides a special form of J-integral analysis with additional safeguards imposed at the plastic collapse limit, while PD 6493 is primarily intended for use with CTOD, although in many cases a K-based analysis is acceptable.

BS 7910

BS 7910 (1999, 2005) is the most widely used standard for assessing flaws in metallic structures. It includes three primary levels of fracture assessment: Level 1 for simplified assessment, Level 2 for normal assessment, and Level 3 for ductile tearing assessment. Within these levels are individual methods that use different amounts of material specific information.

The three levels of ECA defined in BS-7910:2005 are summarized in the following:

Level 1 is a simplified but conservative assessment method, where the area of the FAD for the Level 1 ECA is a rectangle bounded by critical K_r and critical L_r values. If the assessment point lies in the area within the FAD boundary, the flaw is acceptable; if it lies on or outside the boundary, the flaw is not acceptable. In Level 1 ECA, a structure containing a flaw fails only in a totally brittle or in a totally ductile manner. There is no transition region between brittle and ductile failure.

Level 2 is the normal assessment procedure for general application. The FAD for a Level 2 ECA is modified from the rectangular shape in a Level 1 ECA to an assessment curve that accounts for the interaction between the small-scale yielding at the crack tip

and the plastic yielding of the structure. The Level 2 procedure includes two types of assessment: Level 2A and Level 2B. Level 2A utilizes given FAD curves for failure assessment and requires no specific stress-strain data. Level 2B requires the use of specific stress-strain data and generally gives more accurate results than Level 2A. The Level 2 ECA determines if an initial flaw in a structure will grow to a critical size that may result in brittle fracture of the pipe. The procedure depends on linear elastic fracture mechanics (LEFM) together with a limit load analysis to assess failure. The stress intensity factor (K) is used to characterize low-stress fatigue crack growth in LEFM.

Level 3 is an advanced assessment method used for ductile materials that exhibit stable tearing. The Level 3 procedure includes the use of the crack resistance curve (R-curve) and ductile tearing analysis to evaluate the acceptability of a critical flaw on the FAD boundary. The FADs for Level 3A and Level 3B ECA are similar to those for Level 2A and 2B, but a FAD specific to a particular material is obtained by determining the J-integral using both elastic and elastic-plastic analyses of the flawed structure under the loads of interest. If the J-integral for the FAD is material and geometry specific, the procedure is termed Level 3C ECA. The Level 3 ECA takes into account that when a fatigue crack reaches a critical size, the subsequent crack growth may still be stable with consideration of crack tearing resistance and the associated plasticity effect. The procedure is based on elastic-plastic fracture mechanics (EPFM) and a limit load analysis for failure assessment. The J-integral is generally used for high-stress fatigue crack growth in EPFM.

API 1104 Appendix A

API 1104 is the fabrication standard connected to design standards that restrict the allowable axial strain. It does not itself restrict the allowable axial strain. However, the method for alternative acceptance of girth weld imperfections provided in Appendix A covers axial strains of no more than 0.5%. These are the applied strains. A residual strain from the welding residual stress of 0.2% was assumed in developing the criteria.

The method within Appendix A is based on assessment methods from an earlier version of BS 7910, BS PD 6493. The current BS 7910 Level 1 provides similar methods. These methods provide a determination of the resistance to fracture, but do not include the effects of plasticity or allow for a plastic-collapse fracture mode.

DNV-RP-F108

DNV-RP-F108 (2006) [5] gives specific guidance for testing and analysis to ensure fracture control of pipeline girth welds subject to cyclic plastic strains during installation (e.g., reeling). It is based on the results of a joint industry project conducted by DNV, TWI, and SINTEF. It gives recommendations for SENT testing, ECAs, validation testing based on segment tests, and sensitivity analyses.

BS 7448 and ASTM E 1820 describe methods for measuring fracture toughness using high constraint SENB and CT test specimens suitable for use in conservative fracture assessments for a wide range of structures and components. The SENT

specimen is a test specimen that nominally has a similar level of constraint to a circumferential flaw in a girth weld subject to global bending. In the continued absence of a standard method for conducting SENT tests, Section 2 of DNV-RP-F108 gives suitable guidance. It is also noted that SENT specimens may not be appropriate for combined longitudinal loads and internal overpressure, which is consistent with DNV-OS-F101, 2007.

The guidance on conducting ECAs is specifically limited to the "installation phase," that is, longitudinal loads only. The amendments and assumptions in DNV-RP-F108 are consistent with those in Appendix A of DNV-OS-F101, for a "static" and "full" ECA for loading modes that are displacement controlled. The guidance on the treatment of multiple strain cycles (e.g., reeling on and bending over the aligner) is more comprehensive. DNV-RP-F108 also gives a simple method for treating counterboring based on increasing the flaw height and reducing the wall thickness, hence, increasing the stresses by the change in wall thickness due to counterboring.

DNV-RP-F108 recommends that the results of the ECA should be verified by segment testing, as there is only limited experience of applying ECA methods to high cyclic strain situations. Considering the good experience with constraint matched methods, Appendix A of DNV-OS-F101 has now limited the requirement for segment testing to clad or lined pipe; $\varepsilon_{l,nom} > 1.5\%$, for X65 and above carbon steel line pipe or stainless steel line pipe and $\varepsilon_{l,nom} > 2.25\%$, for all line pipe.

DNV-OS-F101

DNV-OS-F101 (2007) adds some comments on the procedure used within BS 7910, since its procedure is designed for stress-based rather than strain-based assessment. A material-specific stress-strain curve is required, as noted in the commentary, so only BS 7910 Levels 2B, 3B, and 3C are accepted. For weld regions, conservative determinations require that the upper bound material-specific stress-strain curve from the base metal be used to determine the stress from the applied strain. Then, the lower bound material-specific stress strain curve from the weld metal is used to determine the resistance on the FAD. This can make the calculated fracture resistance differ markedly between under- and overmatched welds.

The maximum value of the limit-load ratio L_r is allowed to increase to the ratio of the uniaxial ultimate strength to the yield strength. For load-controlled cases, this same ratio cannot exceed the flow strength (average of yield and ultimate strength) divided by the yield strength. Also, the material-specific stress-strain curve is used in its true-stress/true-strain form rather than the more common engineering-stress/engineering-strain form. This allows smooth extension of the FAD to the maximum value of the limit-load ratio.

References

[1] BS7608. Code of practice for fatigue design and assessment of steel structures. London: British Standards Institution; 1993.

[2]   DNV-RP-C203. Recommended practice for fatigue design of offshore steel structures. Det Norske Veritas; 2005.

[3]   DNV-OS-F101. Submarine pipeline systems. Det Norske Veritas; October 2007.

[4]   HSE. Review of low cycle fatigue resistance. Res. Rep. 2004;207, Health Safety Executive, London.

[5]   DNV-RP-F108. Fracture control for pipeline installation methods introducing cyclic plastic strain. Det Norske Veritas; January 2006.

[6]   Dowling AB, Townley CHA. The Effect of defect on structural failure: A two-criteria approach. Int. J. Pressure Vessels and Piping 1975;3(2):77–107.

[7]   Maddox SJ, Pargeter RJ, Woollin P. Corrosion fatigue of weld C-Mn steel risers for deepwater applications: A state of the art review. 2005. OMAE2005–67499, Halkidiki, Greece.

[8]   Connely LM, Zettlemoyer N. Stress concentrations at girth welds of tubulars with axial wall misalignment. In: Proceedings of the Fifth International Symposium of Tubular Structures: Nottingham, UK; 1993.

[9]   Buitrago J, Hudak S, Baxter D. High-cycle and low-cycle fatigue resistance of girth welds in sour service. Portugal: Estoril; 2008. OMAE2008–57545.

[10] Pargeter R, Baxter D. Corrosion fatigue of steel catenary risers in sweet production. Portugal: Estoril; 2008. OMAE2008–57075.

[11] Cordes R. How inspectors can use fracture mechanics. The 2000 API Inspector Summit, Houston, Texas; 2000.

[12] Pisarski H. Fracture toughness testing. Available at www.twi.co.uk/content/kscsw011. html.

[13] Thaulow C, et al. Consequences of defects in stainless steel weldments in subsea pipelines. Underwater Technology Conference 2004, Bergen, Norway.

[14] Nyhus B, Østby E, Knagenhjelm HO, Black S, Røstadsand PA. Fracture control— Offshore pipelines: experimental studies on the effect of crack depth and asymmetrical geometries on the ductile tearing resistance. OMAE2005–67532, Halkidiki, Greece; 2005.

[15] BS7910. Guide on methods for assessing the acceptability of flaws in metallic structures. London: British Standard Institution; 2005.

[16] API RP 579. Fitness-for-service. Washington, DC: American Petroleum Institute; 2000.

[17] R6. Assessment of the integrity of structures containing defects, revision 4. British Energy; UK, June 2005.

[18] PD 6493. Guidance on methods for assessing the acceptability of flaws in fusion welded structures. London: British Standards Institution; 1991.

13 On-Bottom Stability

Chapter Outline

1. Introduction

Pipelines resting on the seabed are subject to the forces in both the horizontal and vertical directions due to wave and current loads. When the loads are large enough, these forces can destabilize the pipe, leading to floatation or lateral movement. The stabilization requirements of the pipeline can be a major cost driver on subsea pipeline projects, especially in some shallow locations around the world, where the wave-induced current is an extremely challenging condition. Sometimes, costly stabilization requirements, such as trenching, anchoring, rock dumping, and mattressing, have therefore been used to ensure the stability of a pipeline on the seabed [1]. Deepwater pipelines are typically stable on bottom due to the absence of wave-generated currents. However, certain deepwater regions around the world experience loop currents that may affect pipeline on-bottom stability. In addition, pipeline on-bottom stability design is critical in the whole life of pipeline design procedure.

The main purpose of pipeline on-bottom stability design is to choose the appropriate pipeline route, materials, size and convenient manufacture, installation, and maintenance method so that the pipeline can withstand probable design current and wave loads at a low cost [2]. On-bottom stability calculations are performed to determine the minimum requirements for pipeline submerged mass. The required pipeline submerged weight has a direct impact on the required pipe laying tensions, installation stresses, and the pipeline configuration on the sea bottom. From the installation viewpoint, especially where spans are not a concern, the priority is to minimize the required pipeline submerged mass.

On-bottom stability design is performed in the following typical conditions for the installation and operational phases.

- **Operational phase:** The pipeline is considered filling with content at the expected lowest density, the following wave combination with current should be used [3]:
  - Wave domain, 100 year wave loading plus 10 year return current loading.
  - Current domain, 10 year wave loading plus 100 year return current loading.
- **Installation phase (temporary phase):** The pipeline is considered filling with air, the recurrence period may be taken as follows:
  - Duration less than 3 days, the environmental parameters for determination of environmental loads may be established based on reliable weather forecasts.
  - Duration in excess of 3 days, (1) no danger of loss of human life; a return period of 1 year for the relevant season may be applied. (2) Danger for loss of human life; the parameters may be defined with a 100 year seasonal return period.

However, the relevant season may not take less than two months. If the empty pipeline is left unprotected on the seabed over the winter season, combinations of 10 year current + 1 year wave and 1 year current + 10 year wave loading are checked, which is required for the temporary phase with a duration less than 12 months but in excess of three days according to DNV-RP-F109 [4]. For the installation condition, a minimum specific gravity of 1.1 is required.

2. Vertical On–Bottom Stability

According to DNV RP F109, to avoid flotation in water, the submerged weight of the pipeline should meet the following criterion:

$$\gamma_W \cdot \frac{b}{w_S + b} = \frac{\gamma_W}{s_g} \leq 1.00 \qquad\qquad [13.1]$$

where

γ_W = safety factor
w_S = pipe submerged weight per unit length
b = pipe buoyancy per unit length

The safety factor depends on the wave and current velocities around the pipe and its relative position to the seabed. In the pipeline empty condition, the safety factor $\gamma_W = 1.1$ can be applied.

Liquefaction generally occurs due to excess pore water pressures being generated within the structure of the soil by wave action directly or through cyclic loading on a seabed structure in contact with the soil. The process of liquefaction reduces the overall relative density of the soil, and as a result, a pipeline buried in a soil subject to liquefaction will undergo floatation or further settlement, depending on the relative density of the pipe. Pipes that are intended to be buried should be checked for possible sinking or floatation. Sinking should be considered with maximum content density, such as water filled, and floatation should be considered with minimum content density, such as air filled. If sinking is also considered, the following formula, given by Ghazzaly and Lim [5], should be used:

$$\gamma_p + R_V \geq \gamma_S \geq \gamma_p - R_V \qquad\qquad\qquad [13.2]$$

where

γ_S = soil saturated density on seabed; $\gamma_S = G \cdot \gamma_W \cdot (1 + W)/(1 + G \cdot W)$
G = specific gravity of solid particles on seabed
W = soil water cut
γ_P = pipeline density
γ_W = seawater density
R_V = floating or sinking resistance of soil; $R_V = 2 \cdot C/D$
C = soil remodelling shear strength
D = external diameter

When calculating the pipeline in the three conditions: installation, operation, and hydrotesting, if the soil saturated density is between the limits of floating and sinking, the pipeline is stable. Otherwise, if larger than the floating limit, the pipeline will float; if smaller than the sinking limit, pipeline will sink. More detailed pipe-soil relationships are described in Chapter 6.

3.   Lateral On-Bottom Stability

Subsea pipelines are subjected to the drag and inertia forces in the horizontal plane due to wave and current loads, except for the lift forces. When these forces are sufficiently large to overcome seabed friction, lateral movement is possible. The pipeline lateral on-bottom stability design focuses mainly on getting a minimum submerged weight of pipeline so that it can resist the design load during the operation period. The main referenced rules are DNV codes [3, 4].

DNV-RP-E305

DNV-RP-E305 [3] presents three design approaches for pipeline lateral on-bottom stability design:

- The simplified stability method.
- The generalized stability method.
- The dynamic stability method.

Simplified Stability Method

This method is based on a quasi-static stability approach, which ties the classical static design approach to the generalized stability method through a calibration of the classical method with generalized stability results. It is suitable for checking stability in all normal design situations by using a calibration factor F_w.

Stability in the quasi-static method is given by the following expression:

$$\left(\frac{W_s}{F_w} - F_L\right) \cdot \mu \geq F_D + F_I \tag{13.3}$$

where

W_S = pipe submerged weight
F_w = calibration factor
μ = soil friction factor (0.7 for sand, Figure 5.11 of DNV RP E305 for clay)
F_L = lift force, calculated by Morison equation
F_D = drag force, calculated by Morison equation
F_I = inertia force, calculated by Morison equation

Then, W_s can be figured out by

$$W_s = \left[\frac{F_D + F_I + \mu F_L}{\mu}\right]_{max} \cdot F_w \tag{13.4}$$

Generalized Stability Method

This method is based on generalization of the results from dynamic analysis, which applies the design curves by using a set of nondimensional parameters to provide a minimum required pipe weight (in terms of the dimensionless weight parameter, L) as a function of the Keulegan-Carpenter number, K, the current to wave velocity ratio, M, and the duration of the storm, that is, the number of waves, T. Figure 13.1 shows the design stability curves of sand soil for pipe lateral movement of 10 diameters (dimensionless lateral displacement, $\delta = 10$) during 1000 waves (approximately two hours for an average wave period of 15 s). The square root of the required weight parameter can be plotted for a given combination of K and M. The curves for a nondimensional strain parameter are also given to enable assessment of the bending of the pipe. It should be noted that the method can be used only under the following condition: $4 < K < 40; 0 < M < 0.8; 0.7 < G < 1.0$ (for sand soil); and $D \geq 0.4$ m. The design stability curves of clay soil are also plotted in DNV-RP-E305 [3] for different K values. The generalized stability design method for clay soil is illustrated in the flow chart of Figure 13.2.

Dynamic Stability Method

The full dynamic analysis stated in the recommended practice [3] means the dynamic simulation of a section of pipeline under the action of waves and current by the use of AGA level III or PONDUS. However, the recommended practice gives little advice on how to design these analyses. A time domain solution is recommended because of the nonlinear behavior of the pipeline.
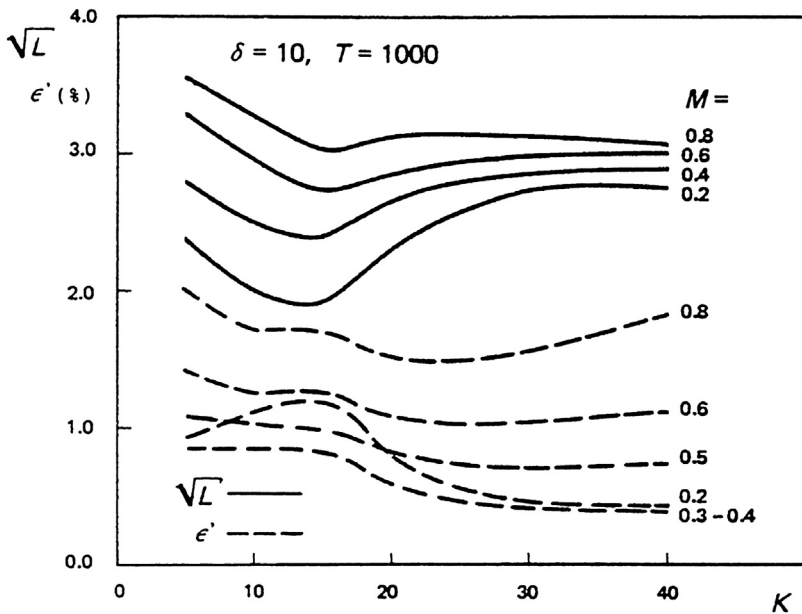
Figure 13.1 Generalized weight parameter *L* versus *K* for various *M* values.
Source: DNV-RP-E305 [3].

The FEA method is usually used to do pipeline dynamic stability analysis. The following issues should be accurately modeled:

- Wave spectrum and corresponding realistic time series.
- Current velocity at the seabed.
- Structural behavior of pipe.
- Hydrodynamic forces.
- Soil resistance forces.
- Restraints (e.g,. riser connections).

DNV-RP-F109

DNV-RP-F109 [4] is an updated version of RP-E305, and many symbols have the same meaning. If no other description is presented, the symbols should be taken as the same definitions.

Generalized Lateral Stability Method

In this method, a dimensionless lateral pipe displacement, *Y*, is used. It is governed by a set of nondimensional parameters,

$$Y = f(L, K, M, N, \tau, G_s, G_c) \qquad [13.5]$$

where

$N = U_s/(g \cdot T_U) =$ spectral acceleration factor

$\tau = T/T_U =$ number of oscillations in the design bottom velocity spectrum

$G_s = \gamma_s'/(g \cdot \rho_w) =$ sand soil strength parameter

$G_c = S_U/(D \cdot \gamma_s) =$ clay soil strength parameter

$U_s =$ near bottom significant velocity perpendicular to the pipeline due to a given surface sea state

$T_U =$ near bottom zero up-crossing period due to a given surface sea state

$T =$ sea state duration

$S_U =$ undrained clay soil strength

$\gamma_s' =$ submerged unit soil weight, for sand normally in the range 7,000 to 13,500 N/m^3

$\gamma_s =$ dry unit soil weight, usually taken as 18,000 N/m^3 for clay.

If end constraints are neglected, the following design criterion for lateral stability can be used:

$$\frac{Y}{Y_{\text{allowable}}} \leq 1.0 \qquad\qquad [13.6]$$

$Y_{\text{allowable}}$ is the allowed dimensionless lateral displacement scaled to the pipe diameter. The following four design criteria are applied in the generalized method:

- 10 pipe diameter displacement on sand.
- 10 pipe diameter displacement on clay.
- A virtually stable pipe on sand.
- A virtually stable pipe on clay.

If other limit states, such as the maximum bending and fatigue, are not investigated, it is recommended to limit the sum of the lateral displacement in the temporary condition and during operation to 10 pipe diameters. A design curve method is used to determine the minimum submerged weight of pipe. The curves are obtained from a large number of one-dimensional dynamic analyses performed by the PONDUS program [6], that is, on a flat seabed and neglecting bending and axial deformation of the pipe. A virtually stable pipe is a pipe that has a weight, denoted L_{stable} in the RP-F109, that is sufficient to avoid significant displacements, typically less than half its diameter.

For sandy soil, the specific weight of a pipe can be obtained by

$$S_g = 1 + \frac{2 \cdot N \cdot K \cdot L}{\pi} \qquad\qquad [13.7]$$

L can be interpolated in Tables 3.2–3.4 of the recommended practice [4] according to the design criteria or looked up from the design curves in Figure 13.3.

For clay soil, the minimum pipe weight required to limit the maximum relative displacement, Y, to less than 0.5 can be calculated by the following formula:

$$L_{\text{stable}} = 90 \sqrt{\frac{G_c}{N^{0.67} \cdot K}} \cdot \left[0.58(\log M)^2 + 0.60(\log M) + 0.47 \right]^{1.1} \qquad\qquad [13.8]$$
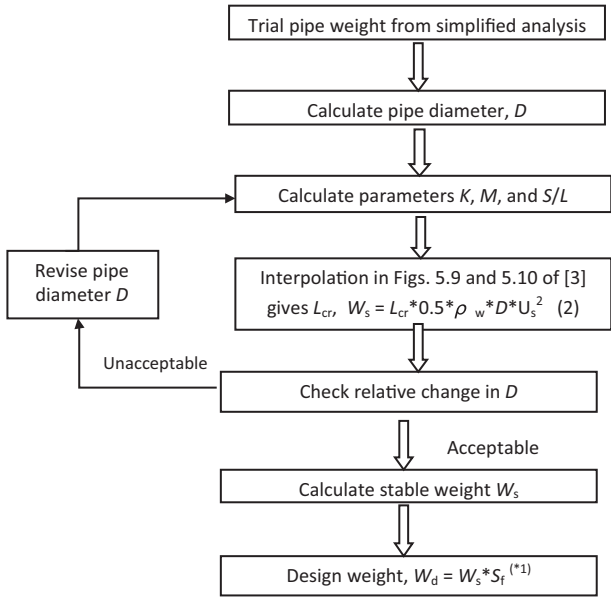
$^{(*1)}$The stable weight, W_s, calculated based on Figs. 5.9 and 5.10 of the RP [3], must be multiplied with a safety factor S_f =1.1 to arrive at design weight.

Figure 13.2 Flowchart of generalized stability design method.
Source: DNV-RP-E305 [3].

For the 10 pipe diameter displacement criteria, the dimensionless displacement, *Y*, to $10 \cdot \tau/1000$ can be calculated by the following formula:

$$\frac{L_{10}}{(2+M)^2} = \begin{cases} C_1 + \dfrac{C_2}{K^{C_3}} & \text{for } K \geq K_b \\[3mm] C_1 + \dfrac{C_2}{K_b^{C_3}} & \text{for } K < K_b \end{cases} \qquad [13.9]$$

where, the coefficients C_1, C_2, C_3, and K_b are tabulated in Appendix A of the RP [4].

Absolute Lateral Stability Method

This method gives an absolute static requirement for lateral on-bottom pipelines based on static equilibrium of forces that ensure that the resistance of the pipe against motion is sufficient to withstand maximum hydrodynamic loads during a sea state. The requirement for absolute stability may be relevant for, say, pipe spools, pipes on narrow supports, cases dominated by current, and on stiff clay.
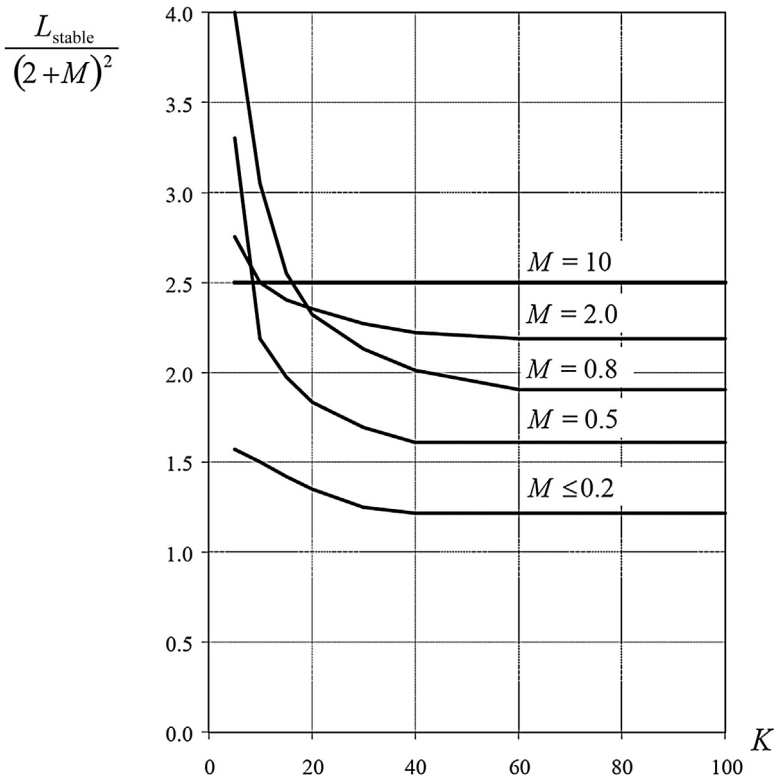
$$\frac{L_{\text{stable}}}{(2+M)^2}$$

Figure 13.3 Design curves of minimum weight, $L_{\text{stable}}/(2 + M)^2$ for a pipe on sand.
Source: DNV-RP-F109 [4].

A pipeline can be considered absolutely static stable if the following requirements can be satisfied:

$$\gamma_{\text{sc}} \cdot \frac{F_Y^* + \mu \cdot F_Z^*}{\mu \cdot w_s + F_R} \leq 1.0 \qquad\qquad [13.10]$$

and

$$\gamma_{\text{sc}} \cdot \frac{F_Z^*}{w_s} \leq 1.0 \qquad\qquad [13.11]$$

where

γ_{sc} = safety factor, from Tables 3-5 to 3-8 of the RP [4]
F_Y^* = peak horizontal load, $= r_{\text{tot,z}} \cdot \frac{1}{2} \cdot \rho_w \cdot D \cdot C_Y^* \cdot (U^* + V^*)^2$
F_Z^* = peak vertical load, $= r_{\text{tot,z}} \cdot \frac{1}{2} \cdot \rho_w \cdot D \cdot C_Z^* \cdot (U^* + V^*)^2$
F_R = passive resistance, can be obtained from Section 3.4.6 of the RP
μ = friction coefficient, 0.6 for sand and 0.2 for clay

$r_{tot,y}$ = total horizontal load reduction
$r_{tot,z}$ = total vertical load reduction
C_Y^* = horizontal peak load coefficients, from Table 3.9 of the RP
C_Z^* = vertical peak load coefficients, from Table 3.10 of the RP
U^* = oscillatory velocity amplitude for single design oscillation, perpendicular to pipeline, from Eq. (3.15) of the RP
V^* = steady current velocity associated with design oscillation, perpendicular to pipeline, from Eq. (3.3) of the RP

The required submerged weight, w_s, can be determined from the preceding equations.

4. Pipe-Soil Interaction

The pipe-soil interaction model consists of a definition of seabed stiffness and equivalent friction to represent the soil resistance to movement of the pipe. It is therefore important to predict the soil contact pressure, equivalent friction, and soil stiffness accurately.

Pipe-soil interaction is an important factor that affects on-bottom stability when pipeline laying on the seabed; however, due to its highly nonlinear property, it is very difficult to analyze using a numerical model. To understand the effects clearly, lots of experiments were carried out in the last decades. Figure 13.4 shows a typical passive resistance force-displacement curve. Based on the model developed by Brennodden et al. [7] and Verley and Sotberg [8], the pipe-soil interaction is divided into four distinct regions:

- Pipe displacements between the origin 0 and y_1 are within the elastic region and no work is done by the pipe on the soil within this region. Therefore, the level of penetration remains unchanged.
- Pipe displacement between y_1 and y_2 cause an increase in penetration. The increase in penetration can be calculated from the work done by the pipe on the soil.
- Breakout is initiated for pipe displacement greater than y_2. Therefore, the penetration and the passive soil resistance decrease.
- For pipe displacement greater than y_3, the penetration and passive soil resistance remain constant.

In the figure,

F_{r1} = peak elastic passive force
F_{r2} = peak passive force
F_{r3} = residual passive force
y_1 = mobilization distance associated with F_{r1}
y_2 = mobilization distance associated with F_{r2}
y_3 = mobilization distance associated with F_{r3}

More detailed pipe-soil interactions for subsea pipelines are described in Chapter 6 of this book.

Allowing the pipeline to undergo small cyclic lateral movements by using the detailed pipe-soil interaction model can significantly reduce the requirements for
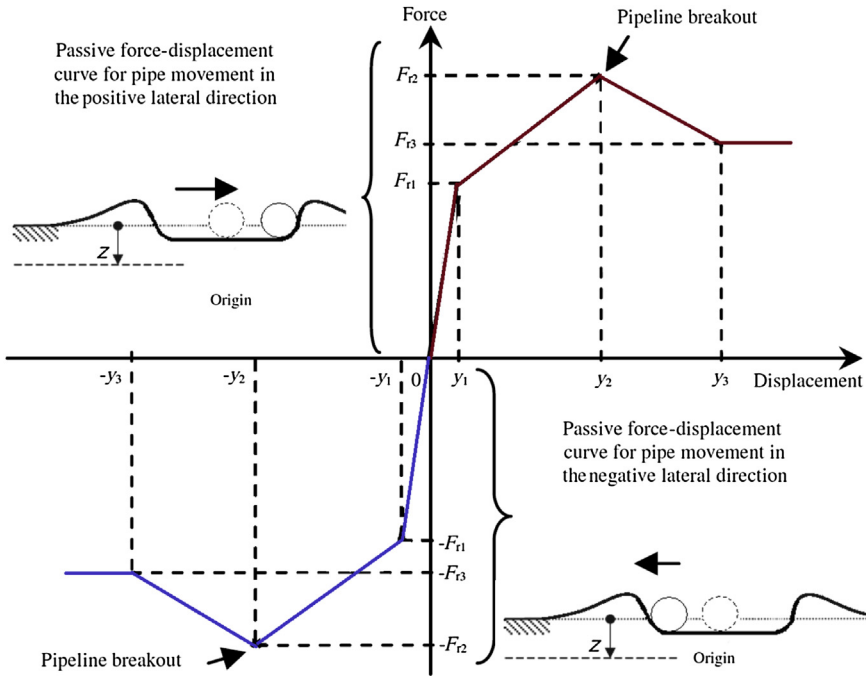
Figure 13.4 Pipe-soil interaction model.
Source: Zeitoun et al. [9]. (For color version of this figure, the reader is referred to the online version of this book.)

concrete weight coating (CWC) in comparison with a design based on the simple force balance method, in which no displacement or movement is allowed [10]. Furthermore, small cyclic movements are likely to lead to increased pipeline embedment into the soil, which in effect can significantly increase the pipe-soil resistance and thus further stabilize the pipeline.

5. Stabilization Measures

The mechanism responsible for subsea pipeline instability mainly arises from the fluid force balance imposed on the pipeline. To protect the pipeline against yielding and local buckling due to excessive displacement, floatation, and the like, additional stabilization beyond that provided by concrete weight coating is sometimes required. A wide range of secondary stabilization methods is available for this purpose. Secondary stabilization methods vary between intervention methods, such as trenching and rock dumping, to pipeline anchoring techniques, such as rock bolts, strategic anchors [1], and gravity anchors. Some of the stabilization methods, including concrete weight coating, are described next.

Concrete Weight Coating

Concrete weight coatings are very often applied to subsea pipelines to maintain the lateral and vertical stability of the pipeline. Usually, the concrete is applied by the impingement method over a pipeline. Basically, in the impingement method, the pipe joint is rotated as concrete is sprayed onto the pipe joint under pressure. Concrete coating thicknesses are limited by practical considerations and range from a minimum of 20 mm to a maximum of approximately 120 mm. Typical concrete densities values are 2040 kg/m^3 for low density concrete, 2540 kg/m^3 for medium density concrete, and 3040 kg/m^3 for high density concrete.

Wall Thickness

Even though concrete weight coating is one of the most commonly used methods for providing additional submerged weight for pipeline on-bottom stability, a thick concrete weight coating has the negative effect of increasing the overall outside diameter of the coated pipe, which in turn leads to higher hydrodynamic forces being generated. Using a thicker pipe wall to increase the submerged weight is a practical option, but this invariably increases the fabrication cost of the pipe.

Trenching and Backfill

Trenching of subsea pipelines is widely used as a means of stability enhancement in that the pipeline within a trench is partially shielded against hydrodynamic loads. In addition, the method is also suitable for providing protection from fishing gear damage, scour, and so forth. In general, sand and clay sea floors are relatively easy to trench with increasing difficulty as the soil becomes harder. Trenching is much more difficult in areas of rock or frequent rock outcrops. When trenching is an option, precutting a trench with a suction dredger or blasting can sometimes be used, depending on environmental impact.

Rock Dumping

Rock dumping is an increasingly common means of protecting a pipeline against floatation, lateral movement, upheaval buckling, and mechanical damage by dropped objects. In areas where local flow velocities are high, rock dump designs must ensure that the material be of a certain particle size that will not be washed away easily. The relative cost of rock dumping is high when compared to trenching. However, it is applicable to seabed conditions, such as hard clay or rock, where trenching cannot be reliably achieved. It is also frequently used as an expansion control system and for span protection.

Checks are required on the possible damage to the pipeline during the rock dumping operation, and if large diameter rock is required for the on-bottom stability, a smaller diameter rock may need to be dumped as an armor layer to protect the pipeline.

Concrete Mattress

Various forms of concrete mattresses offer protection to pipelines against instability. This method is cheap, simple, readily available, and can be taken out on a DSV. Figure 13.5 shows a typical revetment concrete mattress made by Submar Inc. However, the concrete mattress may not be stable in severe sea states, because the mattress is not attached to the pipeline, the edges may lift and the mattress removed from the pipeline.

Anchors or Rock Bolts

Anchors or rock bolts are an option for stabilizing pipelines. They rely on the seabed being able to sustain lateral and vertical loads from the pipeline. Rock bolts are used particularly where the seabed is rocky and trenching cannot be done. Rock bolts are installed after pipe laying by divers and are an extremely expensive solution. Anchors are also diver installed and can either be pushed or screwed into the ground.

Sand and Grout Bags

Sandbags maybe fabricated in various sizes and weights to suit a particular environment. Installation is usually done by divers and may be readily performed from a DSV.

The grout bag system offers significant advantages over sandbags and mattresses because of their ease of handling, prior to grout filling, particularly for installation under pipelines and structures. Flexible nylon or canvas bags with grout are put over or under pipeline to stabilize or protect it.
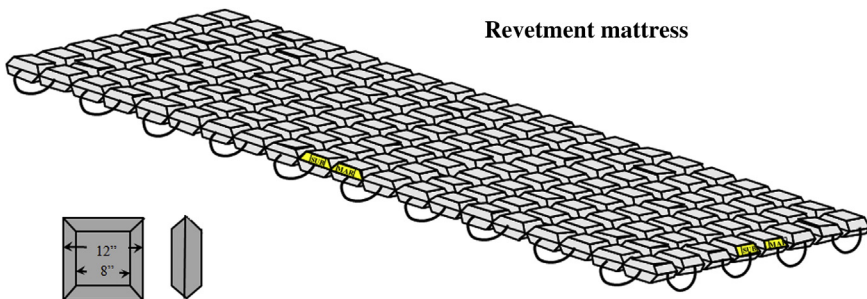
Mattress weight: Air 6200lbs, underwater 3500 lbs
Concrete density: 145 lbs per cu ft

Figure 13.5 Revetment concrete mattress.
Source: Submar, Inc. (For color version of this figure, the reader is referred to the online version of this book.)

6.   Acceptance Criteria

Allowable Lateral Displacement

The selection of the allowable lateral pipeline displacement should be based on several factors, such as

- National regulations.
- Distance from platform or other restraint.
- Seabed obstructions.
- Width of surveyed corridor.

If no further information is available, then the following may be used for the allowable maximum lateral displacement of the pipeline in the operational condition, according to RP-E305 [3]:

- Zone 1 (over 500 meters from a platform or subsea template): 20 meters.
- Zone 2 (less than 500 meters from a platform or subsea template): 0 meters.

These criteria can be relaxed or replaced if other relevant criteria (e.g., limit-state based strength criteria) are available.

Limit-State Strength Criteria

Limit-state based strength criteria have been discussed by Bai and Damsleth [11], who present potential failure modes and design equations as well as design experience on detailed design projects. Details are given in Chapter 4 of this book.

7.   Stability Analysis

The common tools for modeling pipeline stability response has been to either use special purpose pipeline stability finite element (FE) packages, such as AGA PRCI Stability (Levels I, II and III by PRCI, USA) [2] or PONDUS (SINTEF, Norway) [6], or to use special purpose finite element models [12].

Special Purpose Program for Stability Analysis

Simplified stability analysis is based on a quasi-static balance of forces acting on the pipe but has been calibrated with results from the generalized stability analysis. The method generally gives pipe weights that form a conservative envelope of those obtained from the generalized stability analysis.

- **Purpose made spreadsheet software (EXCEL, LOTUS 1-2-3):** Generalized stability analysis is based on a set of nondimensional stability curves, which have been derived from a series of runs with a dynamic response model.
- **PIPE software:** Dynamic analysis involves a full dynamic simulation of a pipeline resting on the seabed, including modeling of soil resistance, hydrodynamic forces, boundary

conditions, and dynamic response. It may be used for detailed analysis of critical areas along a pipeline, such as pipeline crossings or riser connections, where a high level of detail is required on pipeline response or for reanalysis of a critical existing line.

- **PONDUS and AGA software:** The special purpose FE stability packages often impose several disadvantages, including
  - Simplified structural response assumptions, including small deflection, two-dimensional motion, and no consideration of geometric nonlinearity.
  - The seabed assumed to be flat.
  - The modeling capability is inflexible in the sense that nonstandard features cannot be modeled, such as an irregular seabed or presence of trenches or tie-in spools.
  - No capability of modeling additional stabilization measures, such as trenching or anchoring.
  - Pipeline stability is considered in isolation from other design issues, such as free spanning and buckling.
- Finite element models developed using general purpose FE packages, such as ABAQUS or ANSYS, may be associated with [9]
  - Hydrodynamic modeling.
  - Pipe-soil interaction modeling.
  - Requirement for advanced user FE knowledge.

The choice of these analysis methods depends on the degree of detail required in results of the design analysis.

FE Analysis for Intervention Design

Design Procedure

Figure 13.6 shows a flowchart for the seabed intervention design procedure.

Seabed Intervention

There are several types of seabed intervention. Examples of seabed intervention are rock dumping, trenching, burying, and presweeping. The purpose of seabed intervention design is to ensure that the pipeline maintains structural integrity throughout its design life. It is then the premise that good work has been done when the design criteria is established and compared with the simulated pipeline response to a history of loads.

The structural behavior of a pipeline along its route can be analyzed using finite-element simulations of the load history from installation, flooding, hydrotesting, dewatering, to operation. This analysis makes it possible to simulate the pipeline in-place behavior. Based on an understanding of the pipeline behavior from the analysis, it is possible to select a seabed intervention design that is technically feasible and cost effective. The effect of the intervention can then be analyzed in detail for each particular location of the pipeline by finite-element simulations. The finite-element simulations are therefore of great help for developing a rational intervention strategy.
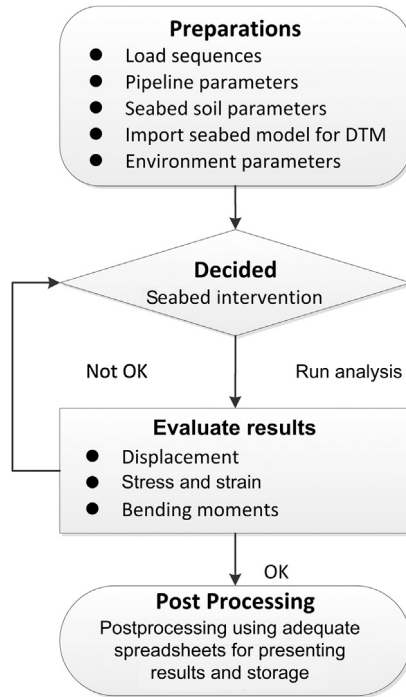
Figure 13.6 FEM analysis procedure.

This kind of simulation has also shown that the results can be quite sensitive to the shape and properties of the seabed. As a result of this, the actual behavior of the pipeline can differ from the simulated behavior. Some factors are

- Deviations between the planned route and the as-laid route.
- Actual lay tension during installation.
- Performance of seabed intervention, primarily trenching.
- Local variations in soil conditions.

It is therefore suggested to make the final decision on whether to perform seabed intervention work at some locations when as-built information becomes available.

Effect of Seabed Intervention

In Figure 13.7, seabed intervention in the form of trenching and rock dumping has been performed on the 3D seabed model, trying to reduce stresses and strains in the pipe from vertical loads. Results are given for maximum axial stress and bending moment, before and after intervention [12].

In Figure 13.8, seabed intervention in the form of rock dumping has been performed on the 3D seabed model, trying to reduce the lateral displacement of the pipe due to hydrodynamic loads.
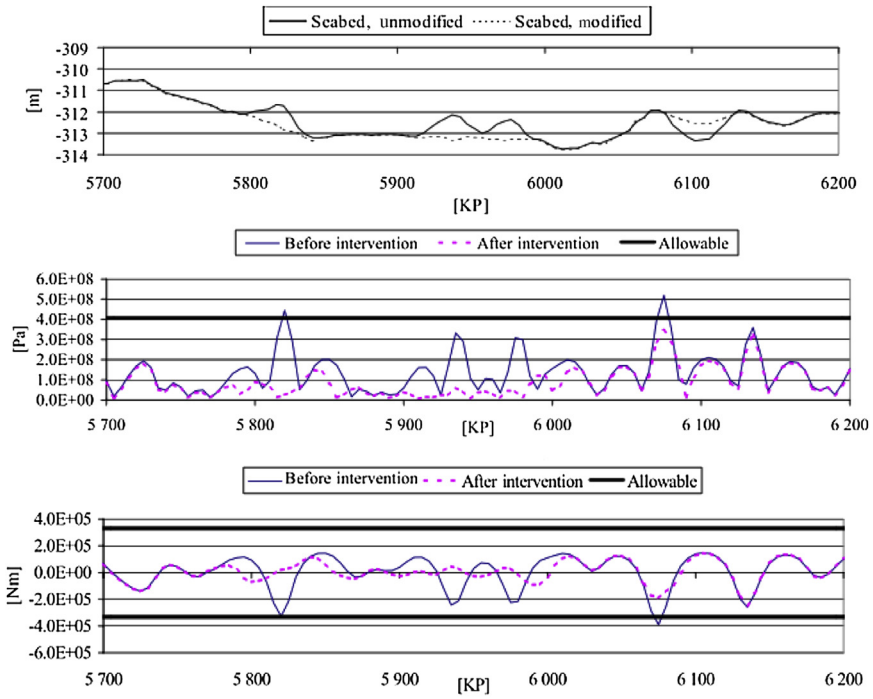
Figure 13.7 Comparison of stress and bending moment, before and after. (For color version of this figure, the reader is referred to the online version of this book.)
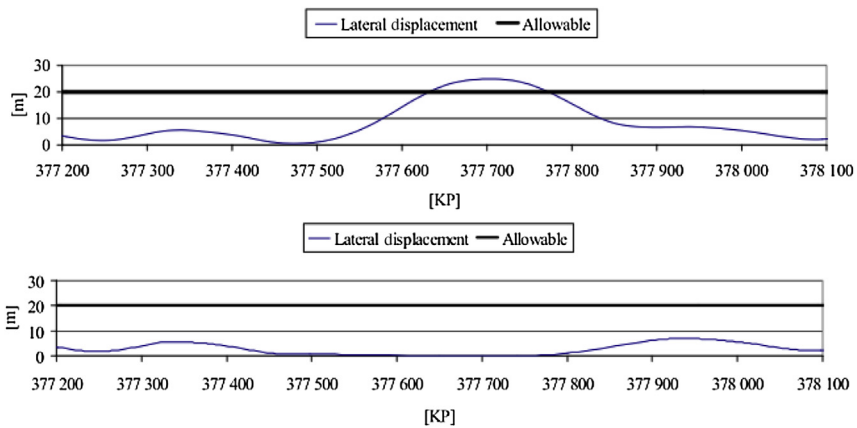
Figure 13.8 Comparison of lateral displacement of pipeline, before and after. (For color version of this figure, the reader is referred to the online version of this book.)

The seabed intervention design through analysis is conducted as follows:

- Calculate stress, bending moment, and displacements, as shown in Figures 13.7 and 13.8, for the two pipelines.
- Compare the calculated stress, moment, and displacements with acceptance criteria.
- For the sections of pipeline where stress, moment, or displacement criteria are violated, a seabed intervention is designed. The stress, moment, or displacements are then recalculated, as shown in Figures 13.7 and 13.8, and compared with the acceptance criteria.
- This iteration is continued until acceptance criteria are fulfilled in all sections, Figure 13.7. From the plots, it can be seen that the load effects are reduced significantly as a result of the seabed intervention performed on the 3D seabed of the analysis model.

References

[1] Brown NB, Fogliani AG. Pipeline lateral stabilisation using strategic anchors. SPE 77849. Proceedings of the SPE Asia Pacific Oil and Gas Conference. Melbourne: Australia; 2002.

[2] AGA. Submarine pipeline on-bottom stability, vols. 1 and 2. Project PR-178–9333. American Gas Association, Houston; 1993.

[3] DNV. On-bottom stability design of submarine pipelines. DNV-RP-E305; Det Norske Veritas; 1988.

[4] DNV. On-bottom stability design of submarine pipelines. DNV-RP-F109; Det Norske Veritas; 2007.

[5] Ghazzaly OI, Lim SJ. Experimental investigation of pipeline stability in very soft clay. OTC 2277; In: Proceedings of the 7th Offshore Technology Conference. Houston, TX; 1975.

[6] Tørnes K, Zeitoun H, et al. A stability design rationale—A review of present design approaches. OMAE 79893. In: Proceedings of the ASME 28th International Conference on Ocean. Honolulu, HI: Offshore and Arctic Engineering; 2009.

[7] Brennodden H, Lieng JT, Sotberg T, Verley RLP. An energy based pipe soil interaction model. OTC6057. In: Proceedings of the 21th Offshore Technology Conference. Houston, TX; 1989.

[8] Verley RLP, Sotberg T. A soil resistance model for pipelines placed on sandy soil. Pipeline Technology. In: Proceedings of the 11th International Conference on Offshore Mechanics and Arctic Engineering. AB, Canada; 1992.

[9] Zeitoun HO, Tørnes K, et al. Advanced dynamic stability analysis. In: Proceedings of the ASME 28th International Conference on Ocean. Honolulu, HI: Offshore and Arctic Engineering; 2009.

[10] Holthe K, Sotberg T, Chao JC. An efficient computer program for predicting submarine pipeline response to waves and current. OTC5502. In: Proceedings of the 19th Offshore Technology Conference. Houston, TX; 1987.

[11] Bai Y, Damsleth PA. Limit-state based design of offshore pipelines. Proc. of OMAE'97; Proceedings of the 16th International Conference on Offshore Mechanics and Arctic Engineering, Yokohama, Japan; 1997.

[12] Ose BA, Bai Y, Nystrøm PR, Damsleth PA. A finite element model for in-situ behavior of offshore pipelines on uneven seabed and its application to on-bottom stability. Proc. of ISOPE '99; Brest, France; 1999.

14 Pipeline Spans and VIV Fatigue

Chapter Outline

---

1.   Introduction

General

The configuration of pipeline on the seabed depends on the topographical features of the seabed, soil type, residual tension, pipe stiffness, and its submerged weight. The pipeline spans are unsupported pipe sections above the seabed. The pipelines tend to form spans rather than follow the topographical features of the seabed if the seabed is very rough. The pipeline spans may be created due to the seabed irregularities during installation or the subsequent scouring and pipeline horizontal movements during the operation. Pipeline spans are not limited to a single span, multiple span configurations are also possible, in which adjacent spans are located in sufficiently close proximity for interaction between them [1]. Figure14.1 illustrates typical pipeline spans formed on a seabed, in which (a) shows a single span and (b) shows multiple spans.

(a) Single span
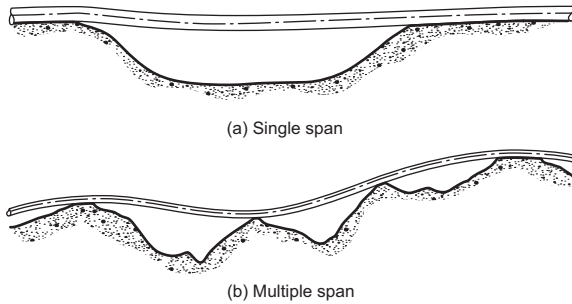
(b) Multiple span

Figure 14.1 Typical pipeline spans.

The tendency of interaction between spans in multiple spans depends on the soil properties and the relative length of two adjacent spans. Figure 14.2 indicates the classification of pipeline span type by DNV-RP-F105 [2]. The relationships of the relative span lengths of adjacent spans to the relative span shoulder length for four soil types are shown in the figure. If the relationship for the multiple spans is above the curve, then the multiple spans should be evaluated as multispans; otherwise, the multiple spans can be evaluated as isolated single spans. A softer soil tends to have shorter and fewer spans and probably less interacting spans than a harder soil.

As a typical feature of many sandy seabeds in shallow water, sand waves tend to propagate, resulting in continuously moving pipeline spans unless the pipeline is lowered to below the trough level. The residual tension on span formation during
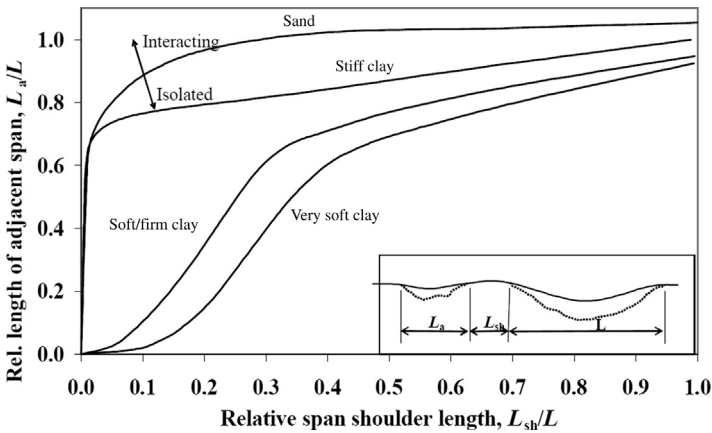
Figure 14.2 Classification of span types.
Source: DNV-RP-F105 [2].

installation is closely related to the pipe's submerged weight. Higher residual tension tends to create more and longer span. Heavier pipes normally form fewer and shorter spans. If the pipe is heavy, higher tension is required during installation to prevent overstress in the pipeline.

The pipeline spans may have a critical influence on the safety and integrity of the pipeline operation. Usually potential spans can be predicted prior to installation by gathering environmental data and subsea surveys along the proposed pipeline route. The basic span length criteria include static stress, vortex shedding induced vibrations (VIV) and fatigue damage, and bar buckling due to the following failure modes of pipeline spans:

- Yield failure due to excessive stress from a long span.
- Fatigue damage due to direct wave loads and pipeline VIVs.
- Local buckling due to high local bending caused by pipeline weight and current loads, VIV and wave loads, and trawl interference; or bar buckling due to effective compressive axial force under internal pressure and temperature loads.

For each of the criteria, the allowable span length should generally be calculated for each of the following four load conditions:

- Installation condition—empty pipe.
- Flood and hydrotest condition—water filled pipe.
- Operating condition—production fluid filled pipe.

The pipeline span loadings for these load conditions are based on the evaluation of environment, construction methods, operational parameters, and test requirements, which include

- Submerged weight of pipe.
- Effective mass of pipe.
- External and internal pressures.
- Temperature.
- Residual lay tension.
- Soil-pipe interaction for unburied and buried pipelines.

In some cases, the environmental loadings also include the following reasons:

- Seawater-pipe interaction, hydrodynamic forces due to current and wave action.
- Loadings due to seismic activity.
- Trawl board pull over or hooking.

The structural properties of the given span configuration are to be characterized in terms of static and dynamic properties. Key parameters and relationships to be deducted are mainly

- Relationship between loading or deflection of span and associated stresses and sectional forces and moments in pipe wall (static analysis).
- Eigen frequencies and mode shapes of span, relationship between vibration amplitudes and stress cycles (dynamic analysis).
- Soil damping in terms of soil static and dynamic interaction with pipe.

Structural Static Model

Structural models of varying complexity, analytical as well as finite element analysis based models, may be applied, ranging from simple models for simplified desk calculation to advanced finite element models for FE analysis.

Basically, the static model is applied to determine the stresses due to static or quasi-static loads, such as the deadweight of span, quasi-static wave and current loads, trawl boards, and anchors. An elastic approach is frequently selected for the pipe itself, whereas elastoplastic soil behavior is most often adopted. This is particularly important in the case of large spans supported on a soft seabed.

For analysis of impact loads, it is usually relevant to consider elastoplastic behavior of the pipe as well as the soil.

Structural Dynamic Model

Basically, the dynamic model is applied to determine the stresses due to flow-induced vibrations for subsequent calculation of fatigue damage (in conjunction with the fatigue model) and for comparison with criteria for the maximum allowable stresses. In-line and cross-flow vibration may be treated in an integrated manner or separately.

Objective

Pipeline spans on the seabed require assessment to determine whether or not remedial action is required to avoid damage to the pipeline. The static and dynamic characteristics of the pipeline spans should be investigated to ensure that the pipeline can be maintained at an acceptably safe state. If the required safety cannot be ensured, then remedial actions in the form of rerouting, span correction, suppression of VIV, and the like are used to make certain that the design criteria regarding stress levels and potential fatigue damages due to VIV are not exceeded.

In the design stage, an assessment of the seabed profile along the proposed route may be performed to identify whether pipeline spans are expected to occur. If pipeline spans may occur, then where and how much of the spans will be calculated must be determined. This assessment of the pipeline route is normally based on survey data using finite element analysis, such as ABAQUS software, or a specialist pipeline package such as Orcaflex or Sage Profile to lay the pipeline over the seabed profile. This analysis gives predictions of the numbers and sizes of expected pipeline spans [3].

DNV-RP-F105 is the main design code available for the evaluation of free spanning pipelines in subsea engineering. Other main offshore standards, such as DNV-OS-F101, PD 8010, and ASME B31.8, have no specific requirements regarding pipe spans, but the stress limits are included for the calculation of allowable span length based on the static stress criteria.

The objective of this chapter is to present the acceptance criteria with respect to static stress limits and fatigue damage limits due to the VIV of free spans and to outline the proposed methodology for the detailed design of pipeline systems.

2. Static Analysis

Analytical Analysis

The static analysis of spanning pipelines is to use simple linear elastic analysis methods and limit the maximum equivalent stress due to pressure, temperature, and bending to a proportion of the specified minimum yield strength (SMYS) of the pipe material. The validity of linear elastic analysis methods becomes highly questionable when the effects such as soil flexibility, pipe-soil interaction, and axial effective tension are considered.

A uniform load, q, due to lateral bending load resulting from the drag and inertia hydrodynamic forces and the vertical bending load resulting from self-weight of pipe and contents and lift from the hydrodynamic forces is applied along the span length. An effective axial load, S_0, resulting from Poisson's effect, internal fluid pressure generating end-cap forces, and thermal expansion, is also included in the analysis.

Figure 14.3 shows a typical configuration of pipeline span and its loads. The following equations are derived from the force equilibrium of pipe elements, assuming the pipe rotations and the initial inclination of the pipe element to the horizontal are small:

$$EI\frac{d^4y}{dx^4} - S_0\frac{d^2y}{dx^2} + k_s y = q \qquad [14.1]$$

where k_s is the soil stiffness. A dimensionless equation from Eq. [14.1] was solved numerically using a computer program with boundary conditions [1]. Because of the nonlinear nature of the equation, an iterative method was employed. The derived results were then used to compute bending moments and axial forces. If the span shoulders are defined as rigid contacts, the spring term in the equation is ignored. The
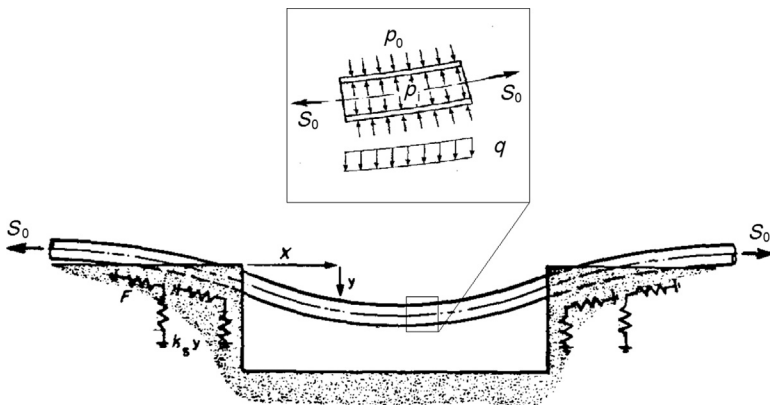
Figure 14.3 Typical configuration of pipeline span and loads.
Source: Kenny [1].

governing equation of the simple beam theory, Eq. [14.1] is reduced to Eq. [11.4], in which y is replaced with $-w$.

The maximum bending moment, M_{max}, induced in a span length of L, by a uniform load along the span length, q, is given by

$$M_{max} = \frac{qL^2}{8} \quad \text{for pinned} - \text{pinned boundary condition} \qquad [14.2]$$

$$M_{max} = \frac{qL^2}{12} \quad \text{for fixed} - \text{fixed boundary condition} \qquad [14.3]$$

$$M_{max} = \frac{qL^2}{10} \quad \text{for fixed} - \text{pinned boundary condition} \qquad [14.4]$$

The pinned-pinned case underestimates the stiffness of the real span supports, while the fixed-fixed model overestimates the fixity for most spans. On the basis that the end fixities of a span are somewhere between the two cases, but it is difficult to determine exactly where, the normal compromise is to model the span with one end fixed and one pinned, as an intermediate and representative value. This generally gives remarkably good results.

The static bending moment may also be estimated following DNV-RP-F105[2]:

$$M_{max} = C \frac{qL_{eff}^2}{\left(1 + \frac{S_0}{P_{cr}}\right)} \qquad [14.5]$$

where C is a boundary condition coefficient, 1/8 for pinned-pinned bound condition, 1/12 for fixed-fixed boundary condition. For a single span on a seabed, $C = 1/24$ at the mid-span, $C = 1/[18(L_{eff}/L)^2 - 6]$ at the span shoulders. The term L_{eff} is calculated using the static soil stiffness; P_{cr} is the critical buckling load; the term S_0/P_{cr} is negative when the effective axial force is in a compressive condition.

The maximum bending stress, σ_b, is given by

$$\sigma_b = \frac{M_{max}D}{2I} \qquad [14.6]$$

where

M_{max} = maximum bending moment
I = pipe moment of inertia
D = pipe outside diameter

Total longitudinal stress, σ_L, for axial restrained end condition, is given by

$$\sigma_L = \sigma_T + \sigma_p \pm \sigma_b \qquad [14.7]$$

where

σ_T = thermal stress, $-E\alpha\Delta T$
σ_p = Poisson stress, $\nu\sigma_h$

Combined Von Mises stress due to the hoop and longitudinal stresses is

$$\sigma_{eq} = \sqrt{\sigma_L^2 + \sigma_h^2 - \sigma_L \sigma_h + 3\tau^2} \qquad\qquad [14.8]$$

where τ is the shear stress, which is normally taken as zero for pipeline spans.

Pipeline spans may be subjected to various loads in different phases, such as installation and operation. The response of pipeline to these loads varies considerably, depending on the degree of interaction with its environment, its conditions of use, and its configuration and geometry. The behavior of pipeline may be considerably more complex than that predicted by the simplified analytical methods. For more accurate evaluation, finite element analysis is suggested.

Static Stress Limits

Pipeline spans increase the stress level in the pipe due to its self-weight and hydro-dynamic loading. The bending stress should account for the combined axial and hoop stresses generated by these loads. The combined stresses due to these loads and operational loads should be checked against the allowable levels of stress given in the relevant design codes.

The usage factors for pipeline according to the relevant design codes are summarized in Table 14.1.

When using DNV-RP-F105, the stress check is replaced by an ultimate limit state check on local buckling. DNV-RP-F105 specifies ultimate limit state (ULS) criteria as specified in the offshore pipeline code DNV-OS-F101. The critical ULS for operational spans is local buckling. Local buckling implies gross deformation of the cross section and DNV OS-F101 requires that checks be made against system collapse, combined loading, and propagating buckle.

Table 14.1 Usage Factors of Different Design Codes for Subsea Pipelines

Design Codes	Equivalent Tensile Stress	Usage Factor		
		Von Mises Stress		
		Installation	Functional	Functional and Environmental
DNV OS-F101	—	0.72/0.96	0.72	0.96
BS8010	—	1.0	0.96	0.96
ASME B31.4	—	—	0.72	
ASME B31.8	0.9	—	—	—
API RP 1111	0.9			

3.   Dynamic Analysis

The natural frequency is one of the most important parameters in the dynamic analysis, because it determines the response of the system to time-dependent excitation forces. For example, as shown in Figure 14.4, the response of free pipeline spans to vortex shedding is dictated by the closeness of the vortex shedding frequency to the natural frequency of the flowline system.

When the vortex shedding frequency, f_V, is very small in comparison to the natural frequency, f_n, the effect of vortex shedding is small and pipe deflections are not very different from those due to static action. However, as the frequency ratio, f_V/f_n, approaches unity, the amplitude of the resulting forced vibrations increases very rapidly, reaching a maximum, which is referred to as *resonance*. These very large deflections of pipeline caused by vortex induced vibrations may cause pipe failure due to yielding, buckling, concrete spilling, or combinations of these. In addition, fatigue damage may also occur due to stress change in the pipe. For these reasons, it is necessary to allow a safety margin between the vortex shedding and natural frequencies to avoid such effects.

Pipeline Natural Frequency

The difference between dynamic and static response is that, in the former, the submerged weight is replaced by an inertia force, which is given by the product of the effective mass, m_e, incorporating added mass effects, and the transverse acceleration of the beam element, $y_t(t)$ [4, 5]. For a pipe element, the dynamic equilibrium equation becomes
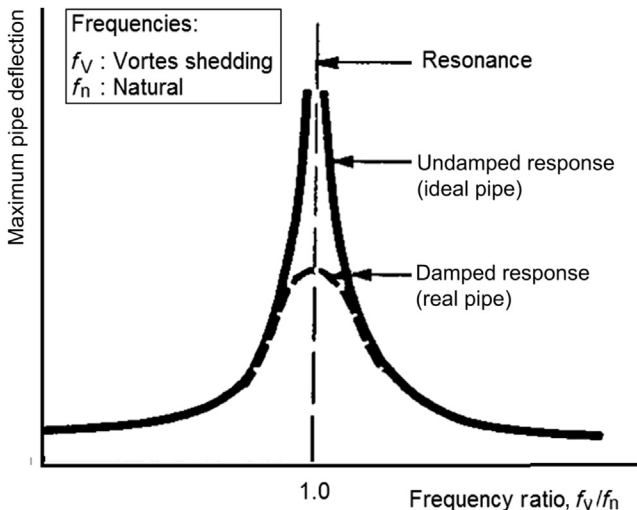
Figure 14.4 Relationship of natural frequency and vortex shedding frequency.

$$EI\frac{d^4y_t}{dx^4} - S_0\frac{d^2y_t}{dx^2} = m_e\ddot{y}_t \qquad [14.9]$$

which is similar to Eq. [14.1] but with the weight replaced by the inertia term. A dot (.) above y indicates derivatives with respect to t.

When a pipe vibrates transversely in one of its natural modes, its deflection, y_t, varies harmonically with time:

$$y_t = y[A\cos(\omega t) + B\sin(\omega t)] \qquad [14.10]$$

where ω is the angular velocity of the vibration. Substitution of Eq. [14.10] into Eq. [14.9],

$$EI\frac{d^4y}{dx^4} - S_0\frac{d^2y}{dx^2} = m_e\omega^2 y \qquad [14.11]$$

Solution of this equation yields a dynamic displacement function, y, and the angular velocity, ω, and thus the natural frequency, f, which is relative to the angular velocity ω, as

$$f = \frac{\omega}{2\pi} \qquad [14.12]$$

The natural frequency, f_n, can be expressed as

$$f_n = \frac{C_1}{L^2}\sqrt{\frac{EI}{m}\left(1 + \frac{S_0}{P_E}\right)} \qquad [14.13]$$

where

L = length of the span
EI = flexural rigidity of pipe
m = mass per unit length, including added mass to account for the surrounding water
C_1 = constant that depends on the end boundary condition, as shown in Table 14.2; 3.56 for fixed-fixed boundary condition
S_0 = effective axial force, positive for tension force
P_E = Euler buckling load, $= 4\pi^2 EI/L^2$ for fixed-fixed boundary condition

Table 14.2 Boundary Conditions Coefficients for Equation of Nature Frequency

Boundary Condition	C_1	C_2	C_3
Pinned-pinned	1.57	1.0	0.8
Fixed-fixed	3.56	0.25	0.2
Single span on seabed	3.56	0.25	0.4

DNV RP-F105 gives an empirical equation for natural frequency as

$$f_\mathrm{n} = C_1 \sqrt{1 + \mathrm{CSF}} \sqrt{\frac{EI}{m_\mathrm{e} L_\mathrm{eff}^4} \left[1 + C_2 \frac{S_0}{P_\mathrm{cr}} + C_3 \left(\frac{\delta}{D} \right)^2 \right]} \qquad [14.14]$$

where CSF is the concrete stiffness enhancement factor, defined as $\mathrm{CSF} = k_\mathrm{c}(EI_\mathrm{conc}/EI_\mathrm{steel})^{0.75}$; P_cr is the critical buckling load, $P_\mathrm{cr} = (1 + \mathrm{CSF})\,(C_2 \pi^2 EI / L_\mathrm{eff}^2)$; and δ is the static deflection. The boundary coefficient coefficients, C_1 to C_3, are defined in Table 14.2.

The correlation of natural frequency for pipelines, Eq. [14.13], is good for the first in-line VIV frequency; Eq. [14.14] is used for the first cross-flow nature frequency. The three terms in the square root of Eq. [14.14] include the contributions of cable, beam, and soil plus pipeline vertical deflection.

Instead of being calculated, the natural frequencies can also be measured by attached accelerometers and use an inertial pig. The most important parameters that affect the natural frequencies are

- Axial force.
- Soil conditions and degree of pipe embedment in soil.
- Seabed geometry.
- Static and dynamic nonlinear effects.
- Multiple spans, separation length.

Free-Span VIV Analysis Procedure

General

Traditionally, the VIV of free spans is not allowed to occur at any time during the design life of a pipeline system based on the onset criterion. In recent years, DNV-RP-F105 has allowed VIV to occur but requires that the fatigue damage due to VIV does not exceed an allowable value. The screening criterion of DNV-RP-F105 is similar to the onset criterion; however, the safety factors applied with the screening criterion allow for some vibrations under extreme environmental conditions.

The inline screening criterion [2] requires that the inline natural frequency, $f_\mathrm{n,IL}$, satisfy

$$\frac{f_\mathrm{n,IL}}{\gamma_\mathrm{IL}} > \frac{U_\mathrm{c,100year}}{V_\mathrm{R,onset}^{IL} \cdot D} \left(1 - \frac{L/D}{250} \right) \frac{1}{\alpha} \qquad [14.15]$$

where $U_\mathrm{c,100\ year}$ is the 100 year return period current flow at pipe level, $V_\mathrm{R,onset}$ is the onset value for inline VIV, D is the outer diameter of the pipe, L the span length, α is the ratio of 100 year return current flow over $U_\mathrm{w,1\ year} + U_\mathrm{c,100\ year}$, and γ_IL is the inline safety factor.

The cross-flow screening criterion requires that the cross-flow natural frequency, $f_{n,CF}$, must satisfy

$$\frac{f_{n,CF}}{\gamma_{CF}} > \frac{U_{c,100year} + U_{w,1year}}{V_{R,onset}^{CF} \cdot D} \qquad [14.16]$$

where $V_{R,onset}$ is the onset value for cross-flow VIV, and γ_{CF} is the cross-flow safety factor. If the preceding criterion for inline or cross flow is violated, then a full inline or cross-flow VIV fatigue analysis is required.

If a pipeline span is critical with respect to full inline or cross-flow VIVs, the span is usually corrected by rock dumping below the pipe to shorten the span lengths and thus increase the natural frequency of the spans. In addition to the cost implication of dumping a large number of rocks on the seabed, the main disadvantage of this approach is that the feed in of thermal expansion into the spans is restricted. It was demonstrated that allowing the pipeline to feed into the spans reduces the effective force, which is the prime factor to initiate pipeline global buckling. It is advantageous with respect to minimizing buckling that the number of rocks dumped for a supporting span is kept to a minimum. Therefore, the VIV criteria for full analysis are proposed as follows:

- Onset of inline VIV is allowed during any phase of the design life, if it is demonstrated that the allowable stress and fatigue damage are not exceeded.
- Onset of cross-flow VIV is allowed during any phase of the design life, provided it is demonstrated that the allowable stress and fatigue damage are not exceeded.

Figure 14.5 is a flowchart of the procedure for VIV assessment [3].

The design criteria for pipeline spans applicable to different environmental conditions are defined as follow:

1. Peak stresses or moment under extreme condition satisfy the dynamic strength criteria.
2. The fatigue damage should not exceed the allowable fatigue damage, η, that is normally 0.1 with a safety factor of 10.

Mørk et al. gave a series of papers on VIV and fatigue of free-spanning pipelines [6], [7], and [8].

Span Dynamics

Reduced Velocity

For determination of velocity ranges where VIV may occur, the reduced velocity parameter, V_R, is used, defined as

$$V_R = \frac{U_c + U_w}{f_n \cdot D} \qquad [14.17]$$

where

$\quad U_c$ = mean current velocity normal to the pipe
$\quad U_w$ = wave-induced flow velocity normal to the pipe
$\quad f_n$ = natural frequency of the span for a given vibration mode
$\quad D$ = total outside diameter of the pipe including any coating or marine growth
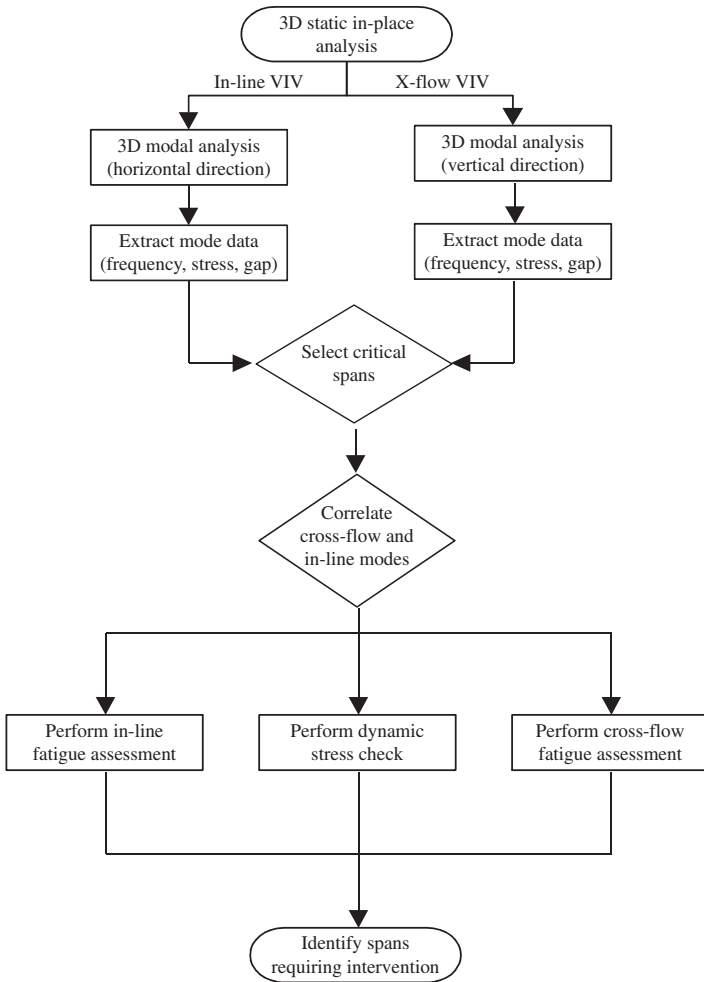
Figure 14.5 Flowchart of pipeline span assessment.

Stability Parameter

The other main parameter controlling the motions is the stability parameter, K_s, which is given as

$$K_s = \frac{4 \cdot \pi \cdot m_e \cdot \zeta_T}{\rho \cdot D^2}$$

[14.18]

where

m_e = mass per unit length (total pipe mass and added mass)
ρ = seawater density

ζ_T = total modal damping ratio at a given vibration

D = hydrodynamic diameter, that is, overall outside diameter

Damping

The total damping, ζ_T, is normally considered to comprise hydrodynamic damping, soil damping, and structural damping.

Hydrodynamic Damping

The hydrodynamic damping ratio accounts for the damping effect of the surrounding water. Hydrodynamic damping is proportional to the water velocity; that is, it reduces to zero as the water velocity tends towards zero. For VIV, the contribution to hydrodynamic damping within the lock-in region is set to zero, since damping is already included in the response model.

Soil Damping

The soil damping ratio is the contribution of the soil to the overall damping ratio of the pipe-soil system. The soil damping is an end effect of the span; therefore, increasing the span length reduces the overall effect to the total damping. The soil damping is larger for the inline direction than the cross-flow direction. For screening purposes, the soil damping of 0.01 may be assumed.

In the guidelines by Grytten and Reid, typical values of soil damping ratios for various types of soil and span length/pipe diameter (L/D) ratios are given. The damping values, as used in VIV analysis, can be interpolated for the correct span length. For continuous spans, taking the largest span length gives the most conservative value for soil damping [3]. It should be emphasized that the determination of pipeline-soil interaction effects is encumbered with relatively large uncertainties stemming from the basic soil parameters and physical models. It is therefore important that a sensitivity study be performed to investigate the effect of these mentioned uncertainties.

Structural Damping

The structural damping ratio is the damping due to internal friction in the pipe steel material. A value of 0.005 (0.5%) is to be used if no other information is available, which is considered to be very conservative. If concrete is present, the sliding at the interface between the concrete and corrosion coating may further increase the damping to 0.01–0.02. Flexible pipe has a high structural damping and is not easy to start VIV.

Effective Mass

The effective mass is defined as

$$m_e = m_{str} + m_c + m_a + m_{con} \qquad [14.19]$$

where

m_{str} = structural mass (including coating)

m_c = mass of content

m_a = added mass, which is a function of the gap between the seabed and the pipe. It may be calculated by

$$m_a = \frac{\pi}{4} D^2 \cdot \rho \cdot C_a \qquad\qquad [14.20]$$

where C_a is the added mass coefficient. Added mass is the increase in effective mass that occurs when the acceleration of the structure is nonzero. It is also called the *hydrodynamic mass*. The added mass is zero when there is no acceleration. The effective mass defined by Eq. [14.19] is based on an assumption that the entire span is oscillating and vortex shedding occurs over the entire length. This assumption contributes to a somewhat lower natural frequency and is considered to be conservative.

The Eigen period increases as the added mass increases. The Eigen period calculation is computed during the Eigen value analysis. Second, K_s, the stability parameter increases as the added mass increases. Thereby, the effect of the damping increases.

Vibration Amplitude and Stress Range Analysis

The results of structural and environmental analysis are used as inputs to the calculation of the response of the free span to the environmental loads. The response may be found through the application of static or quasi-static loads or may be given directly as vibration amplitudes.

Due to the complexity of the physical processes involved, that is, the highly nonlinear nature of the fluid-elastic interaction of the vibrating span, the response of the span generally is determined through the application of a model or full-scale investigation. Therefore, the fluid-elastic properties of the environment and the free span are described by a number of governing nondimensional parameters, which are used to retrieve the relevant response data (force coefficients and oscillation amplitudes).

The response data are subsequently used to calculate

- Stress range distribution.
- Expected number of oscillations.
- Fatigue damages parameter.
- Maximum stress.

Fatigue Damage

To calculate the relationship between stress cycles experienced in pipes and the resulting fatigue damages, and thus the consumption of fatigue life, the relationship of an empirical or semi-empirical nature may be applied. This typically means a determination of the number of cycles that lead to failure for the various dynamic stress ranges (e.g., S-N curves) and subsequently the determination of the

accumulation of partial damages (e.g., Palmer-Miners law). Refer to Chapter 12 for a more detailed description about fatigue damage of pipeline.

Accumulated Fatigue Damage

The fatigue damage is based on the accumulation law by Palmgren-Miner:

$$D_{fat} = \sum_{i=1}^{M_c} \frac{n_i}{N_i} \leq \eta \qquad [14.21]$$

where

D_{fat} = accumulated fatigue damage
η = allowable damage ratio, normally to be taken as 0.1
N_i = number of cycles to failure at stress range ΔS_i defined by the S-N curve
n_i = total number of equivalent stress cycles with stress range ΔS_i

When several potential vibration modes may become active simultaneously at given current velocity, the mode associated with the largest contribution to the fatigue damage should be applied. Otherwise, the multimode span analysis should be carried out.

S-N Curves

When the stress range ΔS (i.e., the double stress amplitude) has been established for a range of values of reduced velocity, V_R, the expected fatigue damage is calculated by means of S-N curves.

In the case in which the stress concentration factor is not applied, it is proposed that the F2 S-N curve for submerged structures in seawater be used in the detailed design; therefoore,

$\log a$ = constant, equal to 11.63
m = fatigue exponent, which is equal to 3

Response Amplitude

Inline VIV in Current-Dominated Conditions
This section applies to current-dominated situations only; that is, for $\alpha > 0.8$.

Onset of Inline Vibrations
The onset value for the reduced velocity in the first instability region is given by DNV. First instability region,

$$V_{R\_onset} \, \gamma_{on,IL} = \begin{cases} 1.0 & \text{for} \quad K_{s,d} \leq 0.4 \\ 0.6 + K_{s,d} & \text{for} \quad 0.4 \leq K_{s,d} \leq 1.6 \\ 2.2 & \text{for} \quad K_{s,d} \geq 1.6 \end{cases} \qquad [14.22]$$
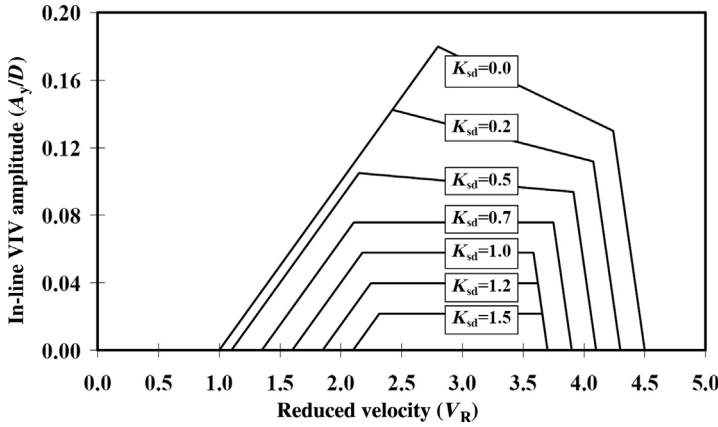
Figure 14.6 Amplitude response model for inline VIV.
Source: DNV-RP-F105 [2].

Where, $K_{s,d} = K_s/\gamma_k$, γ_k, and $\gamma_{on,IL}$ are the safety factors related to damping and onset value for inline reduced velocity, respectively. Second instability region,

$$V_{R\_end} = \begin{cases} 4.5 - 0.8K_{s,d} & \text{for} \quad K_{s,d} \leq 1.0 \\ 3.7 & \text{for} \quad K_{s,d} > 1.0 \end{cases} \tag{14.23}$$

Response
The characteristic maximum response amplitude is shown graphically in Figure 14.6.

Stress Range
The inline response of a pipeline span in current-dominated conditions is associated with either alternating or symmetric vortex shedding. Contributions from both the first inline instability region ($1.0 < V_R < 2.5$) and the second instability region ($2.5 < V_R < 4.5$) are included in this section. The stress range, S, may be approximately calculated by the inline VIV response model:

$$S = 2 \cdot S_{A=1m} \cdot (A_Y/D) \cdot D \tag{14.24}$$

where

$S_{A=1m}$ = unit stress amplitude (stress due to 1 meter inline mode shape deflection), which is to be estimated by a dedicated FE analysis package
(A_Y/D) = nondimensional inline VIV response amplitude

Cross-Flow VIV in Combined Wave and Current

This section applies to all cross-flow loads in all types of regions ($\alpha < 0.5$ and $0.5 < \alpha < 0.8$ wave dominant and $\alpha > 0.8$ current dominant).

Onset of Cross-Flow Lock-On

For steady current-dominated flow situations, onset of a cross-flow VIV of significant amplitude occurs typically at a value of reduced velocity, V_R, between 3.0 and 5.0, whereas maximum amplitude vibrations occur at a value between 5.0 and 7.0. For wave-dominated flow situations, cross-flow vibrations may be initiated for V_R as low as between 2 and 3 and are in this region apparently linked to the inline motions. For high values of V_R, the motions are again decoupled.

$$V_{\mathrm{R,onset}} = \sqrt{\frac{\pi^3 \left(\frac{\rho_s}{\rho} + C_m\right)}{1.5 + \left[0.27 - 0.03 \cdot \left(\frac{e}{D_{\mathrm{pipe}}}\right)\right]^2 \times \left[\pi^3 \left(\frac{\rho_s}{\rho} + C_m\right) - 1.5 K_S^2\right]}}$$

[14.25]

where (ρ_s/ρ) is the specific mass, to be taken as

$$\left(\frac{\rho_s}{\rho}\right) = \frac{m(s)}{\frac{\pi}{4} \cdot \rho_w \cdot D_{\mathrm{pipe}}}$$

[14.26]

The onset of cross-flow motion does not occur if the reduced velocity is below $V_{\mathrm{R,\ onset}}$.

Stress Range

If it is established that cross-flow VIV may occur, the span has to be checked for fatigue damage. An important parameter is the stress range, S, associated with the response amplitude. The stress range may be approximately estimated as

$$S = 2 \cdot S_{\mathrm{FE}} \cdot R \cdot f_Y (V_R, K_c, \alpha)$$

[14.27]

where

S_{FE} = stress amplitude (stress due to unit diameter mode shape deflection), which is to be estimated by a dedicated FE analysis package

R = amplitude reduction factor accounting for damping and gap ratio

The characteristic (maximum) amplitude response in combined current and wave flow may be taken from Figure 14.7.

Characteristic (maximum) amplitude responses with axes: y-axis "Cross-flow VIV amplitude (A_Z/D)" from 0.0 to 1.4, x-axis "Reduced velocity (V_R)" from 0 to 16. Curve annotations: $\alpha > 0.8$; $\alpha < 0.8$; $KC > 30$; $\alpha < 0.8$; $KC < 10$; $\left(\frac{f_{n+1,CF}}{f_{n,CF}}\right) > 2.3$, $\left(\frac{f_{n+1,CF}}{f_{n,CF}}\right) < 1.5$; $V_{R,onset}^{cr}$.
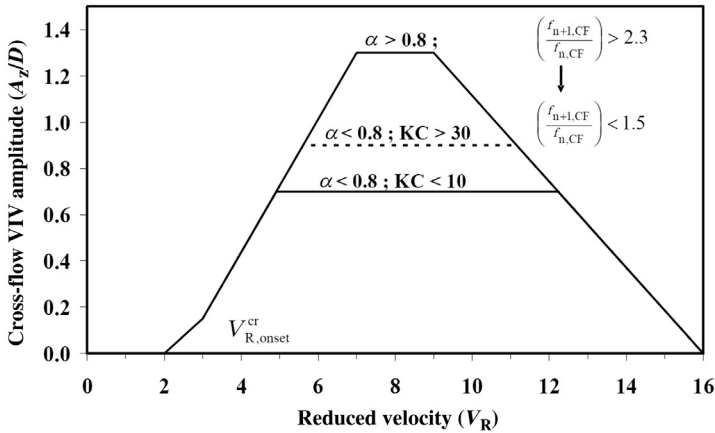
Figure 14.7 Characteristic (maximum) amplitude responses.
Source: DNV-RP-F105 [2].

Modal Analysis

General

To obtain natural frequencies, modal shapes, and associated normalized stress ranges for the possible modes of vibrations, a dedicated FEM analysis program should be used, and at a minimum, the following aspects have to be considered:

1. The flexural behavior of the pipeline is modeled considering both the bending stiffness and the geometrical stiffness.
2. The effective axial force that governs the bending behavior of the span is taken into account.
3. Interaction between the spanning pipe section and the pipe lying on the seabed adjacent to the span should be considered (multispan project).

Due consideration to items 1 and 2 is given in both the single-span and multispan modal analyses:

- In the FEM analyses, the change (increase) in the overall stiffness due to the deflected shape of the as-laid span is taken into account. This includes second order effects such as stress stiffening due to the sagging of the span.
- The axial effective force, that is, the sum of the external forces acting on the pipe, is also accounted for. It should be noted that the effective force changes considerably during the various phases of the design life.

To achieve this, it is important to ensure that a realistic load history be modeled prior to performing the modal analyses [9, 10, 11].

Single-Span Modal Analysis

Single-span analyses are performed to assess the onset of inline and cross-flow VIV as well as to calculate fatigue damage if it is found that onset of VIV may occur.

The modal analyses of a single span with simple boundary conditions are used to assess the onset of inline and cross-flow VIV and associated fatigue damage. The justification for this is as follows:

- The multispan analysis can be carried out on the assumption that the pipeline along the routing is an input to the FEM program and the actual span length is considered. The multispan analysis is used to take into account the interaction between adjacent spans; that is, several spans may respond as a system. Although this may be important for the vertical mode of vibration, where the seabed between adjacent spans may form a fixed point about which the pipeline may pivot during the vibration, this effect is less important for the horizontal mode, where the lateral seabed friction opposes the movement and there is no fixed point about which to pivot. The VIV analysis for the actual span lengths are considered in the in-place analysis.
- The single-span model is adequate for the VIV analysis based on the fact that actual span lengths are unknown, which is one condition to carry out the multispan analysis.

Both fixed-fixed and pinned-pinned boundary conditions have been analyzed, together with a range of axial effective forces.

Multiple-Span Modal Analysis

Two-dimensional multispan analyses are performed to assess the onset of cross-flow VIV as well as to calculate fatigue damage, if it is found that onset VIV may occur. The multispan analyses take account of the interaction between adjacent spans. The multispan analysis can be carried out on the assumption that the pipeline along the routing is an input to the FEM program, and the actual span length is considered. The VIV analysis for the actual span lengths is considered in the in-place analysis report.

The criteria used for cross-flow VIV are to keep the natural frequency of the spans above the VIV frequency corresponding to the onset of cross-flow vibrations. To ensure that the boundary conditions for each individual span are properly accounted for, the cross-flow vortex shedding is subject to a more rigorous modal analysis, in which the longitudinal on-bottom configuration is assessed as part of the 2D static analysis.

The spans' natural frequencies are checked against the corresponding frequency for onset of cross-flow VIV for the various design conditions (installation, water filled, and operation). Those with a potential for experiencing significant cross-flow VIV are identified and measures to prevent or limit fatigue of the pipe evaluated on a case-by-case basis.

4. VIV Mitigation and Span Correction

General

The intervention requirements for pipeline spans is normally decided based on the analysis of spanning pipeline configuration to determine stress levels and span lengths likely to occur when the pipe is laid on the seabed [12]. If the survey data indicate
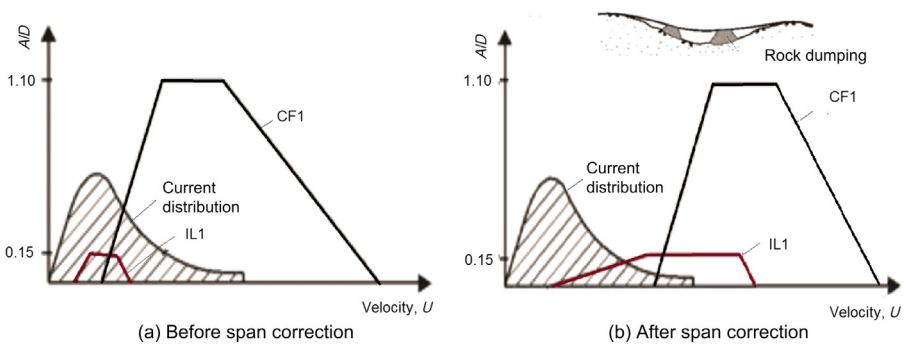
Figure 14.8 VIV response after span correction.

unacceptable spans during the design phase, various methods may be taken to address the problem. The obvious solutions are to reroute the pipeline wherever possible considering any given physical and economic constraints, reduce pipe laying tension, and increase pipe submerged weight. Other approaches are adding on devices for VIV suppression and span corrections by flexible pipe in areas of extreme irregularity, using jet bury barges to presweep areas of irregularity to smooth seabed along route in shallow water, allowing for the use of preinstalled supports, and increasing pipe grade or wall thickness [13].

If postlaying or inspection surveys discover unsupported spans on an existing pipeline, these spans must be evaluated. Spans discovered during such surveys may be compared to allowables calculated during the design. Alternately, they may be analyzed based on site-specific survey and environmental data to determine their acceptability.

Figure 14.8 illustrates VIV responses after the span length is shortened by rock dumping. For the same current distribution, the onsets of both cross-flow and inline VIV are delayed to a higher current velocity, in which the probabilities of higher velocities are lower. Therefore, after span correction, the fatigue damage due to VIV decreases or VIV does not occur.

VIV Mitigation

The suppression of VIV can be achieved with many different methods by modifying either the structure or the flow, as shown in Figure 14.9.

The most commonly used vortex suppression devices are helical strakes. Their function is to trigger separation to decrease the vortex shedding correlation along the pipeline. This method increases the cost of the pipeline and complicates handling during installation. The inline drag coefficient is also increased by introducing strakes. The important parameters for the strake design are the height and pitch of the helical strakes for a given pipeline diameter. The overall performance characteristics of a given strake design vary with the current velocity distributions.
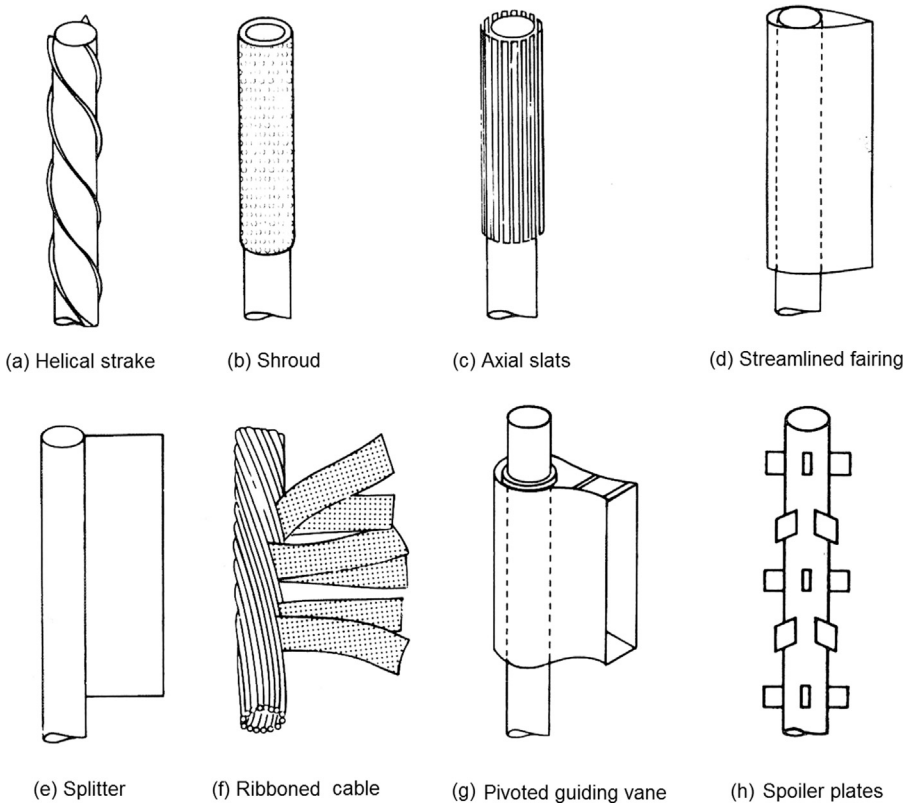
Figure 14.9 Add-on devices for suppression of VIV of cylinders.
Source: Blevins [14].

Span Correction

The following span corrections are used to rectify existing unacceptable spans: sand or grout bags, mechanical supports, jetting or trenching, backfill, and enhanced sedimentation.

Mattresses and Bags

Mattresses, sand or grout bags placed by divers under a span for support and to shorten the span, are a common means of span rectification in shallow waters. Accurate placement in deep water may be difficult and time consuming, and therefore not economical, even though grout bags can be installed using diverless installation.

For a span with a small clearance, sand or grout bags may be built up around and on top of the pipe. Grout bags can also be deployed close to other structures, even at a very small span gap. If scour or an unusually soft bottom is anticipated, a grouted fabric mattress may be installed first as a foundation for the support.

Normally, sand and grout bags are suitable for only postlaying intervention, but mattresses may be used for either pre- or postlaying intervention. However, placement of large numbers of mattresses or bags prior to pipe laying is not a practical method if a lot of spans require intervention along the pipeline route.

Trenching

Trenching seabed below the pipe can be used to change the pipeline profile so that curvature and the span length are reduced. Conventional offshore pipeline trenching methods include the use of ploughs, mechanical cutters, or jetting sleds, which are detailed in Chapter 22, Section 5. All of them can be deployed after the pipeline is laid. Trenching, using these methods, is the most effective way in cohesionless soils or soft clay, when the seabed is relatively soft. Generally, trenching is not a practical option when rock is present in the seabed of the pipeline roue. Many pipelines, especially small diameter lines, are trenched for stability and protection. Trenching is particularly useful in areas of sand waves and other mobile bed forms.

Rock Dumping

Rock dumping may be used for span intervention by modification of the seabed profile prior to pipe laying and by correction of excessive spans after pipe laying.

To fill in depressions in the seabed or to smooth out peaks, the rock dumped area should be equal to the width of the lay corridor, and this requires large volumes of rock. Prelaying rock dumping intervention may be essential and unavoidable in some instances. Specifying reduced lay tolerances in areas of spanning reduces the quantities but generally reduces the progress rate of the pipe laying operations. Postlaying intervention requires a smaller quantity of rock fill-in than prelaying intervention, as the span location is accurately known and rock dumping can be performed as required.

Mechanical Supports

Mechanical supports can be installed by diverless installation; therefore, they can be used in deep water. A two-legged support is lowered over a pipeline span and clamped to the pipeline with a clamping device at the top of the legs. The support is used to elevate the pipe and change the pipe profile so that the pipeline curvature is reduced. In the design of mechanical supports, minimum height, maximum pipe lift, maximum load carrying capacity, foundation size, maximum seabed slope, installation tolerances, and allowances should be considered.

5. Example Case

General

To give an insight into design against free span fatigue, a 40-inch pipeline is assessed under the operating condition as an example. For a complete analysis, the fatigue

Table 14.3 Pipeline Input Parameters

Input Parameters\Pipe Diameter	40 inch
Outer pipe diameter (m)	1.016
Wall thickness (m)	0.030
Corrosion coating thickness (m)	0.006
Corrosion coating density (kg/m^3)	1300
Concrete coating thickness (m)	0.05
Concrete coating density (kg/m^3)	2500
Residual lay tension (kN)	1350
Content density operating (kg/m^3)	180
Internal operating pressure (bar)	175
Operating Temperature (°C)	25
Internal hydrotest pressure (bar)	200

damage during the installation and the hydrotest conditions should be assessed and included in the overall damage accumulation.

Table 14.3 lists the characteristic dimensions of pipeline and flow parameters for the analysis [9].

A typical uneven seabed has been selected to obtain a wide range of span lengths giving high fatigue damage. The soil is medium stiff clay. The configuration and loads from the static analysis are used as the basis for the Eigen mode analysis. The modal analysis is carried out for the horizontal (inline) and the vertical (cross-flow) directions. Figures 14.10 and 14.11 show the mode analysis results for both inline and cross-flow line directions for the 40 inch pipeline. The inline Eigen mode values (natural frequencies) tend to be lower than the cross-flow values due to the stiffness of
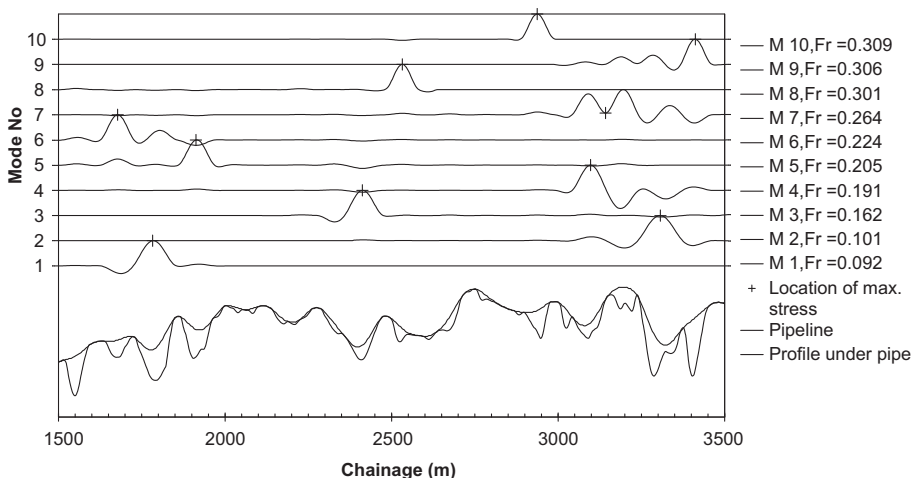
Figure 14.10 Inline modes for a 40-inch pipe.
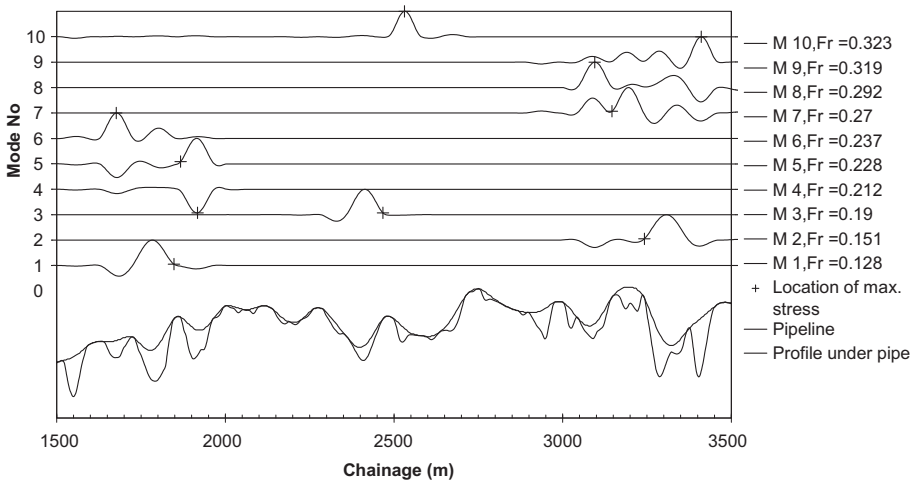
Figure 14.11 Cross-flow modes for a 40-inch pipe.

the span end conditions. To limit the amount of data processed for this exercise, the fatigue is assessed for the first 10 modes.

The modal analyses also generate unit stress amplitude results, that is, the stress of the pipeline for 1 meter of modal deflection for every mode. This is used to find the stresses along the pipe for VIV and wave-induced vibrations. The location of the maximum bending stress over the section is the point where the fatigue damage is evaluated. The maximum stress is normally located on the shoulder or at the mid-span of the dominating free span in each mode.

The cross-flow and the inline mode shapes need to be correlated to take account of the cross-flow induced inline fatigue. For the first three modes in the figures, the inline and the cross-flow modes are clearly linked. There are two clear cross-flow modes at the same location as the fourth inline mode. Both the seventh and the eighth cross flows show large excitations over the same span. The seventh mode is conservatively chosen because the natural frequency is lower. For the tenth inline frequency, the corresponding mode was found to be the twelfth cross-flow mode (not shown in the figures).

Fatigue Assessment

For the long-term environmental description, typical North Sea omni-directional wave and current distributions are applied:

- The joint-frequency spectrum (H_s and T_p) of three hourly sea states.
- Three parameter Weibull current distribution of the 10 minute average current measurement at 3 m above the seabed

The water depth is approximately 120 m so the longer period waves have an effect on the pipeline. The loads are initially considered acting at 90° to the pipe. This is a conservative assumption, which reduces the running time during the first stage of the

Table 14.4 Fatigue Assessment Results

Span Location (KP)	40-inch Pipeline	
	Inline	Cross Flow
1585	N/A	N/A
1718	0.55	0.55
1841	3380	16.7
1956	0.95	2.06
2436	1.61	2.71
2571	0.19	0
2704	N/A	N/A
2970	0.05	0
3136	0.69	0.02
3236	0.39	0.18
3319	943	3.71
3444	0.17	0.003

Note: Span damage given as N/A indicates that the span is not among the first 10 Eigen modes.

analysis. It is used for screening purposes to determine which spans are critical and therefore require a more detailed assessment.

Structural damping of 1% is taken for each of the pipelines. The fatigue resistance is determined from the two-slope F1 S-N curve in seawater with cathodic protection. The damage is found for an operational life of 50 years for all expected environmental conditions. Ten percent of the total fatigue damage is allowed during the temporary phases, that is, empty and water filled conditions, and a further10% for the installation. Table 14.4 shows the analysis results, in which the damage acceptance criterion for the operating condition is 0.48.
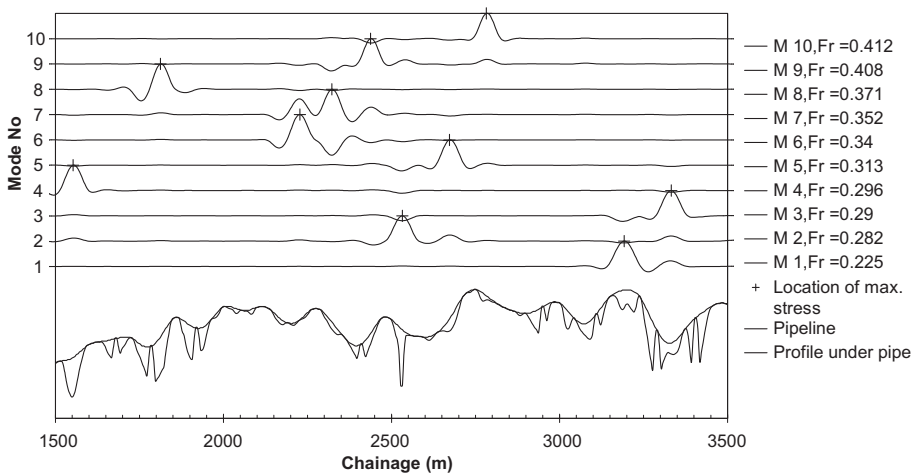
Figure 14.12 Inline mode shapes, 40-inch pipe with supports.
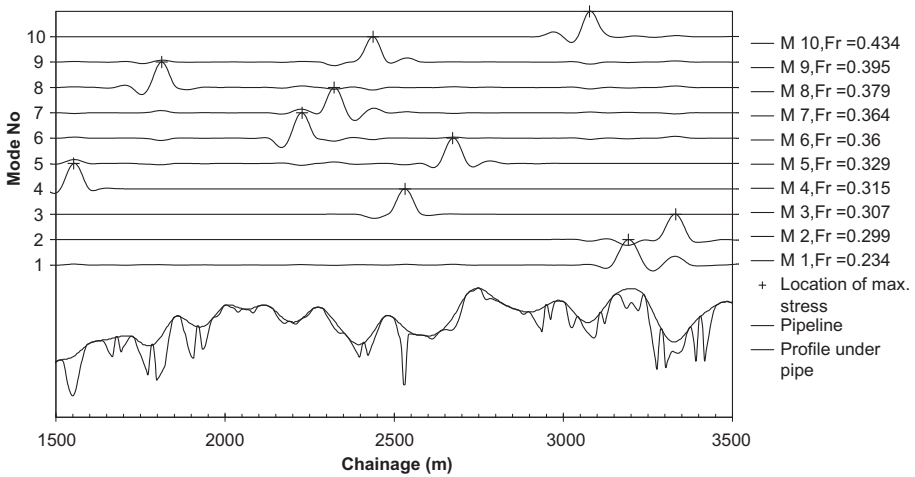
Figure 14.13 Cross-flow mode shapes, 40-inch pipe with supports.

As expected, due to the rough seabed, the pipes experience a high level of fatigue damage and intervention is required. There is unacceptable damage for both the cross-flow and the inline directions. The lowest modes show high force model damage, in particular at KP 1841 and KP 3319. Most of the spans have cross-flow damage and therefore also experience cross-flow induced inline damage.

Supports are placed at the mid-spans of all the unacceptable locations. Optimization of the support location is possible to reduce the rock volume by placing the supports nearer the span shoulders. Further static and modal analyses and a fatigue reassessment are carried out. Figures 14.12 and 14.13 shows the mode analysis results after the supports are added. The frequencies of first several modes in both inline and cross-flow directions increase to above 0.2 [Hz], therefore, the accumulated fatigue damage due to VIV is approved.

References

[1] Kenny JP. Structural analysis of pipeline spans. OTI 93 613. HSE Books, UK; 1993.
[2] DNV. Recommended practice of free spanning pipelines. DNV-RP-F105. Det Norske Veritas; 2006.
[3] Grytten TI, Reid A. VIVA guidelines, vol. 2. Theory. J P Kenny A/S, Norway. 1999.
[4] Kenny JP. Evaluation of vortex shedding frequency and dynamic span response. OTI 93 614. HSE Books, UK; 1993.
[5] HR Wallingford Ltd. Vibration of pipeline spans. OTI 92 555. HSE Books, UK; 1992.
[6] Mørk K, Vitali L, Verley R. Design guideline for free spanning pipelines. OMAE 97. Proceedings of the 16th International Conference on Offshore Mechanics and Arctic Engineering, Yokohama, Japan; 1997.

[7] Mørk L, Fyrileiv O. Fatigue design according to the DNV guideline for free spanning pipelines. OMAE 98. Proceedings of the 17th International Conference on Offshore Mechanics and Arctic Engineering, Lisbon, Portugal; 1998.

[8] Mørk K K, Verley R R, Bryndum M M, Bruschi R. Introduction to the DNV guideline for free spanning pipelines. OMAE 98. Proceedings of the 17th International Conference on Offshore Mechanics and Arctic Engineering, Lisbon, Portugal; 1998.

[9] Reid A, Grytten TI, Nystrøm PR. Case studies in pipeline free span fatigue. Proc. of ISOPE'2000. Seattle, USA; 2000.

[10] Fyrileiv O, Mørk K, Chezhian M, Sigurdsson G. Updated design procedure for free spanning pipelines DNV-RP-F105 Multi-mode Response. OMAE 2006–92098. Proceedings of the 25th International Conference on Offshore Mechanics and Arctic Engineering, Hamburg, Germany; 2006.

[11] Pereira A, Bomfimsilva C, Franco L, Tardelli L, Eigbe U. In-place free span assessment using finite element analysis. OMAE 2008–57272. Proceedings of the 27th International Conference on Offshore Mechanics and Arctic Engineering, Estoril, Portugal; 2008.

[12] Pontaza JP, Menon RG, Swanson RC, Jhingran V, Hill M, Kopp F, Hoffman J. Fluid-structure interaction simulations of a pipeline span exposed to sea bottom currents. OTC 21070. In: Offshore Technology Conference 2010, Houston, TX; 2010.

[13] Wang J, Banneyake R, Huang S, Jukes R, Eltaher A. The span mitigation analysis with use of advance FEA modeling techniques. OMAE 2011–50239. Proceedings of the 30th International Conference on Offshore Mechanics and Arctic Engineering, Rotterdam, The Netherlands; 2011.

[14] Blevins RD. Flow-induced vibrations. New York: Van Nostrand Reinhold Company; 1977.

15 Force Model and Wave Fatigue

Chapter Outline

1.   Introduction

Free-spanning subsea pipelines subject to oscillating environmental loads may fatigue at their welded joints. Remedial seabed intervention by trenching and rock dumping is intended to ensure that the span lengths are acceptable but often at a great cost. Therefore, the spans have to be carefully assessed with respect to fatigue due to vortex-induced vibrations and wave-induced oscillations.

A considerable amount of work has been performed to develop methods for assessment of vortex-induced vibrations [1,2]. However, there is a lack of comprehensive mathematical formulations specifically dealing with wave-induced fatigue. To clearly present the theoretical background, a few equations available from reference books are presented [3,4]. However, the rest of the chapter is devoted to a methodology to assess wave-induced fatigue that the authors think have not been given enough focus in the literature.

When calculating the fatigue damage due to transverse oscillations, it is first necessary to determine the stress amplitudes. This chapter describes the methodology used to calculate the stress amplitudes using a wave force model, based upon

the well-known Morison equation. Two approaches are developed to solve the equation of the motion of the free-spanning pipeline:

- Time domain solution for solving the nonlinear equation of motion numerically.
- Frequency domain solution for linearizing the Morison equation and solving it analytically.

2.   Fatigue Analysis

Fatigue of Free-Spanning Pipelines

Vortex-Induced Vibrations and Wave-Induced Oscillation

A complete fatigue assessment of a free-spanning pipeline should consider the loading due to both vortex-induced vibrations (VIV) and wave-induced oscillations.

While an amplitude response model may be applied when the vibrations of the free span are dominated by vortex-induced resonance phenomenon, a (Morison) force model is used to compute the free span response to waves through application of calibrated hydrodynamic loads.

Fatigue due to free-span oscillations is considered in two directions, as shown in Figure 15.1:

- Inline with the wave and current direction (horizontal plane).
- Cross-flow direction (vertical plane).

Combined Inline Fatigue

There are three sources of inline fatigue:

- Inline motion due to cyclic wave-induced oscillations, which may be simulated using a force model.
- Inline vibrations due to inline vortex-induced resonance, which may be simulated using an amplitude response model.
- Inline vibrations due to coupling from cross-flow vibrations.

Theoretically, it is necessary to add the fatigue damage due to all of these. The accumulated fatigue is obtained by accounting for all sea states and the joint probability of sea state combined with current. Since vortex shedding has been thoroughly discussed in DNV-RP-F105 [5], this chapter focuses on the wave-induced fatigue.

Current Conditions

The current velocity is statistically described by a Weibull distribution as

$$F_{U_{\text{ref}}}\left[U\left(z_{\text{ref}}\right)\right] = 1 - \exp\left[-\left(\frac{U_{\text{ref}} - \gamma_{\text{ref}}}{\alpha_{\text{ref}}}\right)^{\beta_{\text{ref}}}\right] \qquad [15.1]$$
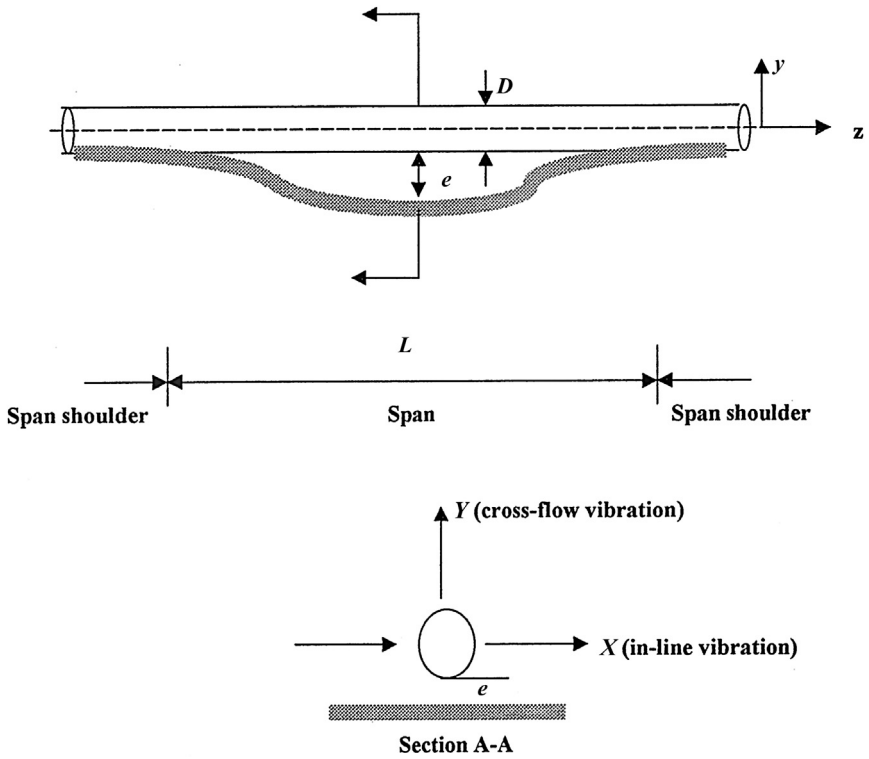
Figure 15.1 Free-spanning pipeline and its inline and cross-flow directions.

where γ_{ref}, β_{ref}, and α_{ref} are Weibull distribution parameters. The current velocity at a given depth $U(z_{\text{ref}})$ is transferred to current velocity at pipe level.

Long-Term Wave Statistics

Long-term statistics are applied in the fatigue damage assessment, whereby the wave climate is represented by a scatter diagram of the joint probability of the sea state vector, $\Theta = \lfloor H_s, T_p, \theta_w \rfloor$ and the wave spectrum, defined by significant wave height H_s, peak period T_p, and main wave direction θ_w.

Short-Term Wave Conditions

An irregular sea state is assumed to be a short-term stationary process represented by a wave spectrum:

$$S_{\eta\eta}(f,\overline{\theta}) = S_{\eta\eta}(f)W(\overline{\theta}) \qquad\qquad [15.2]$$

The directional properties are usually modeled as

$$
W(\overline{\theta}) = \left\{
\begin{array}{ll}
k_{\mathrm{w}} \cos^s(\overline{\theta}) & , |\overline{\theta}| < \dfrac{\pi}{2} \\[4mm]
0 & , |\overline{\theta}| > \dfrac{\pi}{2}
\end{array}
\right\}; \quad
k_{\mathrm{w}} = \dfrac{1}{\sqrt{\pi}} \dfrac{\Gamma\left(\frac{s}{2}+1\right)}{\Gamma\left(\frac{s}{2}+\frac{1}{2}\right)}
\tag{15.3}
$$

The nondirectional spectrum, $S_{\eta\eta}(f)$, adopted in this chapter is the JONSWAP spectrum. The velocity and acceleration spectra at pipe level are derived from the directional wave spectrum through a transformation, using Airy wave theory:

$$
S_{\mathrm{UU}}(f,\overline{\theta}) = G_{\mathrm{U}}^2(f) S_{\eta\eta}(\omega,\overline{\theta}), \ S_{\mathrm{AA}}(f,\overline{\theta}) = G_{\mathrm{A}}^2(f) S_{\eta\eta}(\omega,\overline{\theta})
\tag{15.4}
$$

where

$$
G_{\mathrm{U}}(f) = \frac{2\pi f \cosh[k(D+e)]}{\sinh(kh)}, \ G_{\mathrm{A}}(f) = \frac{(2\pi f)^2 \cosh[k(D+e)]}{\sinh(kh)}
$$

where

f = wave frequency in (1/sec), f = $\omega/2\pi$
k = wave number
D = outer pipe diameter
E = gap between seabed and pipe
H = water depth to pipe

Fatigue Damage Assessment Procedure

The following assumptions are made for the force model:

- The mass, axial force, stiffness, and structural damping are constant over time and along the pipe.
- The mean (main) wave direction is assumed to be perpendicular to the pipe, and all the energy is assumed to be concentrated around the main wave direction.
- The time domain fatigue model can include a statistically distributed current velocity or a fixed current velocity.
- The frequency domain fatigue model does not account for current.

Under these assumptions, the fatigue damage assessment procedure may be summarized as follows:

- **Characterization of sea environment:** The wave environment is represented by the frequency of occurrences of various sea states, defined by the sea state vector $\Theta = \lfloor H_{\mathrm{s}}, T_{\mathrm{p}}, \theta_{\mathrm{w}} \rfloor$ and the wave spectrum. The current is described by a Weibull distribution of current velocity.
- **Dynamic response analysis:** Waves of appropriate frequencies, heights, and directions are selected. The dynamic response and the loading of the pipeline are computed for each wave

condition. The dynamic response analysis that is usually referred to as the force model can be developed based on a time domain approach, hybrid time/frequency domain approach, and frequency domain approach. The results are expressed as the load or displacement transfer function per unit wave amplitude.

· **Structural analysis:** Structural analysis is conducted to determine the stress transfer function per unit load or per unit displacement at each hotspot in the pipeline.

· **Stress transfer function:** The load transfer function per unit wave amplitude as a function of wave frequency is multiplied by the stress transfer function per unit load to determine the stress transfer function per unit wave amplitude as a function of wave frequency.

· **Stress concentration factor (SCF):** The geometric SCF should be considered in the fatigue assessment. The SCF is determined by finite element analysis.

· **Hotspot stress transfer function:** The stress transfer function is multiplied by the stress concentration factor to determine the hotspot stress transfer function.

· **Long-term stress range:** Based on the wave spectrum, wave scatter diagram, and hotspot stress response per unit wave amplitude, the long-term stress range can be determined. This is done by multiplying the ordinate of the wave amplitude spectrum for each sea state by the ordinate squared of the hotspot stress transfer function to determine the stress spectrum. The stress range distribution is assumed to follow a Rayleigh distribution. The long-term stress range is then defined through a short-term Rayleigh distribution within each sea state for different wave directions. This summation can be further used to fit the Weibull distribution.

· **S-N classification:** For each critical location considered, S-N curves are assigned based on the structural geometry, applied loading, and welding quality.

Based on the long-term hotspot stress distribution and the S-N classification, the fatigue analysis and design of free-spanning pipeline may be conducted.

Fatigue Damage Acceptance Criteria

The design philosophy is that vibrations caused by vortex shedding and oscillations due to wave action are allowed, provided that the fatigue acceptance criteria are satisfied for the total number of stress cycles. The fatigue damage assessment is based on the Miner's rule:

$$D_{\text{fat}} = \sum \frac{n_i}{N_i} \leq \eta \qquad\qquad [15.5]$$

where D_{fat} is the accumulated lifetime fatigue damage, η is the allowable damage ratio, and N_i is the number of cycles to failure at stress S_i defined by the S-N curve on the form:

$$N_i = C^* S_i^{-m} \qquad\qquad [15.6]$$

m is a fatigue exponent and C is the characteristic fatigue strength constant. The number of cycles n_i corresponding to the stress range block S_i is given by

$$n_i = P(\cdot) f_v T_{\text{life}} \qquad\qquad [15.7]$$

$P(\cdot)$ is the probability of a combined wave- and current-induced flow event, f_v is the dominating vibration frequency of the considered pipe response. and T_{life} is the time of exposure to fatigue load effects.

Applying the partial safety factors, the preceding equations may be re-expressed as

$$D_{fat} = \frac{T_{life}}{C} \sum f_v \big[\gamma_S S(\gamma_f, \gamma_k, ...) \big]^m P(\cdot) \leq \eta \qquad [15.8]$$

where γ_f, γ_k, and γ_s denote partial safety factors for natural frequency, damping (stability parameter), and stress range, respectively. For the normal safety class, it suggests that $\gamma_f = \gamma_k = \gamma_s = 1.3$ and $\eta = 0.6$.

Time Domain Solution for Fatigue Damage

The fatigue damage may be evaluated independently for each sea state of the scatter diagram in terms of H_s, T_p, and θ_w as follows:

$$D_{fat} = \frac{T_{life}}{C} \sum_{H_s T_p \theta_w} P(\cdot) \int_0^\infty \max \big\{ f_v \big[\gamma_s S(\gamma_f, \gamma_k, ...) \big]^m \big\} dF_{Uc} \qquad [15.9]$$

where $P(\cdot)$ is the joint probability of occurrence for the given sea state in terms of significant wave height, H_s, wave peak period, T_p, mean wave direction. The term dF_{Uc} denotes the long-term distribution function for the current velocity. The notation *max* denotes that the mode associated with the largest contribution to the fatigue damage must be applied when several potential vibration modes may be active at a given current velocity.

In time domain analysis, the irregular wave-induced short-term particle velocity at pipe level is represented by regular waves for a range of wave frequencies.

The stress range is calculated in the time domain force model for each sea state with a constant value of wave-induced velocity amplitude but for a range of current velocities, from zero to a maximum value with nearly zero probability of occurrence. The calculated stress ranges are used when evaluating the integral in Eq. [15.9]. For each sea state, the fatigue damage associated with each current velocity is multiplied by the probability of occurrence of the current velocity. When stress ranges for all sea states are obtained through the force model, the fatigue damage is calculated using Eq. [15.9].

Frequency Domain Solution for Fatigue Damage

Fatigue Damage for One Sea State

For narrow banded response, the accumulated damage of a sea state may be expressed in the continuous form:

$$D_{fat} = \int_0^\infty \frac{n(S)}{N(S)} dS \qquad [15.10]$$

where $n(S)dS$ represents the number of stress ranges between S and $S + dS$. If a stationary response process of duration T_{life} is assumed, the total number of stress cycles are

$$N = v_0 T_{\text{life}} = \frac{T_{\text{life}}}{2\pi} \sqrt{\frac{m_2}{m_0}} \qquad [15.11]$$

in which, one can obtain

$$n(S)dS = Np(S)dS = v_0 T\, p(S)dS$$

where $p(S)$ is the probability density function for stress range S given by

$$p(S) = \frac{S}{4\sigma^2} \exp\left(-\frac{S^2}{8\sigma^2}\right)$$

Then, one can obtain

$$D_{\text{fat}} = v_0 T_{\text{life}} \int_0^\infty \frac{p(S)}{N(S)} ds = \frac{T_{\text{life}}}{2\pi} \sqrt{\frac{m_2}{m_0}} \cdot \frac{1}{m} \int \frac{S^{m+1}}{4\sigma^2} \exp\left(-\frac{S^2}{8\sigma^2}\right) ds$$

using the notation

$$t = \frac{S^2}{8\sigma^2}$$

and gamma function

$$\int_0^\infty e^{-t} t^{m/2} dt = \Gamma\left(1 + \frac{m}{2}\right)$$

We may get

$$D_{\text{fat}} = \frac{T_{\text{life}}}{2\pi} \sqrt{\frac{m_2}{m_0}} \cdot m_0^{m/2} \left(\frac{8^{m/2}}{C}\right) \cdot \Gamma\left(1 + \frac{m}{2}\right) \qquad [15.12]$$

Fatigue Damage for All Sea States

From the damage equation for one sea state, we may easily calculate the damage accumulated for all sea states. If the response process is a widebanded process,

Wirsching's rain flow correction factor is recommended to correct the conservatism due to any narrowbanded assumption [6]:

$$D_{\text{fat}} = \sum_{i}^{\text{all sea states}} \frac{T_{\text{life}}}{2\pi} \sqrt{\frac{m_{2i}}{m_{0i}}} \cdot m_{0i}^{m/2} \left(\frac{8^{m/2}}{C}\right) \cdot \Gamma\left(1 + \frac{m}{2}\right) \cdot \lambda(\varepsilon, m)\gamma_s^m \qquad [15.13]$$

where

$\lambda(\varepsilon, m)$ = rain flow correction factor;
$\lambda(\varepsilon, m) = a + (1 - a)(1 - \varepsilon)^b$
$a = 0.926$–$0.003\ m$
$b = 1.587$–$2.323\ m$
m_{0i} = spectral zero moment of the hotspot stress spectrum
m_{2i} = spectral second moment of the hotspot stress spectrum
ε = band width of the hot spot stress spectrum

Based on Eq. [15.13], the transformation of a stress range spectrum to fatigue damage is straightforward. Applying a spectral fatigue analysis, analytical expressions may be derived as the transfer functions from wave spectra to bottom velocity spectra, to response amplitude spectra, and finally to stress range spectrum.

3.   Force Model

The Equation of Inline Motion for a Single Span

The equation of inline motion for a Bernoulli-Euler beam subject to wave forces represented by the Morison force, damping forces, and the axial force is given by

$$M\frac{\partial^2 z}{\partial t^2} + C\frac{\partial z}{\partial t} + EI\frac{\partial^4 z}{\partial x^4} - T\frac{\partial^2 z}{\partial x^2} = \begin{array}{l} \frac{1}{2}\rho DC_{\text{D}}\left(U - \dfrac{\partial z}{\partial t}\right)\left|U - \dfrac{\partial z}{\partial t}\right| \\[2mm] + C_{\text{M}}\dfrac{\pi}{4}\rho D^2\dfrac{\partial U}{\partial t} \\[2mm] -(C_{\text{M}} - 1)\dfrac{\pi}{4}\rho D^2\dfrac{\partial^2 z}{\partial t^2} \end{array} \qquad [15.14]$$

where

z = inline displacement of the pipe, and it is a function of t and x
x = position along the pipe
t = time
M = mass of the pipe and the mass of fluid inside
C = damping parameter
EI = bending stiffness parameter, where E is the elasticity module and I is the inertia moment for bending

T = effective force (T is negative if compression)
U = time-dependent instantaneous flow velocity
ρ = water density
D = pipe diameter
C_D = drag coefficient
$C_M = (C_a + 1)$, inertia coefficient, and C_a is the added mass coefficient

The terms C_D and C_M are functions of the Keulegan-Carpenter (KC) number and the ratio between the current velocity and wave velocity α. The added mass coefficient is taken from Figure 9-1 of the DNV guideline [5], multiplied by a factor due to the gap between the span and the seabed.

The motion of the beam as a function of time and position along the beam is obtained by solving Eq. [15.14]) with appropriate boundary conditions.

Equation [15.14] is a nonlinear, partial differential equation that cannot be solved analytically. The dependency of the position along the pipe axis can be eliminated from the equation by applying modal analysis. Modal analysis is based on the assumption that the vibration mode shape of the beam is represented by a summation of beam Eigen modes, whereby increasing the number of modes improves the accuracy. Modal analysis reduces the nonlinear, partial differential equation to a set of nonlinear ordinary differential equations.

The nonlinear ordinary differential equations can be solved either numerically or linearized and then solved analytically. The first approach is called the *time domain solution* and the latter one the *frequency domain solution*.

The time domain approach demands more computing power than the frequency domain approach, but the latter approach, in some cases, gives erroneous results. In this context, it should also be mentioned that the Morison force representation is empirical and originally intended to be used on stationary vertical piles. Since the first presentation of the formula, it has been verified to cover other scenarios. The relative velocity model is used to describe the wave forces on a vibrating cylinder. The force coefficients are empirical and probably obtained from experiments with regular waves.

Modal Analysis

The modal analysis method reduces the partial differential equation to a set of ordinary differential equations. The key assumption is that the vibration mode of the beam can be described by a superposition of the Eigen modes. Eigen frequencies and modes are determined from the equation of motion describing free vibrations:

$$M\frac{\partial^2 z}{\partial t^2} + EI\frac{\partial^4 z}{\partial x^4} - T\frac{\partial^2 z}{\partial x^2} = 0$$

Solutions to this equation are expressed as

$$z(t, x) = \psi(x)\chi(t)$$

where

$$\chi(t) = \cos(\omega t + \varphi), \quad n = 1, 2, 3, \dots$$

and

$$\psi(x) = c_1 \cosh(s_1 x) + c_2 \sinh(s_1 x) + c_3 \cos(s_2 x) + c_4 \sin(s_2 x)$$

$$s_1 = \sqrt{\left(\frac{T^2}{4E^2I^2} + \frac{\rho A \omega^2}{EI}\right)^{\frac{1}{2}} + \frac{T}{2EI}}$$

$$s_2 = \sqrt{\left(\frac{T^2}{4E^2I^2} + \frac{\rho A \omega^2}{EI}\right)^{\frac{1}{2}} - \frac{T}{2EI}}$$

The boundary conditions (BCs) for a beam with end springs may be expressed as

BC 1, $EI \dfrac{d^2\psi(0)}{dx^2} = k_{r_1} \dfrac{d\psi(0)}{dx}$

BC 2, $EI \dfrac{d^2\psi(l)}{dx^2} = -k_{r_2} \dfrac{d\psi(l)}{dx}$

BC 3, $T \dfrac{d\psi(0)}{dx} - EI \dfrac{d^3\psi(0)}{dx^3} = k_{t_1} \psi(0)$

BC 4, $T \dfrac{d\psi(l)}{dx} - EI \dfrac{d^3\psi(l)}{dx^3} = -k_{t_2} \psi(l)$

where

k_{t1} = translational spring stiffness, left end of beam
k_{t2} = translational spring stiffness, right end of beam
k_{r1} = rotational spring stiffness, left end of beam
k_{r2} = rotational spring stiffness, right end of beam
l = length of pipe

Applying the boundary conditions in the general solutions, four linear equations are obtained, from which ω is solved as the frequency determinant. When ω is known, the four coefficients, except for an arbitrary factor, can be determined.

The frequency determinant may be derived as

$$
\det
\begin{vmatrix}
s_1^2 & -\dfrac{k_{r_1}}{EI}s_1 & -s_2^2 & -\dfrac{k_{r_1}}{EI}s_2 \\[2ex]
s_1^2\cosh(s_1 l) & s_1^2\sinh(s_1 l) & -s_2^2\cos(s_2 l) & -s_2^2\sin(s_2 l) \\[1ex]
+\dfrac{k_{r2}}{EI}s_1\sinh(s_1 l) & +\dfrac{k_{r2}}{EI}s_1\cosh(s_1 l) & -\dfrac{k_{r2}}{EI}s_2\sin(s_2 l) & +\dfrac{k_{r2}}{EI}s_2\cos(s_2 l) \\[2ex]
\dfrac{k_{t1}}{EI} & s_1^3+\dfrac{T}{EI}s_1 & \dfrac{k_E}{EI} & \dfrac{T}{EI}s_2-s_2^3 \\[2ex]
\left(s_1^3+\dfrac{T}{EI}s_1\right)\sinh(s_1 l) & \left(s_1^3+\dfrac{T}{EI}s_1\right)\cosh(s_1 l) & \left(s_2^3-\dfrac{T}{EI}s_2\right)\sin(s_2 l) & \left(\dfrac{T}{EI}s_2-s_2^3\right)\cos(s_2 l) \\[2ex]
-\dfrac{k_{t2}}{EI}\cosh(s_1 l) & -\dfrac{k_{t2}}{EI}\sinh(s_1 l) & -\dfrac{k_{t2}}{EI}\cos(s_2 l) & -\dfrac{k_{t2}}{EI}\sin(s_2 l)
\end{vmatrix}
= 0
$$

The solution to the original equation of motion, Eq. [15.14], is assumed to be a product between the time response function and the Eigen modes, as follows:

$$
z(x,t) = \sum_{n=1}^{m} Z_n(t)\psi_n(x) \tag{15.15}
$$

Time Domain Solution

The Generalized Equation of Motion

Inserting Eq. [15.13] into Eq. [15.14]) gives

$$
\sum_{n=1}^{m}\left(\psi_n(x)\left[(M+M_a)\frac{d^2(Z_n(t))}{dt^2}+C\frac{d(Z_n(t))}{dt}\right]\right)
$$

$$
+\sum_{n=1}^{m}\left(Z_n(t)\left[EI\frac{d^4(\psi_n(x))}{dx^4}-T\frac{d^2(\psi_n(x))}{dx^2}\right]\right)
$$

$$
=\frac{1}{2}\rho D C_D\left(U-\sum_{n=1}^{m}\left(\psi_n(x)\frac{dZ_n(t)}{dt}\right)\right)
$$

$$
\left|U-\sum_{n=1}^{m}\left(\psi_n(x)\frac{dZ_n(t)}{dt}\right)\right|+C_M\frac{\pi}{4}\rho D^2\frac{dU}{dt}
$$

where

$$
M_a = (C_m - 1)\frac{\pi}{4}\rho D^2
$$

Multiplying the equation through by $\psi_j(x)$ and integrating over the beam length gives

$$\int\limits_{x=0}^{l} \left\{ \sum_{n=1}^{m} \left(\psi_n(x) \left[(M + M_a) \frac{d^2(Z_n(t))}{dt^2} + C \frac{d(Z_n(t))}{dt} \right] \right) \right\} \psi_j^2(x) dx$$

$$+ \int\limits_{x=0}^{l} \sum_{n=1}^{m} \left(Z_n(t) \left[EI \frac{d^4(\psi_n(x))}{dx^4} - T \frac{d^2(\psi_n(x))}{dx^2} \right] \right) \psi_j(x) dx$$

$$= \int\limits_{x=0}^{l} \left\{ \frac{1}{2} \rho D C_D \left(U - \sum_{n=1}^{m} \left(\psi_n(x) \frac{dZ_n(t)}{dt} \right) \right) \right.$$

$$\left. \left| U - \sum_{n=1}^{m} \left(\psi_n(x) \frac{dZ_n(t)}{dt} \right) \right| \right\} \psi_j(x) dx + \int\limits_{x=0}^{l} \left\{ C_M \frac{\pi}{4} \rho D^2 \frac{dU}{dt} \right\} \psi_j(x) dx$$

Using the orthogonality properties results in

$$\left[(M + M_a) \frac{d^2(Z_n(t))}{dt^2} + C \frac{d(Z_n(t))}{dt} \right] \int\limits_{x=0}^{l} \psi_n^2(x) dx$$

$$+ Z_n(t) \int\limits_{x=0}^{l} \left[EI \frac{d^4(\psi_n(x))}{dx^4} - T \frac{d^2(\psi_n(x))}{dx^2} \right] \psi_n(x) dx$$

$$= (\text{for } n = 1, ..., m)$$

$$\int\limits_{x=0}^{l} \left\{ \frac{1}{2} \rho D C_D \left(U - \sum_{n=1}^{m} \left(\psi_n(x) \frac{dZ_n(t)}{dt} \right) \right) \left| U - \sum_{n=1}^{m} \left(\psi_n(x) \frac{dZ_n(t)}{dt} \right) \right| \right\}$$

$$\times \psi_n(x) dx + C_M \frac{\pi}{4} \rho D^2 \frac{dU}{dt} \int\limits_{x=0}^{l} \psi_n(x) dx$$

The generalized equation of motion is therefore given by

$$M_n \frac{d^2(Z_n(t))}{dt^2} + C_n \frac{d(Z_n(t))}{dt} + K_n Z_n(t) = F_n \qquad\qquad [15.16]$$

where

$$M_n = \int\limits_{x=0}^{l} (M + M_a)\psi_n^2(x)dx = (M + M_a) \int\limits_{x=0}^{l} \psi_n^2(x)dx$$

$$C_n = \int\limits_{x=0}^{l} 2\zeta_n\omega_n m\psi_n^2(x)dx = 2\zeta_n\omega_n m \int\limits_{x=0}^{l} \psi_n^2(x)dx$$

$$K_n = \int\limits_{x=0}^{l} \left[EI\frac{d^4(\psi_n(x))}{dx^4} - T\frac{d^2(\psi_n(x))}{dx^2}\right]\psi_n(x)dx$$

$$F_n = \int\limits_{x=0}^{l} \left\{\frac{1}{2}\rho DC_D\left(U - \sum_{n=1}^{m}\left(\psi_n(x)\frac{dZ_n(t)}{dt}\right)\right)\left|U - \sum_{n=1}^{m}\left(\psi_n(x)\frac{dZ_n(t)}{dt}\right)\right|\right\}$$

$$\times \psi_n(x)dx + \int\limits_{x=0}^{l} \left\{C_M\frac{\pi}{4}\rho D^2\frac{dU}{dt}\right\}\psi_n(x)dx$$

When Eq. [15.16] is solved, the motion of the beam as a function of time and position along the pipe is given by Eq. [15.15].

There are two ways of determining the response time history when using the time domain model. One is to solve Eq. [15.16] for a spectrum of representative regular waves; the other is to generate an irregular wave velocity time history from the wave spectrum and use this when solving Eq. [15.16].

Preparation for Numerical Solution

The time domain approach is to construct a time history of the irregular sea surface from a wave spectrum, $S_X(\omega)$. Given such a spectrum, the velocity and acceleration of water particles given by the linear wave theory are

$$U(t) = \sum_{i=-n}^{n} \overline{\omega}_i\sqrt{2S_{hh}(\overline{\omega})\Delta\overline{\omega}}\cos(\overline{\omega}_i t + \theta_i)$$

$$\dot{U}(t) = -\sum_{i=-n}^{n} \overline{\omega}_i^2\sqrt{2S_{hh}(\overline{\omega})\Delta\overline{\omega}}\sin(\overline{\omega}_i t + \theta_i)$$

where

$S_{hh}(\overline{\omega}) = \frac{1}{4} S_{\eta\eta}(\overline{\omega}) =$ the wave height spectrum
$\theta_i =$ the phase angle uniformly distributed from 0 to 2π

Given the preceding equations, a time series of velocity and acceleration can be constructed. The span motion can then be analyzed in the time domain to obtain a time history of the response.

Before Eq. [15.16] can be solved, it is necessary to recast it, because the numerical differential equation solver used handles only first order ordinary differential equations. By introducing a new variable, the equations become

$$\frac{dZ_n(t)}{dt} = \tilde{Z}_n \tag{15.17}$$

$$\frac{d^2 Z_n(t)}{dt^2} = \frac{d\tilde{Z}_n}{dt} \tag{15.18}$$

$$(M + M_a)\frac{d(\tilde{Z}_n(t))}{dt} \int_{x=0}^{l} \psi_n^2(x)dx$$

$$= \int_{x=0}^{l} \left\{ \frac{1}{2}\rho D C_D \left[U - \sum_{n=1}^{m} (\psi_n(x)\tilde{Z}_n(t)) \right] \left| U - \sum_{n=1}^{m} (\psi_n(x)\tilde{Z}_n(t)) \right| \right\} \psi_n(x)dx$$

$$+ C_M \frac{\pi}{4}\rho D^2 \frac{dU}{dt} \int_{x=0}^{l} \psi_n(x)dx - C\tilde{Z}_n(t) \int_{x=0}^{l} \psi_n^2(x)dx$$

$$- Z_n(t) \int_{x=0}^{l} \left[EI\frac{d^4(\psi_n(x))}{dx^4} - T\frac{d^2(\psi_n(x))}{dx^2} \right] \psi_n(x)dx$$

$$\tag{15.19}$$

Equations [15.17] and [15.19] are solved to obtain $Z_n(t)$. The pipe movement is then given by Eq. [15.15].

The spectrum of the pipe response is calculated from the response time history by a Fourier transformation. The advantage of the time history simulation is that non-linearities in the loading and response may be correctly taken into account. However, the calculation of the transfer function also involves a linearization process that is basically appropriate for only the sea state for which the simulation was done.

The accuracy of the solution increases when m increases. Unfortunately, the number of simultaneous equations that are to be solved increases by $2 \times m$. The value of m is therefore determined from test runs.

Stress Calculation

When the beam motion, as a function of time and position along the x-axis, is obtained, the stress range is given by

$$\Delta\sigma = E\frac{\partial^2 z(x,t)}{\partial x^2}D$$

If the beam has elementary supports (pin-pin, fix-fix, pin-fix), the maximum bending moment occurs at the beam middle or ends. If the beam is supported by springs, the maximum moment does not necessarily occur at these positions.

Frequency Domain Solution

The Generalized Equation of Motion

The frequency domain model presented here is based on a linearized version of the Morison equation. To linearize the nonlinear drag term, it is assumed that $U \gg \partial z/\partial t$; the following linearization is then proposed [7]:

$$\left(U - \frac{\partial z}{\partial t}\right)\left|U - \frac{\partial z}{\partial t}\right| \cong U|U| - 2|U|\frac{\partial z}{\partial t}$$

A value for the absolute velocity being used in a statistical sense is averaged over the entire sea state,

$$|U| = \sqrt{\frac{8}{\pi}}\,\sigma_U, \sigma_U = \text{RMS}[U(t)]$$

then

$$\left(U - \frac{\partial z}{\partial t}\right)\left|U - \frac{\partial z}{\partial t}\right| = K_L U - 2K_L\frac{\partial z}{\partial t}$$

The equation of motion can then be re-expressed as

$$(M + M_A)\frac{\partial^2 z}{\partial t^2} + (C + 2K_D K_L)\frac{\partial z}{\partial t} + EI\frac{\partial^4 z}{\partial x^4} - T\frac{\partial^2 z}{\partial x^2} = K_D K_L U + K_M\frac{\partial U}{\partial t}$$

where

$$K_D = \frac{1}{2}\rho D C_D$$

$$K_M = C_M\frac{\pi}{4}\rho D^2$$

$$M_A = -(C_M - 1)\frac{\pi}{4}\rho D^2\frac{\partial^2 z}{\partial t^2}$$

$$K_L = \sqrt{\frac{8}{\pi}}\,\sigma_U$$

The generalized equation of motion becomes

$$M_n\frac{d^2 Z_n(t)}{dt^2} + C_n\frac{dZ_n(t)}{dt} + K_n\,Z_n(t) = F_n(t) \qquad \text{for} \quad n = 1, ..., m$$

where

$$M_n = \int_0^l (M + M_a)\psi_n^2(x)dx = (M + M_a)\int_0^l \psi_n^2(x)dx$$

$$C_n = \int_0^l (C + 2K_D K_L)\psi_n^2(x)dx = (C + 2K_D K_L)\int_0^l \psi_n^2(x)dx$$

$$K_n = \int_{x=0}^l \left[EI\frac{d^4(\psi_n(x))}{dx^4} - T\frac{d^2(\psi_n(x))}{dx^2}\right]\psi_n(x)dx$$

$$F_n = \left(K_D K_L U + K_M\frac{\partial U}{\partial A}\right)\int_0^l \psi_n(x)dx$$

The Transfer Function between Wave Forces and Displacements

Using short-term wave conditions, the forcing function spectrum is given by

$$S_{FF}(f) = K_D^2 K_L^2 S_{UU}(f) + K_M^2 S_{AA}(f)$$

The spectrum for the nth generalized forcing function, $F_n(t)$, is

$$F_n(t) = \int_0^l \psi_n(x)F(t)dx = F(t)\int_0^l \psi_n(x)dx$$

$$S_{F_nF_n}(f) = \left[\int_0^l \psi_n(x)dx\right]^2 S_{FF}(f)$$

The Z_n-nth response spectrum is:

$$S_{Z_nZ_n}(f) = \left|M_{\text{transfer},n}(f)\right|^2 S_{F_nF_n}(f)$$

where $M_{\text{transfer},n}(f)$ is the transfer function between wave forces and displacement response, which is given by

$$\left|M_{\text{transfer},n}(f)\right|^2 = \frac{1}{K_n^2\left\{1 + (4\zeta_n^2 - 2)\left(\frac{f}{f_n}\right)^2 + \left(\frac{f}{f_n}\right)^4\right\}}$$

where

$$\zeta_n = \frac{C_n}{M_n}$$

The Hotspot Stress Spectrum

Between displacement and stress range is the following linear relation:

$$\Delta\sigma(x,t) = -ED\frac{\partial^2 z(x,t)}{\partial x^2} = -ED\sum_{n=1}^{m} Z_n(t)\frac{\partial^2 \psi_n(x)}{\partial x^2}$$

The stress spectrum for a specific point along the beam is therefore given by

$$S_{\sigma\sigma}(f,x) = E^2 D^2 \sum_{n=1}^{m}\left(\frac{\partial^2 \psi_n(x)}{\partial x^2}\right)^2 S_{Z_nZ_n}(f)$$

The hotspot stress spectrum is given by

$$S_{\text{hotspot}}(f,x) = (\text{SCF})^2 S_{\sigma\sigma}(f,x)$$

where SCF is the stress concentration factor.

The resulting hotspot stress response spectrum is numerically integrated to obtain the necessary moments m_n used for calculating the fatigue damage:

$$m_n = \int_0^\infty f^n S_{\text{hotspot}}(f,x)df \quad \text{for} \quad n = 0, 1, 2$$

The zero crossing rate and bandwidth are determined by

$$T_{z} = 2\pi \sqrt{\frac{m_0}{m_2}}, \quad \varepsilon = \sqrt{1 - \frac{m_2^2}{m_0 m_4}}$$

4.   Comparison of Frequency Domain and Time Domain Approaches

A computer program, Fatigue, has been developed. The time domain program consists of two parts:

- Part One solves the differential equation of motion.
- Part Two calculates the fatigue damage.

The Fatigue program has been compared with fatigue calculations by Fyrileiv [8].

Figure 15.2 shows the variation of accumulated fatigue damage with the span length based on the time domain and frequency domain approaches for a 42-inch pipeline in different water depths. It appears that the difference between the results from the time domain and frequency domain approaches is not small, and further investigation is required. The time domain approach is believed to be more accurate
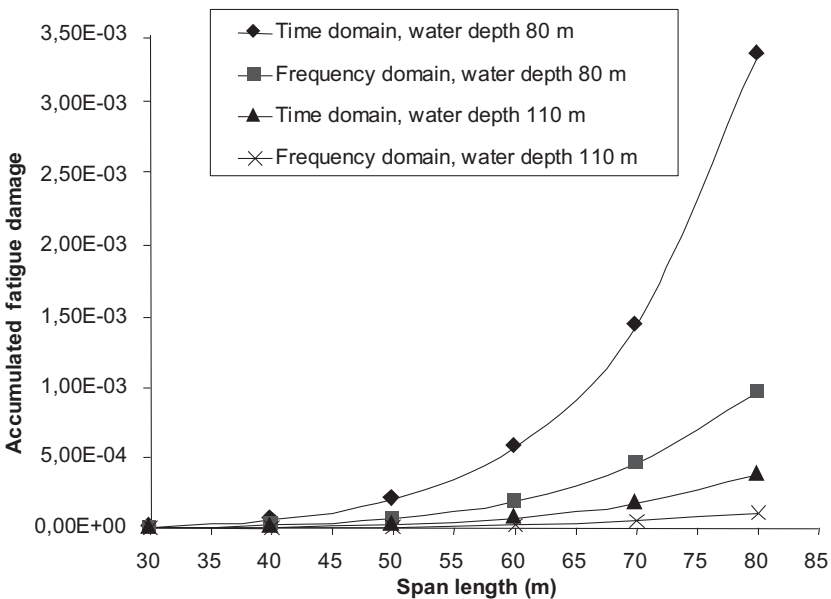
Figure 15.2 Accumulated fatigue damage versus span length based on time domain and frequency-domain approaches.

than the frequency domain approach, because it accounts for the influence of current and nonlinear velocity.

A parametric study on fatigue damage assessment was conducted by Xu et al. [9].

5.   Summary

A general free span may be described in terms of the natural frequencies, modes shapes, damping, and modal mass. Beams with spring boundary conditions are considered in this chapter. However, the developed formulation may be easily used to postprocess the modal analysis results from in-place finite element models of a pipeline that models the seabed and in-service conditions accurately. The Fatigue program may then be used to validate the more detailed models [11].

The chapter presented a methodology for analyzing wave-induced fatigue of free spanning pipelines. In this methodology, the following contents are included:

1. The analytical equations for the dynamic response analysis of free spans in a frequency domain are developed, neglecting current velocity.
2. The equation of motion is solved in the time domain for combined regular waves and current velocities with different probability of occurrence.
3. Fatigue damage is calculated by adding contributions from all sea states and currents using joint probability.
4. The numerical examples illustrate that there is a disturbing difference between the time domain fatigue analysis and frequency domain fatigue analysis. This is due to the nonlinear effects of the Morison equation and current velocity, which is a subject requiring further investigation.
5. The fatigue is calculated at 51 points along the pipe span. The computer program predicts fatigue damages reasonably close to those predicted by Fyrileiv [10].

References

[1] Tura F, Bryndum MB, Nielsen NJR. Guideline for free spanning piplines: Outstanding items and technological innovations. In: Proceedings of Conference on Advances in Subsea Pipeline Engineering and Technology. Scotland: Aberdeen; 1994.
[2] Mørk KJ, Vitali L, Verley R. The Multispan Project: Design guideline for free spanning pipelines. In: Proceedings of OMAE'97; 1997.
[3] Blevins RD. Flow-induced vibration. Melbourne, FL: Krieger Publishing Company; 1994.
[4] Sumer MB MB, Fredsøe J. Hydrodynamics around cylindrical structures. In: Advanced Series on Ocean Engineering, vol. 12. Singapore: World Scientific; 1997.
[5] DNV. Recommended practice of free spanning pipelines. DNV-RP-F105. Det Norske Veritas; 2006.
[6] Wirsching PH, Light MC. Fatigue under wide band random stresses. J. Struct. Div. ASCE 1980;106(7):1593–607.
[7] Verley R. Gudesp—Hydrodynamic force model, in-line. Memo; June 19, 1992.

[8]   Bai Y, Lauridsen B, Xu T, Damsleth PA. Force model and in-line fatigue of free-spanning pipelines in waves. Proc. of OMAE'98; 1998.
[9]   Xu T T, Lauridsen B B, Bai Y. Wave-induced fatigue of multi-span pipelines. J Marine Structures 1999;12:83–106.
[10] Fyrileiv O O, et al. Fatigue calculations using frequency domain approach. Fax; Janiary 30, 1998.
[11] Bai Y, Damsleth PA. Design through analysis applying limit-state concepts and reliability methods. Plenary paper for ISOPE'98; 1998.

16 Trawl Impact, Pullover, and Drop Objects

Chapter Outline

---

1. Introduction

The interaction between fishing gear and a pipeline is one of the most severe design cases for a subsea pipeline system, because the severity of the impact, pullover, and hooking is not well described by the industry today. The damages to the pipeline, the fishing gear, and ship depend greatly on the type of fishing gear and the pipeline conditions, such as the weight and velocity of the fishing gear and the wall thickness, coating, and flexibility of the pipeline. One of the most important issues in designing the pipelines to resist fishing gears is to make a realistic description of the applied loads, their time history, and the pipeline resistance. A summary of loads, response analysis, and acceptance criteria are listed in Table 16.1.

Table 16.1 Summary of Trawl Impact, Pullover, and Hooking

	Time	Load	Solution	Design Acceptance Criteria	Design Parameters
Impact	Seconds	Mass velocity	Mass-spring system dynamics	Dent damage in pipe < 0.035 OD	Energy absorption capacity of pipe coating
Pullover	Seconds	Time history of horizontal and vertical loads	Time domain dynamics	Allowable moment. Allowable stress-strain	Heights and length of free spans
Hooking	Minutes	Vertical displacement	Static solution	Allowable moment. Allowable stress-strain	Fishing gear frequency free spans

2. Trawl Gears

Basic Types of Trawl Gear

Bottom trawling is typically conducted with two types of trawl gear in the North Sea: otter and beam. Otter trawling occurs down to depths of more than 400 m. Generally, beam trawling occurs in water depths down to 100 m. The otter trawl board is a more or less rectangular steel board that holds the trawl bag open, while the beam trawl consists of a long beam that holds the trawl open. The beam has beam shoes on each end and an impact is assumed to be from these beam shoes.

Largest Trawl Gear in Present Use

Table 16.2 indicates presently applicable data for the largest trawl boards in use in the North Sea in 1995.

As for future developments or changes in equipment, these must be accounted for by investigating possible changes within the lifetime of the pipeline. Trends are toward improved design to optimize trawl board shape and, in this way, reduce the

Table 16.2 Data for Largest Trawl Boards in the North Sea

	Consumption		Industrial
	Polyvalent	V-Board	V-Board
Mass (kg)	3500	2300	1525
Length × breadth (m)	4.8 × 2.8	3.8 × 2.25	3.7 × 2.4
Trawl velocity (m/s)	2.8	2.8	1.8

power needed to drag the trawl, hence, minimizing fuel consumption and improving the economy. Although there may be fewer but larger trawlers in the future, this indicates that there will be a negligible increase in the mass of trawl board and the velocity of trawling.

3.   Acceptance Criteria

The acceptance criteria corresponding to accidental loads and environmental loads from NPD (1990) [1] is that no leak should occur. The acceptance criteria "no leak" is interpreted here.

Impact Response Analyses

When the trawl loads are considered accidental loads, a dent depth acceptance criterion is proposed, as follows. In the past, the dent depth was limited to 2% of the outer diameter (OD) according to ASME B31.8 [2]. This was a conservative assumption. A rational criterion on dent acceptability can be argued based on residual strength assessment. Up to 5% of OD can be allowed based on the following considerations:

- **Serviceability limit state:** The limit for allowing pigging operation is 5% OD.
- **Burst strength:** The pipe corrosion coating is not likely to be penetrated by the impact. It is then assumed that no cracks (gouges) affect the pipe's steel wall due to impact. Therefore, the burst strength of the pipeline is not reduced significantly, because the dent depth is 5% OD with no cracks in the dented area.
- **Fatigue strength:** The required fatigue life is that no fatigue failure should occur before the subsequent inspection in which the possible dent damage can be detected and repaired. Based on the information from an American Gas Association (AGA) study by Fowler [3], it can be documented that a dent depth of 5% OD might be acceptable from the point of view of fatigue due to cyclic internal pressure.
- **Buckling or collapse:** The collapse pressure is reduced by dents. The allowable strain is reduced from the viewpoint of strain-based design criteria.

Internal pressure can reduce the dent depth. However, the reduction of dent depth due to internal pressure is neglected.

Strictly, it is necessary to check the local stress and strain to ensure that no leak occurs during the impact process. Since pullover loads are much higher than impact loads, such leak check is to be done only for pullover loads.

Pullover Response Analyses

In the pullover response analyses, *no leak* means satisfaction of the strength requirements to local buckling and fracture or plastic deformation, as discussed in Chapter 4. Especially, girth weld fractureis a governing failure mode, because local buckling strain is considered to be large.

According to STATOIL [4], free spans are generally permitted in areas where trawling occurs, provided that the preceding criteria are satisfied.

4. Impact Response Analysis

General

The impact analysis is carried out to define the impact energy that must be absorbed by the coating and the testing requirements for the coating.

For concrete-coated pipelines, the impact energy is generally assumed protected by the coating and no further analysis is required by STATOIL.

Methodology for Impact Response Analysis

The analysis is carried out following the procedure recommended in the document STATOIL [4]. The finite element model used in this design guide is similar to that proposed by Bai and Pedersen [5].

The analysis is carried out because the traditional impact analysis, assuming the impact energy is totally absorbed by the steel and insulation coating as deformation energies, is too conservative. Kinetic energies absorbed by the trawl board and the pipe can be large. In fact, only a fraction of the kinetic energy of the trawl board is absorbed by the steel pipe locally.

A Level 2 analysis is shown in Figure 16.1. The notations used in this figure are defined as follows:

Trawl board:
- m_a and m are the added mass and steel mass of the trawl board.
- k_b and k_i are the trawl board out-of-plane and in-plane stiffness.

Coating and steel shell:
- k_{c1} represents the coating stiffness.
- k_{c2} denotes the possible effect that the coating has on the steel shell stiffness.
- k_s is the local shell stiffness of the steel pipeline.

Pipe and support:
- m_p is the effective mass of the pipe including hydrodynamic added mass.
- k_{pb} is the effective bending stiffness of the pipe.
- k_{ps} is the effective soil stiffness acting on the pipe.

The local indentation curve including both steel pipe and insulation coating can be obtained by finite element analyses using a static local shell model. The steel pipe
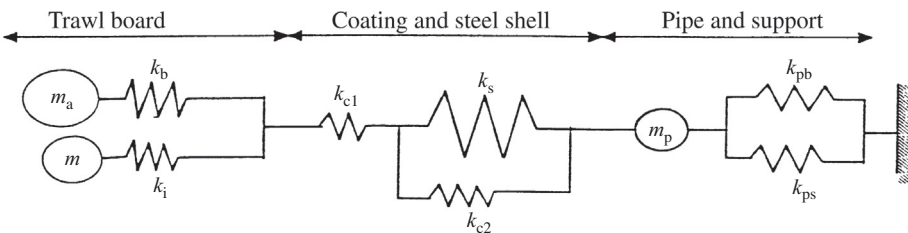
Figure 16.1 Physical model for impact between trawl board and pipeline.

should be modeled using geometrical and material nonlinear elements. Large deflections should be considered but small strain theory might be applied. The sophistication of the elements for insulation coating largely depend on the availability of the material properties from the insulation coating manufacturer.

The energy absorption process is simulated applying the dynamic global pipe model. Nonlinear beam elements with pipe sections can be used for the simulation of pipeline global behavior. The indentation curve for a steel pipe and insulation coating are modeled using nonlinear spring elements capable of accommodating compression forces only. The dynamic analysis is carried out assuming the steel and added masses of the trawl board with an initial velocity. The finite element modeling is similar to finite element description in Chapter 8. The difference is that the pipeline length to be considered can be much shorter for the impact response analyses. Figure 16.2 shows the principle and steps for the analysis of impact between trawl board and pipeline.

As a result of the dynamic global pipe model, a dent size is obtained as the description of the damage to the pipe steel. In addition, analysis results also include time histories of deformation in steel pipe and coating and the impact force between the trawl board and the pipeline.

For a balanced consideration of coating material costs and pipeline safety, the impact energy absorption capability of the coating should be determined based on impact response of pipelines to trawl board loads. An analytical method is developed to determine the initially assumed energy absorption capability of the coating. Detailed impact response analyses of the dynamic system are carried out using nonlinear finite element programs to confirm the assumed energy absorption capability.

Steel Pipe and Coating Stiffness

General

The local stiffness of the pipe is represented by the stiffness of

- Local shell stiffness of the steel pipe, k_s.
- Coating stiffness, k_{c1}.
- Possible effect that the coating has on the steel shell stiffness, k_{c2}. This is because the coating distributes the impact load to a wider area on the steel shell and might transfer certain forces tangentially.

The deformation energy to be absorbed by the steel pipe and the insulation coating are

$$E = E_S + E_{C1} + E_{C2} \qquad [16.1]$$

where

E_S = deformation energy absorbed by the steel pipe while coating is not used
E_{C1} = deformation energy absorbed by coating
E_{C2} = effect of the coating on the energy absorption

Step #1

Perform static analysis. Denting force includes the effect of trawl board geometry at the impact point and the possible coating.

Step #2

Establish the force-dent relationship from the local pipe shell model.

Trawl board stiffness and mass (both in-plane and out of plan/bending). Given initial impact velocity and direction.

Step #3

Perform dynamic analysis: Pipe shell performance included as nonlinear spring. Trawl board stiffness include as springs pipe global bending stiffness included by use of beam elements. Soil stiffness modeled with discrete ground springs (both vertical and lateral).

Step #4

Calculate the impact energy absorbed by the pipe shell, based on the maximum impacting force and the established force-dent relationship.

Figure 16.2 Scheme for impact between trawl board and pipeline.
Source: STATOIL [4].

Steel Pipe Stiffness, k_s

The indentation (δ-F) curve recommended by STATOIL [4] for steel pipe is

$$\delta = \left(\frac{1}{25\sigma_y^2 t^3}\right) F^2 \tag{16.2}$$

where

δ = deformation (indentation) of the steel pipe
F = impact force between trawl board and steel pipe
σ_y = yield stress of the steel pipe
t = wall thickness of the steel pipe

Coating Stiffness, k_{C1}

In general, two types of insulation coating are used in the industry: rubber and plastic. Both rubber and plastic coatings distribute the load to the steel underneath while they absorb part of the impact energy. It is recommended that finite element analysis or experimental tests are carried out to obtained load-indentation curves for insulation coating (k_{c1}) and the possible effect the coating has on the steel shell stiffness (k_{c2}). At an early design stage, no information is available with respect to k_{c1}, it is proposed to represent the coating indentation curve (k_{c1}) by empirical equations as follows. For Case 1,

$$\delta_C = \alpha F^2 \tag{16.3}$$

For Case 2,

$$\delta_C = \beta F \tag{16.4}$$

where α and β are empirical coefficients to be calculated by equating the energy calculated from the preceding empirical equation with the energy absorption capability of the coating, E_C, obtained from the coating tests conducted by the manufacturer:

$$E_C = \int_0^{t_c} F d\delta_C = \frac{2 t_c^{1.5}}{3\alpha^{0.5}} \tag{16.5}$$

and

$$E_C = \int_0^{t_c} F d\delta_C = \frac{t_c^2}{2\beta}$$ [16.6]

where:

　　t_c = coating thickness
　　δ_c = deformation in coating

Solving these energy equations, we may get

$$\alpha = \frac{4t_c^3}{9E_C^2}$$ [16.7]

and

$$\beta = \frac{t_c^2}{2E_C}$$ [16.8]

and the indentation curve (δ_c-F curve) for the insulation coating. For Case 1,

$$\delta_C = \left(\frac{4t_c^3}{9E_C^2}\right) F^2$$ [16.9]

and for Case 2,

$$\delta_C = \left(\frac{t_c^3}{2E_C}\right) F$$ [16.10]

Through finite element simulation, it is possible to know the indentation of coating, $\delta_{coating}$. In such cases, the energy actually absorbed by the coating is, for Case 1,

$$E_{Coating} = \int_0^{\delta_{coating}} F d\delta_C = \frac{2\delta_{coating}^{1.5}}{3\alpha^{0.5}}$$ [16.11]

and for Case 2,

$$E_{Coating} = \int_0^{\delta_{coating}} F d\delta_C = \frac{\delta_{coating}^2}{2\beta}$$ [16.12]

The safety factor in the design of coating energy absorption capacity may then be calculated as

$$\text{Safety factor} = \frac{E_\text{C}}{E_\text{Coating}} \qquad [16.13]$$

We may get, for Case 1,

$$\text{Safety factor} = \left(\frac{t_\text{c}}{\delta_\text{coating}}\right)^{1.5} \qquad [16.14]$$

and for Case 2,

$$\text{Safety factor} = \left(\frac{t_\text{c}}{\delta_\text{coating}}\right)^{2} \qquad [16.15]$$

Coating Effect on Steel Pipe Stiffness, k_{C2}

The coating effect on steel pipe stiffness, k_{C2}, may be established through finite element analysis. However, this requires material stress-strain curves for the coating from the manufacture. The coating effect on steel pipe stiffness is conservatively neglected.

Trawl Board Stiffness, Mass and Hydrodynamic Added Mass

General

Two masses are associated with the trawl board:

- Mass of the steel, m; assuming $m = 3500$ kg for steel mass.
- Hydrodynamic added mass, m_a; assuming $m_\text{a} = 2.14$ m for P-board [4].

Trawl Board In-Plane Stiffness Connected with Steel Mass

The mass of the steel, m, is connected to a spring that simulates the in-plane stiffness, k_i, of the board. It is suggested that [4]

$$k_i = 500 \ (\text{MN/m}) \qquad [16.16]$$

Trawl Board Out-of-Plane Stiffness Connected with Added Mass

The added mass, m_a, is connected to a spring that simulates the bending stiffness, k_b, of the board. It is suggested that [4]

$$k_b = 10 \ (\text{MN/m}) \qquad [16.17]$$

Pipe Stiffness, Mass, and Added Mass

The mass of the activated pipe, m_p, is a function of time. The length of the activated pipe increases during the impact.

The mass of the pipe consists of

- Mass of the content within the pipe.
- Mass of the steel pipe.
- Mass of the coating.
- Hydrodynamic added mass related to the pipe. The added mass is 2.29 times the mass of the displaced water for pipes resting on the bottom, 1.12 times the mass of the displaced water for pipes with 1*m* elevation.

Pipe added mass is calculated for every case using the following equation:

$$M_a = C_m \cdot \frac{\pi \cdot \text{OD}^2}{4} \cdot \rho_w \qquad\qquad [16.18]$$

where

$C_m = 2.29$ (added mass coefficient)
$M_a =$ added mass
$\text{OD} =$ pipe outside diameter, including all coatings
$\rho_w =$ water density

The bending stiffness of the pipe, k_{pb}, is also a function of time and decreases over the time. The pipe stiffness and mass are simulated using beam elements.

The soil is represented by a spring stiffness, k_{ps}, in the vertical direction and friction m in the horizontal direction. The soil stiffness is a function of time and decreases over time. It is be of concern only for impacts with a downward vertical component or when the soil forms a support to the pipeline in the opposite direction of the impact. No soil stiffness is assumed for pipeline free spans, if the pipeline is laid freely on seabed, not trenched or buried. No sticking effect is applied for pipe-soil interaction. In this study, a constant soil spring stiffness is assumed, due to the very small time period of the impact response.

Impact Response

General

The purpose of this section is to model a trawl board impact on a pipeline resting on the seabed. The main acceptance criteria on assessing pipe behavior under dynamic load are pipe shell dent, coating deflection, and forces and stresses in pipe body. The objective is to identify the minimum coating characteristics to provide

sufficient protection of the pipelines against impact load of trawl board/pipeline interaction.

Assumptions and Acceptance Criteria

The acceptance criteria for trawl board impact response under accidental loads are having no leak [4]. This implies that

- No direct contact between trawl board and steel pipe (no gouge occurs due to impact); the deformation of coating should be sufficiently less than the coating thickness.
- The dent depth of the steel pipe should be less than 5% of steel pipe diameter.
- The local equivalent stress in the pipe should be sufficiently small to avoid possible bursting; this failure mode is not considered to govern in the impact analysis.
- The maximum tensile strain should be sufficiently small to avoid possible fracture at girth weld; this failure mode is not considered to govern in the impact analysis.

Detailed modeling of local strain is also necessary, in case we evaluate possible fracture at girth welds during impact process. However, bursting due to overstress and fracture due to overstrain are more critical during the pullover process. These failure modes are therefore not considered in the impact response analysis and are evaluated in the pullover response analysis.

Finite Element Model

In finite element calculations, it is assumed that

- Coating density $r_c = 1200$ kg/m^3.
- Coating indentation curve is $\delta_c = \alpha F^2$.
- A 60 meter long pipe section is fixed at both ends. Pipe shell and coating are modeled by two nonlinear springs acting in the direction of the impact and placed one after the other. The springs provide no reaction force on tensile deformation and the springs are unloaded along a line parallel to the slope at the origin of the loading curve (plastic behavior). The trawl board is modeled by two structural masses: board steel and added mass. Both masses are connected in parallel by springs to the end of a coating spring. These two springs have the stiffness of the trawl board's in-plane and out-of-plane stiffness, respectively. The soil-pipe interaction is modeled in Chapter 6.

In fact, as a result of investigations into the effect of the soil model on dent depth, it can be concluded that, for different soil-pipe models, results are very close. This can be explained by the very short time of impact. At the moment of time when impact force reaches maximum, pipe displacements are very small, so soil reaction is negligible. In the initial condition, all springs and contact elements are not loaded. Both masses have velocities in a direction of 45° to the "soil" plane.

5. Pullover Loads

The maximum horizontal force applied to the pipe model, F_p, is given by [6]

$$F_p = C_F V (mk)^{1/2} \gamma \qquad [16.19]$$

where

    m = trawl board steel mass
    k = warp line stiffness
    d = water depth
    V = tow velocity
    γ = load factor = 1.3

The coefficient C_F is calculated as

$$C_F = 6.6 \left(1 - e^{-0.8\overline{H}} \right) \text{ for polyvalent and rectangular boards} \qquad [16.20]$$

$$C_F = 4.8 \left(1 - e^{-1.1\overline{H}} \right) \text{ for v-shaped boards} \qquad [16.21]$$

where

$$\overline{H} = \text{dimensionless height, } \overline{H} = \frac{H_{sp} + D/2 + 0.2}{B} \qquad [16.22]$$

    H_{sp} = span height
    D = pipe diameter
    B = half height of the trawl board

For trawl boards, maximum vertical force acting in the downward direction can be accounted for as

$$F_Z = F_p \left(0.2 + 0.8 e^{-2.5\overline{H}} \right) \text{ for polyvalent and rectangular boards} \qquad [16.23]$$

$$F_Z = 0.5 F_p \text{ for v-shaped boards} \qquad [16.24]$$

The total pullover time, T, is given by

$$T_p = C_T C_F (m/k)^{1/2} + \delta_p/V \qquad [16.25]$$
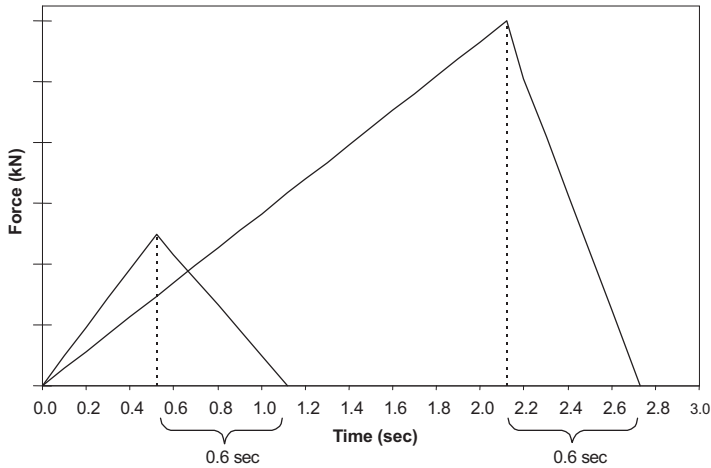
Figure 16.3 Pullover load versus time history.

where

$$\delta_p \approx 0.1 \left[C_T C_F (m/k)^{1/2} \right]$$ [16.26]

C_T = coefficient for the pullover duration; 2.0 for trawl boards

The fall time for the trawl boards may be taken as 0.6 s, unless the total pullover time is less than this, in which case the fall time should be equal to the total time. Figure 16.3 shows a typical time history of vertical forces and horizontal forces.

6. FE Model for Pullover Response Analyses

General

Pullover response analysis procedures are presented in this section. Pullover is the stage of the trawl gear interaction in which the trawl board is held behind the pipeline and, as the warp is tensioned by the movement of the vessel, the trawl gear is pulled over the pipeline.

In general, two base cases are considered:

- Pipeline in full contact with a flat seabed.
- Pipeline suspended in a free span on a real seabed.

In the first base case, an ideally flat seabed profile has been assumed. In the latter base case, a real seabed profile giving free spanning is imported from the most up-to-date pipeline route profiles and has been implemented to establish a span model. In the first base case, the seabed profile has been expanded to create a quasi 3D seabed surface, while in the second base case, a certain width of real seabed has been used to represent the 3D seabed.

The main objectives of these analyses are

- To establish whether a pipeline with continuous contact with the seabed can withstand a pullover load.
- To establish whether a pipeline in a free span can withstand a pullover load, whether it requires protection, or if a maximum allowable span length is required to ensure the structural integrity of the span in the event of a pullover load.
- To investigate the influence of different parameters such as vertical soil stiffness and, seabed friction through sensitivity analyses.

In the analyses presented here, the pipeline is subjected to the most severe pullover loads.

Finite Element Models

The purpose of the analyses presented in this section is to study the pullover response. Nonlinear transient least-plastic finite element analyses using the model described in Chapter 8 are performed to achieve this purpose.

The length of the model has been selected so that full axial anchoring is achieved at a distance away from the pullover point; that is, the effective force is unchanged after the time of impact.

Analysis Methodology

A real 3D seabed surface from on-site survey data, with real spans, which have been determined in in-place analyses, has been adopted for analyses of pullover on spans.

- The pullover load is modeled as a dynamic transient analysis.
- The pipeline has in general been assumed to be in its operating condition prior to pullover that is at its full design pressure and ambient temperature and with operating content. Additional sensitivity analyses on the influence of soil friction, prebuckled pipe, empty condition, different trawl board weight, low seabed stiffness, and a packing condition with different internal temperature has been undertaken for the flat seabed model.
- The pipeline material stress-strain relationship is based on Ramberg-Osgood parametric curves at the design temperature.
- The added mass of the pipeline has been taken into account by attaching point mass elements to the pipeline nodes. An added mass coefficient of 2.29 is assumed in the analysis.
- Due to symmetry, only half of a pipeline section is modeled for the flat seabed cases and thus only half of the total pullover load is applied to the symmetric plane.
- The large-deflection option and material nonlinear option in ANSYS are activated. This means that geometric nonlinearly and material nonlinearly are taken into account, that is, the change in overall structural stiffness due to geometrical changes of the structure as it responds to loading.

- A Coulomb friction model is assumed.
- No additional damping effect has been included in the analysis model.

The pullover load for the flat seabed cases is applied as a force versus time history at the model's second end node (symmetry plane). For the real seabed cases, the pullover forces are applied at the middle of the span investigated. Two force components are applied at the pullover point: one acting in the horizontal (lateral) plane and one acting vertical downward, which tends to punch the pipe into the seabed and thus increases the lateral restraint. The time history of the pullover loads applied to the model are presented in Figure 16.3.

The following main assumptions in the pullover analysis have been made:

- Dents and ovalization are not accounted for in the pipe elements; that is, the pipe cross-section is always circular during deformation.
- An equivalent pipe wall density is used to obtain the correct submerged weight, accounting for the effect of concrete, corrosion coating, and buoyancy.

As in industrial practice, upheaval buckling and lateral buckling have been considered as displacement-controlled situations, and strain-criteria are applied to check load effects. However, free-spanning pipeline and pullover response have been checked as load-controlled structures, and moment criteria are to be applied to check load effects.

For the detailed analysis method of the impact capacities of pipelines, umbilicals from drop objects and typical protection measures refer to DNV code [7].

7. Case Study

General

It has been common industrial practice in the North Sea to trench or cover all pipelines less than 16 inches to protect them from fishing gear interference. To trench a pipeline is costly and may lead to an additional requirement to cover it with backfill plus rock dumping to restrain it from buckling out of the trench.

A 3D nonlinear transient finite element model has been developed to investigate the structural response of pipelines subjected to pullover loads. A realistic 3D model of an uneven seabed is simulated by importing survey data directly into the model [8]. Throughout this case study, it will be shown how a 10-inch HPHT flowline was able to withstand the pullover loads when left exposed on an uneven seabed.

Trawl Pullover for Pipelines on Uneven Seabed

Pipelines installed in areas with an uneven seabed have a number of free spans along the pipeline route. Furthermore, a HPHT pipeline laid on an uneven seabed may have undergone global buckling prior to being exposed to trawl pullover loads. To assess the structural response of the line under these circumstances, it is necessary to apply the pullover loads on a 3D in-place model for a given load case. In the following examples, pullover simulations have been applied to a small diameter, HP/HT
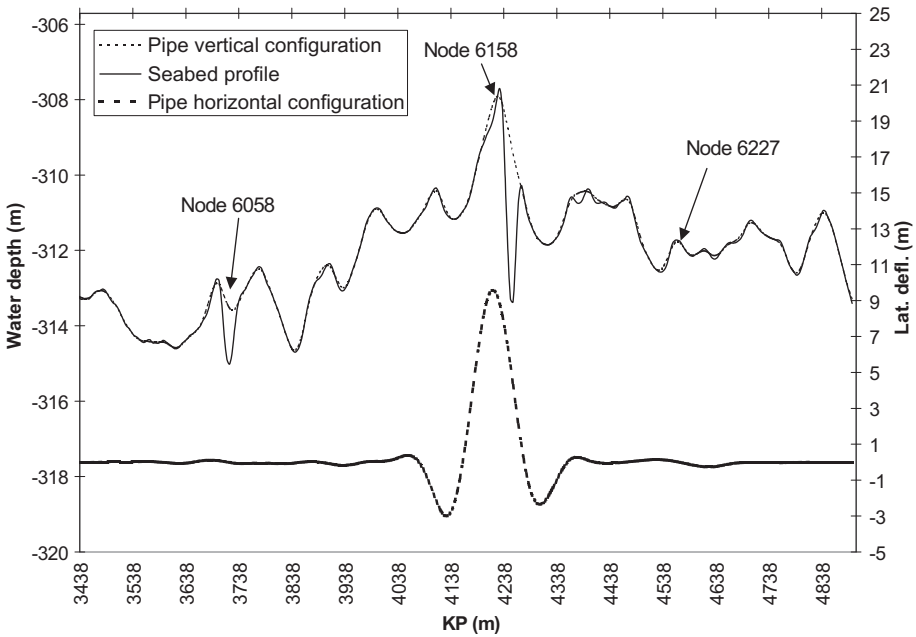
Figure 16.4 Uneven seabed: Flowline configuration prior to pullover.

flowline that has undergone global buckling prior to being exposed to the trawl load. Intermittent rock berms have been applied to control the thermal buckling behavior, and the model is therefore limited to the section of the flowline between two adjacent rock berms.

Figure 16.4 shows the vertical and horizontal configurations of the flowline in its as-laid condition under its maximum pressure (370 barg) and temperature (135°). A large horizontal buckle has formed across the large span at KP 4.25 and a further span has formed at KP 3.70. In this particular design case, the approach has been to use intermittent rock dumping as a means of controlling the buckling behavior. The extent of the model has therefore been limited to approximately 1500 m, that is, the distance between two rock berms. The effective axial compressive force prior to pullover has been reduced to about 5 tonnes (i.e., significantly less than for the flat seabed examples) due to the release of thermal and pressure strain into the lateral buckle. A friction factor of 0.3 has been applied.

Basic Case: Pullover on Section in Contact with Seabed

The pullover load is applied at a point where the pipeline is in full contact with the seabed. Figure 16.5 shows the resulting pipeline configuration as a function of time. It shows how a new "buckle" has appeared at the point of impact with a permanent amplitude of 2.4 m, which is close to the result for the flat seabed (2.8 m).
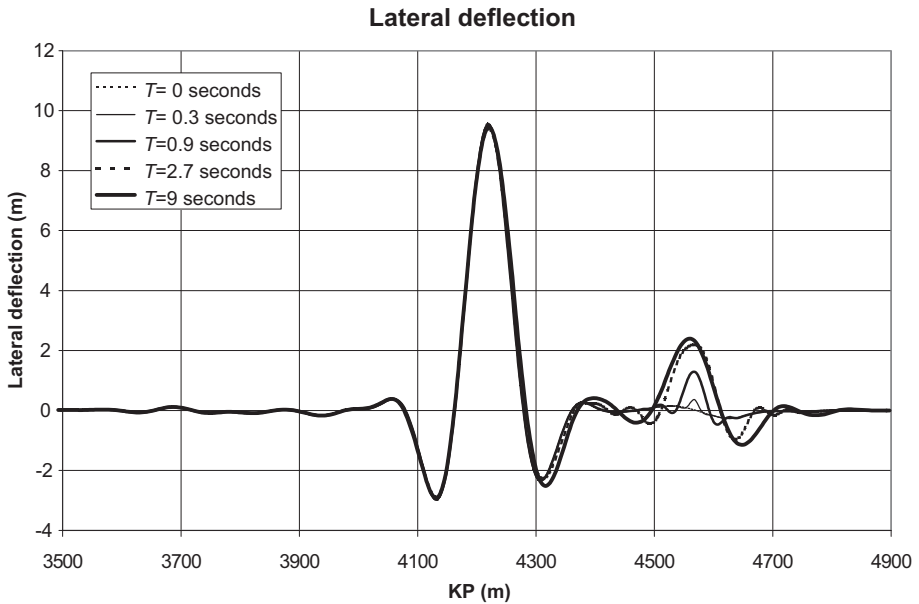
Figure 16.5 Lateral flowline configurations as function of time.

In the example with an uneven seabed, the effective compressive force was only 4 tonnes, which reduced to approximately 2 tonnes after the passage of the trawl board. In other words, global buckling, which is associated with a large release of axial force, does not take place. However, the pipeline is also here being "fed" into the "buckled" area, not because thermal strains are released, but because the axial "slack" in pipeline is being recovered. For an HPHT pipeline, this "slack" is due to existing spans in the adjacent area, as in this case, or in existing buckles adjacent to the point of impact. This is an important observation; When analyzing the flowline on a flat seabed, with the same axial effective force (4 tonnes), a considerably smaller lateral deflection occurred.

The resulting equivalent stress distribution after $t = 0$ second and $t = 0.3$ seconds are presented in Figure 16.6. Figure 16.6(a) shows the stress distribution in the flowline prior to trawl impact. The highest equivalent stress of 385 MPa occurred in the buckled section and approximately 315 MPa at the hit point. In Figure 16.6(b), there is a peak in the equivalent stress of about 395 MPa at the hit point after 0.9 seconds, which reduces to about 320 MPa after the passage of the board.

Span Acceptance Criteria for Pullover Loads for a 10-Inch Flowline

The effective axial force in the line varies from load case to load case. The 10-inch flowline is in effective compression during normal operation and pressure test and in tension in the temporary phases. The feed-in of expansion and resulting buckle
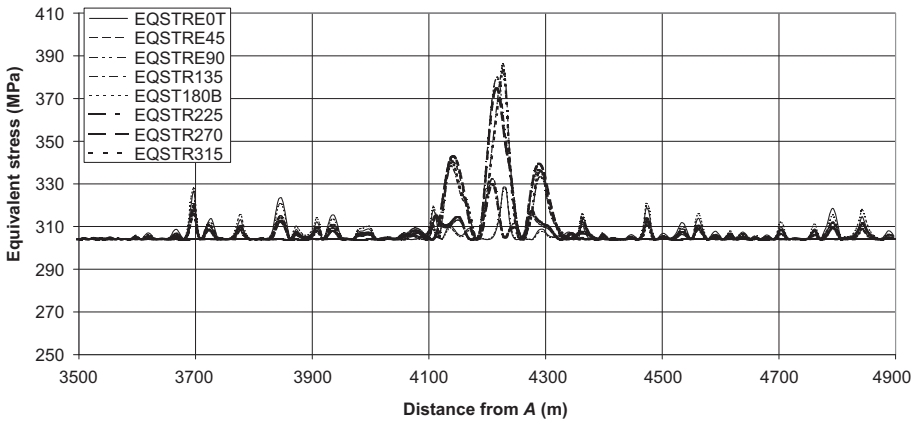
(a) Equivalent stress at $t = 0.0$ [s]
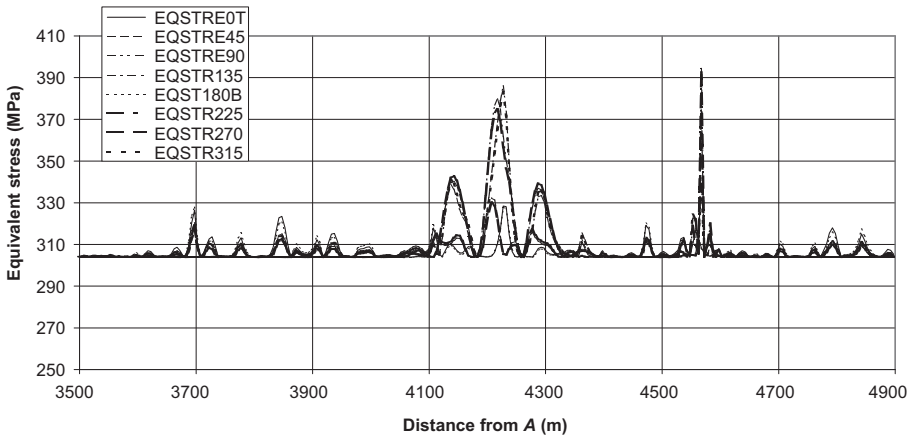
(b) Equivalent stress at $t = 0.3$ [s]

Figure 16.6 Equivalent stress distributions as a function of time.

amplitude during the trawl board pullover is larger when the pipe is in compression prior to being pulled over, which affects the stresses in the pipeline.

The location of the hit point relative to neighboring spans and buckles also affects the amount of feed-in into the buckled sections of the pipe during pullover and, in turn, the flexibility of the pipe. However, for the 10-inch flowline discussed here, it was demonstrated that span height is the governing parameter in structural response to trawl board pullover loads.

To establish the critical span height with respect to trawl board pullover, a series of finite element analyses were performed for the 10-inch flowline. The analyses considered trawl-board pullover loads applied to the flowline at various free spans along the route. The spans analyzed had different heights, ranging from 0.1 to 1.2 m.

Table 16.3 Critical Span Heights for Trawl
Pullover

	Critical Span Height (m)	
		Temporary
Operation	**Cool-down**	**Shutdown**
0.25	0.40	+ 1.00

The critical span heights based on equivalent stresses and axial strains criteria are listed in Table 16.3.

As long as the pullover load used as input to the analysis is a strong function of the gap height, other variables, such as span length and axial force in the 10-inch flowline prior to impact, do not significantly affect the response.

The pullover loads and durations, based on Eqs. [16.1] to [16.26] for a 10-inch flowline, are presented in Figure 16.7.

Among others, the following parameters influence the pullover loads:

• Flexibility, which is governed by pipeline diameter, wall-thickness, span length, and sup-
  porting condition.
• Geometrical effects, for instance, due to the relative position and motion between the trawl
  gear and the pipeline, front geometrical shape of trawl gear, and the location where wire
  rope is attached, as shown in Figure 16.8.
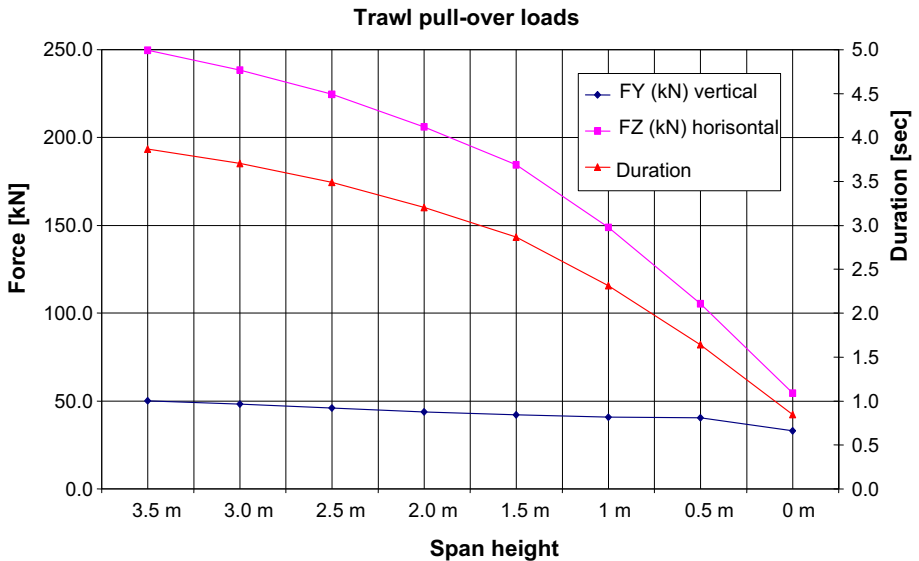
Figure 16.7 Pullover loads and duration for different span heights. (For color version of this figure, the reader is referred to the online version of this book.)
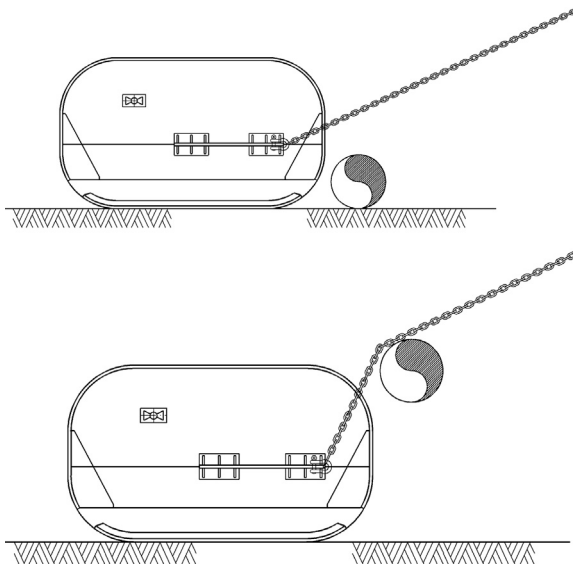
Figure 16.8 Geometrical effects on pullover loads for free-spanning pipeline.

References

[1] NPD. Guidelines to regulations relating to pipeline systems in the petroleum activities. Norwegian Petroleum Directorate, Stavanger; 1990.

[2] ASME B31.8. Code for gas transmission and distribution piping systems. New York: American Society of Mechanical Engineers; 1992. 1994 Addendum.

[3] Fowler JR. Criteria for dent acceptability of offshore pipelines. Project PR-201–914. Pipeline Research Committee of the American Gas Association, Virginia; July 1992.

[4] STATOIL. Design guidelines for trawl loads on pipelines. Document No. UoD/FLT-95051. STATOIL, Norway; 1996.

[5] Bai Y Y, Pedersen PT. Impact response of offshore steel structures. Int J Impact Engineering 1993;13(1):99–115.

[6] DNV. Guideline No.13. Interference between trawl gear and pipelines. Det Norske Veritas; September 1997.

[7] DNV. Risk assessment of pipeline protection. DNV-RP-F107. Det Norske Veritas; 2001.

[8] 1Tørnes K, 1Nystrøm P, Kristiansen NØ, 1Bai Y, Damsleth PA. Pipeline structural response to fishing gear pullover loads. Proceeding of 8th ISOPE 1998 Quebec, Canada; 1998.

17 Pipe-in-Pipe and Bundle Systems

Chapter Outline

1.   Introduction

A pipeline bundle integrates the required flowlines, water injection, gas lift, and control systems necessary for any subsea development and assembles them within a steel carrier pipe. A bundle can be open, with the individual pipes and cables strapped together, or closed, with all of them contained in an outer carrier pipe. Three typical bundle configurations are illustrated in Figure 17.1. Type A is a single wall pipeline with an external bundled line, Type B is a pipe in pipe (PIP), and Type C is a pipeline bundle. The PIP is one of the simplest pipeline bundles, and the main feature of PIP and pipeline bundle systems is that the pipeline comprises concentric inner and outer pipes. The inner pipe or pipes within sleeve pipes carry the production fluids and are insulated, while the outer pipe or carrier pipe provides mechanical protection.

The first known PIP system was installed in 1973 by Pertamina Offshore Indonesia. This pipeline was 8 miles long, extending from shore to a single point mooring facility. The outer and inner diameters of this pipeline were 40 and 36 inches, respectively. Up until 2000, 103 miles PIPs and bundles have been used in North Sea, which is about 1% of total pipeline population; 64 miles PIPs and bundles were used in Gulf of Mexico [1]. Nearly 50 pipeline bundles have been installed in the North Sea by a controlled-depth tow method (CDTM). The first one was installed at the
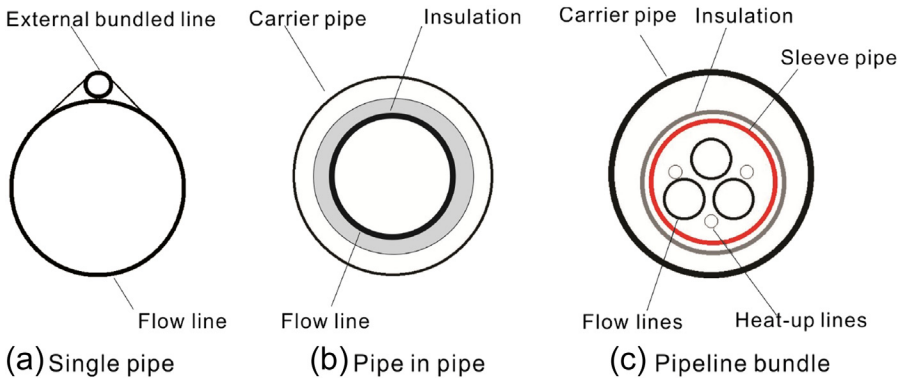
Figure 17.1 Bundle configurations. (For color version of this figure, the reader is referred to the online version of this book.)

Murchison field in 1980. The longest pipeline bundle is the one being designed, constructed, and installed in the Norwegian Sector by Rockwater. This bundle is 14 km long with a 46-inch carrier pipe and three production lines.

PIP and bundle systems may be considered for a particular pipeline application over a conventional or flexible pipeline due to the following several conditions [2]:

1. **Insulation-HPHT reservoir conditions:** HPHT pipelines require thermal insulation to prevent cooldown of the well stream fluid to avoid wax and hydrate deposition. Many thermal coatings are available that can be applied to conventional steel pipe, but they tend not to be particularly robust mechanically and have not been proven at the temperatures now being encountered in the HPHT field, typically 150°C and above. A similar problem exists for flexibility in this respect. An alternative is to place the pipeline(s) inside another larger pipe, often called a *carrier pipe*. The annulus between them can then be used to contain the insulating material, whether granular, foam, gel, or inert gas.
2. **Multiplicity of pipelines:** The bundle concept is a well-established one and a number of advantages can be achieved by grouping individual pipelines together to form a bundle. For specific projects the complete bundle may be transported to the site and installed with a considerable cost savings relative to other methods. The extra steel required for the carrier pipe and spacers can be justified by a combination of the following cost advantages:
   - A carrier pipe can contain more than one pipeline. Common applications have also contained control lines, hydraulic hoses, power cables, glycol lines, and the like.
   - Insulation of the bundle by the use of gel, foam, or inert gas is usually cheaper than individual pipeline insulation.
   - In most cases, no trenching or burial is required, due to the carrier pipe's large diameter. Since there are multiple lines within the carrier, seabed congestion within the field is also minimized.

Bundle installation is commonly carried out through use of the controlled-depth tow method. The main limitation to the CDTM is the permissible length of bundle that can be installed, currently around 7.7 km. This is due to a combination of construction site and onshore launch area size.

3. **Trenching and rock dumping:** Traditionally, pipelines less than 16 inches in diameter are trenched or buried. When contained within a sleeve pipe, which could be anything from 18 to 24 inches in diameter for single PIP systems and much larger for bundles, a reasoned argument for nontrenching can be made, demonstrating that the line will not pose a risk to human life or the environment nor will it become a hazard to other users of the sea. The cost associated with needing to trench, backfill, and rock dump is often greater than that of the installation cost of the pipeline. By not trenching, buckling of the pipeline occurs only in the lateral direction across the seabed, and there are methods to control such an event, for example, laying in a "snaking" configuration or setting buckle mitigation methods (refer to Chapter 10, "Lateral Buckling and Pipeline Walking"). Upheaval buckling through the seabed, which is the more severe situation, can be controlled only through sufficient overburden placed on the line in the form of rock dumping. These issues have been addressed in Chapter 11, "Upheaval Buckling."

In terms of impact from trawl boards or fishing gear, the external pipe acts as the first line of defense, and although it may be breached, the integrity of the pipeline is not compromised. For certain applications, PIP and bundle systems offer significant cost savings over conventional pipelines, particularly when the need to trench, backfill, and rock dump can be eliminated with additional mechanical and structural benefits as well.

Pipelines in PIP configurations were constructed in the Gulf of Mexico primarily to achieve high thermal insulation for flow assurance purposes. Keeping the internal fluid warm helps prevent formation of hydrate plugs and reduces paraffin deposition, which can constrain the production flow. Figure 17.2 shows the applicability of the bundle systems, in which the towed bundles are constructed in water depth below 500 m, while PIP can be used for water depths up to 2000 m, and the U-value of the PIP pipeline is applicable to most required U values.
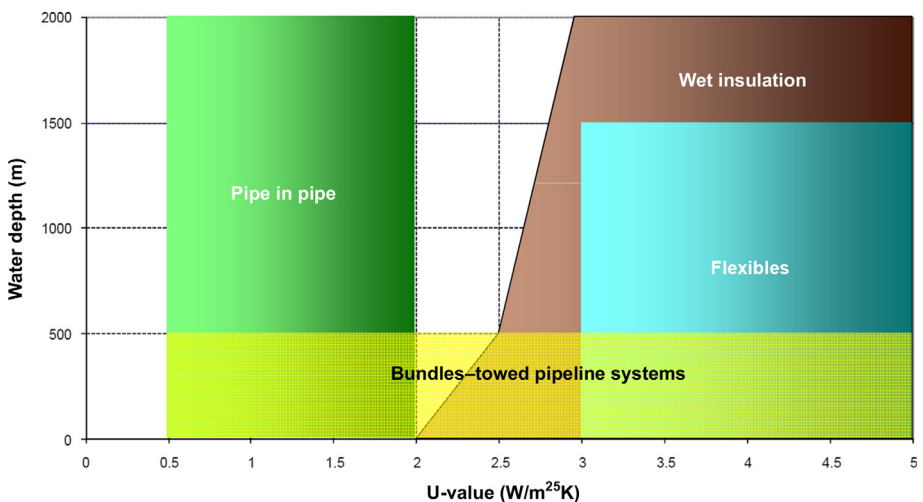
Figure 17.2 PIP and Bundle system applicability.
Source: Watson and Walker [3]. (For color version of this figure, the reader is referred to the online version of this book.)

This Chapter presents the design procedure and strength acceptance criteria for the PIP and bundle systems. The design should ensure that adequate structural integrity is maintained against all possible failure modes. All relevant failure modes for pipelines described in Chapter 4 are to be considered in the design of PIP and bundle systems.

2.   PIP Systems

General

Many of the high pressure/high temperature (HP/HT) reservoirs in the North Sea are being exploited using pipe bundles and PIP configurations as part of subsea tie-backs to existing platforms. Not only are reservoir conditions harsher but also there is a need to insulate the pipelines to prevent wax and hydrate formation as the product cools along the pipeline. However, the PIP systems have some additional design features that are not present in conventional pipeline design. Challenging engineering problems range from structural design of spacers and internal bulkheads to the understanding of the structural behavior both globally and locally under a variety of loads. Due to the increased number of components in PIP systems compared with conventional pipelines, the design process is therefore more iterative in nature as the interactions of the components may necessitate design alteration.

PIP Configuration

For the exploitation of HPHT reservoirs, PIP systems can provide the necessary thermal insulation and integrity for transporting hydrocarbon at high temperature and high pressure. The PIP system comprises a rigid steel inner pipe (flowline) inside a rigid outer pipe (carrier pipe). The two pipes are kept apart by spacers (centralizers) at the ends of each joint and by bulkheads at the ends of the pipeline. The various proprietary systems on the market differ in the details of the spacers and bulkhead arrangements.

Figure 17.3 presents a typical PIP configuration. The air gap between the inner and outer pipes provides the means of achieving the high thermal insulation. This air gap accommodates the insulation, which typically consists of either granular material poured into the inter-pipe annulus or a blanket form, which is wrapped around the inner pipe. In either case, the insulation material needs to be kept dry to maintain its insulation properties.

Various PIP configurations have been used in subsea fields. The following should be considered when determining the PIP configuration:

- Gap thickness between the internal and external pipes, which should be optimized to prevent the heat loss.
- Thermal stability.
- Overall feasibility.
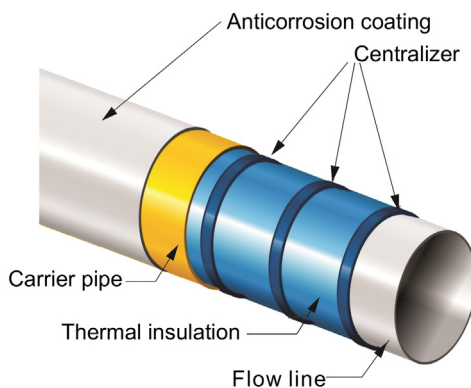
Figure 17.3 Typical PIP configuration. (For color version of this figure, the reader is referred to the online version of this book.)

A typical PIP system mainly includes the following components:

- Flowline (inner pipe).
- Carrier pipe (outer pipe).
- Insulation layer.
- Centralizers (spacers).
- Bulkheads.
- Water stops.
- Buckle arrestor.

The basic functions of each component are discussed next.

Flowline

The function of the inner pipe is to convey production fluids and therefore is designed for internal pressure containment. The bore diameter of the flowline is normally determined by the pipeline operator according to their desired fluid rates and flow assurance requirements. The wall thickness of the flowline is calculated following standard single pipeline design procedures.

Carrier Pipe

The carrier pipe protects the insulation material from external hydrostatic pressure and other mechanical damage. Concrete weight coating is not normally required, due to the high submerged weight and usually low ocean current speeds in deepwater areas. The wall thickness of the carrier pipe also is calculated following standard single pipeline design procedures.

Insulation Layer

Thermal analysis is fundamental to the design of a PIP system. From a flow assurance viewpoint, the main drivers for an insulated flowline system are

- To ensure that the product arrives at the topsides at a temperature above the wax appearance temperature.
- To ensure that hydrates do not form anywhere in the system.
- To reduce the rate of cooldown in the event of an unplanned shutdown to allow sufficient time to re-establish flow or inject wax- and hydrate-inhibiting chemicals before the product reaches the wax or hydrate formation temperature at any point in the system. The required cooldown duration usually ranges from several hours to a few days.

Some of the typical thermal analyses of flowline assurance are briefly described in the following:

- Flashing analysis of production fluid to determine hydrate curve. From these data, the critical minimum temperature is established.
- Global thermal hydraulic analysis of the flowline system to determine the required overall heat transfer coefficient (OHTC, or U-value) at each point in the system and length weighed average overall heart transfer coefficient for the system as a whole, hence, determining if insulation is required and where.
- The required U-value determines the type and thickness of insulation to be used and hence determines the required cross section of the PIP system. At this stage, a trade-off between the cost of insulation and the cost of injecting inhibition chemicals during operation may be feasible.
- Local heat transfer analysis to calculate the mechanical heat transfer coefficient for each component of the PIP system.
- Based on the calculated U-value's performance, a global thermal hydraulic analysis of the insulated flowline system to see if it satisfies the required value.
- Performing a local transient heat transfer analysis at strategic points along the system to develop cooldown curves and hence determine cooldown times to the critical minimum allowable temperature at each location.

Based on the flow assurance analysis results, the minimum required U-values and the operating temperature determine the options of PIP insulation materials. Typical insulation materials are

- Polyurethane foam (PUF).
- Mineral wool.
- Aerogel.

PIP insulation system is a method of achieving U-values of 1 W/(m^2·K) or less. Table 17.1 summarizes some insulation materials used for PIP system, their properties, and U-values for a given insulation thickness. For most insulation systems, thermal performance is based mainly on the conductive resistance. However, heat convection and radiation transfer heat across a gas void in an annulus if there is one. The convection and radiation in the gas in large void spaces result in a less effective thermal system than one that is completely filled with the insulation material. For this reason, PIP systems often include a combination of insulation materials. An inert gas, such as nitrogen or argon, can fill in the gap or annulus between the insulation and the outer pipe to reduce convection. A near vacuum in the annulus of a PIP greatly improves insulation performance by minimizing convection in the annulus and also significantly reduces conduction of heat through the insulation system and the annulus. The difficulty is to maintain a vacuum over a long time.

Table 17.1 Thermal Properties of PIP Insulation Materials

Insulartion Material	Density (kg/m^3)	Conductivity (W/m·K)	Thickness (mm)	Annulus Gap (if any)	Maximum Temperature (°C)	U-value (W/m^2·K) 16-in. Inner Pipe	Comment
Mineral wool	140	0.037	100	Clearance	700	1.6 (40 mm)	Ropckwood or Glava, usually in combination with Mylar reflective film
Aluminum slicate microspheres	390–420	0.1	No limit	None	1000+	3.9 (100 mm)	Commonly referred to as fly ash, injected to fill the annulus
Thermal cement	900–1200	0.26	100	None	200	—	Currently being investigated under a JIP tp provide collapse resistance with reduced carrier pipe wall thickness
LD PU foam	60	0.027	125	None	147	0.76 (100 mm)	Preassembled as a single- or double-jointed system, used on the Erskine replacement
HD PU foam	150	0.035	125	None	147	1.2 (100 mm)	
Microporous silica blanket	200–400	0.022	24	Clearance	900	0.4 (100 mm)	Cotton blanket, calcium-based powder, glass, and titanium fibers
Vacuum insulation panels	60–145	0.006–0.008	10	Clearance	160	0.26 (100 mm)	Foam shells formed under vacuum with aluminum foil and uses gas-absorbing "getter" pills to absorb any free gas thereafter

Polyurethane Foam

A polyurethane foam insulation layer is made by blowing the polyurethane with CO_2, N_2, or water and is one of the most common PIP insulation materials. The density of the foam can be controlled. The thermal conductivity of foams is proportional to the density of the foams. For high density, which means high conductivity and low insulation performance but greater strength, 3.0–6.0 pcf polyurethane foam expanded with a CO_2 blowing agent is a typical insulation material for a PIP system. PIP systems with a PUF insulation layer have been successfully installed with both S-lay and J-lay methods. Reeling lay has more limitations than other installation methods because of potential damage to the insulation during reeling procedure. The insulation procedure may be

- Foam clamshells taped onto the inner pipe, with centralizers spaced 20 ft to 40 ft apart for S-lay or J-lay installation, assembled by sliding the pipes together.
- A foam and hard jacket sprayed onto the inner pipe, with no centralizers, assembled by sliding inner and outer pipes together.
- Foam or ceramic microspheres injected into centralizers. Field joints requiring expensive welding of split sleeves or similar devices as pipes are bonded together.

Mineral Wool

Mineral wool is a fiber made of natural or synthetic minerals or metal oxides. The synthetic form is generally referred to synthetic materials, including fiberglass, ceramic fibers, and stone wool. One of mineral wool's forms is stone wool, which has the main components of inorganic rock or slag as the main component, typically around 98%, the leftover 2% organic content is commonly a thermosetting resin binder or an adhesive and a little oil. Mineral wool insulation is a low-cost material. As listed in Table 17.1, it can provide a good level of insulation performance. Figure 17.4 shows the variation of thermal conductivities of mineral wool with temperature. The mineral wool insulation is suitable for high-temperature applications where polymer coatings are not considered suitable. Typical mineral wool densities are in the range of 120 to 140 kg/m^3.

Aerogel

Aerogel is a synthetic porous material derived from a gel, in which the liquid component of the gel has been replaced with a gas. Aerogels, first produced by Klister in 1931, possess a range of attractive physical properties, such as very low thermal conductivity, high temperature resistance, and good mechanical properties combined with very low density.

The aerogel based system produced by Aspen combines the qualities that suit the reelable PIP system [5]. Figure 17.5 shows an Aspen's insulation panel system, which is based on Aspen's Spaceloft AR5100 series ® flexible aerogel blankets. Aerogel insulation bag is made of a number of blanket layers, typically 3–6 mm thick. It is light, flexible, but has a low thermal conductivity in atmospheric air environment, namely, between 11.0 and 13.5 mW/(m · K) within the typical pipeline temperature range.
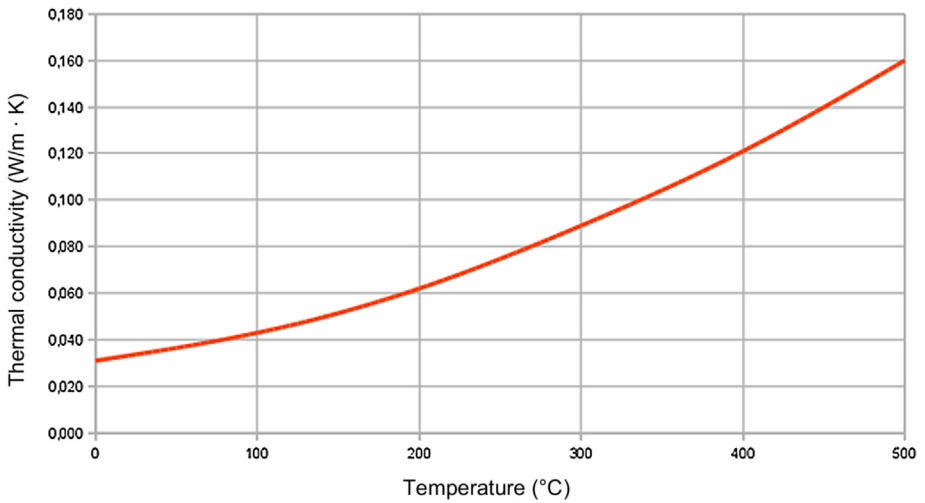
Figure 17.4 Thermal conductivity of mineral wool.
Source: Isover [4]. (For color version of this figure, the reader is referred to the online version of this book.)

Aerogel is a very high-performance material for PIP insulation at attractive cost. The flexibility of the aerogel is very well suited to reeled PIP applications. Extremely low U-values can be reached, due to the lowest thermal conductivity available at atmospheric pressure. Furthermore, PIP size and weight reductions can be obtained when using aerogel instead of other insulation material. These reductions can lead to very attractive cost savings and greater water depth capabilities.

(a) Aerogel layers **(b)** Aerogel insulation blanket
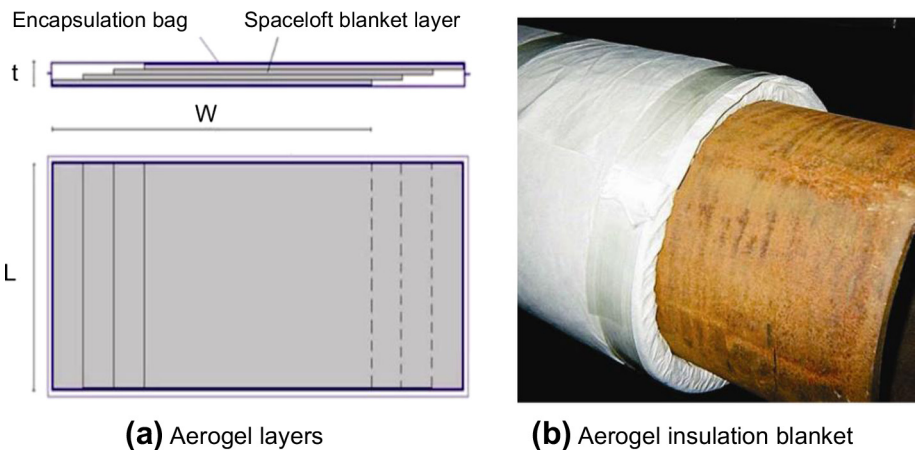
Figure 17.5 Aerogel insulation blanket on a flowline.
Source: Denniel and Blair [5]. (For color version of this figure, the reader is referred to the online version of this book.)

Pipeline Centralizers

The purpose of the centralizers is to effectively centralize the inner pipe to prevent damage to the thermal insulation during installation and to minimize loads on the insulation during installation and operation. The centralizer material must be structurally sound during installation and not deform under operational temperature loads.

Figure 17.6 shows centralizers and an insulation material layer installed on the flowline. The centralizer design consists of two plastic half shells bolted together by a single bolt on each side of the centralizer. The distance between the centralizers depends on the loading to which the section of the PIP is subjected. This spacing between two centralizers may be 2 meters for reeled pipelines, and 20–40ft for S-lay and J-lay installation methods. The presence of centralizers provides heat loss paths and can present cold spots, reducing the overall thermal performance of the PIP system.

Traditional centralizers for lower-temperature conditions are made of a nylon material that exhibits good resistance to abrasive wear. Injection-molded thermoplastic polypropylene can be used in a temperature limitation of about 130°C.

Bulkheads

Bulkheads are forged fittings attached to the PIP pipeline to maintain structural integrity during installation and operation and to serve as installation aids in a variety of ways. Bulkheads, as shown in Figure 17.7, are welded to both the inner and outer pipes at several locations, especially at both ends, to fully constrain relative axial motion. They can also combine the functions of buckle arrestor, water stop, and annulus isolator as well as create an inner pipe inlet when drilled through their web.

Bulkheads are normally welded during pipe laying on the ramp of the installation vessel. The insertion of bulkheads is undertaken on a critical path during pipeline installation, resulting in extended durations for welding the flowline, carrier and half shells at each end of the bulkhead, NDE (non destructive examination), and field joint coating, especially in an application with corrosion-resistant alloy bulkheads. Reelable bulkheads by Technip address these inherent issues, decreasing installation

Figure 17.6 Centralizer and insulation material flowline.
Source: Devol [6]. (For color version of this figure, the reader is referred to the online version of this book.)
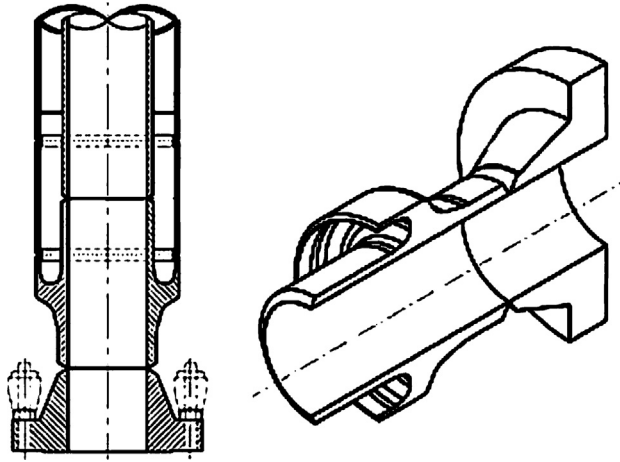
Figure 17.7 End bulkhead configurations.
Source: KW Subsea [7].

duration and allowing NDE to be undertaken in a controlled fabrication environment off the critical path [8].

The following are the challenges in designing bulkheads for a PIP system:

- Transfer of significant compressive and tensile loads in the flowline, due to heat-up and cooldown procedures, into the carrier pipe.
- Bending moments during installation.
- Assessment against more restrictive pressure vessel codes, instead of the pipeline codes.

Water Stops

The purpose of water stops in a PIP design is to avoid the unacceptable result of flooding the entire annulus of a PIP flowline due to a single defect in the outer pipe. The water stop seal resists the maximum external hydrostatic pressure without damage or detriment to long-term integrity should the outer pipe be breached due to impact, corrosion, or other failure. Figure 17.8 shows a field-proven water stop, which comprises two sealing elements and a mechanical clamp assembly. The mechanical clamp anchors the assembly onto the inner pipe to prevent any axial movement of the water stop assembly should a breach of the outer pipe occur. The clamp assembly incorporates integral high-strength precision-locking collets. The mechanical clamp also allows the seals to be positioned at any point along the inner pipe.

The spacing of water stops can be arbitrary, but some practical considerations provide guidance. The first constraint is the maximum tolerable heat loss from a flooded pipeline section or sections. The second constraint is the amount of spare materials (for example, pipe, insulation, or centralizers) available for a single repair. Enough spare material should be available for repairs in an accidental flooding of one segment during construction. It may be unacceptable to lose any reasonable length of insulation, and in that case, the spacing would be governed solely by material constraint [10, 11].

Figure 17.8 A Field-proven water stop.
Source: Subsea Innovation [9]. (For color version of this figure, the reader is referred to the online version of this book.)

Structural Design and Analysis

As detailed in the last section, a PIP system has several structural components. Each component is designed to individual specifications initially, and the combined system must be analyzed to ensure that the local and global response to various loading regimes is satisfactory. In this way, the interaction of all the components is checked, which is important, as one component's behavior may affect the behavior of others. The design of PIP systems is therefore a more iterative process than the systematic approach used for conventional pipelines [12]. Detailed structural design and analysis of a PIP system include

- Determination of pipeline material properties.
- Detailed design of end and midline bulkheads.
- Evaluation of requirements for water stops and optimized spacing.
- Detailed design of field joints.
- Thermomechanical analysis for PIP system, including bulkheads and other components.
- Analysis of sliding pipe systems and the effects of reeling residual strains on in-place behavior.

Limit state and strain-based analysis and assessment include

- Preparation of assessment limits for the required forms of strength limit states.
- The use of finite element modeling for strain-based analysis.
- The preparation of limiting strain levels relating to the flowline and outer pipe materials.
- Evaluation of strain limits for fracture and application of ECA methodologies.
- Thermomechanical analysis under cyclic loading conditions and fatigue limit states.

Wall Thickness Design and Material Selection

Compared to conventional pipelines, several practical considerations are associated with the PIP system, including insulation methods and insulation capabilities currently available, material and construction costs, ease of repair, and structure integrity issues.

Of all the components, the design of the carrier pipe is most flexible for achieving specific system characteristics. Optimization of carrier pipe size and other advantages to be gained from a particular size carrier pipe depend on the global behavior of the system. The carrier pipe is a line pipe but is sized in accordance with the requirements of the overall system. The diameter usually depends on the volume of insulating material required, and wall thickness is generally determined on hydrostatic collapse criteria, that is, the operating water depth. The carrier pipe dimensions have a direct economic impact, in that a larger pipe means more steel and probably longer offshore welding time at each station on the installation barge. As the carrier pipe is not a pressure containing structure, it is not subject to the same design codes as the flowline. In fact, there is no applicable design code, as it is only a structural member, and therefore the design requirement is fitness for purpose. A general basis of 2% strain can be used for the limiting design, as this is on the order of strain seen by reeled pipe. Obviously, it is not desirable for the carrier pipe to be at this level of strain for the duration of its lifetime, but short excursions to this level can be tolerated, such as during installation in the limiting sea states.

For the carrier pipe, the governing criteria are usually collapse and local buckling under combined loading of hydrostatic pressure and bending. Resistance to busting may also be required so that fluid containment can be maintained in case of leakage in the inner pipe. This is a contingency measure and not considered as a normal operating condition. For a deepwater pipeline, the use of buckle arrestors is more economical to limit the extent of a buckle than having a thick wall to resist buckle propagation. This is particularly true for PIP systems, whose self-weight needs to be kept low to ensure that the pipeline is installable.

The inner pipe is designed to resist bursting under internal operating pressure and hydrotest pressure. The inner pipe may also be designed to resist collapse under external hydrostatic pressure and local buckling in case of leakage in the outer pipe.

The factors to be considered in material selection include adequate material toughness for fracture and fatigue performance, practical weld defect acceptance criteria, and whether or not sour service is required throughout the design life.

In-situ stress conditions need to be assessed in wall thickness and material selection. Any stress locked into the inner and outer pipes as a result of installation procedures needs to be accounted for. Also, the tension or towing capacity of the installation vessel needs to be checked for both normal laying and contingency conditions.

The structural behavior of a PIP system depends on both the overall behavior of the system and the mechanism of load transfer between the inner and outer pipes. The overall effective axial force developed in the system depends on the operating conditions of temperature and pressure, and if the pipeline is in the end expansion zone, on the friction forces developed between the outer pipe and the soil. The stresses that develop within the PIP assembly are governed by the type of system used, that is, compliant or noncompliant, and the presence of end bulkheads.

Failure Modes

Failure modes described for single pipeline in Chapter 4 are applicable for the pipe-in-pipe system. The complexity and the differing load-carrying capacity of the system add to the number of failure modes. In addition, the risk and consequence of each particular failure mode and the impact on the PIP system differ from a single pipeline. Additional failure modes need to be considered for the design and assessment of the PIP system.

Bursting

The burst capacity of the PIP system is determined based on the inner pipe subjected to the full internal pressure and the outer pipe subjected to the full external pressure.

Fatigue and Fracture

PIP systems are subjected to both low-cycle and high-cycle fatigue due to daily operational fluctuations and startup-shutdown conditions. One area particularly prone to fatigue is the weld joint. Typically, the weld joint for PIP systems comprise butt weld on the internal pipe and either split shells or some form of sleeve arrangement for the external pipe connection. Special attention should be given to the fatigue assessment for the inner face of the internal pipe, since it is subjected to a corrosive environment, and the outer face of the external pipe, which is subjected to a seawater environment.

Global Buckling

Due to effective axial force and the present of out of straightness (vertically and horizontally) in the seabed profile, PIP systems are subjected to global buckling, namely, upheaval buckling or lateral buckling. Upheaval buckling should be investigated if the PIP system is intermittently rock dumped. Lateral buckling should be investigated in all cases.

Design Criteria

Stress-Based Design Criteria

The stress-based design criterion is that the hoop and equivalent stresses are limited to fractions of the SMYS depending on the considered design cases. The hoop stress criterion may be used with due consideration of material derating factor for both internal and external pipes.

The equivalent stress criterion limits von Mises stress to a fraction of SMYS. For a D/t ratio larger than 20, the biaxial form of equivalent stress should be calculated and the criterion reads as

$$\sigma_e = \sqrt{\sigma_h^2 + \sigma_l^2 - \sigma_h \sigma_l + 3\tau^2} \leq \eta \cdot \text{SMYS} \qquad [17.1]$$

where

    σ_h = hoop stress
    σ_l = longitudinal stress
    τ = shear stress
    η = usage factor

For high-pressure pipes with a D/t ratio less than 20, the triaxial form of equivalent stress should be calculated and the criterion reads as

$$\sigma_e = \sqrt{\frac{1}{2}\left[(\sigma_h - \sigma_l)^2 + (\sigma_l - \sigma_R)^2 + (\sigma_h - \sigma_R)^2\right]} \leq \eta \cdot \text{SMYS} \qquad [17.2]$$

where

    σ_R = radial stress

Strain-Based Design Criteria

For a highptemperature (e.g., above 120°C) pipe, the stress-based design criteria might severely limit the hoop stress capacity, due to internal pressure. In this case, the strain-based design criteria can be applied instead of stress-based criteria. The maximum equivalent plastic strain should be calculated by

$$\varepsilon_p = \sqrt{\frac{2}{3}\left(\varepsilon_{pl}^2 + \varepsilon_{ph}^2 + \varepsilon_{pr}^2\right)} \qquad [17.3]$$

where:

    ε_{pl} = longitudinal plastic strain
    ε_{ph} = hoop plastic strain
    ε_{pr} = radial plastic strain

The accumulated plastic strain should satisfy $\varepsilon_p < 0.5\%$. Otherwise, fracture assessment should be performed.

Local Buckling Design Criterion

Fot local buckling capacity, check that both internal and external pipes are in line with the criterion given in Chapter 3.

Global Buckling Analysis

The global buckling analysis of PIP systems is referred to Chapters 10 and 11.

Fabrication and Field Joints

Depending on the installation method chosen, a PIP flowline system may be the ideal candidate for utilizing onshore fabrication to reduce offshore fabrication time, as any

such offshore operation is fairly time consuming, leading to low production rates in comparison to a single wall flowline. Onshore fabrication site requirements depend on system design and local availability of resources.

Prior to offshore installation, for most PIP systems, onshore fabrication of the individual PIP joints is required. The inner pipe must be placed within the outer pipe and the annulus filled with the insulating material, or the inner pipe precoated with the insulation material must be slid into the outer pipe. The joint fabrication method depends on the PIP system, the installation method, and the vessel selected. As part of the PIP joint fabrication, the joints could be made up as double, quad, or hex joints in single operation to suit the installation method.

The field joint is a critical area for S-lay and J-lay installation. A suitable method that allows the welding of pipe joints in an efficient manner and maintains the integrity of the insulation and mechanical properties is essential. Two basic methods are available. The first, which is more applicable to J-lay, is to allow the outer pipe to slide over the inner pipe after the inner pipe field weld has been made. The outer pipe is then welded after the field joint area has been insulated with suitable insulating material. The technique is required, and the integrity the PIP system during the sliding operation needs to be closely examined. This system may not be used for S-lay, as the outer pie cannot be slid over the inner pipe in the firing line over multiple weld stations.

Installation of PIP

Installation Methods

The total submerged weight of the pipe section suspended in the water column increases at a faster rate than the water depth. A PIP system is generally much heavier than its single-wall counterparts; therefore, the tension capacity of the installation vessel becomes an important design factor, given the generally low tension capacities of the existing installation vessels available on the market.

The methods for the installation of deepwater pipelines are S-lay, J-lay, reeling, and towing. Detailed accounts on these methods have been made by various authors. A brief summary is given here to capture some key characteristics of each method.

The S-lay method is used by S-lay vessels with dynamic positioning and stingers capable of very deep departure angles. With its long firing line and many work stations, an S-lay vessel can be reasonably productive. The S-lay method is characterized by its fast installation process and the applicability of the method over a wide range of water depths. Limitations of the S-lay technique are tension capacity and potential high strains in the overbend region, hence, the restrictions on combinations of large pipe diameter and water depth.

The J-lay method results in a reduction in lay tension requirements. Also, large J-lay vessels have better motion characteristics and hence lower dynamic pipe stress especially at the stinger tip than those used in S-lay. However, productivity can be low, due to the limited number of work stations and rather confined working space. This shortcoming may be offset somewhat by the use of prefabricated quad or even hex joints. J-lay is generally not suitable for shallow water applications.

The reeling method can be very efficient, particularly for relatively short length pipelines, where the number of reloads can be minimized. The method is suitable for outer pipe diameter up to 18 inches with no concrete coating. Plastic strains developing reeling and unreeling; hence, particular attention needs to be given to stress-strain conditions at bulkheads. Until now, its application has been restrained by the relatively low tension capacity currently available. Several large reel laying vessels are under construction. The vessels will have very high tension capacities, large drums, and near vertical departure angles, making reel laying a strong alternative to J-lay for small to medium diameter, short to medium length pipelines.

Towing methods include several arrangements, mid-depth off-bottom and on-bottom tows. It can be very cost effective for flowlines of short length. However, it may be restrained by factors such as the maximum pull of the towing vessels, the ocean current conditions, availability for a suitable onshore fabrication and launching site, and the seabed topography and soil condition along the tow route. Towing is particularly suitable for the installation of pipeline bundles where a large outer pipe can be used to house several flowlines and umbilicals.

Installation Analysis

First of all, layability checks are performed for the worst cases as part of the wall thickness and steel grade selection exercise. Once the wall thickness and steel grade are finalized, detailed pipeline analyses are carried out covering both normal laying and contingency operations.

Static normal laying analysis establishes the optimum lay parameters, that is, barge tension and J-lay tower inclination angle, for various sections along the entire pipeline route. Dynamic analyses on selected static conditions are then performed to confirm that the resultant stress and strain is acceptable and the vessel tensioner capacity is adequate. The cumulative fatigue damage of a weld is estimated, accounting for the various stress ranges it experiences as the pipe is lowered toward the seabed or suspended below the water surface during undesirable weather conditions.

3. Bundle Systems

General

A pipeline bundle system consists of an outer carrier pipe, inner sleeve pipe, several internal flowlines and umbilical components, insulation system, and appurtenances such as spacer, valves, chains, and supports. The carrier pipe is a continuous tubular structure that contains flowlines and a sleeve pipe and is used to provide additional buoyancy to the bundle components during installation, structural strength mechanical protection during operation, and a corrosion-free environment for the flowlines. The sleeve pipe is used to provide a dry, pressurized compartment for internal flowlines. The internal flowlines are continuous line pipes without frequent branches used for the transportation of fluids within the field. Spacers are non-stress-distribution elements provided to locate and support flowlines within the bundle

configuration. Usually, the pipeline bundle is terminated by bulkheads, which are stress-distribution diaphragms. To facilitate the installation, ballast chains are attached to the bundle for submerged weight adjustment and to suit installation by towing. Spools, which are short, rigid pipelines, are needed to facilitate tie-in of the bundles and pipelines to structures.

The advantages of the bundle include [3]

- Elimination of the requirement for heavy lift vessels by incorporating subsea structures within a towed production system.
- Fabrication, testing, and commissioning of complete system onshore, thereby reducing offshore time and allowing fast hookup and commissioning for early first oil dates,
- Low stress installation and reduced number of subsea tie-ins and spool installations by using the controlled depth tow method.
- Protection incorporated in the structure design, and seabed stability using a gravity-based or piled design.
- Improved flow assurance and thermal management.
- Leak mitigation in case of internal pipeline failure by maintaining leaked oil within the carrier annulus.
- Reduction in pipeline safety class when using the DNV-OS-F101 design code.
- Use of CRA (corrosion resistant alloy) lined pipe in place of clad pipe or solid CRA pipe.
- High-temperature pipeline design.

Bundle Configurations

Bundle configurations can be grouped into conventional configurations and innovative configurations. Conventional configurations are mainly a carrier-based system. All the parts of the bundle system are within the carrier pipe, which provides buoyancy and acts as mechanical protection. Innovative configurations have no carrier pipe or inner sleeve pipes. One option is to use external single or multiple buoyancy pipe(s) for all flowlines. Figure 17.9 shows two examples of a pipeline bundle. A typical pipeline bundle system mainly includes the following components:

- Flowlines (inner pipe).
- Carrier pipe (outer pipe).
- Insulation layer.
- Control, chemical tubes.
- Power, signal, and data highway cables.
- Spacers.
- Bulkheads.
- Ballast chains.
- Anodes.

The bundle configuration should fulfill the weight and buoyancy requirements. In addition, the following principles should be considered when selecting the bundle configuration [13]:

- The center of gravity of the bundle has to be situated as near as possible to the vertical center line of the carrier and as far as possible below the horizontal center line of the carrier.
- The bundle should be configured at the bulkhead such that sufficient distance exists between the flowlines to allow for access during fabrication.

(a) Drake F-76 bundle   (b) Subsea 7's bundle
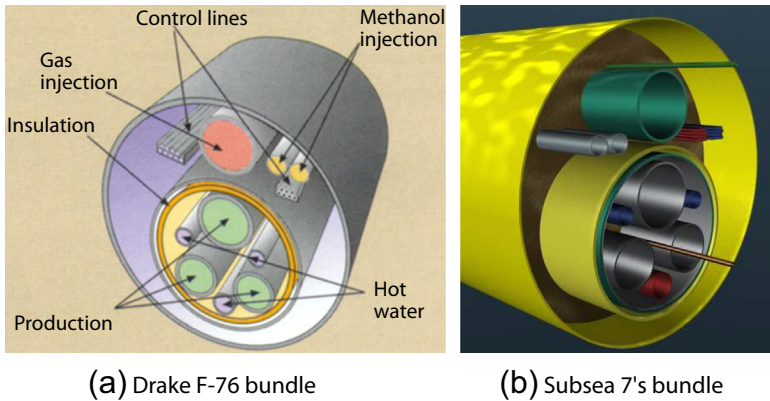
Figure 17.9 Bundle configuration.
Source: (a) McBetn [1]; (b) Watson and Walker [3]. (For color version of this figure, the reader is referred to the online version of this book.)

- The minimum clearance between the flowlines and the sleeve pipe should be selected to allow for heat transfer.
- The configuration must allow for the design of suitable spacers.

Structural Design and Analysis

Design Requirements for Bundle System

As a minimum requirement, the bundle system is to be designed against the following potential failure modes:

- Service Limit State
- Ultimate Limit State
- Fatigue Limit State
- Accidental Limit State

Bundle Safety Class Definition

The safety class for flowlines, sleeve and carrier pipes may be tabulated as in Table 17.2, unless otherwise specified by clients.

Functional Requirements

Design Pressure
The general design pressures for the bundle system should be based on processing data. The internal pressure for carrier and sleeve pipes during installation should be at least 1 bar higher than the expected water depth.

Hydrotest Pressure
The hydrotest pressure of the flowlines, heat-up, and service lines systems should be based on $1.25 \times$ design pressure.

Table 17.2 Safety Class Definition for the Bundle

Pipes	Launch & Installation	Operation
Carrier and Sleeve	Normal	Low
Flowlines	Low	Normal
Heat-Up Lines	Low	Low

Design Temperature

The design temperature should be based on the processing data. A significant temperature drop along the bundle system must be avoided.

Pigging Requirements

If the bundle system is designed for pigging, the geometric requirement should be fulfilled. The minimum bend radius should be 5 times the nominal internal diameter of the pipe to be pigged. The pipe should be gauged as a part of onshore and offshore testing of the system.

Insulation and Heat-up System

The following requirements related to insulation and heat-up functions for the bundle system should be satisfied:

- During normal operation, the temperature should be above the hydrate formation temperature for the system.
- Minimum arrival temperature for the production lines should be above the hydrate formation temperature.
- A minimum of certain hours' shutdown should be accepted before the fluid in the production lines has reached hydrate formation temperature.
- To melt wax, it should be possible to bring temperature in the system up to above a certain degree.

The cooldown time is the critical factor to determine the bundle insulation requirements. Therefore, the design of insulation thickness should be based on the minimum cooldown time. The insulation combined with active heating should satisfy the heat-up requirement where applicable.

The following factors should be considered for the bundle thermal design:

- Maximum and minimum operating temperatures.
- Cooldown time.
- Heat-up time.

The following conditions should be analyzed for bundle thermal analysis:

- **Steady state:** The evaluation of bundle steady state thermal performance includes the calculation of U-value and process fluid properties.
- **Bundle cooldown:** The evaluation of bundle cooldown thermal performance includes transferring initial cooldown properties from steady state analysis and calculating the bundle cooldown time.

- **Bundle heat-up:** The evaluation of bundle heat-up thermal performance includes the calculation of the process fluid properties at initial and final heat-up conditions and calculation of the bundle heat-up time.

The following heat-up system operating parameters have been the subject of the design:

- Maximum heating at medium flow rate.
- Heat-up time.
- Heat-up system volume.

The heat transfer inside the bundle and the bundle heat-up time depend on the following factors:

- Bundle configuration and the relative positions of the components.
- Bundle length.
- Heating medium temperature.
- Properties of the fluid contained inside the flowlines.

Umbilicals in the Bundle

The general functional design requirements for umbilicals are as follows:

- The level of redundancy should be the same as for a system with separate umbilicals.
- The control system should be protected during fabrication and testing period.
- Testing of the system should be catered for during and after fabrication and during and after installation on the seabed.
- Seamless tubing, all welded, should be used.
- The electrical cable should be in continuous lengths to avoid splices and provide suitable outer isolation.
- The electrical connectors should be electrically isolated from the cathodic protection system of the bundle to avoid buildup of calcareous layer on the metal parts.
- Components should be located to minimize their temperature effects.
- It must be possible to individually replace any pipeline or control jumper as well as any electrical jumper.
- The connection system should be compatible with the flowline connection system.
- Future extension of the system should be planned for.

Design Loads

Temporary Phase Loads

The temporary phase loading to be addressed as part of the bundle component analyses are summarized as follows:

- Lifting and support during fabrication.
- Sheathing of the sleeve pipes with applied tension to flowline and sleeve sections.
- Sheathing of the carrier pipe over the sleeve pipe.
- Support of inner bundle on the sleeve pipe.
- Hydrostatic testing of the completed flowlines and subsequent leak testing of the sleeve and carrier pipes.
- Launch after tie-in of the towheads.
- Tow from the fabrication site to the field.

- Installation at the designated in-field locations.
- Flooding of the bundle flowlines and carrier pipe with subsequent hydrotesting of the flow-lines.

Operational Phase Loads

The operational phase loads to be addressed as part of the flowline analyses are summarized as follows:

- Hydrostatic collapse of flowlines considering axial tensions and support conditions.
- Expansion loading during operation, considering thermal- and pressure-induced forces, support conditions within the carrier pipe, and sleeve pipe and carrier free spanning.
- Stability of the bundles, considering environmental forces during extreme wave events, operational conditions within the flowlines, and residual bundle curvature or displacement present after installation.
- Carrier expansion considering existing operational conditions within the bundle, including thermal- and pressure-induced loads, residual installation curvature or displacement of the carrier, and possible free spans.

Additionally, where a sleeved pipe insulation system is present within the bundle, the effect of thermal and pressure effects on the integrity of the sleeve and associated insulation bulkheads are evaluated.

Load Combinations

The most onerous of the following loading conditions should be applied to the bundle design:

- Functional loads alone.
- Functional loads plus simultaneous environmental loading.
- Accidental loads.

Functional loads are described as all loads arising from the flowline bundle system normal function and include, in addition, the loads imposed during launch and installation. Environmental loading is usually direct loading resulting from wave, wind, or current but may also include indirect loads, due to the environment, which are transmitted to the bundle system during installation.

Design Procedure and Acceptance Criteria

The design of bundle system should ensure that the system satisfies the functional requirements and adequate structural integrity is maintained against all the failure modes. In principle, the design procedure and acceptance criteria for a conventional single pipeline could be applied to the bundle system. Some special design considerations are needed, which are presented in this section.

Design Procedure for Bundle System

The first requirement of the bundle design is to determine the carrier pipe size. Having fixed the carrier size the bundle is considered with regard to its on-bottom stability, tow stresses, mechanical protection, and the like. The recommended design procedure is shown in Figure 17.10.
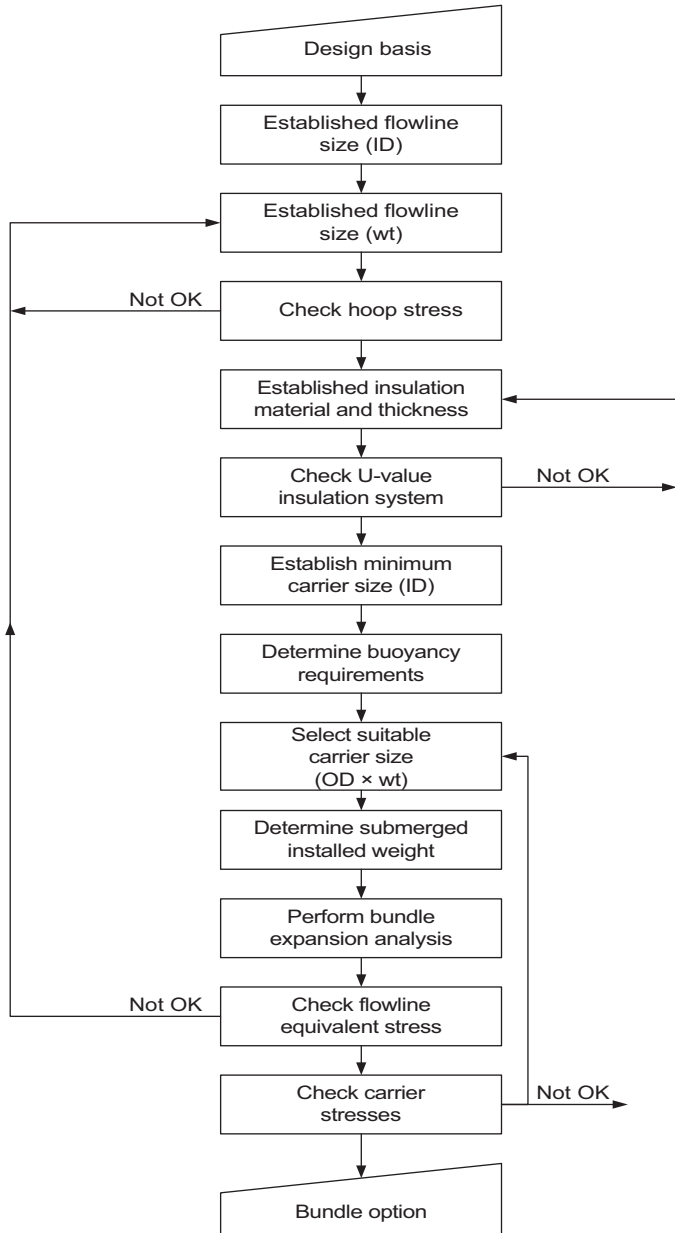
Figure 17.10 Design flowchart for bundle system.

The carrier pipe is generally regarded as an installation aid. After installation, the carrier pipe provides the flowlines with protection from impact. Consideration of this policy is required when carrier pipes contain flowing fluids to provide either a cooldown or heat-up process, as they may be considered as a pipeline.

Flowlines are usually sized according to processing data. The wall thickness of the flowlines depends on the internal pressure containment. However, in high-temperature applications especially with CRA material, thermal loadings must be considered with regard to flowline sizing and more likely material properties that apply at elevated temperatures.

The insulation U value is determined from thermal and processing analysis. The weight and volume of the insulation are needed for bundle design. Thick coatings of polymer insulation can result in carrier pipes of large cross section enclosing relatively small weights, producing excess buoyancy. In such cases, consideration may have to be given to flooding a flowline to provide additional weight.

The weight of all the bundle component parts must be determined. Generally, only carrier pipe displacement is considered in the buoyancy calculation. The displacement of external anodes, clamps, and valves is accounted for by using a submerged weight for these items in the weight calculations. The objective of this weight and displacement determination is to arrive at a carrier pipe diameter that provides a resultant buoyancy of 200 N/m + 3% of steel pipe weight. The 3% figure stems from the weight tolerance, and the 200 N/m figure is suited to carrier pipe diameters of 32 inches or greater. If diameters are less than 32 inches, then 100 N/m should be used. The optimum carrier could be found through a reiterative process to calculate the weights and buoyancy.

The installed submerged weight, expansion analysis, and flowline equivalent stresses are considered to ensure that the bundle design is stable once installed and has no adverse effect on the permanent flowlines.

The submerged weight of the bundle is compared with the minimum submerged weight of the bundle required to satisfy Morison's classical two-dimensional theories. The cyclic varying horizontal velocity in the water particles introduced by the design wave is superimposed on the steady bottom current velocity at the height of the bundle. The bundle is considered stable when the actual submerged weight is greater than the calculated minimum, applying a safety factor of 1.1. Bundle expansion due to the temperature and pressure of the product in the flow-lines should be considered. The geometry of the installed bundle is such that the flowlines are attached to the carrier pipe at the extreme ends only via a solid bulkhead. Over their length the flowlines are supported by spacers, maintaining their positions relative to and parallel with each other and the carrier pipe. The carrier pipe is supported over its length by the seabed. Expansion of the flowlines exerts loads on the bulkhead, which in turn mobilizes the carrier pipe that is itself constrained by seabed friction. The bundle is a system with boundaries at a free end and at the associated anchor point. The bundle expansion analysis includes determining external and internal forces acting on the system, calculating axial strain of system, and integrating the axial strain of unanchored bundle to determine the expansion.

The check on flowline equivalent stresses is important, especially with high-temperature applications, not only for the higher thermal loads produced but also the reduction in yield strength with some materials.

Carrier stresses should be looked at during the carrier selection and reviewed in light of the stresses determined during the expansion analysis.

Design Criteria for Bundle System

The carrier and the sleeve pipes should be designed in accordance with the criteria given in Chapter 4. The deduction of large D/t ratio of carrier and sleeve pipes on bending moment should be accounted for in the maximum allowable bending moment criterion defined in Chapter 4.

Global equivalent stress in the carrier pipe during installation should be limited to 72% of yield stress. Local equivalent stress in the carrier pipe during installation should be limited to 90% of yield stress.

Wall Thickness Design Criteria

The wall thickness design of pipes within the bundle system should take into account the following:

- **Hoop stress:** The hoop stress criterion is in principle applicable for the bundle system with the following special considerations—the allowable hoop stress for flowlines and heat-up lines in Safety Zone 1 and those inside the bundle carrier in Safety Zone 2 should be limited to $0.8 \times$ SMYS.
- **Collapse due to external hydrostatic pressure:** Wall thickness should be designed to avoid pipe collapse due to external hydrostatic pressure. A collapse analysis may be performed in accordance with Chapter 3. The carrier pipe and the sleeve pipe should be pressurized to a pressure 1 bar greater than the maximum external pressure at the deepest point in the installation area to prevent collapse.
- **Local buckling:** The flowlines, sleeve pipe, and carrier pipe should be designed to withstand local buckling due to the most unfavorable combination of external pressure, axial force, and bending. The design may be carried out in accordance with Chapter 4.
- **On-bottom stability:** The wall thickness design should be adequate to ensure the on-bottom stability of the bundle with no additional means.
- **Installation stress:** The wall thickness should be adequate to withstand both static and dynamic loads imposed by installation operations.
- **Hydrotest and operational stresses:** The wall thickness should be adequate to ensure the integrity of the flowlines, sleeve pipe, and carrier pipe under the action of all combinations of functional and environmental loads experienced during hydrotest and operation.
- **Bundle thermal expansion design:** The design should take into account expansion and contraction of the bundle as a result of pressure and temperature variation. Design pressure and the maximum design temperature should be used in bundle expansion analysis. The presence of the sleeve pipe should be taken into account.
- **Bundle protection design:** The bundle system should be designed against trawl loads outside the trawl-free zone around the installations. The flowlines and umbilicals should be protected against dropped objects around the installations. Carrier pipe and bundle towheads should offer sufficient protection against dropped objects with impact energy of 20 kJ. Impact loads from

dropped objects for the protection structure design should be treated as a PLS (plastic limit state) condition.

- **Corrosion protection design:** Cathodic protection design should be performed according to relevant codes. Cathodic protection together with an appropriate protective coating system should be considered for protection of the bundle external steel surfaces from the effects of corrosion. Sleeve pipe is protected from corrosion by provision of chemical inhibitors within the carrier annulus fluid. Flowlines within the sleeve pipe are maintained in a dry environment. Therefore, cathodic protection system is not required.
- **Bulkheads and towhead structure design:** The bulkheads form an integral part of the towhead assemblies. The towhead structures should remain stable during all temporary and operational phases. Stability should be addressed with respect to sliding and overturning with combinations of deadweight, maximum environmental, and accidental loads applied. The design of towhead structure should be in accordance with relevant structural design code, like API RP2A.
- **Bundle appurtenances design:** Relevant design codes should be applied for the design of bundle appurtenances based on their functional requirements.
- **Fabrication and construction design:** Design check and analysis should be performed to confirm the adequacy of the selected pipe wall thickness to withstand loads during fabrication and construction phases and to ensure that the pipe stress values remain within the specified limits.

Bundle Installation

A number of tow methods have been used to tow lines to sites. These are classified by the buoyancy in the pipeline and hence the level in the water at which the tow takes place. Three primary methods of towing bundles to their locations are used:

- Bottom tow.
- Controlled-depth tow.
- Surface tow.

For the bottom tow of bundles, the bundle is pulled along the seabed, usually with some buoyancy tanks attached by one or more towing vessels. This method is used primarily in the Gulf of Mexico. However, this method needs accurately surveyed tow corridors without obstructions, and any pipeline crossing must be protected [14, 15].

For surface towing of bundles, the bundle is towed on the surface of the water, with or without additional temporary buoyancy tanks. It has not been widely used, due to fear of bending fatigue because of weather conditions and the risk of collisions with vessels crossing the path of the bundle during towing. It was developed from bundle technology in towing. Either the flowline or the carrier can be flooded, depending on the relative weights and buoyancy of each, and the on bottom stability requirements. It promises considerable savings over other systems of installation for single or double lines.

Controlled-depth towing, as the name implies, is towing the bundle such that it stays in mid-water between the seabed and the surface. When one considers that bundles may be 5 to 7 km long and the water depth may be 100 meters, it is quite a feat to keep the bundles straight and steady without perturbations, which could take it either to the surface or the seabed. This method is primarily used in North Sea by Subsea 7.

Bundle Installation by CDTM

The most feasible and reliable way of bundle installation is by use of controlled-depth tow method, which is a subsea pipeline installation system.

The principle of the CDTM involves the transportation of the bundle towed between two lead tugs and one trail tug. By controlling the tow speed in combination with the tension maintained by the trailing tug and the trailing towhead, the bundle configuration and its deflections are kept under control during the tow. The essential parameters are continuously monitored during the tow and adjusting if necessary to maintain the desired bundle configuration well clear of the seabed; its nominal position during tow is some 30 m below sea surface.

The complete installation of bundle system includes the following main activities.

Launch
On completion of fabrication and testing, the bundle is outfitted for tow and installation with a ballast chain, telemetry systems, and other installation aids. Breakout and pull forces during various stages of the launch should be calculated and assessed for the bundle system.

Pretow Preparation
The pretow preparation commences with the activities including towhead inspection, trimming, bundle submerged weight check, and tow preparation.

Tow to Field
The bundle system is towed to the field by use of CDTM along a presurveyed route. During towing, the drag on the ballast chain creates a "lift force", and so reduces the bundle submerged weight. This lift force results in a complete lift off from the seabed into CDTM mode. When the tow arrives near the field, the bundle is lowered to the seabed in the designated parking area, situated in front of the bundle installation area.

In-Field Installation
The in-field installation of the bundle system is carried out by remote intervention, which is carried out directly by ROV (remotely operated vehicles). The bundle is towed at a slow speed in off-bottom mode into the installation area. After adding weight to the bundle, the off-bottom tow can commence. During the off-bottom tow, the bundle position must be monitored at all times. The bundle is pulled in at a straight line. A temporary target box is determined for the leading towhead. When the towheads and bundle position have been confirmed, flooding down of the bundle can commence.

CDTM involves the transportation of prefabricated and fully tested flowlines, control lines, and umbilicals in a bundle configuration suspended between two tugs. A further vessel accompanies the tow as a patrol or survey vessel. To maintain control during towing, the bundle is designed and constructed within specified tolerances with respect to its submerged weight.

The bundle is designed to have buoyancy, this being achieved by encasing the bundled pipelines, control lines, umbilicals, and so forth inside a carrier pipe. Ballast

chains are attached to the carrier pipe at regular intervals along its length to overcome the buoyancy and provide the desired submerged weight, as shown in Figure 17.11. The carrier pipe is sized so that the bundle is slightly positively buoyant, then chains are attached to the underside. The bundle is next towed out into a sheltered bay. Being positively buoyant, the carrier pipe rises from the seabed and lifts the chain until enough links are suspended to counteract buoyancy. Chains can be easily cut by ROV to trim bundle for tow, if required.

The tow speed has a direct lift and straightening effect on the bundle. By controlling the tow speed in combination with the tension exerted by the tugs, the bundle tow characteristics and deflections are maintained.

The tow is controlled by adjustment of the tow wire length, tow wire tension, tow speed, and the tug's relative positions. In this manner, the tow depth, catenary shape, stresses, and movement are kept within specified operational limits under given environmental conditions. During towing, the bundle is kept well clear of the seabed to enable a safe and unobstructed passage. The towheads are kept below the surface to minimize the effect of surface waves. The towhead depth is normally about 30 m below the surface, but this controlled depth can be increased or reduced by adjustment of the tow wire lengths.

On arrival in the field, the bundle is gradually lowered by adjustment of the controlling parameters (tow wire length, forward speed, and tension), and the bundle settles in a position of equilibrium above the seabed with the lower portion of the chains resting on the seabed. Once in this position the bundle can easily be
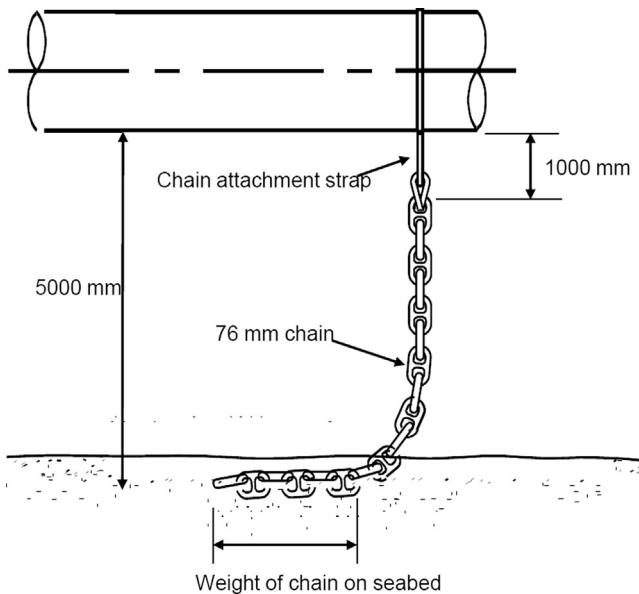
Figure 17.11 Control depth tow method.
Source: Watson and Walker [3].

maneuvered in the off-bottom mode to its final position and the towheads located in the required target areas. The carrier annulus is flooded with inhibited seawater, and the bundle settles on the seabed.

References

[1] McBeth R. An overview of pipeline configuration alternatives. Anchorage, AK: Presentation at the Alaskan Arctic Pipeline Workshop, Minerals Management Service; November 1999.

[2] Carmichael R, Fang J, Tam C. PIP systems for deepwater developments. New Orleans: Proc. of Deepwater Pipeline Technology Conference; 1999.

[3] Watson I, Walker P. Bundle pipeline systems and shell FRAM development. Lunch and Learn with Shell and Subsea 7, Subsea UK; March 21, 2012.

[4] Isover. Available at http://www.isover-technical-insulation.com/MARINE-INSULATION/ Applications.

[5] Denniel S, Blair C. Aerogel insulation for deepwater reelable PIP. OTC 16505 Offshore Technology Conference 2004, Houston, TX; 2004.

[6] Devol JW. PIP centralisers go deep offshore. Oil and Gas Engineer; 2011.

[7] KW Subsea. Available at http://www.kwltd.com/services-kw-PIP-pip.php.

[8] Boi J, Lynch B, Sloan C. Development and application of reelable PIP bulkhead technology. OTC 23112 Offshore Technology Conference 2012, Houston, TX; 2012.

[9] Subsea Innovation. Available at http://www.subsea.co.uk/subsea-sealing-solutions/ waterstop-seals.

[10] Jukes P, Eltaher A, Sun J. Extra high-pressure high-temperature flowlines—Design considerations and challenges. OMAE 2009. Honlulu, HI; 2009.

[11] Jukes P, Delille F, Harrison G. Deepwater PIP qualification testing for 350 F service. IOPF2008-922. Houston, TX; 2008.

[12] Dixon M, Patel M. Analysis methods for PIP systems; 1999.

[13] McKelvie M. Bundles–Design and construction. Integrated Graduate Development Scheme. Heriot-Watt University; 2000.

[14] Brown RJ. Past, present, and future towing of pipelines and risers. OTC 18047 Offshore Technology Conference 2006, Houston, TX; 2006.

[15] Brown RJ. Installation case study: Pipe bundles and risers. Clarion Technical Conferences Marine Pipeline Engineering Course. Houston, TX; 2004.

18 Seismic Design

Chapter Outline

1.   Introduction

When a pipeline system traverses through various seismic damage areas, many potential damages, such as slope instability at scarp crossing, soil liquefaction, and fault movement, may hit the pipeline system. Different kinds of seismic hazards often impose hazardous geotechnical loads on subsea pipeline systems. In some extreme situations, the loads due to those seismic hazards may be so large that the subsea pipeline system yields and suffers plastic deformation. Damages and disruptions of the subsea pipelines caused by an earthquake may have severe effects on service life, since it may lead to significant financial loss due to service interruptions, fires, explosions, and environmental contamination. Examples of such catastrophes include the 1964 Alaska Earthquake, the San Fernando Earthquake of 1971, the Guatemala Earthquake in 1976, the 1987 Ecuador Earthquake, the Kobe Earthquake in 1995, and

the 2003 Algeria Earthquake. A general conclusion drawn from a review of many earthquake events shows that, for buried steel pipelines, the direct effect of seismic ground waves on the integrity of long, straight pipelines is generally not significant. Where there is permanent ground deformation due to soil failure, there may be a severe influence on pipeline integrity. For unburied pipelines, both seismic ground waves and permanent ground deformation can cause severe damage, depending on the pipeline geometry and connected structures.

Seismic ground waves produce strains in buried pipelines. However, because there are little or no inertia effects from dynamic excitation, the strains tend to be small and often are well within the yield rupture threshold of the pipeline material. The direct effect of seismic waves is, therefore, generally not expected to cause rupture or buckling failure to buried pipelines. Nonetheless, seismic waves can cause damage to unburied pipeline systems, especially in the interfacing area, such as in the pipeline transition section from buried to unburied and the pipeline tie-in spool to the subsequent structure. In general, the seismic analyses of the permanent ground deformation for buried pipes and unburied pipes and seismic ground waves for unburied pipes are required for designing pipeline systems.

Many subsea pipelines are often buried for stability and mechanical protection in the shallow water area; otherwise, they are laid on the seabed. This chapter

- Addresses available seismic design codes, standards, and design criteria for subsea pipelines.
- Discusses a general design and analysis methodology for fault crossing and seismic ground waves.
- Presents design and analysis examples using a static model for buried pipe, subjected to permanent ground deformations due to the foundation failure, and a time history dynamic model for unburied pipelines subjected to seismic ground waves.
- Summarizes the mitigation methods for subsea pipelines to avoid seismic hazards.

2.   Seismic Hazards

Damage to pipeline systems during an earthquake, whether onshore or offshore, can arise from the traveling ground waves and permanent ground deformation due to soil failures. The primary soil failures are

- Surface faulting.
- Landslides.
- Liquefaction.
- Differential settlement.
- Ground cracks.
- Seismic wave propagation.

Surface Faulting

Surface faulting is the earth surface deformation associated with the relative displacement of adjacent parts of the surface crust. Surface fault displacements can

occur rapidly during an earthquake. In addition, relatively minor displacements may accumulate gradually over many years as seismic creep.

Surface fault crossing is one of the major hazards to subsea pipelines, whether buried or unburied. Numerous investigations have been carried out for fault crossing with different soil movements. Surface faulting is an important consideration for buried pipelines, because pipelines crossing fault zones must deform longitudinally and bend to accommodate the ground surface offsets. For subsea pipelines laid on the top of the seafloor, fault movements are generally of little, if any, consequence. However, it is possible that subsea faulting could produce a vertical offset that would cause a spanning pipeline to be elevated above the seafloor and may cause vortex-induced oscillations due to water currents, then cause fatigue damages of the pipeline.

Figure 18.1 illustrates the classifications of fault movements, in which the surface faults are classified on the basis of their direction of movement with respect to the ground surface. A strike-slip fault is one in which the predominant component of ground movement is horizontal displacement. Normal-slip and reverse-slip faults are those in which the overlying side moves downward and upward, respectively, in relation to the underlying side of the fault.

The amount and type of ground surface displacement is the main factor for designing pipelines to resist permanent ground deformation at fault crossings. Bonilla (1982) [2] summarizes a simple equation relating the maximum displacement at ground surface to the earthquake surface-wave magnitude as

$$\log L = -6.35 + 0.93 M_s \qquad [18.1]$$

where L is the maximum surface displacement in meters and M_s is the earthquake surface wave magnitude. The earthquake magnitude is one of the design criteria based on historical seismicity and geological data. Displacement data from the fault of similar earthquakes might be used in selecting a value for designing pipelines, because of a big deviation in earthquake surface displacement data, on which the equation is based.

The ability of a pipeline to deform in the plastic range under tension helps prevent rupture at fault crossings. If compression of the pipeline in a fault crossing is un-avoidable, the compressive strain should be limited to within the local buckling criteria.

(a) Strike-slip faulting   (b) Normal-slip faulting   (c) Reverse-slip faulting
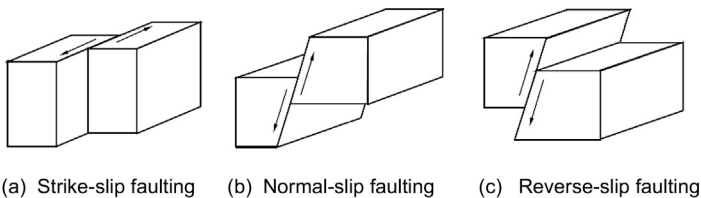
Figure 18.1 Classification of surface fault movement.
Source: Honegger and Nyman [1].

Landslides

Landslides are mostly triggered by strong ground shaking during earthquakes, which include rock falls, disrupted soil slides, rock slides, soil slumps, soil block slides, and soil avalanches, as illustrated in Figure 18.2. The potential threat to pipeline performance includes the following parameters:

- The amount of landslide displacement.
- The depth of the landslide relative to the depth of the pipeline.
- The type of ground displacement associated with the landslide movement.
- The direction of landslide movement relative to the pipeline.

An approximate estimate of potential landslide movement can be made based on the existing slope and a general description of the near-surface material. Several commercial software packages are available for the analysis. Stress-deformation analyses have been used to estimate the permanent deformations caused by inertial instabilities. The strain potential and stiffness reduction approaches allow the estimation of permanent deformations from relatively simple analyses.

Liquefaction

Liquefaction is the transformation of a saturated noncohesive soil from a solid to a more liquid state as a result of increased pore-water pressure and concomitant loss of shear strength. Liquefaction hazards to pipelines include pipeline flotation and sinking, which require the pipe to be located below the ground water table within a zone of liquefiable soil. Ground settlement occurs when a liquefiable soil layer is beneath a layer of competent or hard soil. If the pipeline is located in the layer of competent soil near the surface, it is subjected to displacement associated with subsidence of the ground. Loss of shear strength gives rise to bearing failures and large deformations in surface structures founded on liquefied soil.

Assessing liquefaction potential is based on both peak ground acceleration and earthquake magnitude. Estimating the peak ground acceleration at the site of interest can be performed using probabilistic or deterministic approaches.

3. Pipeline Seismic Design Guidelines

Pipeline Seismic Design

Most loads of seismic hazards on a buried pipeline are due to the ground movements relative to the pipeline. The pipeline is deformed to match the ground movements, and the loads are displacement controlled. Pipelines buried with minimal soil cover or in relatively weak soils and subjected to high axial loads due to the ground movement may experience upheaval buckling. The current design code and guidelines for pipeline systems under displacement-controlled loads are basically strain-based design, in which the acceptable strain levels for the system based on limit-states design are limited (see Chapter 4, "Limit-State Based Design" of this book). The
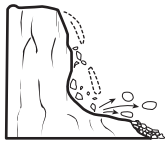
Rock fall (disruptive)   Rock topple (disruptive)
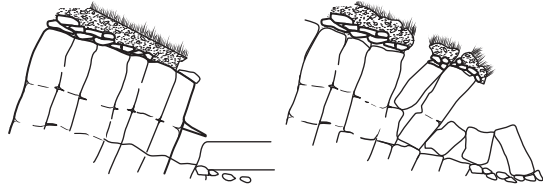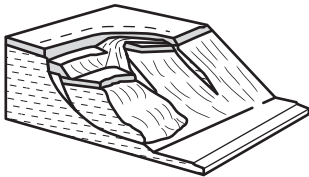
Earth slump (coherent)   Earth block slide (coherent)
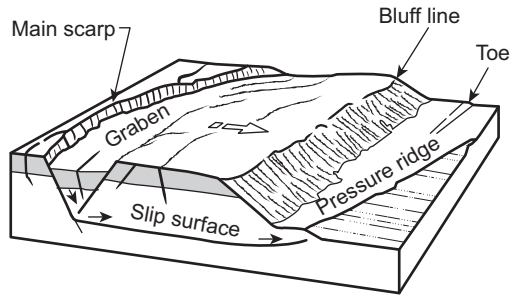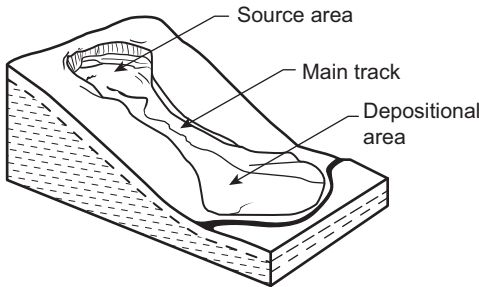
Earth flow (occurs very slow to   Debris avalanche (disruptive and
rapid and can be coherent to   occurs very rapid to extremely rapid)
disruptive in nature)

Figure 18.2 Various types of landslides.
Source: Barnes [3].

limitation of pipeline strains associated with varying levels of performance is an
ongoing area of investigation within the pipeline industry. For buried pipelines, the
parameters of interest in the seismic design are the displacement and strain under the
imposed permanent ground deformation due to foundation failure.

The American Society of Civil Engineers, ASCE (1984) [4], collected some
published systematic papers in seismic analysis and design as a standard, giving
seismic design guidelines for oil and gas pipeline systems. These guidelines provide
valuable information on seismic design considerations for pipelines, primarily

onshore-buried pipelines, and force-deformation curves of the pipe-soil interactions for pipelines buried in both clay and sand. ASCE (2001, 2002) [5], [6] also developed seismic design guidelines for onshore piping systems and buried pipes but not for petroleum pipelines and offshore pipelines. The American Society of Mechanical Engineers (ASME) states that the limit of calculated stresses due to occasional loads, such as wind or earthquake, should not exceed 80% of SMYS of the pipe, but this specification provides no guidance for the design method [7]. DNV in the code of "Submarine Pipeline Systems" [8] classifies the earthquake load into an accidental or environmental load, depending on the probability of earthquake occurrence. It also does not provide an earthquake design method for offshore pipelines [8]. However, in the selection and specification of a pipeline for a seismic design, the pipeline system may not be adequately addressed in a conventional stress-based design but a strain-based design. Considerable research efforts in the pipeline industry have been directed at understanding the behavior of pipe at high strains, with this effort increasing over the last few years with more focus on strain based design.

Pipeline Design Criteria

Longitudinal tensile strains of 3–5% for assessing the ability of pipelines to maintain pressure integrity when subjected to earthquake-generated ground displacement were recommended in ASCE (1984) [4]. The failure strains in the strain-based design are estimated usually by fracture mechanics approaches, advancements have been made from the research and practices about the strain capacities of pipeline. The longitudinal compression strain limit is defined as follows:

$$\varepsilon_{\mathrm{cp}} = 1.76 \frac{t}{D} \quad \text{and} \quad \leq 4\% \qquad [18.2]$$

Test data from the available papers are plotted in Figure 18.3, with calculated strains from Eq. [18.2].

The tests performed by Mohareb et al. (1994) [9] focused on conditions where the axial load was constant, five of the seven analysis cases utilized a constant axial load. The axial force applied in the pipe tests by Mohareb et al. corresponds to a 45°C temperature differential, a tension force equivalent to the force necessary to counteract axial shortening from the Poisson effect of internal pressure, and a compressive force to counteract the tension produced by the closed-end conditions of the test specimens. Ghodsi et al. (1994) [10] repeated the tests of Mohareb et al. but included a girth weld in the center of the test specimen to assess the impact of a girth weld on the initiation of wrinkling. Zimmerman et al. (1995) [11] carried out pipeline tests to examine postwrinkling behavior, including a relationship for compression strain limits for X70 steel. The testing program carried out by Dorey et al. (2001) [12] concentrated on the investigation of strains associated with the initiation of wrinkling. These test data, compared with Eq. [18.2], were taken past the point of wrinkle formation and development of maximum pipe moment capacity.
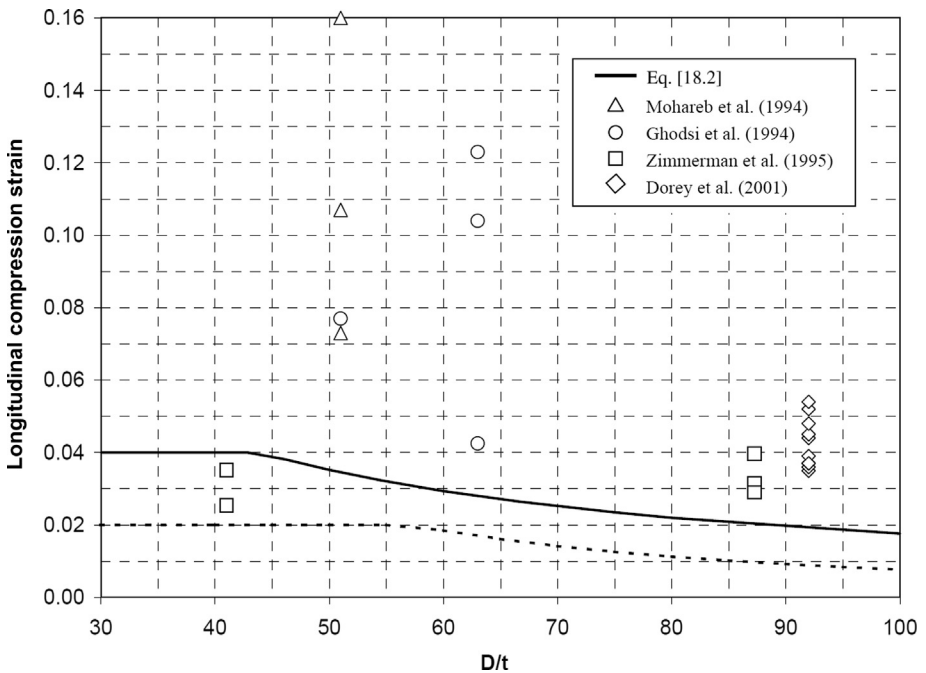
Figure 18.3 Comparison of recommended compression strain limits with test data.
Source: Honegger and Nyman [1].

The longitudinal tension strain limit for pressure integrity when evaluating pipeline response to permanent ground deformation is defined as the follows:

$$\varepsilon_{tp} \leq 4\% \tag{18.3}$$

4. Seismic Design Methodology

Several seismic analysis approaches for pipeline design were developed to predict the pipeline behavior in response to differential ground movements. Two main structural response models are considered:

- A static model for buried pipelines subjected to fault crossing due to soil failure.
- A dynamic analysis model for unburied pipelines subjected to ground wave load.

Static Analysis of Fault Crossing

Two typical analytical methods under certain assumptions were suggested for the fault crossing analysis, Newmark and Hall (1975) [13] and Kennedy et al. (1977) [14]. Kennedy and others extended the ideas of Newmark and Hall and incorporated some

improvements in the method for evaluation of the maximum axial strain. They considered the effects of lateral interaction in their analyses. The influence of large axial strains on the pipe's bending stiffness is also considered. O'Rourke and Liu (1999) [15] report that the Kennedy model for strike-slip faulting, which results in axial tension, provides the best match to ABAQUS finite element results, based on an independent comparison of the available analytical approaches. The ASCE guidelines give a detailed description of both the Newmark and Hall and Kennedy et al. schemes. It must be emphasized that both schemes are valid only for pipe under tension, since this condition may not be guaranteed under other various combined modes of fault movement.

Due to the largely nonlinear nature of the problem, a finite element analysis (FEA) is the most general tool for pipeline fault crossing design. Nonlinear finite element modeling allows accurate determination of pipeline stress and strain at various locations along the pipeline route with a wide range of parameters. The pipe-soil interaction can be modeled as discrete springs in three dimensions. The pipeline is represented as a sequence of finite straight beam elements supported on the bottom by the bearing springs. The imposed fault movement is then input into the FE model as a static displacement boundary condition. The analysis is performed to determine the equilibrium nodal position of the pipe, bending moment, axial force, strains, and stresses. The next section explains a detailed example of finite element analysis for the fault crossing using the ABAQUS software.

Ground Wave Analysis

Both permanent ground deformation and seismic ground wave can cause severe damage to unburied pipelines and connected equipment. Three basic methods are available for analyzing the responses of a structure subjected to seismic ground wave:

- Static analysis.
- Response spectra analysis.
- Time history analysis.

In general, a static analysis is sufficient for the long-term response of a structure to applied loads. However, if the duration of the applied load is short, as in the case of an earthquake, a time history dynamic analysis is required.

For the unburied pipeline, earthquake design motions are typically presented in the form of a seismic time history ground motion or a design response spectrum, which is based on the estimated ground waves and characteristics of the ground structure.

Static Analysis

The pipeline is divided into individual spans or a series of segments. Static seismic loads are considered to be in direct proportion to the weight of pipe segments. The peak acceleration from the response spectrum is applied as a lateral force distributed along the pipe, and bending stresses and support reactions are calculated. The seismic static coefficients are usually obtained from the seismic "zone," which corresponds to

a level of seismic acceleration. Many design software programs can perform static analysis, but these methods are primarily used in building seismic design.

Response Spectra Analysis

In response spectra analysis, the ground motion versus frequency method is used. The maximum acceleration for a given frequency and damping is determined based on seismic maps and soil characteristics. The higher the damping, the lower is its acceleration. The responses of displacements (translations and rotations), loads (forces and moments), and stresses at each point for each natural frequency of the system and for each direction are obtained after analysis. The calculated loads, displacements, and stresses of the piping system are typically calculated by taking the square root sum of squares of the response in each of the three directions. The response spectra method is approximate but often a useful, inexpensive method for preliminary design studies.

Time History Analysis

This analysis method involves the actual solution of the dynamic equation of motion throughout the duration of the applied load and subsequent system vibration, providing a true simulation of the system response at all times. In time history analysis, the seismic time history ground motions (displacement, velocity, or acceleration as a function of time) of seismic ground waves in three directions are applied to a finite element model of a system to obtain time history excitations of the system, including stresses, strains, and reaction forces. Time history analysis is a more accurate, more computationally intensive method than response spectrum analysis and is best suited to the transient loadings where the profile is known.

An example of time history analysis with a finite element model for the ground wave movement with ABAQUS software is detailed in the next section. ABAQUS software is the selected program to develop finite element models of ground soil, pipelines, and the subsea manifold connection because of its capability to accurately simulate solid objects, pipes, elbows, material and geometric nonlinearities, and interactions between soil and pipelines. The ABAQUS software also provides analytical models to describe the pipe-soil interaction. These models describe the elastic and perfectly plastic behavior by defining the force exerted on the pipeline and its displacement. These definitions are suitable for use with sands and clays and can be found in detail in the ASCE guidelines for the seismic design of oil and gas pipeline systems.

Seismic Level of Design

Two design levels are normally adopted for the design criteria:

- Contingency design earthquake (CDE).
- Probable design earthquake (PDE).

CDE represents a higher-level earthquake, established on the basis of a geoseismic evaluation with a typical return period of 200 to 1000 years for pipelines. The

intensity of CDE is taken as the design limits, exceeding causes of pipe failure or at least sufficient damage to cause an interruption of service. On the other hand, PDE is a lower-level earthquake, which assumes only minor damages to the pipeline system without interrupting the service. These events are likely to occur during the life of the pipeline and are therefore incorporated as part of the design environmental load. PDE is usually taken to have a return period of 50 to 100 years.

5.   Analysis Example

To explore the seismic responses of offshore pipeline systems, two study examples are presented [16]:

- The static response of a 42-inch buried pipeline to permanent ground deformations, where the pipeline is fully buried under the natural seabed.
- The dynamic response of a 42-inch unburied pipeline system to seismic waves, where the pipeline is laid on the seabed and connected to a subsea manifold.

Buried Pipeline Responses for a Fault Crossing

A buried steel pipeline with a 42-inch diameter and a 0.875-inch wall thickness, material of API 5L Grade-X65, contains oil at a specific gravity of 0.8. The pipeline is backfilled with a 3-foot sand depth median, with a density of 120 pounds per cubic foot and a friction angle of 35°.

Figure 18.4 illustrates a buried pipeline under a fault crossing due to an earthquake. The fault length in the plan direction is set as 1.2 [m], in the vertical direction, set as 1.0 [m]. A static analysis of buried pipeline was analyzed using the ABAQUS software. Here, the unanchored length varies, depending on the pipeline size and axial pipe-soil interaction force (friction force). The 1000 [m] long pipeline, with both ends fixed, is modeled by using pipe elements in the example.

Nonlinear pipeline-soil interactions in the axial, lateral, and vertical directions are modeled with pipe-soil interaction elements and soil characteristics in f_t-x_t, f_p-y_p, and f_q-z_q force-deformation curves. Based on the formulas suggested in the ASCE guidelines, the maximum axial interaction force per unit length at the pipe-soil interface, f_t, of 36.6 [kN/m], and corresponding maximum deformation, x_t, of 0.004 [m]. The maximum lateral interaction force per unit length f_p of 175.4 [kN/m], and the corresponding maximum deformation y_p of 0.08 [m]. The maximum upward interaction force per unit length f_q of 38.0 [kN/m] and the corresponding maximum deformation z_q of 0.044 [m]. The maximum downward interaction force per unit length f_q is 1450 [kN/m] and the corresponding maximum deformation z_q is 0.13 [m].

Figure 18.5 shows the displacements of the pipeline in the y and z directions under the fault crossing. The corresponding stress distribution at the bottom wall along the pipeline is shown in Figure 18.6. The maximum von Miss stress exceeds 80% of SMYS of the pipe, which does not satisfy the ASME criteria. Therefore, the designed buried pipeline is not suitable for the seismic level that can cause inputted fault distances.
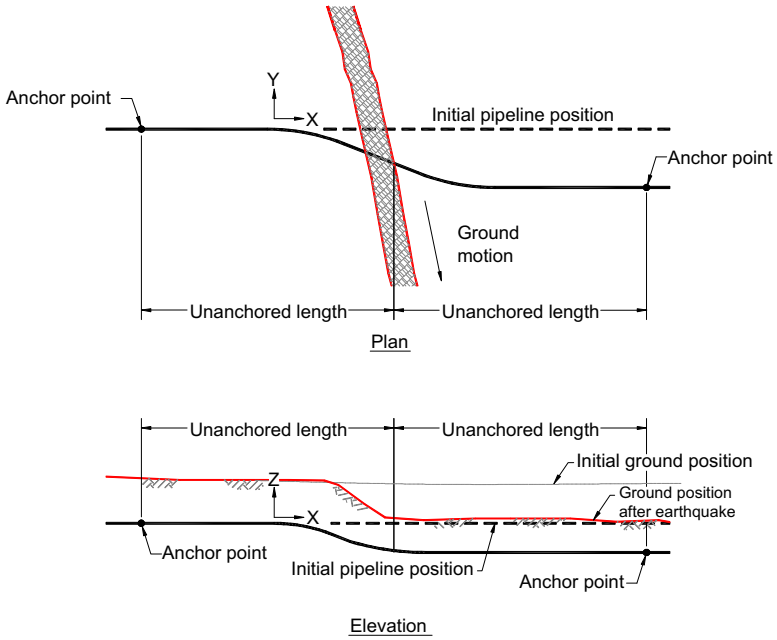
Figure 18.4 Buried pipeline under a fault crossing. (For color version of this figure, the reader is referred to the online version of this book.)
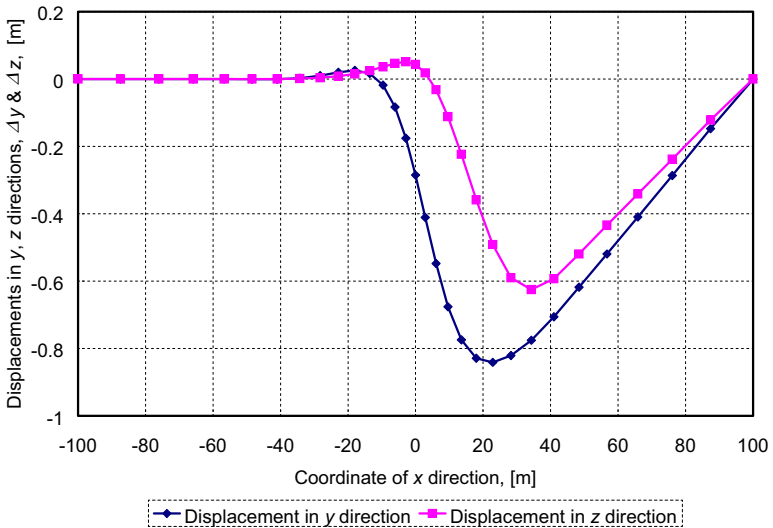
Figure 18.5 Deformations of pipeline in *y* and *z* directions. (For color version of this figure, the reader is referred to the online version of this book.)
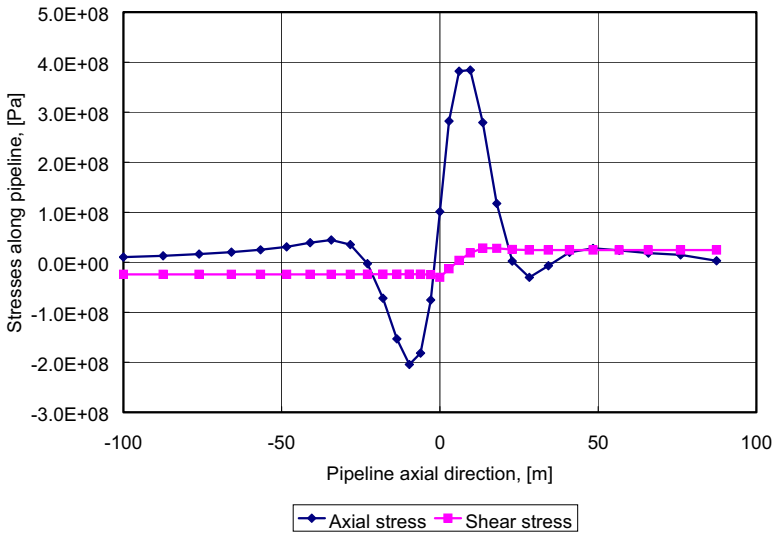
Figure 18.6 Stress distributions at the bottom wall along the pipeline. (For color version of this figure, the reader is referred to the online version of this book.)

Sensitivity calculations of different buried depths of the pipeline also show that the maximum stress and strain of the pipeline are proportional to the buried depth, when other parameters are the same. To decrease the damage of the pipeline, in the possible area of the seismic fault cross, the pipeline should not be buried.

Responses of Unburied Pipelines for a Ground Wave

A seismic dynamic analysis was performed as an example, using the ABAQUS software, for an offshore pipeline system. This pipeline system consists of two 42″ OD × 0.875″ wt (API X65 pipelines) and a 300 tonne subsea manifold, as shown in Figure 18.7. The pipelines contained oil at a specific gravity of 0.8 with an internal pressure of 600 [psi]. A settlement of 0.1 [m] for the subsea manifold due to sand liquefaction in the earthquake is considered.
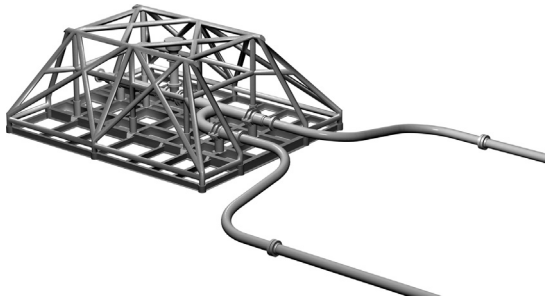
Figure 18.7 Subsea pipeline system, with a subsea manifold.

A 10-second seismic event was used in the dynamic analysis. Figure 18.8 shows the acceleration time history in the E-W, N-S, and vertical directions. The maximum accelerations are 0.34 g, 0.26 g, and 0.25 g for E-W, N-S, and vertical directions, respectively.

In the ABAQUS model, the subsea manifold is modeled as a solid box. The straight and curved pipeline sections are modeled as 3D beam elements and elbow elements, respectively. The seabed is modeled as a rigid surface with frictions in both longitudinal and lateral directions. The pipeline-soil interaction is modeled by a linear contact pressure relationship. The accelerations in three directions are applied to the seabed. As shown in Figure 18.9, the maximum Von Mises stress of 191.9 [MPa] (27.8 [ksi]) occurs at the spools. Figure 18.10 shows the time history of the maximum Von Mises stress in the pipelines.

The maximum Von Mises stress in the time history always occurs in the spool areas. The difference of natural frequencies and weights for the subsea manifold and pipelines causes the response difference between subsea manifold and pipelines. Therefore, the maximum stress occurs in the spool areas.

The seismic design and analysis methodology presented here was developed for subsea pipeline design. It has been successfully applied in seismic analyses of buried pipelines under fault crossing and unburied pipelines with a subsea manifold using a static analysis and a dynamic time history analysis. The sensitivity analysis results show that the buried depth of buried pipeline and the soil stiffness in the pipeline-soil interaction are the primary factors affecting pipeline stress in an earthquake.

6. Mitigation Methods

Several mitigation methods improve postearthquake conditions if the pipeline response is found to exceed the acceptance criteria of pipeline seismic design. The mitigation method of a subsea pipeline under seismic load is selected based on the pipeline location, expected failure mode, potential for collateral damage, risk acceptance

(a) E-W acceleration   (b) N-S acceleration   (c) Vertical acceleration
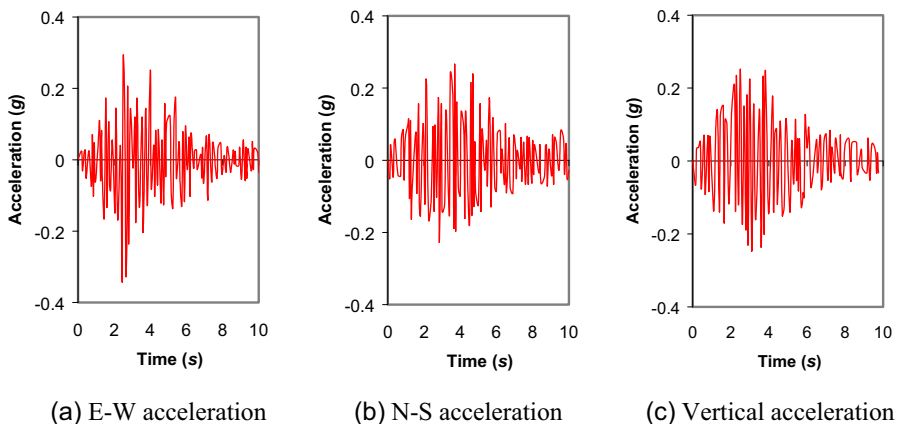
Figure 18.8 Seismic ground motions: E-W, N-S and vertical accelerations. (For color version of this figure, the reader is referred to the online version of this book.)
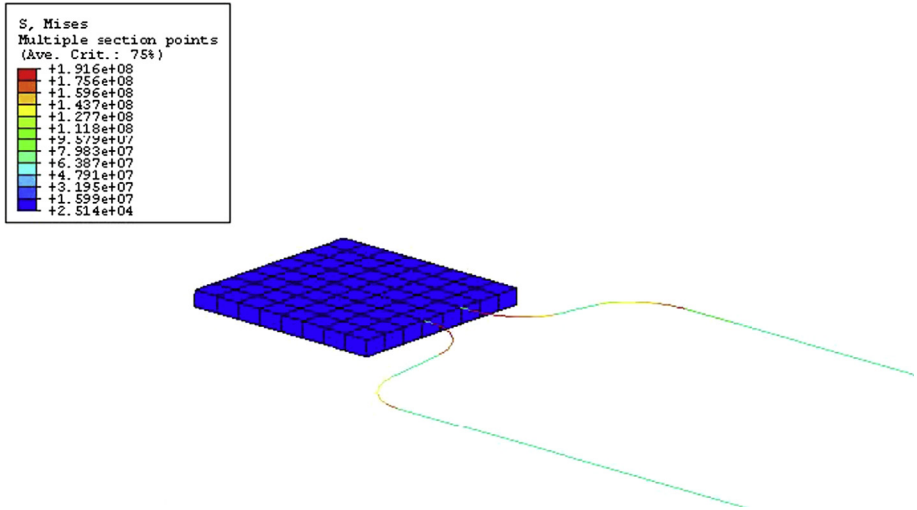
Modifying Loading and Boundary Conditions

The capacity of a buried pipeline to withstand ground displacements can be improved by minimizing the soil resistance to pipe movements, in which the most common approach is to reduce the strength of the soil surrounding the pipeline or the frictional characteristics of the pipeline. The mitigation methods for a buried pipeline include

- Place the subsea pipeline on the seabed instead of burying it to reduce the lateral soil resistance.
- Use smooth, low fiction coatings on the pipeline surface to reduce the axial soil friction resistance.
- Bury the pipeline in a shallow trench with loose backfill to release high restraints for the buried pipeline sections. However, this has limited applicability, due to other specifications and restraints for the subsea pipeline.

For the unburied pipeline, modifying the boundary condition at the pipe end is a suitable method to reduce the pipeline seismic stress.

Modifying Pipeline Configuration

The modifications also can be made by changing the welding condition, increasing the pipe wall thickness, using a high-strength steel grade for the pipe material, replacing sharp bends and elbows with induction bends or gradual pipeline field bends, and the like to increase the ability of subsea pipeline to resist the ground displacement.

The allowable longitudinal compression strain increases with the increase of the pipe wall thickness, as shown in Eq. [18.2]. The bending and axial strength of the pipeline relative to the soil also is improved. Isolation valves, automatic or remotely controlled, may be provided on each side of the zones of ground displacement to mitigate the possible pipeline ruptures.

Modifying Pipeline Route Selection

Soil loads on buried pipelines are the result of relative movement between the pipe and the surrounding soil. Select pipeline routing with suitable soil properties, as the site soil properties play an important role in the seismic analysis. In most cases, the pipeline fails due to soil instability or failure (such as land faulting, landslide, settlement, or liquefaction). Therefore, selecting a suitable pipeline route by maximizing the distance from the ground deformation zone to avoid bad geological areas and hazard helps prevent pipeline failure during strong earthquakes.

Improving Emergency Response

The normal emergency response procedures are typically inadequate for dealing with postearthquake recovery, because multiple emergencies may be occurring simultaneously. Modifying and planning for the postearthquake response procedures to address the consequences of pipeline damage need to be coordinated with local and regional government authorities, as well as key customers.

It is not sufficient to simply have an earthquake response plan. Because of the infrequent nature of earthquakes, regular earthquake simulation exercises are necessary to maintain personnel readiness and identify potential planning deficiencies. These exercises should be coordinated with local and regional planning exercises to identify coordination issues and take full advantage of current information on earthquake hazards and other earthquake damage that could risk a rapid response to pipeline damage.

References

[1] Honegger DG, Nyman DJ. Guidelines for the seismic design and assessment of natural gas and liquid hydrocarbon pipelines. Contract PR-268-9823. Pipeline Research Council International, Inc, Arroyo Grande, CA; 2005.

[2] Bonilla MG. Evaluation of potential surface faulting and other tectonic deformation. Open File Report 82-732. U.S. Geological Survey, Menlo Park, CA; 1982.

[3] Varnes DJ DJ. Slope movement types and processes, landslides analysis and control. Special Report 176. Washington, DC: Transportation Research Board, National Academy of Sciences; 1978.

[4] ASCE. Guidelines for the seismic design of oil and gas pipeline systems. Washington, DC: American Society of Civil Engineers; 1984.

[5] ASCE. Guideline for the design of buried steel pipe. Washington, DC: American Society of Civil Engineers; 2001.

[6] ASCE. Seismic Design and retrofit of piping systems. Washington, DC: American Society of Civil Engineers; 2002.

[7] ASME. Pipeline transportation systems for liquid hydrocarbons and other liquids. ASME 31.4. New York: American Society of Mechanical Engineers; 2006.

[8] DNV. Submarine pipeline systems. DNV-OS-F101. Det Norske Veritas, Norway; 2010.

[9] Mohareb ME, Elwi AE, Kulak GL, Murray DW. Deformational behavior of line pipe. Structural Engineering Report 202. Edmonton, AB, Canada: Department of Civil Engineering, University of Alberta, Canada; 1994.

[10] Ghodsi YN, Kulak GL, Murray DW. Behavior of girth-welded line pipe. Structural Engineering Report 203. Edmonton, AB, Canada: Department of Civil Engineering, University of Alberta; 1994.

[11] Zimmerman TJE, Stephens MJ, DeGreer DD, Chen Q. Compressive strain limits for buried pipelines. In: Proceedings of the 1995 Offshore Mechanics and Arctic Engineering Conference, vol. 5. New York: American Society of Mechanical Engineers; 1995. pp. 365–78.

[12] Dorey AB, Cheng JRR, Murray DW. Critical buckling strains for energy pipelines. Structural Engineering Report 237. Edmonton, AB, Canada: Department of Civil Engineering, University of Alberta; 2001.

[13] Newmark NM, Hall WJ. Pipeline design to resist large fault displacements. Proc. US National Conference on Earthquake Engineering. Ann Arbor, MI; 1975.

[14] Kennedy RP, Chow AW, Williamson RA. Fault movement effects on buried oil pipeline. J Transportation Engineering Division. ASCE 1977;103(TE5):617–33.

[15] O'Rourke MJ, Liu X. Response of buried pipelines subject to earthquake effects. Monograph No. 3. Multidisciplinary Center for Earthquake Engineering Research Buffalo, NY; 1999.

[16] Bai Q, Zeng W, Tao L. Seismic analysis of offshore pipeline systems. Offshore 2004;64(10):100–4.

19 Corrosion Prevention and Advanced CP Design

1. Introduction

Corrosion is the degradation of a metal by its electrochemical reaction with the environment. A primary cause of corrosion is an effect known as galvanic corrosion. All metals have different natural electrical potentials. When two metals with different potentials are electrically connected to each other in an electrolyte (e.g., seawater), current flows from the more active metal to the other, causing corrosion. The less active metal is called the *cathode*, and the more active, the *anode*. Figure 19.1 illustrates a basic principle of cathodic protection of a subsea pipeline system by galvanic corrosion, in which the more active metal, Zn, is the anode and the less active metal, steel, is the cathode. When the anode supplies current, it gradually dissolves into ions in the electrolyte and, at the same time, produces electrons, which the cathode receives through the metallic connection with the anode. As a result, the cathode steel is negatively polarized and, hence, protected against the corrosion.
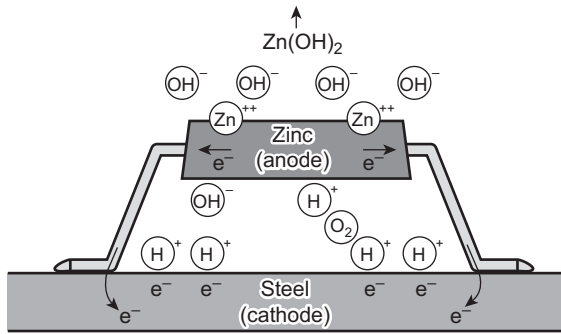
Figure 19.1 Galvanic corrosion.

Subsea rigid pipelines are susceptible to corrosion in seawater. Corrosion has become a major issue in pipeline operation, as major pipeline failures (20–40%) are due to corrosion. Degradation of the pipeline by corrosion reduces the resistance to the pressure difference between the pipeline's internal and external surfaces. The preferred technique for mitigating subsea corrosion is the use of external coatings combined with a cathodic protection (CP) system. External coatings can provide a barrier against moisture reaching the steel surface and therefore a defense against external corrosion. However, in the event of the failure of coatings, a secondary CP system is required, and the prevention of corrosion requires attention throughout the life cycle of the pipeline. The prevention methods for corrosion of subsea pipeline can be summarized as follows:

- Change the materials used for the subsea pipeline, that is, use CRA (corrosion resistant alloys) materials.
- Change the environment of pipeline, that is, use in a bundle or PIP.
- Apply barrier films or coatings.
- Use an electrochemical techniques, such as sacrficial coatings or a CP system.

This chapter deals with pipeline coatings and corrosion protection such as CP systems.

2.   Fundamentals of Cathodic Protection

Carbon steel structures exposed to natural waters generally corrode at an unaccept- ably high rate unless preventative measures are taken. Figure 19.2 shows a cathodic protection system used in subsea pipelines to reduce the corrosion speed by providing a direct current through the electrolyte to the structure.

The basic concept of cathodic protection is that the electrical potential of the subject metal is reduced below its corrosion potential, making it incapable of corroding. Cathodic protection results from cathodic polarization of a corroding metal surface to reduce the corrosion rate. The anodic and cathodic reactions for iron corroding in an aerated near neutral electrolyte are

$$Fe \rightarrow Fe^{2+} + 2e^{-}$$
[19.1]
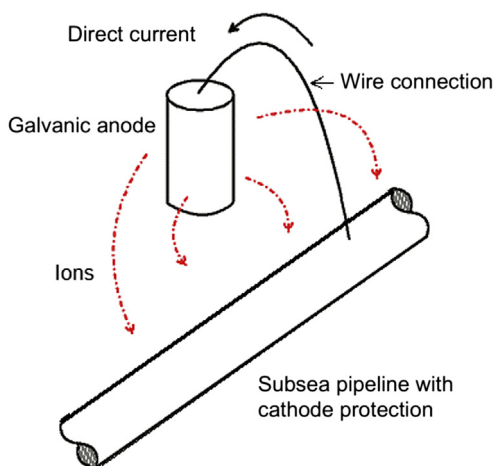
Figure 19.2 Cathodic protection of a subsea pipeline. (For color version of this figure, the reader is referred to the online version of this book.)

and

$$O_2 + 2H_2O + 4e^- \rightarrow 4OH^- \qquad [19.2]$$

respectively. As a consequence of reaction [19.2], the pH of the seawater immediate to a metal surface increases. This is beneficial because of the precipitation of solid compounds (calcareous deposits) by the reactions:

$$Ca^{2+} + HCO_3^- + OH^- \rightarrow H_2O + CaCO_3 \qquad [19.3]$$

and

$$Mg^{2+} + 2OH^- \rightarrow Mg(OH)_2 \qquad [19.4]$$
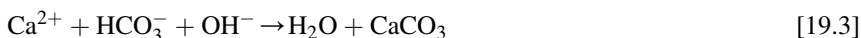
These deposits decrease the oxygen flux to the steel and hence the current necessary for cathodic protection. As a result, the service life of the entire cathodic protection system is extended.

Subsea pipelines can be protected as a cathode by achieving a potential of –0.80 $V_{Ag/AgCl}$ or more negative, which is accepted as the protective potential (E_c°) for carbon steel and low alloy steel in aerated water. Normally, it is the best if potentials negative to –1.05 $V_{Ag/AgCl}$ are avoided, because these can cause a second cathodic reaction [1]:

$$H_2O + e^- \rightarrow H + OH^- \qquad [19.5]$$

which results in (1) wasted resources, (2) possible damage to any coatings, and (3) the possibility of hydrogen embrittlement.

There are two types of cathodic protection systems: impressed current and galvanic anode. An impressed current cathodic protection (ICCP) system consists of an external power source and anodes. The external power source forces current to flow from the anode to the subsea structure through the electrolyte. The anodes used in an impressed current system are usually constructed of a relatively inert material. However, the latter (galvanic anode) has been widely used in the oil and gas industry for offshore platforms and subsea pipeline in the last 40 years because of its reliability and relatively low cost of installation and operation. The effectiveness of the cathodic protection systems allows carbon steel, which has little natural corrosion resistance, to be used in such corrosive environments as seawater, acid soils, and salt-laden concrete. However, the galvanic anodes have disadvantages of low driving voltage/current output; therefore, many anodes may be required for poorly coated subsea structures.

3.   Pipeline Coatings

Internal Coatings

The primary reason of applying internal coatings is to reduce the friction and therefore enhance flow efficiency. In addition, the application of internal coatings can improve corrosion protection, precommissioning operations, and pigging operations. Increased efficiency is achieved through lowering the internal surface roughness, since the pipe friction factor decreases with a decrease in surface roughness. In actual pipeline operation, the improved flow efficiency is observed as a reduction in pressure drop across the pipeline.

The presence of free water in the system is one cause of the corrosion of the inner pipeline. An effective coating system provides an effective barrier against corrosion attack. The required frequency of pigging is significantly reduced with a coated pipeline. The wear on pig discs is substantially reduced due to the smoother pipe's surface.

The choice of a coating is dictated by both environmental conditions and the service requirements of the line. The major generic types of coatings used for internal linings include epoxies, urethanes, and phenolics. Epoxy-based materials are commonly used internal coatings because of their broad range of desirable properties, which include sufficient hardness, water resistance, flexibility, chemical resistance, and excellent adhesion.

External Coatings

Oil and gas pipelines are protected by the combined use of external coatings and cathodic protection for pipeline external surfaces. The coating systems are the primary barrier against the corrosion, therefore highly efficient at reducing the current demand for cathodic protection. However, they do not supply sufficient electrical current to protect for a bare pipeline. Cathodic protection prevents corrosion at areas of coating breakdown by supplying electrons.

Thick coatings are often applied to subsea pipelines to minimize holidays and defects and to resist damage by handling during transport and installation. High electrical resistivity retained over long periods is a special requirement, because the cathodic protection is universally used in conjunction with coatings for corrosion control. Coatings must have good adhesion to the pipe surface to resist disbondment and degradation by biological organisms, which abound in seawater. Pipe coatings should be inspected both visually and by a holiday detector set at the proper voltage before the pipe is lowered into the water. Periodic inspection of the pipeline cathodic protection potential is used to identify the coating breakdown areas.

Coatings are selected based on the design temperature and cost. The principal coatings, in rough order of cost are

- Tape wrap.
- Asphalt.
- Coal tar enamel.
- Fusion-bonded epoxy (FBE).
- Cigarette wrap polyethylene (PE).
- Extruded thermoplastic PE and polypropylene (PP).

The most commonly used external coating for subsea pipeline is fusion-bonded epoxy. These are thin film coatings, 0.5–0.6 mm thick. They consist of thermosetting powders applied to a white metal blast-cleaned surface by electrostatic spray. The powder melts on the preheated pipe (around 230°C), flows and subsequently cures to form thicknesses of between 250 and 650 microns.

4. CP Design Parameters

This section specifies parameters to be applied in the design of cathodic protection system based on sacrificial anodes.

Design Life

The design life of the pipeline cathodic protection system is specified by the operator and covers the period from installation to the end of pipeline operation. It is normal practice to apply the same anode design life as for the offshore structures and subsea pipelines to be protected, since maintenance and repair of CP system are very costly.

Current Density

Current density refers to the cathodic protection current per unit of bare metal surface area of the pipeline. The initial and final current densities give a measure of the anticipated cathodic current density demands to achieve cathodic protection of a bare metal surface. They are used to calculate the initial and final current demands that determine the number and sizing of the anodes.

The initial design current density is necessarily higher than the average final current density, since the calcareous deposits developed during the initial phase reduces the current demand. In the final phase, the developed marine growth and calcareous layers on the metal surface reduce the current demand. However, the final design current density takes into account the additional current demand to repolarize the structure if such layers are damaged. The final design current density is lower than the initial one.

The average (or maintenance) design current density is a measure of the anticipated cathodic current density, once the cathodic protection system has attained its steady-state protection potential. This simply implies a lower driving voltage, and the average design current density is therefore lower than both the initial and final design values. Table 19.1 gives the recommended design current density used for the cathodic protection system of nonburied offshore pipelines under various seawater conditions in different standards. For bare steel surfaces fully buried in sediments, a design current density of 20 mA/m^2 is recommended irrespective of geographical location or depth.

Coating Breakdown Factor

The coating breakdown factor describes the extent of current density reduction due to the application of coating. The value $f_c = 0$ means the coating is 100% electrically insulating. $f_c = 1$ implies that the coating provides no protection.

Table 19.1 Recommended Design Current Densities for Bare Steel

Organization	Location	Water Temp. (°C)	Design Current Density (mA/m^2)		
			Initial	Mean	Final
NACE	Gulf of Mexico	22	110	55	75
	U.S. West Coast	15	150	90	100
	N. North Sea	0–12	180	90	120
	S. South Sea	0–12	150	90	100
	Arabian Gulf	30	130	65	90
	Cook Inlet	2	430	380	380
	Buried/mud zone	All	10–30	10-30	10-30
DNV	Tropical	>20	150/130	70/60	90/80
	Subtropical	12–20	170/150	80/70	110/90
	Temperate	7–12	200/180	100/80	130/110
	Arctic	<7	250/220	120/100	170/130
	Buried/mud zone	All	20	20	20
ISO	Nonburied	>20	—	70/60	90/80
		12–20	—	80/70	110/90
		7–12	—	100/80	130/110
		<7	—	120/80	170/130
		All	20	20	20

Note: DNV and ISO format: (depths less than 30 m)/(depth greater than 30 m).
Source: NACE Standard RP 0176 [2].

The coating breakdown factor is a function of the coating properties, operational parameters, and time. The coating breakdown factor, f_c, can be described as

$$f_c = k_1 + k_2 \cdot t \qquad [19.6]$$

where t is the coating life time and k_1 and k_2 are constants dependent on the coating properties.

In seawater, to account for the effect of a coating system on coating breakdown factor, four paint coating categories have been defined for practical use, based on the coating properties in DNV RP B401 [3]:

- **Category I:** One layer of primer coat, about 50 μm nominal DFT (dry film thickness).
- **Category II:** One layer of primer coat, plus a minimum of one layer of intermediate top coat, 150–250 μm nominal DFT.
- **Category III:** One layer of primer coat, plus a minimum of two layers of intermediate/top coats, minimum 300 μm nominal DFT.
- **Category IV:** One layer of primer coat, plus a minimum of three layers of intermediate top coats, minimum 450 μm nominal DFT.

The constants k_1 and k_2 used for calculating the coating breakdown factors are given in Table 19.2.

In designing the cathodic protection system, the average and final coating breakdown factors are to be calculated by introducing the design life t_r:

$$f_c(\text{average}) = k_1 + k_2 \cdot t_r / 2 \qquad [19.7]$$

$$f_c(\text{final}) = k_1 + k_2 \cdot t_r \qquad [19.8]$$

Anode Material Performance

All metals have different natural electrical potentials and corrosion potentials. When two metals with different potentials are electrically connected to each other in an

Table 19.2 Constants (k_1 and k_2) for Calculation of Paint Coating Breakdown Factors

	Coating Category			
Water Depth (m)	I $k_1 = 0.1$ k_2	II $k_1 = 0.05$ k_2	III $k_1 = 0.02$ k_2	IV $k_1 = 0.02$ k_2
0–30	0.1	0.03	0.015	0.012
>30	0.05	0.02	0.012	0.012

Source: Sunde [4].

Table 19.3 Corrosion Potentials of Metals in Seawater

Metals	Corrosion Potentials
Magnesium	High potential (most active)
Zinc	
Aluminum	
Low carbon steel	
Cast iron	
Copper	
Stainless steel	
Silver	Low potential (least active)
Gold	
Platinum	

electrolyte (e.g., seawater), the metal with high corrosion potential (anodic) is more rapidly corroded, while the metal with less corrosion potential (cathodic) tends to be protected and corrodes less. The performance of a sacrificial anode material depends on its actual chemical composition. As the potential difference between these two metals increases, the rate of galvanic corrosion increases. Table 19.3 lists the relative corrosion potentials for common metals in seawater with the most easily corroded (highest corrosion potential) on the top and the least easily corroded (lowest corrosion potential) at the bottom.

The most commonly used anode materials in subsea oil and gas production system are aluminum (Al), magnesium (Mg), and zinc (Zn). The efficiency of a galvanic anode depends on the alloy of the anode and the environment in which it is installed. The consumption of any metal is directly proportional to the amount of current discharged from its surface. Table 19.4 gives the electrochemical efficiency ε of anode materials applied in the determination of required anode mass.

The closed circuit anode potential used to calculate the anode current output should not exceed the values listed in the Table 19.5.

Resistivity

The salinity and temperature of seawater influence its resistivity. In the open sea, the salinity does not vary significantly. The temperature becomes the main factor. The

Table 19.4 Design Electrochemical Efficiency Values Sacrificial Anode Materials

Anode Material Type	Electrochemical Efficiency (Ah/kg)
Al-base	2000 (max 25°C)
Zn-base	700 (max 50°C)

Source: DNV RP B401 [3].

Table 19.5 Design Closed Circuit Anode Potentials for Sacrificial Anode Materials

Anode Material Type	Environment	Closed Circuit Anode Potential ($V_{Ag/AgCl}$ at seawater)
Al-base	Seawater	−1.05
	Sediments	−0.95
Zn-base	Seawater	−1.00
	Sediments	−0.95

Source: DNV RP B401 [3].

resistivities of 0.3 and 1.5 ohm · m are recommended to calculate the anode resistance in seawater and subsea sediments, respectively, when the temperature of surface water is between 7 and 12°C [3].

Anode Utilization Factor

The anode utilization factor indicates the fraction of anode material that is assumed to provide cathodic protection current. Performance becomes unpredictable when the anode is consumed beyond a mass indicated by the utilization factor. The utilization factor of an anode depends on the detailed anode design, in particular the dimensions and location of anode cores. Table 19.6 gives the anode utilization factor for different types of anodes [3].

5. Galvanic Anodes System Design

Selection of Anode Type

Galvanic anodes come in a variety of sizes and shapes. For subsea applications, the anodes are often sized to fit the size of the subsea structures. The ends of the anodes are equipped with welding tabs for electrical connection to the structure. Pipeline anodes are normally of the half-shell bracelet type, as shown in Figure 19.3. The

Table 19.6 Design Utilization Factors for Different Types of Anodes

Anode Type	Anode Utilization Factor
Long, slender standoff, $L > 4r$	0.90
Long, flush-mounted, $L >$ width and thickness	0.85
Short, flush-mounted	0.80
Bracelet, half-shell type	0.80
Bracelet, segmented type	0.75
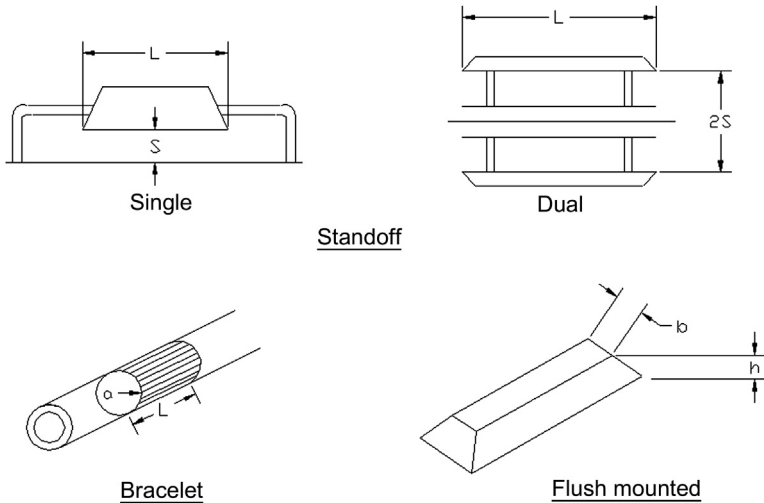
Figure 19.3 Commonly used anodes.

bracelets are clamped or welded to the pipe joints after application of the corrosion coating. Stranded connector cables are used for clamped half-shell anodes. For the anodes mounted on the pipeline with concrete, measures are taken to avoid electrical contact between the anode and the concrete reinforcement.

The major types of galvanic anodes for offshore applications are slender standoff, elongated flush mounted, and bracelet. The type of anode design to be applied is normally specified by the operator, and various factors should be taken into account, such as anode utilization factor and current output, cost of manufacturing, and installation, weight, and drag forces exerted by the ocean current. The slender standoff anode has the highest current output and utilization factor among these commonly used anodes.

Galvanic anodes must be directly attached to the subsea structures through a metallic conductor. This is achieved by one of the following methods:

- Using insulated copper wire provided by the manufacturer and welded or attached to the structure.
- Bracelet anodes clamped around the pipeline and connected to it with a welded pigtail connection.

Normally, the bracelet anodes are distributed at equal spacing along the pipeline. Adequate design calculations should demonstrate that anodes can provide the necessary current to the pipeline to meet the current density requirement for the entire design life. The potential of pipeline should be polarized to –0.8 $V_{Ag/AgCl}$ or more negative. Figure 19.4 shows the potential profile of a pipeline protected by galvanic bracelet anodes.

Since installation expense is the main part of CP design, larger anode spacing can reduce the overall cost. However, the potential is not evenly distributed
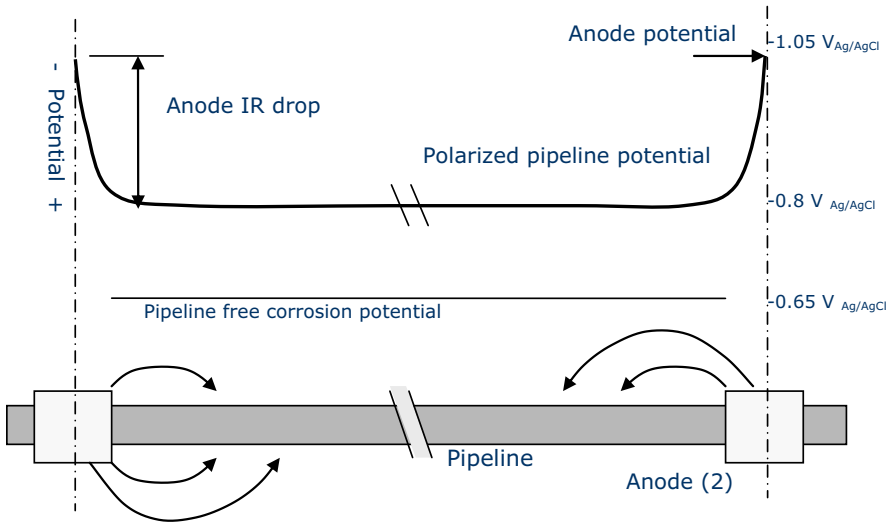
Figure 19.4 Potential profile of a pipeline protected by bracelet anodes.

along the pipeline. The pipeline close to the anode has a more negative potential. The potential of a middle point on the pipeline between two anodes is more positive and must be polarized to -0.80 $V_{Ag/AgCl}$ or more negative to achieve the cathodic protection for the whole pipeline. Increased anode spacing brings bigger mass per anode and, therefore, cause more uneven potential distribution. The potential close to the anode could be polarized to more negative than -1.05 $V_{Ag/AgCl}$, which should be avoided because of reactions. Figure 19.5 schematically illustrates the anticipated potential attenuation for situations of large anode spacing [5].

CP Design Practice

Subsea pipeline CP design includes the determination of the current demand, I_c, required anode mass, M, and number and current output per anode, I_a. The current demand is a function of cathode surface area, A_c, a coating breakdown factor, f_c, and current density, i_c; the function can be expressed as [3]

$$I_c = A_c \cdot f_c \cdot i_c \qquad\qquad [19.9]$$

where i_c depends on water depth, temperature, seawater versus mud exposure, and whether or not the mean or final life of the CP system is being evaluated. The current density i_c is normally in the range 60–170 mA/m^2 [3]. As the initial polarization period preceding steady-state conditions is normally quite short compared to the design life, the mean (time-averaged) design current density, i_c, becomes very close to the steady-state current density. Therefore, it is used to calculate the minimum mass
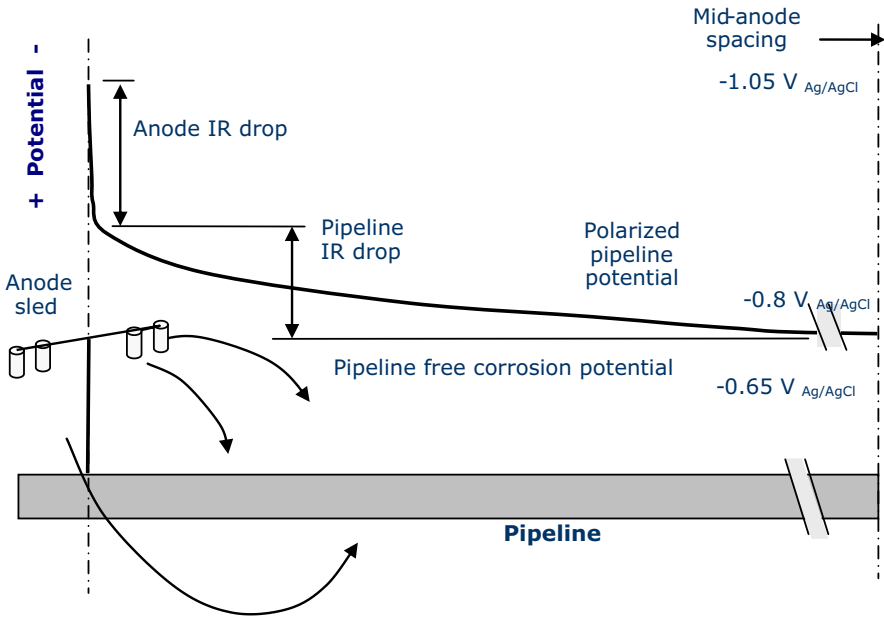
Figure 19.5 Pipeline potential profile for large anode spacing.

of anode material necessary to maintain cathodic protection throughout the design life. Correspondingly, M can be calculated as

$$M = \frac{8760 \cdot i_m \cdot T}{u \cdot C} \qquad [19.10]$$

where u is a utilization factor, C is anode current capacity, and T is design life. The cathode potential is assumed to be spatially constant. Therefore, the current output per anode can be calculated by

$$I_a = \frac{\phi_c - \phi_a}{R_a} \qquad [19.11]$$

where ϕ_c and ϕ_a are the closed circuit potential of the pipe and anode, respectively, and R_a is the anode resistance.

Anode Spacing Determination

Bethune and Hart (2000) [6] propose a new attenuation equation to modify the existing design protocol interrelating the determination of the anode spacing L_{as}, which can be expressed as

$$L_{as} = \frac{(\phi_c - \phi_a)}{\phi_{corr} - \phi_c} \cdot \frac{\alpha \cdot \gamma}{2\pi \cdot r_p \cdot R_a} \qquad [19.12]$$

where

ϕ_{corr} = free corrosion potential
α = polarization resistance
γ = reciprocal of coating breakdown factor f
r_p = pipe radius

The following assumptions are made for this approach:

- Total circuit resistance is equal to anode resistance.
- All current enters the pipe at holidays (or defects) in the coating (bare areas).
- ϕ_c and ϕ_a are constants with both time and position.

The ISO standards recommend the distance between bracelet anodes should not exceed 300 m [7].

Pipeline CP System Retrofit

Cathodic protection system retrofits become necessary as the pipeline systems age. An important aspect of such retrofitting is the determination of when such action should take place. Assessment of cathodic protection systems on pipelines is normally performed based on potential measurements. As galvanic anodes waste, their size decreases; and this causes a resistance increase and a corresponding decrease in polarization. Anodes' depletion is time dependent in the model.

Bracelet anodes have been used for cathodic protection of subsea pipelines, especially during the "early period" (roughly 1964–1976), when many oil companies had construction activities in the Gulf of Mexico. According to recent survey data, many of these early anode systems have depleted or are now depleting. Retrofitting of old anode systems on pipelines installed in the 1960s and 1970s and even newer ones is required, since these are still being used for oil transportation. Anodes can be designed as multiples or grouped together to form an anode array (anode sled). Anode arrays typically afford a good spread of protection on a subsea structure. They are a good solution for retrofitting old cathodic protection systems.

6. Internal Corrosion Inhibitors

Corrosion inhibitors are chemicals that can effectively reduce the corrosion rate of the metal exposed to the corrosive environment when added in small concentration. They normally work by adsorbing themselves to form a film on the metallic surface [8].

Inhibitors are normally distributed from a solution or dispersion. They reduce the corrosion process by either

- Increasing the anodic or cathodic polarization behavior.
- Reducing the movement or diffusion of ions to the metallic surface.
- Increasing the electrical resistance of the metallic surface.

Inhibitors used in subsea oil and gas production system are introduced into the "downhole" tubing to isolate the walls of the tubing from saltwater, corrosives gases,

crude oil, and drilling fluids often associated with oil and gas production. Inhibitors may also be used in pipeline system to mitigate internal corrosion, which are carried by oil and gas production into storage tanks and ultimately affect the coating performance of the system.

Inhibitors can be generally classified as follows [8]:

- Passivating inhibitors.
- Cathodic inhibitors.
- Precipitation inhibitors.
- Organic inhibitors.
- Volatile corrosion inhibitors.

The key to selecting an inhibitor is to know the system and anticipate the potential problems in the system. System conditions include water composition (such as salinity, ions, and pH), fluid composition (percentage water versus hydrocarbon), flow rates, temperature, and pressure. Application of the inhibitors can be accomplished by batch treatments, formation squeezes, continuous injections, or a slug between two pigs.

Inhibitor efficiency can be defined as

$$\text{Inhibitor efficiency } (\%) = \frac{\text{CR}_{\text{uninhibited}} - \text{CR}_{\text{inhibited}}}{\text{CR}_{\text{uninhibited}}} \times 100 \qquad [19.13]$$

where

$\text{CR}_{\text{uninhibited}} = $ corrosion rate of an uninhibited system
$\text{CR}_{\text{inhibited}} = $ corrosion rate of an inhibited system

Typically, the inhibitor efficiency increases with an increase in inhibitor concentration.

References

[1] Jones DA. Principles and prevention of corrosion. New York: Macmillan; 1992. pp. 437–45.
[2] NACE Standard RP 0176. Corrosion control of steel-fixed offshore platforms associated with petroleum production. Houston, TX: NACE; 1994.
[3] DNV RP B401. Cathodic protection design. Hovik: Det Norke Veritas Industry AS; 1993.
[4] Sunde ED. Earth conduction effects in transaction systems. New York: Dover Publishing; 1968. pp. 70–3.
[5] Hartt WH, Zhang X, Chu W. Issues associated with expiration of galvanic anodes on marine structures. Presented at Corrosion, paper no. 04093; 2004.
[6] Bethune K, Hartt WH. A novel approach to cathodic protection design for marine pipelines. Part II. Applicability of the slope parameter method. Presented at Corrosion, paper no.00674; 2000.
[7] ISO/TC 67/SC 2 NP 14489. Pipeline cathodic protection. Part 2. Cathodic protection of offshore pipelines. Washington, DC: International Organization for Standardization; 1993.
[8] Available at www.corrosion-doctors.org/Inhibitors/lesson11.htm.

20 Arctic Pipelines

Chapter Outline

1. Introduction

Arctic pipelines refer to the pipelines that cross permafrost terrain, where the soil or rock remains below 0°C throughout the year and is formed when the ground cools sufficiently in winter to produce a layer that persists throughout the following summer. The occurrence of permafrost depends on the heat transfer balance in the ground surface. Normally, the permafrost can be categorized in two ways [1]:

- Continuous permafrost, an area with permafrost almost everywhere.
- Discontinuous permafrost, the temperature of the permafrost just below the depth of seasonal variation is above 23°F (–5°C) or an area without permafrost greater than 10%.

The permafrost regions currently occupy about one quarter of the Earth's land area. Figure 20.1 shows the distributions of permafrost areas in Alaska with vast areas of permanently frozen ground [2]. The area underlain by permafrost and its thickness generally decrease from north to south, because the permafrost temperature generally increases. The arctic area also coves the offshore area, which mainly includes Barents Sea, the Russian Arctic, Beaufort Sea, the Canadian Arctic Islands, and the Caspian Sea. Different areas have different challenges, mostly related to the climatic and environmental conditions.

In recent decades, temperature measurements in the continuous and most of the discontinuous permafrost zones in Alaska reveal an increase in temperature. Arctic pipelines require considering heat transfer, geotechnical factors, and structural engineering factors. Freezing and thawing of water within soils along the pipeline route for a buried pipeline result in frost heave, where frost heave is the raising of a surface caused by ice in the underlying soil; generally frost heave generates stress in vertical support members of pipelines in the arctic [3]. The thaw settlement is known to be a result of ice melting in the soil. The results and loads from frost heave and thaw settlement to the arctic pipeline should be considered during pipeline design, construction, and operation.

Climate Data and Topography

The climate data could be obtained from various government stations. All these data are the basis for the arctic pipeline design, construction, and operation planning. Normally, the annual mean ground temperatures are about 2–5°C higher than the annual mean air temperatures. The ground temperatures in specific sites are affected
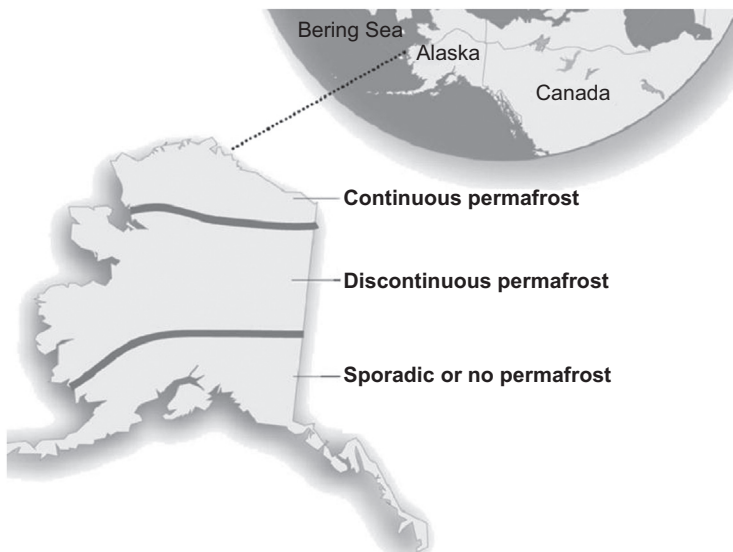
Figure 20.1 Arctic areas of Alaska permafrost coverage.

by altitude, aspect, vegetative cover, and the surface organic layer depth. Topographic data were initially obtained from the topographic maps. However, the data may be currently acquired from aerial photography.

2. Arctic Pipeline Considerations

The arctic pipeline designs of pipeline configuration, thermal insulation, and trenching requirements are influenced by the arctic environmental loading conditions. The main features of the pipeline design in arctic regions or arctic environments include pipeline environmental loadings and the limit state design for the extreme loading conditions, resulting from ice scour. *Ice scour* is generally known as a geological term for long, narrow ditches in a seabed, created by the collision of fast ice, pack ice, or the grounding of icebergs. The differences between arctic pipelines and other conventional pipelines include

- Operating temperature.
- Geotechnical loads, resulting from thaw settlement and frost heave.
- Construction surface disturbance impacts on permafrost terrain.
- Seasonal constrains on construction and maintenance activities.
- Civil construction techniques in permafrost.

The differences due to the climate conditions and ice coverage require the consideration of certain challenges in the design of arctic pipelines, which include

- Ice gouging or icebergs in shallow water.
- Strudel scour.
- Frost heave.
- Permafrost thaw settlement.
- Upheaval buckling.

Ice Scour

Ice scour, or ice gouging, of the seabed is a near-shore feature for most of the northern continents. Ice gouging faces a process through which a moving ice feature comes into contact with the seabed, as shown in Figure 20.2. As a result of environmental forces on the gouging ice feature, the keel, the lowest regions of the ice feature, interacts with the seabed and physically deforms the soil structure.

Figure 20.3 presents a schematic of the ice gouging process, where sea ice is driven by wind and current forces and tends to pile up, creating a pressure ridge. This pressure ridge has a keel extending below the water surface, and it moves with the ice sheet. Occasionally, these ice keels intrude into water with depths less than the ice keel draft and form a gouge in the seafloor soil. The ice keel not only removes soil within the gouge depth zone but also can result in plastic deformation of the soil below the base of the gouge depth.

Subsea pipelines on the seabed in such an environment may not be able to withstand the ice contact loadings and typically must be buried below predicted extreme
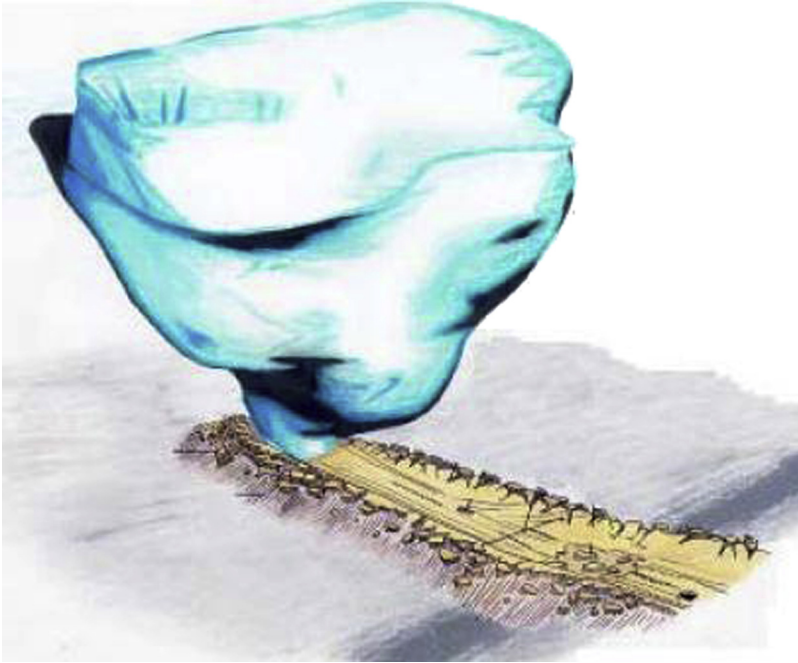
Figure 20.2 Iceberg gouging the seabed.
Source: Woodworth-Lynas [4].
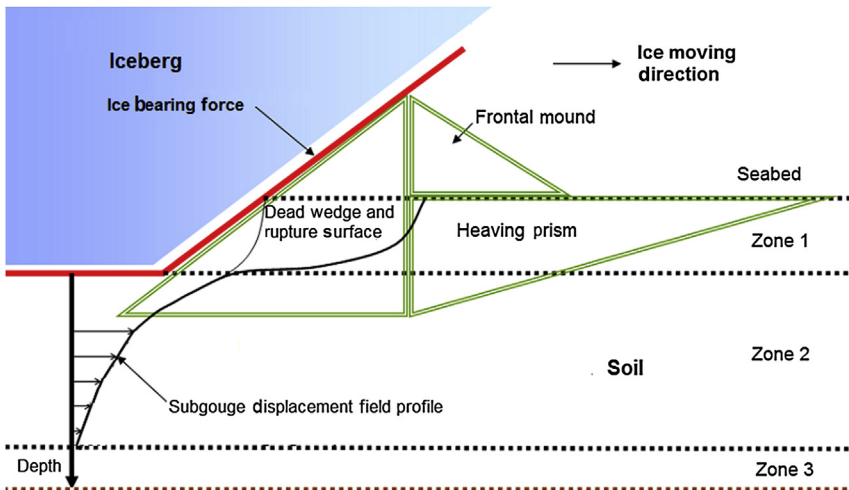
Figure 20.3 Ice-soil interaction during ice gouging.
Source: Davies et al. [5]. (For color version of this figure, the reader is referred to the online version of this book.)

ice keel scour depths for protection. Further, the pipe must be trenched sufficiently far beneath the influence zone of soil displaced below the ice keel to control pipe bending to acceptable limits. In addition, adequate route selection avoids or minimizse passage through the affected areas.

Strudel Scour

Strudel drainage may occur through holes and cracks in the ice during the overflow phase of the breakup process. The impact of the water jets induced by strudel drainage on the seabed is known as *strudel scour* [6]. Figure 20.4 illustrates a representative circular strudel drainage and scour. Strudel scours also form when a bottom fast ice sheet is typically developed near shore in arctic zones, especially during the winter. If onshore riverwater overflows the bottom fast ice sheet in the near shore zone area, it spreads offshore and drains through cracks or holes in the ice sheet. High velocity currents on the seafloor can scour seabed sediment and potentially expose and impose high current loads on a pipeline. This phenomenon, also known as *strudel scour*, results in unacceptable pipeline spans.

Frost Heave

Frost heave is the volumetric expansion of frozen soil caused by moisture migration along a temperature gradient. Water travels in thin liquid films next to soil particles from a relatively warm area to a relatively cold area. Cumulative ice expansion from the freezing of migrating water can be significant. Variables that affect the amount of expansion include freeze depth, moisture content, soil gradation (or grain size), temperature gradient, and soil pressure.
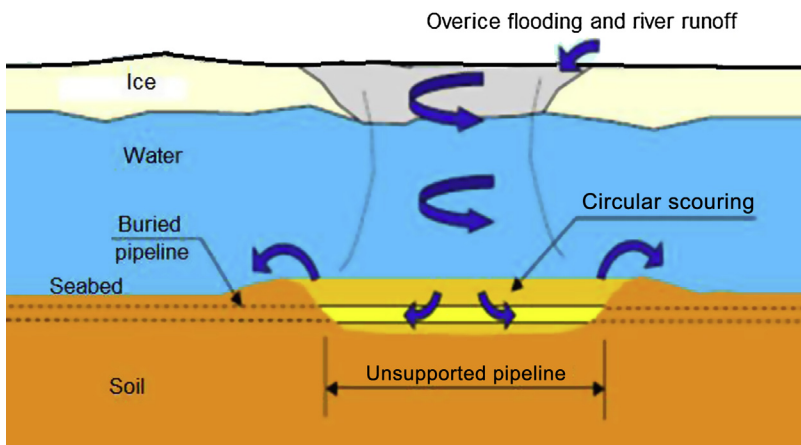
Figure 20.4 Representative circular strudel drainage and scour.
Source: Dickins et al. [7]. (For color version of this figure, the reader is referred to the online version of this book.)

Profile of cold pipeline crossing unfrozen span
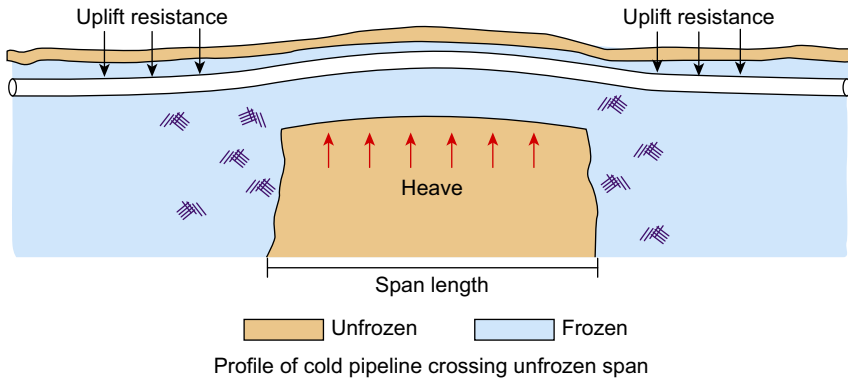
Figure 20.5 Frost heave. (For color version of this figure, the reader is referred to the online version of this book.)

As a free bulb grows around a cold buried pipeline, ice lenses form just behind the freeze front and volumetric expansion gradually pushes the pipeline upward. This movement is resisted by the frozen soil surrounding the pipe in the adjacent frozen span, as shown in Figure 20.5.

Frost heave is anticipated where unfrozen frost-susceptible soils exist in combination with other critical conditions, such as available water. Frost heave mitigation may involve removing or replacing frost-susceptible soils within the influence zone of the pipeline or providing insulation or heat to prevent the frost-susceptible soils below the pipe from freezing. A heater may be installed to raise the pipeline operating temperature above freezing and mitigate potential frost bulb development.

Thaw Settlement

Thaw settlement is a significant issue for pipeline design in the arctic area. It occurs in shallow waters and at the shore crossing, where soil-ice bonded permafrost underlies the pipeline. When the pipeline becomes operational, the temperature of the pipeline typically increasingly warms the surrounding soil and creates a permafrost thaw bulb. This may result in permafrost thaw consolidation and pipeline settlement. The settlement of pipeline depends on the thaw depth, ice content, and soil gradation. A pipeline span forms if the settlement area is adjacent to a stable thaw area. Along the settling span, the weight of the pipe, internal fluid, and soil overburden push the pipe down as the soil beneath the pipe settles. Resistance is provided by the pipe's stiffness, while outside of the settling, the span is resisted by soils beneath the pipe during the downward movement. Figure 20.6 is a schematic of thaw settlement. The differential settlement can induce considerable bending strain in the pipeline and must be accounted for in design.

Arctic pipelines in the continuously chilled regions and discontinuously permafrost regions may be operated above freezing at some time of a year. There is a potential for thaw settlement to occur in frozen, ice-rich soils where the pipeline

Profile of warm pipeline crossing unfrozen span
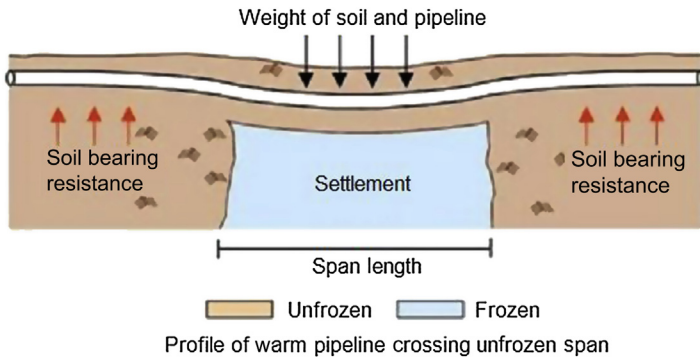
Figure 20.6 Thaw settlement. (For color version of this figure, the reader is referred to the online version of this book.)

operating temperature is above freezing. To reduce these potential impacts along the pipeline, the production may be chilled before entering the regions.

Upheaval Buckling

Arctic pipelines attempt to expand longitudinally when a buried pipeline is operated at a certain temperature higher than the installation temperature. Due to the restraint provided by the surrounding soil, the pipeline is not free to expand; hence, an axial compressive force develops. When the axial force is higher than the critical buckling load for the pipeline imperfection, this axial force moves the pipeline upward at the points of pipeline imperfections with vertical curvatures, as shown in Figure 20.7. Such points might represent imperfection of the trench bottom during the installation. The combination of pipeline stiffness, soil cover, and pipeline weight creates upheaval buckling, especially when the upward force exceeds the downward forces. The upheaval buckling is highly imperfection sensitive and may lead to high pipe bending
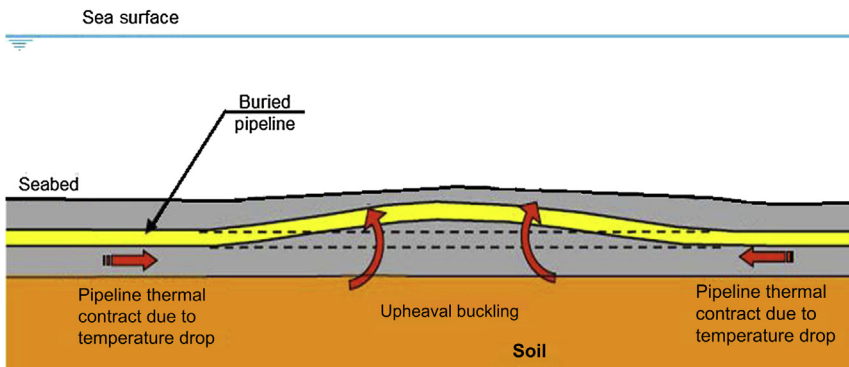
Figure 20.7 Upheaval buckling. (For color version of this figure, the reader is referred to the online version of this book.)

stresses and loss of soil cover, thus it causes the pipeline to be exposed at the mud-line level and at increased risk of impacts by ice keels [8].

It should be noted that the analysis of upheaval buckling as a potential loading condition is also applicable to pipeline design in other geographic areas; however, the great difference between installation and operation temperatures is unique to the arctic environment. To minimize the risk of upheaval buckling, several methods may be used, such as backfill or additional weight over imperfections and using limits on the pipeline profile during installation. Upheaval buckling of subsea pipelines is detailed in Chapter 11 of this book.

3. Arctic Pipeline Design Approach

General

In the 1970s and 1980s, the oil discoveries in offshore of the arctic area initiated subsea pipeline construction studies to develop installation methods of subsea pipelines through the ice to the seabed. Except for the standard operating pressure containment, the unique loading conditions associated with the arctic suggest that the traditional stress-based design would not be economically possible and the conventional pipeline design methods are impractical for arctic pipelines, in which potentially large ground movements are associated with frost heave, thaw settlement, and ice gouging, and that a certain amount of plastic deformation must be anticipated and accepted. However, the possible ground movements are a displacement-controlled loading process, and a strain-based limit state design approach can be applied.

The pipeline is designed to satisfy safety, reliability, and environmental requirements while balancing capital, operating, and maintenance costs. Some arctic pipelines are elevated to avoid warm operations in soils susceptible to high thaw strains. The pipe displacements and strains resulting from frost heave and thaw settlement may be reduced by selecting the operating temperatures for the buried pipeline design. The arctic pipeline designs to manage the effects of frost heave and thaw settlement include

- Controlling the pipeline operating temperatures.
- Changing pipeline burial depth.
- Using a thicker-walled pipe.
- Selecting pipe material that is capable of sustaining high levels of applied strain.
- Insulating the pipe.
- Using non-frost-susceptible and thaw-stable soil for overexcavating and backfilling.

Pipeline Configurations

Figure 20.8 illustrates some types of arctic pipelines, which include

- Single-walled, insulated pipelines.
- Pipe-in-pipe pipelines.
- Bundled pipelines.
- Flexible pipelines.
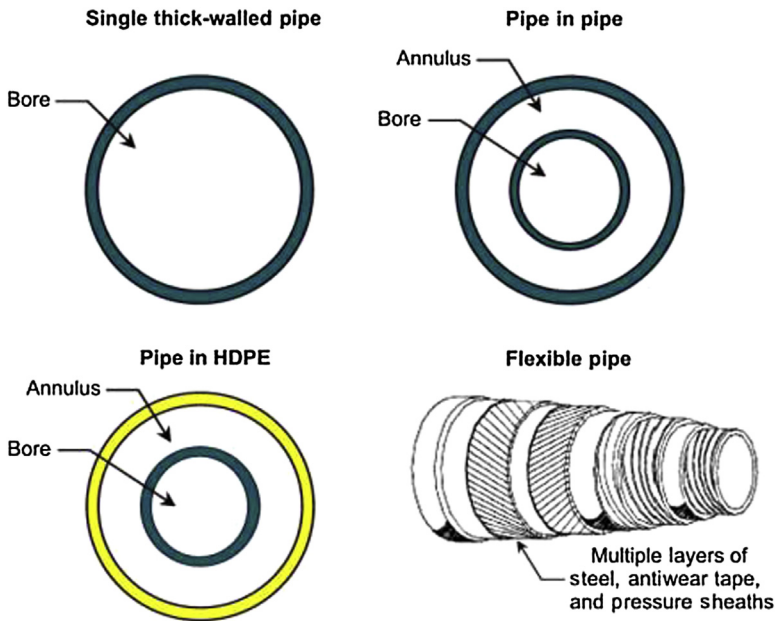
Figure 20.8 Types of arctic pipeline.
Source: DeGeer and Nessim [9]. (For color version of this figure, the reader is referred to the online version of this book.)

The most common application is the single-walled rigid pipe, consisting of a steel pipe, with external and internal corrosion coating. Internal cladding is necessary for products with corrosive content, but this is not the case for a pipeline dedicated to export oil, assuming that prior treatment has been made to permit loading on export tankers.

Pipe in pipe (PIP) and bundled flowlines have been the primary HPHT flowline design concept. The PIP and multipipe bundle systems mechanically connect one or more product inner pipes to an outer jacket pipe with structural bulkheads. The bulkheads transfer thermal expansion loads from the inner pipe to the jacket pipe. While the inner pipe expands, the jacket pipe resists expansion loads through the bulkheads. Spacing and configuration of bulkheads and internal spacers depend on the buckling potential of the inner pipe, ease of fabrication, and installation methods. PIP and bundle systems are detailed in Chapter 17 of this book.

Flexible pipe can be utilized to absorb the expansion loads and displacements at the ends of the flowline, or they can be utilized for the entire flowline to absorb expansion and relieve axial stress. Flexible pipelines have an order of magnitude higher material cost, particularly in short lengths, as a significant percentage of the cost is associated with the manufacturing setup and termination. However, installation costs are generally much lower when compared to rigid flowlines, which can exceed material costs. Flexible pipeline is detailed in Chapters 24 to 30 of this book.

Pipeline Loads

The design of subsea pipelines in arctic and northern ice environments must evaluate environmental and geotechnical load effects for potential large deformation ground movement events that may affect pipeline's mechanical integrity.

In addition to the primary loads, such as internal or external pressure to a conventional pipeline, the secondary geotechnical loads apply to arctic pipelines. However, the secondary loads of the arctic pipeline, generated by the bending deformations due to frost heave, thaw settlement, and iceberg gouging, are the displacement-controlled loads. Arctic pipelines may use the strain-based design to mitigate the secondary loads A requirement for a combination of primary and secondary loads can use a strain-based limit state design approach. Large axial strains and beyond yield are acceptable, since the pipe can safely withstand the stress-limited primary loads and the strain-limited secondary loads. The use of strain-based design codes and limit-state based design have cost savings benefits [10].

Strain Capacity and Design Criteria

The main concerning limit states to be investigated during the design of arctic pipelines are two types of limit states. One is the limit state of the rupture of a pipe wall that causes leakage of hydrocarbons, in which the ultimate limit state is thresholds beyond which pressure containment, safety, or the environment is threatened. Another one is the limit state of accident conditions where the pipeline no longer meets one or more design requirements. The serviceability limit states are reached and the normal operations are restricted, which leads to economic damage to the operator.

The goal of the limit state design is to verify the adequacy of the pipeline design against limit states and failure modes relevant to the events. The criteria from DNV OS-F101 and API RP 1111 may be considered. Criteria from these references are based mostly on the risk principles and limit state methodology.

The following limit states are to be considered for the design of arctic pipelines: compressive strain limit states for local buckling, tensile strain limit states for strain capacity, and fracture.

Compressive Strain Limit States

A local buckle or wrinkle does not result in a loss of pressure containment in a pipeline. The onset of local buckling is considered a serviceability limit state when the loading is secondary, such as displacement-controlled frost heave and thaw settlement. The strain at which the onset of local buckling or wrinkling occurs is significantly less than that required to produce a buckle of sufficient magnitude to affect the pipeline operations, such as the passage of in-line inspection tools (pig). There is also a large deformation saving between the onset of local buckling and the ultimate limit state of a rupture in a buckle. The strain capacity under compression is higher than that of the onset of local buckling, in which the limit state is determined

using empirical models and finite element structural analysis. DNV OS-F101 and API RP 1111 design codes may be applied for the calculation criteria.

Tensile Strain Limit States

When the pipe wall is under tension, the design should be based on the ultimate limit state of a tear or plastic collapse at a girth weld flaw. A longitudinal tensile fracture in a plastically strained pipeline typically initiates at a girth weld anomaly. To prevent fracture in the weld, welding procedures are developed to ensure that the weld exhibits a higher strength than the adjacent pipe. This weld strength overmatching and combining with suitable high weld toughness and pipe tensile properties results in a weld anomaly failure strain that exceeds the allowable tensile strain of 1–2% used in the pipeline design. If the weld has no anomaly, the stronger weld forcs deformation to the pipe, which has much higher strain capacity [11]. The strain capacity under tension should be determined based on fracture mechanics modeling and full-scale curved wide-plate test results.

For these strain limit states, DNV OS-F101 and API RP 1111 provide detailed calculation criteria that can be used for the arctic pipeline designs. SAFEBUCK also presents the following criterion to limit the imposed strain on a pipeline:

$$\varepsilon \le 0.3(0.97 - \mathrm{YT})$$

where ε is the applied equivalent plastic strain and YT is the maximum specified yield to tensile strength ratio of the pipeline steel.

Fracture Mechanics and Material Selection

Pipelines operating in an arctic environment require material properties suitable for operating in permafrost terrain, which include

- Fracture toughness requirements for lower operating temperatures.
- Pipe properties, including yield strength limit, stress-strain behavior, uniform elongation, yield to tensile ratio, aging effect, girth welds being stronger than the pipe.

Selection of line pipe material and specification of welding procedures are extremely important for successful arctic pipeline projects [12], [13]. For arctic service based on limit state design, the behavior of the line pipe under bending must be fully understood. An engineering criticality assessment (ECA) is usually required to establish an allowable strain level and specify allowable flaw size during welding of the line pipe. Allowable flaw sizes are increased by specifying a combination of pipe with a low SMYS, which typically provides good ductility, a special pipe chemistry, and a slight grade overmatch of the weld electrode material.

Experimental testing may be necessary to validate the limit state design capacity of the pipeline. A dedicated bend test program may be performed to check collapse and fracture limit states. Pipeline nondestructive testing (NDT) capabilities and procedures are an integral component of the design process.

For the fracture mechanics and ECA, refer to Chapter 12 for details.

Arctic Pipeline Design Procedure

The arctic pipeline design for frost heave and thaw settlement may be carried out through an iterative process in the following steps:

1. Hydraulic analysis for establishing the relationships among the pipe size, material grade, wall thickness, operating temperature, and pressure profiles.
2. Geothermal analysis to predict the potential for frost heave and thaw settlement by using an operating temperature profile. A range of route conditions based on the statistics in terrain analysis are considered as well.
3. Structural modeling to predict pipeline strain and displacement distributions resulting from predicted frost heave and thaw settlement effects over time.
4. Determination of the pipe's capability to sustain the strain and displacement through the analysis of finite element modeling and full-scale test results.
5. Comparison between the strain demands over time with the strain capacity to ensure the pipeline integrity.
6. Testing and checking the heave frost and thaw settlement displacements and freeze bulb growth to assess the environmental impacts.
7. Evaluation of the following factors to the design and maintenance of the arctic pipeline, such as temperature limits, material grade of pipeline, pipeline size, and wall thickness.
8. Repeating Step 1 until Step 7 as required.

Arctic pipeline designs also need to include parameters such as ice impact, gouging by icebergs or ice keels, assessment of uncertainty related to ice scour events, and ice-soil-pipe interaction.

Monitoring and Maintenance

Thaw settlement can occur toward the upstream station discharge where the pipeline is in a warm condition, while frost heave can occur in unfrozen sections when the operating temperature of pipeline is below 0°C.

The considerations of the pipeline integrity by establishing operating temperature guidelines include

- Pipe strain demand resulting from frost heave and thaw settlement must be less than the pipe's strain capacity.
- Material specifications must ensure the ductile properties at the minimum design temperature.

Operating, monitoring, and maintenance practices are integral to the design approach. A strain-based limit state design for an arctic pipeline requires considering the operational phase as well as the design and construction phases.

The potential monitoring and maintenance methods for managing the frost heave and thaw settlement in the pipeline integrity monitoring plan include

- Varying the operating pipeline temperature temporarily to heat the overburden and reduce the uplift resistance.
- Controlling the freeze size or thaw bulb by locally heating or cooling the soil.
- Excavating and repositioning the pipeline.

The pipeline movements may be monitored by in-line inspection tools of inertial guidance technologies. After the pipeline construction has been completed, a baseline survey should be conducted. The survey for the variations of the pipeline centerline coordinates in relation to the baseline serves as input to analysis and to identify the locations of potential excessive strain.

Other monitoring activities focus on assessing ground temperatures and ground movements leading to pipeline deformation and strain. Geotechnical loads resulting from frost heave and thaw settlement occur gradually over several years. Pipeline deformation monitoring during operations may detect local areas of frost heave and thaw settlement. An instrumented internal inspection tool, such as a "smart pig" may be used periodically to monitor the pipeline. The instrumentation includes inertial guidance and caliper capability. Monitoring should be scheduled to provide adequate time to perform maintenance to limit strain buildup resulting from displacement [14], [15].

4.   Geothermal Analysis

Geothermal Design

The mechanism of pipeline frost heave has been investigated in detail for many years. Frost heave is usually observed for pipelines carrying a product below the water freezing point. Although gas pipelines are more likely to be chilled, oil pipelines may also carry products at subfreezing temperatures. Frost heave occurs when a chilled pipeline freezes water in the frost-susceptible soil in which it is buried. As the soil freezes, it expands and forms a frost bulb around the pipe. Upward heave of the pipe is produced by swelling at the bulb face as the bulb grows. Significant pipe stresses and deformations can occur when the buried pipeline runs between a stable soil and a frost-susceptible soil. Because the pipe heaves in the frost-susceptible soil section but remains stationary in the adjacent stable soil section, a differential vertical heave displacement profile is produced across the transition between the stable and frost-susceptible soil sections.

Geothermal design considers the coupled effect of soil mechanics and heat transfer principles that the drive physical processes can affect the operational reliability and performance of the arctic pipelines [16]. Examples of these processes are

- Frost bulb formation.
- Frost heave beneath the pipe.
- Thaw bulb formation.
- Thaw settlement of the soils supporting the pipe.

The approach to frost heave analysis should combine the pipeline route soil data with climate data and pipeline thermal predictions and pipe deformation analysis. Thermal conditions of the pipeline and ground may be predicted using a coupled hydraulics -geothermal model. The geotechnical information is used to predict frost heave, and the hydraulics model predicts temperatures along the pipeline for a given throughput, inlet temperature and pressure, initial soil temperatures, and production fluid properties. The pressure and temperature of the production fluid depends on the heat flux
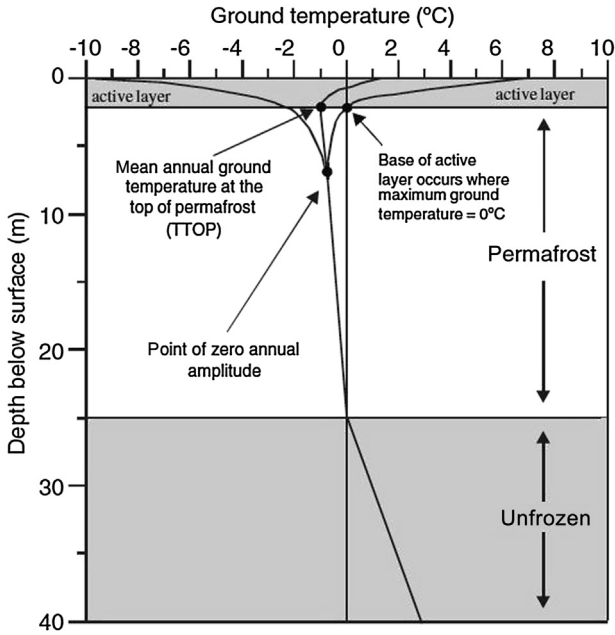
Figure 20.9 A ground temperature profile through permafrost.
Source: Wright et al. [17].

through the pipe wall, which in turn depends on the pipe interaction with the subsurface thermal state. TTOP [17] and PIPLIN [18] are industry software used for the geothermal pipeline analysis.

Figure 20.9 shows an analysis result of soil temperature distribution, which indicates that the mean annual temperature at the top of permafrost corresponds closely to the minimum temperature observed in the mean annual ground temperature.

Structural Analysis

The stresses and strains of arctic pipelines caused by the primary and secondary loads can be simulated by finite element analysis software, such as PIPLIN, or the general purpose FE software ABAQUS. The software should include the following functions:

- Anisotropic material behavior.
- Large and elastic-plastic pipe deformations.
- Elastic-plastic soil deformation.
- Load functions to characterize pipe-soil interactions.
- Transient temperature and loads.

Frost Heave

Time-dependent structural analyses were undertaken for frost heave. Loads considered in the analyses include

- Permanent loads, such as weight of pipe and soil overburden.
- Operating loads, such as temperature, pressure, and weight of fluid.
- Environmental loads, such as soil displacement as a result of frost heave.

A sensitivity analysis of the pipeline design parameters and soil properties may be conducted. These parameters include

- Soil frost susceptibility.
- Mean annual pipe temperature.
- Seasonal temperature variation.
- Peak and residual uplift resistance.
- Creep resistance.
- Longitudinal resistance.
- Wall thickness.
- Span length.

Thaw Settlement

The permanent and operating loads considered for thaw settlement were similar to frost heave. Thaw settlement is greatest in ice-rich soils. A sensitivity analysis of the design parameters may be conducted, which include

- Soil ice content.
- Compressor station discharge temperature.
- Overburden load.
- Span length.

5. Ice Scour Analysis

General

Ice scour is a complicated phenomenon that involves interaction between hydrodynamic forces, ice feature, soil medium, and the pipeline. At an earlier time, it was believed that, if direct contact between the ice and the pipeline could be avoided by setting the pipeline below the maximum gouge depth, the pipeline would be sufficiently protected. Later, experimental study revealed that, even with no direct contact with the ice, the surrounding subgouge soil deformations could affect the buried pipeline severely. Over the last two decades, the ice scour problem has been dealt with using different methods based on the available tools at the time. These include analytical and empirical formulations [19], simplified structural analyses [20], and advanced numerical techniques [21], [22].

The pipeline located in an ice scour zone is likely to be damaged by ice scour due to large soil displacement during the ice scouring process. In the ice scour load, the buried pipeline is generally considered a flexible structure and is carried by the movement of the soil. Stresses induced in seabed soil during scour are of less importance, because these are limited to the soil strength; and subsea pipelines are expected to withstand this level of stresses without excessive strains. Therefore, it is crucial to understand the mechanism of soil failure and the associated soil displacements. An ice gouge model can be used to predict the forces and the

deformations encountered by the gouging ice feature, to determine the soil displacements around or near the ice feature, and to determine the deformations and stresses encountered by a pipeline that happens to cross the ice gouge track.

The selection of the discretization method is one of the most important decisions in the development of a numerical model for the ice gouge problem. The FE method has become the most popular, advanced numerical method in the solving solid mechanics and geomechanics problems. Improving the numerical method to address large deformation pipeline-soil interactions in designing arctic pipelines narrows the margins of engineering model uncertainty and reduces target burial depth requirements, thus lowering cost and establishing improved risk estimates.

In solid mechanics, Lagrangian formulations, where a coordinate system moves with the material, are most commonly used, whereas in fluid dynamics, Eulerian formulation is almost universal. The arbitrary Lagrangian-Eulerian (ALE) formulation does not experience the mesh distortion issues encountered by the Lagrangian formulations, it is particularly well-suited for very large deformations problems. In recent years, the coupled Eulerian Lagrange (CEL) method, introduced in ABAQUS FE explicit software, has been used to study some of the important aspects of the ice gouging process, such as the subscour deformation and the ice-soil interaction forces. This method has the capacity to model fully coupled pipe-soil-ice interactions with reliable results.

ALE Method

The ALE FE ice scour model developed by Konuk et al. [22] was utilized to study the effects of the pipeline trench on the scour process and the forces transmitted to the pipeline. ALE is one of the few rigorous numerical methods for solving problems combining large deformations and large mass movements along with significant density variations. In the ALE method, the analysis undergoes three major steps:

- Conduct standard large deformation explicit Lagrangian FE analysis.
- Remap the FE mesh based on smoothing criteria.
- Compute descretized strain, mass, and momentum for each node of the new mesh using an advection algorithm based on laws of conservation.

The ALE FE ice scour model shown in Figure 20.10 was implemented in the LS-DYNA Explicit software. Typical graphical outputs from the model are illustrated in Figure 20.11. The dark color elements indicate ambient seabed soil and the trench soil is designated by a lighter color. Empty void elements are removed, and only partially or completely full soil elements are shown in the figure. It was concluded that the subscour deformations and the ice-soil reaction forces are very sensitive to the ice ridge angle, the loads transferred to the pipeline depend on the infill soil properties placed in the trench. It was shown that loads experienced by the pipeline are less for the softer infill than stiffer soils.

CEL Method

The CEL-FEA model developed by Jukes et al [23] for simulating the ice-gouging events consists basically of the following components as shown in Figure 20.12.
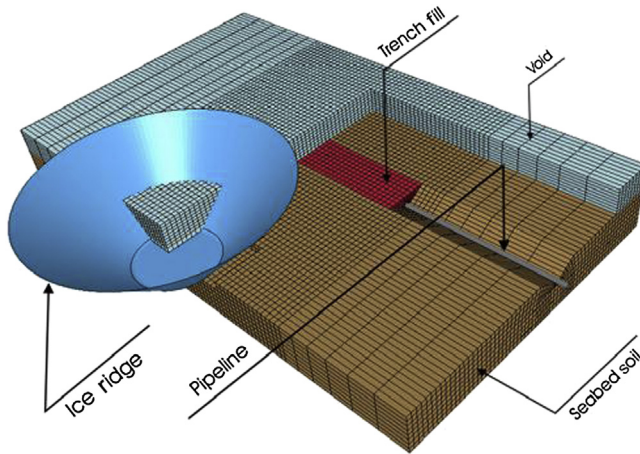
Figure 20.10 ALE FE ice scour model.
Source: Konuk et al. [22]. (For color version of this figure, the reader is referred to the online version of this book.)
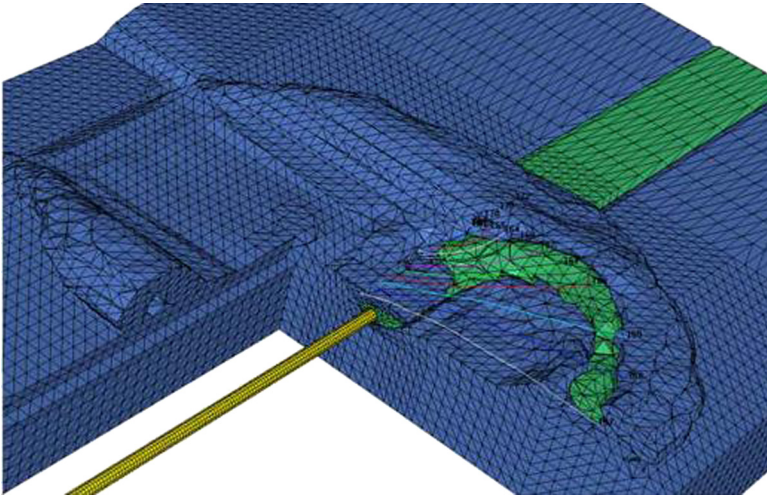
Figure 20.11 Visualization of typical output from the ALE FE model.
Source: Konuk et al. [22]. (For color version of this figure, the reader is referred to the online version of this book.)

- **Eulerian domain:** This domain encloses all materials and Lagrangian parts. In ABAQUS, initial locations of different materials may be defined within the Eulerian domain using the Volume Fraction tool. Material displaced by the translation of the iceberg may then occupy the elements that were once assigned void in subsequent time steps.
- **Lagrangian part:** The pipeline extends outside the seabed and trench material but not beyond the Eulerian domain. The pipe was modeled as a 3D deformable, homogenous,
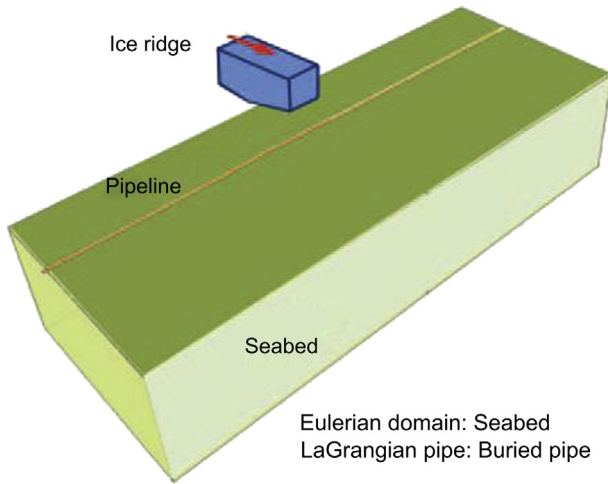
Figure 20.12 Ice-seabed-pipeline model components in CEL-FEA. (For color version of this figure, the reader is referred to the online version of this book.)

  doubly curved, general-purpose shell using a four-node, reduced integration with hourglass control (linear quadrilateral element type S4R).
- **Ice ridge:** The ice ridge was modeled as a 3D solid rigid shape. The motion of the ice ridge was determined by initial penetration depth and a prescribed velocity. A general contact with penalty-based friction was defined between the ice ridge and the soil.

Due to the quick nature of an ice-gouging even, it occurs in an undrained mode for clayey soil. A pressure independent von-Mises, Tresca, or Mohr-Coulomb plastic model with appropriate shear strain hardening is quite adequate. For sand, the response is mostly drained, despite the short duration of the event. Therefore, using a model that can capture volume change and hardening is rather essential. Drucker-Prager/Cap models and Cam Clay models that are modified to account for deformation characteristic of sand are suitable for this purpose.

In the dynamic step, the simulation of the gouging process was initiated and completed by applying the keel scouring motion at a specified gouge depth. An illustration of a gouging simulation is shown in Figure 20.13. The simulation results verify that subgouge soil and pipeline displacements are indeed influenced in varied degrees by the parameters: ice keel gouge depth, attack angle, base width, pipe diameter, pipe burial depth, and seabed soil type.

6.   Installation Techniques

Installation methods for arctic pipelines must be evaluated to identify the best candidate method with respect to many factors [24], such as

- Size and length of the pipeline.
- Duration of ice free and ice coverage seasons.
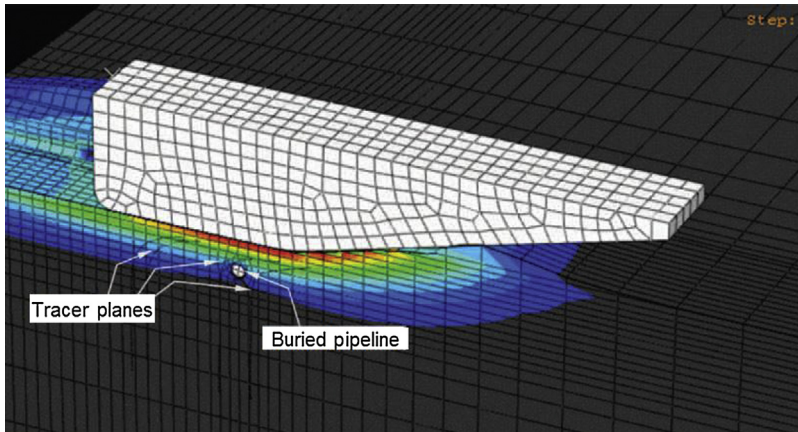
Figure 20.13 Ice gouging simulation using a 3D CEL-FEA model.
Source: Jukes et al. [23]. (For color version of this figure, the reader is referred to the online version of this book.)

- Bathymetry and ice features of the crossed areas.
- Type of shore approach.
- Underwater soil type.

Trenching

Trenching is a major technical and economic factor in arctic pipeline engineering design. For example, in the deeper waters of the Beaufort Sea, cover depths of 2 m and greater, avoiding direct ice contact, are expected. Several trenching techniques could be used during the water-open season. Some are applicable only to pretrenching, before the pipeline is installed, whereas others are best suited to post-pipeline installation. These methods include

- Conventional excavation.
- Hydraulic dredging.
- Plowing.
- Jetting.
- Mechanical trenching.

Detailed pipeline trenching and burying methods are detailed in Section 5, "Flowline Trenching and Burying," of Chapter 22.

Installation Methods

The installation methods are detailed in Chapter 33 of this book. The possible installation methods include

- Lay vessel.
- Towing and pulling.

In areas where the ice is land fast or grounded, the arctic pipelines can be assembled completely on ice and either lowered through an ice trench or towed to their final location. The ice must be thickened so that it can bear the weight of the construction equipment during pipeline installation.

An alternative method is to utilize towing and pulling under the ice through holes that are drilled through the ice along the route. Using a remotely operated vehicle, guide cables are passed and connected in advance from hole to hole before the pipe is laid on the seabed.

References

[1] Brown RJE. Distribution of permafrost in the discontinuous zone of western Canada. In: Proceedings of the Canadian Regional Permafrost Conference; December 1964.

[2] Larsen PH, Goldsmith S, Smith O, Wilson ML, Strzepek K, Chinowsky P, Saylor B. Estimating future costs for Alaska public infrastructure at risk from climate change. Burlington, MA: Elsevier: Global Environment Change; 2008.

[3] Imperial Oil Resources Ventures Limited; Application to the National Energy Board for approval of the MacKenzie Valley pipeline; IPRCC.PR.2004.05. Calgary, Canada: Imperial Oil Resources Ventures Limited; August 2004.

[4] Woodworth-Lynas CMT. The geology of ice scour. PhD thesis, University of Wales; 1992.

[5] Davies G, Marey M, Mork K. Limit state design methodology for offshore pipelines against ice gouging—Industry guideline from the ICEPIP JIP. OTC 2011; 22037.

[6] Reimnitz E E, Rodeick CR. CR, Wolf SC. Strudel scour: A unique marine geological phenomenon. J Sedimentary Petrology 1974;44:409–20.

[7] Dickins D, Hearon G, Morris K. Mapping sea ice overflood along the Alaskan north coast. ICETECH10, USA' 2009.

[8] Abdalla B, Jukes P, Eltaher A, Durron B. The technical challenges of designing oil and gas pipelines in the arctic. OCEANS 2008, Houston, TX, USA; 2008.

[9] DeGeer D, Nessim M. Arctic pipeline design considerations. In: Proceedings of the ASME 27th International Conference on Offshore Mechanics and Arctic Engineering. Estoril, Portugal: OMAE; 2008; 57802.

[10] Paulin MJ, Nixon D, Lanan GA. Environmental loadings and geotechnical considerations for the Northstar offshore pipelines. Canada: International Pipeline Conference, Calgary, AB; 2002.

[11] Wang X, et al. Strain based design—Advances in prediction methods of tensile strain capacity. International Society of Offshore and Polar Engineers. Vol. 21; No. 1, March 2011. pp. 1–7.

[12] Timms C, DeGeer D, McLamb M. Effects of a thermal coating process on X100 UOE line pipe. In: Proceedings of the ASME 24th Int. Halkidiki, Greece: Conference on Offshore Mechanics and Arctic Engineering, OMAE2005–67401; 2005.

[13] Mohr W W, Gordon R R, Smith R. Strain based design guidelines for pipeline girth welds. Proc 14th Int. Toulon, France: Offshore and Polar Eng Conference; 2004. ISOPE, Vol. 2.

[14] Smith MW, Riseborough DW. Permafrost monitoring and detection of climate change, Permafrost and Periglacial Processes, John Wiley & Sons, Ltd. vol. 7. 1996. pp. 301–9.

[15] Smith MW, Riseborough DW. Climate and the limits of permafrost: A zonal analysis. Permafrost and Periglacial Processes. vol. 13. 2002. pp. 1–15.

[16] Goodrich LE. An introduction review of numerical methods for ground thermal regime calculations. No, 106. Division of Building Research: National Research Council of Canada, Ottawa; 1982. p. 133.

[17] Wright JF, Duchesne C, Cote MM. Regional scale permafrost mapping using the TTOP ground temperature model. Ottawa, ON: Geological Survey of Canada; 2003.

[18] PIPLIN software. Available at http://www.ssdinc.com/services.htm.

[19] Reece AR, Grinsted TW. Soil mechanics of submarine ploughs. Houston, TX: Eighteenth Annual Offshore Technology Conference (OTC); 1985. Vol. 2, pp. 283–91.

[20] Palmer AC, Konuk I, Comfort G, Been K. Ice gouging and the safety of marine pipelines. OTC 1990; 6371. Houston: Offshore Technology Conference; 1990.

[21] Jukes P. Innovative pipeline and subsea engineering experience. St. Petersburg, Russia: Paper presented at the International Conference on Subsea Technology; June 2007.

[22] Konuk I, Yu S, Garcia R. A three-dimensional continuum ALE model for ice scour—Study of trench effects. OMAE 2005–67547, Halkidiki, Greece; 2005.

[23] Jukes P, Eltaher A, Abdalla B, Duron B. The design and simulation of arctic subsea pipelines—Ice gouging formulations. Oslo, Norway: Fourth annual Arctic Oil and Gas conference; 2008.

[24] Busetto G G. Arctic offshore pipelines design and installation challenges. Brussels: ARCOP Workshop, No. 4; 2004.

21 Subsea Survey and Positioning

Chapter Outline

1.   Introduction

General

The study of the subsea soil, including the subsea survey, positioning, and soil investigation, is one of the main activities for subsea field development. This chapter provides the minimal functional and technical requirements for the subsea soil issue, but these guidelines can be used as a general reference to help subsea engineers make decisions.

As part of the planned field development, a detailed geophysical and geotechnical field development survey and a soil investigation, based on the survey results, are to be performed. The purpose of the survey is to identify potential human-made hazards, natural hazards, and engineering constraints when selecting a subsea field area and flowline construction; to assess the potential impact on biological communities and to determine the seabed and subbottom conditions.

This chapter explains briefly about

- Establishing vertical route profiles, a contour plan, and the seabed features, particularly any rock outcrops or reefs.
- Obtaining accurate bathymetry, locating all obstructions, and identifying other seabed factors that can affect the development of the selected subsea field area, including laying, spanning, and stability of the pipeline.
- Carrying out a geophysical survey of the selected subsea field and route to define the shallow subseabed geology.
- Carrying out geotechnical sampling and laboratory testing to evaluate precisely the nature and mechanical properties of soils at the selected subsea field area and along the onshore and subsea pipelines and platform locations.
- Locating existing subsea equipment (for example, manifold, jumper, and subsea tree), pipelines, and cables, both operational and redundant, within the survey corridors.
- Determining the type of subsea foundation design normally used for subsea field development.

2. Subsea Survey

The subsea survey is described as a technique that uses science to accurately determine the terrestrial or 3D space position of points and the distances and angles between them in the seabed area for subsea field development.

Subsea Survey Requirements

Geophysical and geotechnical surveys are conducted to evaluate seabed and subsurface conditions to identify potential geological constraints for a particular project.

Survey Pattern for Selected Subsea Field and Each Pipeline Route

The base survey covers the whole subsea field development, which includes the infield pipelines, mobile offshore drilling unit (MOPU) footprints, pipeline end manifolds (PLEMs), manifolds, Christmas tree, umbilicals, and so forth.

The nominal width of the pipeline route survey corridor is generally 1640 ft (500 m) with a maximum line spacing of 328 ft (100 m). Different scenarios can be proposed, provided full route coverage is achieved.

Geotechnical Study

A geotechnical study is necessary to establish data that allows selecting an appropriate trenching design and equipment. It is also important to identify any possibility of hard ground, reefs, shallows, and human-made debris.

The electromagnetic properties of the soil are also of interest, and the potential effect that the ferrous content may have on the sacrificial anodes of certain subsea equipment, such as manifolds and PLEMs, needs to be assessed. A grab sample/cone penetration test (CPT) is conducted at locations determined from review of the geophysical survey. Based on the test, the characteristics of the seabed soil around the

subsea field development area can be determined. If there is a drastic change in one of the core samples, additional samples are taken to determine the changes in condition. A piezocone penetration test (PCPT) should be obtained at the MODU and PLEM locations and FSO (floating storage and offloading) anchor locations.

Samples of the geotechnical gravity core, piston core, or vibracore are obtained 5–10 m from the seabed of the subsea equipment locations, such as pipeline and PLEMs. Samples should be suitable for a laboratory test program geared toward the determination of strength and index properties of the collected specimens. On board, segments (layers) of all samples at 1-m intervals are classified by hand and described. Samples for density measurements are also taken. At least one sample from each layer is adequately packed and sent to the laboratory for index testing or sieve analysis and unconsolidated, undrained triaxial testing. Cohesion is measured on clayey parts of the core by torvane and a pocket penetrometer on board and by unconfined compression tests in the laboratory. The minimum internal diameter of the samples is generally 2.75 in. (70 mm).

Survey Vessel

The vessel proposed for survey should be compliant with all applicable codes and standards (see Figure 21.1). The vessel must follow high safety standards and comply with all national and international regulations, and the marine support must be compatible for survey and coring operations.

The survey vessels provided are collectively capable of the following:

· Minimum offshore endurance of two to three weeks.
· Operating in a maximum sea state of 2.5 to 3.5 m.

Figure 21.1 Survey vessel.
Source: GEMS [1].

- Survey at speed of 3 to 10 knots.
- Supplying the necessary communication and navigation equipment.
- Supplying minimum required survey equipment—multibeam echosounder, precision depth sounder, side-scan sonar, subbottom profiler, grab sampler/CPT, piston/vibracore coring equipment, and differential GPS (dual system with independent differential corrections).
- Supplying lifting equipment capable of safely deploying, recovering, and handling coring and geophysical equipment.
- Supplying adequate AC power to operate all geophysical systems simultaneously without interference.
- Accommodating all personnel required to carry out the proposed survey operations.
- Accommodating a minimum of two representative personnel.
- Providing office space/work area. The area is fitted with a table or desk large enough to review drawings produced on board and to allow the installation of notebook computers and printers.
- The vessel should have radio, mobile telephone, and fax equipment. This equipment should be capable of accepting a modem hookup.
- The vessel should have a satellite or cellular phone link to report the progress of the work on a daily basis. Communications with this system should not cause interference with the navigation or geophysical systems.
- At the time of mobilization, a safety audit is carried out of the nominated vessel to ensure compliance with standards typical for the area of operations or as agreed. A current load certificate is supplied for all lifting equipment to be used for the survey operations (i.e., deep towfish, coring). Safety equipment, including hard hats, safety boots, and safety glasses, should be worn during survey operations.

Survey Aides

The survey vessel is normally equipped with an A-frame and heave-compensated offshore cranes that are capable of operating the required survey equipment. Winches are used for handling sampling and testing equipment in required water depths. The winches have a freefall option if required, such as for hammer sampling and chiselling. However, the winch speed should be fully controllable to achieve safe deployment. Geotechnical sampling and testing equipment are remotely operated. The tools are guided remotely and in a safe manner off and onto the deck. The vessels have laboratory facilities and equipment that can perform routine laboratory work.

A vessel in the soil drilling mode should include the following:

- Sampling and testing equipment that is fully remotely operated.
- A pipe centralizer in the moon-pool is used.
- A pipe stab guide that is used when pipe stringing.

Gyrocompass

A gyrocompass is similar to a gyroscope, as shown in Figure 21.2. It is a compass that finds true north by using an electrically powered, fast-spinning wheel and friction

Figure 21.2 Cutaway of Anschütz gyrocompass.
Source: Anschütz [2].

forces in order to exploit the rotation of the Earth. Gyrocompasses are widely used on vessels. They have two main advantages over magnetic compasses:

A gyrocompass is similar to a gyroscope. It is a compass that finds true north by using an (electrically powered) fast-spinning wheel and friction forces to exploit the rotation of the Earth. Gyrocompasses are widely used on vessels. They have two main advantages over magnetic compasses:

- They find true north, that is, the direction of Earth's rotational axis, as opposed to magnetic north.
- They are far less susceptible to external magnetic fields, for example, those created by ferrous metal in a vessel's hull.

The gyrocompass can be subject to certain errors. These include steaming errors, in which rapid changes in course speed and latitude cause deviations before the gyro can adjust itself [3]. On most modern ships, the GPS or other navigational aid feeds into the gyrocompass, allowing a small computer to apply a correction. Alternatively, a design based on an orthogonal triad of fiberoptic or ring laser gyroscopes eliminate these errors, as they depend on no mechanical parts, instead using the principles of optical path difference to determine rate of rotation [4].

A dedicated survey gyro is installed on the vessel and interfaced to the navigation computer. During mobilization, calibration of the gyros is carried out while the vessel is at the dock.

Navigation Computer and Software

The navigation computer and software is capable of

- Simultaneous acquisition of all navigation and sensor data as interfaced.
- Generation of closures to all geophysical acquisition equipment recorders simultaneously.
- Helmsman display showing vessel and fish position, proposed pipeline route, and intended survey line.
- Producing a header sheet and fix printout containing all relevant survey constants with bathymetry and position fix information.

Personnel

In addition to the full complement of vessel operations personnel normally aboard a survey vessel, additional qualified personnel may be utilized to safely and efficiently carry out the survey and geotechnical operations. The number of personnel should be adequate to properly interpret and document all data for the time period required to complete the survey work, without operational shutdown due to operator fatigue.

Qualified personnel interpret data during the survey and make route recommendations or changes based on the information gathered. This geophysical data interpretation should be performed by a qualified marine engineering geologist or geophysicist experienced in submarine pipeline route analysis.

Subsea Survey Equipment Requirements

For the main survey vessel, survey equipment is used to meet this specification. Vessels must follow high safety standards and comply with all national and international regulations, and marine support is compatible for survey and coring operations. All survey systems are able to operate simultaneously with minimal interference.

Multibeam Echo Sounder (MBES)

The MBES, or swath echo sounder, is a high-precision method for conducting bathymetric surveys obtained at water depths and seabed gradients over the corridor along the proposed pipeline routes, as shown in Figure 21.3. During data acquisition, the data density should be sufficient to ensure that 95% of the processed bins contain a minimum of four valid depth points.

The following issues are required for subsea survey equipment:

- Equipment specifications.
- Method of integrating the system with the vessel's.
- Surface positioning system.
- Method of calibration.
- Method of postprocessing of data.
- On- and offline quality control, with particular reference to overlap swaths.

The swath bathymetric system provides coherent data across the full width of the swath. Alternatively, the portion of the swath that does not provide coherent data should be clearly identified. and the data from that portion are not be used.

Figure 21.3 MBES working model.
Source: Mayer et al. [5].

A 50% overlap of adjacent swaths is arranged to provide overlap of acceptable data for verifying accuracy. In areas where swath bathymetry overlaps occur, the resulting differences between data after tidal reduction are less than $\pm 0.5\%$ of water depth. Line spacing is adjusted according to the water depth to provide sufficient overlap (50%) between adjacent swaths to facilitate correlation of the data of the adjacent swaths.

Consideration should be given to installing a tidal gauge(s) or acquiring actual tidal data from an existing tide gauge in the area. If no nearby benchmarks of known height are available for reference, the tide gauge must be deployed for at least one lunar cycle.

Side-Scan Sonar

Side-scan sonar is a category of sonar system used to efficiently create an image of large areas of the seafloor. This tool is used for mapping the seabed for a wide variety of purposes, including creation of nautical charts and detection and identification of underwater objects and bathymetric features. Side-scan sonar imagery is also a commonly used tool to detect debris and other obstructions on the seafloor that may be hazardous to shipping or to seafloor installations for subsea field development. In addition, the status of pipelines and cables on the seafloor can be investigated using side-scan sonar. Side-scan data are frequently acquired along with bathymetric soundings and subbottom profiler data, thus providing a glimpse of the shallow structure of the seabed.

A high-precision, dual-frequency side-scan sonar system can obtain seabed information along the routes, for example, anchor/trawl board scours, large boulders, debris, bottom sediment changes, and any item on the seabed having a horizontal

dimension in excess of 1.64 ft (0.5 m). Side-scan sonar systems consist of a dual-channel tow-fish capable of operating in the water depths for the survey and contain a tracking system. The equipment is used to obtain complete coverage of the specified areas and operates at scales commensurate with line spacing, optimum resolution, and 100% data overlap.

The height of the tow-fish above the seabed and the speed of the vessel are adjusted to ensure full coverage of the survey area. The maximum tow-fish height is 15% of the range setting. Recorder settings are continuously monitored to ensure optimum data quality. Onboard interpretation of all contacts identified during the survey is undertaken by a geophysicist suitably experienced in side-scan sonar interpretation.

Subbottom Profilers

The subbottom profilers are tested under tow at each transmitting frequency available using maximum power and repetition rates for a period of half an hour.

During mobilization, the outgoing pulse from the transducer-seismic source is monitored to ensure a sharp, repeatable signature utilizing a suitably calibrated hydrophone. The monitored pulse is displayed onboard on an oscilloscope with a storage facility and a copy generated for approval. The pulse should conform to the manufacturer's specifications and a printout of the signature should be included in the final report.

A static or dynamic pulse test may be used to demonstrate a stable and repeatable seismic source signal producing a far-field signature at a tow depth of 3.28 ft (1 m):

- Pulse in excess of 1 bar meter peak to peak.
- Pulse length not exceeding 3 ms.
- Bandwidth of at least 60 to 750 Hz (–6 dB).
- Primary to secondary bubble ratio > 10:1.

High-Resolution Subbottom Profiler

A high-precision subbottom profiler system is provided and operated to obtain high-resolution data in the first 10 m of sediment. The operating frequency and other parameters are adjusted to optimize data within the first 5 m from the seafloor. Vertical resolution of less than 1 m is required.

A dual-channel "chirp" subbottom profiler may be capable of operating within the 3.5 to 10 kHz range with a pulse width selectable between 0.15 and 0.5 m and transmitting power selectable between 2 and 10 kW. The system is capable of transmitting repetition rates up to 10 Hz. Transmitting frequency, pulse length, power output, receiving frequency, bandwidth, and TVG (time varying gain) are adjustable. A heave compensator is required when using a subbottom profiler.

The system may either be collocated with the side-scan sonar system utilizing the same tracking system or hull mounted/over the side and reference the ship's navigation antenna. Onboard interpretation of sub-bottom profiler records is carried out by a geophysicist suitably experienced in interpretation of such records.

Low-Resolution Subbottom Profiler

The generic term *mini air gun* covers a range of available hardware that uses explosive release of high-pressure air to create discrete acoustic pulses within the water column of sufficient bandwidth and high-frequency components to provide medium-resolution data for engineering and geohazard assessment.

The system is capable of delivering a stable, short-duration acoustic pulse at a cycle repetition rate of 1 sec. The hydrophone comprises a minimum of 20 elements, linearly separated with an active length not exceeding 32.8 ft (10 m), with a flat frequency response across the 100 to 2000 Hz bandwidth.

Magnetometer

A magnetometer is a scientific instrument used to measure the strength and direction of the magnetic field in the vicinity of the instrument. Magnetism varies from place to place because of differences in Earth's magnetic field caused by the differing nature of rocks and the interaction between charged particles from the sun and the magnetosphere of a planet.

Magnetometers are used in geophysical surveys to find deposits of iron because they can measure the magnetic field variations caused by the deposits. Magnetometers are also used to detect shipwrecks and other buried or submerged objects.

A towed magnetometer (cesium, overhauser, or technical equivalent) has a sensor head capable of being towed in a stable position above the seabed. The sensor head comprises a three-component marine gradiometer platform synchronized to within less than 0.1 m and able to measure 3D gradient vectors. The tow position should be far enough behind the vessel to minimize magnetic interference from the vessel.

In normal operation, the sensor is towed above the seabed at a height not exceeding 5 m. In the case of any significant contacts, further profiles across such contacts may be required. In these circumstances, the magnetometer should be drifted slowly across the contact position to permit maximum definition of the anomaly's shape and amplitude.

The magnetometer has field strength coverage on the order of 24,000 to 72,000 gammas with a sensitivity of 0.01 nanotesla and is capable of a sampling rate of 0.1 sec. The equipment incorporates depth and motion sensors and operates in conjunction with a tow-fish tracking system. Onboard interpretation of all contacts made during the course of the survey should be carried out by a geophysicist suitably experienced in magnetometer interpretation.

Core and Bottom Sampler

The gravity corer, piston corer, or vibracore can be deployed over the side or through the A-frame of a vessel or operated from a crane configured with a 70 mm ID core barrel and clear plastic liners. The barrel length has 5 to 10 m barrel options.

The grab sampler can be of the Ponar or Van Veen type, which can be handled manually. Both systems are capable of operating in a water depth 135% deeper than the maximum anticipated water depth. At all core locations, up to three attempts are

made to acquire samples to the target depth of 5 to 10 m. After three unsuccessful attempts, the site is abandoned.

Positioning Systems

Offshore Surface Positioning

A differential global positioning system (DGPS) is utilized for surface positioning. A DGPS is capable of operating continually on a 24-hour basis. Differential corrections are supplied by communications satellites and terrestrial radio links. In either case, multiple reference stations are required. A dual-frequency DGPS is required to avoid problems associated with ionospheric activity.

A secondary system operates continuously with comparison between the two systems recorded along with the bathymetry data (geophysical vessel only). The two systems utilize separate correction stations, receivers, and processors. The system is capable of a positioning accuracy of less than ± 3.0 m with an update rate of better than 5 sec.

During geophysical operations, the receiver can display quality control (QC) parameters to the operator via an integral display or remote monitor. The QC parameters to be displayed include the following items:

- Fix solution.
- Pseudo-range residuals.
- Error ellipse.
- Azimuth and altitude of satellite vehicles (SVs) tracked.
- Dilution of position (DOP) error figures for fix solution.
- Identity of SVs and constellation diagram.
- Differential correction stations, position comparisons.

A transit fix at a platform, dock, or trestle near the survey area is carried out to ensure the DGPS is set up and operating correctly. The transit fix is carried out in both the clockwise and counterclockwise directions.

Underwater Positioning

An ultrashort baseline (USBL) tracking system is provided onboard the offshore survey vessel for tracking the positions and deployments of the towed, remote, and autonomous vehicles or the position determination of geotechnical sampling locations.

The positioning systems interface with the online navigation computer. All position tracking systems provide 100% redundancy (a ship-fit USBL may be backed up by a suitably high-precision portable system), encompassing a fully backed up autonomous system. In addition, a complete set of the manufacturer's spares are kept for each piece of positioning instrumentation, such that continuous operations may be guaranteed.

The system, including the motion compensator, is installed close to the center of rotation of the vessel. It incorporates both fixed and tracking head transducers to allow

the selection of the most optimum mode of performance for the known range of water depths and towing or offset positions.

The hull-mounted transducer is located so as to minimize disturbances from thrusters, machinery noise, air bubbles in the transmission channel, and other acoustic transmissions. In addition, the transponder-responder mounted on the ROV or AUV requires suitable positioning and insulation to reduce the effects of ambient noise.

A sufficient number of transponders-responders, with different codes and frequencies, are used to allow the survey operation to be conducted without mutual interference. The system should perform to an accuracy of better than 1% of slant range.

3.   Subsea Metrology and Positioning

Metrology is defined by the International Bureau of Weights and Measures (IBWM) as "the science of measurement, embracing both experimental and theoretical determinations at any level of uncertainty in any field of science and technology" [6]. This section describes the subsea positioning systems, which are integrated with the main survey computer to provide accurate and reliable absolute positioning of the surface and subsurface equipment.

Transducers

A transducer is a device for transforming one type of wave, motion, signal, excitation, or oscillation into another. Transducers are installed on board the vessels accordingly. A plan is created for the locations of all acoustic transducers and their coordinates that refers to a fixed reference point. A high-quality motion sensor (motion reference unit) is used to compensate for transducer movement.

Calibration

Calibration is the process of comparing a measuring instrument with a measurement standard to establish the relationship between the values indicated by the instrument and those of the standard. Calibration of the positioning systems, including all spare equipment, is carried out to ensure that each piece of individual equipment is working properly. Field calibration is performed during both prefield and postfield work. Depending on the length of the field work, additional field calibrations may be required during the course of the work. The following general procedures and requirements are adopted during the calibration process:

- No uncalibrated equipment, including cables and printed circuit boards, is used during any part of the position fixing.
- Each calibration setup should last for at least 20 min and the resulting data is logged for processing and reporting.
- The results of the calibrations, including relevant information on equipment settings, are presented for review and acceptance. The report includes measured minimum, maximum, mean, and standard deviations for each measurement and recommendations for operating

figures. Any odd figures, anomalies, or apparent erroneous measurements are highlighted and explained in the report. If, after further examination of results, doubt still exists as to the integrity of any equipment, the faulty equipment is replaced with similarly calibrated equipment prior to the start of the survey.

- In the event that positioning equipment must be repaired or circuit boards changed, and if such actions alter the position information, recalibration is performed.

Water Column Parameter

A water column is a conceptual column of water from surface to bottom sediments. The application of the correct speed of sound through seawater is critical to the accuracy of the acoustic positioning. Sound velocity is a function of temperature, salinity, and density. All three properties change randomly and periodically; therefore, regular measurements for velocity changes are required.

A salinity, temperature, and depth profiler is used to determine the propagation velocity of sound through seawater. The computed sound velocity value or profile is then entered into the appropriate acoustic system. All procedures need to be properly followed and the results applied correctly.

Field Procedure

A velocity value or profile is obtained at the beginning of the survey and thereafter. Observations are made at a suitable depth or intervals during descent and ascent through the water column. The velocity profile is determined with the value at common depth agreed to within ±3 m/sec; otherwise, the observation has to be repeated. The sound velocity at the sea bottom level is determined within ±1.5 m/sec. Having observed and recorded these values, a computation of the speed of sound is made.

Calibration

The temperature-salinity-depth probe has a calibration certificate verifying that it has been checked against an industrial standard thermometer in addition to testing against a calibrated saline solution. A strain gauge pressure sensor certificate is supplied.

Acoustic Long Baseline

Acoustic long baseline (LBL), also called *range/range acoustic*, navigation provides accurate position fixing over a wide area by ranging from a vessel, towed sensor, or mobile target to three or more transponders deployed at known positions on the seabed or on a structure. The line joining a pair of transponders is called a *baseline*. Baseline length varies with the water depth, seabed topography, and acoustic frequency band being used, from more than 5000 m to less than 100 m. The LBL method provides accurate local control and high position repeatability, independent of water depth. With the range redundancy that results from three or more range measurements, it is also possible to make an estimation of the accuracy of each position fix.

These factors are the principal reasons for a major increase in the utilization of this method, particularly for installation position monitoring.

LBL calibration and performance can be improved significantly by using "intelligent" transponders. These devices calibrate arrays by making direct measurements of the baselines and acoustically telemetering the data to the surface equipment for computation and display. They also reduce errors inherent in the conventional LBL due to ray-bending effects, as measurements are made close to the seabed, where propagation changes are generally slight. In addition, they can be supplied with environmental sensors to monitor the propagation conditions.

Field Procedure

The system is operated by personnel who have documented experience with LBL operations, to the highest professional standards and manufacturers' recommendations. Local seabed acoustic arrays consist of networks with at least six LBL transponders. Ultrahigh-frequency (UHF) arrays are used for the installations with the highest requirements for accurate installations.

The system includes

- A programmable acoustic navigator (PAN) unit for interrogation of LBL.
- Transponders.
- A transducer for vessel installation.
- All necessary cables and spare parts.

All equipment is interfaced to the online computer. The online computer system is able to handle the LBL readings without degrading other computation tasks. The software routines allow for the efficient and accurate use of all LBL observations and in particular deal with the problems encountered in surveying with a LBL system. The vessel's LBL transducer is rigidly mounted. The operating frequency for the required medium-frequency (MF) system is typically 19 to 36 kHz. The operating frequency for the required UHF system is typically 50 to 110 kHz. A minimum of five lines of position for each fix are available at all times.

MF-UHF LBL Transponder

The latest generation LBL transponder has the following minimum requirements (data presented as MF-UHF):

- Transducer beam shape: hemispherical-hemispherical.
- Frequency range: 19 to 36 kHz/50 to 110 kHz.
- Acoustic sensitivity: 90 dB re 1 μPa/90 to 125 dB.
- Acoustic output: 192 dB re 1 μPa at 1 m/190 dB.
- Pulse length: 4 ms/1 ms.
- Timing resolution: 1.6 μsec/8.14 μsec.
- Depth rating: according to project requirements.

At least two of the transponders in each array include depth, temperature, and conductivity options. The MF transponder includes anchor weights (minimum of 80 kg) attached to the release mechanism on the base of the unit by a strop

(preferably nylon to avoid corrosion) 1.5 to 2 m in length. A synthetic foam collar is used for buoyancy.

The UHF array setup includes frames with transponders rigidly installed in, for example, baskets 2.0 to 2.5 m above the seabed. The deployment is performed following a special procedure in accordance with the sea bottom depth. The setup is visually inspected by an ROV after installation. Concrete reference blocks or other transponder stands for MF arrays may be required.

Acoustic Short Baseline and Ultrashort Baseline

Acoustic Short Baseline

A short baseline (SBL) acoustic positioning system [7] is one of the three broad classes of underwater acoustic positioning systems used to track underwater vehicles and divers. The other two classes are ultrashort baseline and LBL systems. Like USBL systems, SBL systems require no seafloor-mounted transponders or equipment and are thus suitable for tracking underwater targets from boats or ships that are either anchored or under way. However, unlike USBL systems, which offer a fixed accuracy, SBL positioning accuracy improves with transducer spacing [8]. Therefore, where space permits, such as when operating from larger vessels or a dock, the SBL system can achieve a precision and position robustness similar to that of seafloor-mounted LBL systems, to make the system suitable for high-accuracy survey work. When operating from a smaller vessel, where transducer spacing is limited (i.e., when the baseline is short), the SBL system exhibits reduced precision.

Ultrashort Baseline

A complete USBL system consists of a transceiver, which is mounted on a pole under a ship, and a transponder-responder on the seafloor, or on a tow-fish, or ROV. A computer, or "topside unit," is used to calculate a position from the ranges and bearings measured by the transceiver.

An acoustic pulse is transmitted by the transceiver and detected by the subsea transponder, which replies with its own acoustic pulse. This return pulse is detected by the shipboard transceiver. The time from the transmission of the initial acoustic pulse until the reply is detected is measured by the USBL system and converted into a range.

To calculate a subsea position, the USBL calculates both a range and an angle from the transceiver to the subsea beacon. Angles are measured by the transceiver, which contains an array of transducers. The transceiver head normally contains three or more transducers separated by a baseline of 10 cm or less. A method called *phase differencing* within this transducer array is used to calculate the angle to the subsea transponder.

Description

SBL systems conventionally replace the large baselines formed between transponders deployed on the seabed with baselines formed between reference points on the hull of

a surface vessel. The three or four reference points are marked by hydrophones, which are typically separated by distances of 10 to 50 m and connected to a central control unit.

Seabed locations or mobile targets are marked by acoustic beacons, whose transmissions are received by the SBL hydrophones. It is more convenient than the LBL method because multiple transponder arrays and their calibration are not required; however, position accuracy is lower than the LBL method and decreases in deeper water or as the horizontal offset to a beacon increases. Additional factors such as vessel heading errors and roll and pitch errors are significant in the accuracy measurements.

In the USBL, the multiple separate SBL hull hydrophones are replaced by a single complex hydrophone that uses phase comparison techniques to measure the angle of arrival of an acoustic signal in both the horizontal and vertical planes. Thus, a single beacon may be fixed by measuring its range and bearing relative to the vessel. Although more convenient to install, the USBL transducer requires careful adjustment and calibration.

Field Procedure

A USBL system, with tracking and the latest generation fixed narrow transducer, can be used. A high-precision acoustic positioning (HIPAP) or similar system can also be used. This subsurface positioning system is integrated with the online computer system to provide an accurate and reliable absolute position for the transponders and responders.

All necessary equipment is supplied so that a fully operational USBL system can be interfaced to an online computer for integration with the surface positioning systems. It must also meet the operational requirements set forth in this section. The installation of equipment should comply with manufacturers' requirements, and special attention should be given to the following requirements:

- A system check is performed within the last 12 months prior to fieldwork. Documentation must be submitted for review.
- The installation and calibration of the acoustic positioning system should provide accuracy better than 1% of the slant range.
- The hull-mounted USBL transducer should be located so as to minimize disturbances from thrusters and machinery noise or air bubbles in the transmission channel or other acoustic transmitters.
- The USBL equipment is supplied with its own computer and display unit, capable of operating as a stand-alone system.
- The vertical reference unit (VRU) is fabricated based on recommendations by the USBL manufacturer and installed as recommended.
- The system is capable of positioning at least nine transponders and responders.

Calibration of the USBL System

Calibration and testing of the USBL and VRU should be performed according to the latest revision of the manufacturers' procedures. If any main component in the USBL

system has to be replaced, a complete installation survey and calibration of the system must be performed.

In the USBL, the multiple separate SBL hull hydrophones are replaced by a single complex hydrophone that uses phase comparison techniques to measure the angle of arrival of an acoustic signal in both the horizontal and vertical planes. Thus, a single beacon may be fixed by measuring its range and bearing relative to the vessel.

Although more convenient to install, the USBL transducer requires careful adjustment and calibration. A compass reference is required, and the bearing measurements must be compensated for the roll and pitch of the vessel. Unlike the LBL method, there is no redundant information from which to estimate position accuracy.

4.   Subsea Soil Investigation

Subsea soil investigations are performed by geotechnical engineers or engineering geologists to obtain information on the physical properties of soil and rock around the subsea field development for use in the design of subsea foundations for the proposed subsea structures. A soil investigation normally includes surface exploration and subsurface exploration of the field development. Sometimes, geophysical methods are used to obtain data about the field development. Subsurface exploration usually involves soil sampling and laboratory tests of the soil samples retrieved. Surface exploration can include geological mapping, geophysical methods, and photogrammetry, or it can be as simple as a professional diver diving around to observe the physical conditions at the site.

To obtain information about the soil conditions below the surface, some form of subsurface exploration is required. Methods of observing the soils below the surface, obtaining samples, and determining physical properties of the soils and rocks include test pits, trenching (particularly for locating faults and slide planes), boring, and in situ tests.

Offshore Soil Investigation Equipment Requirements

General

The general requirements for soil investigations are as follows:

- Drill, sample, and downhole test to a minimum of 120 m below the seabed.
- Carry out relevant seabed in-situ testing, for example, a cone penetration test to a maximum of 10 m depending on soil conditions.
- The actual sampling and subsequent handling are carried out with minimum disturbance to the sediments. The choice of sampler and sampling tubes reflects the actual sediment conditions and the requirements for the use of the sediment data. Therefore, different types of equipment are required.
- All equipment capable of electronic transmissions is designed to sustain the water pressure expected in the field.
- Records of experience with the use of the equipment and routines and procedures for interpretation of measurements for assessment of sediment parameters are documented and made available.

A detailed description of the sampling is provided as is testing equipment, which includes the following:

- Geometry and weight in air and water of all sampling and testing equipment.
- Handling of the seabed equipment over the side, over the stern, or through the moon-pool as applicable.
- Required crane or A-frame lifting force and arm length.
- Any limitations as to crane and A-frame capacity, water depth, sediment type, penetration depth, and the like.
- Zeroing of the PCPT before deployment.
- During testing, recording of the zero readings of all sensors before and after each test.

Calibration certificates for all cones are presented on commencement of operations. Sufficient spare calibrated cone tips should be provided to ensure work can be completed.

Seabed Corer Equipment

The coring equipment used should be of well-proven types and have a documented history of satisfactory operation for similar types of work. The seabed corers have a nonreturn valve at the top of the tube to avoid water ingress and sample washing out when pulling the sampler back to the surface. Both penetration and recovery are measured and recorded.

The main operational requirements for the corers are as follows:

- The corer is capable of operating on the seabed.
- The corer is monitored continuously in the water column using a transponder.

Piezocone Penetration Test

The main operational requirements for the PCPT are as follows:

- PCP equipment is capable of operating on the seabed.
- All cones are of the electric type, and cone end point resistance, sleeve friction, and pore water pressure are continuously recorded with depth during penetration.
- The PCP rig is monitored continuously in the water column using a transponder.
- Typical penetration below the seabed is up to 5 m, pending soil conditions.
- During PCPT operations, prior to the start of the penetration of the push rods into the soil, the following data are recorded—water head, the resistance at the penetrating probe, the lateral friction, and the pore pressure starting from an elevation of 1 m above the seabed.
- The penetrometer is positioned in such a way as to provide the perfect verticality of push roads.

A typical scheme for a PCPT is shown in Figure 21.4.

Drill Rig

Figure 21.5 illustrates a typical jack-up drilling rig. The drilling rig should be provided with all drill string components: the drill pipe, drill bits, insert bits, subs, crossovers, and so on. The capability for the drill string on the drilling rig to be heave
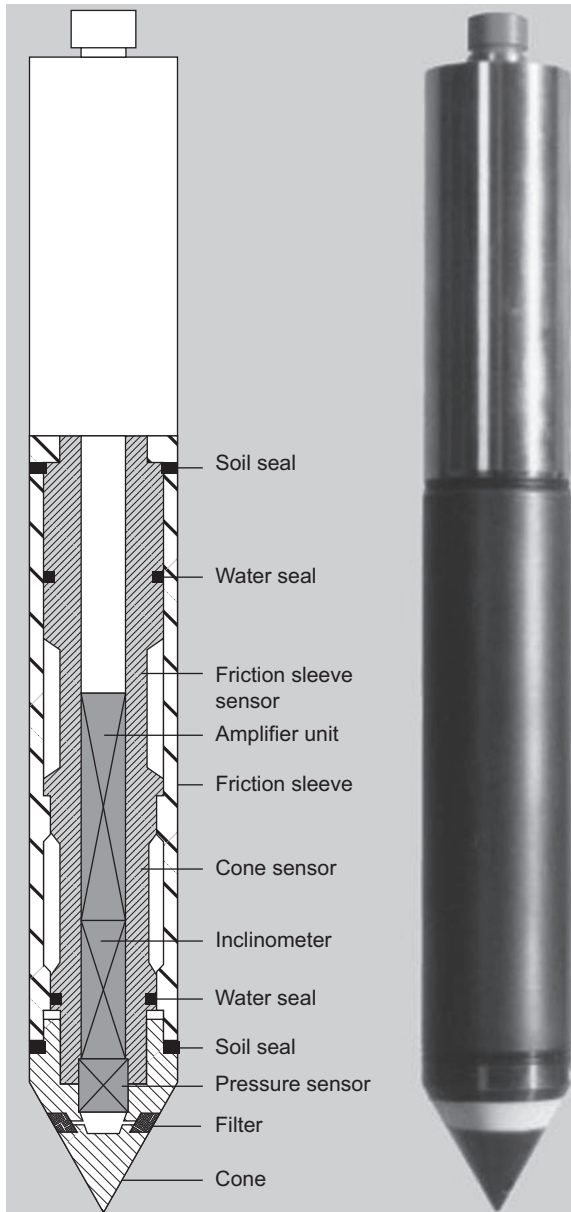
Figure 21.4 Piezocone penetration.
Source: Fugro Engineers B.V. [9].
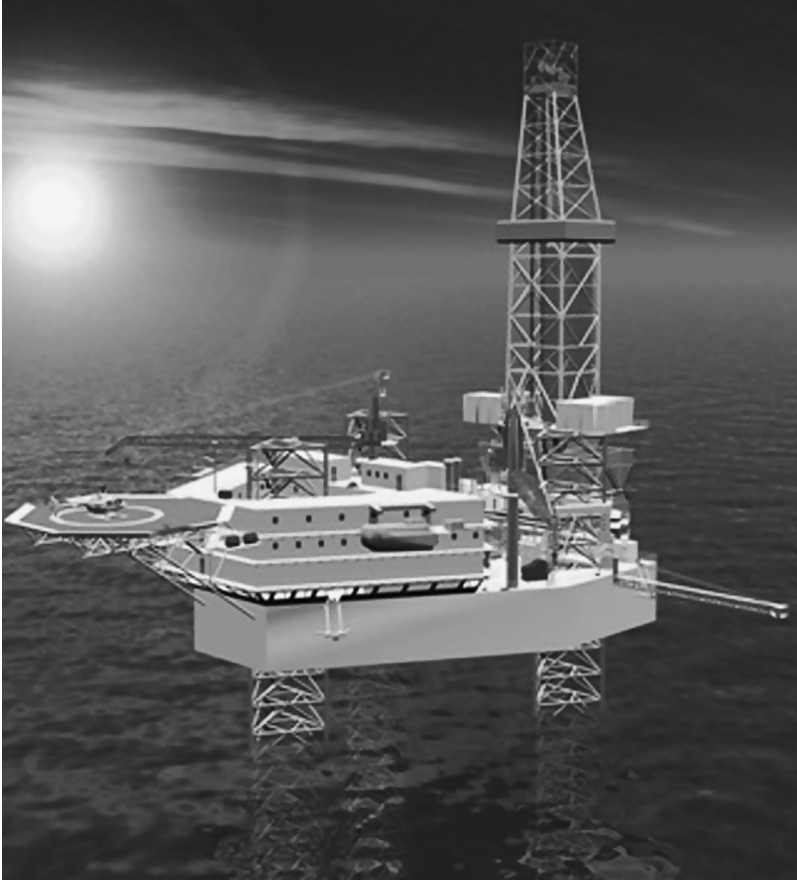
Figure 21.5 Jack-up drilling rig.

compensated, such that the drill bit has a minimum of movement while drilling and performing downhole sampling and testing, is very important.

Borings are drilled, using rotary techniques with a prepared drilling mud, from the seabed to the target depth. The objective of the borings is to obtain high-quality samples and perform in-situ testing.

Downhole Equipment

Equipment for performing sampling and testing in downhole operation mode through a drill string is relevant to the investigation:

- PCPT.
- Push sampling.
- Piston sampling.
- Hammer sampling.

An ample number of cones and sample tubes should be available. Push sampling is performed with thin-wall or thick-wall sample tubes, depending on the soil conditions. The main operational requirement for downhole equipment is that the equipment be used in the maximum relevant water and drilling depths.

Laboratory Equipment

The vessel is provided with either a room or a container to act as an offshore soil testing laboratory with sufficient equipment and personnel for 24 hour per day operation. All necessary supplies and equipment for cutting liners and sealing and waxing samples, including transportation boxes for shipping of samples to the onshore laboratory, have to be carefully provided for.

The offshore laboratory varies depending on the nature of the project. Equipment is required for performing the following types of standard laboratory tests:

- Extrusion of samples.
- Description of samples.
- Bulk density.
- Specific gravity.
- Water content.
- Shear strength of cohesive sediment.

Subsea Survey Equipment Interfaces

Sound Velocity Measurement

Velocity profiles are recorded whenever necessary to ensure that the correct speed of sound in seawater is utilized for the calibrations of the geophysical and bathymetric instruments. The velocity of sound in seawater can be calculated with a recognized formula.

All equipment is operated in accordance with manufacturers' published instructions and conforms to manufacturers' specifications. The velocity probe and winch system are capable of operating efficiently in survey water depths. Data are to be recorded on the descent to the seabed and recovery to the surface.

The instrumentation is calibrated to the standards set by the National Bureau of Standards within the 12 months prior to the mobilization date. Calibration certificates should be included with the survey procedures.

Sediment Handling and Storage Requirements

Sediment samples are carefully marked, handled, and transported. Samples from the corer are cut in 1-m sections. The core samples are then stored in a cool place but not frozen where shaking and shock are limited to a minimum. The sealed cylinders or waxed samples are clearly labeled with

- Top (nearest seabed).
- Bottom.

- A "Top Up" indicator (arrow pointing upward).
- Core location, attempt number, date, and company project number.
- Section number and depths at top and bottom.
- Length of core in meters.

An identification label is placed inside the top cap.

The sealed and marked sample cylinders and waxed samples are placed in boxes suitable for transportation. If possible, the core barrels should be stored vertically. Rooms adjacent to heavy engines or generators, which generate excessive vibrations, are avoided.

The boxes with sealed sediment material are transported to the onshore laboratory with caution and handled with care. Special precautions are made to prevent shock and impact loads to the sediment material during handling of the boxes.

The sediment must not be exposed to temperatures below $0°C$. Whether samples are air freighted or trucked to the onshore laboratory must be decided in each case.

Each cylinder and waxed sample is registered and stored for convenient retrieval.

On completion of the fieldwork, a sample log for each sample is prepared. The sample log includes the following information:

- Project number.
- Site area.
- Borehole or core number.
- Sample number.
- Water depth.
- Date of sampling.
- Type of sampler.
- Diameter of sampling tube.
- Length of core material.
- Length of sediment penetration.
- Core catcher material.
- Whether core material is extruded onboard or sealed in a tube or liner.

A short description of sediment type should be prepared based on contents in the core catcher and in each end of the liners.

Onboard Laboratory Test

The cores are cut into sections no more than 1 m in length. Disturbance of the cores is avoided during cutting and at other times. The following tests are conducted at each end of the 1-m samples:

- Pocket penetrometer.
- Torvane.
- Motorized miniature vane.

Sediment samples obtained by the Ponar or Van Veen grab sampler are described, bagged, and sealed for transportation with the cores. A motorized miniature vane measurement is conducted within the box core sample near the center of the core where the soils are undisturbed.

Core Preparation

Prior to sealing, a visual classification of the sediment types is performed. Pocket penetrometer and shear vane tests are undertaken at the top and bottom of each core section. All cores are then labeled and sample tubes are cut to minimize air space, sealed to prevent moisture loss, and stored vertically. Minimum labeling includes this information:

- Company.
- Project name.
- Core location reference number.
- Date.
- Water depth.
- Clear indications of the top and bottom of the core (e.g., use different colored caps or mark the cores "Top" and "Bottom").
- An "UP" mark indicates proper storage orientation.

Onshore Laboratory Tests

The following tests, as applicable, depending on soil types and locations, are carried out in a geotechnical laboratory on core samples sealed and undisturbed in the field as soon as possible after recovering the samples:

- Sample description.
- Sieve analysis.
- UU (unconsolidated, undrained) and triaxial (cohesive soil).
- Miniature vane (cohesive soil).
- Classification tests (Atterberg limits, water content, submerged unit weight).
- Carbonate content.
- Ferrous content.
- Thermal properties.
- Organic matter content.
- Hydrometer.

The onshore laboratory program is approved prior to commencement of testing.

Near-Shore Geotechnical Investigations

To carry out geotechnical investigations in near-shore areas, a self-elevating jack-up is fully utilized or, as an alternative, an anchored barge for drilling operations in up to 20 m of water depth (WD) and as shallow as 2 m of WD. The general requirements for certification, integrity, and safe, efficient working described in preceding sections are applied. In addition, the acceptable sanitary conditions and messing conditions are guaranteed, which can reduce the impaction of environment in near-shore areas.

For support of the geotechnical drilling unit, any small boat operations should comply with the following guidelines:

- Small boats are equipped with spare fuel, basic tool kit, essential engine spares, radar reflector, portable radio, mobile telephone, potable water, first aid kit, and distress signals or flares (secure in a waterproof container).

- Small boats are driven only by members of the crew or other personnel who have undergone a specialized small boat handling course.

References

[1]   GEMS. Vessel specification of MV Kommandor Jack. Available at: www.gems-group. com.
[2]   Anschü tz KF. Cutaway of Anschütz gyrocompass. Available at: en.wikipedia.org /wiki/ Gyrocompass.
[3]   Gyrocompass. Available at: www.navis.gr/navaids/gyro.htm.
[4]   House DJ. Seamanship techniques: Shipboard and marine operations. Elsevier Butterworth-Heinemann. UK: Oxford; 2004.
[5]   Mayer L, Li Y, Melvin G. 3D visualization for pelagic fisheries research and assessment, ICES. J Marine Sci 2002:59.
[6]   Isaev BM. Measurement techniques, vol. 18, no 4. New York: Plenum Publishing Co; 2007.
[7]   Milne PH. Underwater acoustic positioning systems. Houston, TX: Gulf Publishing; 1983.
[8]   Christ RD, Wernli RL. The ROV Manual, advantages and disadvantages of positioning systems. Butterworth-Heinemann. UK: Oxford; 2007.
[9]   Fugro Engineers BV. Specification of piezo-cone penetrometer. Available at: www.fugro-singapore.com.sg.

22 Route Optimization, Shore Approach, Tie-In, and Protection

Chapter Outline

1.   Introduction

Over the last several decades the installation equipment used in the subsea shallow and deepwater engineering has been developed to meet the needs of the industry and the harsh environmental conditions. The available equipment and its associated capabilities and limitations play a major role in the construction of subsea pipelines [1].

This chapter outlines some of the construction items of subsea pipelines, which are discussed in the following sections:

- Route optimization.
- Shore approach.
- Pipeline tie-ins.
- Pipeline trenching and burying.
- Pipeline rock dumping.

2.   Pipeline Routing

Introduction

The selection of a subsea pipeline route involves technical and economic assessments of alternative routes performed during the conceptual design phase. The actual selection of a final pipeline route in the detail design phase is usually an iterative process, often involving discussion with several third parties, and this process may continue well into the whole design phase. If the routing selection lacks sufficient data, a preliminary route survey is often required to fulfill that need.

General Principles

Route selection is a complex procedure, which can be governed by numerous factors. Apparently, the shortest distance between the terminal points is likely to be the most economic from a material standpoint. However, in practice, many factors may influence the final selection and optimization of a subsea pipeline route, and each must be considered during the conceptual or detailed project design phases. Typically, the route selection is affected by

- End point locations and seabed obstructions (such as platforms, wells, wrecks, other pipelines and cables). For fixed obstructions, 500 m minimum clearance is suggested, The number of pipeline and umbilical crossings should be minimized, and the existing pipelines are preferably crossed perpendicularly with the minimum angle of 30°. Pipelines should be corridored with a separation of 50 to 100 m, if possible, and anchoring and dropped object zones should be avoided.
- Water depths and topography of the seabed (to avoid such features as sand waves or ridges, rocks, mud slides, mud volcanoes, and iceberg scars, where possible).
- Presence of adverse environmental features, such as high currents, shoaling waves. In designing a shore approach, normally the pipeline route is a curved line with the pipeline being perpendicular to the shoreline, which gives the shortest beach pull between the laying barge and shoreline, and the wave loads on the pipeline are minimized.
- Presence of other fields, pipelines, structures, large rocks, and prohibited zones (e.g., military exercise zones and minefields).
- Presence of unfavorable shipping or fishing activity.
- Construction constraints with regards to maximum water depths layable for specific type of laying barge, minimum lay radius of curvature, and the like. The typical minimum lay radius

for pipeline diameters of less than 10 inch, 10–18 inch, and greater than 18 inch are 1000 m, 2000 m, and 3000 m, respectively.

Cost Considerations

The cost to install a pipeline is directly affected by the chosen route, and it incurs a significant proportion of the total cost during fabrication and installation. The associated activities are

- Length of fabricated pipeline pipe or coated pipe.
- Presweeping of route.
- Prelaying installed free-span correction supports.
- Postlaying installed free-span correction supports.
- Trenching, burying, or rock dumping.

Some or all of these activities are related with the selected pipeline route. As a general rule, the design should be performed to

- Minimize the length of pipeline required.
- Avoid requirement for presweeping.
- Avoid prelaying installed free-span correction supports.
- Minimize postlaying free-span correction supports.
- Minimize trenching, burying, and rock dumping.

Route Survey

The route survey includes the surveys for design, preinstallation, and as-laid conditions. The width of the survey corridor is to be large enough to cover the installation tolerance. The route survey required for the design purposes includes the following aspects:

- Seabed profile along the pipeline route centerline.
- Seabed features and irregularities, especially for uneven seabed topography.
- Specific soil conditions in the suspected problem areas.
- Current and wave measurements.
- Locations and descriptions of seabed obstacles, including existing pipelines or umbilical crossings.

Detailed descriptions related to the pipeline route survey are discussed in the next chapter.

Route Optimization

Optimization of pipeline routing is usually not performed, as the route probably has no obstruction, the seabed is flat and in an accessible water depth. Therefore, a straight line between the two termination points suffices. However, on a seabed with onerous terrain, significant savings on fabrication and installation costs can be made if route optimization is performed.

To perform a route optimization, reasonably accurate costs for the following activities are required:

- Presweeping a corridor, including cost of reduced laying rate due to a smaller laying corridor.
- Prelaying free-span correction supports, again including cost of reduced laying rate due to smaller laying corridor.
- Postlaying free-span correction supports.
- Trenching, burying, and rock dumping.

Based on these derived costs, a total cost for each route can be derived. It is worth noting that the optimization cannot be completed until all the pipeline design parameters are finalized (for instance, the number of free-span correction supports is not known until the allowable free spans have been determined).

Pipeline Alignment Sheet

Alignment sheets are used to record a wide range of information required to produce the material takeoff and required by the installation contractor. For major pipeline systems, a preliminary set of subsea alignment sheet drawings are usually prepared during the conceptual design phase. During the detail design, additional information and revisions are incorporated, sufficient to give a full description of the works for pipeline construction. Typically, an alignment sheet covers in the region of 2–3 km of pipeline, with a portion overlapped between sheets. Subsea pipeline alignment sheets typically include the following three parts, as shown in Figure 22.1:

1. Route plan view and bathymetry map
   - Coordinate grid system.
   - Pipeline route corridor.
   - Pipeline route centerline with kilometer point (KP) markers and earings.
   - Route geometry (curvature radii, tangent points and pipeline headings).
   - Locations of subsea obstacles.
   - Pipeline and umbilical crossings.
   - Seabed features.
   - Seabed bathymetry contours.
   - Restricted anchor areas.
2. Route seabed and subseabed profiles
   - Seabed profile along route centerline.
   - Subseabed profile along route centerline.
   - Soil core or CPT data.
3. Pipeline and installation data
   - Pipe diameter, wall thickness, and material grade.
   - Internal and external corrosion coating type and thickness.
   - Pipe weight coating type (concrete coating) and thickness.
   - Anode details and spacing requirements.
   - Buckle arrestor details and spacing requirements.
   - Field joint coating details.
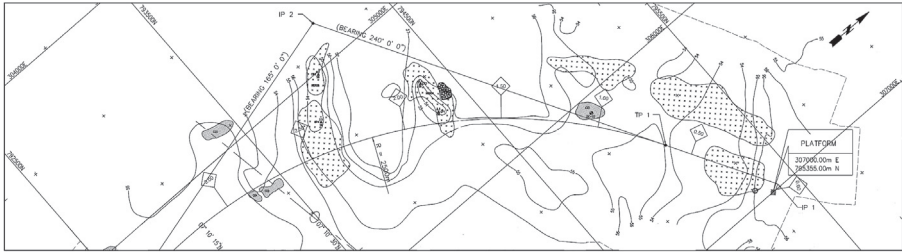
(1) Route plan and bathymetry map

(2) Route seabed and subseabed profiles

(3) Pipeline and installation data.

Figure 22.1 Typical alignment sheet of subsea pipelines.

- Trenching and backfilling details.
- Fittings and special features.

Seabed bathymetry and soil data properties are to be investigated and provided based on the route survey results. Seabed properties, including different soil layers, are to be included in the route survey maps.

3. Shore Approach

Introduction

The shoreline is an extremely complex interface of sea, land, and air. The configuration of shorelines is formed by the interaction of hydrodynamics from water, aerodynamics from air, geotechnics, and biological and human activity. It changes with time under the environmental loads. A subsea pipeline reaches the landfall by way of a shore approach. In the selection of the preliminary pipeline routes, the shore approach forms part of the route selection process. In shallow water, the pipeline is particularly exposed to higher wave action and longshore currents. Experience has shown that serious problems and cost overruns have occurred in the past due to the

difficult environment of very shallow water, and the engineering of pipeline shore approaches has to be carried out with special care to consider all these factors. Every shore approach is different; the choice of shore approach location takes into account the following factors:

- Geotechnical conditions, long-term erosion of the shore, and changing nature of the shorelines.
- Environmental loads to shorelines.
- Complexity of sea-land interface.
- Existing pipelines, cables, and outfalls in the area.
- Installation issues, such as enabling the installation and trenching vessels to come close inshore and providing adequate space onshore for the pulling operation or pipe string fabrication.

Adequate site investigation of environmental conditions is required in planning shore approaches. A marine survey is to be carried out to determine the shore profile, the ocean and tidal currents, and the seabed bathymetry. Geotechnical site investigation is to be carried out to determine the geotechnical description and strength properties of the seabed soil.

Design of Shore Approach

The choice of a shore approach location is critical and demands a very careful engineering review of the coastal hydraulics, geotechnics, and environment, in parallel with a study of the proposed construction method. Normally, the following design issues are discussed in the shore approach design:

- Coastal environment.
- Pipe wall thickness.
- Pipeline stability.
- Cover depth.
- Cathodic protection.
- Environmental concerns.
- Installation considerations.

Coastal Environment

As waves move toward a shore they become higher and steeper. A wave moving toward a shelving shore eventually becomes so steep that it breaks. Most waves break when the wave height is about 0.8 of the local water depth, although there is a variation between waves and an interaction with the flow created by the previous wave. The form of the breaker varies and depends primarily on the beach slope. Refraction alters the direction of propagation.

Waves that approach the shore obliquely induce a longshore current, which transports sediment stirred up by the wave-induced movement of the water close to the seabed. These currents modify the seabed topography through sediment transport processes, and these changes in turn modify the pattern of the breaking waves.

Pipe Wall Thickness

The selection of pipe wall thickness of subsea pipelines for the shore approach and landfall section can also be affected by pipeline on-bottom stability.

Pipeline Stability

The shore approach is usually characterized by relatively high environmental forces, due to waves and tidal currents. Pipelines in the shore approach are usually installed within a predredged trench and the sheltering effect of the trench should be taken into account in the stability analysis. In addition, significant embedment of the pipeline can be expected in sandy seabeds, which should also be considered in the analysis. Negative buoyancy of the pipe should take into account the increased soil density (liquefaction) during the artificial backfilling operations.

Cover Depth

Subsea pipelines should be buried in the shore approach; otherwise, alternative protection measures, such as rock dumping, are required. The depths of pipeline cover influence whether postinstallation trenching of the pipeline is feasible or preinstallation dredging and excavation should be performed. Unless a specialist trenching machine is to be used, which is confidently expected to achieve the specified cover requirements, preinstallation dredging is usually preferred.

Normally, it is suggested that the minimum depth of cover be 2.0–3.0 m to ensure that the pipeline stays buried well below any future erosion of the beach, and this has generally been adopted as a standard industry practice. The cover should extend to the location seaward at least 500 m from the beach or the final water depth of the cover is approximately 12 m below the lowest astronomical tide (LAT) to ensure the laying barge has an adequate draft. The cover seaward of this location should either be compatible with the offshore cover requirements or sufficient to provide long-term stability to the pipeline by decreasing exposure to environmental forces.

A typical backfill system comprises sand and gravel to a minimum of 800 mm on top of the pipe, a further layer (minimum 0.8 m) of rock on top of the sand, gravel of average size of 100 mm, and then a further layer of rock of average size of 350 mm.

Shore Approach Method

Common methods of shore approach are categorized into the following three groups:

- Bottom pull.
- Horizontal drilling.
- Tunneling method.

Bottom Pull Method

The most common method used in the shore approach is the bottom pull, which can be divided into onshore pull and offshore pull methods, respectively.
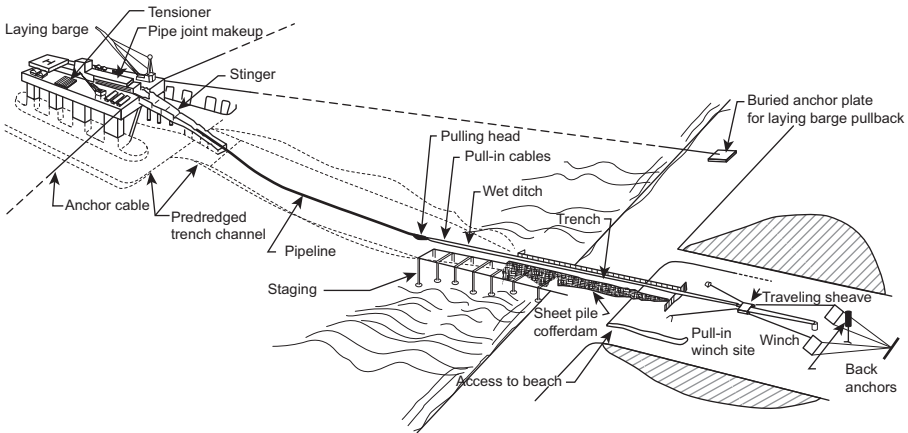
Figure 22.2 Layout of onshore pull.
Source: Palmer [2].

Onshore Pull

A winch is often installed onshore at the head of the trench in the shore pull method. A pull cable is needed to connect the laying barge and pull head, which is welded on the pipe end. The laying barge keeps its original position in the operation procedure, while the pipe section is pulled ashore by the winch. The curvature of the pipeline under the water should be controlled to keep the stress level of the pipeline in the allowable range. Figure 22.2 shows a typical layout of shore pull.

Building a causeway for the pull corridor may be a solution to a restricted site area or difficult topography. The pipeline is pulled off the laying barge into a predredged trench in a synchronized manner until it reaches a cofferdam installed near the high water mark. The cofferdam forms an integral construction with a steel sheet piled retaining wall installed down the beach to the low water mark. Following pipeline installation, the dredged trench and the beach trench are backfilled in combination with steel sheet pile removal. The cofferdam is utilized for tie-in to the landline to be installed.

The pulling system used for the onshore pull may be of two-, four-, or six-wire systems with a traveling sheave unit. For a two-wire system, the pull capacity may be 400 tonnes, and for a four wire system, the pull capacity may be 800 tonnes. The multiwire pull system requires a larger beach area. The two factors that primarily influence the pulling capacity required for an onshore pull are the laying barge location or the pull length and the concrete thickness, which determines pipe weight. Buoyancy can be provided to reduce pulling loads, but this measure should provide for refinement during construction rather than be a premise for determining the pulling capacities. Excessive buoyancy is undesirable, as it represents potential stability problems. Additional marine work needs to be
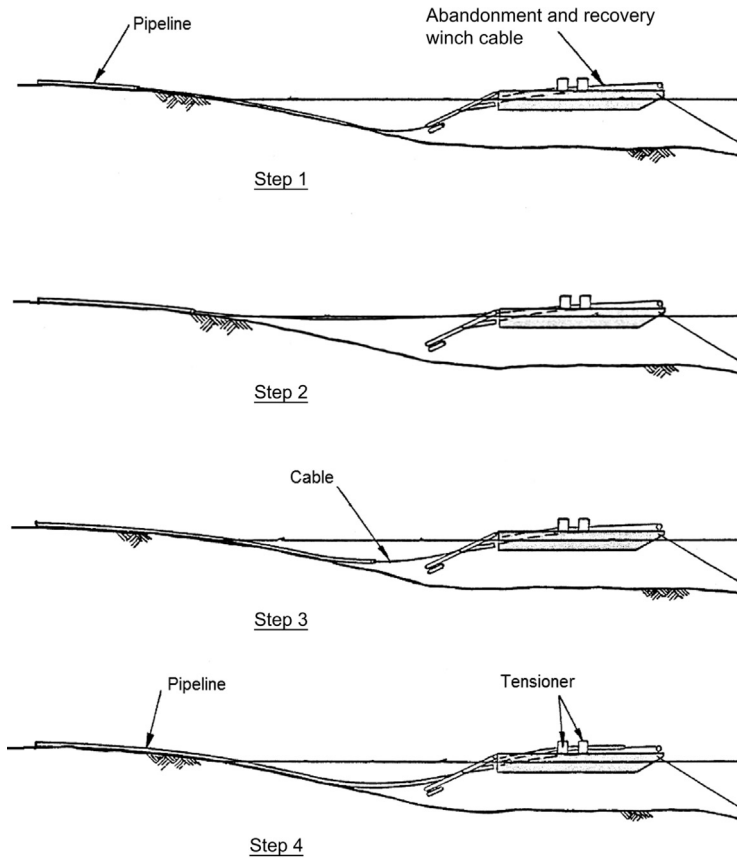
Figure 22.3 Offshore pull method.
Source: Brown [3].

performed where the attachment and removal of buoyancy aids can be problematic
and unreliable.

Offshore Pull

Offshore pull, shown in Figure 22.3, is another bottom pull method, which involves the
fabrication of pipe strings onshore to be pulled into position by a pulling barge anchored
offshore. Pipe strings are fabricated on the construction site onshore, and a pulling
corridor is formed from the fabrication area to the beach. The pulling wires are laid from
the barge along the pulling corridor to the pipe fabrication area and attached to the pulling
head on the first pipe string. The pipes are then pulled offshore. The pipeline would have
to be installed to a point offshore where a laying barge could pick up the pipeline to
commence the offshore pipelay. Hence, the length of pull and pulling capacity consid-
erations are similar to the onshore pull. The laying barge could also be a pulling barge.

Directional Drilling Method

Horizontally controlled directional drilling involves the drilling of a small-diameter pilot hole using a custom designed drilling rig. When drilling of the pilot hole is complete, a reamer is attached. The reamer is pulled along the path of the pilot hole, reaming out a larger-diameter hole with wash pipe being added behind the reamer. Figure 22.4 illustrates the installation steps of the directional drilling method for shore approach.

The physical features of the landfall zone is one of the main factors having the significant impact on the shore approach, especially for zone with huge ecological value that cannot be disrupted or damaged in the construction procedure. Horizontal controlled directional drilling is preferred to overcome this kind of
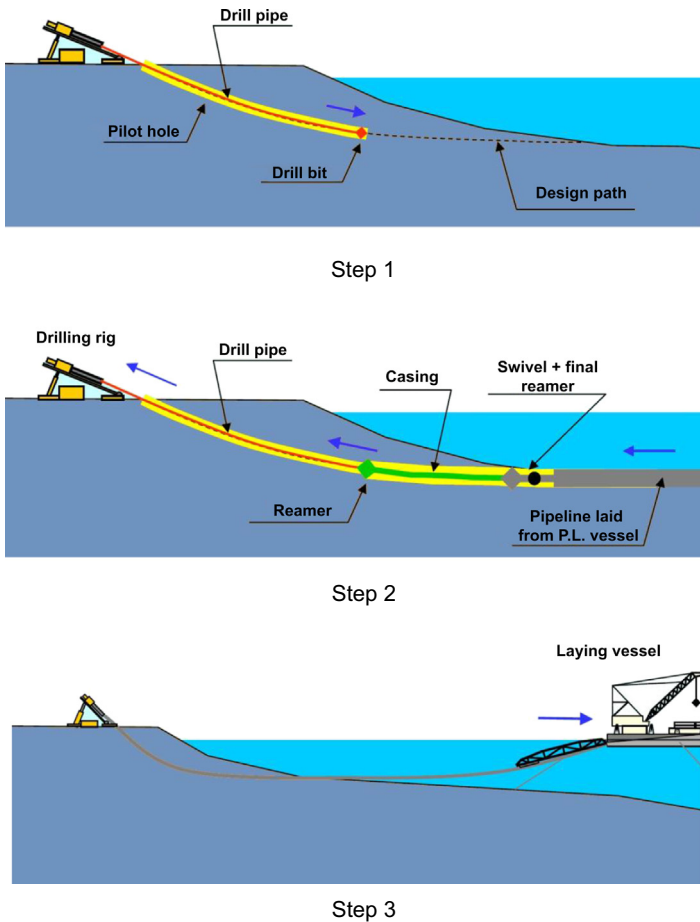
Figure 22.4 Directional drilling method.
Source: Technomare [4]. (For color version of this figure, the reader is referred to the online version of this book.)

problem. Compared with the other shore approach methods, the feasibility of directional drilling depends on the ground conditions and installation procedure carried out under the water, the weather and ocean factors having minimal impact on the pipeline; meanwhile, it is suitable for hard soils and irregular shorelines, the adverse impact on the ecological features is avoided in this installation procedure.

Tunneling Method

For shore approaches that involve the crossing of a coastal cliff, conventional tunneling methods may be used to alleviate substantial cuttings through the cliff and avoid cliff disturbance and reinstatement. Normally, the mini-tunnel method is the most cost effective. Mini tunneling involves the installation of concrete segments to form a casing into which the pipeline is then installed.

4. Pipeline Tie-Ins

Figure 22.5 shows some typical methods of pipeline tie-in to platform:

- Spool piece.
- Lateral pull.
- J-tube.
- Connect and lay away.
- Stalk on.

In the following subsections, the general principles and installation capabilities and constraints are discussed for these tie-in methods.

Spool Pieces

This method is probably the most popular method of tie-in for flowlines and pipelines. Divers measure and assist the installation of a piece of pipe to fit in between the two ends of flowline to be tied together.

This method is popular because of the flexibility of the method. Misalignment of the two pipes can be accommodated by installing bends in the spool, and inaccuracies in placing the pipelines can be accommodated when the spool is made up after diver measurements.

The connection method can either be by flanges or welding. The welding method requires a hyperbaric habitat. From the design viewpoint, if there is a large pipeline expansion, the spool pieces can be accommodated by incorporating a dogleg in the spool, which permits pipeline expansion without transmitting high loads into the adjacent pipe. The obvious disadvantages of this method are that remedial work is required after pipeline installation to tie the line in. Additional work requires divers. This could limit this option if the tie-in is required in very deep waters.
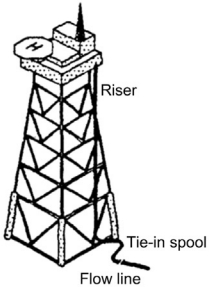
Spool piece
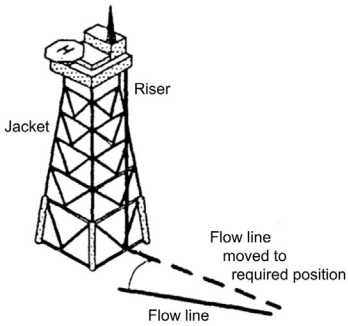
Lateral pull

Pipeline is initially installed
past the jacket

Pipeline is lifted and moved
across to the tie-in point
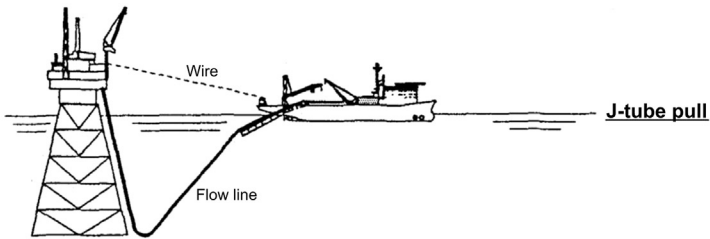
J-tube pull
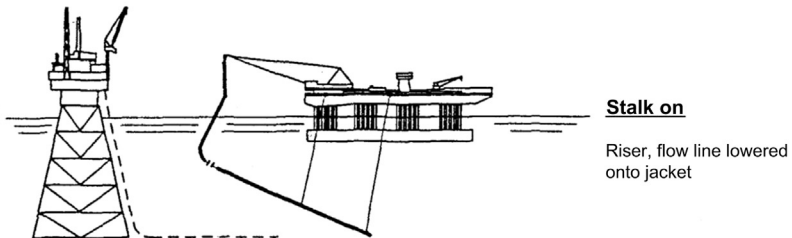
Stalk on

Riser, flow line lowered
onto jacket

Figure 22.5 Tie-in methods.

Lateral Pull

Lateral deflection involves positioning the pipeline end to one side of the target structure then pulling it laterally into position. This has two disadvantages compared with a direct pull-in:

- Alignment is more difficult to achieve.
- A clear (swept) area is required to one side of the tie-in site.

The pipeline may be pulled toward the target by a single wire, or a series of wires may be developed through deadman anchors to give greater control of alignment. A bell mouth or stab-in guides usually assist final alignment. For large diameters, such as export lines or bundles, it is necessary to make a length of pipeline neutrally buoyant. This gives greater flexibility and reduces the pull forces but can expose the pipe to large current forces.

A progress of this technique is the use of vertical deflection rather than lateral deflection. The required initial shape could be attained by local adjustments to buoyancy, pull-in being again by a system of wires. The principal advantage of this method is that it does not require the same amount of seabed space.

In addition, it should be possible to devise initial configurations that it would be difficult to create laterally by laying or towed installation. Direct pull for second-end tie-ins may then become available by creating a vertical slack loop behind the pullhead.

This method is usually utilized when direct pull-ins (i.e., J-tube, connect and lay away. or stalk on) are not feasible options. However, this method is frequently used, as direct pull-ins are usually not possible. For instance, J-tube pull-in, connect and lay away can be performed only by a vessel laying away and not when a vessel lays down. Stalk-ons can be performed only in shallow water.

The main disadvantages of this method are

- Requires extensive diver intervention.
- Difficult operation to perform; several experienced diving operators have buckled pipelines using this method.
- If connected directly to the tie-in point, then all the pipeline expansions are fed into that point. The tie-in point must either take high axial loads or large deflections.

J-Tube Pull-In

The J-tube pull-in method is to connect the pipeline to a wire and, by pulling the wire, to pull the pipeline through a J-tube up to the topsides of the platform. This method requires the J-tube to be of a reasonably large diameter compared to the pipeline [5].

The J-tube pull-in method requires the pipeline to have a capacity to easily move axially over a relatively large distance. This limits the option to pulling the pipeline directly from the pipe laying vessel.

The principal advantage of this system is that the pipeline is tied in directly to the jacket topsides, so avoiding subsea tie-in work. However, the main disadvantages are

- Normally used for small-diameter lines; the loads involved with large-diameter lines become too high.
- The line is directly tied into the jacket, with no system to accommodate pipeline expansion. Large deflections and axial forces are fed into the J-tube during operation.

This method is very popular for small-diameter pipelines, when the pipe laying starts at the jacket.

Connect and Lay Away

This method is very similar to the J-tube pull-in method, with the exception that the tie-in is performed subsea. This method is usually applied in diverless operations, where a mechanical connecting system is utilized to perform the connection.

Two examples of diverless pull-in and connection tools, McEVOY and FMC, are presented in Figures 22.6 and 22.7, respectively. There are also diverless connection systems for bundled lines, two such systems, VETCO and CAMERON, are presented in Figures 22.8 and 22.9, respectively [6].

This system is used mainly at subsea manifolds and wellheads, where the water depth prohibits the use of divers. This is the only system developed for performing diverless connection of pipelines.

The principal advantage is that this system can be adapted to perform diverless connections.

The main disadvantages are

- Expensive technology to perform diverless work.
- The connection is subjected to the pipeline axial loads, when it cannot accommodate expansion.

Stalk On

The stalk-on method is primarily used in shallow water applications (less than 40 m) and, hence, applicable only in the southern North Sea. The method involves laying the pipeline down adjacent to the jacket into which it is tied. The vessel maneuvers over the pipeline, lifts it up, and welds on or flanges on the jacket riser. The pipeline and riser are then lowered onto the seabed or jacket. The jacket clamps are subsequently closed around the riser, as illustrated in Figure 22.5.

The primary advantage of this method is that the same vessel that installs the pipeline can also perform the stalk on. However, the disadvantages are

- The riser is subjected to the expansion of the pipeline, as no expansion spool is used.
- The operation can be used only in shallow waters.
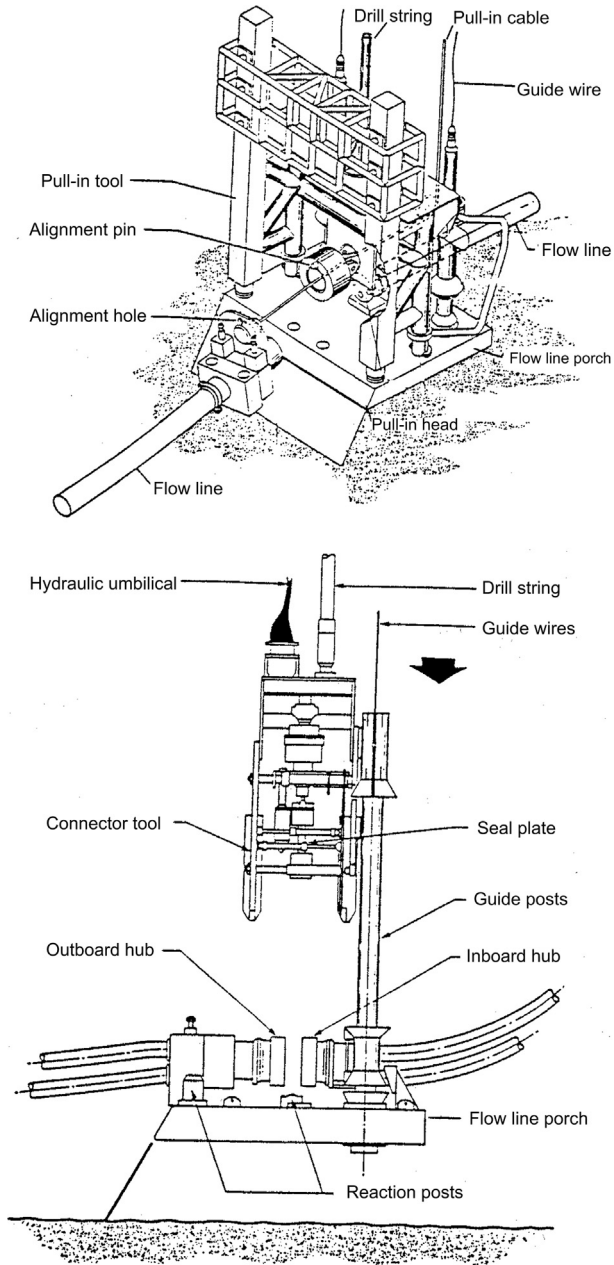
Figure 22.6 McEvoy flowline connection system.

Connector
Guide post
Electrical umbilical
Flow lines

Flow line running tool

Alignment structure

Section A-A   Flow line bundle hub
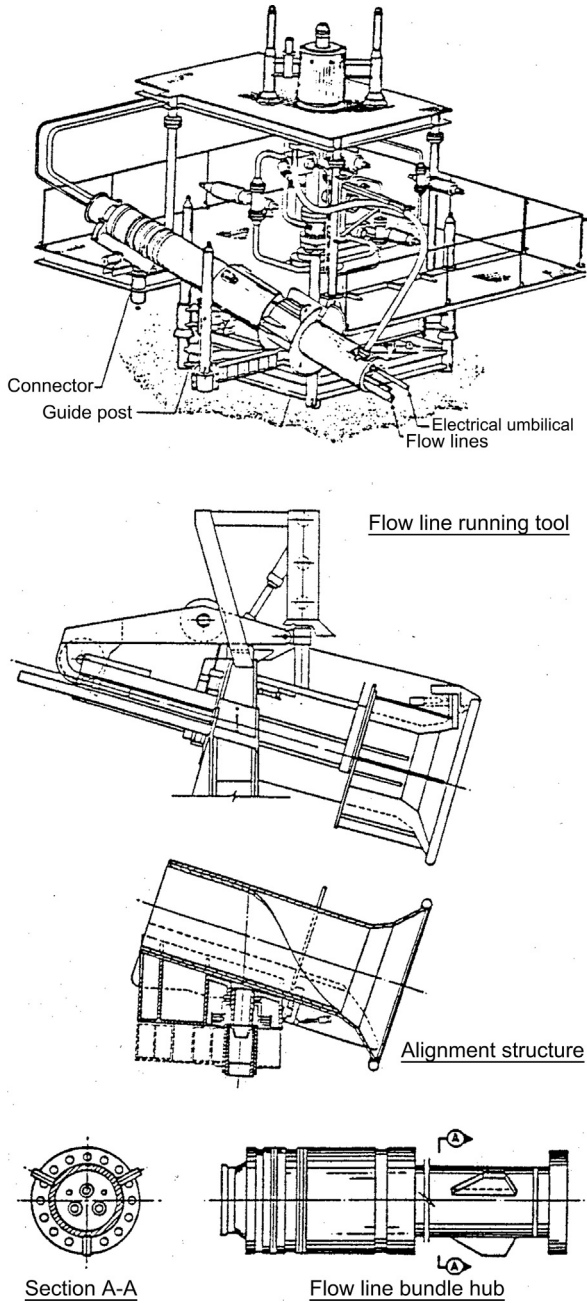
Figure 22.7 FMC diverless flowline connector system.

Tree flange

Hydraulic
supply port

Flow line port

Seal sub

Seal plate

Final alignment post

Tree flange assembly

Flow line port

Hydraulic supply
line

Electrical
connector

Alignment holes

Flow line flange assembly

Guidelines

Drill string

Flow line
carrier

Blanking
flange

Flow line
flange

Permanent
guide base
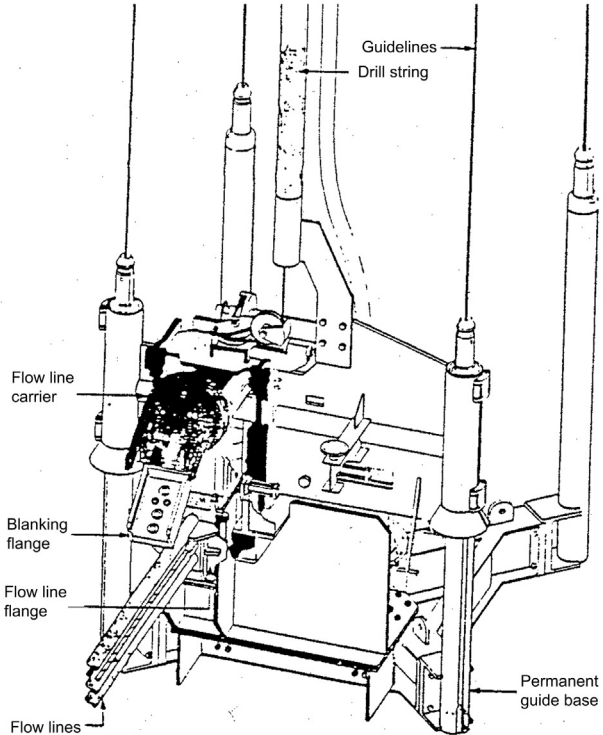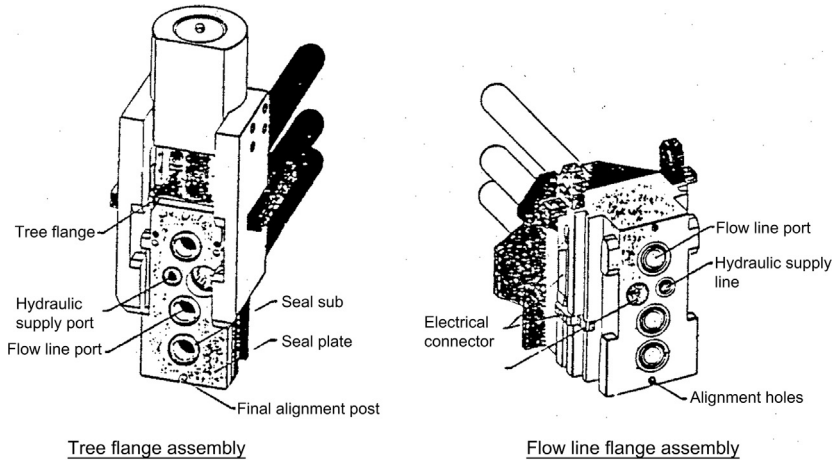
Flow lines

Figure 22.8 VETCO diverless flowline connection tool.
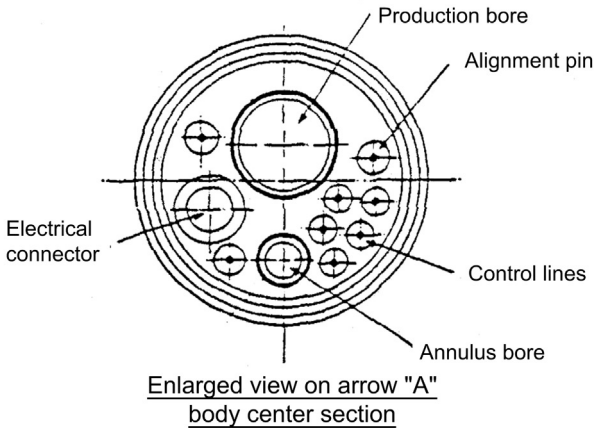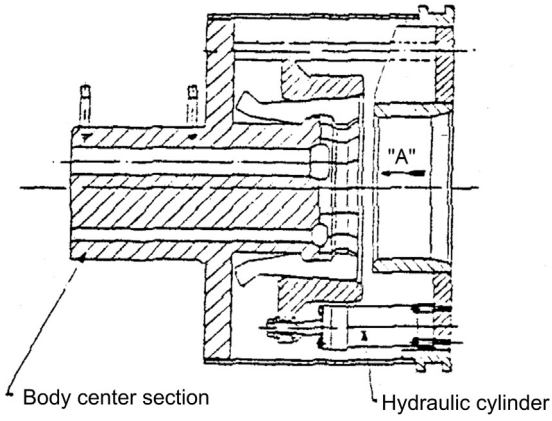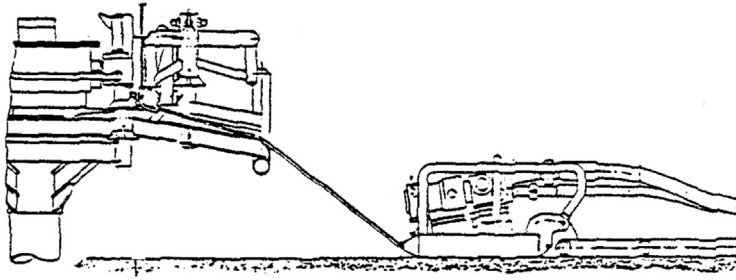
Figure 22.9 CAMERON multibore connector system.

5. Pipeline Trenching and Burying

The purposes of pipeline trenching are to reduce the hydrodynamic force and increase the stability of the pipeline section; protect the pipeline section from the external damage due to anchors, heavy dropped objects or fishing gear; and improve other pipeline structural performance, such as free span, lateral buckling, and insulation performance. Trenching pipelines is one main part of the shore approach design, and posttrenching is more popular than predredged trenches. The development of trenching and burying equipment has, like the pipeline installation equipment, changed significantly over the last several decades [7], [8]. The trend has been to move away from dedicated trenching vessels to equipment that can be used from diving support vessels (DSVs). The pipeline trenching and burying equipment is discussed next:

- Jet sled.
- Plowing.
- Mechanical cutter.

Jet Sled

This method is a traditional method of trenching a pipeline. Dedicated vessels with turbine engines were built to provide jet sleds that would trench through most soils, as shown in Figure 22.10.
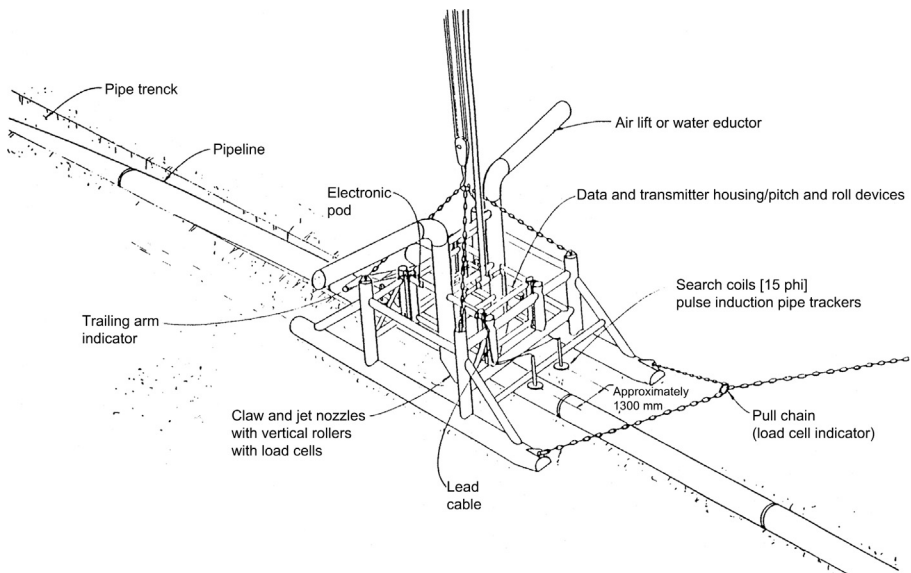
Figure 22.10 Jet sled.

The jet sled straddles the pipeline and extends into the seafloor to the desired depth of burial. Water and air are supplied to the machine from the surface. It works on the following two principles:

- High pressure jet nozzles power water to break up the soil.
- Air is pumped into pipes, which generates lift force, which lifts the broken soil away from the trench.

The pipeline settles into the trench after the machine passes, and natural action eventually backfills the trench.

The size of jet sleds and associated costs vary considerably. The largest one can weigh up to 80 tonnes and are controlled by dedicated vessels, and the smallest one can fit onto a DVS and weigh up to 0.5 tonne. The associated capabilities also vary. The large ones can trench through sand, silt, and clay and even through soft rock (sandstone); the trench rates vary depending on the soil conditions. The small jet sleds are suitable for only sand, silt, and soft clay.

The main constraint of the jet sleds is that they cannot bury the pipelines. They can excavate a hole into which the pipeline sinks, but they cannot backfill the hole. Another disadvantage is the large amounts of power required. As much as 32,000 HP has been used to power the jets and evacuators of a large pipeline burial system used to trench boulder clay in the North Sea. However, jet sleds are still a popular means of trenching pipes, as the method is well proven and little damage to the pipeline occurs compared to the damage caused by other methods. This system usually requires divers but may be operated diverless.

Trenching Plowing

Trench plowing was first developed in 1980 for the North Sea to provide a cheaper alternative to trenching of pipelines. Since then, it has become a popular method of pipeline trenching, as shown in Figure 22.11.

The general principle of pipeline plowing has been adapted from the technique used in agriculture to plow fields. The pipeline plow consists of a very large "share," on top of which the pipeline rests. The pipeline is pulled along (usually by the surface vessel), and as the plowshare passes, the pipeline settles in the trench. If a backfill plow also is employed, this reverses the process by pushing the soil back into the trench, so burying the pipeline.

The main advantage of the trenching plow is that it can trench a large range of pipeline sizes (up to 24 inch diameter) operated from a DVS. The trench rates can be very high, depending on the soil conditions. The shape of the ditch can be precisely controlled, because a mechanical excavation method is employed, allowing the ditch to be narrower and deeper.

This is probably the only system that can bury pipelines in one operation, if so required. It should be noted, however, that some operators prefer rock or imported material to be used as backfill.

The main disadvantage of this system is that it has a limitation on the depth that can be excavated. To date, the maximum trench depth is 1.5 m. An additional
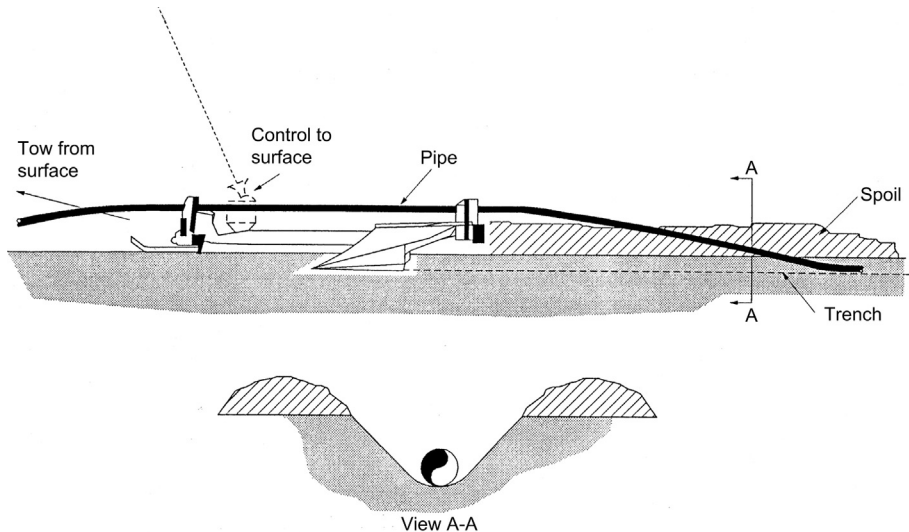
Figure 22.11 Pipeline plow.

disadvantage is that the plow system can cause damage to pipelines, especially those lines not protected by a concrete coating. However, this system is better than most. This system usually requires divers for plow placement and retrieval, but in some cases, it can be performed without divers.

Mechanical Cutters

Mechanical cutters have been developed as a diverless option to trenching for small-diameter pipelines, as shown in Figure 22.12.

Many different types of mechanical diggers are available for subsea pipeline trenching. However, all the methods are based on the same basic principle. The controls and power source are onboard a surface vessel, which via an umbilical powers a subsea machine. This machine moves along the seabed on tracks.

These machines can usually handle only small-diameter pipelines and preferably flexible ones. Since they provide their own traction, the machines require reasonably firm soil. They cannot trench in very soft soil or very hard clay or rock.

Fluidization Trenching Equipment

The fluidization trenching method is designed for noncohesive soil conditions where conventional methods have been ineffective. For sandy soil, the operation efficiency for both the jet and hinge suction ditcher is very low. This is mainly because the trenching gap needed is very wide and a large amount of sand should be excluded, sometimes repeated ditching is needed to achieve the designed depth. For that reason, fluid trenching equipment is designed according to the characteristics of

View A-A
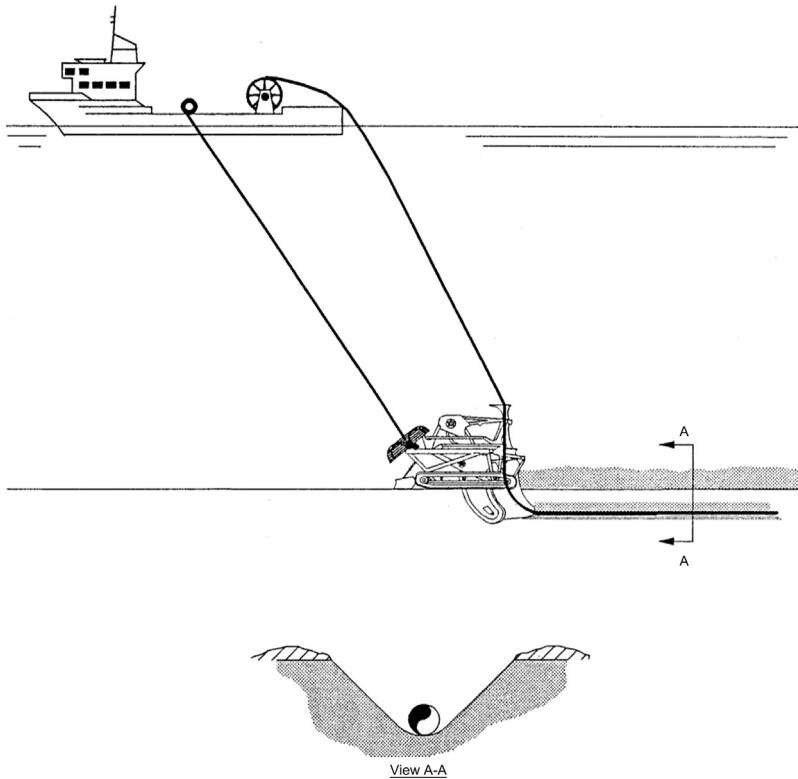
Figure 22.12 Mechanical cutter.

sandy soil. As illustrated in Figure 22.13, by introducing water and air under the pipeline along a length, the sand is fluidized, allowing the pipeline to sink of its own weight.

The main advantage of this method is that the pipeline is protected immediately after sinking into sand, due to soil fluidization. However, the fatal disadvantage is that it is effective only for a very low viscosity in the sand or silty clay. This method is not suitable for the deepsea area, where the soil types change rapidly.

6. Pipeline Rock Dumping

Rock dumping, like the other installation activities for offshore, has become more specialized. The rock dumping vessels are designed to deposit large quantities of rock in localized areas. Along with the requirement of small quantities of rock being placed over pipelines, new vessels have been developed, as shown in Figure 22.14.
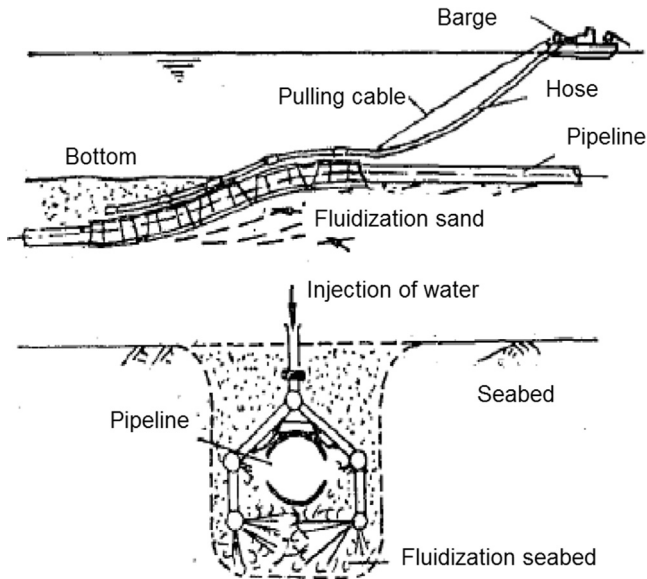
Figure 22.13 Fluidization trenching equipment.
Source: Mousselli [8].

The main rock dumping techniques for subsea pipelines include

- Side dumping.
- Fall dumping.
- Bottom dropping.

Side Dumping

This method involves loading selected stone onto a flat-decked ship, positioning the ship over the required location to dump rock, and pushing rock over the side by hydraulic rams that clear the rock from the centerline of the vessel and drop it overboard.

This rock dumping method is very efficient at dumping large quantities of rock in short lengths. This is suitable for protecting the bases of jackets or subsea manifolds but is wasteful of rock for dumping on pipelines.

Fall Pipe

The method is based on loading the selected stone onto the vessel, mobilizing offshore to the selected location to dump the rock, and dropping the rock through a tube to the location. To provide further accuracy, the "fall pipe" has a remote operated vehicle at the end so the location of the rock can be monitored and controlled.

Side dumper

Fall pipe

Bottom dropper
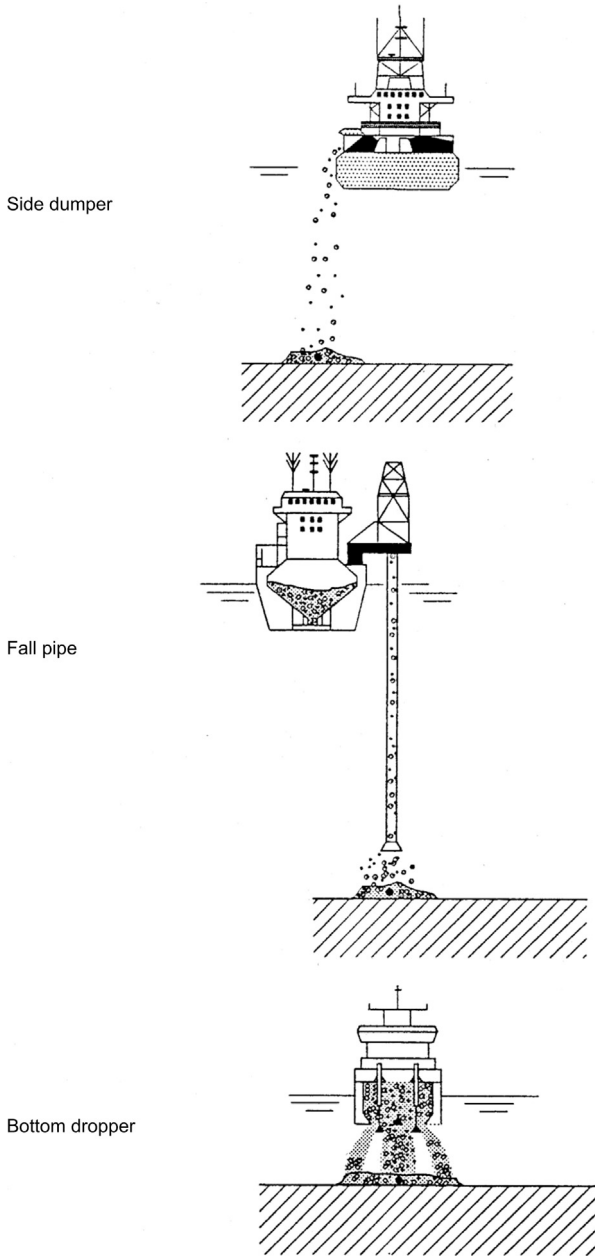
Figure 22.14 Rock dumping methods.

This rock dumping method was developed for dumping rock on pipelines and flowlines. It provides accurate dumping, which minimizes wastage and permits long stretches of rock to be dumped during one trip.

Bottom Dropping

There are two methods of bottom dropping. One method incorporates ports that open at the bottom of the hold; the second is to apply a split barge that drops all the rock at once.

Both methods are again suitable for dropping large quantities of rock, when great accuracy is of less importance. This method is not suitable for dumping rock on pipelines.

References

[1] Langford G, Kelly PG. Design, installation and tie-in of flowlines. JPK Report Job No. 4680.1. Norway: Stavanger; 1990.
[2] Palmer AC. Trenching and burial of submarine pipelines. In: Proceedings of the Subtech 85 Conference. Scotland: Aberdeen; 1985.
[3] Brown RJ. Past, present, future pipeline trenching systems operating capabilities and limitation; 1976.
[4] Tecnomare SPA. Arctic offshore pipelines design and installation challenges. Brussels: ARCOP Workshop No F; June 2004.
[5] Ellinas CP. J-Tube method of riser installation. Offshore Pipeline Engineering, Park Lane Hotel, London; 1986.
[6] Raven PWJ. The development of guidelines for the assessment of submarine pipeline spans. Overall summary report, OTH 86 231, HMSO, England; 1986.
[7] Brown RJ. Latest developments for subsea pipeline plowing. Pipeline Industry 1987;66(4).
[8] Mousselli AH. Offshore pipeline design, analysis and methods. Tulsa, OK: Pennwell Publishing; 1981.

23 Åsgard Flowlines Design Examples

1.   Introduction

The Åsgard Field is a joint effort by Statoil and Saga Petroleum to develop the Smørbukk, Smørbukk Sør, and Midgard fields located in the Haltenbanken area of the Norwegian Sea. Floating production and offloading vessels are linked to 300 km of flowlines in a two-phase field installation. This chapter focuses on the Åsgard Flowlines Project Phase 1 development, consisting of 90 km of 10-inch insulated flowlines operating at 120° to 145°C and 390 bar [1], [2]. These were installed in spring 1998 and tied back to the Åsgard A FPSO for early recovery of oil [3].

J P Kenny A/S in Stavanger was contracted in October 1995 by the joint Statoil-Saga development project to perform the conceptual and detailed engineering of the flowlines [4]–[6]. The integrated project team benefited from recent developments in subsea equipment, pipeline research, and codes to continuously improve the design. The early engineering phases identified several aspects of the design where

innovation would have an important impact on the performance of the project and the capital expenditure (CAPEX):

- Selection of 13% chrome as a flowline material.
- Using the limit-state approach to developing strength criteria.
- Using the design through analysis method to optimize seabed intervention.

The combination of these aspects influenced the course of the flowline design, which focused on minimizing the main CAPEX cost drivers: procurement and marine operations. This presentation outlines the evolutionary design process and highlights the choices made along the way.

2.   Wall Thickness and Line Pipe Material Selection

General

The Smørbukk and Smørbukk Sør well streams are highly corrosive, due to the presence of CO_2 combined with 140°C temperature and 390 bar pressure, which places extraordinary demands on material performance. The careful selection of line pipe and coating benefited from recent development work by Statoil's materials research department in cooperation with the suppliers [7].

Line Pipe Material Selection

Four flowline materials were considered for the 10-inch flowlines: X65 steel, duplex, Inconel-cladded carbon steel, and 13% chrome. More commonly used for well casing, 13% Cr had not been used previously as a flowline material, and there was little experience in how the material would perform when subject to production welding methods and elastic-plastic deformation during installation and operation. While Statoil was engaged in a qualification program for welding 13% Cr line pipe, the conceptual engineering compared several different flowline materials, each of which involved cost trade-offs.

   A carbon steel line could be expected to need at least one replacement during the field lifetime due to the high corrosion rate. The significant strength derating of duplex above 100°C meant that a high-integrity pressure protection system (HIPPS) is required to limit the pressure in the lines to 170 bar. Availability of sufficient quantities of the material was also a problem. The cladded pipe was considered to be too costly to weld offshore and unsuitable for the reeling installation method. The material and welding qualification program carried out by Statoil confirmed that 13% Cr was suitable for the Åsgard flowlines due to its resistance to CO_2 corrosion, high strength at elevated temperatures, and availability.

Wall-Thickness Design

The primary requirement of the pipe wall is to sustain stresses from the internal pressure. The tensile hoop stress is due to the difference between internal and external

pressure and is not to exceed the permissible value of 0.8 SMYS. This higher utilization value achieves a 5% reduction in wall thickness over the previous 0.72 usage factor and represents about 1 mm reduction in wall thickness for the Åsgard flowlines.

The analysis results of wall thickness were in the range 11.6 mm to 12.6 mm for the Åsgard flowlines and 15.3 mm for the gas injection lines. As these were compatible with the reeling pipe laying method, it was also the most cost-effective combination of material and wall thickness.

3. Limit State Strength Criteria

General

This section presents limit-state based strength criteria for typical flowlines under consideration in the Åsgard flowlines, Phase 1 detail engineering design. Development of the limit-state based strength criteria specific to the Åsgard flowlines was carried out by Bai and Damsleth [8], [9], before the DNV 1996 rules were issued [10].

The most severe case (thinnest wall thickness, largest D/t) is chosen to demonstrate that these failure modes do not govern the Åsgard Phase 1 flowlines. The most severe design case regarding strength criteria is considered to be the following production flowlines:

- Pipeline Systems: P101, P102, S101, S102.
- Area: Smørbukk Sør.
- Design pressure: 370 barg.
- Wall thickness: 11.6 mm.
- Outside diameter: 251.8 mm.

Bursting under Combined Loading

For a 10-inch flowline subject to pullover loads, finite element analyses revealed that a plastic hinge occurs at the location where a pullover load is applied [11]. It was therefore concluded that the pullover response of the 10-inch flowlines is predominately load controlled. Investigation of fishing activities documented that there is very little fishing activity in the area where the flowlines are to be installed. Because the flowlines in the Åsgard field are doubled up for roundtrip pigging, the consequences of a structural failure in one of the flowlines is not considered to be as severe as structural failure of an export pipeline. Therefore, an equivalent stress criterion is used with allowable stress of 1.0 SMYS for the bursting failure mode.

Local Buckling and Collapse

An allowable bending moment was defined for load-controlled situations. It was, however, concluded that local buckling for external overpressure is not a governing failure mode, because the D/t values are low and the water depth (300 m) not deep

enough for external pressure to be dominant. Calculations also show that propagation buckling will not occur for the Phase 1 flowlines.

Allowable axial compressive strains are estimated for displacement-controlled situations. A pipeline is made up of 12-m long pipe joints welded together. The difference in the stiffness of the pipe at the welded joint due to the discontinuity of the external coating and possibly the effect of local heat treatment can be significant. This is accounted for in the displacement-controlled situations by applying a strain concentration factor (SNCF).

Fracture

The stress-strain curves used in converting stress to strain are very conservative, because stress-strain curves are usually based on the lowest yield stress and lowest ultimate stress. In addition, PD6493 has been derived for load-controlled situations, and the allowable strain is applied to deformation-controlled situations. The stress is defined as the average of yield and tensile stress, which is also conservative.

Low-Cycle Fatigue

Tests at SINTEF in 1997, based on the author's definition, have established the fatigue performance of the welded pipes for the Åsgard Phase 1 flowlines [12]. The tests simulated loading from reeling installation, vortex-induced vibrations, temperature, and internal pressure. The results, as shown in Table 23.1, were used to generate fatigue life design curves.

Constant amplitude sinusoidal loads with a frequency range of between 0.5 Hz and 1.0 Hz were used and the specimens were subjected to an internal pressure of 330 bar. All tests were carried out in air. Based on the laboratory tests on the given loading sequence of 8-inch pipe with weld undercuts, a design curve—with the common 97.5% probability of survival—was established. The design curve was slightly on the conservative side of the AWS-2 $\Delta\varepsilon$-N curve [13]. It is therefore concluded that the AWS-2 $\Delta\varepsilon$-N curve should be applied to low-cycle fatigue design of Phase 1 lines. The AWS $\Delta\varepsilon$-N curves are expressed as follows:

$$\Delta\varepsilon = 0.055N^{-0.4} \quad \text{for} \quad \Delta\varepsilon \geq 0.002$$

and

$$\Delta\varepsilon = 0.016N^{-0.25} \quad \text{for} \quad \Delta\varepsilon \leq 0.002$$

The Åsgard Phase 1 flowlines are designed to the following cyclic strains:

- Two strain cycles during reel on and reel off.
- One strain cycle during bending over stinger and bending in sag bend.
- 200 cycles of planned and unplanned shutdowns.

Table 23.1 Low-Cycle Fatigue Test Results for Pipes with a Butt Weld

Specimen no.	Internal Pressure (bar)	$\Delta\varepsilon_{nom}$ [%]	ε_{max} [%]	ε_{min} [%]	R ratio	N_1[1]	N_f[2]	Remarks
1	330	0.29	0.59	0.30	0.51	9600	24768	Surface as welded
2	330	0.47	0.69	0.22	0.32	1900	3600	Surface as welded
3	330	0.30	0.60	0.30	0.50	2021	5620	Simulated undercut in weld
4	330	0.46	0.69	0.23	0.33	1800	3490	Simulated undercut in weld
5	330	0.48	0.70	0.22	0.31	2800	4665	Simulated undercut in weld
6	330	0.17	0.53	0.36	0.68	30175	49045	Simulated undercut in weld
7	330	0.30	0.60	0.30	0.50	3100	7853	Simulated undercut in weld
8	0	2.07	1.80	−0.27	−0.15	91	101	Simulated undercut in weld

Notes: $\Delta\varepsilon_{nom}$, ε_{max}, ε_{min} are nominal strain range, maximum strain, and minimum strain, respectively. $R = \varepsilon_{min}/\varepsilon_{max}$.
[1]N_1 is first indication of crack by gauges.
[2]N_f is leakage through crack.

The planned cycles of shutdowns are estimated 40–50. However, there will be an unknown number of unplanned production cooldown-restart cycles. Conservatively, an upper limit of the total shutdown cycles during the entire operation period is assumed to be 200. It is conservatively assumed that the strain range during shutdowns is a constant.

Based on the AWS curves and the laboratory tests conducted for this project, it is found that the allowable strain range for low-cycle fatigue is 0.3%.

Ratcheting

Industrial codes state that ratcheting of high-pressure and high-temperature (HPHT) flowlines during startup and shutin or shutdown cycles places a stringent limit, and tge allowable equivalent plastic strain is 0.1%. This allowable limit is conservative, because it neglects the effect of strain hardening and large deflection [14], [15].

D = 251.8 mm, t = 11.6 mm, 13 % Cr.
P_c/P_o = 0.5, K_c/K_1 = 0.21 ($\Delta\varepsilon_b$ = 0.75 %)
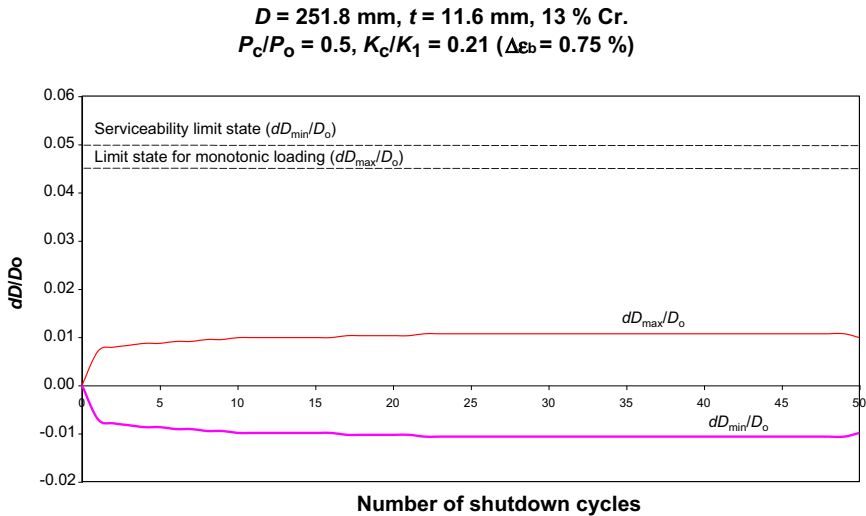
Figure 23.1 Effect of cyclic curvature on ovalization. (For color version of this figure, the reader is referred to the online version of this book.)

A finite element simulation of a flowline subjected to pressure and curvature cycles from installation and repeated shutdown-startup cycles shows a gradual accumulation of ovalization and circumferential strain. The accumulation of plastic deformation occurs during the initial stages of the cyclic loading and stabilizes before the end of the series of load cycles, demonstrating characteristic "shakedown" behavior.

The results are illustrated for the cyclic load case $P_c/P_o = 0.5$ and $\kappa/\kappa_1 = 0.21$ [15]. The changes in minimum and maximum diameters, are recorded in Figure 23.1. The minimum and maximum diameter increase and decrease with number of applied cycles, respectively, and the accumulation of ovalization stabilizes after approximately 30 load cycles.

In Figure 23.2, strain versus number of shutdown cycles is illustrated for combined cyclic bending and internal pressure loading. The circumferential strain increase to approximately 0.60% in 28 load cycles and stays constant thereafter. Hence, the limiting strain of 1% that control brittle fracture of pipes under circumferential tension is not reached. For the combined curvature and internal pressure case (Figure 23.2), the axial strain increases for the first seven load cycles before stabilizing at approximately 0.3% strain.

The fabrication ovality tolerance given by the Statoil specifications "Seamless Linepipe-Austenstic Steel" (1990) and "Welded Linepipe-Ferritic Steel" (1990) is 0.75%. Ovality increases due to the reeling installation process, where the pipe is subject to reverse bending and the effect of this on subsequent straining should be considered. Generally, numerical methods (e.g., finite element methods) must be used to predict the reeling-induced ovality, in which bending against a surface, axial load, and repeated bending are considered. The fabrication tolerance given

D = 251.8 mm, t = 11.6 mm, 13 % Cr.
P_c/P_o = 0.5, K_c/K_1 = 0.21 ($\Delta\varepsilon_b$= 0.75%)
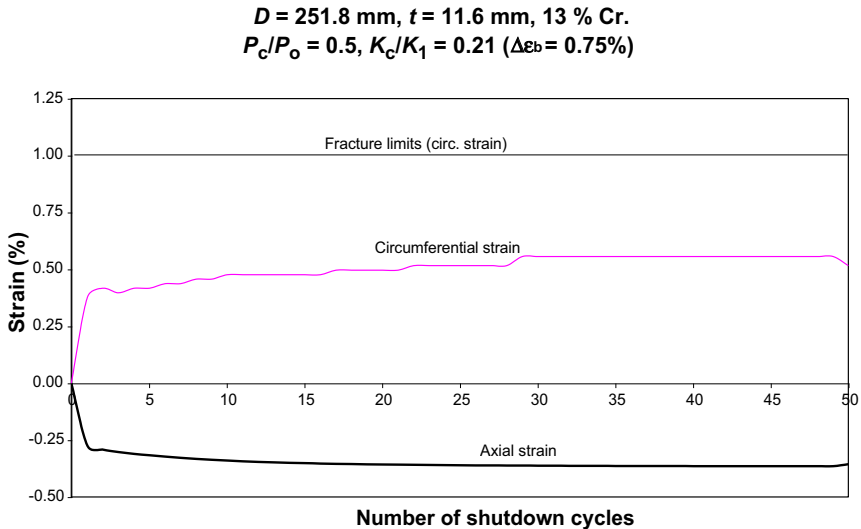
Figure 23.2 Effect of cyclic curvature on axial and circumferential strain. (For color version of this figure, the reader is referred to the online version of this book.)

by the Statoil specification (0.75%) is applied as the initial ovalization prior to reeling [3]–[5].

The most severe case is chosen for the ratcheting analysis. It has been found that the maximum ovalization of the flowlines at the end of design life is 1.5%, significantly less than the 3% limit. Therefore, it is concluded that the ovalization for the serviceability limit state will not be violated.

4.   Installation and On-Bottom Stability

Installation Design

The vessel Apache was used to install the flowlines using the reeling method. During the reeling process, the pipeline undergoes plastic deformation on the reel. The pipeline is plastically deformed in the opposite direction during off-reeling, as it passes through the straighteners located on the adjustable stern ramp. The installation analysis was carried out by use of the OFFPIPE computer program, where the 60° ramp angle was considered to be the base case for the Åsgard flowlines.

The design criterion used is that the pipeline strain is to be within the allowable 0.15% for the static installation analysis, and there should be no pipeline-support contact (i.e., a small gap) on the lower support (lower roller box). The pipeline configuration and residual lay tension in the pipeline is then calculated as an input to the in-place analysis.

The installation analysis shows that the 10-inch Åsgard Phase 1 flowlines can be installed by the reel method with relatively low residual lay tension, as presented in

Table 23.2 Installation Analysis Results for Phase I Flowlines

Pipeline	Zone	Pipeline Section (Kp.)	Steel Data OD/WT (mm/mm)	Coating Data WT/Density (mm/ kg/m^3)	Pipeline Submerged Weight (kg/m)	Residual Lay Tension (kN)
P101 and	2	0–0.36	258.8/15.6	53/1190	46.4 (24.7)	121
P102	1	0.36–1.5	251.8/11.6	53/190	24.7	83
	1	1.5–8.6	251.8/11.6	53/1000	15.1	53
S101 and&	2	0–0.36	258.8/15.6	53/1000	37.0 (15.6)	94
S102	1	0.36–7.4	251.8/11.6	53/1000	15.6	54
	1	7.4–11.6	251.8/11.6	53/1220	26.2	85

Table 23.2. Some of the lines required different coating density along the route, which resulted in tension variations.

The pipeline strains are less than 0.05% for all cases of the pipeline, both on the ramp and in the sagbend. The results show that the pipeline residual lay tensions in general are in the area of 5 to 9 tonnes, depending on the coating characteristics, and up to 12 tonnes in zone 2 sections.

As the residual lay tension has a considerable impact on the seabed intervention, possible ways of reducing the residual lay tension were investigated. The flowline departure angle could be increased by bending the pipeline over the lay ramp roller supports or by adding a ramp extension, whereby the residual lay tension could be reduced by 46–58%. Because the sensitivity analyses showed that considerable reductions in the pipeline residual tension were feasible by modifying the standard ramp configuration, the requirement for low lay tension was included in the installation contract to reduce the postinstallation seabed intervention.

On-Bottom Stability

The purpose of the analysis is to recommend coating thickness and equivalent coating density to ensure on-bottom stability of the untrenched flowline throughout its design life. The following design conditions are considered:

- Installation phase:1 year wave + 10 year current or 10 year wave + 1 year current.
- Operational phase: 10 year wave + 100 year current or 100 year wave + 10 year current.

In the analysis, the shear strength of the clay is varied between 2 to 20 kPa, 5 kPa at critical locations, while the corresponding coefficient of friction may vary between 0.15 and 0.3, depending on the pipe penetration. The flowlines are subjected to environmental loads, spring-autumn wave and current and all year wave and current, corresponding to installation and operation phases, respectively. Both wave and current flow are assumed to act perpendicular to the flowline.

The long-term extreme sea states are transformed to water particle velocity data at the seabed level. Since only the longest period (14 to 25 [s]) surface waves have any

significant effect at 300 m depths, the two-peaked Torsethaugen wave spectrum is used. The peak combined wave and current velocities form the basis for the long-term hydrodynamic loading.

Two principally different design checks are made for the stability control of the pipeline.

The first design check is a static equilibrium calculation of a pipeline trenched or buried in the soil, sand, or clay. The design check is based on static equilibrium between the hydrodynamic design loads and the soil capacity.

The second check is based on a specified permissible pipeline displacement for a given design load condition (return period), generated through series of pipeline response simulations with PONDUS, a purpose-made FE stability program. For the on-bottom design check on clay, a critical weight is calculated to fulfill the "no breakout criteria." The results in Table 23.3 represent the worst case. where directional wave and current flows are applied concurrently. The extreme wave and current data correspond to all-year directional conditions.

Compared to the observed pipe penetration into the seabed, the calculated values shown in Table 23.3 are underestimated. The effect of concentrated loads at free-span shoulders is not modeled by PONDUS. An ABAQUS model was later developed to account for the effect of local seabed penetration on stability, including the reduction in lift force where the flowline is in a free span. It was demonstrated that, while there was local movement, the overall pipeline remained in position and could be considered as stable [16].

5.   Design for Global Buckling, Fishing Gear Loads, and VIV

General

The seabed intervention design through analysis is conducted as Figure 23.3:

Global Buckling

A pipeline may buckle as seabed friction builds up to resist axial expansion caused by temperature and pressure loads [17], [18]. The compressive forces set up by the seabed friction, in addition to any other external forces, such as restraint forces at tie-in points, is commonly referred to as the *effective axial force*.

Other important parameters that govern the buckling behavior are the size and shape of any out of straightness (OOS), the structural stiffness, and the seabed friction coefficients. For the flowlines resting on a very uneven seabed terrain, the vertical seabed imperfections result in more abrupt curvature than the horizontal imperfections created during laying. As a result, the axial load that initially forces the pipe vertically is found to be lower than the corresponding load needed to buckle the pipe laterally. It is observed that the pipe initially moves in the vertical plane as a gradual magnification of the initial imperfection due to its large initial OOS. As the pipe lifts off the seabed, a length of the pipe becomes laterally unrestrained and therefore the

Table 23.3 Equivalent Insulation Coating Density for Stability of KP Production Lines

								PONDUS	
				On-Bottom Stability Results According to RP E305					
Pipeline Section	Flowline	Soil Shear Strength Su (kPa)	Water Depth (m)	Water Depth used in Analysis (m)	Pipeline Submerged Weight (kg/m)	Coating Thick. (mm)	Min. Coating Density (kg/m^3)	Pipeline Movement Su = 20 kPa (m)	Pipeline Penetration in Clay Soil Su = 20 kPa (mm)
0–1.5	P101/102	20	306–322	306	31.0	53	1170	0.26	3
1.5–8.6	P101/102	20	306–322	306	22.4	53	1000	0	2
0–7.4	S101/102	20	299–322	299	22.9	53	1010	0	2
7.4–11.6	S101/102	20	299–322	299	33.5	53	1220	0	3
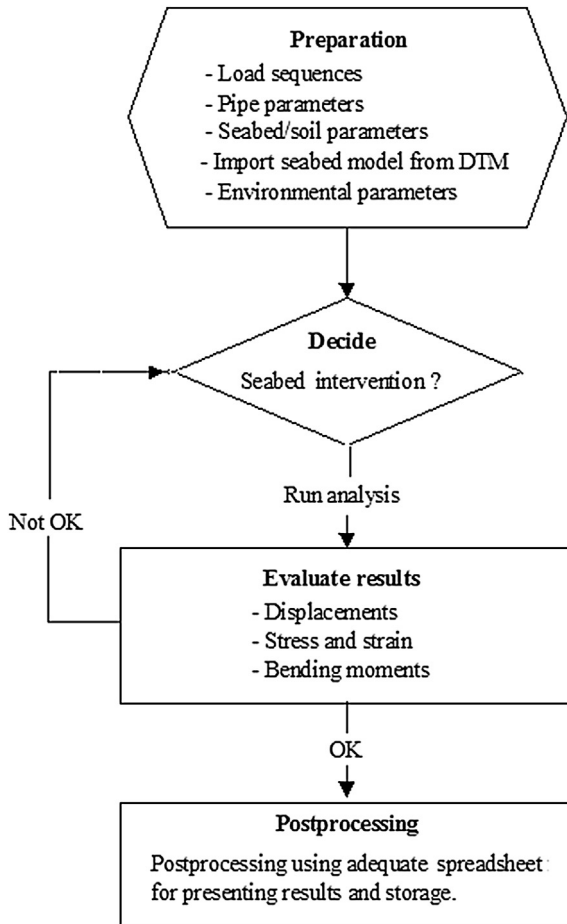
Figure 23.3 Flowchart for seabed intervention design through analysis.

critical axial force needed for lateral buckling decreases. Eventually, if sufficient pipe has lifted off the seabed, the lateral buckling force becomes less than the force required to lift the pipeline further in the vertical plane. At that moment, an interaction with the horizontal mode occurs and the pipe goes through dynamic "snap" movement.

On an uneven seabed, it appears that the critical lateral buckling force is little affected by the lateral friction coefficient. The 3D lateral buckling results show significantly lower stresses and strains in the buckles compared to 2D vertical buckling results for the same seabed and loads.

The cyclic shutdown-startup (or cooldown-heatup) analyses show that the flowline bending tends to "shake down" to an elastic state after a few cycles. For all cases, the largest stresses and strains are found to occur during the first operation startup. For the
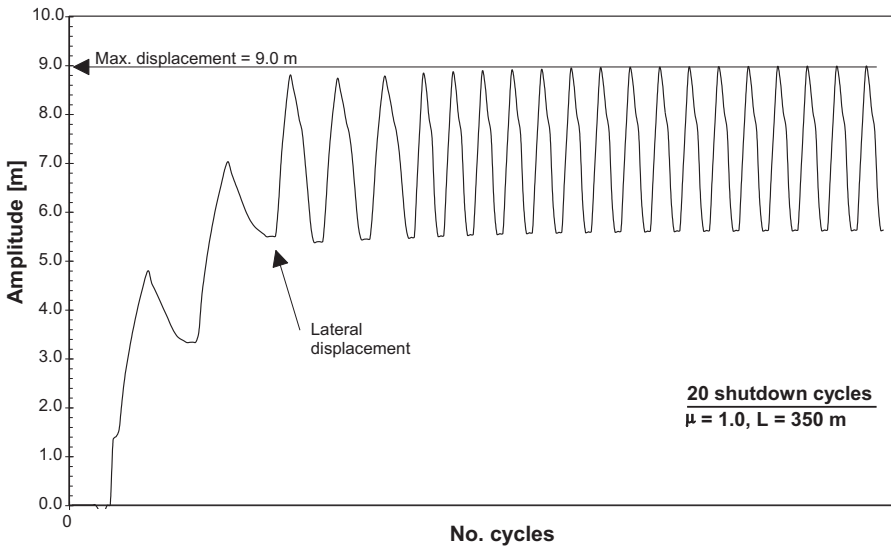
Figure 23.4 Displacement versus number of shutdown cycles.

case with a higher lateral friction coefficient ($\mu = 1.0$), the lateral displacement converges toward a maximum level of approximately 9.0 m after approximately 10 cycles, as shown in Figure 23.4 [19].

A buckling force of 220 kN represents only approximately 10% of the fully restrained axial effective force, which indicates that the flowlines are closer to being unrestrained than to being restrained. This important finding indicates that, unless the flowlines are restrained by other means (trenching, rock dump protection), the forces into the templates, riser bases, and the like are relatively low.

In-place analysis of the 10-inch production flowlines was conducted for P02 and SSP2. The latter line has many small imperfections, ranging in size between 1 and 2 m, and experiences buckling forces from 200 to 260 kN; while the P02 line, with larger seabed imperfections from 2 to 4 m, experiences buckling forces ranging between 140 and 180 kN.

If the vertical imperfection is of a size and a shape that the vertical buckling force stays lower than the lateral buckling force, even when the pipe has lifted off, the buckle should theoretically remain in the vertical plane. However, interaction with the lateral plane will certainly occur at some stage due to current forces, side slopes, and so forth. The effect of current and wave forces can be incorporated into the 3D in-place analysis using Morison's equations [20].

Trawl Board

In areas where fishing with bottom trawl equipment is likely, the industrial practice in the North Sea has been to protect all pipelines with diameter less than 16-inch from

trawl interaction loads by trenching or cover. Larger-diameter pipelines are left exposed on the seabed and protected by concrete coating. The 16-inch rule of thumb stems from the considerable amount of research conducted in the 1970s, Moshagen and Kjeldsen based theirs on trawl tests and analyses of simple beams subjected to transverse pullover loads [21].

To trench a pipeline is costly and may lead to an additional requirement to cover with backfill plus rock dumping to restrain the pipeline from buckling out of the trench.

The pullover load is a result of a dynamic interaction between the fishing gear and the pipeline. An increased flexibility (longer span length or reduced pipe diameter or wall thickness) is expected to reduce the pullover load. However, the geometrical effect is believed to be the governing parameter influencing the pullover load. Therefore, pullover loads are expressed as a function of span height [22].

A 3D nonlinear transient FE model has been developed to investigate the structural response of pipelines subjected to pullover loads. The analysis results indicated that this particular flowline would be able to withstand pullover loads when the impact point on the flowline was in full contact with the seabed prior to the load being applied [10]. However, further investigation was required to establish whether any limit should be defined for maximum allowable span length or span height. To investigate this, a vertical and horizontal pullover force of 105 kN and 40 kN, respectively, were applied at the large span at KP3.720, which corresponds to a span height of 0.5 m. (The span height is actually 1.5 m, however preliminary analyses had showed that the resultant stresses were far above acceptable levels).

Figure 23.5 shows an elevated view of the flowline configuration on the seabed as a function of time. As the pullover load is applied to the span, the adjacent section of the flowline is set in tension, so that a new span appears on the right-hand side of the existing span. In other words, the "slack" in the neighboring section is being pulled in toward the point where the pullover load is applied, very much in the same way as was found in the previous example, where the pipe was in full contact with the seabed. For this span the resulting equivalent stress of 520 MPa was found to exceed the allowable stress of $1.0 \times$ SMYS of 500 MPa.

A number of further analyses of spans with different heights and lengths revealed that the resulting stresses were not much influenced by span length, which agrees with the observations made by Verley (1994). The strong influence of the span gap is due to the way the load is specified by the DNV guideline [23]. Both the vertical and horizontal load components increase dramatically with the gap between the seabed and the pipeline. However, for the 10-inch flowline discussed, it was demonstrated that span height is the governing parameter in structural response to trawl board pullover loads.

The main conclusions from a large number of pullover simulations are

1. **Span height:** For a small-diameter pipeline, the span height is a governing parameter in the assessment of pipe structural behavior during trawl board pullover. For the high-strength 10-inch pipeline considered, it was concluded the maximum allowable gap should be
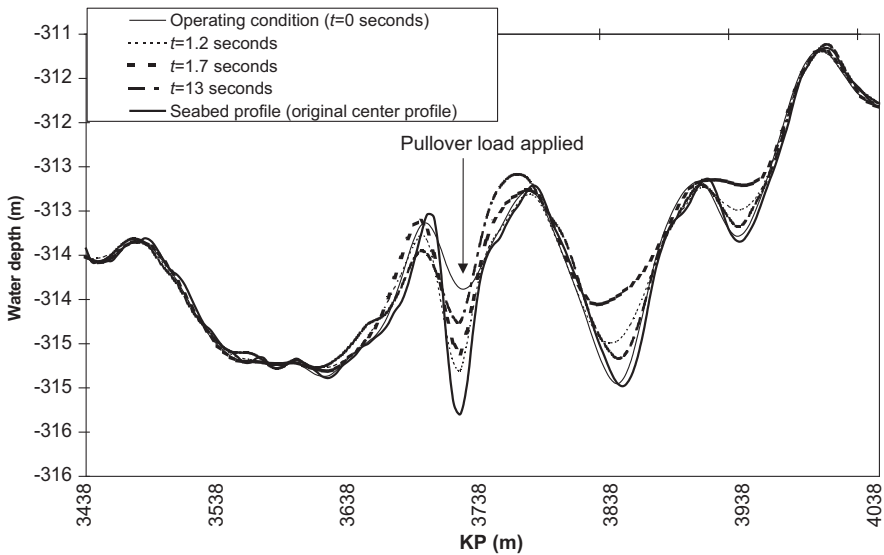
Figure 23.5 Flowline deflected shape (elevated view) as function of time.

limited to 0.25 m under permanent operating conditions. The span length was not found to be an important parameter for the structural pullover response.

2. **Trawling frequency:** Based on detailed information, it has been found that the trawling frequency with in the Åsgard field is less than one impact per km × year. Therefore, trawling frequency may be classified as "low."

3. **Impact response:** Through dynamic nonlinear analyses, it has been demonstrated that only a fraction of the impact energy is absorbed locally by the steel pipe. The flowlines can accommodate the identified impact loads, provided that the insulation coating has an energy absorption capability of 12 KJ and a minimum thickness of 30 mm. The flowlines will experience denting (plastic deformation) but within allowable limits.

4. **Pullover response of pipelines on a flat seabed:** Where the flowlines are in contact with a flat seabed, they can accommodate the maximum trawl board pullover loads, even while they are subject to high compressive effective force.

5. **Pullover response of pipelines on uneven seabed:** While it was confirmed that the pipelines resting on the seabed can resist the highest pullover loads considered for this area, the effect of span height on pullover loads and structural response was analyzed. For flowlines in operating conditions, it was found that the allowable span height is 0.25 m if both the equivalent stress (with usage factor 1.0) and strain criteria are applied; the allowable span height is 0.6 m if only strain criteria are applied. The length of the finite element model is limited by the length of flowline between two intermittent rock berms. In the seabed intervention design, the rock berm is designed such that the highest axial load may be resisted. The rock berm may be considered as fixing the ends of the pipelines.

6. **Soil sensitivity study:** The effect of varying the axial friction coefficient is small on trawl pullover response because the axial feed-in of pipe to the deflected zone is already limited by the low axial force and intermittent rock dumping. The peak stress and strain values reduce as the lateral friction coefficient increases. For the base case with an axial friction

coefficient of 0.3, increasing the lateral friction component from 0.3 to 0.6 results in a reduction in peak equivalent stress and strain of 18% and 6%, respectively. During trawl board pullover, the pipe is pushed downward, resulting in an increased lateral resistance locally near the hit point. Increasing the lateral friction to 2.0 over a length of 50 m with axial friction coefficients at 0.1 and 0.3 results in a reduction in the peak stress and strain of up to 30 and 40%, respectively. In both cases, the growth in the amplitude of the global buckle induced by trawl pullover was limited by the higher lateral friction. Therefore, the final bending configuration was less severe than with low friction.

7. **Generalization of trawl pullover analysis results:** It has been demonstrated that span height is the governing parameter in the assessment of pipe behavior during trawl board pullover. The critical span heights based on equivalent stress and axial strain criteria are listed in Table 23.4.

As long as the pullover load used as input to the analysis is a strong function of the gap height, other variables, such as span length and axial force in the line prior to impact, do not significantly affect the response.

Vortex-Induced Vibrations

The in-place analysis of the flowlines simulates the behavior of the lines on the seabed from the installation phase, including flooding and pressure testing, to operation and repeated shutdown cycles. The 2D FEM multispan modal analysis provides the cross-flow natural response frequencies of free spans while the in-line mode frequencies are determined from 3D span analyses [14]. The free spans present during the installation and shutdown periods tend to disappear when in operation, because the flowlines expand. Therefore, any proposed seabed intervention measures need to consider the consequences to later stages of operation, including startup and shutdown cycles.

The criteria applied in design of the Phase 1 flowlines are

- Onset of in-line VIV may occur during any phase of the design life provided the accumulated fatigue damage is acceptable.
- Onset of cross-flow VIV will be allowed during any phase of the design life provided allowable stress and fatigue limits are not exceeded.

Spans that are found to be critical with respect to VIV are usually rectified by placing rock berms below the pipe to shorten the span lengths and thus increase the natural

Table 23.4 Critical Span Heights for Trawl Board Pullover

| | Critical Span Height (m) | | |
| | | Temporary | |
Line	Operation	Cooldown	Shutdown
R101	0.30	0.40	+ 0.80
P101	0.25	0.40	+ 1.00

frequency of the spans. In addition to the cost implication of placing a large number of rock berms on the seabed, the main disadvantage of this approach is that feed-in of expansion into the spans is restricted. It was demonstrated through in-place analysis that allowing the flowline to feed into the spans reduces the effective force, which is the prime factor in the onset of pipeline buckling. It is therefore advantageous with respect to minimizing buckling that the number of rock-berm free-span supports is kept to a minimum.

The span analysis methodology and criteria are based on the design guideline from DNV for steady current loading and combined wave and current loading [24]. In-house Excel spread sheets and MATHCAD validation sheets have been prepared to process the large number of span assessments anticipated for the detail design of the Åsgard Phase 1 flowlines.

Two types of VIV assessment have been performed: a Level 2 assessment and a more advanced Level 3. The Level 2 assessment uses simplified single-span FE models and conservative VIV onset criteria to derive critical span lengths. The Level 3 assessment uses full multispan FE analysis to establish natural frequencies and associated mode shapes and fatigue analysis to calculate the fatigue lives due to in-line and cross-flow vibrations.
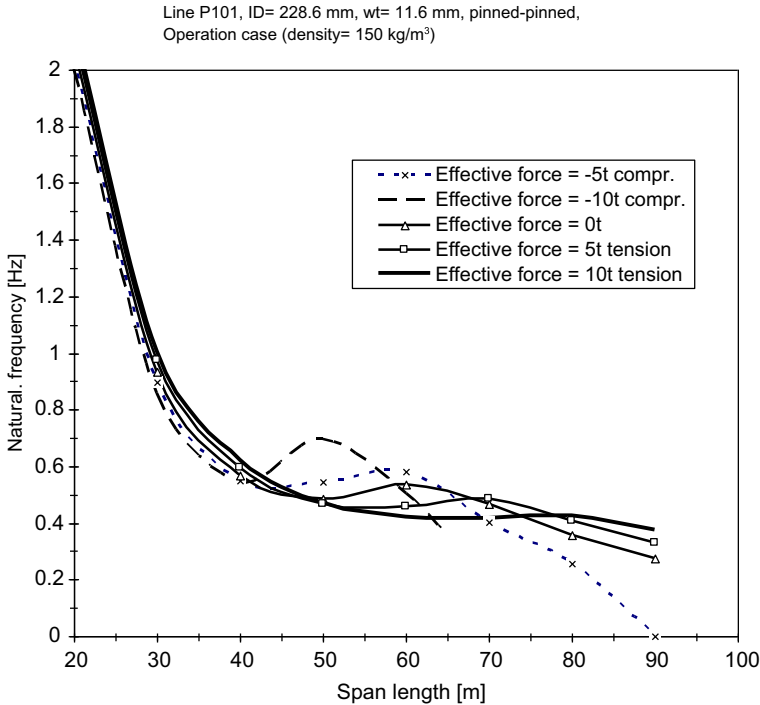
Figure 23.6 First vertical natural frequency as a function of span length and effective force (single-span Level 2 model).

When the nonlinear effect of sagging is ignored, the effect of axial tension is to stiffen the pipe and increase the natural frequency, while axial compression has a tendency to lower it. The effect of varying the effective force on the frequency versus span length behavior is illustrated in Figure 23.6 [25]. The results are obtained for the P101 line under operational loading. It can be seen that varying the tension or compression does not alter the frequency significantly for short span lengths. However, for span lengths longer than 40 m, where nonlinear geometry effects come into play, the natural frequency is strongly influenced by the effective force. This is particularly the case for long spans in compression.

It can be concluded that, when the axial tension cannot be estimated accurately, it may not be conservative to calculate the natural frequency for zero tension. In the case of axial compression, increasing the loading has a lowering effect on the natural frequency for very long spans (>40 m). A conservative estimate of natural frequency associated with maximum allowable span length can be obtained only if the maximum axial compression is adopted in the calculations.

The effect of the axial stiffness on the frequency is illustrated in Figure 23.7 [10], where single-span results with pinned-pinned boundary conditions and different axial restraints are illustrated. Curves representing the frequency versus span length for the three stiffnesses—zero, infinite, and a stiffness equal to the axial stiffness of the spanning pipe—are illustrated in Figure 23.7. For span lengths longer than 20 m, axial restraint is obviously an important variable.
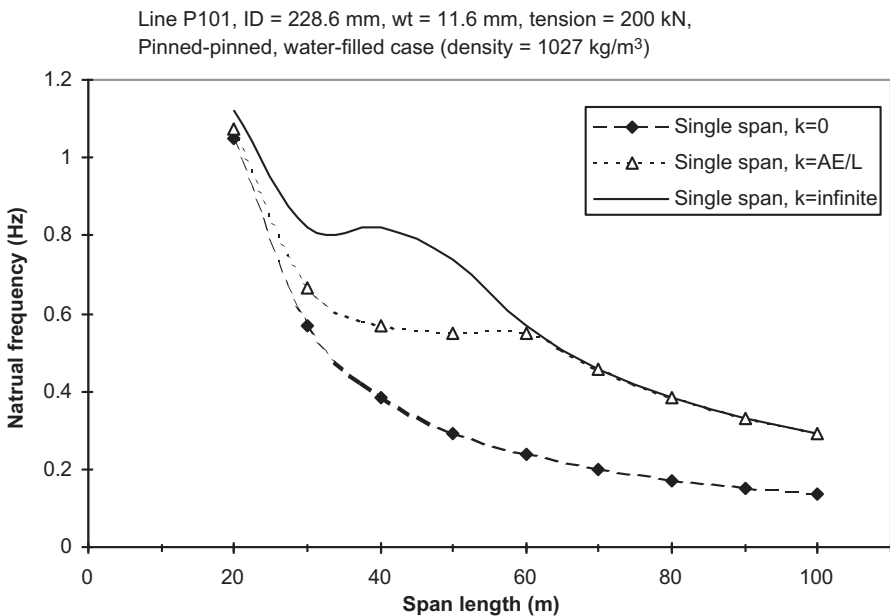
Figure 23.7 First vertical natural frequency as a function of span length and axial restraint (single-span Level 2 model).

From Figure 23.7, it can be seen that reducing the axial stiffness results in a reduction in the frequency and, hence, a lower allowable span length for a given critical frequency. The axial stiffness is represented by the two components; structural stiffness of the connecting pipe system and the pipe-soil interaction. The first component, which is significantly larger than the second, is a function of the pipe axial stiffness, shoulder length, and span interaction.

References

[1] Damsleth P, Dretvik S. The Åsgard Flowlines—Phase 1 design and installation design. In: Proc. of Offshore Pipeline Technology Conference, The Holmenkollen Park Hotel, Oslo, Norway; 1998.

[2] Bai Y, Damsleth PA, Dretvik S. The Åsgard Flowlines Project—Limit-state design experience. Oslo: IBC Conference on Risk-Based and Limit-State Design and Operation of Pipelines; October 4, 1999.

[3] Holme R, Levold E, Langford G, Slettebø H. Åsgard transport—The design challenges for the longest gas trunkline in Norway. Amsterdam: OPT'99; 1999.

[4] Statoil Technical Specification R-SF-260. Pipeline welding specification; 1991.

[5] Statoil Technical Specification R-SP-230. Welded linepipe-ferritic steel; 1990.

[6] Statoil Technical Specification R-SP-233. Seamless linepipe-austenstic ferritic stainless steel; 1990.

[7] Andersen O. Overview of Åsgard and Gullfaks satellite flowlines systems. Yokohama: OMAE'97; 1997.

[8] Bai Y, Damsleth A. Limit state design of flowlines. In: Yokohama: OMAE' 97; 1997.

[9] Damsleth P, Dretvik S. The Åsgard Flowlines—Phase 1 design and installation design. In: Proc. of Offshore Pipeline Technology Conference. The Holmenkollen Park Hotel, Oslo, Norway; 1998.

[10] DNV. Rules for submarine pipelines. Oslo: Det Norske Veritas; December 1996.

[11] Tørnes K, Nystrøm PR, Kristiansen NØ, Bai Y, Damsleth P. Pipeline structural response to fishing gear pull-over loads by 3D transient FEM analysis. Montreal, Canada: ISOPE'98; 1998.

[12] SINTEF. Åsgard flowlines—Fatigue testing of Cr13 tube. Trondheim, Norway: SINTEF; May 1997.

[13] Marshall PW PW. Design of welded tubular connections—Basis and use of AWS code provisions. Amsterdam: Elsevier; 1992.

[14] Kristiansen NØ, Bai Y, Damsleth PA. Ratcheting of HP/HT pipelines. Yokohama: OMAE'97; 1997.

[15] Bai Y, et al. Simulation of ratcheting of HP/HT flowlines. Brest, France: ISOPE'99; 1999.

[16] ABAQUS Version 5.5. Users manual, theory manual, verification examples manual. Hibbitt, Karlsson and Sorensen, Inc, Providence, Rhode Island: USA; 1995.

[17] Hobbs RE. In-service buckling of heated pipelines. J Transportation Eng 1984;110(2).

[18] Pedersen PT, Jensen JJ. Upheaval creep of buried heated pipelines with initial imperfections. J Mar Structures 1988;1:11–22.

[19] Nystrøm PR, Tørnes K, Bai Y, Damsleth P. 3-D dynamic buckling and cyclic behaviour of HP/HT flowlines. Honolulu, Hawaii: ISOPE'97; 1997.

[20] Ose BA, Bai Y, Nystrøm PR, Damsleth P. A finite element model for in-situ behavior of offshore pipelines and its application to on-bottom stability. Brest, France: ISOPE'99; 1999.

[21]   Moshagen H, Kjeldsen SP. Fishing gear loads and effects on submarine pipelines. In: Proc 12th Int. Offshore Technology. Conference. Houston: OTC 3782; 1980.

[22]   Verley RLP, Moshagen BH, Moholdt NC. Trawl forces on free-spanning pipelines. Int. J. Offshore and Polar Engineering 1994;2:24–31.

[23]   DNV. Interference between trawl gear and pipelines. Oslo: Det Norske Veritas; 1997.

[24]   DNV. Guideline no. 14. Free spanning pipelines. Oslo: Det Norske Veritas; 1998.

[25]   Kristiansen NØ, Tørnes K, Nystrøm PR, Damsleth D. Structural modeling of multi-span pipe configurations subjected to vortex induced vibrations. Montreal, Canada: ISOPE'98; 1998.

24 Flexible Pipe

Chapter Outline

---

1.   Introduction

The origin of flexible pipes can be traced to pioneering work carried out in the late 1970s. Initially, flexible pipes were used in relatively benign weather environments, such as offshore Brazil, the Mediterranean, and the Far East. However, the technology of flexible pipes advanced so rapidly that nowadays they have been used in various areas in the North Sea and gained popularity among designers in the Gulf of Mexico. The flexible pipe can be applied in the environments with water depths down to 8000 ft, high pressure reaching to 10,000 psi, and high temperatures above 150°F, as well as withstanding large vessel motions in adverse weather conditions. Figure 24.1 illustrates typical flexible risers used in deep water, in which different configurations are designed for different water depths. This type of dynamic application is typically used for floating production systems with high-pressure production risers, export risers, chemical/water/injection lines, and gas lift lines.

The applications of flexible pipe result from its composite structure, which combines helical steel armor layers with high stiffness to provide strength and polymer sealing layers with low stiffness to provide fluid integrity. As a result, this kind of pipe has low bending stiffness in comparison to axial tensile stiffness, which allows a much smaller radius of curvature than the homogenous pipe with the same antipressure capacity. This particular structure gives the flexible pipe a number of advantages over other types of pipelines and risers, such as steel catenary risers, which include reduced transport and
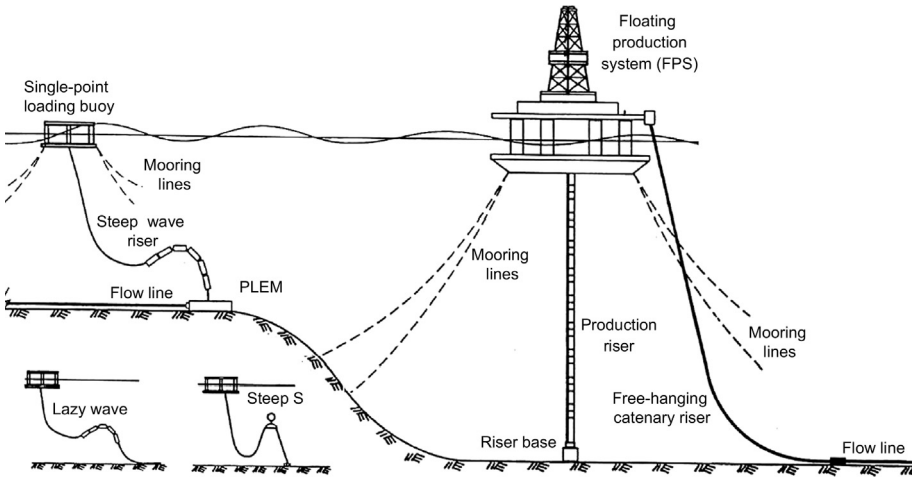
Figure 24.1 Typical flexible riser configurations.
Source: Ismail et al. [1].

installation costs by prefabrication in long lengths stored on reels and suitability for use with compliant structures, which allow permanent connection between a floating support vessel with large motions and subsea installations.

2. Applications of Flexible Pipe

The deepest water depth in which a flexible riser is installed is about 6234 ft (1900 m) with a flexible pipe internal diameter (ID) of about 7.5 in., as shown in Figure 24.2. Although flexible risers with ID of more than 16 in. have been installed offshore, these are in water depths not exceeding 1312 ft (400 m).

Figure 24.3 shows design pressure versus internal diameter for flexible pipes in operation, in which the data of flexible pipes are gathered from worldwide industry applications in the SurFlex Joint Industry Project (JIP) deliverables completed by the end of 2010. The database shows that 76% of all flexible pipes have design pressure below 345 bar (5000 psi), 90% below 10 in., and 70% used for design temperature less than 80°C. The pressure by internal diameter ($P \times$ ID) is an important characteristic for flexible pipes, and four lines of constant $P \times$ ID are plotted on the data collected from the database. The largest $P \times$ ID value in operation is 80,000 psi-inch, which is for a 12-inch flexible pipe. The majority of flexible pipes in use is below a $P \times$ ID value of 50,000 psi-inch. Figures 24.2 and 24.3 provide a good indicator of the current capacities of flexible pipes in operation.

The past and present applications of flexible pipes are cataloged as follows:

- Riser lines for connecting subsea equipment with the above-water production facilities. This includes the free-standing hybrid riser systems with flexible pipes used as jumper lines from rigid pipe risers to floating platforms,
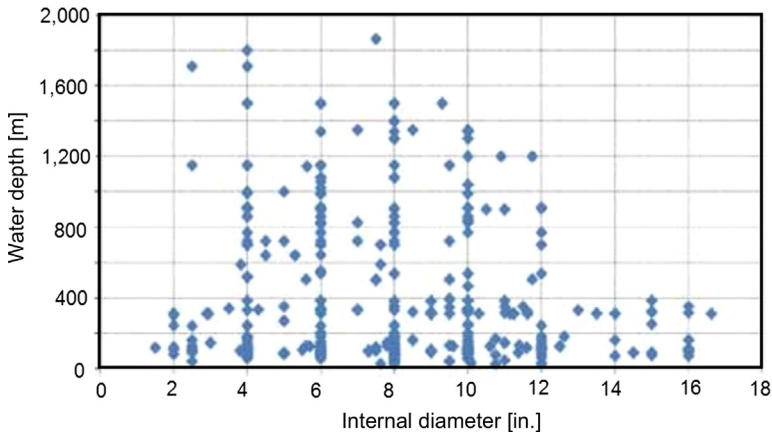
Figure 24.2 Water depth versus internal diameter for flexible pipes.
Source: O'Brien et al. [2]. (For color version of this figure, the reader is referred to the online version of this book.)

- Flowlines for intra-field connection of wellheads, templates, loading terminals, and the like.
- Loading hoses for offshore loading terminals,
- Jumper lines between fixed and floating platforms,
- Small-diameter service lines, such as kill and choke lines, umbilicals, and so forth.

The description of applications, functional requirements, and typical configurations are given in the following sections.

Flexible Risers

Except for the requirements of pipelines with long life, mechanical strength, internal and external damage resistance, and minimal maintenance, flexible risers are used as
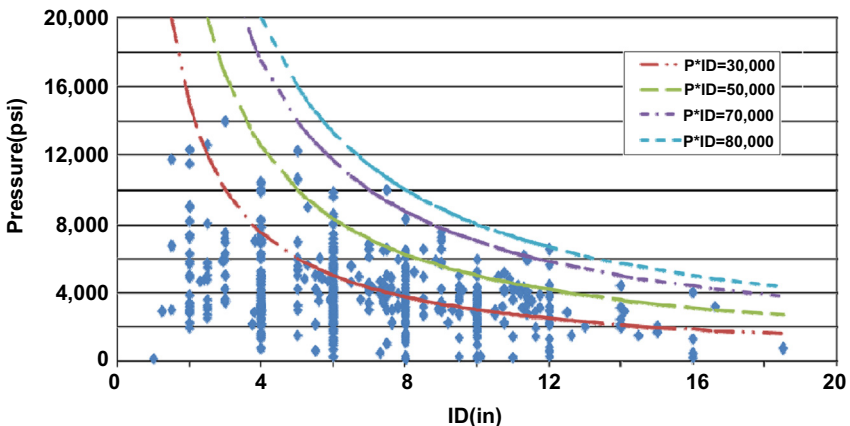
Figure 24.3 Design pressure versus internal diameter for flexible pipes.
Source: O'Brien et al. [2].

dynamic service pipes that require pliancy and high fatigue resistance. And flexible pipes are sometimes the only solution for risers in dynamic environments. Based on the JIP database, 58% of installed flexible pipes are risers and 70% of operating ones are in a water depth of less than 3281 ft. Industry practice requires several types of riser configurations typically used in conjunction with floating production-loading systems, as described before. Figure 24.4 illustrates six typical types of main riser configurations.

The configurations generally used are

- **Free-hanging catenary:** This is the simplest configuration for a flexible riser. It is also the cheapest to install, because of the minimal subsea infrastructure and easy installation. However, a free-hanging catenary is exposed to severe loading due to high vessel motions. And the riser is simply lifted off or lowered down onto the seabed. As a result, the free-hanging catenary is likely to suffer from compression buckling at the riser touchdown point (TDP) and tensile armor wire "birdcaging." The riser is appropriate for water depths from medium to deep water in medium environmental conditions. However, in deeper water, the top tension is large due to the long suspended riser length.
- **Lazy wave and steep wave:** In the wave type, buoyancy and weight are added along a longer length of the riser to decouple the vessel motions from the TDP of the riser. Lazy
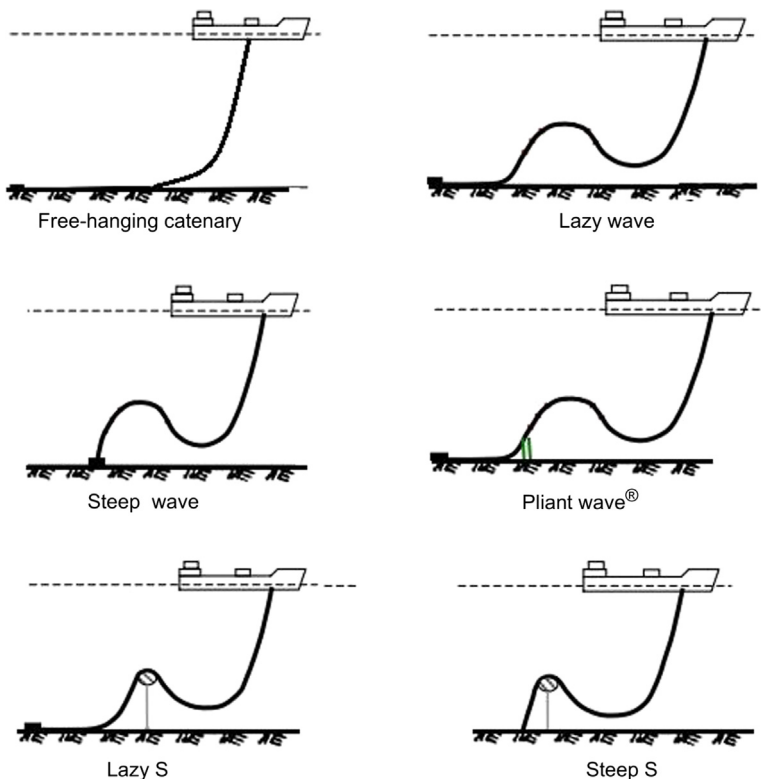
Figure 24.4 Flexible riser configurations.
Source: Bai and Bai [3].

waves are preferred to steep waves, because the former require minimal subsea infrastructure. However, lazy waves are prone to configuration alterations if the internal pipe fluid density changes during the riser lifetime, while steep wave risers require a subsea base and subsea bend stiffener and yet are able to maintain their configuration even if the riser fluid density changes. The wave type risers are appropriate for water depth from shallow to deep water. The steep wave risers are suitable for congested seabed developments and have a good dynamic response.

- **Pliant wave:** The pliant wave configuration is almost like the steep wave configuration, except a subsea anchor controls the TDP; that is, the tension in the riser is transferred to the anchor and not to the TDP. The pliant wave has the additional benefit that it is tied back to the well, located beneath the floater. This makes well intervention possible without an additional vessel. This configuration is able to accommodate a wide range of bore fluid densities and vessel motions without causing any significant change in configuration and inducing high stress in the pipe structure. Due to the complex subsea installation that is required, it would be required only if a simple catenary, lazy wave, or steep wave configuration is not viable. Moreover, this configuration is appropriate for a wide range of water depths and retains the advantages of both lazy wave and steep wave.
- **Lazy-S and steep-S:** In the lazy-S and steep-S riser configurations, there is a subsea buoy, either a fixed buoy, which is fixed to a structure at the seabed, or a buoyant buoy, which is positioned by cpreviously. The subsea buoy absorbs the tension variation induced by the floater, and the TDP has only small variation in tension, if any. Lazy-S configurations are considered only if catenary and wave configurations are not suitable for a particular field. This is primarily due to the complex installation required. A lazy-S configuration requires a mid-water arch, tether, and tether base, while a steep-S requires a buoy and subsea bend stiffener. The riser response is driven by the buoy hydrodynamics, and complex modeling is required, due to the large inertial forces in action. In case of large vessel motions, a lazy-S might still result in compression problems at the riser touchdown, leaving a steep-S as a possible alternative. This configuration is good at shallow water and for satellite tiebacks with several risers with a good dynamic response.

The feasible configurations differ in the use of buoyancy modules and the methods of anchoring to the seafloor. Configuration design drivers include a number of factors, such as water depth, host vessel access/hang-off location, field layout such as the quantity and types of risers and mooring layout, particular environmental data, and the host vessel motion characteristics.

The dynamic response of a particular riser system is directly related to the environmental loadings due to the combined wave-current flow field and the dynamic boundary conditions of the riser top end at the water surface, coupled with the interaction arising from the structural nonlinear behavior of the riser itself. Due to the low bending stiffness, all the external forces have to be balanced by geometric bending deformation and variability in the tension.

The design of a riser system must be closely integrated with the design of the support vessel and its station-keeping system, which governs motions together with the offset of the supporting point. The essential tasks for design and analysis of flexible risers should be as follows:

- Host layout and subsea layout.
- Wind, wave, and current data; vessel motion design codes; and company specifications.

Flexible Flowlines

Flexible flowlines are used in the intra-field to connect subsea wells, templates, wellhead platforms, or loading terminals to processing platforms, as shown in Figure 24.5. The flexible flowlines belong to the static categories, in which the flexible pipe is used to simplify the design or installation procedures or for the

1. Wellhead to steel platform flexible pipe through J tube

2. Wellhead to steel platform flexible pipe clamped along platform

3. Wellhead to concrete platform flexible pipe to rigid riser

4. Platform to platform

5. Wellhead to manifold

6. Platform to riser base

7. Platform to shore

8. Riser base to riser base
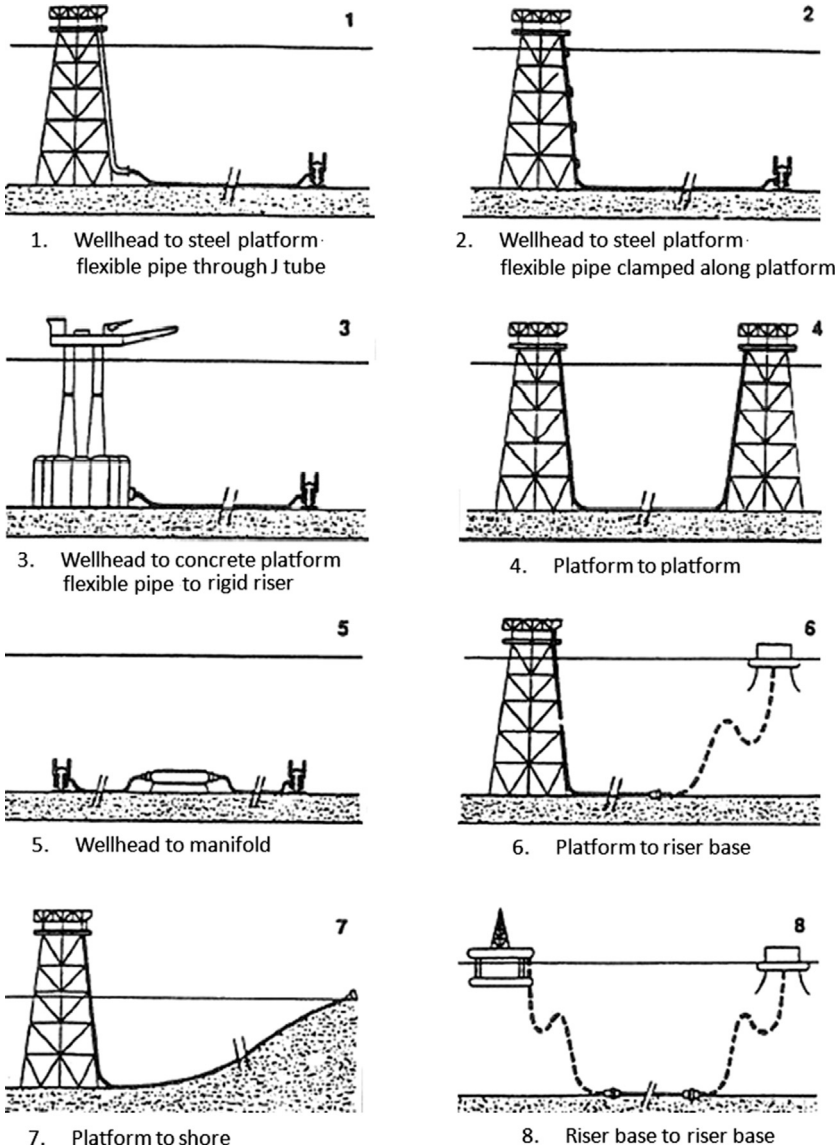
Figure 24.5 Flowline configurations.
Source: Berge and Olufsen [4].

inherent insulation or corrosion-resistant properties. The functional requirements to a flexible flowline are generally the same as a steel one.

Loading and Offloading Hoses

Offshore loading hoses are used as temporary connections between shuttle tankers and a storage tanker or loading buoy. The loading hoses may be submerged or pulled into the supporting vessel either straight or reeled. These hoses allow unrestricted moving of the tanker during the loading procedure even under severe weather conditions. Therefore, the loading hoses are subjected to vessel motions and wave loading. Handling involved in connecting and disconnecting operations attach additional loads. Robustness with respect to handling is a major concern for flexible pipes intended for offshore loading.

In most cases, these hoses connect the loading buoy with the tanker. The hoses can either float on the water surface or, as is also practiced, be suspended between the boom of a mooring buoy and the tanker bow. With the development of offshore LNG (liquefied natural gas) projects, cryogenic flexible pipes are also used as the loading and offloading hose in the several offshore LNG transfer systems, as shown in Figure 24.6. In this system, operational reliability and safety are key issues.

In shallow water, a pipeline between two surface floaters separated by 1500 m is simply laid on the seabed. However, in water over 1000 m deep, this would significantly increase the total length of the line between the two floaters. It is therefore preferable to suspend the export line between the two floaters (for example, FPSO and the CALM buoy) without contact with the seabed.

Figure 24.7 shows some possible configurations of flexible pipes to link the two floaters with an oil offloading line. In these options, the amount of buoyancy needed to support the pipeline has an important impact on the final costs of the export system. On the other hand, the loads applied on the CALM buoy also have an important impact and should be as vertical as possible to avoid disturbing the equilibrium of the buoy. The buoyancy modules spread along the line, as shown in (a), (b), and (c) of the figure, give the possibility of obtaining a broad range of different shapes. This is the most common solution in shallow water, where buoyancy waves are required to give sufficient compliance to the system. Another option is to use a single catenary without intermediate buoyancy, as shown in (d) of the figure. This has an important impact on the size of the CALM buoy but can be a valuable solution in some cases, in
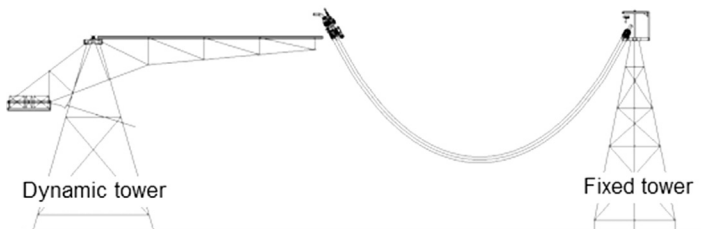
Figure 24.6 Flexible hose used in LNG transfer system.
Source: Rombaut et al. [5].

(a)

Large diameter pipe with one buoyancy wave
or W configuration

(b)

Pipe with several buoyancy waves

(c)

Pipe with a subsurface offloading buoy

(d)

Single catenary shape or U configuration
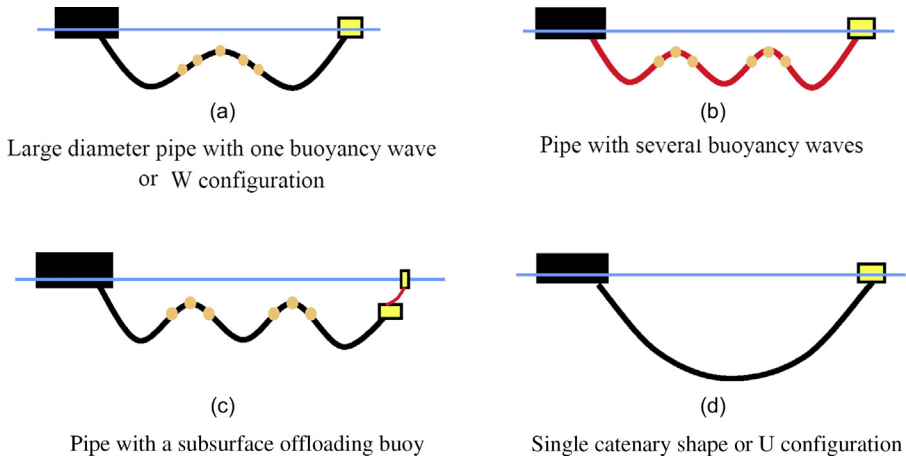
Figure 24.7 Possible configurations for oil export system.
Source: Lebon and Remery [6]. (For color version of this figure, the reader is referred to the online version of this book.)

which large density variations in the internal fluid are considered. In these cases, the shape of a single catenary with a fixed suspended length is not modified by a change in the linear weight of the line.

Jumper Lines

The functions of jumper lines are in many respects similar to riser systems. However, the two operations are somewhat different. The lines are more exposed to wave loading and the configuration is different in the connected condition compared to a standoff condition, which introduces extra requirements at the end of connectors, such as bending stiffeners [3]. The examples of flexible pipes used as jumper line applications include

- Intrafield connection of wellheads and manifolds (typically in lengths less than 100 m).
- Connection of topside wellheads and platform piping on TLPs.
- Connection of wellhead platforms and floating support vessels.
- Lines in FPSO turret motion transfer systems.

Drilling Risers

Flexible pipes can also be used as drilling risers, especially for drilling with downhole motors. In this operation, a controllable weight is applied to the drill bit. Dynamic bending of the suspended part is moderate, and the dynamic support loads are related to the repeated rolling over sheaves. If the heave compensator is based on a taut system, bending fatigue is a major design consideration.

3.   Flexible Pipe System and Components

Flexible pipes are composite structures with two types of basic components:

1. Armour components, which are usually of spiral steel wire construction, providing strength.
2. Polymer or compliant steel tubes, which are sealing components, providing containment of fluid.

Generally, two types of flexible pipes are in use: bonded and unbonded flexible pipes. In bonded pipes, different layers of fabric, elastomer, and steel are bonded together through a vulcanization process. Flexibility is obtained by axial and shear deformation of the elastomer matrix in which the reinforcing elements are embedded. However, bonded pipes are used only in short sections, such as jumpers. On the other hand, unbonded flexible pipes, whose layers are able to slip past each other under external and internal loads, can be manufactured for dynamic applications in lengths of several hundred meters. Unless otherwise stated, the rest of this chapter and the next one deal with unbonded flexible pipes. The unbonded flexible riser may either be designed as a rough bore or smooth bore, as shown in Figure 24.8.

The rough bore structures employ an inner steel carcass and are used whenever gas may be present in the transported fluid. In such cases, a rapid pressure drop may lead to collapse of the inner liner unless it is stiffened by a carcass. The smooth bore pipe constructions are used for applications that do not cause gas diffusion through the internal thermoplastic layer, such as water injection and chemical injection. It is also suitable for the fluid with gas, if the annulus is vented. A smooth bore structure consists of the same layers as the rough bore, except that the inner interlocked carcass is omitted.

The various applications result from the characteristics of the flexible pipe system, which include the pipe body and related ancillaries. Figure 24.9 shows a typical cross section of an unbonded flexible pipe. This figure clearly identifies the five main components of the flexible pipe cross section. And the space between the internal polymer sheath and the external polymer sheath is known as the *pipe annulus*. The five main components of the flexible pipe wall are dealt with in the following sections.

(a) Rough bore   (b) Smooth bore
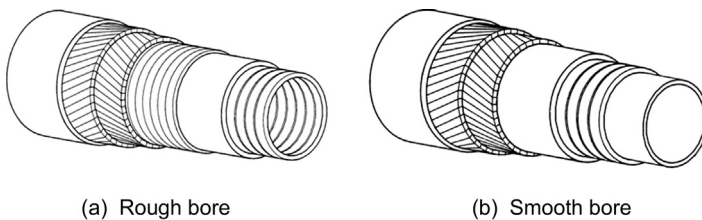
Figure 24.8 Inner surfaces of unbonded flexible pipe.

1. Carcass
2. Internal fluid barrier
3. Pressure armor
4. Antiwear layer
5. Tensile armor
6. Antiwear layer
7. Armor wire
8. Antibirdcaging layer
9. External fluid barrier
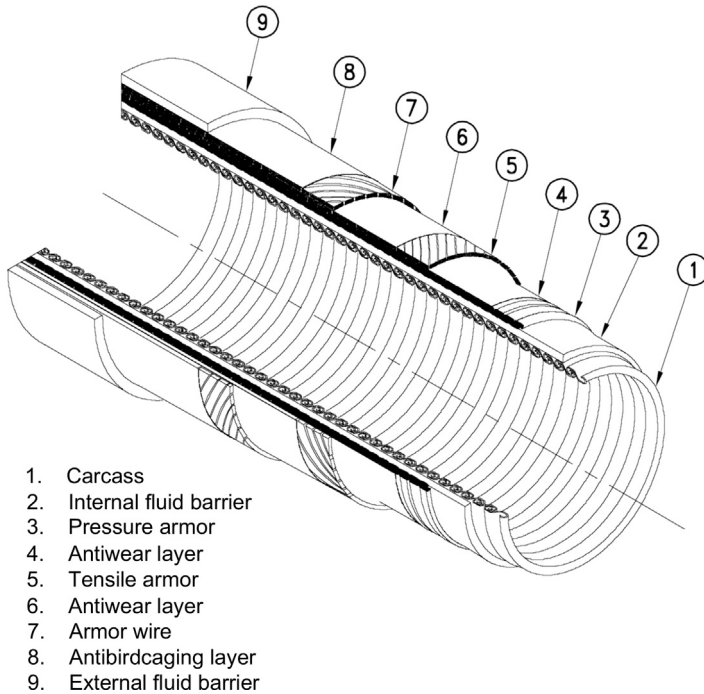
Figure 24.9 Typical cross section of an unbonded flexible pipe.
Source: Zhang et al. [7].

Interlocked Steel Carcass

The carcass forms the innermost layer of the flexible pipe cross section. It is commonly made of a flat stainless steel strip that is formed into an interlocking profile, as seen in Figure 24.9. Different steel grades can be used to form the carcass, and the choice of material usually depends on the internal fluid characteristics. The most common grades used to manufacture the carcass are AISI grades 304 and 316 and duplex. The inner bore fluid is free to flow through the carcass profile, and therefore the carcass material needs to be corrosion resistant to the bore fluid.

An example of a carcass profile is shown in Figure 24.10. The main function of the carcass is to prevent pipe collapse due to hydrostatic pressure or a buildup of gases in the annulus. The buildup of gases in the annulus could be a potential failure mode for the pipe and occurs in hydrocarbon-carrying pipes when gases from the inner pipe bore diffuse through the internal polymer sheath into the annulus. In the case of a well shutdown and subsequent depressurization and evacuation of the inner bore, the annulus gas pressure could cause the pipe to collapse. Therefore, the steel carcass is designed to withstand this collapse pressure. Pipes that do not carry any hydrocarbon fluid (e.g., water injection pipes) can be constructed without a carcass if there is no
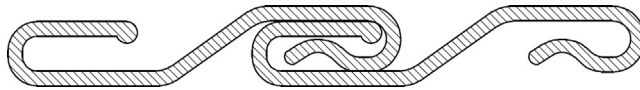
Figure 24.10 Carcass layer profile.
Source: API [8].

potential for gas buildup in the annulus to cause pipe collapse, which are known as smooth bore pipes, described previously.

Internal Polymer Sheath

The internal polymer sheath provides a barrier to maintain the bore fluid integrity. Exposure concentrations and fluid temperature are the key design drivers for the internal sheath. Common materials used for the internal sheath include polyamide-11 (commercially known as Rilsan®), high-density polyethylene (HDPE), cross-linked polyethylene (XLPE), and PVDF (polyvinylidene fluoride). Polyamide-11 and HDPE are the two materials most commonly used. These two materials can withstand temperatures up to about 149°F (65°C) and have an allowable strain of 7%. PVDF can be used for applications that require a higher temperature tolerance. This material can withstand the temperature of 266°F (130°C), but its allowable strain is only 3.5%. The polymer sheath layer thickness is a function of various parameters, such as inner bore fluid temperature, composition, and inner bore pressure. The average size of this sheath is about 5∼8 mm, but pipes with up to 13 mm of internal polymer sheath have also been manufactured.

Armor Layers

Pressure Armor

The pressure armor is to withstand the hoop stress in the pipe wall, which is caused by the inner bore fluid pressure. The pressure armor is wound round the internal polymer sheath and is made of interlocking wires. This is an interlocked metallic layer that supports the internal pressure sheath and system internal pressure loads in the radial direction. Some example profiles for the pressure armor wires are shown in Figure 24.11. These profiles allow bending flexibility and control the gap between the armor wires to prevent internal sheath extrusion through the armor layer. To best resist the hoop stress in the pipe wall, the pressure armor is wound at an angle of about 89° to the pipe longitudinal axis. The "zeta"-shaped helical or interlocked pressure armour layers have reinforcement effects against internal and external pressure and support hoop loading. This layer provides support outside the fluid barrier layer by resisting ovalization of the underlying structure such as carcass layer. The "zeta"-shaped layer is not capable of withstanding either axial or bending loads significantly. This is because it is wound in a helix with a short pitch with a lay angle close to 90° and with a gap between turns of an interlocked metal profile wires.

a) Z-shape   b) C-shape

c) T-shape 1   d) T-shape 2
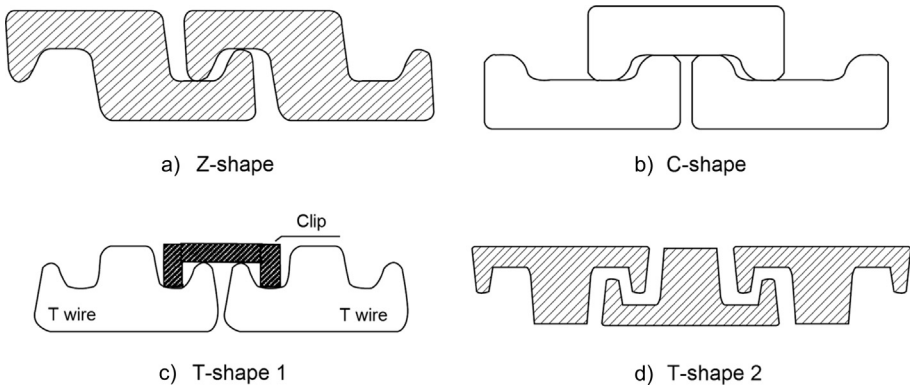
Figure 24.11 Pressure armor interlock profile.
Source: API [8].

The material used for the pressure armor wire is typically high-strength carbon steel. The choice of wire typically depends on whether the pipe is qualified for "sweet" or "sour" service ("sour" service as defined by NACE MR 01-75). The highest-strength steel wires used in flexible pipe applications have an ultimate tensile strength (UTS) of 1400 MPa (200 ksi). However, these high-strength wires are prone to hydrogen-induced cracking (HIC) and sulfide-stress cracking (SSC). Hence, it might not be possible to use such high-strength steel wires for "sour" pipe applications. The alternative would be to use additional steel layers with a UTS as low as 750 MPa (105 ksi).

Tensile Armor

The tensile armor layers are always cross wound in pairs. As their name implies, these armor layers are used to resist the tensile load, torsional, and bending moments on the flexible pipe. The tensile armor layers, as shown in Figure 24.12, are typically made of flat rectangular wires and laid at about $30° \sim 55°$ to the longitudinal axis. Flexibility in bending of unbonded pipes originates from the ability of the tendons (wires) of helical layers to slip with respect to each other. This leads to wear and ultimately the fatigue of the tendons. The amount of slip is inversely proportional to the lay angle of the tendons. A lay angle of $55°$ results in a torsionally balanced pipe,

t=3 mm

b=6 mm
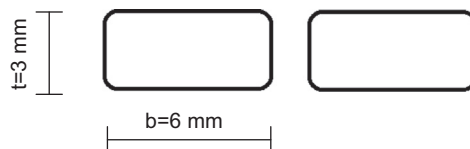
Figure 24.12 Typical profile of tensile armors for helical layers.

and this angle is used in pipe designs where the hoop stress is also resisted by the tensile armor layers, and no pressure armor layer exists.

The tensile armor layers are used to support the weight of all the pipe layers and transfer the load through the end fitting to the vessel structure. High tension in a deepwater riser may require the use of four tensile armor layers, rather than just two. The tensile armor wires are made of high strength carbon steel, like the pressure armor wires. "Sweet" or "sour" service conditions are determining factors on the wire strength that can be used, because high-strength wire is more prone to HIC and SSC.

Composite Armor

With the increasing water depth of offshore field developments, the suspended weight and the fatigue performance of dynamic risers become more and more often driving design factors. The advantages of composite armor may include

- Higher strength to weight ratio, resulting in a lighter weight pipe structure for equivalent structural capacity.
- Improved fatigue resistance.
- Resistance to corrosion and degradation by most oilfield chemicals and seawater.

With properly selected fiber, matrix, and process, typical tensile strength of more than 3000 MPa (435 ksi) has been recorded for carbon fiber composite (CFC) material. Figure 24.13 shows the highest specific strength (UTS to density ratio, where UTS is 3000 MPa and density is 1700kg/m^3) of such CFC when compared to conventional carbon steel and, in particular, steel grades suitable for sour service (presence of H_2S and associated risk of hydrogen embrittlement), which are used for conventional flexible pipes.
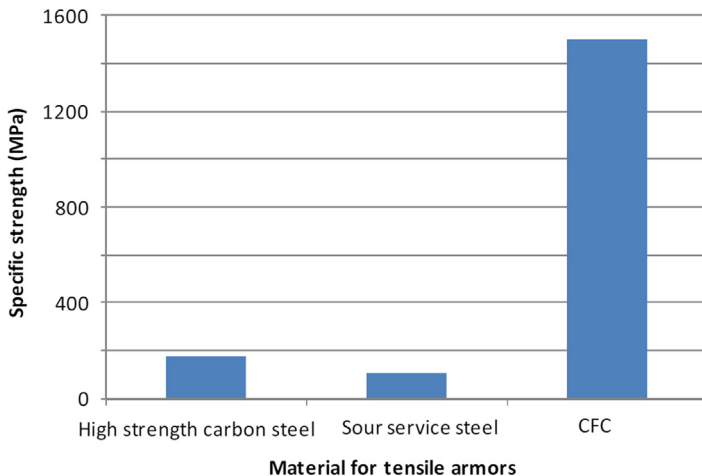
Figure 24.13 Specific strength of various materials usable for tensile armours.
Source: Do and Lambert [9]. (For color version of this figure, the reader is referred to the online version of this book.)
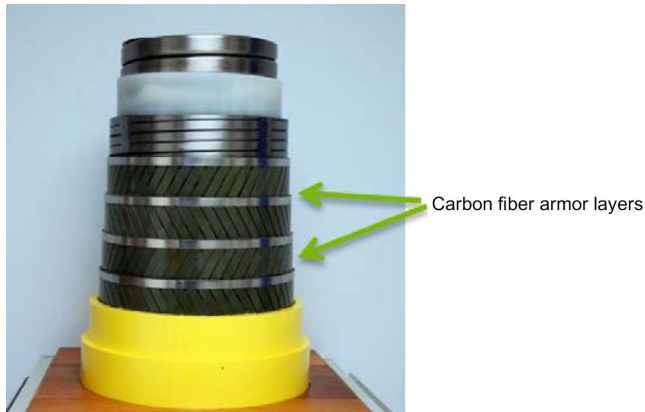
Figure 24.14 Crosswound four CFA layers flexible riser.
Source: Do and Lambert [9]. (For color version of this figure, the reader is referred to the online version of this book.)

Replacing the metallic pressure and tensile armors of unbonded flexible pipe with fiber reinforced polymer (FRP) materials or composite armor is becoming a tendency because of their advantages.

Figure 24.14 shows a flexible pipe using four layers of carbon fiber armour (CFA) by Technip. The high level performance of the qualified flexible pipe integrating CFA allows a light weight flexible riser solution and reducing or removing the requirement for buoyancy elements for ultra-deepwater configurations.

Figure 24.15 provides a cross-sectional view of a typical pipe structure of Deep-Flex FFRP. The flexible fiber reinforced pipe (FFRP) with a noninterlocked hoop strength layer is an unbonded flexible pipe structure employing composite pressure and tensile armor.

External Polymer Sheath

The external polymer sheath can be made of the same materials as the internal polymer sheath. The main function of the external sheath is as a barrier against seawater. It also provides a level of protection for the armor wires against clashing with other objects during installation.

Other Layers and Configurations

In addirion to these five main layers of the flexible pipe are minor layers that make up the pipe cross section. These layers include antifriction tapes wound around the armor layers, whose purpose is to reduce friction and hence wear of the wire layers when they rub past each other as the pipe flexes due to external loads. Antiwear tapes can also be used to make sure that the armor layers maintain their wound shape. These tapes ensure that the wires do not twist out of their preset configuration,
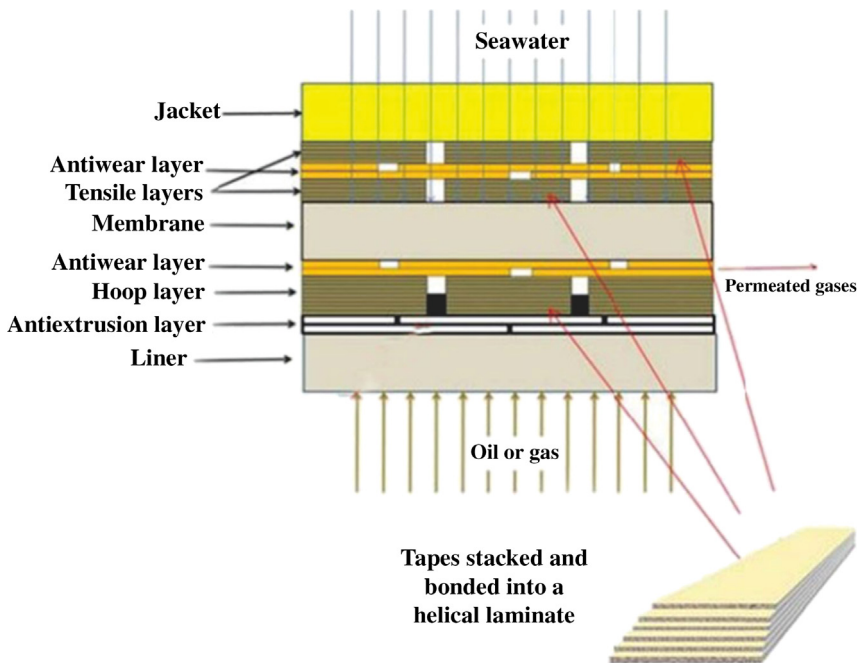
Figure 24.15 Flexible fiber reinforced pipe.
Source: Kalman et al. [10]. (For color version of this figure, the reader is referred to the online version of this book.)

a phenomenon called *birdcaging*, which results from hydrostatic pressure causing axial compression in the pipe.

In some flexible pipe applications, due to high tensile loads, high-tensile wires are required for the tensile armor layers, and yet the presence of a sour environment means that these wires suffer an unacceptable rate of HIC and SSC. A solution to this situation is to fabricate a pipe cross section with two distinct annuli rather than one. The inner annulus could contain the pressure armor layer, which need not be made of very high-tensile steel and would therefore not suffer serious corrosion problems due to a high concentration of H_2S. An extra polymer sheath could then be laid between the pressure armor layer and the tensile armor layers. This polymer sheath would prevent a high H_2S concentration in the outer annulus. A certain amount of H_2S would still be able to diffuse through this polymer sheath from the inner to the outer annulus. However, the concentration of H_2S in the outer annulus could now be low enough to permit the use of high-tensile wires for the tensile armor layers.

Main Ancillaries

The following integral ancillaries assist the pipe body to make up the complete flexible pipe system.

End Fittings

The end fittings are designed to terminate the ends of each flexible pipe layer and provide the required connection to mate with the customer's production facilities. Each of the flexible pipe layers is individually terminated and sealed to sustain the imposed loads and maintain fluidtight integrity. The characteristics are listed as follows:

- End fittings are custom designed for each flexible pipe structure.
- Terminations can be any design—API/ANSI flanges, hubs, welded, or other.
- Stronger than pipe in burst and failure tension.
- The most common structural material is AISI 4130 low alloy steel.
- Common coatings include electrolysis nickel plating and various epoxies.
- Assembly is a manual process.

It is obvious that the effective barrier seal system is a key issue for the design of end fittings. Figure 24.16 is a schematic illustration of an end fitting barrier seal.
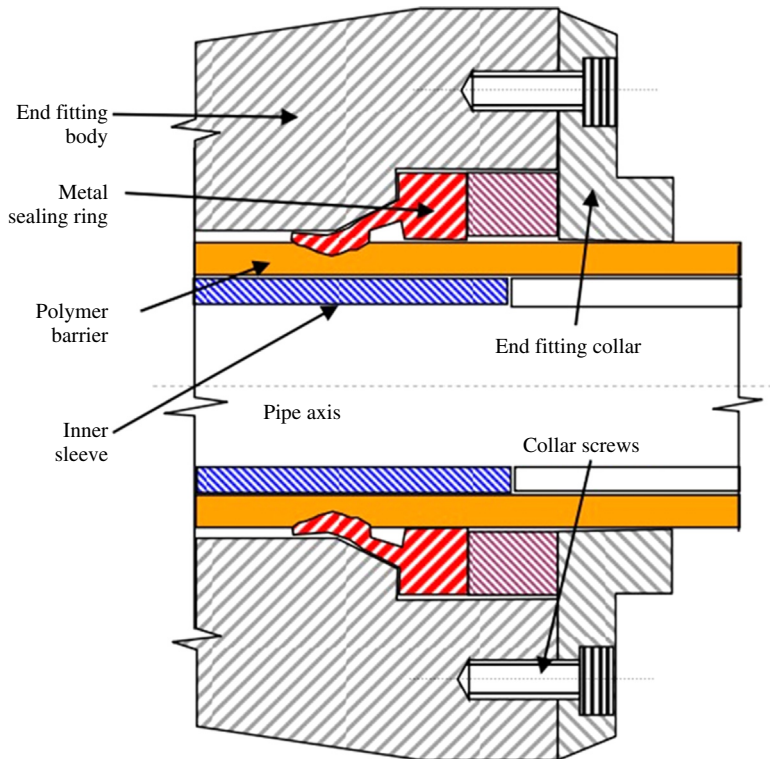
Figure 24.16 An end fitting barrier seal.
Source: Fernando et al. [11]. (For color version of this figure, the reader is referred to the online version of this book.)

A number of critical issues need to be considered during the design and manu-
facture of end fitting arrangements. Tight manufacturing tolerances are essential for
the pressure sheath and sealing ring dimensions, pressure armor termination, and bolt
torque to ensure the adequate transfer of load from the steel layers of the pipe onto the
vessel structure. Epoxy filling should be carried out using the appropriate techniques
to ensure no air gaps are produced. The correct positioning and functioning of the
annulus vent ports are also important to ensure no build-up of gases in the annulus. To
prevent corrosion, the anode clamp design is usually used to protect flexible pipe end
fittings. Before the installation, the ROV needs to clean the end fitting surface using a
steel brush to guarantee a better electrical contact of the anode clamp.

Bend Stiffener and Bell Mouths

One of the critical areas of a flexible riser is the top part of the riser, just before the
hang-off arrangement. This area is prone to overbending and hence an ancillary
device is incorporated into the design to increase the stiffness of the riser and
prevent bending of the riser beyond its allowable bend radius. The two devices used
for this application are bend stiffeners and bell mouths. Figure 24.17 illustrates both
devices.

Flexible pipe manufacturers tend to have a preference for one or the other device,
yet bend stiffeners are known to provide a better performance in applications with
high-motion vessels. Bend stiffeners also provide a moment transition between the
riser and its rigid end connection. The ancillary devices are designed separately
from the pipe cross-section analysis, and specialized software is used for this pur-
pose. Global loads from the flexible riser analysis are used as input to the ancillary
device design.

(a) Bend stiffener   (b) Bell mouth
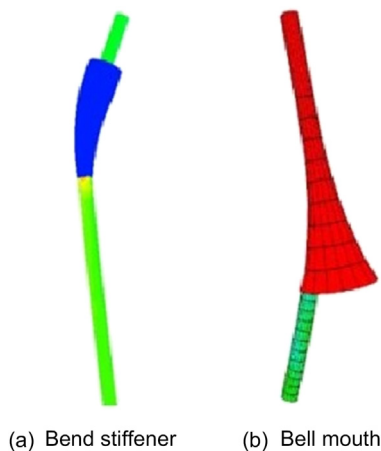
Figure 24.17 Bend stiffener and bell mouth.
Source: Bai and Bai [3]. (For color version of this figure, the reader is referred to the online
version of this book.)
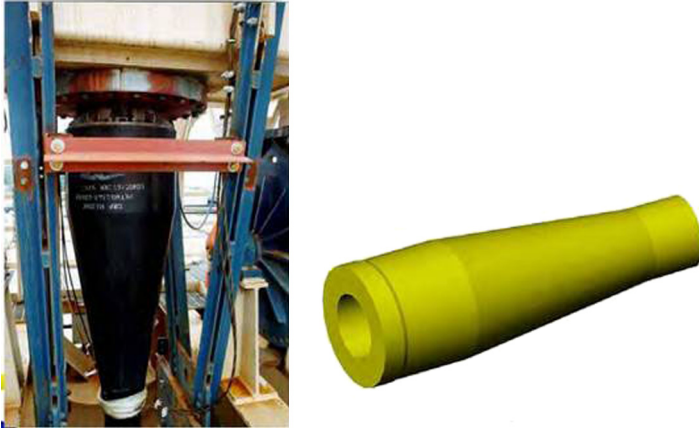
Figure 24.18 An example of a bend stiffener.
Source: Clevelario [12]. (For color version of this figure, the reader is referred to the online version of this book.)

Bend stiffeners are normally made of polyurethane material, and their shape is designed to provide a gradual stiffening to the riser as it enters the hang-off location. The bend stiffener polyurethane material is itself anchored in a steel collar for load transfer. Bend stiffeners are sometimes utilized subsea, such as in steep-S or steep-wave applications to provide support to the riser at its subsea end connection and to prevent overbending at this location. Design issues for bend stiffeners include polyurethane fatigue and creep characteristics. The cone dimensions are determined with the most severe tension and angles combination to satisfy a minimum bending radius acceptance criteria and an acceptable fatigue life for the pressure vault and the armour wires of the flexible structure. Figure 24.18 shows an example of a bend stiffener. Note that bend stiffeners longer than 20 ft have been manufactured and are in operation in offshore applications.

Bell mouths are steel components that provide the same function as bend stiffeners, that is, to prevent overbending of the riser at its end termination topside. The curved surface of a bell mouth is fabricated under strict tolerances to prevent any kinks on the surface that might cause stress concentrations and damage the pipe external sheath.

Bend Restrictor

The bend restrictors are normally located at the bottom and top connections. The purpose is to provide additional resistance to overbending of the riser at critical points (such as the ends of the riser, where the stiffness is increased to infinity).

Bend restrictors are designed to limit bending on flexible pipelines and used for quasi-static purposes and installation. They are made of a hard plastic material and typically used at wellhead tie-ins and riser bases to restrain the riser tension, bending, and shear loads. Steel solutions are also available at lower cost but must be packaged
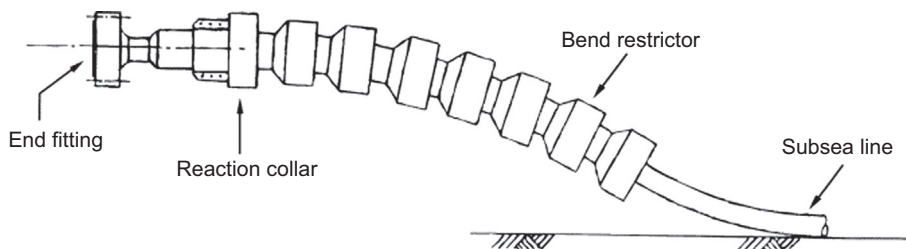
Figure 24.19 Bend restrictor.
Source: API [8].

in plant and protected by paint and anodes. Bend restrictors provide mechanical locking to prevent overbending. Figure 24.19 illustrates a bend restrictor used at the end termination of a flexible pipe subsea.

Buoyancy Modules

Buoyancy modules can be attached to the riser to decrease the tension required at the surface and obtain the desired riser configuration, including lazy, steep, and reverse configurations. These modules may be thin-walled air cans or fabricated syntactic foam modules that are strapped to the riser. These buoyancy modules require careful design, and the material for their construction needs to be selected appropriately to ensure that they have a long-term resistance to water absorption.

Annulus Venting System

Over time, the fluids that are transported in the pipe bore diffuse through the internal polymer sheath into the pipe annulus. These diffused gases include water, CO_2, and H_2S; and their presence in the annulus could have a deleterious effect on the steel layers. Water and CO_2 have a tendency to cause general or pitting corrosion in the pressure and tensile armor layers. The presence of water could also have a negative effect on the fatigue life of the steel layers. The presence of H_2S causes HIC and SSC in steel, and its concentration is carefully assessed during the design stage, because a pipe qualified for sweet service could use high-strength tensile steel that would otherwise suffer unacceptable corrosion in a sour environment.

Apart from the negative corrosion and fatigue effects caused by the presence of these diffused gases on the steel layers of the pipe, the buildup of pressure in the annulus due to the presence of the gases could also trigger collapse of the internal polymer sheath of the pipe. In case of a sudden pressure loss in the inner bore of the pipe (for instance, an emergency shutdown of the system), the pressure in the annulus due to these diffused gases might be greater than the pressure in the inner bore. This could lead to collapse of the internal polymer sheath, loss of fluid integrity, and failure of the pipe. The steel carcass is designed to withstand this collapse pressure due to gas buildup in the annulus. And this failure mode has been documented to occur in flexible pipes.

To prevent the buildup of gases in the annulus due to diffusion, a venting system is incorporated into the pipe structure to enable the annulus gases to be vented out to the atmosphere. The vent valves in both end fitting arrangements are located subsea, directly connected to the annulus, designed to operate at a preset pressure of about 30–45 psi, and sealed to prevent any ingress of seawater into the annulus.

References

[1] Ismail N, Nielsen R, Kanarellis M. Design considerations for selection of flexible riser configuration. PD-Vol. 42. Offshore and arctic operations. New York: ASME; 1992.

[2] O'Brien P, et al. Outcomes from the SureFlex joint industry project—An international initiative on flexible pipe integrity assurance. Houston: OTC 21524, Offshore Technology Conference; 2011.

[3] Bai Y, Bai Q. Subsea pipelines and risers, Chapter 22 2nd ed. Oxford, UK: Elsevier Science Ltd; 2005.

[4] Berge S, Olufsen A. Handbook on design and operation of flexible pipes. Trondheim, Norway: SINTEF Report STF70. A92006; 1992.

[5] Rombaut G, et al. LNG trials of a new 16″ flexible hose based LNG transfer system. Houston: OTC 19405, Offshore Technology Conference; 2008.

[6] Lebon L, Remery J. Bonga: Oil off-loading system using flexible pipe. Offshore Technology Conference, Houston: OTC 14307; 2002.

[7] Zhang Y, Chen B, Qiu L, Hill T, Case M. State of the art analytical tools improve optimization of unbonded flexible pipes for deepwater environments. Houston: OTC 15169, Offshore Technology Conference; 2003.

[8] API. Recommended practice for flexible pipe. API RP 17B. American Petroleum Institute; 2002.

[9] Do A, Lambert A. Qualification of unbonded dynamic flexible riser with carbon fibre composite armours. Houston: OTC 23281, Offshore Technology Conference; 2012.

[10] Kalman M, Yu L, Seymour M, Erni J. Qualification of composite armors materials for unbonded flexible pipe. Houston: OTC-23185, Offshore Technology Conference; 2012.

[11] Fernando, et al. Experimental evaluation of the metal-metal seal design for high pressure flexible pipes. Houston: OTC 23110, Offshore Technology Conference; 2012.

[12] Clevelario J. Introduction to unbonded flexible pipe design and manufacturing. Wellstream do Brasil; 2011.

25 Cross-Sectional and Dynamic Analyses of Flexible Pipes

1. Introduction

The flexible riser configurations are designed to absorb floater motions by change of geometry as shown in Figure 25.1, without the use of heave compensation systems in offshore applications. The required flexibility is normally obtained by arranging unbonded flexible pipes with low bending stiffness and low critical radius of curvature. The desired cross-sectional properties of the unbonded flexible pipes are normally obtained by the introduction of a flexible layered pipe, where each layer has a dedicated function. Although the layers are independent, they are designed to interact with each other. The number of layers and properties of each layer are selected to meet the design requirements.

The cross section of a flexible pipe is a combined construction of armour components (usually of spirally wound steel tendons) and sealing components, which are polymers of thermoplastic materials or compliant steel tubes, providing containment of fluid. The helix armour components are applied in layers with a given
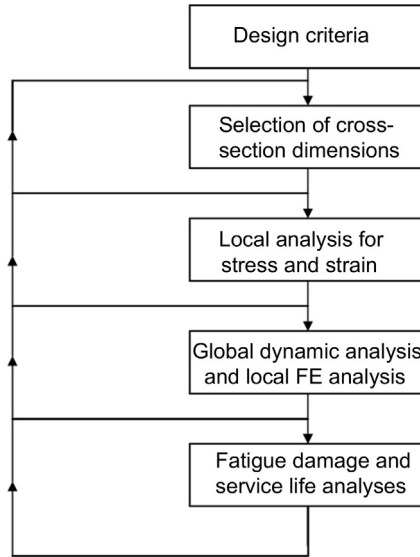
Figure 25.1 Design and analysis flowchart.

lay angle, which is different significantly in the different armour components. The helically wound steel tendons at the spiral armor layer give a high-pressure resistance and excellent bending characteristics to the whole assemble system, which results in the flexibility and a superior dynamic behavior. However, the complex design of unbonded flexible pipe leads to the difficulty in its analysis. To capture its structural response under different loads, local cross-section analysis and global dynamic analysis are required.

2. Flexible Pipe Guidelines

Flexible pipes have been used for decades. The early pipes and hoses were of the bonded type (vulcanized rubber and armoring). The designs were governed primarily by the ratio of burst to the design pressure.

From the early 1970s, large resources were put into the development of reliable unbonded flexible pipes. As a result of the product development work, the confidence in flexible pipes increased, and flexible pipes are considered attractive for many applications. The use of flexible pipes was, however, still limited, partially because no general industry standard was available. In the middle 1980s, Veritec [1] developed a general design standard for flexible pipes, based on a JIP. These guidelines were based on the design methods used by the manufacturers and the offshore design codes. The design codes represented the state of the art of flexible pipe design in the 1990s. With the exception of Brazil, the use of flexible pipes was still moderate during this period. There was, however, a continuous growth in demand and requirements of

temperature, pressure, and diameter to flexible pipes. Many oil companies developed their own specifications for flexible pipes, and the industry faced the following problems:

- Many operators had their own design standards.
- The manufacturers used their in-house standards for design. To prepare additional documentation conforming with the operators' standards was often cumbersome and expensive.
- The general design standards were not updated and were considered to be increasingly inadequate.

The design requirements were divided into two categories [2]:

- Mandatory requirements that are auditable should be included in the specification (API Spec 17J [3]).
- Recommendations with respect to how to satisfy the mandatory requirements, as well as guidance for the design of flexible pipe systems, are included in a separate recommended practice (RP). such as API RP 17B [4]. The RP includes the methodology for the design of flexible risers outside the experience range. Deep water is one of the such area.

API Specification 17K

The design of flexible pipe is according to API Specification 17J for unbonded pipes and API Specification 17K for bonded pipes. These documents provide a checklist of all the essential parameters and guidelines that pipe operators need to verify when ordering flexible pipes from pipe manufacturers. The rest of this section deals with API Spec 17J for unbonded pipes, but API Specification 17K contains essentially identical information and specifications for bonded pipes.

API Specification 17J

API 17J [3] describes the parameters that need to be determined before carrying out a flexible pipe design. These essential parameters (in addition to the external environmental conditions) are the internal bore characteristics, such as pressure, temperature, and fluid composition. These parameters determine much of the pipe design, such as material selection, and layer thickness.

API 17J lists the flexible pipe system requirements, such as inspection and condition monitoring, gas venting, and installation. Another section deals with the allowable loads that can be imposed on the pipe during its lifetime. Once a pipe cross section is established during design work, calculations are carried out to ensure that all allowable loads are not exceeded throughout the pipe design life. Any anomalies in this work require a new pipe cross section to be established. As shown in Table 6, Flexible pipe layer design criteria of API 17J, during normal operational conditions, the tensile armor layer maximum load cannot exceed 0.67 of the ultimate tensile strength (UTS) of the armor material. The pressure armor layer is allowed a maximum load of 0.55 of UTS. During abnormal and installation conditions, the allowable load may be increased to 0.85 of UTS, and during factory acceptance tests, the load may be increased up to 0.91 of UTS.

Further sections of API 17J describe other conditions and limitations that need to be considered during design work. One of the most important of these requirements is the minimum bend radius that the pipe is able to withstand without unlocking the pressure armor layer. An important aspect of design work is the calculations for ensuring that the pipe does not exceed its minimum bend radius under extreme load conditions. The two areas of pipe most susceptible to overbending are the touchdown zone and the upper region just before the hang-off location. Once the minimum bend radius is known, ancillary devices, such as bend stiffeners or bend restrictors, can be designed to ensure that the pipe does not exceed this minimum bend radius under all possible extreme loading conditions.

API 17J contains useful information for the design of the various layers that make up the flexible pipe. Details are also available on the design of the end-fitting arrangement, bend stiffeners, and bend restrictors. In addition to the local cross-section design, the flexible pipe also needs to be verified under a global static and dynamic analysis. Since unbonded flexible pipes have a large damping factor (due to the presence of a number of unbonded layers), they do not suffer from fatigue damage induced by vortex-induced vibration (VIV). Hence, flexible pipes do not need to be installed with strakes or fairings to limit VIV. This means that fatigue damage is primarily due to wave motions and installation damage. A detailed fatigue life analysis is required, and the pipe manufacturer needs to prove that the pipe fatigue life is 10 times the pipe's required service life.

Procedures are required for pipe installation, since incorrect installation induces a greater risk of exceeding the tensile limits of the armor layer material, overbending, and causing impact damage to the flexible pipes. There are documented cases of flexible pipe damage during installation, for example, the piercing of the pipe's outer sheathing that required expensive mitigation measures to be undertaken to prevent the replacement of the whole pipe before commencing operations.

API 17J also includes guidelines for the manufacture of the flexible pipe, and the qualification testing required before the pipe is issued to the operator.

Safety against Collapse

API Spec 17J is based on working stress design. Present standards have been based on a permissible utilization of 67% of the pipe capacity for external pressure. In practice, this means that the stresses in the carcass must be less than 67% of the stresses required to collapse the carcass.

API Spec 17J uses the formulae shown in Table 25.1 to limit stress in the internal carcass from local buckling.

Table 25.1 Permissible Utilization of Stress for Local Buckling

Water Depth (D)	Permissible Utilization
$D \leq 300$ m	0.67
300 m $< D <$ 900 m	$(D - 300)/600 * 0.18 + 0.67$
$D >$ 900 m	0.85

For water depths less than 300 m, the permissible utilization is as before. Due to the negligible uncertainty related to hydrostatic pressure in deep water, the permissible utilization is gradually increased with water depth. The maximum value of 0.85 is reached at 900 m water depth.

Design Criteria

The design criteria for unbonded flexible pipes are given in the following terms [3], [4]:

- Strain for polymer sheath.
- Creep for internal pressure sheath.
- Stress for metallic layers and end fitting.
- Hydrostatic collapse due to buckling load.
- Mechanical collapse due to stress induced from armor layers.
- Torsion.
- Crushing collapse and ovalization during installation.
- Compression (axial and effective).
- Service-life factors.

API RP 17B

Another useful document for flexible pipe operators is API Recommended Practice 17B [4]. This document is not a specification; hence, it is not binding on any party. However, many of the recommendations in API 17B are enforced in practice, since they provide additional measures to maintain the integrity of the flexible pipes and ensure a more efficient and safe operation. API 17B contains useful information on integrity management procedures and inspection and monitoring measures that can be undertaken to manage any risk of damage or failure modes of the flexible pipes. This document also contains useful information on the design and analysis methods that can be used to verify the pipe design and service life. Figure 25.1 shows a simplified design and analysis flowchart of unbonded flexible pipes. More detailed process charts for static flowlines and dynamic risers are illustrated in Figures 19 and 20 of API 17B. The recommended practice discusses various methods for carrying out these design calculations and is a useful tool for pipe operators and manufacturers to ensure an efficient and cost-effective solution for many flexible pipe applications.

3. Material and Mechanical of Properties Flexible Pipes

The characteristic properties and requirements of flexible pipes can be classified based on the sealing and armor components, as shown in Table 25.2 [5].

Properties of Sealing Components

Due to the complex wall structure and the interaction with the transported fluid, material properties of sealing components are particularly important for the flexible pipes. The materials usually used in flexible pipes are

Table 25.2 Properties and Requirements of Flexible Pipe Components

Components	Properties	Requirements
Sealing components	Materials, composition Pressure capacity Dimensions	Transport capacity Pressure ranges Resistance against internal flow Prevention of diffusion and leakage
Armor components	Bending flexibility Weight Axial force capacity, and torque behavior	Entire motivation for using flexible pipe Governs requirement to tension capacity Relevant with respect to static and dynamic loading

- Polymer.
- Steel.
- Foam.
- Synthetic fiber.

Polymers are used for sealing and as spacer elements for keeping the strength armoring in place. Steel fibers and synthetic fibers are used for strengthening, too. Foam materials are used for buoyancy and thermal insulation. An example of insulation material as an integral part of the pipe wall is the integrated production bundle (IPB) developed by Technip [6]. The IPB allows for high-level flow assurance of hydrocarbon fluids in adverse conditions (viscous oil, deep water, pressure constraints, etc.) from wellheads to surface treatment units. However, the materials of polymer and steel are mainly dealt with in this chapter.

Polymer

Polymer materials should have sufficient strength to retain their shape and position relative to the armor elements and be resilient to maintain tightness and integrity under the required bending of pipe wall for the sealing purpose.

The key requirements to the polymer materials are

- High long-term allowable static and dynamic strains.
- Internal and external fluid tightness.
- Required long-term chemical resistance.
- Low permeability.
- Low swelling.

Depending on the type of construction, additional requirements may be

- Required resistance against blistering.
- Good wear resistance.
- Good abrasion resistance.
- Good adhesion to other structural components of the pipe.

Steel

Steel materials are used in different layers of flexible pipes for different purposes:

1. Inner carcass:
   - As a ring stiffener to prevent collapse of the inner liner in case of rapid pressure drop of inner fluid.
   - To protect the inner liner against abrasion.
2. Strength armoring, both tensile armoring and pressure armoring.
3. Outer carcass, if required, to protect the outer liner against abrasion or other damage.
4. Metallic inner liner, to prevent gas permeation into polymeric material.

Interlocked sheet steel is used for the inner and outer carcass. For strength armoring, drawn steel wires of appropriate cross section are used. Because the pipe flow may contain sand particles, the resistance to mechanical wear is of particular importance for the liner material.

Fibers

The main function of the fiber armoring is to prevent the unwanted deformation and extrusion of elastomers relative to the steel armor layers. The fibers are mainly used in the form of yarns or woven fabric for strength armoring in the bonded structures and are not discussed further here.

Properties of Armor Components

The properties of armour components are related to the mechanical properties because of their function. Figure 25.2 illustrates three typical cases of subsea flexible pipes in the operating or installation condition, in which the relationships of tension and bending curvature are shown under the submerged weight [5].

Case a shows a straight configuration, demonstrating that required support force is the product of the submerged weight and the suspended length. Case b shows a catenary configuration, where the curvature is governed by the horizontal tension, T_H.

(a) Straight line   (b) Tension-controlled curvature   (c) Stiffness-controlled curvature
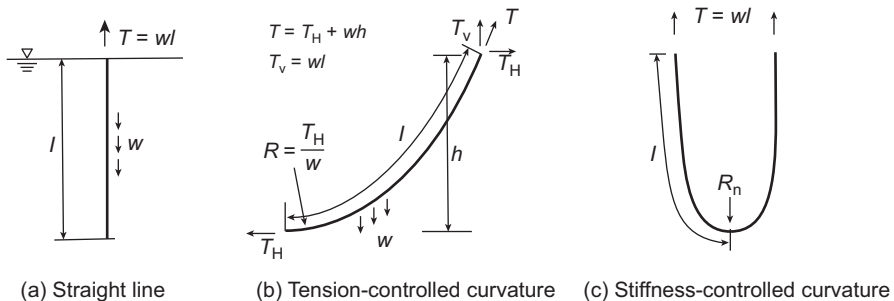
Figure 25.2 Relationship among weight, tension and bending curvature.
Source: Burge and Olufsen [5].

Case c shows the interaction between the tension and the bending stiffness; the curvature radius is entirely controlled by bending stiffness and submerged weight without horizontal force. In deepwater applications, it may be difficult to maintain a tension-controlled curvature of flexible pipe, because the suspended pipe submerged weight, T_V, is too large compared to the required horizontal force, T_H. It may be easy to design a flexible pipe in the configuration of Case c, in which the curvature is limited by the bending stiffness.

Submerged Weight

As shown in Figure 25.2, the submerged weight of flexible pipe is a critical parameter to control the flowline configuration in the installation or operating condition. However, the weight is a function of design pressure and diameter, because these two parameters determine the ratio of steel in the whole flowline system. According to the production statistical results of subsea unbonded flexible pipes, the dimensionless weight ratio, $mg/(p_d \text{ ID}^2)$, is summarized in Table 25.3. In the ratio expression, m represents the mass of pipe, p_d represents the design pressure of pipe, and ID represents the inner diameter of flexible pipe.

Bending Stiffness and Curvature Radius

The bending stiffness EI of flexible pipe is determined by the pipe wall composition, where E is the elastic modulus and I is the area moment of inertia. It is an important parameter with respect to the required tension, bending moment at the end fitting, the point loads (such as load from the guide sheaves during handling), and discrete buoyancy or clamping load. The stiffness, EI, is to a large extent governed by the polymeric components and may be more or less pressure and temperature sensitive. The basic reasons for the nonlinearity of stiffness are the material nonlinearity and the stick-slip, friction between layers of the unbonded flexible pipe.

The nonelastic behavior of pipe stiffness can affect both the static and dynamic responses. The dynamic stiffness for moderate curvature amplitudes may be much higher than the static stiffness, due to locking of layers. Furthermore, the frictional damping of large amplitude bending is large.

For the static curvature of unbonded flexible pipe during transport and installation, the minimum allowable bending curvature radius (MBR) is in a range of $5.5 \sim 7$ times the external diameter of the pipe, while the minimum allowable dynamic curvature

Table 25.3 Ratio Range and Application

Application	Ratio Range
Static flexible pipes	$0.7 \cdot 10^{-3} \sim 1.0 \cdot 10^{-3}$
Dynamic flexible pipes	$1.1 \cdot 10^{-3} \sim 2.0 \cdot 10^{-3}$
Low-pressure dynamic pipes	$3.0 \cdot 10^{-3} \sim 7.0 \cdot 10^{-3}$

radius is on the order of 1.5 times the minimum static radius, or typically 10 times the outer diameter .

Axial Stiffness and Tension Capacity

The axial stiffness of flexible pipe is normally fairly high. And the range of allowable elongation is on the order of 0.5–1.5%.

Compression is generally not allowed. And the effective tension is required to be positive. The tension capacity of flexible pipe can be designed according to the requirements.

Torque Stiffness and Torque Capacity

The torque stiffness often refers to a torsion given as [deg/m]. Flexible pipes have high torque stiffness because of the cross-wound tensile armor. The ratio of torque stiffness to bending stiffness for steel pipe is about 0.77, but for flexible pipe that may be up to 60. The allowable torsion of flexible pipe is in the range of 0.5–1.5 [deg/m].

4.   Analytical Formulations in Flexible Pipe Design

Overview of Analysis and Design

The analyses for flexible pipe design include (1) local cross-section analysis for predicting the cross-section mechanical properties and determining the load shearing between individual elements of the designed flexible pipes, (2) global dynamic response analysis for flexible pipes with the load distributions when effected by wave loads and installation barges, and (3) fatigue analysis of flexible pipe due to cyclic loads and its stress response concerning loads distribution of overall response analysis. The local cross-section analysis is the basic analysis for all analyses in the design of flexible pipes to predict the pipe's mechanical properties, the distribution of stress in the structure, the failure model, and so on. This section discusses the local cross-section analysis in the flexible pipe design.

Analytical Modelling of Flexible Pipes

In the past 30 years, lots of papers dealt with the local analysis of flexible pipes. All the analytical models made many simplified assumptions and hypotheses, and most of them neglected the friction effects that cause highly nonlinear behavior of unbonded flexible pipes, which significantly limit the range of applicability of the analytical results.

Witz [7] discusses a case study analysis of flexible risers, comparing results from the works carried out by 10 institutions with available Coflexip experimental data for a flexible riser design. The stress analysis of marine cables in rotary bending by Witz and Tan [8] was used by the author. It was shown that, if layer interaction is considered, the results from the 10 institutions' methods agree with the experimental

data for the axial-torsional structural response. This supports the argument that internal pressure does not significantly affect the full slip bending stiffness. It was concluded that, in the case of axis-symmetric loading, suitable methods existed for predicting the structural response of a flexible pipe, including interaction effects between the component layers. Furthermore, the models that did not consider this interaction might give erroneous results for some axis-symmetric load cases.

Saevik [9] utilized the kinematic restraints present when the tendons of a helix layer slid only in the curvilinear plane of the supporting pipe to develop an eight degree of freedom curved beam element. His approach uses the Green stain tensor to obtain strain and stress measures in the nonlinear finite element formulation based on an updated Lagrange formulation for arbitrarily large displacements and rotations but with small strains. The interaction between pipe and tendons was handled by a combination of hyperelastic (bonded pipes where the tendon was surrounded by an elastomer) and elastoplastic (unbonded pipes to simulate friction) springs in the nodal points.

Zhang et al. [10] discusses analytical tools for improving the performance of unbonded flexible pipe. This work uses an equivalent linear bending stiffness, which was derived from experimental data, to calculate the maximum bending angle range. It contains reports on irregular wave fatigue analysis, collapse, axial compression, and birdcaging for riser systems. It is believed that the combined bending, axial compression, and torsion could lead to the tendon being separated from the cylinder in a helix layer and might lead to out-of-plane buckling. However, the assumptions of equivalent linear bending stiffness neglects all the interactions between layer components of an unbonded flexible riser and makes it to behave as a bonded riser.

Tan et al. [11] investigated the higher-order geometrical effects by taking into consideration of the effect of the tendon cross-section characteristics. A rather accurate analytical strain energy model had been developed, although frictional effects were ignored. The paper also discusses a brief structural coupling between bending and axial-torsional behavior of the pipe. Comparison between their analytical and numerical results shows that numerical results are conservative in nature, allowing for confidence in use of a finite element model for practical designs. This conservative nature of the numerical model originates from the stronger constraint condition adopted by the model.

In summary, up to now, two approaches have been used to analytically model the unbonded flexible pipes: the classical approach and a multilayer modeling approach. In the classical approach, an equivalent beam element model is used to represent all layers by summing up the contributions of all the layers in the cross-sectional and material properties of the beam. The advantage of this approach is in its computational efficiency. In this method, the unbonded flexible pipe is modeled as one homogeneous structure, and this method is currently being used as an industry standard dynamic analysis method in the software, such as Orcaflex, Flexcom, and Abaqus. On the other hand, in the multilayer modeling approach, the loads of tension, shear, and moment in each layer are fully captured; and the interaction between layers is considered to study the behavior of unbonded flexible pipes. In the

following sections, the methodology of the multilayer approach is introduced, based on the recent researches and development of software for the design of unbonded flexible pipes [12]–[14].

Analytical Method of Unbonded Flexible Pipes

The physical behaviors of flexible pipe under axis-symmetric loads and bending loads depend on the cross-section properties. The axis-symmetric loads are due to the effective tension, torsion moment, and internal and external pressure. The main purpose of the cross-sectional analysis is to predict the stresses in all interior elements under an applied external loading. To establish efficient response models for the cross-sectional analysis, it is convenient to distinguish the responses due to the two loads, axis-symmetric loads and bending loads, and assume the bending and axial loads applied on helically wound armor to be uncoupled, as shown in Figure 25.3.

For the flexible pipe, the tensile armor layers carry most of the axial loads. When exposed to tension and torsion loads, the unbonded flexible pipes respond linearly within the relevant range, the same as the bonded pipes. However, the response to a bending load is completely different from the bonded pipe, which is one of the most important properties of flexible unbonded pipes. For an unbonded flexible pipe, this property is ensured by the slip between the armor tendons and the supporting structure. The unbonded flexible pipe has a nonlinear moment-curvature relationship, as illustrated in Figure 25.4 in a dimensionless form. The behavior of the pipe under a cyclic bending load is shown in (b) of the figure.
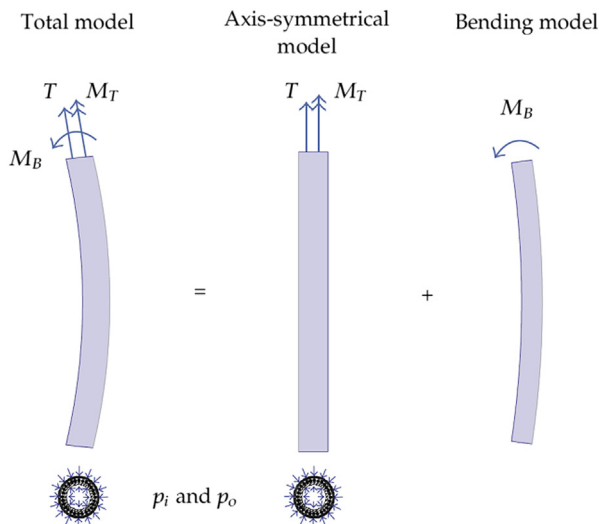
Figure 25.3 Models for cross-sectional analysis.
Source: Skeie et al. [14].
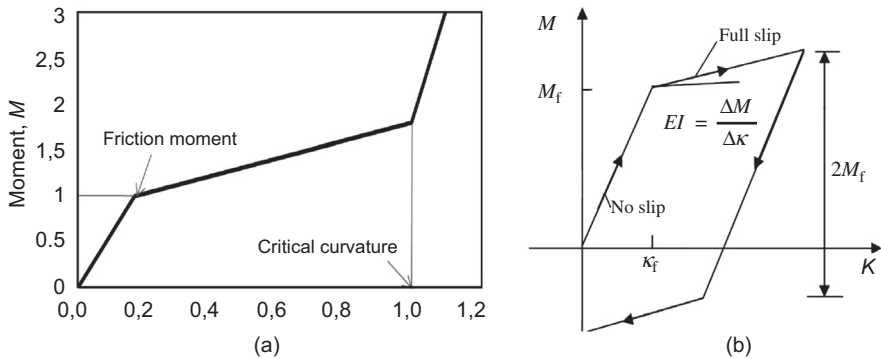
Figure 25.4 Bending behavior of unbonded flexible pipes.

The bending behavior of the unbonded flexible pipes can be divided into three ranges: small curvature range, intermedium curvature range. and large curvature range.

1. **Small curvature range:** The cross section of tendon remains plane. No slip exists between the tendon and the supporting structure. The pipe bends with a stiffnes similar s to a bonded pipe with the same cross section.
2. **Intermedium curvature range:** In this range, the bending stiffness is low. As the moment applied on the flexible pipe increases, slip occurs when the bending moment overcomes the friction moment between the layers of the pipe, due to the development of shear stress in armor layer and the supporting structure. The bending stiffness in this step drops significantly, and it is govern by the stiffness of the plastic tubules and strain energy in each armor tendon.
3. **Large curvature range:** When the curvature is higher than the critical one, the bending stiffness increases deeply. In this phase, the gap between each tendon is closed, no sliding is allowed anymore. The critical curvature corresponds to the critical radius, and it should be avoided in any operation.

Several commercial software programs have been developed for the local cross-section analysis and dynamic analysis of unbonded flexible pipes. For example, the program modules BFLEX by MARINTEK [15] for cross-section design and stress analysis of the armors and components, HELICA and UFLEX by DNV [16] for the cross-sectional bending characteristics of moment curvature, including relative motion between layers and components, friction, and stick-slip behavior.

Axis-Symmetric Behavior

The purpose of the axis-symmetric response analysis is to establish the load sharing between the individual components of the cross section as well as contact forces between the layers under axis-symmetric loading: effective tension, torsion, and hydrostatic pressure loads. The axis-symmetrical response model is built of concentric layers to model the entire cross sections to predict the cross-sectional stiffness, deformations of the pipe, stress, and strains of each component under the axis-symmetric loads. All layers are assumed to have the same axial and torsional

deformation, while the radial deformation is described separately for all layers. Each layer has one or two radial degrees of freedom, depending on whether the radial deformation of the layer itself is considered or not.

The cylinder layers may include the concentric plastic or metallic sheaths, such as the inner and outer pressure barriers of flexible pipes, and the cross-wound tensile armors. The helix layers may be modeled as equivalent thin cylinder layers in the axis-symmetrical analysis. The equivalent cylinder layer is established by assembling the stiffness contributions from each helix component in the layer. The stiffness matrix of each helix element is derived based on slender beam theory, assuming the as-produced nominal helix geometry as initial stress-free condition.

The deformations and stresses of each helix component due to axis-symmetrical loading are uniquely determined by the global axial, torsional, and radial deformation of each layer. Full details for all elements are given in Skeie et al. [14], while the kinematics of the cylindrical and helix element are described next.

Kinematic Restraint

The kinematic description of the cylindrical and helical layers is essential for the response analysis of the composite cross section. The configuration may be described in parametric form, as shown in Figure 25.5.

The cylinder is given by

$$x_c(x, \theta) = xi_x + R\cos\theta i_y + R\sin\theta i_z$$

where i_j denotes the global coordinate system. A helix is a curve on the cylindrical surface following a fixed trajectory defined by the inclination angle, α. This also yields a relation between the helical axis, s, and the polar angle, θ. The helix geometry is thus a one-parameter specialization of the cylinder.

It is assumed that the tendon is forced to slide along the curvilinear axes and transverse direction only. Then, the full three-dimensional description can be eliminated into a two-dimensional problem. Thus, a restraint on the rotation of the rod
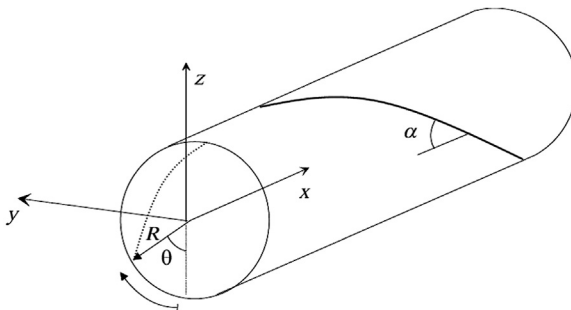
Figure 25.5 Model of pipe and tendon geometry.

around the longitudinal axis is obtained as a function of tendon's longitudinal and transverse displacement along the local curvilinear axes.

Governing Equations

Each layer of the unbonded flexible pipe has its own formula in the model. The equilibrium equations for the helical armor layer are derived in a manner similar to that outlined for the isotropic layer. Appropriate strain expressions may be derived from the kinematic relations. The Green-Lagrange strain measure is used. The general linear strain in the helix elements in the direction of tendon's axis is expressed in the form [12]

$$\varepsilon = \frac{\Delta u_z}{L}\cos^2\alpha + \frac{\Delta u_z}{R}\sin^2\alpha + R\frac{\Delta\phi}{L}\sin\alpha\cos\alpha + R\sin\theta\frac{\Delta\psi_x}{L}\cos^2\alpha$$
$$+ R\cos\theta\frac{\Delta\psi_y}{L}\cos\alpha \qquad\qquad\qquad [25.1]$$

where

   Δu_z = change of axial displacement
   Δu_r = change of radial displacement
   $\Delta\psi_x, \Delta\psi_y$ = change of rotation
   R, I = geometric parameters, shown in Figure 25.6
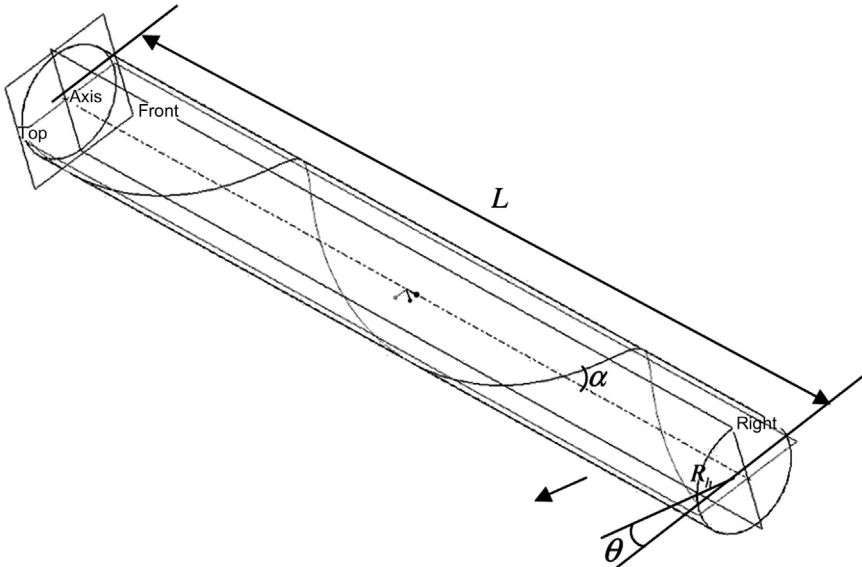
Figure 25.6 Geometric schematic diagram of tender.
Source: Bahtui [12].

α = winding angle of the tensile armour layer

θ = angular position of the tensile in the section of the cylindrical shell

The global assembled system of equations for the axis-symmetrical analysis can hence be expressed as

$$\mathbf{K}r = R \qquad\qquad [25.2]$$

where

$\mathbf{K}$ = the stiffness matrix assembled from all layers

r = the displacement vector for all the unknown degrees of freedom in the system

R = the external load vector

with the constraint: $g_i(r) = r_{i+1}^{\text{inner}} - r_i^{\text{outer}} \geq 0$ for $i = 1 \sim m$

This equation expresses global equilibrium of the cross section, while the constraint states the impenetrability condition of the *m* interface layers, as shown in Figure 25.7.

Bending Behavior

When an unbonded flexible pipe is bent, a longitudinal slip of the tendon always occurs from the compressive side to the tension side, as shown in Figure 25.8(a). However, the tendon has transverse curvature if the transverse slip relative to the core is prevented by friction force. The tendon follows a loxodromic path if there is friction between the tendon and core, but the tendon follows the geodesic solution if the friction is zero. In this case, a certain transverse slip occurs to eliminate transverse curvature, as shown in Figure 25.8(b).

The geodesic curve is defined as the minimum one between two sufficiently close points on the surface and has no transverse curvature. For two sufficiently close points, only one such curve exists. The loxodromic curve is defined as that the tendon is glued to the supporting core under infinite friction condition. The tendon along the loxodromic curve has neither longitudinal nor transverse slip. However, when a pipe
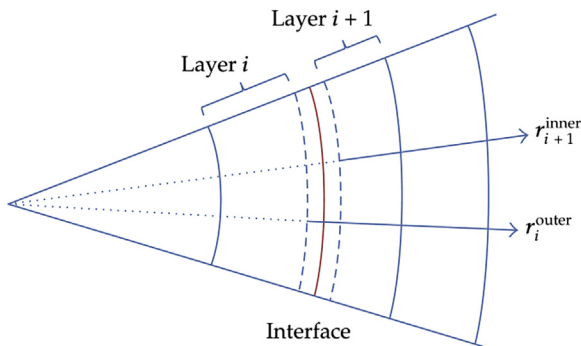
Figure 25.7 Constraints at layer interfaces.
Source: Skeie et al. [14].

(a) Slip from compression to tensile side   (b) Two limited curves
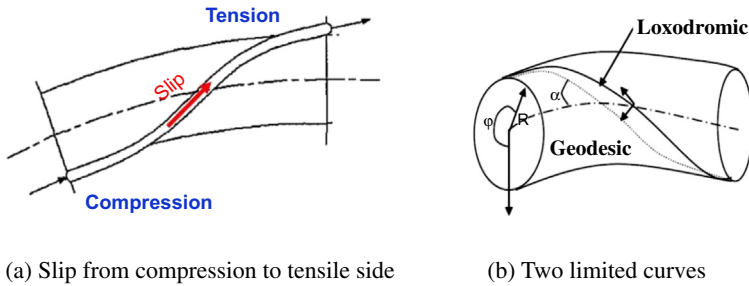
Figure 25.8 Slip direction of tendon under bending load.

is bent, no matter the friction coefficient, the axial strain from the compression side to the tension side is too large and needs to be eliminated by a longitudinal slip along the loxodromic curve path.

The additional stresses due to bending can be derived by assuming that the helix follows a loxodromic curve during cross-sectional bending. This means that the helix remains in its original position on the supporting cylinder surface during bending, and it slips in the axial direction when the tension gradient exceeds the available friction. The stress components in tendons during bending are the local bending stresses due to bending and the friction stress from the stick-slip behavior in bending.

The equations for stress and strain of tendons under bending can be found in the papers given by Bahtui [12], Li [13], and Skeie et al. [14] for slip behavior of tendons. In these models, the stresses in helix elements due to cross-sectional bending are analytically calculated. The stick-slip model is based on contact forces established by the axis-symmetrical analysis. A major advantage of the analytical bending model is that the bending analysis of helix elements can be carried out one by one without considering a complete model of the whole cross section, as in the axis-symmetric behavior analysis. This ensures a very flexible and efficient computation scheme. The assumptions made in the analytical bending model follow:

- Constant interlayer contact pressure found by axis-symmetrical analysis, additional contact pressure induced by bending itself is neglected.
- Friction and contact between helical elements in the same layer is neglected.
- No end effects are included; that is, bending takes place well away from terminations.
- Constant global cross-sectional curvature is assumed.

5. FE Analysis of Unbonded Flexible Pipe

Static Analysis

The analytical analyses for unbonded flexible pipes are based on the two-dimensional formulations with average constant properties in the longitudinal direction. Normally, layered analysis models are used with assumptions of linear material properties, no

end effects, and constant curvature in the bending condition. The analytical analyses is used for load sharing analysis for axis-symmetric loads, calculation of cross-sectional stiffness properties of axial, bending, and torsion. It can also be used for calculation of consistent fatigue stresses by direct application of global response time series as external loading. However, for complex, nonlayered cross sections, local constraints, such as clamps, complex loads of contact loads caused by caterpillars and tensile load during installation, buckling-instability of components, and other complicated conditions, full three-dimensional finite element analysis is required.

Almost all the weakness of analytical methods can be overcome using detailed, three-dimensional FE analysis. The disadvantages of FE analysis are as follows:

- The calculating models are limited to shorter length and fewer layers because of computer memory and speed limitations.
- The calculation needs computers of high performance and long calculating time.
- The calculation is limited to simple issues of the load cases.

The unbonded flexible riser problem is well-suited to Abaqus and Explicit, which can readily analyze problems involving complex contact interaction between many independent bodies. They are also very efficient in solving highly nonlinear classes of problems that are essentially static. Quasi-static process simulation problems involving complex contact generally fall within this class.

Fatigue Analysis

The tensile armor and the pressure armor layers of subsea flexible pipes are most prone to fatigue damage, which limits the service life of the flexible pipes [10]. Compared to the curvature and effective tension, the variation of internal pressure is very low. Thus, the contribution of internal pressure to the fatigue damage is often neglected.

Fatigue analysis methodology guidelines for flexible risers were developed by the Real Life Joint Industry Project (JIP) [17]. The suggested analysis method for flexible pipes is similar to the procedure employed for rigid risers, which involves the following five steps:

1. Collection of environmental loading data and definition of the load case matrix.
2. Global analysis of the riser system, that is, the evaluation of axial forces (tension, as torsion is usually neglected) and bending moments (curvatures) that act on the pipe due to the loads defined in Step 1.
3. Transposition of the tensions and moments determined in the global analysis to theoretical local models devoted to calculate the stresses in each layer of the pipe.
4. Local stress analysis of the pipe, focusing on the evaluation of the stresses in the tensile armor wires.
5. Estimation of the fatigue life, relying on the stresses calculated in the last step.

This procedure is not easy to apply for the fatigue analysis of flexible pipes. For rigid pipes, stresses are calculated directly in the global analyses; but for flexible pipes, the evaluation of stresses in their internal layers is not simple, due to their multilayered structures and complex responses to mechanical loads, mainly when friction between

their internal layers is considered. Thus, specific programs have to be employed. Recently, several papers, [13, 14, 18], developed theoretical approaches to predict the fatigue life of flexible pipes, focusing on the calculation of stresses in the tensile armours.

Skeie et al. [14] gave an example of fatigue analysis for rectangular cross-wound tensile armors of an umbilical operated from a turret-moored FPSO in typical Norwegian environmental conditions, as shown in Figure 25.9.

The main steps in the fatigue analysis are the following:

- Discretize the wave scatter diagram into representative number of blocks. Each block covers several sea states in the wave scatter diagram.
- Perform global response analyses for all blocks in the wave scatter diagram.
- Perform helix fatigue analysis for all fatigue loading conditions using simultaneous time histories of biaxial curvature and effective tension from the global analysis as input.

Figure 25.10 shows short-term helix fatigue analysis for each fatigue load case with the following procedure:
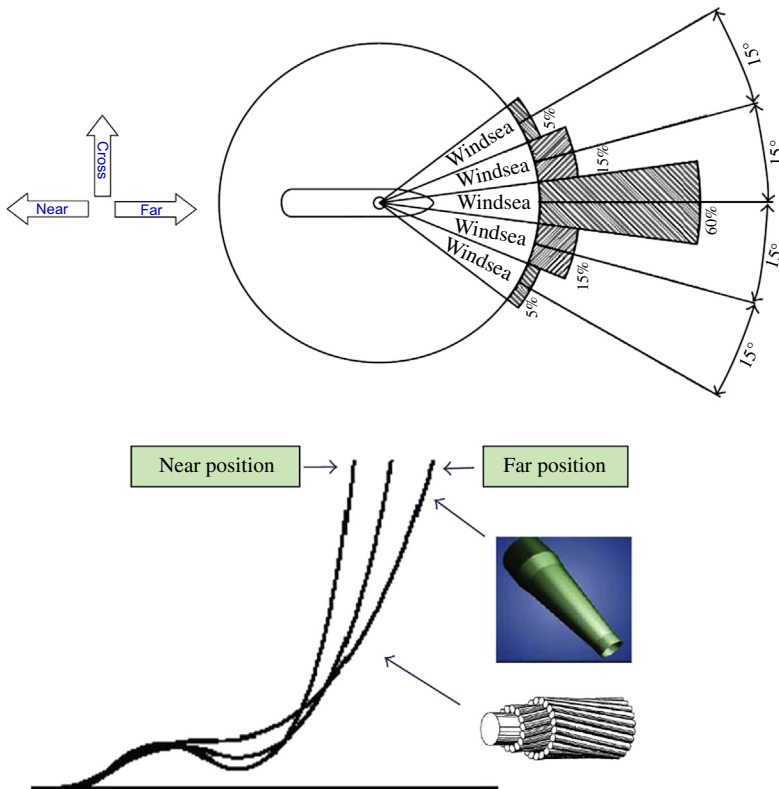
Figure 25.9 Umbilical operated from a turret-moored FPSO.
Source: Skeie et al. [14].
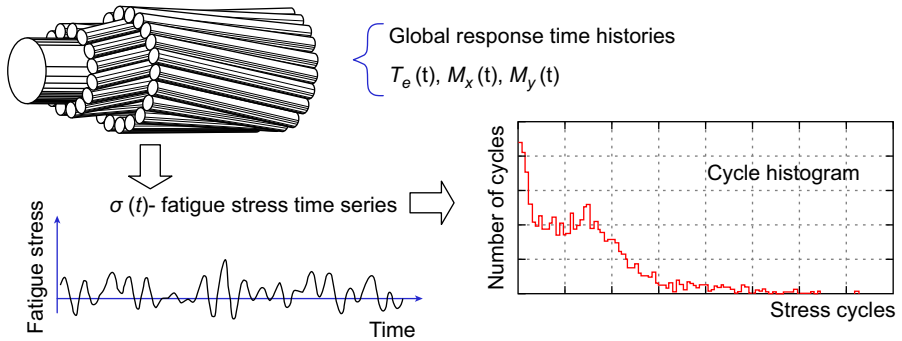
Figure 25.10 Short-term fatigue analysis for one hotspot-helix location.
Source: Skeie et al. [14].

- Establish fatigue stress time histories at all locations and hotspots. This analysis is performed by combined axis-symmetrical analysis and bending analysis at each time step. In this way, the interlayer contact forces governing the stick-slip bending response are updated according to the instantaneous effective tension loading;
- Establish a cycle histogram by rain flow counting of the generated fatigue stress time.

References

[1] Veritec. JIP guidelines for flexible pipes. Veritec; 1987.

[2] Bai Y, Bai Q. Subsea pipelines and Risers. 2nd ed. Oxford, UK: Elsevier Science Ltd; 2005.

[3] API. Specification for unbonded flexible pipe. 3rd ed. ANSI/API Spec 17J or ISO 13628-2. Washington, DC: American Petroleum Institute; July 2008, effective January 2009.

[4] API. Recommended practice for flexible pipe. 4th ed. API RP 17B/ISO 13628-11. Washington, DC: American Petroleum Institute; June 2008.

[5] Berge S, Olufsen A. Handbook on design and operation of flexible pipes. SINTEF Report STF70, A92006. SINTEF, Trondheim, Norway; 1992.

[6] Secher P, Felix-Henry A. Thermal performances of the flexible bundled risers. Houston, Offshore Technology Conference: OTC 14322; 2002.

[7] Witz JA. A case study in the cross-section analysis of flexible risers. Marine Structures 1996;9:885–904.

[8] Witz JA, Tan Z. Rotary bending of marine cables and umbilicals. Eng Structures 1995;17(4):267–75.

[9] Saevik S. A finite element model for predicting stresses and slip in flexible pipe armouring tendons. Comput Structures 1993;46(2):219–30.

[10] Zhang Y, Chen B, Qiu L, Hill T, Case M. State of the art analytical tools improve optimization of unbonded flexible pipes for deepwater environments. Houston, Offshore Technology Conference: OTC 15169; 2003.

[11] Tan Z, Case M, Sheldrake T. Higher order effects on bending of helical armour wire inside an unbonded flexible pipe. In: Proceedings of 24th International Conference on Offshore Mechanics and Arctic Engineering. Halkidiki, Greece: OMAE2005-67106; 2005.

[12] Bahtui A A. Development of a constitutive model to simulate unbounded flexible riser pipe elements. PhD thesis. London, United Kingdom: Brunel University; 2008.

[13] Li H H. Flexible pipe stress and fatigue analysis. Master thesis. Trondheim, Norway: Norwegian University of Science and Technology; 2010.

[14] Skeie G, Sødahl N, Steinkjer O. Efficient fatigue analysis of helix elements in umbilicals and flexible risers: Theory and applications. J Applied Mathematics 2012, Article ID 246812.

[15] Sævik S. BFLEX2010- user manual. Trondheim, Norway: Marine Technology Centre; 2010.

[16] Sødahl N, Steinkjer O, Bahiense R. Helica users manual. Oslo: Det Norske Veritas; 2009.

[17] Grealish F, Smith R, Zimmerman J. New industry guidelines for fatigue analysis of unbonded flexible risers. Houston, Offshore Technology Conference: OTC 18303; 2006.

[18] Sousa JRM JRM. A theoretical approach to predict the fatigue life of flexible pipes. J Applied Mathematics 2012, Article ID 983819.

26 Tensile and Compressive Strengths of RTP Pipeline

Chapter Outline

1.   Introduction

Reinforced thermoplastic pipe (RTP) is a nonmetallic, multilayer pipe with a reliable high strength synthetic fiber in the middle, initially developed in the early 1990s by Akzo Nobel, who developed the first reinforced pipe with synthetic fiber to replace medium-pressure steel pipes in response to the growing demand for noncorrosive conduits for application in the onshore oil and gas industry. As shown in Figure 26.1, typical construction of RTPs includes a polymeric liner or barrier, a structural layer, and an outer polymeric cover. The function of inner liner is to offer leakproof capacity, corrosion resistance, and contain the transported fluid. The function of the structural layer is to provide the mechanical strength to withstand the loads applied during service and installation. The structural layer typically consists of an even number of balanced helical windings of continuous aramid or other types of fiber reinforcement, applied as helically wound yarns, or fiber-reinforced preformed tapes, in which the encapsulation is a thermoplastic resin. The outer cover is added atop of the structural layer to protect the structure during installation and operation.

Materials of RTP

The materials of the inner liner and cover of RTP might be polyethylene (PE), Polyamide-11, or PVDF. The maximum allowable temperatures for typical
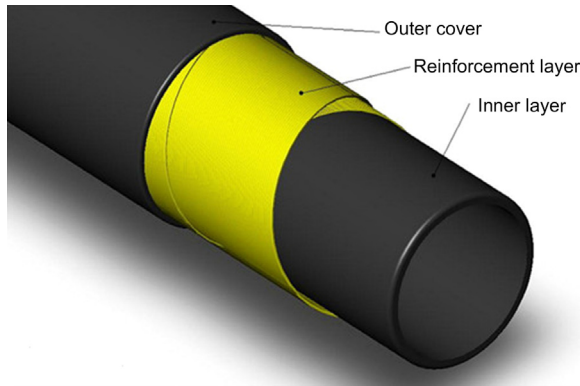
Figure 26.1 Typical construction of RTP. (For color version of this figure, the reader is referred to the online version of this book.)

thermoplastic materials are listed in Table 26.1. The maximum allowable operating temperature for the thermoplastic inner liner, however, may be lower than the values listed in the table, depending on the aggressiveness of the production fluid and its concentration.

The materials typically used for the reinforced layers are

- **Carbon fiber:** This is used for low weight, high strength, and high stiffness reinforced in structures.
- **Glass-fiber:** This has limited chemical resistance and typically must be protected by the resin from direct exposure to the fluid; it is relatively inexpensive and has good mechanical properties.
- **Aramide, para-aramids:** These are used for low weight, high strength and moderate stiffness for reinforced structures.
- **Steel strips, wires, or cords:** These are used in pneumatic tires, hoses, and the like, in accordance with ASTM D 2969.

End-Fitting Design

The end fitting terminates the RTP, maintaining the integrity of the pipe structure, sealing the inner layer and outer cover, and providing a fixture to transmit tension and pressure loads to the pipe structure. Figure 26.2 shows typical end fitting of RTP. Normally, it forms an interfaces between the pipe and a connector, but it also works as

Table 26.1 Allowable Temperature for Typical Thermoplastic Materials

Material	Temperature Range
Polyethylene (PE)	65°C
Polyamide-11(PA-11)	80°C
Polypropylene (PP)	80°C
Polyvinylidene fluoride (PVDF)	130°C
Polyvinyl chloride (PVC)	65°C

Figure 26.2 Typical end fitting of RTP.
Source: FlexSteel [1].

a midline connection, in which the end fitting is used to connect two RTPs together without having an intermediate flange.

Advantages and Applications

Flexible pipelines and RTPs are two kinds of composite pipes, which are applied in different subsea engineering fields. Usually, the flexible pipelines are employed in deepwater applications, even to depths of thousands of meters, while RTPs are often employed in onshore and offshore applications, capable of being made in long continuous lengths and easily reeled for storage, transport, and installation. RTP pipe can hand pressure grade of 300, 400, 600, and 900 ANSI product in 2-inch, 3-inch, 4-inch, and 6-inch ID sizes at normal operating temperature.

Compared to rigid steel pipe, the main technical advantages of RTP for the transportation of oil and gas are

- RTP is flexible and supplied on long-length coils, allowing a simple and very fast installation.
- Corrosion resistance, including sour applications (H_2S) and sweet service (CO_2).
- Very high impact strength.

Tensile strength and compression-bearing capacity are fundamental properties of RTPs. Without enough tensile strength, the pipeline yields and eventually fractures. Without enough compression-bearing capacity, the pipeline is unstable under compression and eventually collapses. Hence, the study on the mechanical properties of RTP under axial loads is of much significance to the popularization of RTP.

2. Code Requirements

Recognized industry norms for flexible pipes have been developed by the American Petroleum Institute (API). Generally accepted codes for flexible pipe are API RP 15S,

"Qualification of Spoolable Reinforced Plastic Line Pipe" [2]; API RP 17B, "Recommended Practice for Flexible Pipe" [3]; API 17J, "Specification for Unbonded Flexible Pipe" [4]; and API 17K, "Specification for Bonded Flexible Pipe" [5].

API RP 15S covers (1) product construction, (2) raw material selection, (3) qualification requirements, and (4) quality control requirements. It prescribes an extensive program of product testing, including regression testing, cyclic testing, joint testing, gas testing, bent testing, and axial load testing.

Performance-based design has been adopted to meet minimum performance criteria, and it requires a careful evaluation of the link between failure mechanisms and failure modes.

3. RTP Pipe Under Tension

In this section, the main features of the failure of RTP under tension are illustrated experimentally.

Axial Tensile Test

Prototype axial tensile tests are conducted for different kinds of RTPs, including RTPs containing glass-fiber reinforcement and RTPs containing aramid-fiber reinforcement. Normally, the tested specimens are provided by the manufacturers with end fittings. Before the test, the dimensions of specimens are measured and the measured data used as an input for the theoretical and finite element analyses. The RTPs used in the tests consist of two HDPE layers and twisted aramid wires. During the manufacturing process the inner and external HDPE layers are formed by heat extrusion and the HDPE matrix is fused with the wires. The dimensions of the five specimens are summarized in Table 26.2.

Experimental Facilities and Procedure

The tests are conducted according to ASTM D2105-2001 [6]. All the tensile tests are conducted in a 3000 kN capacity universal electromagnetism servo control testing machine. The specimen end fittings are connected to the testing machine by flange connections. The specimen axis is aligned with the grips of the testing machine to ensure the specimens are concentrically and uniformly loaded.

Table 26.2 Dimensions of Tensile Test Specimens

Specimen No.	Specimen Length [m]	Mean External Diameter, [m]	Mean Wall Thickness, [mm]
AT 1	0.82	0.14	14.9
AT 2	0.82	0.14	15.0
AT 3	0.82	0.14	15.2
AT 4	0.81	0.14	14.7
AT 5	0.81	0.14	14.9

Experimental Findings

Two failure modes are found in the tests for different kinds of RTPs due to the differences in the materials and components:

- Mode 1. Rupture of reinforcing fibers.
- Mode 2. Yielding of elastomers.

According to API SPEC 17J [4], the maximum allowable strain for PE is 7.7%. Therefore, if the reinforcing fibers rupture before the axial strain reaches 7.7%, the failure mode of the pipe is deemed as Mode 1 and the failure symbol is the sudden break of the reinforcing fibers. Figure 26.3 shows a RTP with glass-fiber reinforcement; the rupture of glass-fiber RTP normally shows the failure mode of Mode 1.

Figure 26.4 shows the measured load-extension curve of a glass-fiber RTP. The rupture of the RTP occurs at a tension force of 820 kN. The RTP with glass-fiber reinforcement layers may fail in Mode 1, while the RTP with aramid-fiber reinforcement layers may fail in Mode 2.

If the axial strain of pipe reaches 7.7% prior to the breaking of the reinforcing fibers, then the failure mode of pipe can be deemed as Mode 2. Normally, the RTP containing aramid-fiber reinforcement has the failure mode of Mode 2. In this chapter, the research focuses on the RTP pipe with failure Mode 2. Unlike Mode 1, the whole failure process for Mode 2 is preceded by a cascade of events. As shown in Figure 26.5, as the elongation increases, the elastomer yields (referring to the point A), then tearing occurs on the outer surface of the pipe. When the elongation is large enough, apparent necking occurs and the inner layer of the pipe collapses (referring to point B). As the elongation keeps increasing, the connection between the pipe ends and the end fittings fails (referring to the point C).

Figure 26.3 Rupture of the glass-fibers in Mode 1. (For color version of this figure, the reader is referred to the online version of this book.)
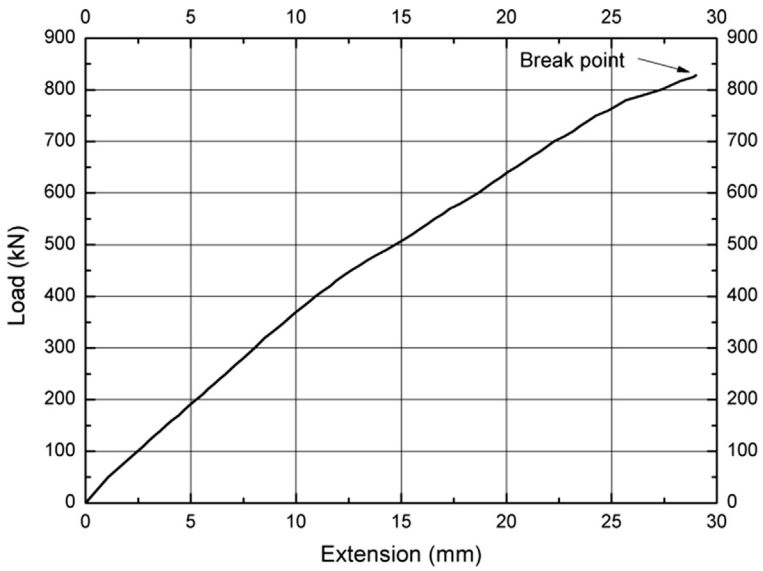
Figure 26.4 Load-extension curve in Mode 1.
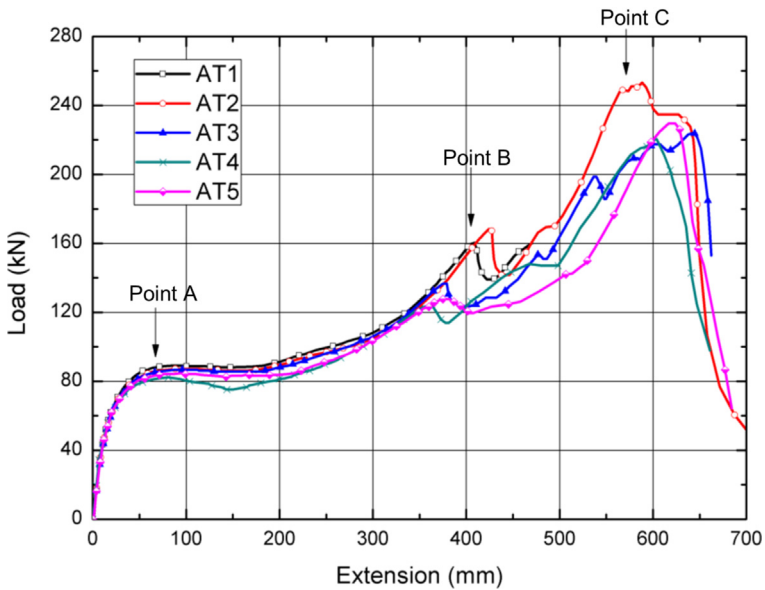
Figure 26.5 Load-extension curves in Mode 2. (For color version of this figure, the reader is referred to the online version of this book.)
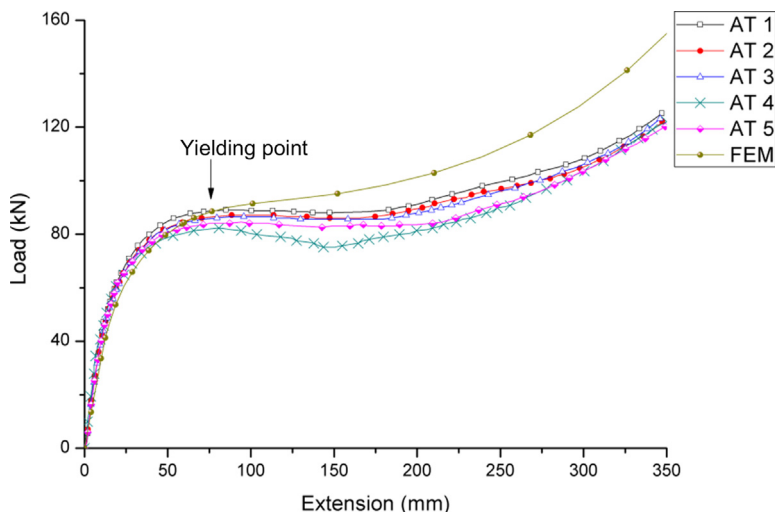
Figure 26.6 Comparison of load-extension curves between test and FEA. (For color version of this figure, the reader is referred to the online version of this book.)

Because the pipes yield at the point A, the sections of curves from the point A to the point C are viewed as invalid in the practical engineering applications.

Comparison of Test Results with FE Analysis

The load versus extension curves from the tests and FE analysis are shown in Figure 26.6. All the curves in the figure show an identical tendency. The mean yielding load from FEA is 88 kN, while from the tests, it is 85kN with a 3.4% relative error, which is very small.

4. RTP Pipe Under Compression

Axial Compressive Test

Prototype axial compressive tests are conducted for the specimens provided by the manufacturers with end fittings. Before the tests, the dimensions of the specimens are measured for the theoretical analysis and numerical simulation.

Experimental Facilities and Procedure

The length of the specimens is chosen to be two times the nominal outer diameter of the pipe for forming a representative distribution of geometric imperfection and minimizing the end effects, while being suitably short enough to avoid global buckling.

The tests are conducted by a 250 kN electronic testing machine. The load versus shortening relationship is recorded throughout the test, including the postultimate

Figure 26.7 Axial compressive test arrangement. (For color version of this figure, the reader is referred to the online version of this book.)

stage. During the test, the specimens are centered in the testing machine to ensure that the compressive axial load is applied without any eccentricity. The tests shown in Figure 26.7 are carried out following the standards ASTM D2105-01 [6] and BS EN ISO 527 [7].

Experimental Results

Figure 26.8 shows the measured load versus shortening curves for two specimens. Expansion occurs near the pipe ends and the outside surface of the pipe wrinkles.
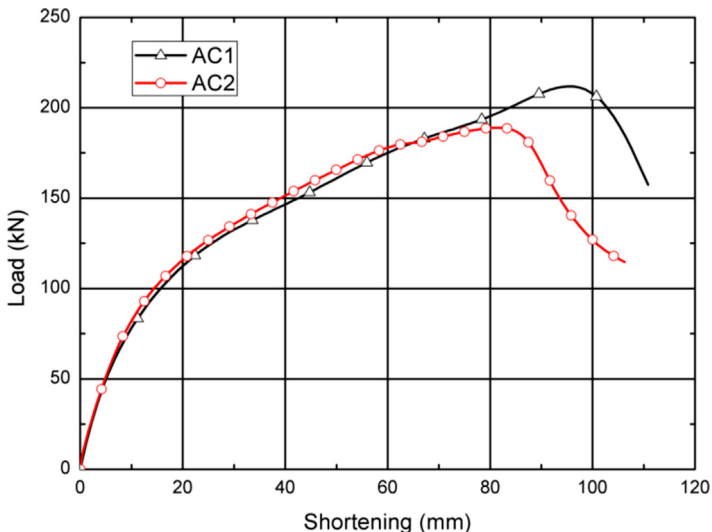
Figure 26.8 Experimental load-shortening curves. (For color version of this figure, the reader is referred to the online version of this book.)
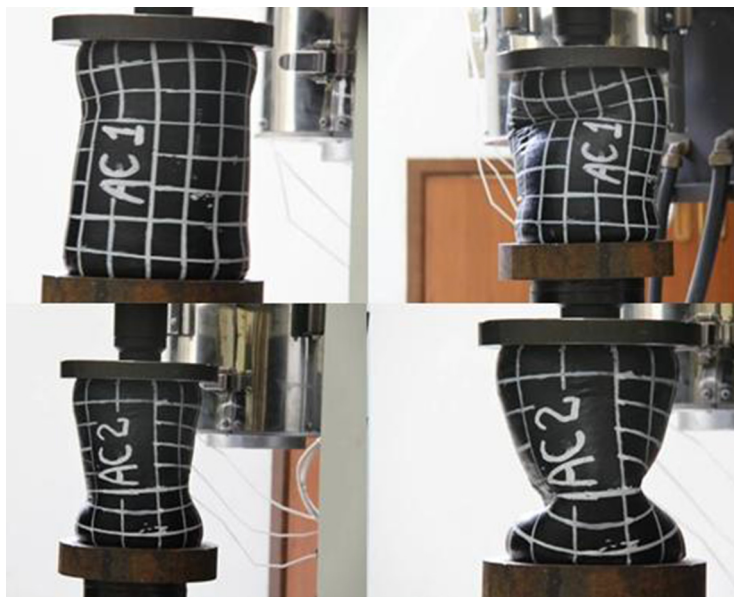
Figure 26.9 Deformations and collapse of the specimens. (For color version of this figure, the reader is referred to the online version of this book.)

When the deformation reaches a certain point, collapse occurs. The deformations of the specimens are shown in Figure 26.9.

The collapse load of the specimen AC2 is lower than that of the specimen AC1, because specimen AC2 has a larger initial imperfection. The larger initial imperfection of the specimen makes it collapse more quickly and ultimately reduces the compression-bearing capacity.

Comparison of Test Results with FE Analysis

Failure Mode Shape

The failure mode shapes from the numerical simulation and axial compressive tests are shown in Figure 26.10.

Load-Shortening Curves

The load-shortening curves from axial compressive tests and numerical simulation are compared in Figure 26.11. The curves have the identical shape and show close agreement at the initial stage. The collapsed loads of the numerical results and experimental results are compared in Table 26.3.

Theoretical and FE simulations of RTP including two reinforced layers with $\pm 55°$ winding angles were carried out under axial loads. The analysis results are compared with experimental data. A reasonable correspondence from the comparison results is obtained in the failure mode and the collapse load.
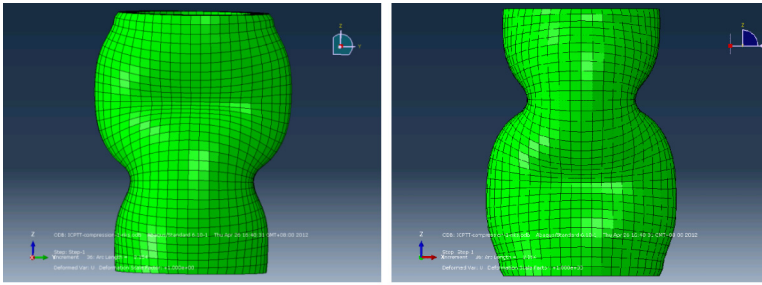
a) Buckling mode of abaqus analysis

b) Failure mode shape of AC 1

Figure 26.10 Comparison of failure modes between experimental and FEM results. (For color version of this figure, the reader is referred to the online version of this book.)
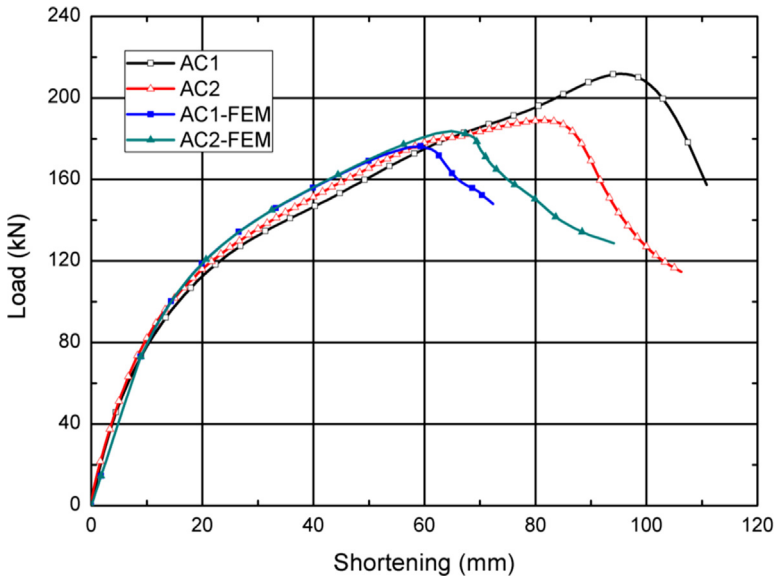
Figure 26.11 Load-shortening curves from experiments and FEM. (For color version of this figure, the reader is referred to the online version of this book.)

Table 26.3 Collapsed Loads of Numerical and Experimental Results

Specimen Number	Numerical Result, [kN]	Experimental Result, [kN]	Relative Error, [-]
AC1	176	212	17.0%
AC2	184	189	2.6%

References

[1] FlexSteel. Available at www.flexsteelpipe.com/products.

[2] API RP I5S. Qualification of spoolable reinforced plastic line pipe. Washington, DC: American Petroleum Institute; 2006.

[3] API RP 17B. Recommended practice for flexible pipe. Washington, DC: American Petroleum Institute; 2002.

[4] API Specification 17J. Specification for unbounded flexible pipe. Washington, DC: American Petroleum Institute; 2001.

[5] API Specification 17K. Specification for bonded flexible pipe. Washington, DC: American Petroleum Institute; 2001.

[6] ASTM D 2105–01. Standard test method for longitudinal tensile properties of 'fiberglass' pipe and tube. Philadelphia: American Society for Testing and Materials; 2001.

[7] BS EN ISO 527. Plastics—Determination of tensile properties. London, United Kingdom: British Standards Institution; 2012.

27 Burst Strength of RTP Pipeline

Chapter Outline

1. Introduction

Due to its high cost effectiveness, excellent corrosion resistance, and ease of installation, reinforced thermoplastic pipe (RTP) is now increasingly being used for onshore and offshore applications. Normally, RTP consists of one polyethylene liner, two layers of reinforced tape overwrapping the liner, and one outer polyethylene coating, as shown in Figure 27.1. The inner liner pipe and outer coating pipe are made of high density polyethylene (HDPE).

The mechanical response of filament-wound structures under internal pressure has been studied by many researchers. Xia et al. [1] performed a stress analysis of multilayered filament-wound composite pipes under an internal pressure based on a 3D anisotropy elasticity theory. Kruijer et al. [2] developed a multilayer "generalized plane strain" model based on a plane strain characterization for RTP under hydrostatic pressure. Kobayashi et al. [3] proposes an elastic-plastic analysis model on the filament-wound carbon-fiber reinforced composite pipes by applying partially plastic thick-walled cylinder theory. Zheng et al. [4] presents an analytical procedure to predict the short-term burst pressure of PSP (plastic pipes reinforced by cross helical-wound steel wires) based on 3D anisotropic elasticity and the maximum stress failure criterion. An elastic solution procedure based on Lekhnitskii's theory was developed by Onder et al. [5] to predict the burst failure pressure of the pressure vessels using the Tsai-Wu failure criterion, the maximum strain, and stress theories.

A material degradation model based on the ply-discounting approach was implemented in a UMAT subroutine and applied to analyze the progression failure of a two-dimensional plate by Knight [6]. A 3D parametric finite of the cylindrical part
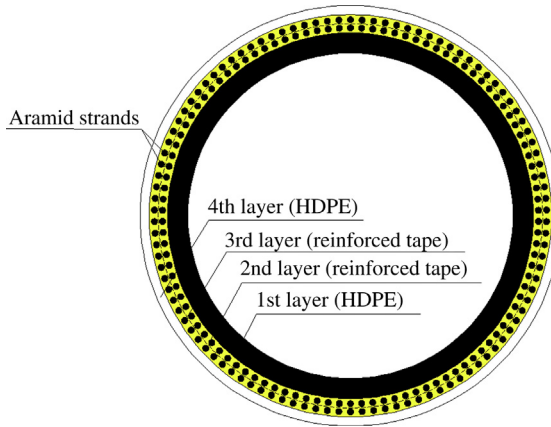
Figure 27.1 Cross section of RTP. (For color version of this figure, the reader is referred to the online version of this book.)

of a composite vessel was established by Xu et al. [7] to explore the failure evolution behavior and the failure pressure of composite vessels. Different failure criteria, such as the maximum stress by Hoffman, Tsai-Hill, and Tsai-Wu, are integrated in the main program. A comprehensive review on the recent developments of the damage and failure evolution using finite element analysis of composite laminates was reported by Liu et al.[8].

In this chapter, RTP is considered a thick cylinder, and the stress distribution is characterized as a generalized plane strain. Since the thicknesses of two reinforced tapes are relatively thin compared to that of the pipe, an assumption of uniform stresses through the thickness of the two layers is made to simplify the analysis. The material of the two reinforced tapes is considered as transverse isotropic. It is assumed that the strains in the reinforcing layers are equal to the strains in the isotropic material. The fiber failure and the matrix failure, the two failure modes used as the failure criterion, are used to determine the failure pressure of RTP. A 3D finite element RTP model is established to evaluate the relationship between the mechanical properties and the final failure pressure. To predict the damage evolution and the failure strength of RTP, the behavior of the reinforcing tape is simulated using a model proposed by Linde et al. [9], which is implemented in a user subroutine (UMAT) of the ABAQUS-standard nonlinear finite element analysis tool. The failure pressure calculated from finite element method and theoretical method are compared with the experimental burst pressure of RTP.

2. Experimental Analysis

Material Properties

In this analysis, two kinds of HDPEs are used for the liner, coating, and matrix. The reinforced tapes are manufactured by embedding the aramid strands in the HDPE. The HDPEs are modeled as linear elastic materials. Table 27.1 lists the secant

Table 27.1 Mechanical Properties of PE

Material	PE100 (k = 1)	PE100 (k = 4)	PE100 (k = 2, 3)
Secant modulus, E_k (MPa)	$350(E_1)$	$390(E_4)$	$460 (E_m)$
Poisson's ratio, μ_k	$0.4(\mu_1)$	$0.4 (\mu_4)$	$0.4 (\mu_m)$

modulus and Poisson's ratio used for modeling HDPEs. The secant modulus is determined based on the loading speed, temperature, and maximum strain during the burst test. Poisson's ratio is assumed to be 0.4 according to Kruijer et al. [10].

The reinforced tapes were modeled to be linear-elastic transverse isotropic. The five independent constants (E_L, E_T, G_{LT}, G_{TT}, μ_{LT}, where E denotes Young's modulus, G denotes the shear modulus, μ denotes Poisson's ratio, subscript L denotes the longitudina, fiber, direction, and subscript T denotes the two transverse directions orthogonal to the longitudinal direction) are listed in Table 27.2. The damage initiation properties of the reinforced tapes are shown in Table 27.3.

Burst Tests

Burst tests are carried out according to ASTM D 1599-99 "Standard Test Method for Resistance to Short-Time Hydraulic Pressure of Plastic Pipe, Tubing, and Fittings" [11]. As per procedure A, a short-time loading process was applied, such that the time to failure for all the specimens was between 60s and 70s. The RTP samples are 760 mm long and terminated by steel swage fittings. The RTPs are free to deform during the tests. In addition, the pressure applied to the internal pressure of RTP is increased uniformly and continuously until the specimen fails. The experimental temperature was controlled at $23 \sim 24°C$.

Table 27.4 summarizes the measured burst pressures of RTP pipes. The average burst pressure of 35.3 MPa is obtained for the RTP samples. It was noted that failure of each tested specimen occurred at the RTP close to the end fittings (Figure 27.2). From

Table 27.2 Transverse Isotropic Elastic Properties of Reinforced Tapes

E_L (MPa)	E_T (MPa)	G_{LT} (MPa)	G_{TT} (MPa)	μ_{LT}	μ_{TT}
20,390	170	160	60	0.38	0.4

Table 27.3 Damage Initiation Properties of Reinforced Tapes

$\sigma_L^{f,t}$ (MPa)	$\sigma_T^{f,t}$ (MPa)
770	6.0

Table 27.4 Measured Burst Pressure of RTP Samples

Specimen no.	Time to Failure (min)	Burst Pressure (MPa)
1	31	37.0
2	30	37.2
3	28	32.2
4	31	33.5
5	27	36.9
Average		35.3
S-SD		1.98

Figure 27.2 Burst samples after testing. (For color version of this figure, the reader is referred to the online version of this book.)

the burst tests, it was observed that the failure of fiber strands of the inner reinforced layer (layer 2) occurs first, which causes catastrophic damage to the entire pipe. The orientation of the crack is almost parallel to the outer reinforced layer (layer 3).

3. Analytical Analysis

Introduction

In the analytical analysis, RTP was considered as a thick cylinder. The deformation in the axial direction was assumed to be uniform. The stresses and strains (except for ε_{zz}

and σ_{zz}) of the two isotropic layers are not uniform, but a function of the radius of the layer. The analysis is carried out using the following procedure:

- First, the strain and stress functions of the two isotropic layers are deduced using elastic mechanics theory.
- Second, the strain and stress functions can be obtained through the strain continuum condition.
- Finally, the unknown constants in the strain equations are determined by interface conditions and equilibrium equations.

Coordinate Systems

A cylindrical coordinate system, as shown in Figure 27.3, is used for the analytical analysis. The coordinate axis r, θ, and z denote the radial, circumferential, and axial directions of RTP pipe, respectively. The local material coordinate system of the reinforced tape layers is designated as (L, T, r), where L is the wound direction, T is the direction perpendicular to the aramid wire in plane, and r is the normal direction, same as in the cylindrical coordinate system. The term α is the wound angle of reinforced layer, the angle between L direction and z direction.

The mathematical solutions are based on the model developed by Zheng et al. [4] for predicting the short-term burst pressure of PSP, by applying the 3D anisotropic elasticity and the maximum stress failure criterion, to calculate the short-term burst pressure of RTP pipe, except for the maximum strain failure criterion.

Provided that the interfaces between the fiber yarn and PE are perfectly bonded, the strain of the aramid wire and PE in the aramid-wound direction can be considered to be equal. Because Young's modulus of the aramid fiber is far greater than that of PE, the stresses in the aramid fiber are much greater than those in the PE. When the
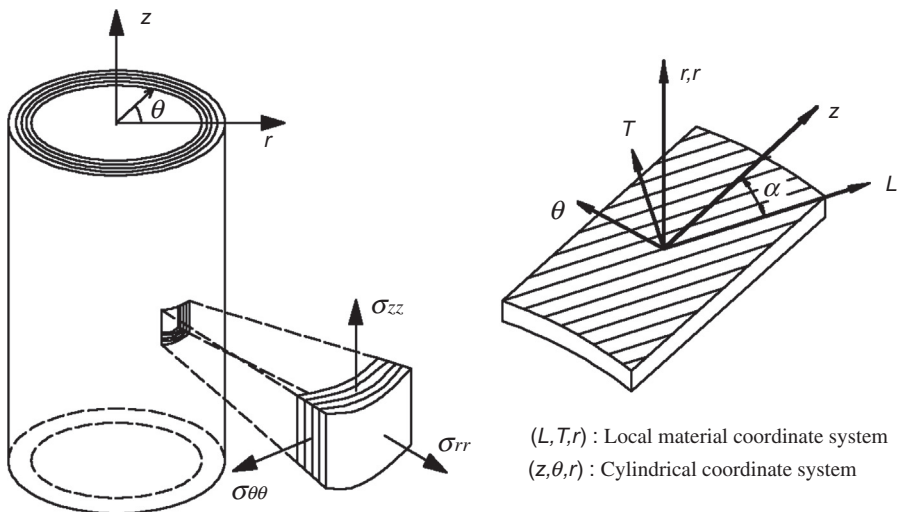
Figure 27.3 Coordinate systems. (For color version of this figure, the reader is referred to the online version of this book.)

RTP is subjected to internal pressure, aramid wires first reach their strength limits and break, resulting in the RTP losing the reinforcement of the fibers yarn and bursting in the short term.

The detailed mathematical equations for the strains of each layers are found in the Bai et al. paper [12].

4.   Finite Element Analysis

A finite element model is also developed to simulate the mechanical properties of RTP under internal pressure. The damage of reinforced tapes is simulated using a model proposed by Linde et al. (2004) [11], which is implemented in the ABAQUS subroutine UMAT. Failure initiation and damage progression law are two major parts of the UMAT model. The failure initiation criterion is the same as failure criterion used in the theoretical analysis. In the following section, the damage progression law is described.

When a fiber failure initiates, the fiber damage variable, d_{f}, evolves according to the following equation:

$$d_{\mathrm{f}} = 1 - \frac{\varepsilon_{11}^{f,t}}{f_{\mathrm{f}}} e^{\left[-C_{11}\varepsilon_{11}^{f,t}\left(f_{\mathrm{f}}-\varepsilon_{11}^{f,t}\right)L^{c}/G_{\mathrm{f}}\right]}, \qquad\qquad [27.1]$$

where L^{c} is the characteristic length associated with the location. The evolution law of the matrix damage variable, d_{m}, is expressed as

$$d_{\mathrm{m}} = 1 - \frac{\varepsilon_{22}^{f,t}}{f_{\mathrm{m}}} e^{\left[-C_{22}\varepsilon_{22}^{f,t}\left(f_{\mathrm{m}}-\varepsilon_{22}^{f,t}\right)L^{c}/G_{\mathrm{m}}\right]} \qquad\qquad [27.2]$$

The reinforced layers are assumed to be transversely isotropic. When the damage is progressive, the effective elasticity matrix is reduced by the two variables d_{f} and d_{m}, as shown in Table 27.5. To improve the convergence speed, a technique based on the viscous regularization is used to regularize the damage variables. The regularized damage variables are stored as solution-dependent variables, SDV3 and SDV4, respectively.

Table 27.5 Degradation Factors

Components of the Elasticity Matrix	Degradation Factors
C_{11}, C_{13}, and C_{31}	$1 - d_{\mathrm{f}}$
C_{22}, C_{23}, and C_{32}	$1 - d_{\mathrm{m}}$
C_{12}, C_{21}, and C_{44}	$(1 - d_{\mathrm{f}})(1 - d_{\mathrm{m}})$
C_{33}, C_{55}, and C_{66}	1
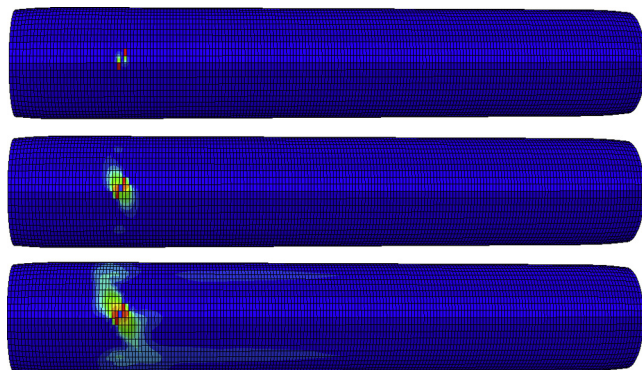
Figure 27.4 Fiber damage evolution of layer 2 (SDV3 contour plot). (For color version of this figure, the reader is referred to the online version of this book.)

A 760 mm long finite element model was built in a cylindrical coordinate system using the ABAQUS/standard nonlinear finite element analysis software. The eight-node linear brick, reduced integration element C3D8R was adopted to mesh the RTP pipe. The HDPE was modeled as an isotropic elastic material. The failure of HDPE is not considered in the analysis because the reinforced layers are damaged first. The mesh of the model includes 10,000 liner elements, 20,000 composite elements, and 10,000 coating elements. Kinematic coupling was used to constrain all six degrees of freedom of each ends at a reference point.

For a perfect FEA model without defect, the failures normally initiate near the boundary of the model, and many failure modes initialize at the same time. It is difficult to determine which mode causes the failure. To study the failure mode, an initial defect was added to the failure initiation area of the perfect FEA model before the analysis. For the FEA model with a defect, initial failure and failure progression of the finite element model occurred at the area around the defect. The fiber damage of the reinforce tape layer 2 in the longitudinal direction happened first, then a matrix damage of the reinforce tape layer 3 in the transverse direction happened. Compared with the experimental results, it can be concluded that the failure mode of RTP can be predicted from the fiber damage evolution, as shown in Figure 27.4, and the matrix damage evolution, as shown in Figure 27.5. The damage angle of the fibere and the matrix is close to 45°, which is similar to the failure angles of the tested specimens, as shown in Figure 27.2.

5. Results and Comparison

The mechanical behavior of RTP before the initiation of failure is evaluated by analytical analysis and finite element analysis. The predicted tangential strains, axial strains, and torsion angles are presented in Figure 27.6. The calculated values from the analytical and finite element analysis agree with each other when pressure is lower
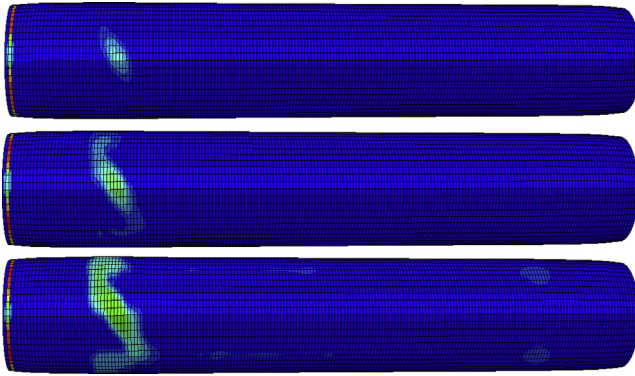
Figure 27.5 Matrix damage evolution of layer 3 (SDV4 contour plot). (For color version of this figure, the reader is referred to the online version of this book.)
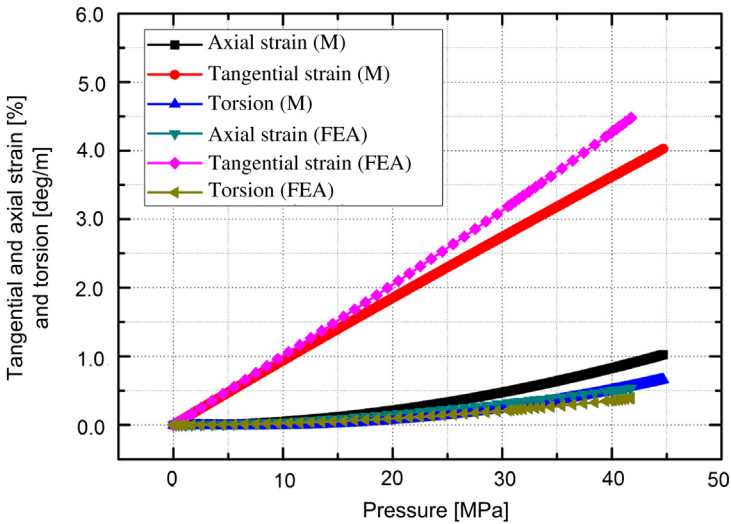
Figure 27.6 Comparison of analytical analysis with FE analysis for RTP under internal pressure. (For color version of this figure, the reader is referred to the online version of this book.)

Table 27.6 Burst Pressure Obtained from Different Methods

Methods	Analytical Analysis	Finite Element Analysis	Burst Test
Results (MPa)	44.7	41.8	35.4

than 10 MPa. The deviations increase when the internal pressure increases, which may be due to the different boundary conditions and the definition of initial defect used in the finite element model, also they may be due to the assumptions used in the analytical analysis. Although the inner and outer reinforced layers generate a positive and a negative torsion moments, respectively, they are not balanced with each other, as indicated by the existence of torsion angle.

Table 27.6 shows a comparison of the burst pressures from analytical analysis, FE analysis, and experimental data. Burst pressure predicted from analytical analysis is 26% higher than that from the experimental data. However, the burst pressure from FE analysis is much closer to the experimental results, only 18% larger than the experimental results. The deviation between the analytical analysis and the test data may be caused by the boundary condition used in the analytical analysis, which is not consistent with the experimental condition. In the FE method analysis, six degrees of freedom at the both model ends are constrained, which is more similar to the actual experimental condition.

The analytical analysis shows that the fiber of layer 2 fails first. The same behavior is observed from the both FE method and experimental data. FE analysis can also predict the progression of crack after the failure initiation. The orientation of the crack predicted from FE method is close to the experimental results, indicating that the FEA model is capable of predicting the post failure behavior.

References

[1] Xia M, Takayanagi H, Kemmochi K. Analysis of multi-layered filament-wound composite pipes under internal pressure. Composite Structures 2001;53:483–91.
[2] Kruijer MP, Warnet LL, Akkerman R. Modelling of the viscoelastic behavior of steel reinforced thermoplastic pipes. Composites, Part A 2006;37:356–67.
[3] Kobayashi S, Imai T, Wakayama S. Burst strength evaluation of the FW-CFRP hybrid composite pipes considering plastic deformation of the liner. Composites, Part A 2007;38:1344–53.
[4] Zheng JY, Li X, Xu P. Analysis on the short-term mechanical properties of plastic pipe reinforced by cross helically wound steel wires. J Pressure Vessel Technology 2009;131.
[5] Onder A, Sayman O, Dogan T, Tarakcioglu N. Burst failure load of composite pressure vessels. Composite Structures 2009;89:159–66.
[6] Knight NF. User-defined material model for progressive failure analysis. NASA/CR-2006–214526, Virginia; 2006.
[7] Xu P, Zheng JY, Liu PF. Finite element analysis of burst pressure of composite hydrogen storage vessels. Materials Design 2009;30:2295–301.
[8] Liu PF, Zheng JY. Recent Developments on damage modeling and finite element analysis for composite laminates: A review. Materials Design 2010;31:L3825–34.
[9] Linde P, Pleitner J, Boer H, Carmone C. Modelling and simulation of fibre metal laminates. ABAQUS Users' Conference 2004:421–39.
[10] Kruijer MP, Warnet LI, Akkerman R. Analysis of the mechanical properties of a reinforced thermoplastic pipe (RTP). Composites, Part A 2005;36:291–300.

[11] ASTM D 1599-99. Standard test method for resistance to short-time hydraulic pressure of plastic pipe, tubing, and fittings. Philadelphia: American Society for Testing Materials; 2003.

[12] Bai Y, Xu F, Cheg P, Badaruddin MF, Ashri M. Burst capacity of reinforced thermoplastic pipe under internal pressure. OMAE 2011-49325. Rotterdam, The Netherlands: OMAE; 2011.

28 Collapse of RTP Pipelines

Chapter Outline

1.   Introduction

The reinforced thermoplastic pipe (RTP) has been extensively used in onshore oil transportation over the past 10 years; however, RTPs face many challenges in offshore applications due to their low collapse resistance. More attention should be paid to the collapse of RTP under external pressure [1]. Normally, RTP consists of an external coating, reinforced tapes, and internal liner, as shown in Figure 26.1. The internal liner and external coating are made of high density polyethylene (HDPE), the reinforced layers in the middle are formed using reinforced tapes (usually two tapes in each layer) by a helical wrapping method [2]. A certain amount of aramid strands are embedded in the tapes to enhance their tensile strength and to resist the internal pressure of pipe. The external coating of pipe is used as a protective layer. Figure 27.1 shows a typical cross-section of RTP, in which two reinforced layers are used.

    The buckling or collapse and the post-buckling behavior of pipelines made of laminated composite materials subjected to an external pressure have received much attention in the past few decades. A two-dimensional nonlinear formulation was used

to analyze the buckling response of steel pipe under external pressure. Initial geometric imperfections, residual stress, and initial inelastic anisotropy were found to affect the external pressure resistance of pipeline [3]. First-order laminated anisotropic plate theory and the Ritz method were used to construct a model for the buckling of thick-walled composite pipe under external pressure. A lower buckling load was obtained because of the inclusion of shear deformation, especially for the pipe with a thick wall [4]. Effects of pre-buckling deformations on the failure pressure of arch-type structure were investigated. Mathematical formulations were proposed to calculate the pre-buckling deformation [5]. To calculate the equivalent stiffness parameters for the pipes reinforced with steel fibers, a rectangular model or rectangular outside and circle inside model were often employed [6]. Theoretical models based on thick-walled pipe are built to investigate the collapse of pipe under combined tension, bending, and external pressure. The J2 flow theory with isotropic hardening was used to model the plastic property of steel. The theoretical prediction showed agreement with finite element solution [7].

The collapse of RTP pipe subjected to external pressure, discussed in this chapter, is based on the analytical analysis and FE analysis of the papers by Bai et al. [8, 9].

2.   Analytical Analysis of RTP Collapse

Kinematics

The analytical analysis of collapse was carried out for a two-dimensional RTP ring with a mean radius of R and a total thickness of t, as shown in Figure 28.1 [10]. The RTP ring comprises four layers, and no relative slip is assumed to exist between layers. External pressure, P, is uniformly applied on the external surface of the RTP cross section. The origin of the polar coordinate system is located at the center of the ring. The coordinate z is the radial distance measured from the mid-surface (shown as a dashed line in the figure) of the pipe. Figure 28.2 illustrates the deformation of pipe cross section under shear load. In the model, the displacement of points on the mid-surface can be expressed with variables w and v. The variable w denotes the
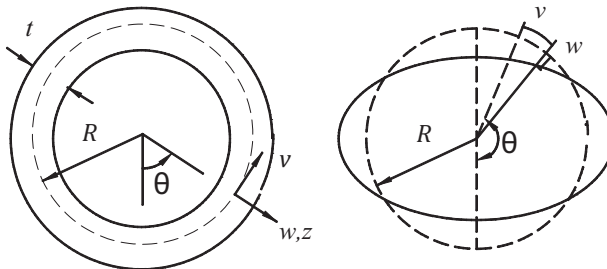
Figure 28.1 Coordinate system and geometric parameters.
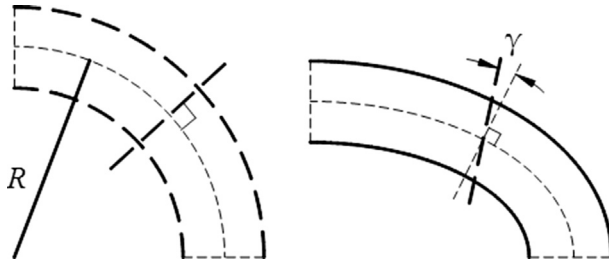
Figure 28.2 Shear deformation.

displacement along the radial direction, and v denotes the displacement in the circumferential direction.

The relationships between displacement and strain are given as follows [11]–[14]:

$$\varepsilon_\theta^L = \frac{v' + w}{R + z} \tag{28.1}$$

$$\varepsilon_\theta^N = \frac{1}{2}\left(\frac{v' + w}{R}\right)^2 + \frac{1}{2}\left(\frac{v - w'}{R}\right)^2 \tag{28.2}$$

$$k_\theta = \frac{v' - w''}{R^2} \bigg/ \sqrt{1 - \left(\frac{v - w'}{R}\right)^2} \tag{28.3}$$

$$\varepsilon_\theta = \varepsilon_\theta^L + \varepsilon_\theta^N + z\left(k_\theta + \frac{\gamma_\theta'}{R}\right) \tag{28.4}$$

$$\gamma_{r\theta} = \gamma \tag{28.5}$$

where $(\gamma)'$ indicates the differential of variables with respect to θ. The normal strain and shear strain in the analysis are denoted by ε_θ and $\gamma_{r\theta}$, respectively. The terms ε_θ^L and ε_θ^N denote the linear and nonlinear parts of the normal strain in the circumferential direction, while k_θ denotes the curvature variation of the cross section. The total normal strain is finally expressed by Eq. [28.5].

Layer Materials of RTP

PE

Polyethylene (PE) has become one of the most widely used and recognized thermoplastic piping materials since its first application as a piping material in the mid 1950s. Considering its mechanical properties, PE is a complicated combination of

elasticity, viscosity, plasticity, and some other components, only elastic strain and
plastic strain are taken into account for simplification in the constitutive model [15].

Reinforced Layer

The reinforced layers shown in Figure 28.3, consisting of PE and aramid strands, are
taken as homogenous layers. The reinforced layers are divided into uniform repre-
sentative volume elements as shown in Figure 28.4. The areas of aramid are the same
in the two forms of elements. An equivalent stiffness is used to get the stiffness pa-
rameters of the reinforced layers expressed in their local coordinate system, which are
the stiffness parameters of PE multiplied by a scale factor. It should be noticed that the
compression stiffness and shear stiffness of aramid strands are ignored, and the ratio
of stiffness parameters in different directions is assumed to be constant.

The mechanical parameters of the reinforced layer are thus expressed in Eqs.
[28.6]–[28.8]:

$$E_1 = E_{PE} V_{PE}$$
$$E_2 = E_{PE}(1 - V_I)$$
$$E_3 = E_{PE}\left(1 - \frac{V_A}{V_I}\right)$$

[28.6]
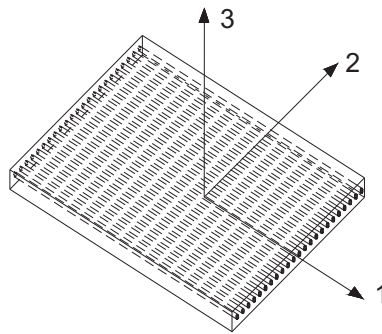
Figure 28.3 Local coordinate system for reinforced tape.
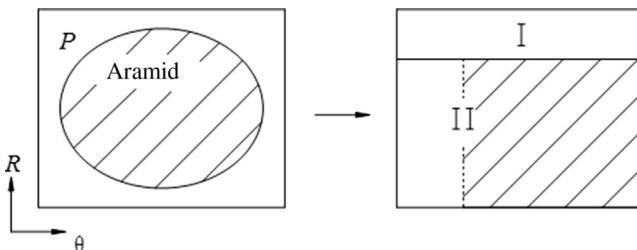
Figure 28.4 Representative volume element.

$$G_{12} = G_{PE}\left(1 - \frac{V_A}{V_I}\right)$$

$$G_{23} = G_{PE}(1 - V_I)$$

$$G_{31} = G_{PE}\left(1 - \frac{V_A}{V_I}\right)$$

[28.7]

The flexibility matrix of the reinforced layer is expressed as

$$\overline{S} = T \cdot S \cdot T^T$$

[28.8]

The detailed expressions of matrix S and T can be found in Bai et al.'s paper [8,9].

The Material Plasticity

Plane stress is used for the reinforced layers (σ_1, σ_3, τ_{13}, and τ_{23} equal to zero) and the stress-strain relationship in the θ direction is given as follows:

$$\varepsilon_\theta = \overline{S}_{2,2} \cdot \sigma_\theta + \overline{S}_{2,6} \cdot \tau_{12}$$

[28.9]

The incremental J2 flow theory of plasticity with isotropic hardening is used to model the plastic behavior of PE:

$$d\varepsilon_{ij}^p = \frac{1}{H}\frac{9}{4\sigma_e^2}(s_{ij} \cdot d\sigma_{ij})s_{ij}$$

[28.10]

where

$$\sigma_e^2 = \frac{3}{2}s_{ij}s_{ij}$$

[28.11]

and H in Eq. [28.10] can be determined by calibrating from a uniaxial tensile test.

Figure 28.5 shows a measured stress-strain relationship of HDPE in the test. The unloading path is shown with a dashed line. In the analytical model, it is assumed that, when the material is unloaded, it reverts to an elastic state and yields again when the equivalent stress grows to the maximum equivalent stress it had experienced.

The stress-strain relation in the incremental form is

$$\dot{\varepsilon}_\theta = \frac{1}{E}\left[-v + Q\left(-2\sigma_\theta^2\right)\right]\dot{\sigma}_\theta$$

[28.12]

where

$$Q = \begin{cases} 0, & \sigma_e \leq \sigma_{max} \\ \frac{1}{4\sigma_e^2}\left(\frac{E}{E_t} - 1\right), & \sigma_e \geq \sigma_{max} \end{cases}$$

[28.13]
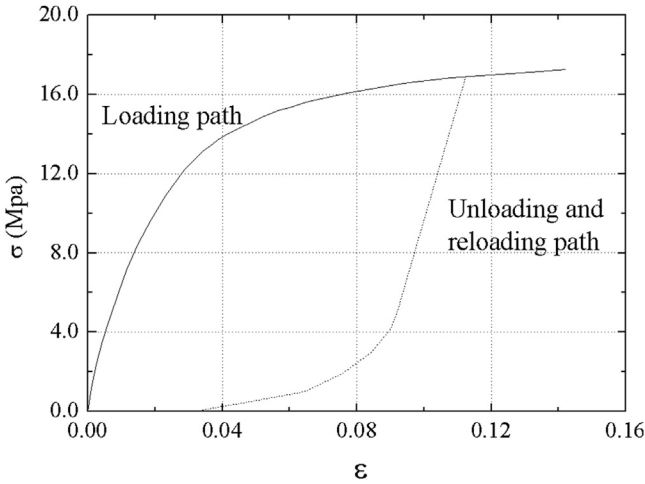
Figure 28.5 Stress-strain relationship of HPDE.

The plastic strain due to the shear strain is neglected, because this part of plastic strain is small; in addition, the calculation efficiency is improved.

Principle of Virtual Work

The principle of virtual work can be used in statics for solution of equilibrium problem of RTP. The equations that follow must be satisfied when the RTP pipe is in an equilibrium state:

$$2R \int_{0}^{\pi} \int_{-\frac{\ell}{2}}^{\frac{\ell}{2}} \left(\hat{\sigma}_\theta \delta \dot{\varepsilon}_\theta + \tau_{r\theta} \delta \dot{\gamma}_{r\theta} \right) d\theta dz = \hat{P} \delta \dot{V} \qquad [28.14]$$

where $(\dot{V})$ denotes the virtual increment of variables. The right-hand side of Eq. [28.14] is the virtual work increment due to the pressure load, that is, the product of pressure and virtual volume change:

$$\delta \dot{V} = R \int_{0}^{2\pi} \left[\delta \dot{w} + \frac{1}{2R} \left(2\hat{w} \delta \dot{w} + 2\hat{v} \delta \dot{v} + \hat{w} \delta \dot{v}' + \hat{v}' \delta \dot{w} - \hat{v} \delta \dot{w}' - \hat{w}' \delta \dot{v} \right) \right] d\theta$$

$$[28.15]$$

It is assumed that the deformations of the pipe are symmetric about the axis, $\theta = 0$. The variables (w, v, and γ) are the functions of θ, and they can be approximated by the following series of expansions:

$$w \cong Ra_0 + R\sum_{n=1}^{N} a_n \cos(n\theta) + R\sum_{n=1}^{N} b_n \sin(n\theta)$$

$$v \cong R\sum_{n=2}^{N} c_n \cos(n\theta) + R\sum_{n=2}^{N} d_n \sin(n\theta)$$ [28.16]

$$\gamma \cong R\sum_{n=1}^{N} e_n \cos(n\theta) + R\sum_{n=1}^{N} f_n \sin(n\theta)$$

Substituting Eqs. [28.15] and [28.16] into Eq. [28.14], 6N-1 nonlinear algebraic equations can be obtained by solving for unknowns: $\{\dot{a}_0, \dot{a}_1, \ldots, \dot{a}_N, \dot{b}_1, \dot{b}_1, \ldots, \dot{b}_N, \dot{c}_2, \dot{c}_3, \ldots, \dot{c}_N, \dot{d}_2, \dot{d}_3, \ldots, \dot{d}_N, \dot{e}_1, \dot{e}_2, \ldots, \dot{e}_N, \dot{f}_1, \dot{f}_2, \ldots, \dot{f}_N\}$.

To properly identify the limit of pressure instabilities, pressure loading can also be accomplished by prescribing the increments of the volume enclosed by the pipe in the unit length. Then, P becomes an additional unknown variable with the following additional equation:

$$\hat{v} = \pi R^2 + R \int_0^{2\pi} \left[\hat{w} + \frac{1}{2R}\left(\hat{v}^2 - \hat{v}\hat{w}' + \hat{v}'\hat{w} + \hat{w}^2 \right) \right] d\theta$$ [28.17]

Therefore, a series of nonlinear algebraic equations containing 6N unknowns $\{\dot{a}_0, \dot{a}_1, \ldots, \dot{a}_N, \dot{b}_1, \dot{b}_1, \ldots, \dot{b}_N, \dot{c}_2, \dot{c}_3, \ldots, \dot{c}_N, \dot{d}_2, \dot{d}_3, \ldots, \dot{d}_N, \dot{e}_1, \dot{e}_2, \ldots, \dot{e}_N, \dot{f}_1, \dot{f}_2, \ldots, \dot{f}_N, \dot{P}_1\}$ are established.

Amendment of Radius and Wall Thickness

The mean radius of pipe decreases while the wall thickness increases during the deformation due to the external pressure, and both changes contribute to the collapse resistance to the external pressure. Ignoring the prebuckling change of mean radius and wall thickness, which is normally used in the analysis of thin-walled pipe, may produce significant errors for the RTP design because of its thickness. Therefore, the prebuckling deformations in the form of mean radius change and wall thickness change are added to the analytical model.

The change of mean radius produced by the increments of internal pressure $\dot{p}_i$ can be calculated by,

$$\dot{\varepsilon}_{Ri} = \frac{\dot{p}_i R_{i-1}}{E_t A_{i-1} + \frac{E_t I_{i-1}}{R_{i-1}^2}}$$ [28.18]

where EA is the tensile rigidity and EI denotes the bending stiffness of the pipe. The mean radius and wall thickness are

$$R = R_0\left(1 - \sum_{i=1}^{N} \varepsilon_{Ri} \right)$$ [28.19]

$$t_j = t_{j0}\left(1 + \nu \sum_{i=1}^{N} \varepsilon_{Ri}\right) \qquad [28.20]$$

where, subscript 0 denotes the initial value of variables and j is the layer number. At the beginning of each loading step, R and t are amended.

Analytical Method

The Gauss integration method is used to simplify the operation of integration. The cross section is discretized to l and m elements along r and θ directions, respectively. One quarter of the cross section is shown in Figure 28.6.

Initial imperfections are introduced by adding small initial displacements, that is, $\overline{w}$ and $\overline{v}$, to the perfect pipe. The initial displacements produce a certain degree of initial ovality (Δ_0), and they are given by

$$\overline{w} = \Delta_0 \cos(2\theta), \quad \overline{v} = \frac{\Delta_0}{2}\sin(2\theta) \qquad [28.21]$$

The Newton-Raphson method is used to solve the $6N$ nonlinear algebraic equations iteratively. As shown in Figure 28.7, the required parameters should be defined in advance, including geometric dimensions, material parameters, initial imperfections, and the distribution of Gaussian integral points. In the first loading step, the $6N$ equations are originally balanced by the initial values. When new values of volume are prescribed, new values of the variables in the braces are solved iteratively until the convergence criterion is met. In each loading step, the mean radius and wall thickness are updated, as well as strain, stress, and equivalent stress.

At the beginning of each loading step, the values of displacements, strains, and stress are updated; and the maximum equivalent stress, $\sigma_{e,max}$, is recorded. Variable values at the end of the previous loading step are set as the initial value for the next
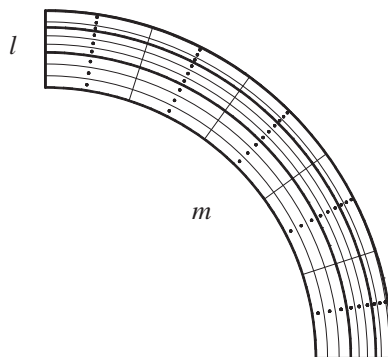
Figure 28.6 Distribution of Gaussian integral points.
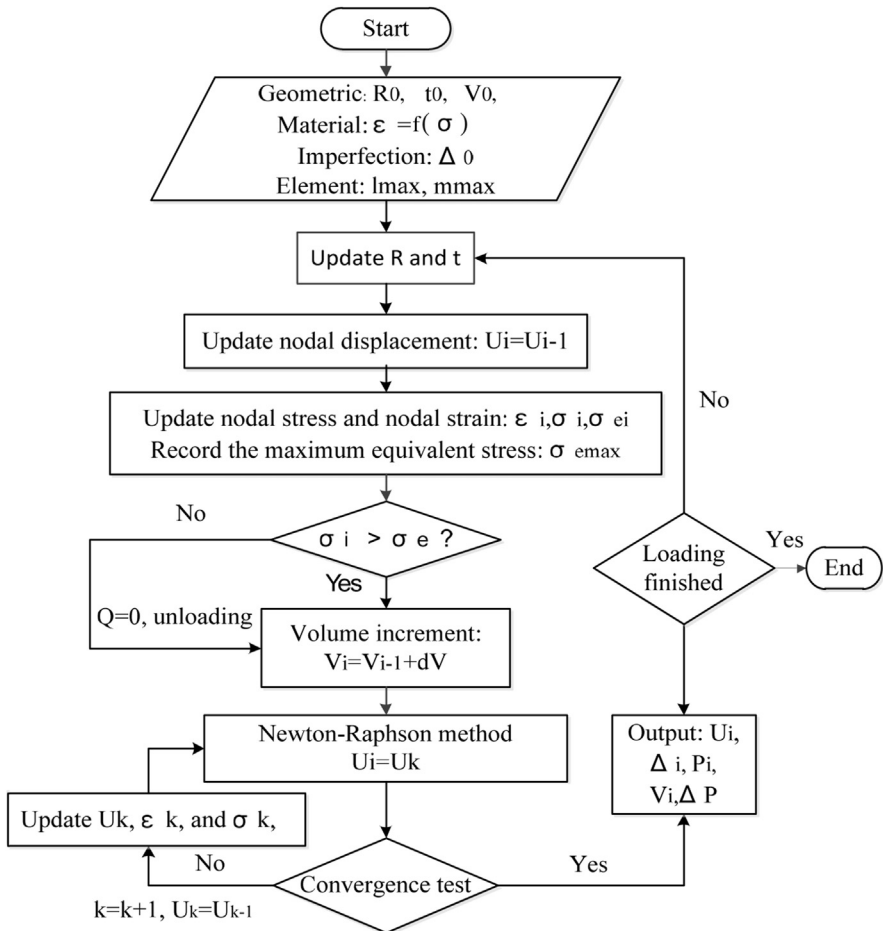
Figure 28.7 Flowchart of analytical analysis procedure.

step. The loading or unloading for an element in the next step is chosen by comparing the values of σ_e with $\sigma_{e,max}$. MATLAB is used to solve the analysis following the flowchart.

3.   FE Analysis of RTP Collapse

Introduction

The collapse of RTP is analyzed using an FE method for comparison with the analytical method. A general commercial FE program, ABAQUS, is selected to simulate the collapse of RTP.

FE Modeling

The ABAQUS finite element model is developed to verify the analytical analysis. An eight-node, second-order, reduced integration plane stress element, CPS8R, is chosen to model the pipe cross section. Just as in the analytical analysis, the axial stress is ignored. Figure 28.8 shows that the cross section is meshed into 6 elements through thickness, 160 elements around the circumference.

Two symmetry boundary conditions are established along the axis of the cross section with a hydrostatic pressure applied on the external surface. J2 flow theory of plasticity with isotropic hardening is adopted to describe the plastic behavior of the material. The fibers are neglected in this model because they are compressed and their compression stiffness is very small.

According to the eigenvalue analysis, the mode shape corresponding to the lowest eigenvalue is in the shape of an oval. The nodal displacements of this mode shape are added to the perfect pipe to produce an initial imperfection in the pipe, after multiplication by a small scaling factor. The Riks method is used to analyze the buckling response of structures exhibiting large prebuckling deformations and material plasticity.
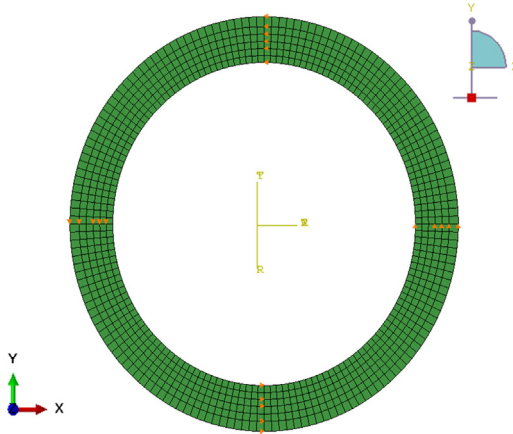
Figure 28.8 FE model of RTP cross ection. (For color version of this figure, the reader is referred to the online version of this book.)

4.   Analysis Example of RTP Collapse

Introduction

An example of collapse analysis for RTP pipe was performed by using both the analytical method and FEA.

Input Data

The RTP with a mean radius of 55.6 mm and a total wall thickness of 13.8 mm ($D/t =$ 8.06) was used for the example. An initial ovality of 0.1% is introduced in the pipe.

Table 28.1 Key Parameters of RTP Pipe for Collapse Analyses

Layer no.	Thickness (mm)	Number of Strands	Winding Angle of Strands (°)	Poisson's Ratio	Δ_0
1	6.3	—	—	0.45	0.001
2	2.25	106	−55	0.45	0.001
3	2.25	106	55	0.45	0.001
4	3	—	—	0.45	0.001

The analysis results of analytical approach and FE approach are presented for comparison. Some important parameters used in the analysis are shown in Table 28.1. The Poisson's ratio of each layer is taken as a constant.

Pressure-Ovality Curves

Figure 28.9 shows the collapse pressure-ovality curves of RTP obtained through the analytical approach and FE approach. Before the maximum collapse pressure is reached, the pressure increases obviously while the ovality is small. After the maximum collapse pressure is reached, the pressure drops as the ovality continues to increase. The results obtained through the two approaches show good agreement, with a maximum difference of 1.0% when the ovality is 2%. The collapse pressure calculated by the analytical analysis is higher than that of the FE model. This can be explained by use of the plane section assumption in the analytical model.

Figure 28.10 shows the variations of strains at four key locations with the change of ovality during the deformation of RTP. The four key locations on the cross section
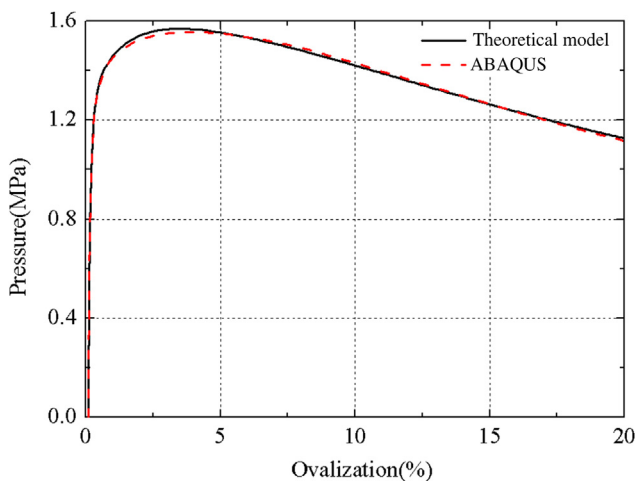
Figure 28.9 Collapse pressure-ovality curves. (For color version of this figure, the reader is referred to the online version of this book.)
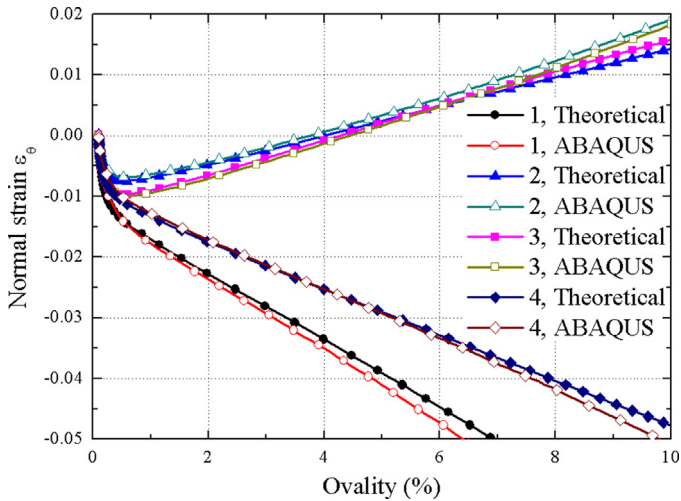
Figure 28.10 Variation of normal strains with ovality at key locations. (For color version of this figure, the reader is referred to the online version of this book.)
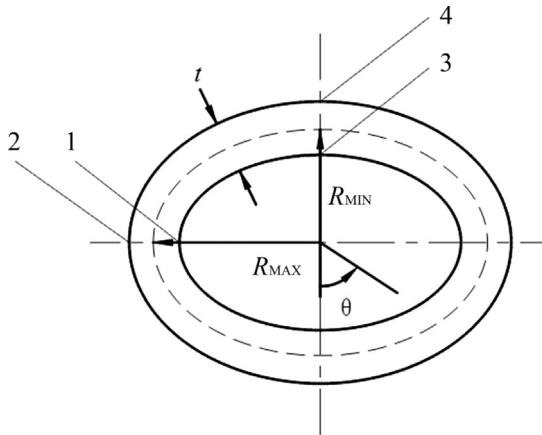
Figure 28.11 Possible locations of the maximum strain.

in which the maximum strain is most likely to occur are shown in Figure 28.11. It can be seen that the elements at point 1 and point 4 are compressed during the loading process; the elements at point 2 and point 3 are found to be compressed at first then elongated. The results obtained through the analytical approach and FE approach show the same tendency, but the strains of the analytical model are less than that of the finite element model. This is because the extra constraints from the plane section assumption restrict the deformation to a certain extent in the analytical model. The maximum difference of the strains between the two approaches is below 6% when the strain is less than 10%.

5. Sensitivity Analysis

The analytical model is used to study the effects of several important factors on the collapse pressure, including initial imperfections, shear deformation, and prebuckling deformations.

Effect of Initial Imperfections

All the pipes used in engineering practice have initial imperfections. In this section, the effect of initial geometric imperfections is studied based on the analytical method.

Figure 28.12 shows the effect of initial imperfections on the collapse pressure-ovality responses of the RTP with the dimensions defined in Table 28.1. The ovality of the pipe with larger initial imperfections grow faster. Meanwhile, the ultimate pressure becomes lower. The collapse pressure for the pipe with $\Delta_0 = 0.01\%$ is 20% higher than pipe with $\Delta_0 = 1.0\%$.

Effect of Shear Deformation

It is well known that shear deformation has a great influence on the pipe's collapse pressure when its wall thickness is large. Ignoring the shear deformation, which is normally used in the analysis of thin-walled pipe, may induce a significant error for RTP. The model shown in Figure 28.2 includes the shear deformation by allowing an angle, γ, to change freely. To illustrate the effect of the shear deformation, an analytical model without the shear deformation is established for comparison. In this model, the planes perpendicular to the mid-surface before the deformation are supposed to remain perpendicular to the mid-surface ($\gamma \equiv 0$), and thus the normal strain in hoop direction is expressed as Eq. [28.22]:
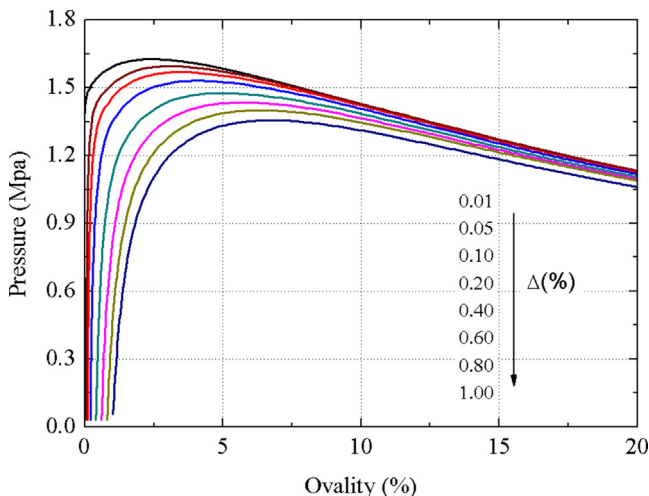
Figure 28.12 Effect of initial imperfections on pressure-ovality curves of RTPs. (For color version of this figure, the reader is referred to the online version of this book.)

$$\varepsilon_\theta = \varepsilon_{\theta L} + \varepsilon_{\theta N} + \frac{z}{1 + \frac{z}{R}} k_\theta \qquad [28.22]$$

Figure 28.13 shows the collapse pressure-ovality curves obtained from the two methods. The RTP with three D/t ratios (D/t = 6.0, 8.06, and 10.0) are analyzed. The thickness and structure of these pipes are the same, but their mean radii are different. It can be seen that when the deformation is small; the curves obtained from the both methods coincide. Higher collapse pressures are calculated for the model without shear deformation. Larger difference is observed for the pipe with higher D/t ratios, and the differences are 4.5%, 3.6%, and 2.8% from D/t = 6.0, 8.06, and 10.0, respectively.

Effect of Prebuckling Deformation

During the loading process, the mean radius of the pipe decreases while the wall thickness increases. Both these changes result in the decrease of diameter-to-thickness ratio, which contributes to the external pressure resistance. In this section, the effects of the prebuckling deformations in the form of the change of mean radius and wall thickness are analyzed with analytical method. The model shown in Figure 28.1 includes the amendment of R and t in the loading steps. To illustrate the effect of prebuckling deformations, another analytical model, which excludes the amendments, is established for comparison.

Figure 28.14 shows the effects of amendment of pipe radius and wall thickness on the collapse pressure-ovality curves. The pressure-ovality curves shown in the figure are calculated based on the three ratios of diameter over wall thickness for RTP (D/t =
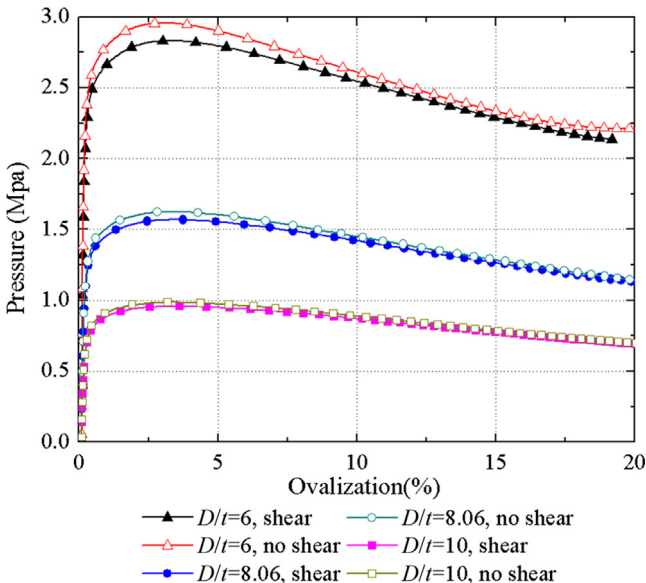
Figure 28.13 Effects of shear deformation on pressure-ovality curves. (For color version of this figure, the reader is referred to the online version of this book.)
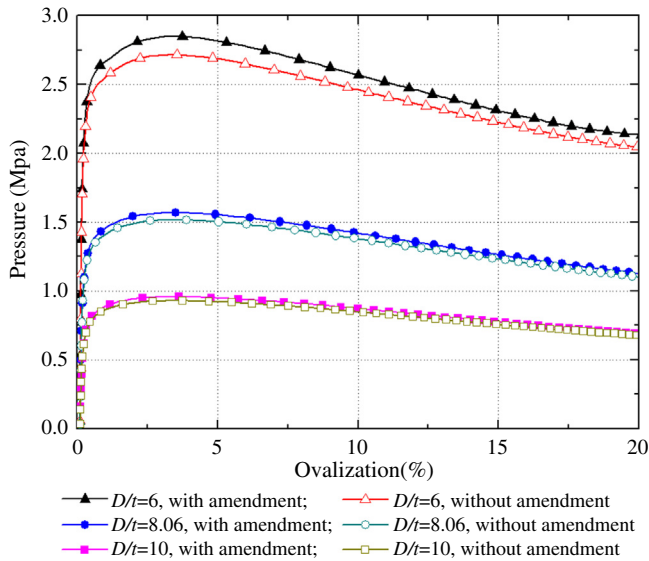
Figure 28.14 Effects of amendment of *R* and *t* on pressure-ovality curves. (For color version of this figure, the reader is referred to the online version of this book.)

6.0, 8.06, and 10.0) using analytical models of with and without amendment of *R* and *t*. The thickness and structure of RTP for all cases are the same, which are given in Table 28.1, but the mean radii are different. When the deformation is small, the effect of amendment of *R* and *t* on the curve configuration is very small. For the same ovality, higher pressure is calculated when the amendment of *R* and *t* is included, and the difference becomes larger for the RTP pipe with a higher *D/t* ratio. As the diameter-to-thickness radio, *D/t* varies from 6.0, 8.06, to 10.0, the pressure differences are 5.3%, 3.4%, and 2.1%, respectively.

References

[1] Dalmolen LGP, et al. Offshore applications of reinforced thermoplastic pipe (RTP). Petromin Pipeliner; January–March 2009:14–8.
[2] Kruijer MP, Warnet LL, et al. Analysis of the mechanical properties of a reinforced thermoplastic pipe (RTP). J Composites Part A: Appl Sci Manufacturing 2005;36(2):291–300.
[3] Yeh MK, Kyriakides S. On the collapse of inelastic thick-walled tubes under external pressure. J Energy Res Technol 1986;108:35.
[4] Yang C, Pang SS, et al. Buckling analysis of thick-walled composite pipe under external pressure. J Composite Materials 1997;31(4):409–26.
[5] Cheng P. In-plane nonlinear theory and elastic-plastic stability of pined circular arches. PhD thesis. Hangzhou, China: Zhejiang University; 2005.
[6] Zhu Y. Investigation on the instability of plastic pipe reinforce by steel wires under the load of external pressure. Master thesis. Hangzhou, China: Zhejiang University; 2007.

[7] Gong S, Yuan L, et al. Buckling response of offshore pipelines under combined tension, bending, and external pressure. J Zhejiang Univ—Science, A 2011;12(8):627–36.

[8] Bai Y, Wang N, Cheng P, Yu B, Fauzi Badaruddin M, Ashri M. Collapse of reinforced thermoplastic pipe under external pressure. OMAE 2011-49324; Rotterdam, The Netherlands; 2011.

[9] Bai Y, Wang N, Cheng P. Collapse of RTP subjected to external pressure. ICPTT2012; Wuhan, China; 2012.

[10] Arjomandi K, Taher F. A new Look at the external pressure capacity of sandwich pipes. J Marine Structures; 2011.

[11] Corona E, Kyriakides S. Asymmetric collapse modes of pipes under combined bending and external pressure. J Eng Mechanics 2000;126:1232.

[12] Kyriakides S, Corona E. Mechanics of offshore pipelines. Vol. 1. Buckling and collapse. Oxford, UK: Elsevier; 2007.

[13] Tabiei A. Buckling of moderately thick composite cylindrical shells under destabilizing loads. J Thermoplastic Composite Materials 1995;8(4):365–74.

[14] Aydogdu M. A new shear deformation theory for laminated composite plates. J Composite Structures 2009;89(1):94–101.

[15] Zhang C, Moore ID. Nonlinear mechanical response of high density polyethylene. Part II. Uniaxial constitutive modeling. J Polymer Eng Sci 1997;37(2):414–20.

29 Offshore Installation of RTP

Chapter Outline

1.   Introduction

Flexible pipes, as a technical alternative to the traditional rigid steel pipes, have been used in oil and gas fields for more than 30 years. The major offshore applications include risers in floating production systems (FPSs) and transportation lines from satellites to subsea manifold center. Especially, composite pipelines, which are a kind of flexible pipeline, are now increasingly being used as transport pipelines in selected offshore projects. Several materials, such as Kevlar fiber, glass fiber, and carbon fiber, are available for fiber-reinforced plastic composites (RTP). The application of composites in marine field for oil and gas industry is encountering big boom currently.

Unlike steel pipes, flexible pipes are usually lightweight and flexible as well as corrosion resistant. These merits provide fast and low-cost installation of flexible pipe. Flexible pipe can be manufactured in long lengths, thus it can be supplied by reels on the vessel. A sufficient top tension by tensioners is needed to avoid over-bending of pipe near the touchdown zone. As shown in Figure 29.1, flexible pipe can be lowered onto the seabed along a ramp or a wheel. Due to the unique construction of flexible pipe, special attentions should be paid for a successful installation [1]. In contrast with rigid steel pipes, flexible RTP pipes do not have a particularly high collapse resistance, so special precautions must be made to ensure no significant positive external pressure difference occurs. The external collapse resistance of pipe must be taken as a primary consideration in selecting subsea pipelines. Flooding the
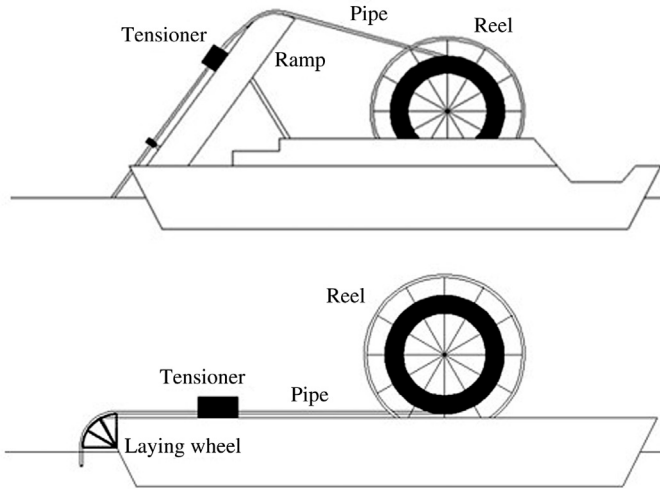
Figure 29.1 Installation method of flexible pipes.

pipeline with water during installation is often used to mitigate the collapse problem. The virtue of the light weight mitigates the required top tension, but it may also bring about problems of submerged weight and stability during laying process. As shown in Figure 29.2, the RTP pipeline is often filled with water before installation and additional weight modules are always attached to pipeline to gain its submerged weight and ensure stability, other methods such as rock bolts or a mattress can also protect the pipeline.

Figure 29.3 illustrates the float and sink method for the installation of RTP in shallow water. The sinking operation basically consists of the controlled addition of water from the onshore end of the pipe and the release of the entrapped air from the opposite end. The sinking is conducted so that it starts at the shore, where the pipe enters the body of water, and gradually progresses into deeper waters. To achieve this, an air pocket is induced by lifting the floating pipe close to the shore. As the water is
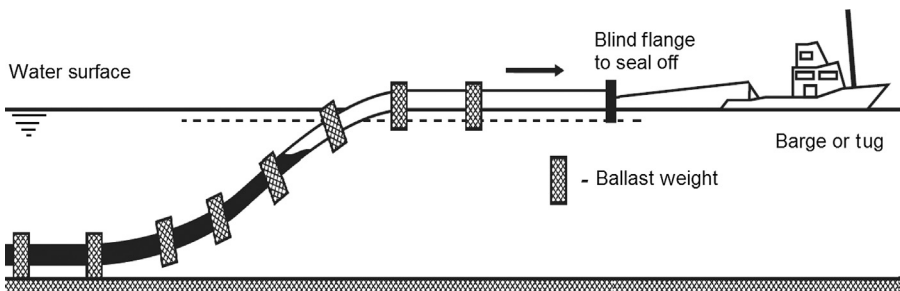
Figure 29.2 Pulling pipe to minimize local buckling.
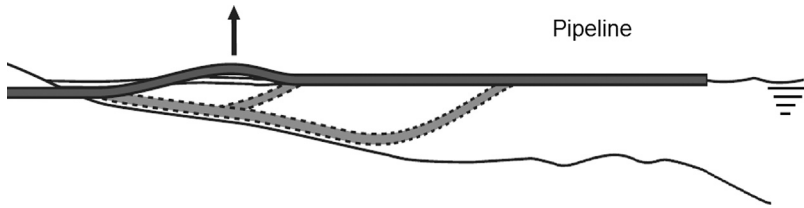
Figure 29.3 Float and sink method of RTP.
Source: PPI [2].

allowed to enter the pipe from the shore side, the added weight causes this initial air pocket to move outward and the intermediate section of pipe between the air pocket and the shore end to sink. As additional water is added, this pocket moves to deeper waters causing the sinking to progress to its terminal point in the body of water.

A potential risk during the submersion operation is that the bending of the pipe between the water-filled and air-filled portions may be deformed sharply enough to risk the development of a kink, a form of localized pipe buckling, when the pipe sinking occurs too quickly. As a pipe is bent, its circumferential cross section at the point of bending becomes increasingly ovalized. This ovalization reduces the pipe's bending moment of inertia. On sufficient ovalization, a kink may form at the location of the maximum bending and lead to a sudden reduction of the bending capacity. The risk of local buckling may be minimized by applying a suitable pulling tension during the installation, as illustrated in Figure 29.2. Therefore, special designs should be used to provide a good grip of RTP as well as to avoid the RTP crushing at the tensioners. Some measures, such as lubricating the ramp, may be needed to avoid the abrasion damage of RTP. Figure 29.4 shows an installation of RTP through a laying wheel to avoid kinks due to overbending in the overbend segment.

The offshore installation analysis of pipelines is to obtain the pipeline configuration and stress and strain distributions along the pipeline to verify the security of installation. The mechanical properties of a flexible pipeline are much more complicated than that of a metallic pipeline, the sectional properties of flexible pipeline must be predetermined before the offshore installation analysis. The following properties are relevant to installation of RTP:

- Axial loading capacity.
- Bending loading capacity.
- Tensional loading capacity.
- Crushing capacity.
- Hydrostatic resistance.

During the installation phase, the following critical parameters must be constantly monitored to help control the states of pipeline:

- Top tension at tensioners.
- Departure angle.
- Bending radius near the TDP.
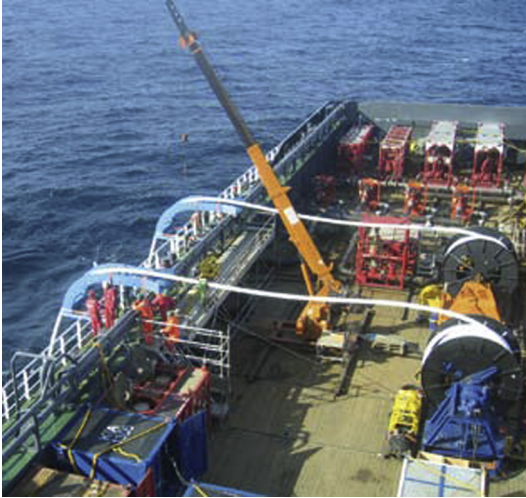
Figure 29.4 Installation of RTP through a laying wheel. (For color version of this figure, the reader is referred to the online version of this book.)

This chapter details an offshore installation analysis of reinforced thermoplastic pipe, which is a kind of composite flexible pipe. The works of theoretical analysis and FEA in the section are quoted from Bai et al. "Offshore Installation of Reinforced Thermoplastic Pipe (RTP)" [3].

2. Code Requirements

Generally accepted codes for RTP flexible pipe are API RP 15S, "Qualification of Spoolable Reinforced Plastic Line Pipe" [4]; API RP 17B, "Recommended Practice for Flexible Pipe" [5]; API 17J, "Specification for Unbonded Flexible Pipe" [6]; and API 17K, "Specification for Bonded Flexible Pipe" [7]. Performance based design has been adopted to meet the minimum performance criteria, and it requires a careful evaluation of the link between failure mechanisms and failure modes.

3. Analytical Analysis of RTP Installation

Introduction

The pipeline is subjected to a combined loading environment, including axial tension, bending moment, external pressure, and ocean currents during installation. In the last few decades, great efforts have been devoted to the analysis and improvement of pipeline installation. Several analytical methods, such as the natural centenary theory and finite element method, have been used to solve the installation problem.

Table 29.1 Parameters of RTP

Item	Value
Outside diameter (OD)	0.125m
Inside diameter (ID)	0.097m
Wall-thickness	0.014m
Unit weight in air	4.8 kg/m
Unit weight with water filled	24.5 kg/m
Unit weight of ballast modules	12.0 kg/m

The flexibility of RTP facilitates the use of catenary theory to establish the pipeline configuration. The catenary model ignores the flexural rigidity of pipeline to calculate the relation between axial tension and curvature. A modified numerical method using catenary theory is introduced. The suspended pipeline is assumed to behave as catenary and the laid part of pipeline is assumed to rest on a Winkler-type deformable soil. A numerical solution is proposed to provide efficient and reliable predictions for actual laying setting.

As mentioned previously, the axial loading and bending loading behaviors are directly related to installation; therefore, these section properties of pipe should be determined before global installation analysis. In this chapter, the adopted parameters of RTP are listed in Table 29.1 and the corresponding axial loading behavior and bending loading behavior are shown in Figure 29.5.

Static Configuration

Assuming RTP is unreeled and lowered into water along a ramp, the installation analysis is simplified as a J-lay problem. To focus on the key points, the following assumptions are made:

- The seabed is a horizontal and flat with soil stiffness.
- The submerged weight is calculated as the average weight of RTP (including water content, if it is flooded) and its rock bolts for weight coating.
- A planar problem is considered, which means the pipeline is restricted to move in vertical plane.

Suspended Pipeline Segment

Under the loads of axial tension and self-weight, the RTP pipeline exhibits a large deflection during installation. Due to the high flexibility of RTP and if the length of suspended pipe is long enough, the curvature of RTP of the suspended part is governed by the applied axial tension. The simplest model for calculating the relationship between tension and curvature is the catenary model, which ignores the effect of bending stiffness.

Figure 29.6 illustrates the overall configuration of RTP pipeline during installation. An orthogonal coordinate system is set up by locating the origin at the position of tensioner, WD represents the water depth from the origin to seabed. For a small
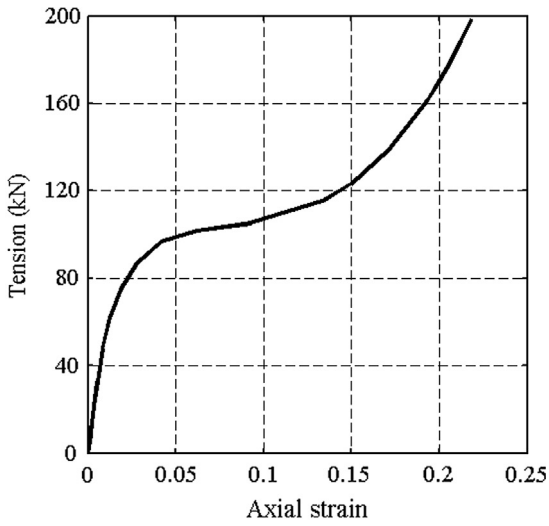
(a) Axial loading behavior
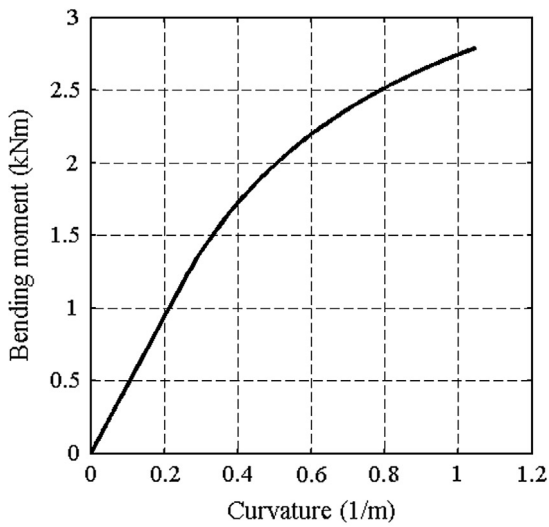
(b) Bending loading behavior

Figure 29.5 RTP mechanical properties.
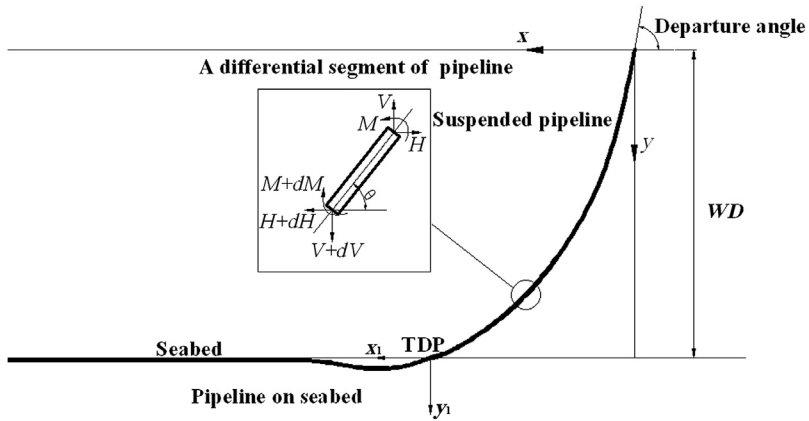
Figure 29.6 Pipeline configuration for RTP installation.

segment of RTP pipeline, the equilibrium of force and bending moment can be derived as

$$dH = 0 \tag{29.1}$$

$$dV = -wds \tag{29.2}$$

$$dM = Vds\cos\theta - Hds\sin\theta - w(ds)^2\cos\theta/2 \tag{29.3}$$

where H and V represent the horizontal and vertical force, respectively; M is the bending moment of pipe segment; w is the unit submerged weight of pipeline.

By neglecting the effect of bending stiffness, Eq. [29.3] is simplified as

$$\tan\theta = V/H \tag{29.4}$$

The curvature can be expressed as

$$\Phi = d\theta/ds \tag{29.5}$$

Obviously, the inclination angle is controlled by the tension along pipeline, which is the classical catenary theory. Although ignoring the bending stiffness in determining the pipeline configuration, the actual bending moment can be approximately obtained by curvature using the relations between bending moment and curvature. For a small segment, the increment of displacement is obtained as

$$dx = ds\cos\theta \tag{29.6}$$

$$dy = ds\sin\theta \tag{29.7}$$

Laid Pipe Segment

To guarantee a smooth transition at the TDP, the assumption of rigid seabed is relaxed and the laid part of pipeline is supposed on a Winklerlike foundation, as shown in Figure 29.7.

The embedment of pipeline is small due to the great stiffness of soil; therefore, the liner theory of beam is proposed to solve the part:

$$EIy_1''''(x_1) - Ty_1''(x_1) + ky_1(x_1) = w \qquad [29.8]$$

where x_1 and y_1 in the equation are the coordinates of this section, as shown in Figure 29.7; T is the axial tension at the TDP, which is assumed remain constant along the laid part of pipeline to neglect the friction effect between the pipeline and seabed; k is the soil stiffness. To ensure the continuity at the TDP, EI is the tangent stiffness at the TDP of the suspended pipeline. This may induce larger, conservative results in the neighborhood of TDP but has little influence on the other part, because the embedment of pipeline is dominated by its self-weight far from the TDP. For $T \leq 2\sqrt{EIk}$ and $x_1 \leq 0$, the general solution of Eq. [29.8] is

$$y_1 = w/k + c_1 e^{-\alpha x_1} \cos(\beta x_1) + c_2 e^{-\alpha x_1} \sin(\beta x_1) \qquad [29.9]$$

where

$$\alpha = \frac{1}{2}\sqrt{2\sqrt{\frac{k}{EI}} + \frac{T}{EI}}; \quad \beta = \frac{1}{2}\sqrt{2\sqrt{\frac{k}{EI}} - \frac{T}{EI}};$$

and two constants vanish due to the boundary conditions at $x_1 \rightarrow +\infty$.
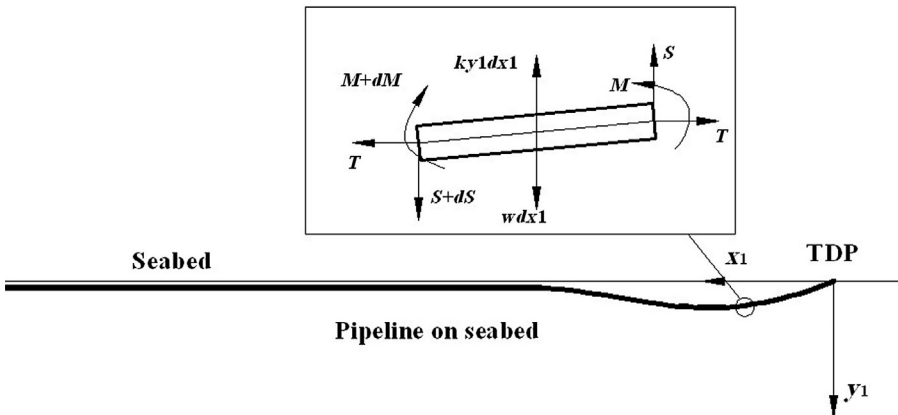
Figure 29.7 Pipeline laid on the seabed.

The pipeline continuity at the TDP is the boundary condition of Eq. [29.9]. The continuity of coordinates and the slope are adopted:

$$y_1(0) = y_{n1} - \text{WD} \qquad\qquad [29.10]$$

$$y_1'(0) = \tan\theta_{n_1} \qquad\qquad [29.11]$$

where n_1 is the point at which y_i reaches the seabed.

The embedment along the pipeline can be easily obtained by Eq. [29.9] and the corresponding bending moment is

$$M_1(x_1) = -EIy_1''(x_1) \qquad\qquad [29.12]$$

Numerical Solution

The key point in numerical solution is to determinate a reasonable top tension to guarantee the continuity at the TDP. The pipeline configuration can be easily obtained once the top tension is found; an iteration program is developed to calculate the top tension and corresponding configuration and internal loads, the following are the main steps:

- An assumption of initial top tension.
- The pipeline is divided into small segments with lengths of ds, the axial tension, increment of displacement and curvature for every segment can be obtained from Eqs. [29.1]–[29.7].
- The unknown variables c_1 and c_2 in Eq. [29.9] should be determined before solving the displacement and bending moment along the pipe. The continuity of displacement, Eq. [29.10], and slope at the TDP point, Eq. [29.11], are used as boundary conditions to solve the variables c_1 and c_2.
- The difference of bending moment of the suspended part, Eq. [29.12], and the part laid on seabed at the TDP are used as the control conditions to get a reasonable top tension, if the difference is small enough, the top tension is determined.

4. FE Analysis of RTP Installation

A general commercial FE software program, ABAQUS [8], is employed to solve the installation analysis. A sketch of the ABAQUS model is shown in Figure 29.8, and the main characteristics of the model are the following:

- **RTP pipeline**: RTP is modeled by beam elements (B31H). For RTP, nonlinear generalized beam section behavior is used; the behavior of axial strain and axial force, bending curvature, and bending moment are applied to B31H instead of stress-strain relationships.
- **Seabed**: A 3D analytical surface is used to model the seabed, an interaction between the pipeline and seabed is defined to simulate the contact during installation. The friction effects are neglected in model.
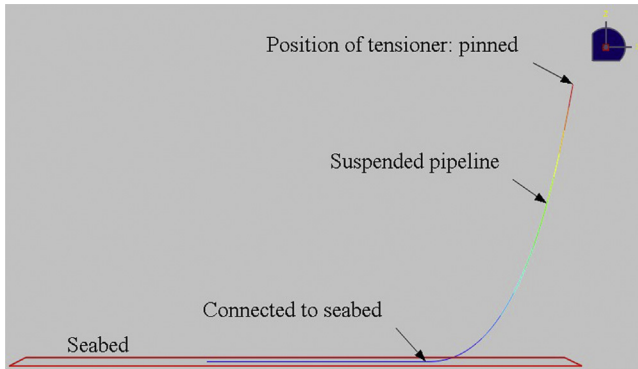
Figure 29.8 Sketch of ABAQUS model. (For color version of this figure, the reader is referred to the online version of this book.)

- **Boundary conditions**: The pipeline is linked to the laying vessel at the tensioner, setting this hang-off end pinned; a concentrated load equal to the residual pulling force is applied at the end node of pipeline on the seabed.

In addition to the parameters of RTP listed in Table 29.1, other required parameters for the installation analysis are summarized in Table 29.2.

Figure 29.9 shows a comparison of pipeline configurations between the analytical solution detailed in Section 3 and the FE simulation in this section. The overall configurations are almost the same, but some differences appear in the magnified neighborhood of TDP, shown in Figure 29.9(b), due to the different treatment of boundary conditions at the TDP. In the analytical model, the tension, displacement, slope, and bending moment are continuous at the TDP, but the continuity of shear force cannot be guaranteed, because the suspended pipeline is treated as a cable, which also induces differences in bending moment at the zone near the TDP, as shown in Figure 29.10. Table 29.3 lists a comparison of M_{max}, T_{TOP}, and T_{TDP} from the two methods. As shown in Figures 29.10 and 29.11, the analytical method provides a good estimation of pipeline behaviors during installation, except for some differences in the area close to the TDP.

Table 29.2 Basic Parameters for Calculation

Parameter	Value
Water depth	70 m
Density of seawater	1025 kg/m^3
Laying angle at the top	80°
Current velocity	0 m/s
Seabed stiffness	2×10^5 N/m^2
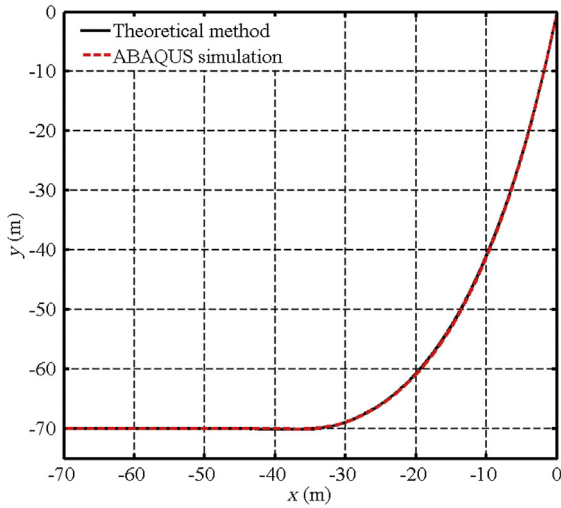
(a) Overall scale
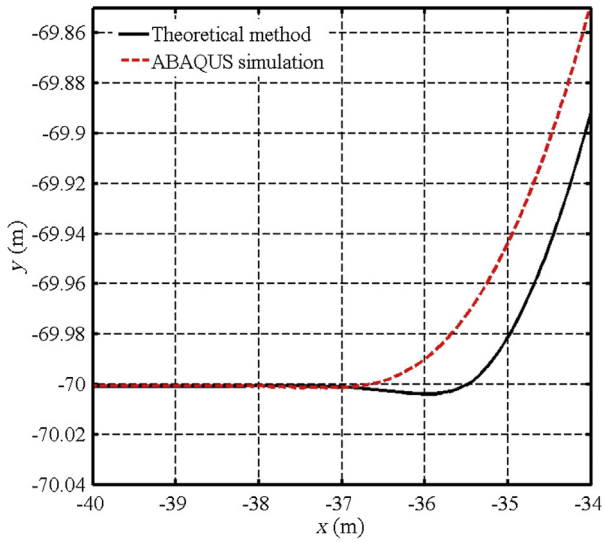
(b) Nearby TDP

Figure 29.9 Pipeline configurations. (For color version of this figure, the reader is referred to the online version of this book.)
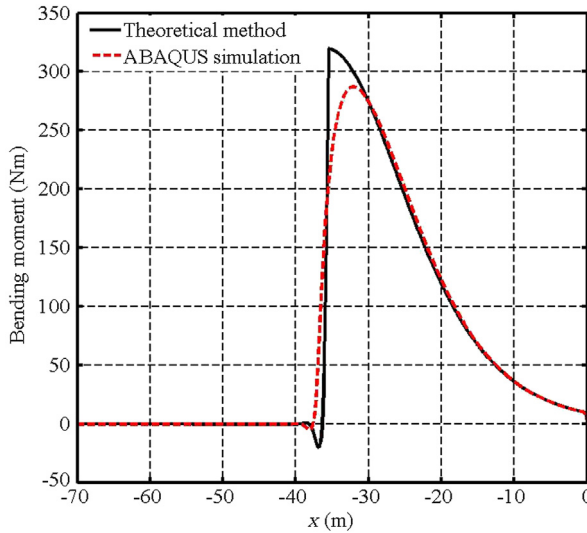
Figure 29.10 Comparison of bending moment. (For color version of this figure, the reader is referred to the online version of this book.)

Table 29.3 Comparison of M_{max}, T_{TOP}, and T_{TDP} between Analytical and FE Methods

Item	M_{max} (Nm)	T_{TOP} (N)	T_{TDP}(N)
Analytical method	320	9872	1714
ABAQUS simulation	287	9848	1698
Difference	10.3%	0.24%	0.93%
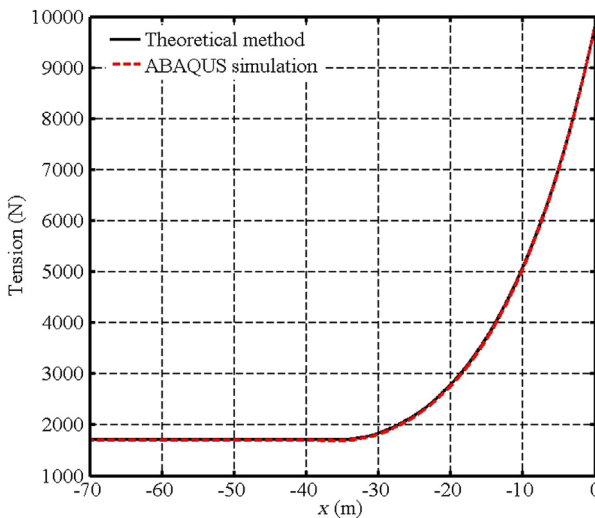
Figure 29.11 Comparison of axial tension. (For color version of this figure, the reader is referred to the online version of this book.)

5.   Parametric Studies

In this section, several examples are presented to figure out the effects of water depth, top laying angle, submerged weight, and seabed stiffness to the RTP installation.

Water Depth

Unlike special offshore flexible pipe, RTP designed for onshore use initially does not have a particularly high collapse resistance. The difference between external and internal pressures for RTP in offshore application limits the use of RTP because of pipeline collapse. Up to now, the main offshore applications of RTP have been in shallow water. Therefore, to avoid special disposal of RTP, four water depths (70 m, 100 m, 150 m, and 200 m) are selected. As shown in Figures 29.12 and 29.13, the pipeline configuration becomes steeper and the bending moment of the suspended part increases more smoothly with the increase of water depth; the difference of moment distribution between the two solutions becomes smaller for deeper water; this is because the length of suspended pipeline is longer for deeper water, which reinforces the flexibility of pipeline. The required top tensions, listed in Table 29.4, grow rapidly with the increase of water depth; this is also due to the longer length of suspended pipeline for deeper water.

Top Laying Angle

The top laying angle is one of the key factors directly related with the pipe bend stress at the sag bend location. The analysis results of the selected laying angles of 78°, 80°, 82°, and 84° are presented in Figures 29.14 and 29.15. Figure 29.14 shows the change
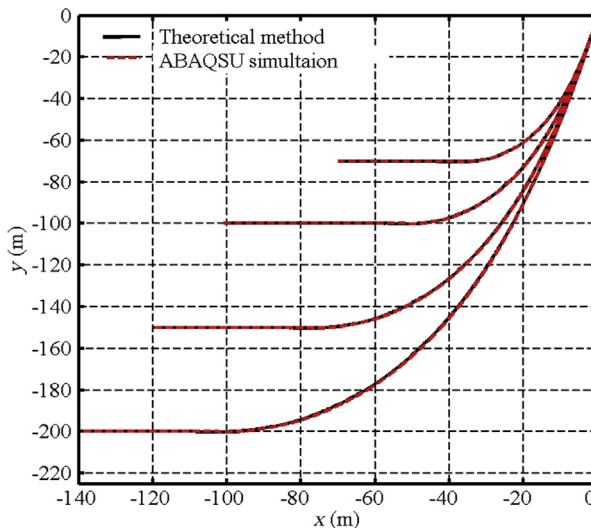
Figure 29.12 Configuration of pipeline for different water depths. (For color version of this figure, the reader is referred to the online version of this book.)
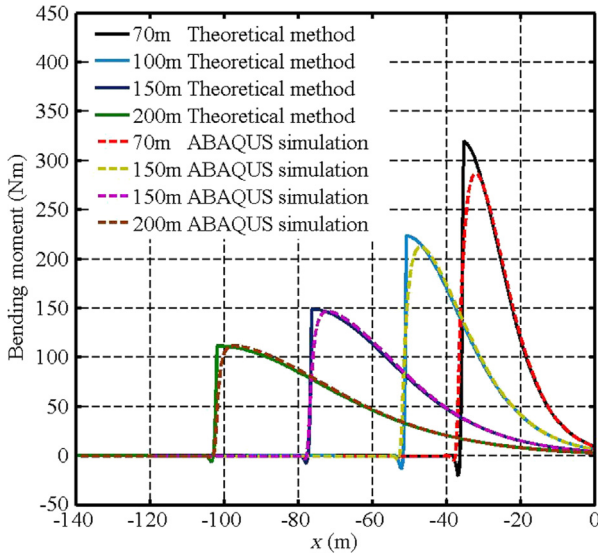
Figure 29.13 Distribution of bending moment for different water depths. (For color version of this figure, the reader is referred to the online version of this book.)

of RTP configuration with the variation of top laying angle. The RTP configuration becomes sharper and the distance between the tensioner and TDP decrease with the increase of the top angle. As the top angle gets larger, the top tension required to support the suspended span decreases, as shown in Table 29.5, while the maximum bending moment near the TDP increases considerably. The difference between analytical and FE analyses becomes larger, as shown in Figure 29.15, because the pipe configuration changes sharply near the TDP and the difference in boundary conditions becomes more obvious. In general, the pipe nearby the TDP is subjected to a larger bending moment for a larger top laying angle, which is a potential dangerous zone during installation. Therefore, a suitable top angle should be selected.

Table 29.4 Comparison of Tension for Different Water Depths

WD (m)	Analytical Method		ABAQUS Simulation	
	T_{TOP} (N)	T_{TDP} (N)	T_{TOP} (N)	T_{TDP} (N)
70	9872	1714	9847	1698
100	14014	2489	14071	2433
150	21157	3673	21101	3655
200	28210	4898	28120	4875
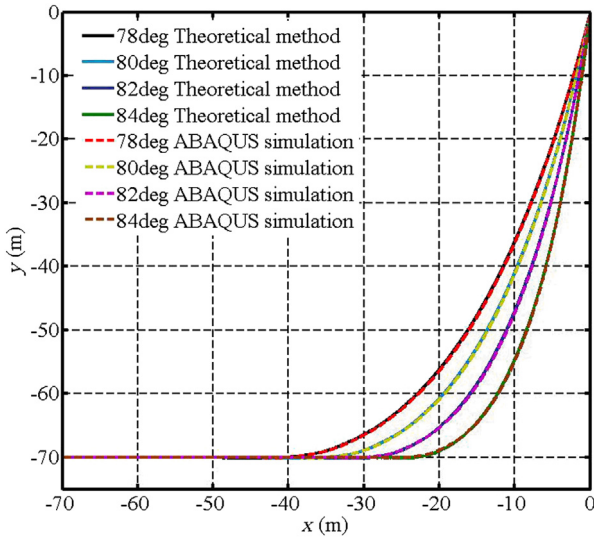
Figure 29.14 Configuration of pipeline for different top laying angles. (For color version of this figure, the reader is referred to the online version of this book.)
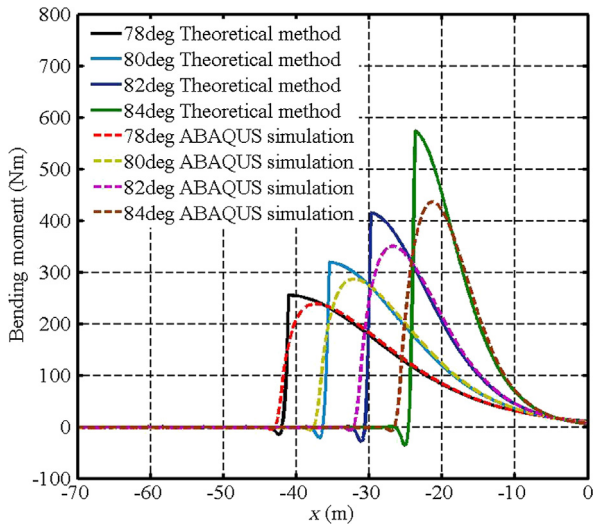
Figure 29.15 Distribution of bending moment for different top laying angles. (For color version of this figure, the reader is referred to the online version of this book.)

Table 29.5 Comparison of Tension for Different Top Laying Angles

Top Laying Angle (deg)	Analytical Method		ABAQUS Simulation	
	T_{TOP} (N)	T_{TDP} (N)	T_{TOP} (N)	T_{TDP} (N)
78	10,299	2142	10,266	2119
80	9872	1714	9847	1698
82	9477	1319	9456	1305
84	9110	952	9096	942

Submerged Weight

Because of the light weight of RTP, additional weight must be attached to it during installation. Enough submerged weight helps to sink the pipe and improve its stability, but it also requires higher tension. Considering the minimal submerged weight required for the on-bottom stability of RTP, three submerged weights, 116 N/m, 175 N/m, and 244 N/m, are chosen for this analyses. Table 29.6 shows that the top tension increases rapidly with the increase of pipe's submerged weight. Figures 29.16 and 29.17 show that the pipeline configurations are almost the same and the bending moment distribution varies a little for different submerged weights. The submerged weight has a big effect on the required tension but a small influence on the bending moment distribution.

Seabed Stiffness

The comparison of analytical and ABAQUS FE analyses shows that the boundary conditions of seabed stiffness at the TDP have significant influence on the behavior of pipe near the TDP. Therefore, four soil stiffness (k1 = 2×10^4 N/m², k2 = 1×10^5 N/m², k3 = 2×10^5 N/m², and k4 = 5×10^5 N/m²) are selected for the sensitivity analysis. Figure 29.18 shows the pipeline configuration near the TDP with different soil stiffnesses. The discrepancy between the analytical method and ABAQUS FE simulation due to boundary conditions was explained previously. The overall tendency is the same with the variation in seabed stiffness. The maximum embedment

Table 29.6 Comparison of Tension for Different Submerged Weights

Unit Submerged Weight (N/m)	Analytical Method		ABAQUS Simulation	
	T_{TOP} (N)	T_{TDP} (N)	T_{TOP} (N)	T_{TDP} (N)
116	9872	1714	9847	1698
175	14,821	2574	14,765	2548
244	20,631	3583	20,528	3546
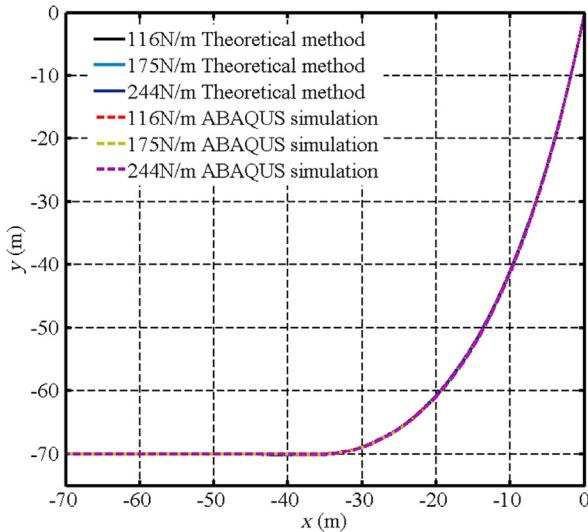
Figure 29.16 Configuration of pipeline for different submerged weights. (For color version of this figure, the reader is referred to the online version of this book.)

appears close near the TDP, decreasing with the increase of seabed stiffness. Because of different boundary conditions at the TDP, the analytical method may overestimate the maximum embedment, but the embedment far from TDP, which is dominated by pipe's submerged weight, is the same for the two methods. Table 29.7 lists several
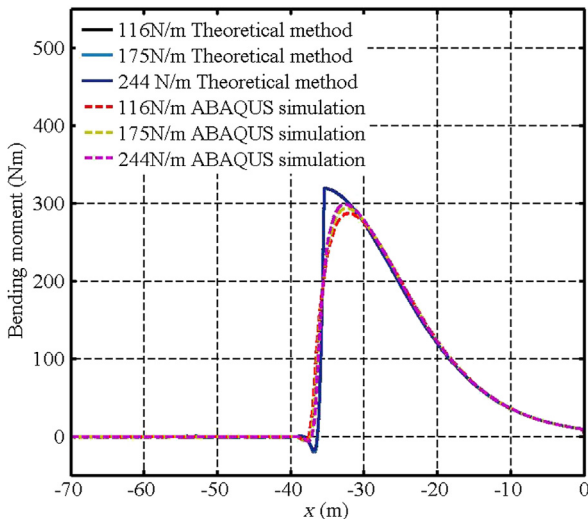
Figure 29.17 Distribution of bending moment for different submerged weights. (For color version of this figure, the reader is referred to the online version of this book.)
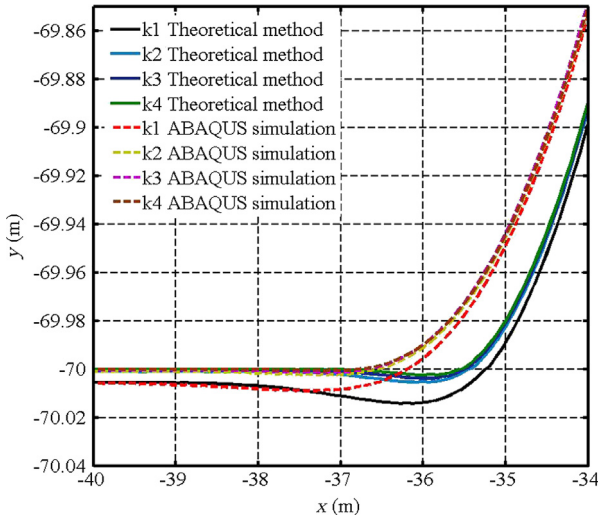
Figure 29.18 Pipeline configuration near the TDP for different seabed stiffnesses. (For color version of this figure, the reader is referred to the online version of this book.)

primary loads, and apparently the seabed stiffness has little effect on tension and the bending moment.

6. Summary

Due to its unique material composition, small bending stiffness, and great nonlinearity, the behavior of RTP is different from that of rigid steel pipeline during installation. A simple analytical method for RTP installation based on the natural catenary theory is developed, owing to the flexibility of RTP. A numerical iteration solution is applied to obtain the pipeline configuration and stress and strain distribution. Meanwhile, a nonlinear FE model is developed to analyze the behavior of RTP during installation. The analysis results from the two methods show good agreement, which demonstrates the validity of the analytical method. Therefore, the proposed

Table 29.7 Primary Loads for Different Seabed Stiffnesses

Seabed Stiffness (N/m^2)	Analytical Method			ABAQUS Simulation		
	M_{max} (Nm)	T_{TOP} (N)	T_{TDP} (N)	M_{max} (Nm)	T_{TOP} (N)	T_{TDP} (N)
k1 = 2 × 10^4	319	9873	1716	287	9846	1696
k2 = 1 × 10^5	320	9872	1715	288	9845	1696
k3 = 2 × 10^5	320	9872	1714	287	9847	1698
k4 = 5 × 10^5	320	9872	1714	288	9845	1696

analytical method can be served as an easy, effective, and time-saving way to study the installation of RTP compared with the FE method. However, the assumptions made for simplicity in analytical method limits its application range, and more complicated models such as FEA may be needed.

A sensitivity analysis based on the analytical method and ABAQUS FE simulation is carried out for the pipeline's behavior by changing several important factors. The laying water depth and top laying angle are critical factors for the overall pipeline configuration and load distribution. The submerged weight and seabed stiffness have effect only on the top tension and the maximum embedment of pipe, respectively. The coincidence of the two methods further verified the reliability of the analytical method.

References

[1] Dalmolen LGP, Kruyer M, Cloos PJ. Offshore applications of reinforced thermoplastic pipe (RTP). Pipelife Nederland B. V: MERL Conference; 2009.

[2] PPI. Handbook of PE pipe. 2nd ed. Available at http://plasticpipe.org/cart/pe_handbook.html.

[3] Bai Y, Yu BB, Cheng P. Offshore installation of reinforced thermoplastic pipe (RTP). Rhodes, Greece: 22nd International Offshore and Polar Engineering Conference; June 2012.

[4] API RP 15 S. Qualification of spoolable reinforced plastic line pipe. Washington, DC: American Petroleum Institute; 2006.

[5] API RP 17B. Recommended practice for flexible pipe. Washington, DC: American Petroleum Institute; 2002.

[6] API RP 17J. Specification for unbonded flexible pipe. Washington, DC: American Petroleum Institute; 2001.

[7] API RP 17K. Specification for bonded flexible pipe. Washington, DC: American Petroleum Institute; 2000.

[8] ABAQUS 6.10. ABAQUS analysis user's manual. Providence, USA: Dassault Systems; 2010.

30 On-Bottom Stability of RTP

Chapter Outline

1.   Introduction

RTP has unique advantages, such as anticorrosion, large allowable plastic strain, and ease of installation, which make it stand out in the onshore oil and gas industry. In recent years, because of the high corrosion products detected in some subsea fields, steel pipes have been easily corroded and need to be replaced within a short lifetime, which involves a high cost for the field operators. RTP is one of the best choices as an anticorrosion transportation methodology. However, RTP has disadvantages that restrict its applications in the subsea fields. Such disadvantages include light weight, low collapse resistance to external pressure, and additional on-bottom stability measures. Some differences in pipeline on-bottom stability between rigid steel pipe and RTP in subsea applications are because of these unique characteristics.

Subsea RTPs are subjected to distributed loading due to current and waves; hence, the objective of the on-bottom stability analysis and design is to limit resultant pipe deflection so that the resultant maximum RTP bending stresses and strains are within the allowable limits. To stabilize the RTP on the seabed, additional weights, such as attached ballasts, are required to restrict or limit the movement of the pipe. The ballast spacing is different among RTPs with different diamesr and wall thicknesses. The ballast spacing of 3 m (10 ft) is commonly used for RTPs with diameters smaller than

10 in. However, shorter spacing of ballasts better distributes anchoring loads on the sea bottom and minimizes local deformation of pipeline. For shorter spacing, the ballasts are more manageable both in size and weight.

Chapter 13 of this book details the on-bottom stability of rigid pipe; this chapter concentrates on the differences in the stability behavior and analysis methods between rigid pipe and RTP flexible pipe; the same parts of on-bottom stability for both types of pipe are not repeated in this chapter.

2.   Stabilizing Methods

Table 30.1 lists the pipe weights per unit length of a typical RTP in various conditions. It is obviously that the pipe submerged weight is insufficient to stabilize the RTP under installation conditions with an empty pipe in seawater. To stabilize the RTP on the seabed, external weight is required. The stabilization methods for RTP are used to restrict or limit the pipe movement. The additional weight is either strapped on concrete blocks at regular intervals or a heavy steel wire. Sometimes, concrete weight mattresses are used.

A wide range of additional stabilization methods are available for subsea RTPs, which vary from the intervention methods such as trenching and rock dumping to pipeline anchoring techniques such as rock bolts, strategic anchors, and gravity anchors. The following stabilization methods can be used for keeping RTP on -bottom stability:

- Strategic and gravity anchors.
- Rock bolts.
- Mattresses.
- Rock dumping.

Strategic and Gravity Anchors

Figure 30.1 illustrates the strategic or gravity anchor method for pipeline on-bottom stability. This method has also been used in steel pipelines that have insufficient on-bottom stability. The main advantage of the method is that the anchor can prevent pipeline from moving out of the stable position throughout the pipeline's life.

Rock Bolts

Due to the disadvantages of gravity anchors method, such as local buckling from RTP contact with the anchor and the high cost of fabrication and installation, a new

Table 30.1 Pipe Weights of RTP

Item	Unit	Value	Remarks
Pipe weight in air per unit length	kgf/m	7.1	
Pipe weight filled with water per unit length	kgf/m	11.5	
Pipe submerged weight per unit length	kgf/m	–2.3	Empty pipe
Pipe submerged weight of flooded RTP	kgf/m	2.2	
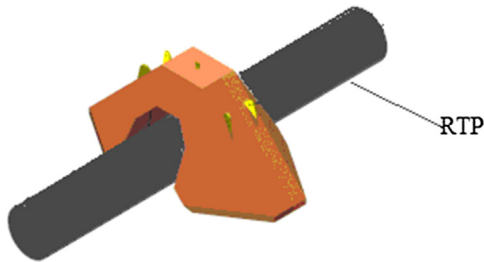
Figure 30.1 Strategic or gravity anchor. (For color version of this figure, the reader is referred to the online version of this book.)

stabilizing method, rock bolts, was introduced in recent years. This method, shown in Figure 30.2, is to assemble two portions of rock with bolts and nuts to form the ballast block. The ballast block is part of the RTP, the environmental load effects on the ballast block should be included in the on-bottom stability analysis.

The rock bolt method has several advantages, such as low cost of fabrication and installation, less damage to RTP, full contacted with RTP, size that can be changed according to actual condition. The main disadvantage is that the bolts and nuts should be protected from corrosion in seawater and local "free span" may exist if the space of ballast block is too large [1].

Concrete Mattresses

Figure 30.3 illustrates a RTP pipe covered with concrete mattresses. The mattress method follows the same principle, with rock bolts for on-bottom stability of pipeline, and compared with the rock bolts method, it improves the current field condition
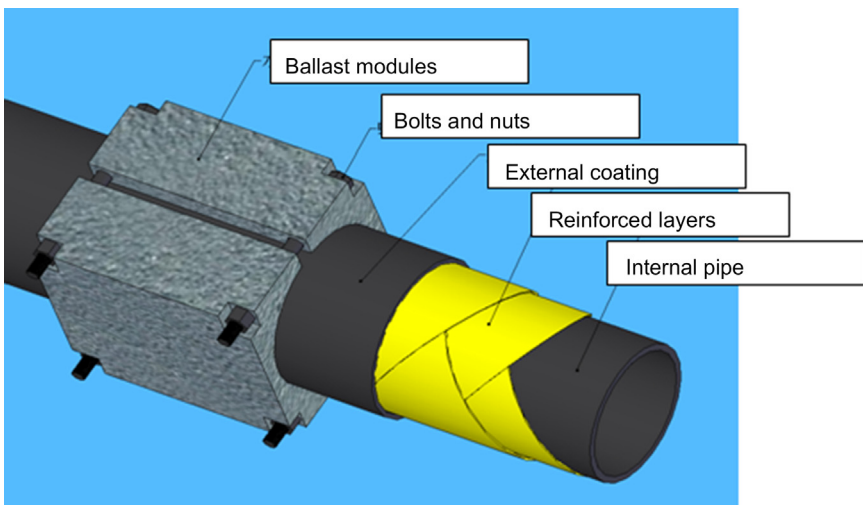
Figure 30.2 Rock bolt. (For color version of this figure, the reader is referred to the online version of this book.)
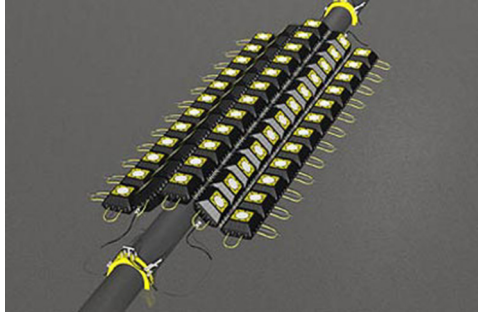
Figure 30.3 Concrete mattress. (For color version of this figure, the reader is referred to the online version of this book.)

around the RTP. The current can flow smoothly above the RTP, and the RTP is in full contact with the seabed. The disadvantage is that fabrication and installation cost more.

Rock Dumping

The rock dumping method, shown in Figure 30.4, belongs among intervention methods that stabilize the RTP. Use of this method is not recommended, because it is difficult to ensure the stabilization of RTP and may also cause damage to the RTP. Should the soil liquefaction easily occur, the RTP may float up and break down.

To choose a suitable method for the RTP stabilization, the pros and cons of the four methods are listed in Table 30.2 [2].

3.   On-Bottom Stability Analysis of RTP

In this section, the following three on-bottom stability analysis methods for RTP are discussed:

- The quasi-static and dynamic analytical methods, which include DNV RP F109, and PRCI/ AGA Level 2 for assessing RTP on-bottom stability.
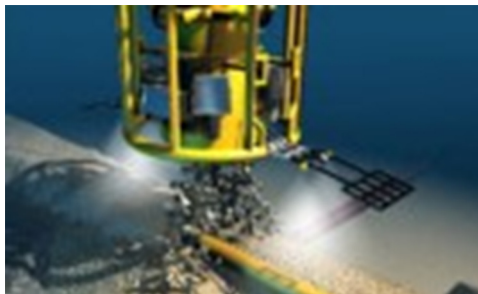
Figure 30.4 Rock dumping. (For color version of this figure, the reader is referred to the online version of this book.)

Table 30.2 Comparison of Stabilization Methods for RTP

Methods	Advantages	Disadvantages
Strategic and gravity anchors	Can be used throughout the RTP life	Costly to fabricate and install Easily causes local buckling
Rock bolts	Easy to fabricate and install Can be taken as part of RTP Size can be designed to fit actual condition	Bolts and nuts should be protected from corrosion in seawater May cause local "free span" if the space is too small.
Concrete mattresses	Improves the current field around the RTP "Free span" is not considered unless seabed is flat	Costly to fabricate and install Stiffener fails easily in seawater
Rock dumping	Easy to install and low cost	May damage the RTP RTP may easily float up and break down in liquidating soil

- FE simulation following DNV RP F109, which models the RTP on the seabed under hydrostatic and hydrodynamic loads.
- Experimental tests, in which the RTP is measured under wave and current loads in laboratory tests.

According to the pros and cons of the stabilization methods listed in Table 30.2, the concrete mattress method is chosen as the measure to perform the analytical analysis, FE analysis, and laboratory tests for the on-bottom stability of RTP.

Design Parameters

Due to lack of a special rule about RTP on-bottom stability analysis, DNV RP F109 (2010) [3] is used as the design criteria and guideline. The main difference of the stability analysis, between the steel rigid pipe and the nonmetallic pipe is the weight coating method. The continuous concrete weight coating method is commonly used as the on-bottom stability mitigation measure of steel rigid pipeline; therefore, the pipeline hydraulic loads can be calculated by the Morison force equations, as suggested in DNV RP F109. However, the ballast methods are normally used for nonmetallic pipeline, and the Morison equations may not be suitable in this case due to inaccuracy.

Table 30.3 shows the environment data for the RTP on-bottom stability analysis, and the basic required parameters of RTP for the analysis are listed in Table 30.4.

Design Criteria

According to DNV RP F109 (2010) and other equal design practices [4]–[6], the pipe is considered to satisfy the requirements of on-bottom stability if the following criteria are satisfied. For lateral stability,

Table 30.3 Wave and Current Data

Parameters	Unit	Value
Seawater density	kg/m^3	1025
Seawater temperature	°C	25
Water depth	m	75
Highest astronomic tide	m	2.1
Mean astronomic tide	m	1.2
Lowest astronomic tide	m	0
Significant wave height, Hs(10 year)	m	4.0
Significant wave period, Tp (10 year)	s	9.7
Current (100 years)	m/s	0.63

$$\gamma_{SC} \cdot \frac{F_Y + \mu F_Z}{\mu W_s + F_R} \leq 1.0 \qquad\qquad [30.1]$$

For vertical stability,

$$\gamma_{SC} \cdot \frac{F_Z}{W_s} \leq 1.0 \qquad\qquad [30.2]$$

$$SG = \frac{W_s + b}{b} \geq 1 \qquad\qquad [30.3]$$

where

γ_{SC} = safety factor, 1.5 is taken
F_Y = lateral force
F_Z = vertical force
SG = specific gravity

Table 30.4 Basic Input Data for RTP On-Bottom Stability Analysis

Item	Unit	Value	Remarks
Inner diameter	mm	75	
External diameter	mm	110	
Pipe weight in air	kgf/m	7.1	
Flooded pipe weight in air	kgf/m	11.5	
Pipe submerged weight	kgf/m	–2.3	Empty pipe
Flooded pipe submerged weight	kgf/m	2.2	
Equivalent density	kg/m^3	1396	
Soil type			Sand
Submerged weight of sand	kN/m^3	10	
Wave attack angle	Deg	90	
Current attack angle	Deg	90	

F_R = soil resistance force
W_s = pipe unit submerged weight
b = pipe buoyancy

Analytical Analysis

The analytical analysis of the on-bottom stability of RTP is carried out according to DNV RP F109. The environmental condition (wave and current) and the pipe's parameters are given in the last section. The additional ballast weight for the stability is averaged in a unit length of the RTP.

The following load conditions of RTP are included:

- Empty pipe in the installation condition.
- Flooded pipe with water in the hydrotest condition.
- Pipe with production in the operating condition.
- Empty pipe in the operating condition.

The analytical results, based on the design criteria of Eqs. [30.1]–[30.3], are summarized in Table 30.5. A minimum additional weight of 11.7 kgf/m is required to satisfy both vertical and lateral stability criteria.

FE Analysis

Time domain dynamic analysis of pipelines on the seabed is the most detailed and accurate method for the pipeline on-bottom stability analysis. Normally, 3 hours of irregular waves is used for on-bottom stability analysis of pipelines. This time is used to evaluate the stability of pipe when the analytical methods, described in the last section, are not suitable for the on-bottom stability analysis. The analytical methods were developed based on rigid pipes with the weight coating method. However, the weight coating methods for RTP belong to intervention or pipeline anchoring techniques, which are not applied in a continuous way but locally. For the option by adding ballast weights locally along the RTP, analytical methods are not accurate, because the RTP does not move at the ballast weight locations, and large deforms in RTP between the ballast weights are allowable if the stress and strain design criteria are satisfied.

Table 30.5 Analytical Analysis Results

SG of empty pipe	0.76
Required ballast weight	3.274 kgf/m
Safety factor	0.15
Lateral stability check	Failure
Required ballast weight	11.7 kgf/m
SG of pipe with ballasts	1.96
Vertical stability check	OK
Final ballast result	11.7 kgf/m

Since the pipeline on-bottom stability was first analyzed with ABAQUS FE analysis using subroutines to model the pipe-soil interaction based on the Coulomb friction models with passive resistance and to apply the wave and current loads on the pipeline [7], several papers were published using similar methods [8]. However, a sounder theoretical basis and more understanding are still required for the pipe-soil mechanism and wave loads in shallow water.

Figure 30.5 illustrates variation in pipeline penetration under cyclic lateral loads. In this case, soil berms are formed in front of the pipeline when the pipe is moving back and forth laterally. The relationship between soil lateral resistance to the pipeline and the pipeline lateral displacement is shown in Figure 30.6. The lateral resistance increases deeply when the berm is formed in front of the pipe, which can greatly increase lateral resistance force on pipeline for preventing lateral motion.

For small amplitude waves in shallow water or long waves in deep water, the wave loading on RTP may be modeled using the standard wave theories available within the ABAQUS/Aqua module, including the Airy wave model and fifth-order Stoke wave model. Three hours of random irregular waves are simulated using a wave subroutine in ABAQUS/Aqua module. However, these models could not be applied to certain water depths, because the extreme environmental conditions, encountered in the pipeline, for on-bottom stability analysis were beyond the limits of the available theories in ABAQUS/Aqua.

Dean [9] introduces an approach by developing a purely numerical procedure to solve the boundary value problem (BVP) for a nonlinear wave, known as the *stream function theory*. One major advantage of this method is that the free surface becomes a streamline itself, and it follows that the free surface kinematic boundary condition, demanding a smooth motion of water particles at the surface, is automatically satisfied. Dean's stream function theory has the advantage that it is applicable in a

(a) Initial settlement

(b) Lateral movement

(c) Reversed lateral movement
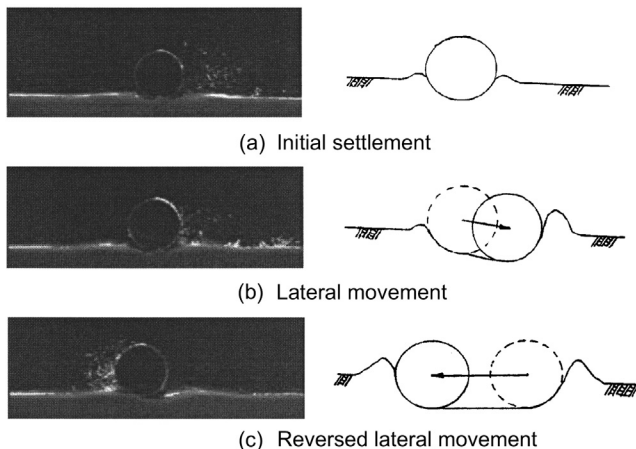
Figure 30.5 Pipeline penetration on soil under cyclic loads.
Source: Zeitoun et al. [8].
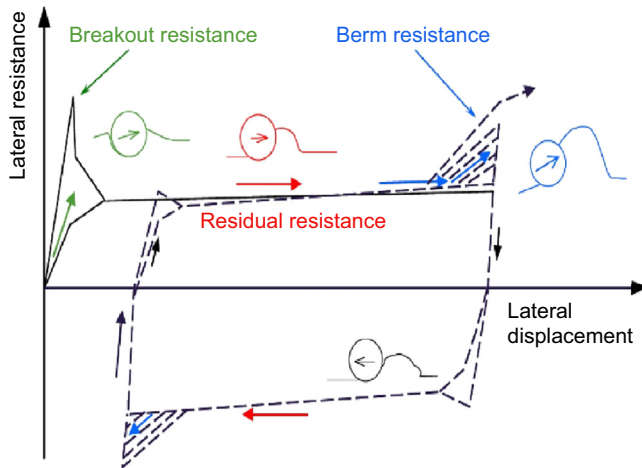
Figure 30.6 Lateral resistance on pipeline under cyclic lateral movements. (For color version of this figure, the reader is referred to the online version of this book.)

much wider range of water depths than the Stokes or Cnoidal theory. Furthermore, the iterative solution process allows for a simultaneous calculation of the nonlinear equations instead of solving the problem successively based on a previously calculated lower-order theory.

Fenton [10] proposes a theory based on Dean's stream function approach. Rather than using the least square error approach taken by Dean, Fenton solves the nonlinear equations by Newton's method and, with this approach, is able to make the calculation numerically more efficient. Its domain includes both those of the Stokes and Cnoidal theories, which are effective in shallow water, as shown in Figure 7.3 of this book. A stream function approach using the Fenton theory was chosen as the fundamental theory for the ABAQUS/Aqua user subroutine to model nonlinear waves on RTP on-bottom stability analysis.

Figure 30.7 shows the ABAQUS FE model for RTP with a ballast mattress along the pipe. The length of RTP in the model is 150 m, simulated with 1500 PIPE31H elements. The water depth is 75 m. An even seabed with pipe-soil frictions is used in the model. In the ABAQUS model, the RTP is mainly subject to submerged weight, temperature, internal and external pressure loads, and the 100-year current with 10-year wave loads. The ABAQUS model includes the following four parts:

- Pipeline → 3D beam element → 1500 elements.
- Seabed → rigid surface with a subroutine ofa pipe-soil contact model to simulate the pipe-soil interaction shown in Figure 30.6;
- Water environment (water depth, 100-year current, and 10-year wave) by a subroutine to simulate wave and current loads using the stream function approach or 3 hours of irregular waves.
- Submerged weight, temperature, and internal and external pressures loads applied at each steps.
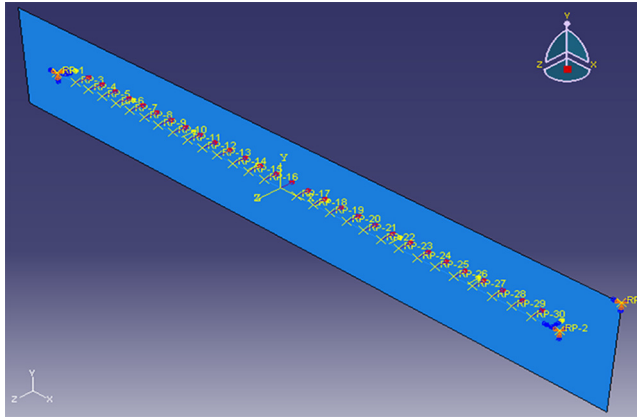
Figure 30.7 Model of RTP with ballast weights. (For color version of this figure, the reader is referred to the online version of this book.)

To compare with the wave test results, 60s regular wave condition is forced on the RTP. Figure 30.8 shows the simulation results of strain distribution. The maximum principal strain is 0.8%, which is much less than the RTP allowable strain of 3.5%. The corresponding displacement distribution is shown in Figure 30.9. The maximum lateral displacement of 1.12 m is calculated.

Experimental Tests

Experimental tests were carried out to study the effects of a mattress for the RTP on-bottom stability, the scaled prototypes were tested in a cyclic water tank, which can create regular waves with different wave heights and time periods.
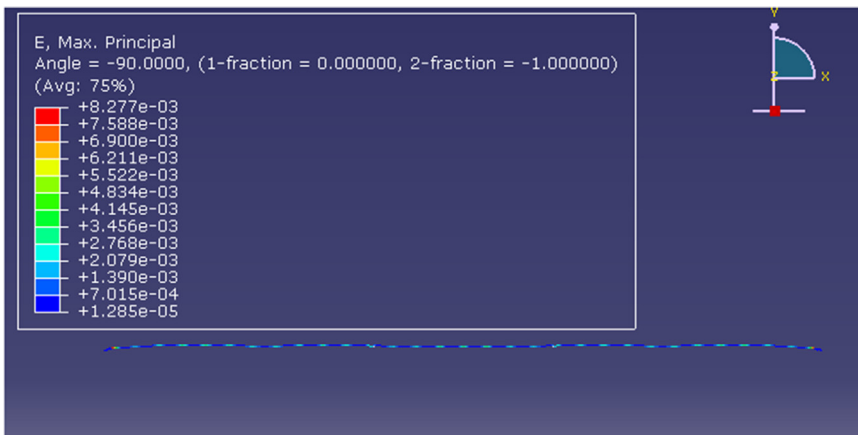
Figure 30.8 RTP strain distribution under 60-s wave load. (For color version of this figure, the reader is referred to the online version of this book.)
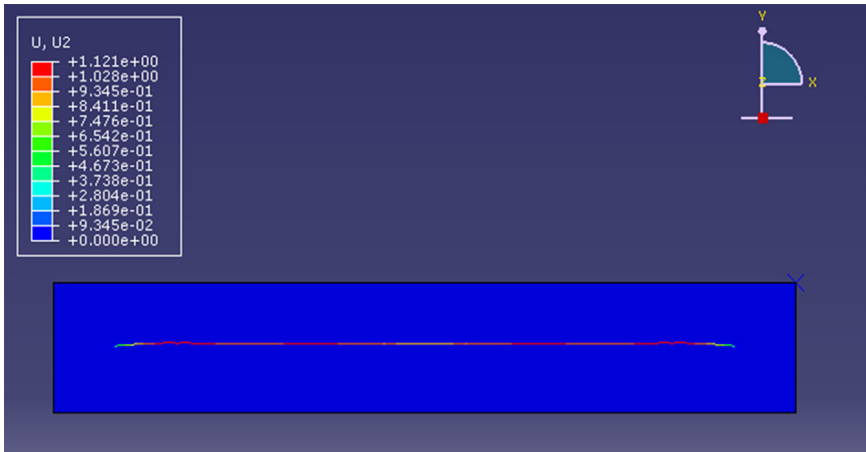
Figure 30.9 RTP lateral displacement under 60-s wave load. (For color version of this figure, the reader is referred to the online version of this book.)

Table 30.6 summarizes the test results for the RTP without a concrete mattress. The regular wave time period is 2 s. With the increase of wave height, the lateral movement also increases. For a water depth of 0.4 m, the RTP become unstable when the maximum wave height is higher than 50 mm. Figure 30.10 shows the relationship between the maximum wave height and lateral movement of RTP, in which the lateral movement increases sharply when the RTP becomes unstable laterally.

Figure 30.11 shows the initial and final positions of RTP for the wave height of 50 mm. The RTP is moved clearly by current due to the wave. The RTP is unstable in this case.

Table 30.7 lists the test results for the RTP with a mattress weight of 3.4 kgf. At the water depth of 0.4 m and a wave period of 2 s, when the maximum wave height

Table 30.6 Test Results for RTP without Mattress and Wave Period of 2 s

Water Depth of Test Region = 0.4 m		Water Depth of Test Region = 0. 6m	
Maximum Wave Height (mm)	Lateral Displacement (cm)	Maximum Wave Height (mm)	Lateral Displacement (cm)
10	0.0	10	0.0T
20	0.5	20	0.0
30	0.8	30	0.0
40	1.2	40	0.0
50	4.2	50	0.1
		60	0.6
		70	4.5

Note: Mattress gravity = 0 kg, wave period = 2 s.
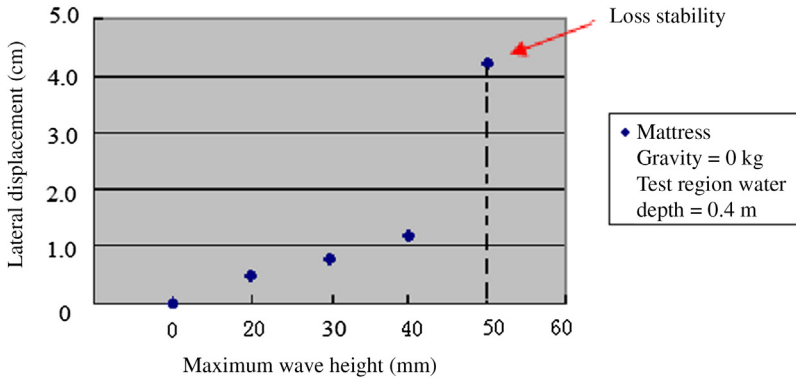
Figure 30.10 Wave height versus lateral displacement for RTP without a mattress. (For color version of this figure, the reader is referred to the online version of this book.)

increases to 150 mm, the RTP become unstable, while at the maximum wave height of 50 mm, the RTP without a mattress becomes unstable. Figure 30.12 shows the picture of RTP position when the mattress is applied, which corresponds to the test results of Table 30.7.

Table 30.8 lists the test results for the RTP with a mattress weight of 3.45 kgf. At the water depth of 0.4 m and wave period of 2 s, when the maximum wave height increases to 180 mm, the RTP becomes unstable, while at the maximum wave height

(a) Initial position of RTP

(b)   Final position of RTP

Figure 30.11 Initial and final positions corresponding to Figure 30.10. (For color version of this figure, the reader is referred to the online version of this book.)

Table 30.7 Test Results for RTP with Mattress Weight of 3.4 kgf and Wave Period of 2 s

Water Depth of Test Region = 0.4 m		Water Depth of Test Region = 0.6 m	
Maximum Wave Height (mm)	Lateral Displacement (cm)	Maximum Wave Height (mm)	Lateral Displacement (cm)
70	0.0	70	0.0
75	0.0	75	0.0
80	0.1	80	0.0
90	0.3	90	0.0
100	0.5	100	0.0
120	0.8	120	0.1
150	13.7	150	0.5
		180	4.5

Note: Mattress gravity = 3.4 kgf, wave period = 2 s.

of 50 mm, the RTP without a mattress becomes unstable. Figure 30.13 shows the RTP position when the mattress is applied, which corresponds to the test results of Table 30.8.

Effect of Water Depth

Tests for the RTP with a mattress weight of 3.4 kgf are done to verify the influence of water depth on the maximum wave force when the RTP is stable. According to experimental results, the RTP pipeline becomes unstable when a 150-mm wave is applied in the specified weight, but the pipeline's lateral displacement is larger in a 0.4-m water depth than in a 0.6-m water depth. This shows that the water depth has a certain influence on pipeline lateral displacement, because the wave induced current velocity is higher in the shallower water for the same wave height.

Effect of Mattress Interval

Tables 30.7 and 30.8 compare the experimental results to verify the influence of weighting form. Two weighting forms are illustrated in Figure 30.14.

Figure 30.12 Position corresponding to test results of Table 30.7. (For color version of this figure, the reader is referred to the online version of this book.)

Table 30.8 Test Results for RTP with a Mattress Weight of 3.45 kgf and Wave Period of 2 s

Water Depth of Test Region = 0.4 m		Water Depth of Test Region = 0.6 m	
Maximum Wave Height (mm)	**Lateral Displacement (cm)**	**Maximum Wave Height (mm)**	**Lateral Displacement (cm)**
70	0.0	70	0.0
75	0.0	75	0.0
80	0.0	80	0.0
90	0.0	90	0.0
100	0.2	100	0.0
120	0.8	120	0.0
150	1.0	150	0.0
180	13.7	180	0.1
		200	0.6
		250	1.5
		280	13.7

Note: Mattress gravity = 3.45 kgf, wave period = 2 s.

From the experimental results, it can be seen that the RTP becomes more stable when a heavier mattress interval is applied.

Summary

The analytical analysis based on DNV RP-F109 is compared with the experimental tests, and the following conclusions are obtained:

- The analysis results of the DNV absolute method are too conservative, although both ends of RTP are free; the minimum required ballast weights in the experimental tests for the on-bottom stability are far less than those calculated from the analytical method.
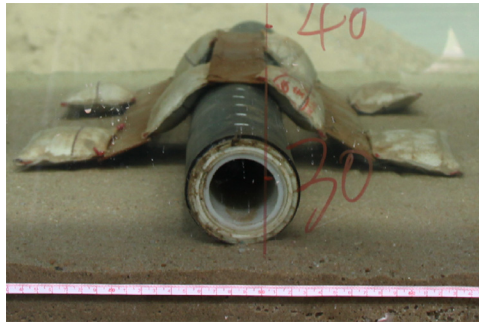
Figure 30.13 Position corresponding to Table 30.8 (For color version of this figure, the reader is referred to the online version of this book.)
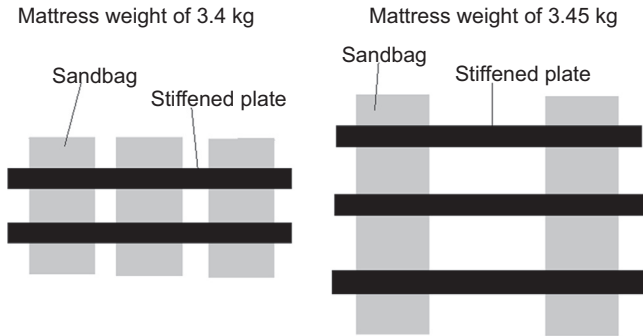
Figure 30.14 Different weighting forms with similar mass. (For color version of this figure, the reader is referred to the online version of this book.)

- The mattress interval and shape have significant effects on RTP on-bottom stability.
- Water depth has an obvious effect on pipe on-bottom stability. The effect reduces when the water depth increases. A mattress can satisfy the RTP on-bottom stability requirement.
- Erosion around the RTP is observed during the experimental tests.

However, there are some disadvantages for the scaled RTP test, such as RTP end effect and lateral displacement measurement. A full-scale RTP on-bottom stability test should be carried out to get more accurate results.

References

[1] Borgman L, Hudspeth R. The effect of random seas on pipeline stability. In: Pipeline Research Publication, Vol 1 and 2. Arlington, VA: American Gas Association; 1984.
[2] Dean RG, Perlin M. Inter-comparison of near-bottom kinematics by several wave theories and field and laboratory data. Coastal Eng 1986;9:399–437.
[3] DNV RP F109. On-bottom stability design of submarine pipelines. Oslo, Norway: Det Norske Veritas; 2010.
[4] DNV RP E305. On-bottom stability design of submarine pipeline. Oslo, Norway: Det Norske Veritas; 1988.
[5] DNV. Environmental conditions and environmental loads. Oslo, Norway: Det Norske Veritas; 1991.
[6] DNV Guideline 14. Free spanning pipelines. Oslo, Norway: Det Norske Veritas; 1998.
[7] Ose BA, Bai Y, Nystrøm PR, Damsleth PA. A finite element model for in-situ behavior of offshore pipelines on uneven seabed and its application to on-bottom stability. In: Proc. of ISOPE'99, Brest, France; 1999.
[8] Zeitoun HO HO, et al. Advanced dynamic stability analysis. OMAE 2009-79778; 2009.
[9] Dean RG. Stream function representation of nonlinear ocean waves. J Geophysical Res 1965;70(18):4561–72.
[10] Fenton JD. The numerical solution of steady water wave problems. Computers Geosciences 1988;14(3):357–68.

31 Use of High-Strength Pipeline Steels

Chapter Outline

1.   Introduction

The increasing demand for oil and gas worldwide requires the construction of high-pressure gas transmission lines with the greatest possible transport efficiency, so the cost of pipeline construction and gas transportation are minimized, especially for long distance pipelines. Therefore, the tendency is toward using line pipe of larger diameter or higher operation pressure, which leads to using higher-strength steel grades to avoid large wall thickness. In the early 1970s, grade X70 was introduced for use as line pipe in gas transmission pipelines. Since then, grade X70 material has proven a very reliable material in the implementation of numerous pipeline projects. Following the satisfactory experience gained with X70 in the subsequent period, grade X80 line pipe came into use for the first time as a 3.2-km pipeline section in 1985 on a trial basis [1].
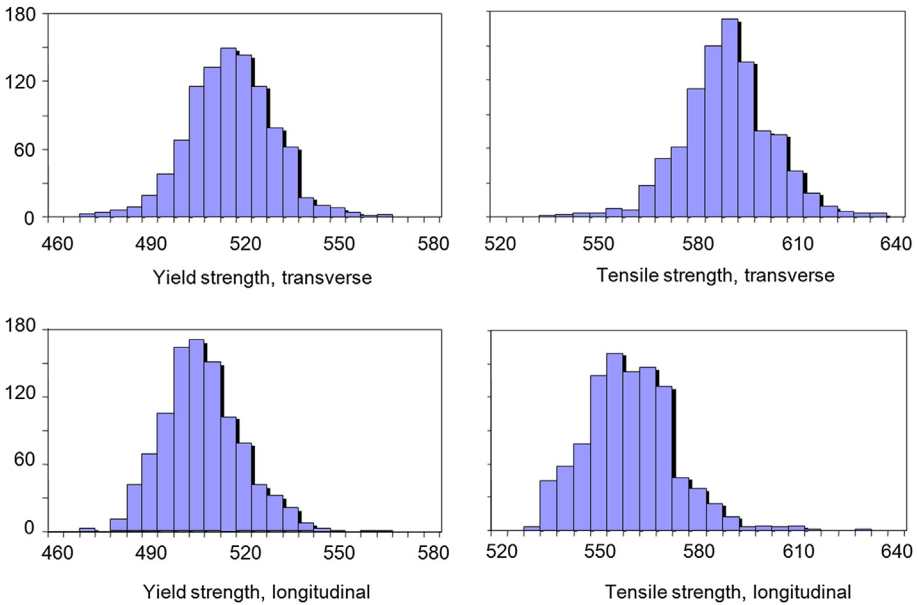
Figure 31.1 Distributions of 24-in. X65 linepipe (WT of 0.563-in) for sour service. (For color version of this figure, the reader is referred to the online version of this book.)

The research and development of new steels are carried out for both sour and nonsour service. The materials being developed for subsea pipelines and risers are grades X70 and X80 for nonsour service and grades X65 and X70 with a wall thickness of up to 40 mm for sour service. Figure 31.1 shows, by way of example, the distribution curves determined on a production lot of grade X65 pipe intended for sour service. As can be seen, the distributions in the transverse direction are shifted to the right relative to those for the longitudinal direction.

In this chapter, we review the use of high-strength steel for subsea pipelines, its technological challenges and solutions.

2. Usage of High-Strength Steel Line Pipes

Usage of X70 Line Pipes

General

For offshore pipelines, the current trend is toward line pipe in grade X70 with a wall thickness up to 40 mm. Fulfillment of the requirements for DWTT (drop-weight tear test) transition temperature is progressively difficult as the wall thickness increases. For wall thicknesses in excess of 30 mm, low transition temperatures can be achieved only by means of highly expensive rolling processes. Figure 31.2 shows the mechanical properties of X70 line pipe.

Mechanical properties	Requirement	Average $\bar{X}$	Stand. dev. S
Transverse yield strength R $_{t0.5}$ [MPa]	> 482	525	12.6
Tensile strength R$_m$ [Mpa]	> 565	635	14.0
Yield-to-tensile ratio R $_{t0.5}$/R$_m$ [%]	< 92	82.6	1.6
Elongation A2" [%]	> 25	34.8	1.6
CVN toughness, -20 °C Weld metal [J] *) HAZ [J] Base metal [J]	> 50 > 50 > 80	172 146 220	36 64**) 45

*) Mn Mo Ti B alloyed
**) No normal distribution

142 heats

97.14255

EUROPIPE

Production results on 682.4 mm O.D. x 15.9 mm W.T., API grade X 70 line pipe

Figure 31.2 Properties of 682.4-mm OD × 15.9 mm WT, API Grade X70 linepipe.

A large offshore project in grade X70 is the pipeline in the North Sea operated by Statoil, connecting Karstø, Norway, with Dornum, Germany. This pipeline has a length of 600 km and it is built of pipe 42 in. × 25–30 mm WT.

In the 1990s, Europipe completed the development of grade X80 pipe 48- in. OD and 18.3 mm to 19.4 mm wall thickness for onshore pipelines. It has been demonstrated that it is feasible to commercially manufacture large-diameter X80 pipe consistently for long transmission pipelines [2].

As regards offshore applications, a series of pipes have been supplied for qualification testing with respect to pipe laying. Use of X80 line pipe for export pipelines was qualified by a joint industry project called EXPIPE.

For low-alloy steel pipelines operating in sour service, X65 is currently the established material. Special treatment in the steelmaking shop and fulfillment of special requirements for chemical composition help prevent the formation of nucleation sites for hydrogen-induced cracking (HIC). Production trials show great potential for the development of higher grades, up to X80, for slightly sour conditions [3].

For high-pressure transmission land lines, Grade X70 is now widely used for high-pressure transmission lines in many countries. The supplier reference lists summarized in Table 31.1 provide 94 project references for four suppliers. This list is indicative rather than comprehensive, as other manufacturers have supplied this grade of material. A pipeline project installed in July 1997 for BP in the North Sea involves the laying of a grade X70, 24-in. diameter pipeline with a wall thickness of 25.8 mm.

Table 31.1 Supply Record of Major Line Pipe Producers

Supplier	Grade and Location	No of References	OD Range (in.)	Thickness Range (mm)	Comments
Europipe	All X70	35	30–48	11–25	All nonsour gas in nine countries
	X80	2	48	18.3	For Ruhrgas, Germany, nonsour gas
Sumitomo	X70 land pipeline	33	20–56	7.9–35	Gas lines: USSR 17, USA: 4, Canada 2, Malaysia 1, Bangladesh 1.
	X70 subsea p/line	2	18–24	22–32	Both for water injection
	X70 other/misc	2	28	31	TLP tethers for Shell USA
	X80	1	21	22	Drilling riser for Vetco/Shell.
Nippon Steel[1]	X70 land pipeline	6	24–42	7.4–20.6	Major orders for USA, UAE, Columbia, Malaya; other minor orders.
	X70 subsea p/line	1	32	14	Small orders only
	X70 other/misc	1	44	38	Conoco Norway, 5000 tonnes, use not stated
	X80	None			
NKK[2]	All X70	8	24–56	9–34	
	X80	3	26–48	10.5–16	42- and 48–in. orders for Canada, 26–in. for Vetco Gray

[1]Nippon Steel references are hard to interpret. Russian orders are omitted as the grade is not known. Structural steel orders also are omitted.
[2]All NKK references are believed to be land pipelines.

The reference list also shows only limited subsea use of X70 material, refer to Table 31.2.

Oman-India Gas Pipeline

In June 1993, a study was initiated to establish the feasibility of installing a subsea pipeline to connect the gas reserves in Oman to markets in India. The preliminary route of over 1100 km would provide a direct link between Oman and India across the Arabian Sea with water depths up to 3500 m. The Oman-India Gas Pipeline (O-IGP) project is currently on hold and design has not progressed past the preliminary stages.

The recommended pipe grade for the Oman-India Gas Pipeline is X70 for a 24-in. pipeline with constant internal diameter. Calculations have shown that the wall thickness along the majority of the route is predominately dictated by the prevention of external pressure collapse, as shown in Table 31.3. For details on the development of design methods for hydrostatic collapse in deep water, see Tam et al. [5].

Britannia Pipeline

The Britannia Field is a gas condensate reservoir in the central North Sea, approximately 200 km northeast of Aberdeen and 45 km north of Forties. Britannia Operator Ltd. (BOL) is a joint venture established by Chevron and Conoco for the operatorship of Britannia on behalf of the coventurer.

Dry gas is exported in dense phase mode through a pipeline to an extension of the Mobil SAGE terminal at St. Fergus. At the terminal, the gas is processed for delivery into the British Gas National Transmission System. Offshore condensate is delivered to the Forties Pipelines System through a condensate export pipeline from the Britannia platform to the Forties Unity platform.

The gas export pipeline is nominally 28-in. diameter, 186 km long, with a bore of 650.6 mm. The pipeline design pressure is 179.3 barg and the design life of the pipeline is 30 years. The pipe grade is X70. The 14-in. condensate pipeline is 45 km in length. The Britannia pipelines were completed in 1997.

Onshore lines are specified on the basis of transverse yield strength. The method of manufacturing these steels (TMCP (thermo-mechanically controlled processing), UOE (U-ing, O-ing, Expanding process)) means that the axial yield strength is around 4–5 ksi ($\sim$30 MPa) lower.

Usage of X80 Line Pipe Onshore

High-strength, large-diameter pipes are available from steelmakers such as Europipe for pipe diameter 20–60 in. and wall thickness of 12–32 mm [4]. Five onshore projects have been identified in which X80 pipe has been used. A period of 7 years elapsed before Ruhrgas AG in Germany began in 1992 to place an order for linepipe for the construction of the world's first grade X80 pipeline.

The 260-km, 48-in. Ruhrgas pipeline from Schlüchtern to Werne in Germany was designed and built entirely to X80 capabilities and requirements. This pipeline, installed in 1992–1993, connects existing pipelines in new federal states in the former

Table 31.2 X70 Subsea Pipeline Projects in 1997

Date	Location	Onshore or Offshore	Length (km)	OD (in.)	WT (mm)	Steel Source, Type	Welding Method	Notes
1997	Shell Oil Mensa[1] Gulf of Mexico	Offshore	100	12	19, 21, 32	—	Phoenix mechanized GMAW with shaw mechanized UT	[2]
August 1997	BP ETAP, UK North Sea	Offshore	74	24	25.8	UOE	Passo GMAW	[3]
July 1997	Britannia, UK North Sea	Offshore	190	28	17.5	—	Passo GMAW	[3]
1997	Norfra Pipeline, Norway to Franla, North Sea	Offshore	840	42	—	—	—	[4]

Notes:
[1]Information shown is based on available data.
[2]Completed by Allseas.
[3]Completed by EMC.
[4]Refer to Thorbjornsen et al. (1997) [4] for details.

Table 31.3 Required Wall Thickness Based on Collapse of Pipeline

Water Depth (m)	Wall Thickness (mm)		
	API 5L X65	API 5L X70	API 5L X80
3500–3000	44.0	41.0	38.0
3000– 500	39.0	37.0	36.0
2500–2000	35.0	34.0	33.0
2000–1500	31.0	30.0	29.0
1500–1000	27.0	26.5	26.0
1000	22.7	22.0	22.0

East Germany and started operations in late 1993. Considerable information has been published about this pipeline [6, 7].

Europipe GmbH, Ratingen, Germany, supplied the entire line pipe for the project. The material, specified as GRS 550 TM by Mannesmannroehren-Werke AG (MRW), Muelheim, Germany, has a specified minimum yield stress (SMYS) of 550 MPa and a minimum tensile strength of 690 MPa. The comparable API 5L X80 grade has an SMYS of 551 MPa and a minimum tensile strength of 620 MPa.

A test program was undertaken to determine the properties of the pipe steel and the weldment. The specified minimum values of yield and tensile strengths were exceeded in the tests. The impact energy values measured on the base material exceeded 95 J, thereby exceeding the minimum value for crack arrest recommended by the European Pipe Research Group (EPRG). The ductile-brittle transition temperatures measured on the drop-weight tear test specimens were well below the specified test temperature of 0°C. The impact energy values of the longitudinal weld metal measured at 0°C, the commonly specified test temperature in Germany, varied between 100 and 200 J. The average values of the impact energy for the base material and weld metal were 190 J and 158 J, respectively [7].

The strength of the seam weld was checked by means of flattened transverse weld specimens with the weld reinforcement removed by machining. For all specimens, failure occurred in the base metal, outside the weld region. The field welding for GRS 550 TM required the development of a new concept to achieve the mechanical-technological properties for the welding metal and welding joint. For this project, it proved necessary to implement a combined manual welding technology, using cellulose-coated electrodes for root and hot pass welding, and lime-coated (basic) electrodes for filler passes and cap pass welding.

NOVA Pipeline Projects

Pipe supplied to the two Canadian projects were CSA Z245.1, typical compositions are given in Table 31.4. The first Canadian project was a short (126 welds) cross over section of the 42-inch diameter pipeline at the Express East Compressor

Table 31.4 Chemical Compositions for X80 Line Pipe and Induction Bends

Typical Values in Weight %	Ruhrgas 48″ Schlüchtern to Werne		Empress East Compressor Station, Canada	Mitzihwin Project, Canada
Element	Line Pipe TMCP [7]	Bends Q&T [6]	Japanese 42″ OD UOE Line Pipe [8]	Canadian 48″ DSAW Spiral Line Pipe [8]
C	0.09	0.12	0.06	0.04
Si	0.04	0.45	0.3	0.35
Mn	1.91	1.75	1.81	1.77
P	0.016	0.015	0.008	0.014
S	0.0009	0.003	0.003	0.005
Cu	0.04		0.16*	0.38*
Cr	0.05		0.02*	0.06*
Ni	0.04		0.09	0.15
Mo	0.01	0.22	0.18	0.26
V	—	0.06	0.08	0.00
Nb	0.042	0.035	0.03	0.09
Ti	0.018		0.01	0.03
Al	0.036	0.04	0.026	0.032
N	0.0035			
B	0.0003			
CE (IIW)	0.43	0.48		

*The original reference has a typographical error, these values are all given as Cr so they are unreliable.

Station in Alberta, Canada, completed in 1990. A Japanese steel mill supplied the pipe. The second Canadian project was 53.8 km of 48-inch diameter pipeline for the Mitzihwin project in Alberta, Canada, completed in 1994. A Canadian steel company supplied the pipe.

These three projects have demonstrated that large diameter X80 pipe can be manufactured consistently for long pipelines. The approach to the X80 projects was significantly different when the welding procedure and consumables were selected. The field welding of the X80 pipe did not present any difficulty for the Ruhrgas and Mitzihwin projects. These projects demonstrated that conventional mechanized welding using the GMAW process could produce consistent, high quality welds for onshore pipelines.

Grades Above X80

Available yield strength levels have doubled in the past 50 years. The overlapping development periods for each grade are presented in Figure 31.3 [9]. Higher grades are currently under active development. X100 grades are being actively developed by several companies, but at the present time, no project use has been identified or
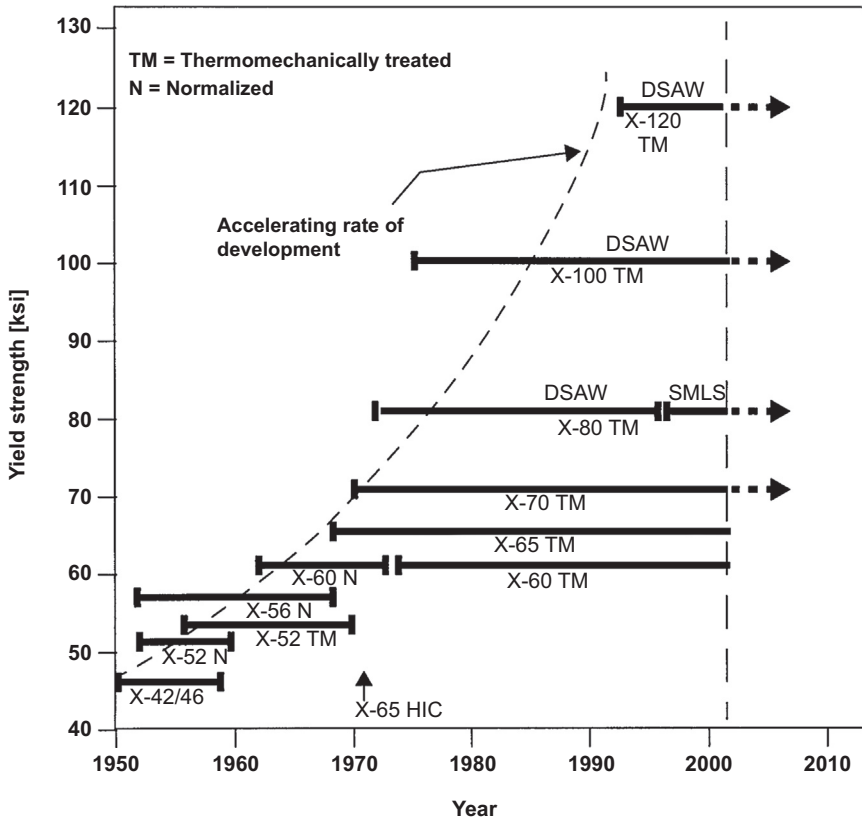
Figure 31.3 Development and history of high-strength line pipes.

indicated [5], [10]–[12]. Views of the future developments of high-strength steel, up to X100, are given by a consortium of companies and documented in Graf and Hillenbrand [2]. The supply capabilities of UOE line pipe as per 1997 are listed in Table 31.5.

3. Potential Benefits and Disadvantages of High-Strength Steel

Potential Benefits of High-Strength Steels

Potential Cost Reduction

The cost reduction is based on the premise that increasing material yield strength reduces the wall thickness required for internal (or external in the case of deep waters) pressure containment and hence the overall quantity of steel required. Price considers

Table 31.5 UOE line Pipe Supply Capabilities in 1997

Supplier	Max Single Joint Length Available (ft/m)	OD Range (in.) at Max Thickness[1]	Max Thickness by Grade (mm, Rounded)					Supply History (Pipelines)	
				X60	X65	X70	X80	X70	X80
British Steel	45/13.7	30–42	49 (X52)		37	35	32	No	No
Europipe	60/18.3	20–64	40 (X52)	36	36	34	30	Yes	Yes
Sumitomo	60/18.3	30–48			38	38	32	Yes	No
Nippon Steel	60/18.3	29–56	40 (GrB)		38	36	33	Yes	No
Kawasaki	60/18.3	20–64		38	36	33	24	Not provided	
NKK[2]	60/18.3	16–56		33/29	33/27	32/26	29/26	Yes	Yes

[1]OD range may vary with grade, value is for X65.
[2]Wall thickness given are for 18-m lengths first, then for shorter lengths down to 13 m.

both the direct and indirect consequences of using a high-strength steel and estimates a 7.5% overall project saving for a 42-in. offshore line laid with X80 instead of X65 [14]. Although the X80 pipe cost 10% more per ton, it was 6% less per meter. Further savings were identified for transportation, welding consumables, welding equipment rental, and overall laying time.

On the recently completed Britannia gas pipeline, cost studies during detailed engineering showed that, by increasing the line pipe material grade from X65 to X70, an approximate cost reduction of $3.5 million could be achieved. The project CAPEX is approximately $225 million. Although not directly related to the use of high-strength material, other potential cost savings identified include

- Tighter than normal API 5L [14] definition of dimensions. Consideration should be given to reducing tolerances on ovality and wall thickness from the API 5L requirements. The cost of reducing tolerances should be compared to the expected increase in pipeline construction rates and wall thickness reductions for mechanical design.
- Use of ECA based acceptance criteria for determination of maximum allowable defect sizes in pipeline girth welds. Traditionally, the acceptance criteria for weld defects are based on workmanship standards. ECA procedures typically rely on the application of crack tip opening displacement (CTOD) test results. The values of defect length are founded on plastic collapse calculations based on assumptions regarding the flow stress and the yield/tensile strength ratio of girth and parent metal welds.
- Nonstandard pipeline diameters should be considered. Optimization of the pipe ID based demonstrated that the line pipe cost could be reduced by procuring pipe of the exact ID required as opposed to selecting the larger standard sizes.
- Elimination of mill hydrostatic testing with appropriate increased NDE.

Pipeline welds are traditionally inspected using visual examination and radiography. Radiography systems are available that produce a real-time image of the weld being inspected. Normally, a radiograph of the weld is produced by exposing a suitable piece of film. The film is then processed and developed prior to viewing for interpretation. The real-time systems produce the image of the weld on a screen that can be viewed without the need for film processing. The radiographic image is stored on digital laser disc as a permanent archive and offers instant retrieval. The time to inspect each weld is reduced compared to traditional methods.

As an alternative to radiography, high-speed ultrasonic inspection is available. This method has become a standard NDT method for inspecting GMAW (onshore) pipeline girth welds in Canada. Currently available high-speed ultrasonic equipment is capable of inspecting a 40-in. diameter girth weld in 90 sec. The inspection can be performed immediately on completion of production welds. A limitation of this technique is that it is not reliable for wall thickness below 10 mm. For project wall thickness above 10 mm, ultrasonic inspection is a viable option. The use of automated ultrasonic inspection for onshore and offshore pipeline welding may reduce construction costs.

Wall Thickness and Construction

Given two similar design conditions, increasing the grade of line pipe in simplistic terms correspondingly decreases the wall thickness and therefore provide cost

benefits. In addition to this, a thinner wall also has various impacts on construction activities. A thinner wall requires less field welding and therefore, in theory, has the potential to reduce construction and laying time.

By increasing the material grade, it is possible to lay pipeline in deeper waters. A thinner wall has a direct impact on this installation method, since the requirements for laying barge tensioners are related to the water depth and weight of pipe. For the Oman-India Gas Pipeline project, the question was how this pipeline could be laid with a massive top tension of 10,600 kN, during normal laying operation, necessary for controlling the catenary. It is recommended that a laying barge that has a tension capability of at least 26,700 kN be used. This requirement is dictated by a wet buckle abandonment-recovery scenario, that is, a buckle together with rupture leading to pipeline flooding. J-lay techniques may be used but the laying rate can be low.

Weldability

Thick walls create additional problems related to weldability. As the wall thickness of the line pipe increases, the cooling rate of the weld increases, leading to possible problems with hardness, fracture toughness, and cold cracking (when non-hydrogen-controlled welding processes are used). A thinner wall, due to increase in material strength, means that the cooling rate of the weld also decreases.

Pigging Requirements

The thicker-walled sections of the pipeline in deeper waters may restrict the full capabilities of intelligent pigging. There is a limitation on the wall thickness, depending on the type of pigging tool used.

Potential Disadvantages of High-Strength Steels

Increase in Material Costs per Volume

Generally, an increase in material grade equates to an increase in the cost of material. See Figure 31.4. However, it is also interesting to note that, for a given design case, an increase in the material grade equates to a slight decrease in cost per meter.

Limited Suppliers

The worldwide availability of proven suppliers for material grades above X70 is still relatively limited.

Welding Restrictions

With regards to the weldability of X80 steel, there is a medium risk of schedule extension and cost increase, since it has been used on only a small number of onshore projects and there is no experience offshore. Welding to the required quality may be slowed by more process restrictions and more complex controls. Due to the limited worldwide experience of welding X80 line pipe, certain
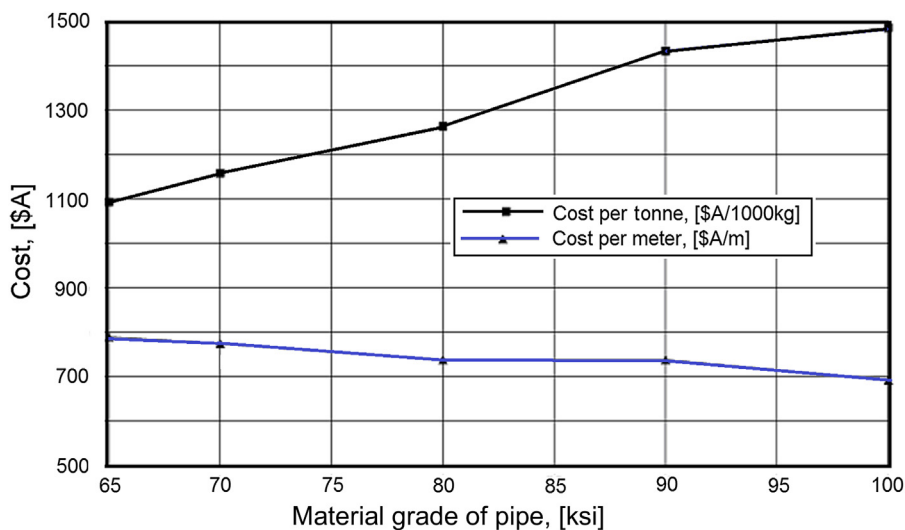
Note: Base case of 46" with wall thickness of 1" for material grade of X65

Figure 31.4 Cost variation of high-grade line pipe. (For color version of this figure, the reader is referred to the online version of this book.)

key welding issues have to be addressed in further studies, particular that of welding consumables.

Limited Offshore Installation Capabilities

The number of offshore pipe installation contractors with proven experience in welding X70 steel line pipe is limited. Additionally, the experience of laying deep-water pipelines by the J-lay method is limited to relatively small-diameter pipelines.

Repair Problems

Repair techniques for any pipeline depend largely on the water depth. At diverless water depths, (that is, at water depths without the use of divers), excluding the use of diverless hyperbaric welding systems (that is, diverless subsea welding systems), the current state of the deepwater repairs involves the use of mechanical connectors. These connectors are attached to the open end of a pipeline by a metal-to-metal sealing arrangement.

Repair by hyperbaric welding, whether at diverable or diverless water depths, for material grades of X70 or above has not been undertaken; therefore, currently, no information is available regarding its behavior under hyperbaric conditions. Research programs should be monitored and initiated to develop understanding in this area.

An alternative repair method is to use the hot tap technique to bypass the area of pipeline damage. However, for offshore use, this experience is limited and certainly unproven in high-strength material pipelines.

Hot tap repairs are regularly performed onshore for API 5L X65 pipe grades and lower. BS 6990 [15] states that hot tap welding of material above X65 yield strength should not be performed without welding trials. The inferior weldability of high-grade line pipe combined with the high cooling rates experienced during welding onto a live pipeline increase the safety risks associated with hot tapping operations. For line pipe grades above API 5L X70, it is recommended that hot tapping is not performed unless extensive weld testing can be conducted.

Additionally, the subsea hot tap technique is limited to a maximum size of 24/36-in. (i.e., 24-in. bypass into 36-in. pipeline) at a limited water depth of 100 m for relatively low pressure lines (1000 psi). This technique needs to be further evaluated.

4. Welding of High-Strength Line Pipe

Applicability of Standard Welding Techniques

The range of welding techniques used for pipeline construction includes shielded metal arc welding (SMAW), gas metal arc welding (GMAW), submerged arc welding (SAW), flux cored arc welding (FCAW), and gas tungsten arc welding (GTAW). All these techniques have been applied successfully to API 5L X65 line pipe and lower in accordance with internationally recognized pipeline construction codes and standards.

When welding higher-strength grades of line pipe (X70 and above), special techniques are generally specified to avoid defects in high-strength welds. Some of the additional measures that are necessary include

- Control of joint preparation and lineup.
- Using adequate preheating.
- Additional inter-run grinding.
- Careful selection of electrical characteristics.
- No movement of the pipe until completion of the root pass.

The specific application of standard welding technology to onshore and offshore pipeline construction is discussed in the following subsections.

Onshore

The SMAW process is the standard welding method for onshore pipelines. Low-hydrogen SMAW has been used on pipelines up to API 5L X80 grade. Cellulosic SMAW is not generally used on line pipe above API 5L X70 strength, due to problems with hydrogen cracking. For onshore pipelines above API 5L X70 grade, low-hydrogen processes, such as GMAW or FCAW, are required. Details of project welding experience are presented later in this chapter.

Offshore

The semi-automatic GMAW process is used extensively on laying barges for offshore pipe laying. GMAW is sensitive to changes in the carbon equivalent of the material.

Generally, the carbon equivalent of line pipe increases as the grade is increased. GMAW is also sensitive to boron alloying in the line pipe; however, control of boron in Japanese and European mills is very good and hence this is not considered to be an issue, provided high-quality line pipe is used. It is possible that development of GMAW procedures will take significantly longer for line pipe above API 5L X70 strength.

SAW is used on third generation laying barges for double jointing. SAW is a high-heat input, high-dilution process. Therefore, the chemistry of the line pipe being welded has a large influence on the properties of the final weld.

Welding API 5L X70 and X80 line pipe with SAW requires careful control of the alloying elements to ensure that the final properties of the weld are satisfactory. There have been problems with poor root toughness of SAW welds due to picking up elements such as aluminum from the line pipe. The construction contractor should be given the opportunity to review chemistry requirements prior to line pipe manufacture to ensure compatibility with proposed SAW procedures.

FCAW is currently used for structural welding and performing certain types of repairs on pipeline welds. Properties of FCAW welds are generally good; however, there have been historical problems in obtaining consistent weld toughness. FCAW consumables have been developed for welding line pipe up to API 5L X 80 grades.

GTAW produces very high-quality welds with excellent properties. However, the process is slow and not generally used offshore (with the exception of hyperbaric welding and welding of corrosion-resistant materials).

In principle, all the standard pipeline welding methods (with the exception of cellulosic SMAW) should be suitable for welding API 5L X70 and X80 line pipe provided additional time is allocated for the weld procedure and consumable development.

Field Welding Project Experience

Manual Welding

The quality requirements of the Megal II and Ruhrgas lines required development of a welding procedure to overcome concerns over cold cracking of the high-strength weld metal during conventional vertical-down welding with cellulosic electrodes. The technique adopted used conventional cellulosic electrodes for the root and hot passes and basic electrodes for the fill and cap passes. The root was welded with an undermatched consumable, while overmatched consumables were used for the fill. All welding was downhill. Table 31.6 lists the consumables for different pass.

It should be noted that downhill welding is the norm for pipelines, at least outside of Japan, because it is fastest overall. Downhill welding is conventionally used with cellulosic electrodes, which have a finite moisture content and are therefore not "low hydrogen" but can be used on conventional line pipe steels when other suitable precautions are taken to prevent hydrogen cracking. Apart from pipelines, downhill welding is regarded as a poor practice for high-quality welding, so it appears that the Japanese uphill practice is more cautious.

Table 31.6 Different Pass Consumables

Pass	Consumable		
	Type	AWS Designation	Diameter (mm)
Root pass	Cellulosic	E6010	4
Hot pass	Cellulosic	E9010-G	5
Filler passes	Basic	E10018-G	4, 4.5
Cap passes	Basic	E10018-G	4

Note: The data are as per Graf et al. [6]; Chaudhari et al. [7] gives root and hot pass consumables differently, as E7020-A1.

High-strength steels and weld metals are more sensitive to hydrogen cracking. They cannot be reliably welded with cellulosic electrodes, so "low-hydrogen" consumables are required, such as basic electrodes, which are normally used in the uphill practice as per Japanese practice. It appears that cellulosic electrodes were used vertical down on the Ruhrgas line but only after two weeks special training of welders.

This approach allowed conventional welding of the first two passes without loss of productivity or risk of cold cracking. Chaudhari et al. [7] states that the use of basic electrodes caused only a small loss of productivity for the subsequent passes. This is based on an overall welding cycle time of 5–6 hours, which includes 3.3 hours for moving equipment between joints, setting up, and the like. If only the welding time is considered, Chaudhari et al. shows the time to complete a joint was 103 minutes using cellulosic electrodes (for all passes), compared with 137 minutes using basic, low-hydrogen electrodes [8]. At 33%, the increased welding time is significant and a consequence of requiring the improved mechanical properties obtainable from the basic electrodes. The increased time was due to more "arc off" time for removal of the basic slag between passes.

The repair rate for manual field welding is reported to have been less than 3%. Maximum hardness of 350 HV10 is reported in the cap HAZ (heat affect zone).

Mechanized Welding

A general discussion of mechanized welding of X80 is provided in Price [13]. Experience with the use of mechanized welding on three projects is presented in Chaudhari et al. [7] and Laing et al. [8]. The CRC Evans GMAW mechanized system was used in all three cases:

- An internal root pass was used in conjunction with external passes deposited into a narrow gap bevel.
- The Empress Project used pulsed GMAW for all external passes, which resulted in improved weld metal and HAZ toughness compared to conventional GMAW.
- All three projects used titanium treated wire, the Thyssen wire used in Germany contained 1% Ni, 0.4% Mo, which was not used in Canada.

The Mitzihwin project achieved an average rate of 103 butts at 48-in. OD × 12.1 mm WT in an 8 hour day, though the repair rate was considered high at 6%, compared with

4% achieved on the other two projects [8]. It is stated that repair rates have been less than 1% in comparable subsequent projects.

Properties of Field Welds

A detailed review of the interrelation of welding process and properties is beyond the scope of this study. In the present context, the main point to be noted is that project specifications for weld quality, strength, and toughness were met in all cases for X80 with wall thickness in the range 10.6–18.3 mm and that techniques have been developed sufficiently to allow consideration of X80 for both land and offshore pipelines.

5. Cathodic Protection

Subsea pipelines require compatibility with CP in seawater. High-hardness steels are at risk of brittle failure caused by hydrogen embrittlement. Compatibility is conventionally satisfied by hardness values below 350HV10. The limit applies to parent metal and all weld zones. Chaudhari et al. [7] and Laing et al. [8] report the maximum values of 350HV10 for manual welding (Ruhrgas project) and 303HV for mechanized welding (three projects, test load not given. The value of 350HV10 (10 for 10 g load in Vickers hardness test) has been shown to be an acceptable maximum hardness for avoiding hydrogen embrittlement of structural steels and welds under CP in seawater (to minimum negative potential, maximum polarization) of conventional sacrificial anodes. In all cases, maxima were in the HAZ. These data indicate that X80 can be welded within the conventional limit for compatibility with CP.

In the context of future developments beyond X80, it is worth noting two points:

1. Marine sacrificial CP systems are available with potential control (as opposed to the full open circuit potential capability of normal systems) to allow the use of steels with higher hardness values. Open circuit is the condition of maximum negative potential (or polarization) of protected steel from a conventionally mounted sacrificial anode when no current flows as can (almost) occur in practice at low-current demands. This condition is the worst for hydrogen evolution and consequent hydrogen cracking. Steels conventionally need to be compatible with this potential, which is more negative than that required for corrosion protection. Smart CP systems now exist that have local, potential sensing devices to control the applied potential only to the value required for corrosion protection, thus, risk of hydrogen cracking is minimized. These systems have been used on high-strength steels of jackup rigs which previously have been known to crack due to hydrogen uptake.
2. Developments of line pipe for sour service impose lower hardness limits, typically 250–275HV10.

Corrosion fatigue in the presence of CP is a secondary consideration, so the pipelines would not normally be designed against a specified fatigue life. However, fatigue concerns may arise in the event of spanning of subsea pipelines, so it is prudent to confirm that candidate materials do not have degraded fatigue properties relative to established grades. The concern arises from the unwanted uptake of hydrogen under the influence of CP. Hydrogen uptake adversely influences toughness and fatigue

crack growth rates. Healy and Billingham indicate that fatigue properties of high-strength grades under CP are comparable to conventional steels, but information should be obtained that is specific to candidate line pipe steels [16].

Pipelines on land similarly require compatibility with CP and the preceding hardness criteria are also conventionally applied. Occurrences of external stress-corrosion cracking (SCC) do not correlate with steel grade. Hydrogen embrittlement is associated with hydrogen uptake, normally in seawater. External SCC is fundamentally different and is a known risk for land pipelines and can be potentially a problem for all lines.

6. Fatigue and Fracture of High-Strength Steel

It is recommended to obtain fatigue data for the proposed materials and apply the data to mechanical design. Fatigue life is used as the basis for many of the limits placed on offshore pipeline strength design. These limits have often been established based on empirical data from tests on low-strength steels, with a safety margin applied. In general, the ability of steels to resist fatigue failure increases with increasing yield strength. Fatigue analysis data from line pipe manufacturers can be used to challenge the requirements of pipeline codes in the areas of thermal buckling analysis and free-span and pipeline stability analysis.

As the strength of line pipe increases, weld metals of increased strength and sufficient toughness are required to ensure overmatching behavior of girth welds.

7. Material Property Requirements

Circumferential Direction

Necessary CTOD value requirements for the heat affect zone and weld metal are to be established that are relevant for the specific design conditions with regard to the type and extent of longitudinal weld defects likely to exist. Typically, the required CTOD value is established through ECA (engineering criticality assessment) using British Standard BS 7910 [17].

The extent of longitudinal weld defects likely to exist is defined in the operators' welding qualification specifications. Typical values are depth 3 mm and width minimum of 25 mm and pipe wall thickness.

Practical experience from field use of the line pipes has demonstrated that very little structural failure occurs due to lack of CTOD value in the hoop direction for line pipes. Similar observations may be made on the CTOD requirements for the longitudinal direction. It is therefore suggested to closely evaluate the following:

• CTOD testing methods, scatters, and statistical evaluation of scatters.
• Possibility to reduce the number of CTOD tests.
• Safety factors used in ECA determination of CTOD requirements.
• ECA design equations and analysis methods.

It is likely that fracture occurs in the weldments. Weldability of the pipe is a more important parameter than CTOD value.

Longitudinal Direction

The CTOD value for line pipes in longitudinal direction is influential for fracture limit state when ECA such as BS 7610 is applied to calculate the limiting loading condition to avoid fracture.

The CTOD value needed to avoid fracture depends on the extent of girth weld defects likely to exist and the applied load. For a defect depth of 3 mm, a wall thickness of 25.4 mm, and loading up to 0.5% total strain, a defect length of 177 mm (7 × wall thickness) was shown to be safe when CTOD is a minimum 0.10 mm, see Knauf and Hopkins [12]. The discussions on unstable fracture and CTOD for hoop direction are also valid for longitudinal direction.

The fact is that the yield stress in the longitudinal direction does not significantly affect pipe strength, as long as strain-based design is applicable to the design situation. The reasoning for this statement is that strain acting on pipelines in operating condition is typically as low as 0.2% unless the pipeline is under a high pullover load.

With exception of some special material problems, the Y/T (SMYS/SMTS) ratio requirements can be replaced by introducing strain-hardening parameters, such as σ_R and n used in a Ramberg-Osgood equation. The level-2 and level-3 failure assessment diagrams in BS 7610 also account for strain-hardening effects.

Comparisons of Material Property Requirements

Which material properties are the dominant factors in local buckling and collapse? The answer is depends on the loads as follows:

- For internal pressure containment, hoop SMTS.
- For external-pressure induced buckling, hoop SMYS.
- For bending collapse, longitudinal SMYS.
- For combined internal pressure and bending, hoop SMTS, longitudinal SMYS, and SMTS.
- For combined external pressure and bending, hoop SMYS, longitudinal SMYS, and SMTS.

Raising hoop SMYS directly results in a proportional reduction of the required wall thickness of the line pipe for water depths shallower than 350 m. As a conclusive remark on material property requirements, it is believed that

- The minimum CTOD values in both hoop and longitudinal directions typically should be 0.1 mm; the applicability of lower CTOD values can be validated by ECA methods.
- It is economically beneficial and technically justifiable that, for pipe grades X60 to X80, yield and tensile strengths in longitudinal direction can be lower by up to 10% than those in the transverse direction for water depths shallower than 450 m.
- For fracture and local buckling failure modes, the Y/T value requirement can be removed if the strength analysis explicitly accounts for the difference of strain hardening whose parameters (σ_R and n) are a function of SMYS and SMTS, as the equations given in Bai et al. [3].

As a further study, it is proposed to compare the *Y/T* ratio requirements from alternative codes (e.g., 0.93 from API for onshore pipelines, 0.85 from EPRG). It is perhaps possible to find some other rational criteria that can replace the *Y/T* ratio requirement in strength design. To develop alternative criteria, it is necessary to understand the reasons of using *Y/T* ratio as a design parameter.

References

[1] Hillenbrand HG, Heckmann CJ, Niederhoff KA. X80 linepipe for large-diameter high strength pipelines. Available at www.europipe.com/; 2002.

[2] Graf M, Hillenbrand HG. Production of large diameter linepipe—State of the art and future development trends. Europipe GmbH; 1995.

[3] Bai Y, Knauf G, Hillenbrand HG. Materials and design for high strength pipelines. Seattle, USA: Proc. of ISOPE'2000; 2000.

[4] Tam C, et al. Oman-India Gas Pipeline: Development of design methods for hydrostatic collapse in deep water. Amsterdam: OPT '96; 1996.

[5] Thorbjornsen B, Dale H, Eldoy S. The NorFra pipeline shore approach: Engineering environmental and construction challenges. Honolulu: Seventh International Offshore and Polar Engineering Conference; 1997.

[6] Graf MK MK, Hillenbrand HG HG. Niederhoff KA. Production of large-diameter linepipe and bends for the world's first long range pipeline in Grade X80 (GRS 550). Houston, TXL: PRC/EPRG Ninth Biennial Joint Technical Meeting on Linepipe Research; May 1993.

[7] Chaudhari V, Ritzmann HP, Wellnitz G, Willenbrand HG, Willings V. German gas pipeline first to use new generation linepipe. Oil Gas J; January 1995.

[8] Laing BS, Dittrich S, Dorling DV. Mechanized field welding of large diameter X-80 pipelines. In: Pipeline technology, proceedings Second International Conference September 1995, Vol. 1. New York: Elsevier; 1995. pp. 505–12.

[9] Gray JM. An independent view of linepipe and linepipe steel for high strength pipelines: How to get pipe that's right for the job at the right price. Hobart, Australia: API X-80 Pipeline Cost Workshop; October 2002.

[10] Nakasugi H, Tamehiro H, Nishioka K, Ogata Y, Kawada Y. Recent development of X80 grade linepipe. Welding-90, Hamburg, Germany; October 1990.

[11] Tamehiro H. High strength X80 and X100 linepipe steels, Nippon Steel Corporation. Australia: Int. Convention Pipelines: The Energy Link; October 1996.

[12] Knauf G, Hopkins P. The EPRG guidelines on the assessment of defects in transmission pipeline girth welds. 3R International; 1996, 35(10–11): 620–4.

[13] Price C. Welding and construction requirements for X80 offshore pipelines. Houston, TX: 25th Annual Offshore Technology Conference; May 1993.

[14] API 5L. Specification for line pipe. 41st ed. Washington DC: American Petroleum Institute; 1995.

[15] BS 6990. Code of practice for welding on steel pipes containing process fluids or their residuals. London: British Standard Institution; 1989.

[16] Healy J, Billingham J. Increased use of high strength steels in offshore engineering. Welding Metal Fabrication; July 1993.

[17] BS, BS7910, Guide on methods for assessing the acceptability of flaws in metallic structures. London: British Standard Institution; 2005.

32 Welding and Defect Acceptance

Chapter Outline

1. Introduction

During offshore pipeline installation, the occasional weld defect repair may be carried out just after the sternmost tensioner and before the next roller support in the repair station. The weld defect is removed by grinding and subsequent rewelding. Aft of the tensioner, the pipe undergoing excavation is highly loaded by bending and tension. The local stresses at the weld repair are intensified during the weld excavation process. Defects in the girth weld are located and measured by radiography or ultrasound. Defects exceeding the project criteria are thoroughly removed; however, the removal of excess material should be minimized to minimize local stresses. The determination of safe weld excavation sizes for repair is one of the more difficult evaluations in pipeline installation engineering. This subject has attracted much attention from pipeline owners, installation contractors, and operating companies because of personnel safety and the risk of the pipeline parting or buckling on the ramp during excavation.

    This chapter presents an analytical method of determining safe weld excavation lengths, preventing both plastic collapse (buckling) and fast fracture of the pipe during weld defect repair.

2. Weld Repair Analysis

The weld excavation and repair procedure has been analyzed and performed successfully for the major Gulf of Mexico operators and many contractors in the past

years due to their awareness of risk and increased focus on safety [1], [2]. Many factors affect the safe weld repair at the laying ramp, for example, plastic collapse of section, brittle fracture, or cracking growth and fatigue. Fatigue is an extension of the present subject and is treated by the fracture mechanics approach. This topic is the subject of a separate chapter. Plastic collapse and fast fracture are both considered in the following weld repair analysis:

1. Stress analysis is performed on the excavated pipeline weld under the most severe tension and bending moment loading conditions experienced during repair on the laying ramp. This analysis is performed to determine the maximum allowable excavation lengths and depths to avoid plastic collapse.
2. Given that the allowable excavation length and depth have been established by stress analysis, fracture mechanics analysis is performed. This ensures that the weld and heat affected zone (HAZ) do not fracture quickly, given the material properties of the weld region.

Allowable Excavation Lengths for Plastic Collapse

The B31G criterion [3] is widely used to assess corroded pipelines for fitness evaluation. This part of the analysis ensures that the pipe does not suffer plastic collapse of the section during repair. The maximum allowable weld repair length and depth is established to ensure that the stress at the root of the excavated area is kept below the yield strength of the pipe during the repair process. API 1104 [4] and BS 4515 [5] are typical guidelines required for welding and weld acceptance standards for construction of offshore pipelines and flowlines. In accordance with British Standard 4515, which considers the welding of steel pipelines on land and offshore, the following criteria should be considered during repair:

1. For a full penetration repair, the maximum weld repair length is 20% of the girth weld length.
2. For a partial penetration repair, the maximum allowable repair length is 30% of the girth weld length.

These guidelines begin to address the issue under discussion but do not necessarily speak to a particular loading condition for a specific excavation or material toughness.

When pipeline repairs are made between the sternmost tensioner and the next roller support on the laylng ramp, the pipe butt weld is excavated under high loads caused by the curvature bending moment and laying tension. With elastic stress analysis [6], the stress distribution in the pipe may be calculated by

$$\sigma_{ax} = \frac{N}{A} + \frac{M_x}{I_x} y + \frac{M_E}{I_y} x \tag{32.1}$$

where the cross section of pipe is assumed to be in an *x-y* plane and σ is stress; N is tension force; A is the pipe cross section area; M is the bending moment; and I is the second moment of area of the cross-sectional area about the neutral axis.

The plastic collapse behavior of an excavated girth weld can be predicted using a local collapse failure criterion proposed by Kastner et al. [7]:

$$\frac{\sigma_{ax}}{\sigma_{flow}} = \frac{\eta[\pi - \beta(1 - \eta)]}{\eta\pi + 2(1 - \eta)\sin\beta} \qquad [32.2]$$

where

$\eta = 1 - d/t$
$d =$ defect depth
$t =$ wall thickness
$\beta = c/R$ (in radians)
$c =$ half defect (circumferential) length; $R =$ pipe radius
$\sigma_{flow} =$ flow stress
$\sigma_{ax} =$ the total axial stress

For a simple excavation geometry, the stress estimate may be calculated based on the formula in BS 7910 [8]. For real-life repair geometries, however, the excavation profile is too complicated to obtain an accurate result of stress distribution using Eq. (32.1). Figure 32.1 shows the geometries of typical grinder forms used in the excavation. The radii may be as large as 6 in. and as small as 2 in. The general defect position and its corresponding excavation forms are shown in Figure 32.2.

Finite element analysis (FEA) is a powerful tool to analyze the complex stress map for this kind of problem. The excavated pipelines are modeled and analyzed with finite elements to provide an accurate assessment of the stresses due to the applied
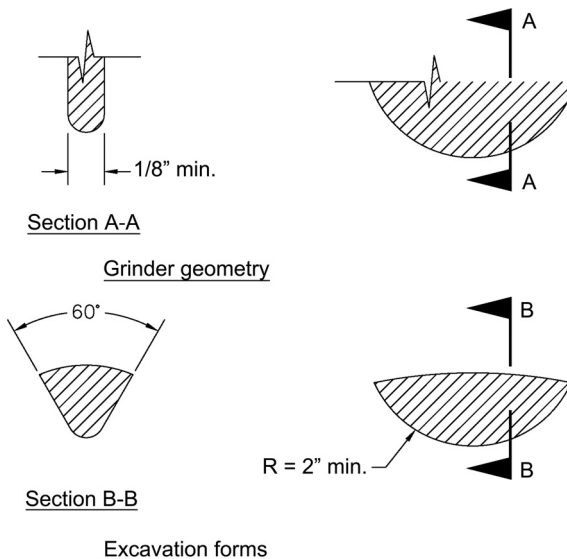
Figure 32.1 Geometries of grinder and excavation.

Defect ≤ 1/3 wall

Defect ≤ 2/3 wall

Defect at root
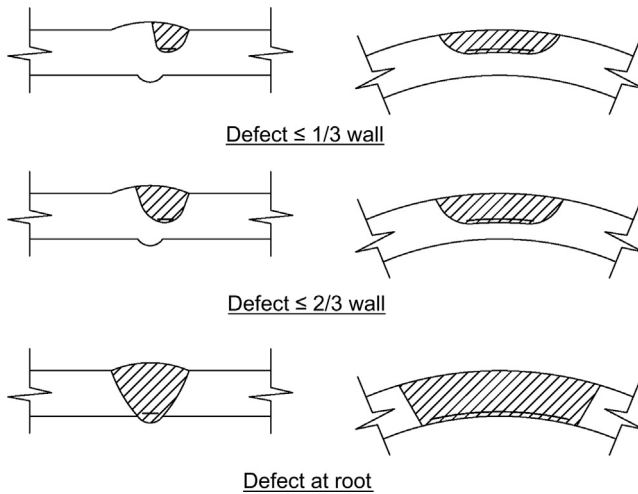
Figure 32.2 Defect positions and its corresponding excavation forms.

bending and tensile loads of the pipe cross section for the conditions of varying excavation lengths and depths.

The loads of bending moment and tension force during repair are chosen from the installation simulation with installation software widely used, such as OFFPIPE. A dynamic factor of 1.20 is included with the static analysis results to account for the effects of vessel and pipe motion. This factor depends on the vessel motion, pipe properties, and the sea states acceptable for pipeline installation. The sea states can be resolved by utilizing dynamic OFFPIPE or similar software sensitivity analyses. Based on the stress distribution from the FEA, the allowable excavation lengths for plastic collapse at various positions and depths of excavation are determined directly.

Allowable Excavation Lengths Using Different Assessments

The stresses resulting from the tensile and bending load and the residual weld stresses, combined with an excavation in the weld-zone is of a critical value with respect to the fracture failure mode. Allowable flaw length of offshore pipelines may be assessed by using different methods, as follows.

Level 1 Assessment: Workmanship Standards

Pipeline welding codes in the United States and elsewhere establish minimum weld quality standards based on the inspection of a welder's workmanship. The initial flaw acceptance criteria evolved through industry experience over many decades. Most workmanship standards are similar, though not identical, in terms of imperfection types and sizes. The advantage of workmanship standards is that they are time tested, compatible with normal levels of NDE quality, easy to apply, and require no material strength or weld toughness data. However, it has been recognized that some rejectable

flaws may not pose a real threat to pipeline integrity but still are rejected solely on the basis of workmanship standards. That is, the workmanship standards tend to be conservative. A girth weld with a defect assessed unacceptable by a workmanship standard may be extremely costly to repair or replace and yet with additional assessment may be shown to be safe and fit for service. Still the basic workmanship standard approach is time tested and has been proven over more than 30 years, as shown by applications on the Alaskan pipeline.

The principal workmanship standards recognized by U.S. gas pipeline regulations are those contained in API Standard 1104. Weld workmanship standards are also contained in other specifications, such as the ASME B&PV Code, CAN/CSA-Z184, and BS 4515, but these are not recognized by U.S. pipeline regulations.

Level 2 Assessment: Alternative Acceptance Standards

Alternative acceptance standards were developed to facilitate acceptance of flaws that do not meet workmanship standards. Incentives for alternative standards are usually economic, arising due to the inaccessibility or quantity of welds that would otherwise require repair. Alternative standards recognize that the true severity of a flaw depends on material toughness and applied stress levels and can be determined only by using fracture mechanics principles. The crack tip opening displacement (CTOD) test is most commonly used as the weld toughness assessment method when alternative acceptance methods are utilized.

Three alternative criteria that are recognized by their respective national regulating agencies and are often cited: Appendix A of API Standard 1104, Appendix K of CSA-Z184, and BSI PD 6493 [9] (PD 6493, Level 1 and revised BS 7910). All three standards are based on the CTOD design curve approach developed by The Welding Institute, and they extend linear elastic fracture mechanics (LEFM) concepts into the elastic-plastic regime. In spite of their common origins, they differ in their treatment of residual stresses, summation of stress components, minimum toughness level, and factors of safety.

Level 3 Assessment: Detailed Analysis Using Fracture Mechanics

Flaws that are not permitted by Level 2 assessment may be further evaluated by detailed fracture mechanics analysis. PD 6493 provides an appropriate Level 3 procedure based on R-6 failure assessment diagram (FAD) methodology. This diagram is broadly used; however, it is generally more representative to plot defect length versus stress field.

The allowable excavation length for weld excavation in this chapter is determined by using the British Standard PD 6493, "Guidance on Some Methods for Assessing the Acceptability of Flaws in Fusion Welded Structures," or its revision, BS 7910, "Guide on Methods of Assessing the Acceptability of Flaws in Structures." Using fracture mechanics, a CTOD-based design curve is generated to ensure that failure by unstable fracture will not occur for a given defect size, applied stress, and critical CTOD toughness. These codes involve a two-parameter assessment depicted by an FAD, which considers the independent possibility of plastic collapse and fast fracture.

FractureGraphic is a typical software that uses the analytical approach detailed in the BSI PD 6493 and BS 7910 codes. As discussed in BS 7910, both the primary and secondary stresses must be considered in determining the allowable crack length. The primary stresses result from the tensile and bending load, and the secondary stresses result from residual weld stresses. FractureGraphic calculates the secondary weld residual stresses based on the material strength and the weld heat input. The relationship between the permissible crack depth and length as a function of applied stress and calculated secondary stress is obtained. Based on these results, the allowable excavation lengths for fracture mechanics at various positions and depths of excavation are determined.

3.   Allowable Excavation Length Assessment

Description of Pipeline Being Installed

A 12.75 in. diameter by 0.625 in. wall thickness X52 pipeline was chosen as an example to evaluate the allowable excavation length in weld repair during laying. The OFFPIPE installation analysis provided the worst stress case during installation, resulting from tension forces and moments including dynamic effects. For this example, tension force and moment were 29.35 kips and 81 ft-kips, respectively. It was assumed that any defects would be removed by grinding using a 4 in. disc or slightly larger. A CTOD value of 0.008 in. was used for the fracture mechanics analysis.

Analysis Method

Finite Element Analysis

FEA analysis was performed using ALGOR software. The pipe under consideration was located aft of the tensioner on the laying barge and was subjected to a bending moment of 81 ft-kips with a tensile load of 29.35 kips. The analysis considered defects removed at one-third, two-thirds, and through-wall thickness. These conditions are shown in Figure 32.3. The excavation profile following defect removal had a combined angle of 60° with a root radius of 0.125 in. The bevel that was modeled is the minimum size necessary for weld repair following removal of the defect. The length of the groove was taken as just slightly larger than the length of the defect. In addition to the length of the defect, the excavated groove includes a curved section required to accommodate the grinder.

In addition to varying the depth of the defect, the length of the defect was altered, along with the position on the circumference of the pipe. As the circumferential position varies, the pipe stresses vary. The bending stress at the top center results in a pure tensile load and at the bottom center normally a pure compressive load, since tension stresses are much smaller than bending stresses. Four circumferential positions are shown evaluated. Top center, 45° off of top center, 90° off of top center, and bottom center. A fifth position, 45° above bottom center, is shown analyzed by interpolation between the two adjacent locations. Each change in a variable requires a new model to be created for stress analysis.
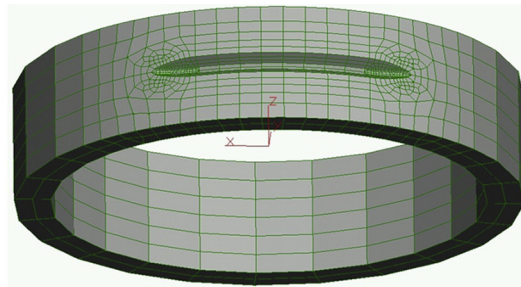
(a) One-third pipe thickness
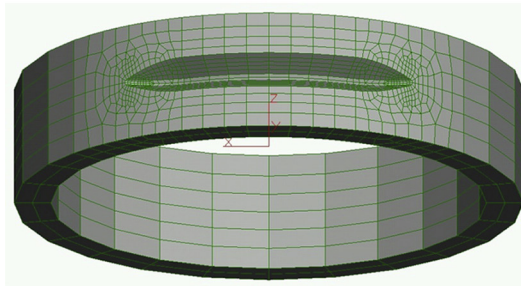
(b) Two-thirds pipe thickness
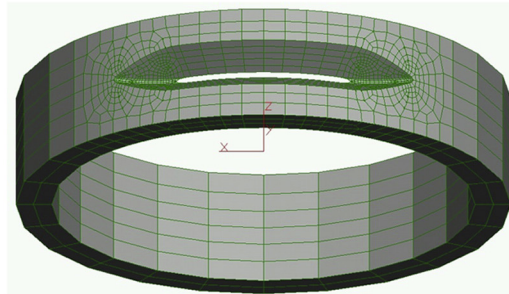
(c) Through-pipe thickness

Figure 32.3 Groove shapes and mesh distribution for the FEA. (For color version of this figure, the reader is referred to the online version of this book.)

Fracture Mechanics Analysis

The fracture mechanics investigation is demonstrated using the Fracture Graphic software, with manual checking using BSI PD 6493 and BS 7910. The defects with depth of one-third wall thickness, two-thirds wall thickness, and through-wall, which were considered, are shown in Figure 32.3. A CTOD value of 0.008 in. was maintained for all positions for these analyses.

Defects may be surface breaking or mid-wall defects. Surface breaking defects are more severe from a fracture standpoint. A mid-wall defect behaves the same as a surface-breaking defect once the top ligament is removed. The limiting length of the

crack for this part of the evaluation is the actual crack length measured by ultrasound or by radiography.

Analysis Results

Typical FEA results are shown in Figure 32.4, which are presented as Von Mises stresses and displacement distributions. The stresses as a function of crack depth and pipe position for all cases are shown in Table 32.1.

   The fracture mechanics analysis results are shown in the form of permissible crack depth and length as a function of applied stress. Figure 32.5 shows the results for the applied stress levels of 25, 30, 35, 40, 45, and 50 kips, respectively, where the stresses are perpendicular to the excavation.

   The FEA results in Table 32.1 are compared to the fracture mechanics analysis results to determine the governing condition. The failure condition limit, either plastic collapse or fast fracture, is determined by the least loading condition and determines the maximum allowable amount of material that can be excavated. The

12" pipe, 0 degree, h=0.667t, L=2 in

(a) Von Mises stress distribution

12" pipe, 0 degree, h=0.667t, L=2 in

(b) Displacement distribution
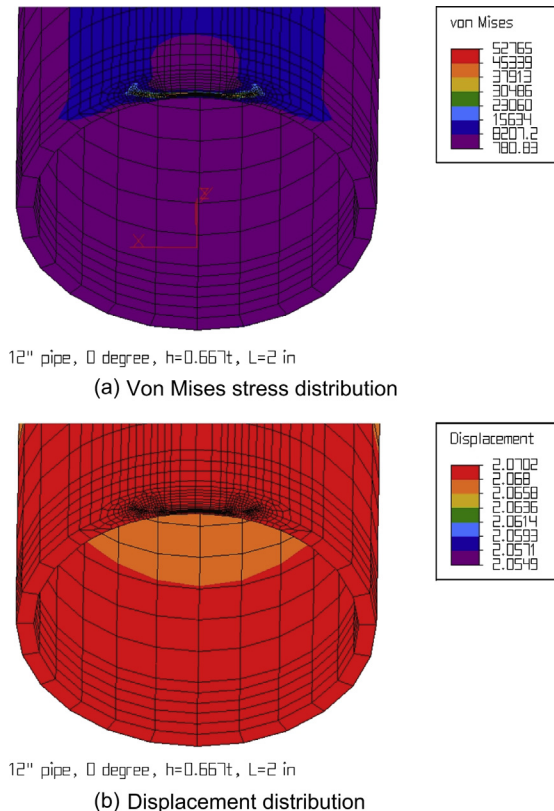
Figure 32.4 Stress and displacement distributions for top center case. (For color version of this figure, the reader is referred to the online version of this book.)

Table 32.1 Variations of Maximum Von Mises Stress with Groove's Position and Depth

Position/Depth	$^1/_3t$	$^2/_3t$	$1t$
0°	$L = 12$ in.	$L = 2$ in.	$L = 1$ in.
	$\sigma_{max} = 42.9$ksi	$\sigma_{max} = 52.7$ ksi	$\sigma_{max} = 54.0$ ksi
45°	$L = 12$ in.	$L = 2$ in.	$L = 1$ in.
	$\sigma_{max} = 44.4$ ksi	$\sigma_{max} = 52.2$ ksi	$\sigma_{max} = 54.0$ ksi
90°	$L = 12$ in.	$L = 3$ in.	$L = 2$ in.
	$\sigma_{max} = 43.4$ ksi	$\sigma_{max} = 19.5$ ksi	$\sigma_{max} = 45.3$ ksi
180°	$L = 12$ in.	$L = 3$ in.	$L = 2$ in.
	$\sigma_{max} = 32.9$ ksi	$\sigma_{max} = 51.9$ ksi	$\sigma_{max} = 52.6$ ksi

Figure 32.5 Permissible crack depth versus length for fracture mechanics analysis.

summary of the allowable length excavation for the example is presented in Figure 32.6.

It is noted that, in general, the limiting failure mechanism is fast fracture rather than plastic collapse. For a through-thickness crack at the top center, a crack length of only ½ in. can be tolerated for this example. Serious consideration is warranted if planning any repair of through-thickness or root defects after the tensioner. If such repairs are attempted, they should be performed only under close supervision. Means of modifying the ramp configuration for a "repair area" can be accommodated on larger vessels to reduce or minimize bending loads. In other cases, only the material and weld toughness can be increased to permit larger excavation.

When the defect length is found to be more than the allowable groove length at that defect depth, either a multistage repair can be undertaken or the joint may be backed up to the front of the tensioner. Backing up is a costly operation offshore. In a multiple repair situation, the first weld repair groove is excavated from one end of the defect up

Maximum weld excavation length
versus pipe position
CTOD = 0.008 in.

Depth	Length (in.)
1/3 wall	8.0
2/3 wall	0.5
Full wall	0.5

Depth	Length (in.)
1/3 wall	8.0
2/3 wall	0.5
Full wall	0.5

0°
Top
of pipe
45°

12.750" x0.625"
X52 pipeline
maximum excavation
lengths
versus angle

90°

Depth	Length (in.)
1/3 wall	8.0
2/3 wall	2.0
Full wall	1.5

135°

180°

Depth	Length (in.)
1/3 wall	12.0
2/3 wall	3.0
Full wall	2.0

Depth	Length (in.)
1/3 wall	12.0
2/3 wall	3.0
Full wall	2.0
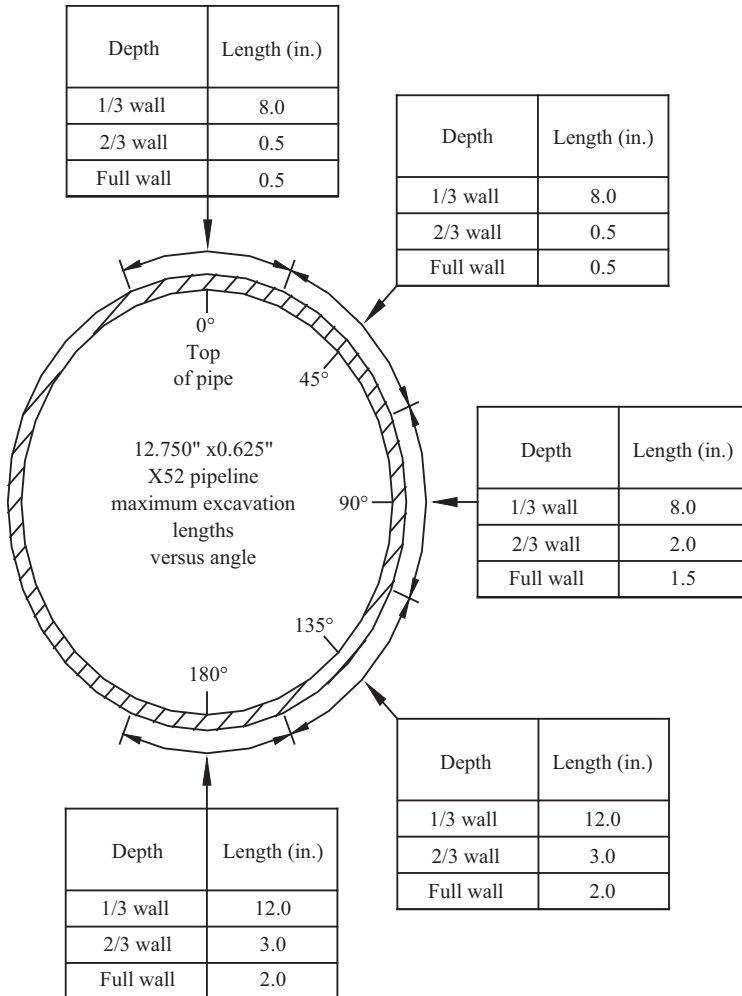
Notes:
1. 1/3 wall means excavation depth from 0 to 3/16 deep.
2. 2/3 wall means excavation depth from 3/16 to 3/8 deep.
3. Full wall means excavation depth to 9/16 deep.
4. Between 2/3 and full wall linear interpolate.
5. Lengths noted are centered at angle shown.
6. 12-in. length is set as a maximum limit for all cases.
7. Excavation length does not equal defect length.
   Lengths shown are measured at pipe surface
8. Use a 4-in. grinding disk or closest possible size to minimize metal removal.
9. No full wall repairs can be made post tensioner.

Figure 32.6 Summary of allowable length and depth of excavation for 12-in. pipeline.

to the allowable length. This section is then weld repaired. The subsequent weld repair grooves are then excavated and repaired without exceeding the allowable repair groove length. The procedure continues until the entire defect length is repaired. Radiographic procedures are performed to demonstrate that the acceptance criteria are met.

4. Conclusions

A procedure for repairing offshore pipeline welds after the tensioner is presented. This procedure has been utilized many times in actual practice. Within the discussion, broadly used and available software are identified, and steps for problem resolution are described. The example problem is taken from an actual project case study to demonstrate defect size limitations.

References

[1] Bai Q, Haun R, Sumner K. Assessment of allowable pipeline weld excavation lengths on the lay ramp. OPT 2003, Houston, TX; 2003.
[2] Anderson TL, Belloni A, Willoughby AA. Plastic collapse analysis of girth weld repair grooves in pipe subjected to offshore laying stresses. Int J Pressure Vessels Piping 1988;31:105–30.
[3] ASME. B31G. Manual for assessing remaining strength of corroded pipes. New York: American Society of Mechanical Engineers; 1996.
[4] API 1104. Field welding pipelines and related facilities. Washington, DC: American Petroleum Institute; 1999.
[5] BS 4515. Specification for welding of steel pipelines on land and offshore. London: British Standards Institute; 1996.
[6] Young WC, Budynas RD. Roark's formulas for stress and strain. 7th ed. New York: McGraw-Hill; 1989.
[7] Kastner E, Roehrich E, Schmitt W, Steinbuch E. Critical crack sizes in ductile piping. Int J Pressure Vessels Piping 1981;9:197–219.
[8] BS 7910. Guide on methods for assessing the acceptability of flaws in fusion welded structures. London: British Standards Institute; 1999.
[9] BSI-PD 6493. Guidance on some methods for assessing the acceptability of flaws in fusion welded structures. London: British Standards Institute; 1991.

33 Installation Design

Chapter Outline

1.   Introduction

Subsea pipeline installation is performed by specialized laying vessels. There are several methods to install a pipeline, the most common methods being S-lay, J-lay, and reeling lay. Figure 33.1 illustrates the typical S-lay pipeline configuration of subsea pipeline installation. In addition, pipeline towing installation methods, as shown in Figure 33.2, including bottom towing, off-bottom towing, mid-depth towing, and surface towing, are also appropriate for some specific projects. Some methods are better suited for a particular application than others. Depending on the method, a subsea pipeline is exposed to different loads during installation from a laying vessel. Generally speaking, these loads include hydrostatic pressure, tension, and bending.

   The pipe-laying ability of a laying vessel relates primarily with the weight of the pipeline. As the water depth increases, so does the total weight of the pipeline, in free span, between the laying vessel and the sea floor touchdown point; consequently, greater tension capacity or different methodology is required. However, the weight can be reduced by either adding extra external buoyancy or increasing the angle of departure of the pipe from the laying vessel. Since it is very expensive to add and retrieve buoyancy tanks, particularly in very deep water, it preferred to increase the departure angle to reduce the length of the free
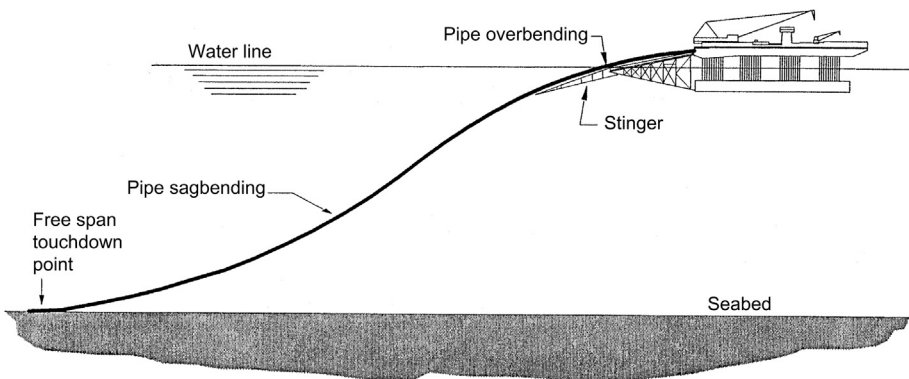
Figure 33.1 Typical pipe configuration during installation.

Controlled depth toe method
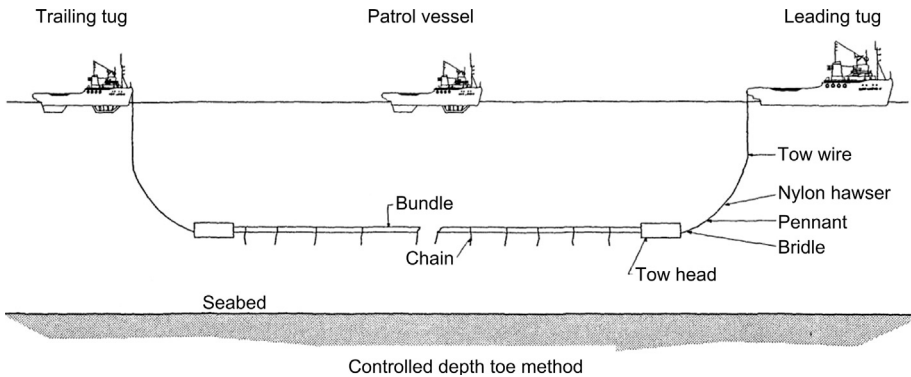
Figure 33.2 Pipeline tow method.

suspension pipeline and consequently the weight of the pipeline. With the increase in water depth, the departure angle of about 45° for an S-lay installation increases to over 80° for J-lay and reel laying. The installation analysis is conducted to estimate the minimum required laying tension for the pipeline for a given radius of curvature to ensure that the load effects on the pipeline are within the strength design criteria.

Commercial pipeline installation analysis software can be used as an effective tool for analyzing the static and dynamic configurations of a pipeline during installation. The static configuration of the pipeline is the shape of the pipeline from the laying vessel to the seabed when it is in static equilibrium. The software should be capable of analyzing the load effects on the pipeline when a section, like a valve, is installed and be capable of letting the pipeline slide over the stinger.

A commonly used FEM computer program for pipeline installation analysis is OFFPIPE. This program can give indicative global results for most situations but not the effects of stress or strain concentration and point loads due to changes in stiffeners.

This chapter first describes the pipeline installation methods, then the installation analysis methods are summarized, finally, examples of installation analysis are presented for the engineering applications.

2.   Pipeline Installation Vessels

Introduction

Pipeline installation methods have significantly changed over the last several decades. This is pertinently enforced by the recent replacement of the BP Forties 170 km trunk line. When it was first installed in 1974, it took two laying barges more than two summer days, and each laying barge suffered 60% downtime due to weather. In 1990, it took one (relatively old) pipe laying vessel to install the

replacement pipeline (and the pipe wall was significantly thicker, 28.5 mm compared to the original 19 mm). The significant increase in laying rate is due to a combination of factors, including

- Improved welding techniques.
- Improved survey capabilities.
- Improved anchor handling techniques.
- Improved procedure.

Figure 33.3 shows typical pipe laying vessels operating in the North Sea. The methods available to install pipelines are discussed in the following sections. Typical pipe laying vessels include

- S-lay and J-lay semisubmersibles.
- S-lay and J-lay ships.
- Reeling ships.
- Towing or pulling vessels.

Different vessel types are used depending on the pipe laying method and site characteristics (such as water depth, weather etc.).

Pipe Laying Semi-Submersibles

Pipe laying semisubmersibles are floating factories that weld line pipe joints together and install the pipe accurately on the seabed. They were developed as a direct response to the large weather downtime experienced by the monohull pipe laying barges (especially in the North Sea). These vessels have excellent weather adaptabilities and can provide a stable platform for pipe laying, even in seas experiencing the Beaufort force 8 wind conditions. It is usually the limitations of the anchor handling vessels that prevent the semi-submersibles from operation in rough weather.

Figure 33.4 shows a typical pipe laying semi-submersible used in the North Sea (SEMAC of ENI). Pipe laying semisubmersibles can install pipes in a wide range of diameters (6 in. to 40 in.) in water depths from 10 m to 1500 m. They usually have following capabilities:

- Stable platform and constant tension to guarantee the pipeline is laid into the sea in an S shape, as shown in Figure 33.1. If the vessel moves too much (i.e., due to weather) in the dynamic condition, the pipeline may suffer overstress and possibly buckle.
- Handles joints quickly. These vessels can install up to 5 km of pipeline a day (an average of 3.5 minutes for each joint).
- Welding and nondestructive testing of joints with sufficient speed to average 3.5 minutes per joint.

The main disadvantage of the pipe laying vessels is the high cost; they typically require 400 personnel, two anchor handling vessels, a survey vessel, and supply vessels for transporting line pipes.

Figure 33.3 shows four diagrams. Text labels in the figure:

Water line — S lay — Seabed

Semi-submergible laying barge
-Semac   (EMC)
-Castoro SEI   (EMC)
-LB 200   (McDermott)

Water line — S lay — Seabed
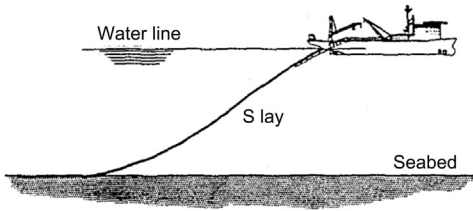
Pipe laying ships
-LoreLay   (Allseas)
-ETPM DLB 1601   (ETPM)
 (No DP, requires anchor)

Water line — S lay — Seabed
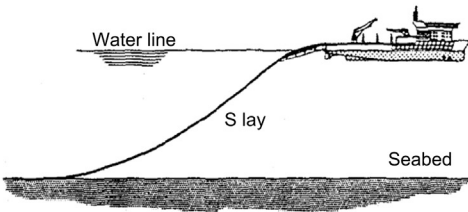
DSV pipe laying
-Any diving support
 vessel with DP system
 capable of constant pulling

Water line — J lay — Seabed
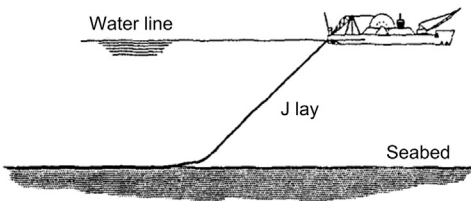
Reeling ship
-Apache   (Technip)

Figure 33.3 Pipe laying vessels available in the North Sea (in 1990).

Pipe Laying Ships and Barges

Pipe laying ships and barges install pipelines in the same manner as the pipe laying semi-submersibles. The principal difference is that these vessels are monohulls, and hence do not have as good sea keeping capabilities as the semi-submersibles. This means longer periods of downtime and reduces the total time per season during which pipe can be installed. Flat barges have worse sea keeping abilities than the ships and are used only in the calmer wave climates. Apart from this the handling, welding and
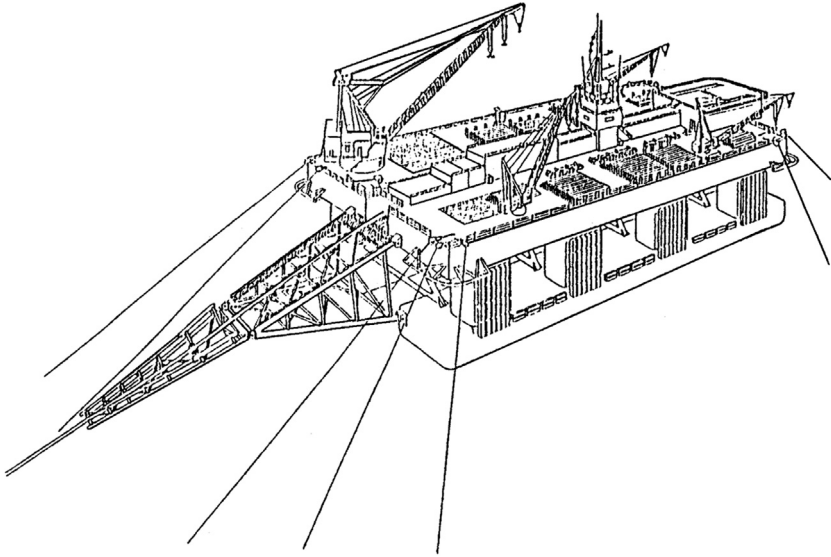
Figure 33.4 Pipe laying semi-submersible.

laying down of line pipes are performed in the same manner as discussed for semi-submersibles.

Pipe laying ships have very similar installation capabilities as pipe laying semi-submersibles. This includes the wide range of pipeline diameters in water depths from 15 m to over 1000 m.

The main advantage of the pipe laying ship is the cost: The relatively smaller, dynamically positioned ships can operate without the assistance of anchor handling vessel.

Pipe Laying Reel Ships

Pipe laying reel ships provide an economical tool for installing short, small diameter pipelines and umbilicals with line sizes up to 16 in. The pipeline is welded onshore and reeled onto a large drum on the reel laying vessel. During the reeling process, the pipe undergoes plastic deformation on the drum. During the installation, the pipe is unreeled and straightened using a special straight ramp. The pipe is then lowered onto the seabed in a similar configuration to that used by the pipe laying barge.

A major consideration in pipeline reeling is that the plastic deformation of the pipe must be kept within limits specified by the relevant codes. The existing reeling ships reflect such code requirements. According to the requirement of reeling the pipeline onto a small diameter drum, the pipeline experiences some plastic strain. The permissible amount of strain and ovalization of the pipe limits the maximum diameter of the pipeline that can be installed by using this method. Usually, depending on the wall thickness, the maximum diameter is about 18 in. Also, due to the limited size of drum,

only short lengths of pipe can be laid (usually 3–15 km depending on pipe diameter). However, it is possible to install longer pipelines if more drums of pipe are available.

Regardless of the constraints of this method, the reeling method of installation has been proven to be a reliable and economical method for installing pipelines. The main advantages of the system include short offshore installation duration, minimum offshore spread (without anchor handlers), low operating risk since all pipe segments in the reel can be laid continuously, cheap cost, and more safety and convenience because all welding, testing, heat preservation, and corrosion prevention are done on land.

The analysis of reeled pipe laying can be achieved using the same techniques as for the laying barge. Special attention must be given to the compatibility of the reeling process with the pipeline steel grade and the welding process. Recent tests have indicated that the reeling process can cause unacceptable work hardening in higher-grade steels.

Towing or Pulling Vessels

In towing lay, the pipe is made up at some remote location onshore, transported to the offshore installation site by towing, and layed down. The buoyancy of the line is selected and designed to verify that a controlled-depth towing can be performed. The towing is either on the water surface (surface towing), at a controlled depth below the surface (control depth towing method, or CDTM), or on the sea bottom (bottom towing), where the different water depths are mainly to reduce the fatigue damage due to waves. The towing method is mainly applied to short lines, usually less than 4 km, (even though 7 km has been laid). Usually, two tugs tow the pipeline to the location, one leading and one trailing. On location, the pipeline is positioned and flooded.

The main advantages of fabricating a pipeline onshore are

- Low equipment costs compared to fabricating offshore.
- Long fabrication durations, permitting more difficult fabrication techniques to be applied. Some fabrication techniques, such as using bundling, cannot be performed by offshore vessels.
- Pipeline fabrication is not prone to weather interruptions.

However, the constraints of using the tow/pull methods are

- Limited fabrication length of pipe strings due to the size (length) of the fabrication yard and the difficulty of controlling a long line during towing out. The maximum line length to date using this method is about 7 km.
- The line should be installed in a straight line. A substantial amount of intervention s required to install bends in the system.

3. Pipe Laying Methods

The pipe laying methods use a series of professional pipe laying devices mounted on the vessel to lay pipelines on the subsea. It can be subdivided into, S-lay, J-lay, reeling lay and towing methods, with detailed description in the following subsections

S-lay Method

The traditional method for installing subsea pipelines in relatively shallow water is commonly referred to as the *S-lay method*, shown in Figure 33.1, because the profile of the pipe segment between the stinger and seabed forms an elongated S shape during the normal pipe laying. As the pipeline moves across the stern of the lay barge, the pipe is supported by a trusslike circular structure equipped with rollers and known as a *stinger*. The purpose of the stinger in the S-lay installation is to control the deflection of the pipe in the overbending region. The curvature radius of the stinger corresponds to the maximum bending stress. To avoid overbending at the last roller, the pipe must lift off smoothly from the stinger well ahead of the lowest two or three rollers. The practical water depth limit for a large, conventionally moored laying barge that uses the S-lay method is about 1000 ft, based on a ratio of anchor line length to water depth of about five to one.

The S-lay method is also commonly used in all kinds of deepwater pipe laying projects nowadays. In extremely deep water, the departure angle of the pipe becomes so steep that the required stinger length may not be feasible. Deeper water depths result in a steeper liftoff angle of the suspended pipe span at the stinger tip, which requires the stinger to be longer or more curved to accommodate the greater arc of reverse curvature in the overbending region. Accordingly, greater stinger buoyancy or structural strength is required to support the increased weight of the suspended pipe span. As for S-laying in ultradeep water, compared with axial tension and dynamic response, the pipeline bending stiffness is not a big concern. Therefore, the pipeline's dynamic response should be taken into consideration; For S-laying in ultradeep water, pipelines are designed and made very huge and heavy to resist external pressure caused by deep water, which need huge tension from the tensioner on the vessel.

A typical side view of S-lay pipe laying is shown in Figure 33.5. The pipe segments between the "inflection point" and the stinger are called the *overbending* region, while the pipe segments between the "inflection point" and the seabed are called the *sag-bending* region.

In generally, the installation equipment on S-lay vessels include a positioning system, windlass system, tensioner, stinger, abandonment and recovery winch, pipe crane, transfer roller, wielding station, groove machine, weld assembly device, inspection station, and corrosion-preventive device. The process of S-lay is shown as in Figure 33.6.

The S- lay vessel is continuously improved with the oil and gas development going deeper and deeper. The first generation S-lay vessels were flat-bottom barges fitted for shallow water, swamps, and inland waters; the second generation S-lay vessels were also barges but mooring system with points from 4 to 14 were added; the third generation S-lay vessels were semi-submersibles using a mooring system for position keeping [1]. The fourth generation pipe-laying vessels adopted the newest dynamic positioning technology to realize precisely controlling of the vessel position. Owing to their high maneuverability and powerful dynamic system, such vessels have advantages like short starting time, high speed in abandoning and recovering pipes, no
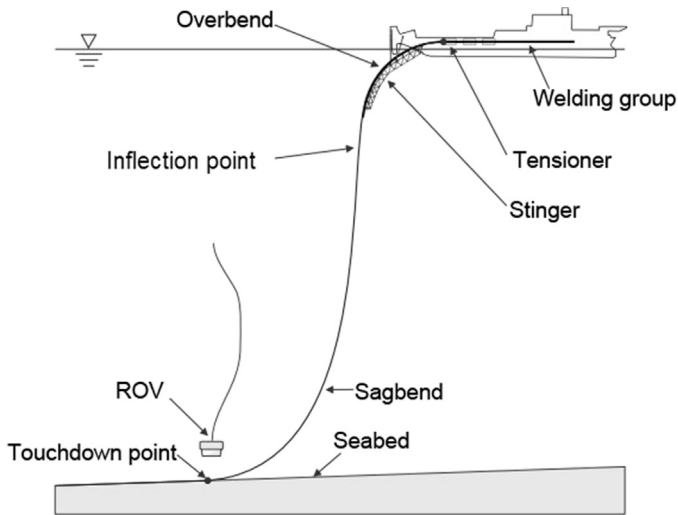
Figure 33.5 S-lay pipe laying.

restriction in water depth, and adaptability in areas intense with oil production systems. Nowadays, their deepest laying depth is up to nearly 3000 m. Table 33.1 lists a detailed comparisons and development process of S-lay vessels [2].

J-lay Method

J-lay method was born with frequent use of deepwater and ultradeepwater pipelines. The earliest J-lay method was started in 1980s and improved later
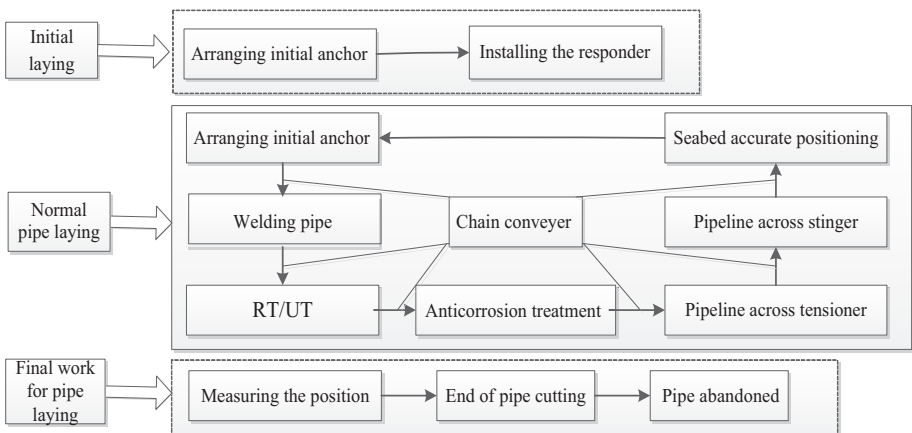
Figure 33.6 Construction process of the S-lay method.

Table 33.1 Development Process of Four Generations of S-lay Pipe-Laying Vessels

S-lay Pipe Laying Vessels	Forms	Main Performance	Pipe Laying Ability	Advantages	Disadvantages
First generation	Converted abandoned warships	Poor stability, enduring wave height of only about 1 m	Working water depth less than 30 m Pipe diameter max 10 in.	Cheap	Low speed of pipe laying and poor working environment
Second generation	Barges	General stability, enduring wave height of 1.5 m to 3 m	Working water depth about 100 m Pipe diameter max 18 in.	Simple structure, easy to construct, stingers are starting to be used	No improvement in pipe laying speed compared with first generation
Third generation	Semi-submersibles	Good stability, can work in waves with height more than 5 m	Working water depth less than 500 m Pipe diameter max 30 in.	Good stability, tensioners are used, pipe diameter becomes larger	No self-power, tugs are needed and speed is limited
Fourth generation	Dynamically positioned	Excellent stability, the max enduring wave height is 10 m	Working water depth less than 2750 m Pipe diameter max 60 in.	Good dynamic performance, flexible, fast pipe laying speed	Expensive, high cost for maintenance
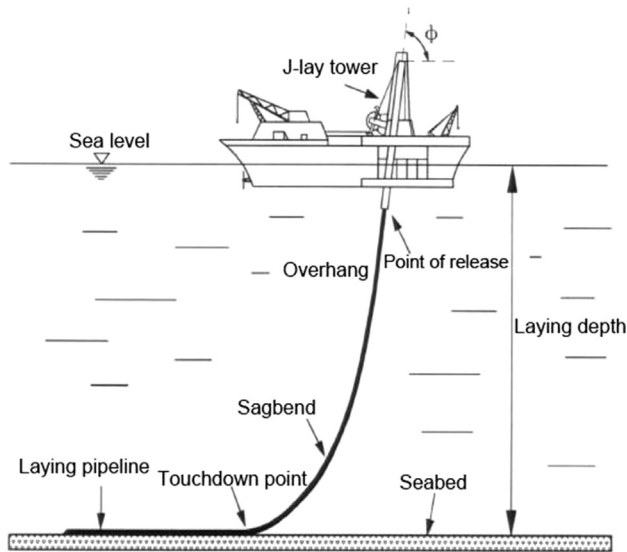
Figure 33.7 J-lay pipe laying.

with deeper and deeper laying depth. At present, there are mainly two J-lay methods: one is drilling vessel J-lay and the other is side slide way J-lay. J-lay is widely used in deep water and has already become one of major deepwater laying methods.

The J-lay method is so called because of the configuration of the pipe resembling a J shape during installation, as shown in Figure 33.7. Line pipes are joined to each other by welding in a vertical or near vertical welding station. As more and more line pipes are connected together, a string is formed and lowered onto the subsea floor. Hence, the J-lay method is inherently slower than the S-lay method and is therefore more costly.

J-Lay method has been used to many subsea pipe-laying projects internationally, particularly in deep water of the Gulf of Mexico, which has a great potential and will play a more and more essential role in future.

Reel Laying Method

Reel laying is a new pipe laying method emerging in the late 20th century. An advantage of this method is that the line pipes can be connected on land to a great length, then reel up to a drum mounted on a reel laying vessel [3]. The main devices for this pipe laying method include reeling drum, straightener, and laying vessel. Figure 33.8 shows a typical reeling vessel.

Table 33.2 compares the S-lay, J-lay, and Reel-laying methods [4].
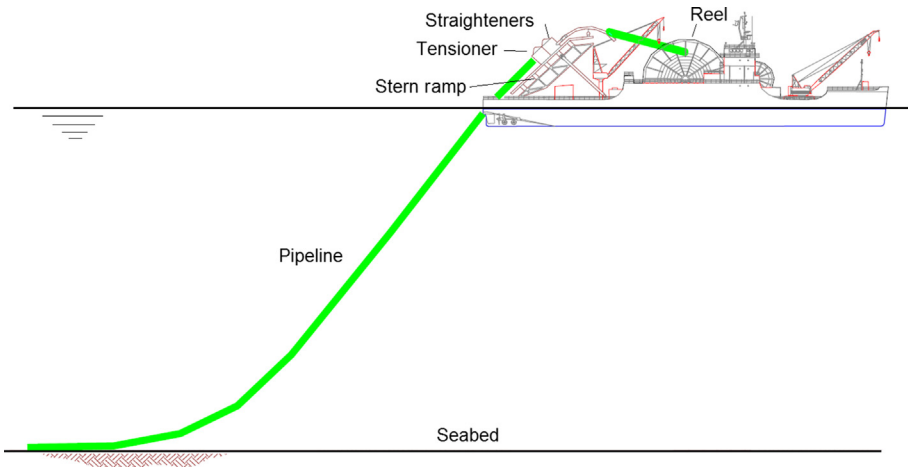
Figure 33.8 Reel laying method. (For color version of this figure, the reader is referred to the online version of this book.)

Towing Methods

The towing methods can be subdivided into the following four categories, as shown in Figure 33.9: surface towing, bottom towing, off-bottom towing, and mid-depth towing.

1. **Surface towing method:** Surface towing method utilizes buoys to adjust the buoyancy of the pipeline to make it float on the water surface. A few tugs are needed to pull the pre-fabricated pipelines to the installation site. This method is used mainly for sea areas with relatively calm water. Restricted by factors like pipe size, speed of current, and size of tug boats, the laying length is normally no more than several kilometers.
2. **Bottom towing method:** For this method, the pipeline segments are laid on the seabed directly and drawn to the installation site by surface tug boats; therefore, it can avoid the influence of wind, waves, and current as well. However, this method is restricted by undulation of seabed terrain and types of seabed soil, which makes it mainly suitable for a relatively flat seabed.
3. **Off-bottom towing method:** Off-bottom towing method utilizes buoys and dragging chains to suspend pipelines above the seabed at a certain height and pull them ahead by a surface tug. Not only can it reduce the influence of waves, it can avoid all kinds of submarine barriers. Therefore, although this method has complicated installation procedures, it can be widely used.
4. **Controlled-depth towing method:** For the controlled-depth towing method, like surface towing, the pipeline line segment is put in a certain depth for towing. Since this towing method can be little influenced by surface wind and waves, it is quite safe for pipeline towing.

4. Installation Software and Code Requirements

OFFPIPE

For pipeline installation analysis, the fit-for-purpose computer program OFFPIPE has been widely used. OFFPIPE is a finite element method program specifically

Table 33.2 Comparison Among Three Major Pipe Laying Methods

	S-lay	**J-lay**	**Reel Laying**
Allowable water depth	0–1800 m	500–3000 m	500–3000 m
Tensioners	Required	Not necessary	Required
Auxiliary device	Stinger	J-lay tower	Drum
No. of welding stations	3–4	1	0
Laying speed	3–5 km per day	1–1.5 km per day	12–24 km per day
Advantages	Well-developed technology, applicable for both Deep and shallow water; fast laying speed; parallel welding station, high laying efficiency	Relatively well-developed technology, especially applicable for the operation in deep water; small tension; no need of stern stinger	Most welding jobs done on land; small tension, easy to control; high laying efficiency; low cost; continuously laying of whole pipeline; low risk
Disadvantages	Stinger and tensioner are needed; big challenge for deepwater mechanic properties ensurance; laying vessel requires high power performance	Only one welding station, low laying speed and efficiency; mainly applicable for deep water; high requirement for vertical stability of laying vessels	Incapable of laying pipes with concrete coating; limited pipe laying diameters; need on land prefabricate sites; high requirement of plasticity of steel

(a) Surface towing method

(b) Bottom towing method

(c) Off-bottom towing method

(d) Mid-depth towing method
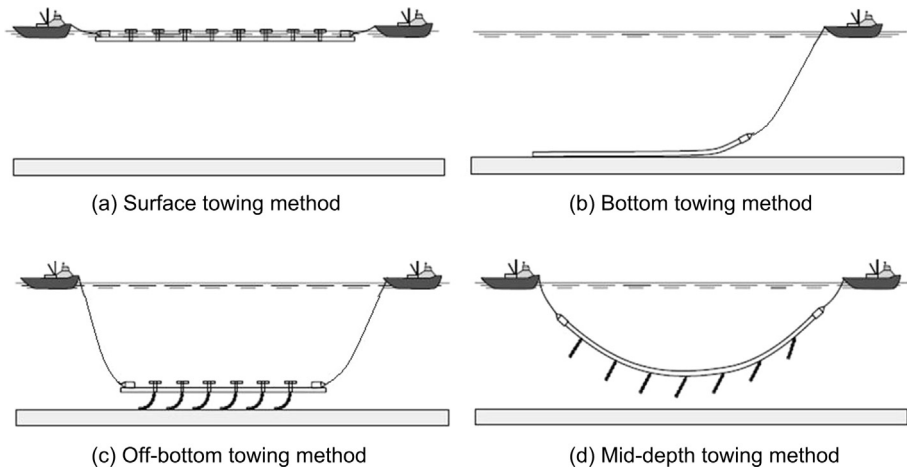
Figure 33.9 Subsea pipeline towing methods.

developed for the modeling and analysis of nonlinear structural problems encountered in the installation of offshore pipelines.

For static installation analysis of subsea pipelines, the following loads have been considered in the OFFPIPE software:

- Tension at laying barge tensioners.
- Buoyancy uniformly distributed.
- External hydrostatic pressure.
- Reaction forces from the laying barge rollers.
- Vertical seabed reaction (assumed to be continuous elastic foundation).

Typical S-lay, J-lay, and reel laying installations of subsea pipeline can be simulated with the OFFPIPE software. The analysis can be carried out both by static and dynamic analysis to determine the effect of the weather conditions.

The material modeling used in the OFFPIPE software is a Ramberg-Osgood material model, which is expressed as follows:

$$\frac{\kappa}{K_y} = \frac{M}{M_y} + A \left(\frac{M}{M_y}\right)^B \qquad\qquad [33.1]$$

where

κ = pipeline curvature
M = pipeline bending moment
$K_y = 2 \cdot \sigma_y/(E \cdot D)$
$M_y = 2 \cdot I_c \cdot \sigma_y/D$
E = modulus of elasticity of the pipe steel

D = diameter of the pipe steel
I_c = cross-sectional moment of inertia of the pipe steel
σ_y = nominal yield stress of the pipe steel
A, B = Ramberg-Osgood equation coefficients

Ocraflex

Orcaflex is a nonlinear, time domain, finite element software program principally used for the static and dynamic modeling of systems used in an offshore construction environment, including subsea pipelines and risers (flexible and rigid types) and mooring systems. Environmental effects, such as the seabed profile, different types of wave spectra, wind, and currents, can be applied to the model. The visualization of the Ocraflex software is based on Windows OS, which has better presentation effects than the OFFPIPE software.

Flexcom

Flexcom software uses a specialized FE formulation, incorporating a hybrid beam-bar element with fully coupled axial, bending, and torque loads, well suited for modeling subsea pipelines, risers, and mooring lines. Sea state modeling options are provided, and hydrodynamic loads is based on Morison's equation. Although originally a time domain analysis tool, more recently, the software has incorporated frequency domain analysis capabilities. It is also capable of performing modal analysis and estimating damage caused by fatigue.

For special consideration of local constraints or loads, more generalized computer software, like ABAQUS or ANASYS, may also be used for special installation methods, where OFFPIPE and Ocraflex software may not be applicable.

Code Requirements

For pipeline installation analysis, code requirements may be related to the pipeline curvature on the stinger and in the sagbending section for S-laying. Typical codes for subsea installation are API RP 1111 and DNV OS F101.

The stress or strain criteria used for the installation analyses are different, based on specific projects. In most cases, the strain criteria are used for the analysis. During pipeline installation, to avoid buckling, the allowable bending strains are limited by safety factors, f_1 and f_2, which are the bending safety factors for installation bending plus external pressure and in-place bending plus external pressure, respectively. These safety factors are determined by the designer with appropriate consideration of the magnitude increases that may occur for installation bending strain, ε_1, and in-place bending strain, ε_2. A value of 2.0 for safety factors f_1 and f_2 is suggested. Safety factor f_1 may be larger than 2.0 for cases where installation bending strain, ε_1, could increase significantly due to nonnominal conditions or smaller than 2.0 for cases where bending strains are well-defined.

However, in some projects, the stress criteria are also required to be used. For example, the acceptable stress criteria are 72% SMYS and 96% SMYS for pipeline sagbending area and overbending area, respectively, according to DNV OS F101. The stress analysis during the pipeline installation procedure should be carried out in detail to check the stress criteria.

5. Physical Background for Installation

S-lay Method

The S-lay vessel can be either a normal or semi-submersible vessel. What makes the laying vessel special is that it has a long ramp extension or "stinger" at the stern. There is a horizontal ramp on the vessel, which includes equipment like welding stations and tensioners. For this method, the welded pipe sections are laid on the seabed by moving the vessel forward with its anchors. A number of rollers are placed at the stinger of the vessel, which provides support for pipeline when it moves from the vessel and into the sea. The pipeline segment over the stinger is named the *overbending* section, as shown in Figure 33.5. The stinger radius controls the overbending curvature.

The number, position, and capacity of tensioners are usually different for pipe laying vessels. The last tensioner is normally placed at the stern of the vessel, close to the stinger. The first tensioner is placed somewhere on the horizontal ramp. The purpose of applying tension to the pipeline through these tensioners is to control the curvature of the pipeline to an acceptable limit to avoid overbending, as shown in Figure 33.10. The tension capacity for the vessel depends on the capacity of each tensioner and the total number of tensioners.

The required tension is a function of water depth, the submerged weight of the pipeline, the allowable radius of curvature at overbending, the departure angle, and the allowable curvature at the sagbending.
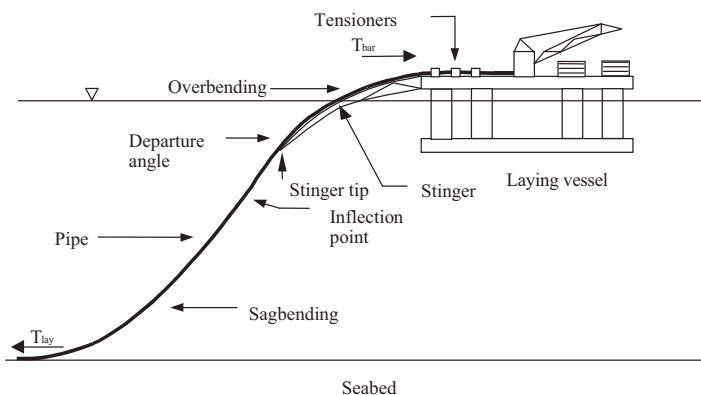
Figure 33.10 S-lay configuration.
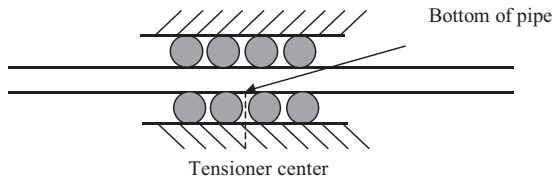
Figure 33.11 Typical tensioner support.

The stinger is normally made up of several sections. The position of the rollers relative to the section to which they belong can also be adjusted, which means that a vessel can be adjusted for a number of different radii of curvature. Generally speaking, the stinger on a laying vessel has an interval for the minimum and maximum radii of curvature. Because of this, each laying vessel also has an upper and lower limit for the pipeline angle of departure from the stinger. Through trimming the vessel, small changes can be made to the departure angle for a specific radius of curvature. The necessary laying tension is greatly influenced by the departure angle from the stinger. Moreover, the curvature of the supported pipeline is very often referred to as the *radius of curvature of the stinger*. This does not mean that the stinger has a constant radius of curvature equal to this value. It is more likely an average value for the radii of curvature that are caused by moveable rollers at the stinger and vessel.

The tensioners normally consist of upper and lower track loops. Wheels within the track loops apply squeeze forces to the tracks, which in turn grip the pipeline, as shown in Figure 33.11.

Static Configuration

During installation, the pipeline experiences a combination of loads. These loads mainly include tension, bending, pressure, and contact forces perpendicular to the pipe axis at the supports on the stinger and seabed. The static configuration of the pipeline is governed by following parameters:

- Tension at the laying vessel.
- Radius of curvature for the stinger.
- Roller positions.
- Departure angle from stinger.
- Pipe weight.
- Pipe bending stiffness.
- Water depth.

Curvatures in Sagbending and Overbending

Sagbending

Under the combined action of tension and pipe weight, the pipeline exhibits large deflection from its stress-free state. The curvature of the pipeline in the sagbend is

governed by the applied axial tension. The simplest model for presenting the relationship between tension and curvature is the catenary model. The catenary model ignores the flexural rigidity of the pipeline. The horizontal component of the tension (T_h) is constant from the point where the pipeline touches the seabed and up to the stinger tip. The vertical component of this force (T_v) increases from the touchdown point on the seabed up to the stinger, because of the submerged weight of the suspended part, see Figure 33.12.

The shape of the catenary can be expressed as

$$z = \frac{T_h}{w_s}\left(\cosh\frac{xw_s}{T_h} - 1\right)$$ [33.2]

where

x = horizontal distance from touch down point;
z = height above seabed;
T_h = horizontal force at seabed;
w_s = submerged weight per unit length.

The curvature is then

$$\frac{d\theta}{ds} = \frac{d^2z}{dx^2}\cos\theta = \frac{w_s}{T_h}\cosh\frac{xw_s}{T_h}\cos\theta$$ [33.3]

where

θ = angle to the x-axis
s = arc length
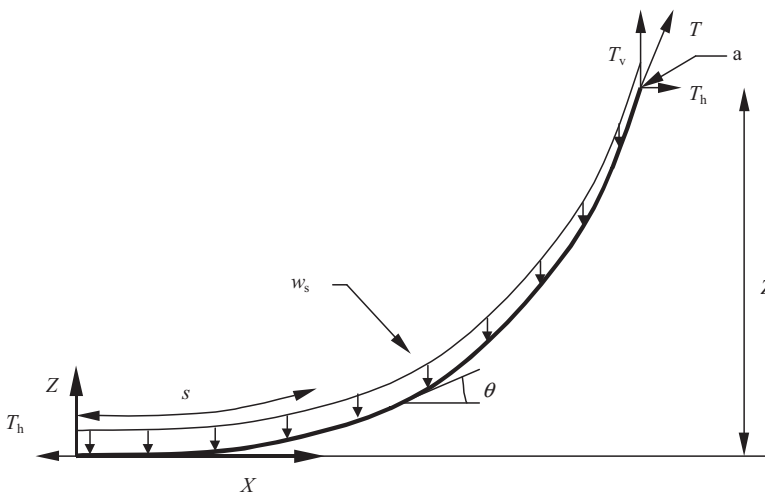
Figure 33.12 Catenary model.

The greatest curvature is at the touchdown point:

$$\frac{1}{R} = \frac{w_s}{T_h}$$
[33.4]

The relationship between curvature and strain for the pipe is

$$\varepsilon = \frac{r}{R}$$
[33.5]

The vertical component, T_v, is equal to the weight of the suspended part of the pipeline:

$$T_v = w_s s$$
[33.6]

where s is the length of the suspended part of the pipeline and can be expressed as

$$s = z\sqrt{1 + 2\frac{T_h}{zw_s}}$$
[33.7]

The angle between the pipeline and the x-y plane is

$$\tan(\theta) = \frac{T_v}{T_h}$$
[33.8]

The term T_h can be expressed through θ, w_s, and z by setting T_v into the expression for $\tan\theta$:

$$T_h = \frac{zw_s}{\tan^2\theta}\left(1 + \sqrt{1 + \tan^2\theta}\right)$$
[33.9]

The departure angle and the height above seabed at the stinger tip are given for a specific laying vessel and stinger radius, while the location of the inflection point is unknown. In deep water, it is reasonable to say that the departure angle from the stinger tip and the angle in the inflection point are approximately the same. The inflection point shown in Figure 33.10 is the same as point a in Figure 33.12. The horizontal tension can therefore be estimated using Eq. [33.9]. Since the inflection point and its location are unknown, the tension can be estimated through using the departure angle and height above seabed at the stinger tip. The predicated tension is overestimated, because θ is smaller and z is greater at the stinger tip than in the inflection point. The tension is also overestimated because the flexural rigidity of the pipeline has been neglected. The calculated curvature and strain in the sag-bend area conservative because of the neglect of the flexural rigidity of the pipeline.
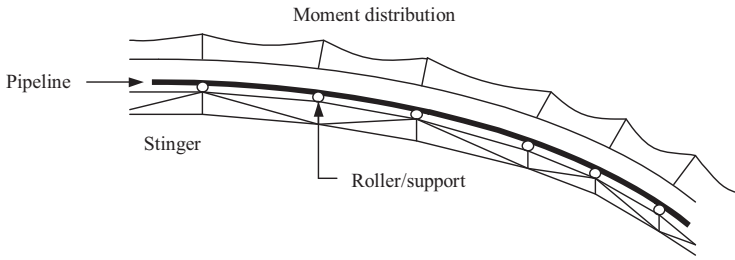
Figure 33.13 Moment distribution over the stinger.

Overbending

The part of the pipeline supported by the laying ramp that is made up of the rollers placed on the stinger and the vessel has the same curvature as the laying ramp. A target for installation analysis is to find the best laying ramp configuration for the pipeline that is going to be installed. The function of the laying ramp is to provide a curved support with an appropriate radius of curvature, which is used to control the overbending strain in the pipeline within an acceptable level.

The configuration and curvature of the pipe section in overbending are controlled mainly by the stinger. This means that the pipeline displacement is governed by the stinger and roller particulars.

The bending moment is not constant along the pipeline, due to the changing radius of curvature of stinger. In fact, the rollers and supports do not create a continuous support for the pipeline, which can trigger peak moment at the position of each roller. The moment distribution over the stinger is illustrated in Figure 33.13. Hence, it is very important to represent the stinger geometry as accurate as possible in the finite element model.

Hydrostatic Pressure

The pipeline is exposed to hydrostatic external pressure when it is submerged. There is no internal pressure during installation. The external pressure has an effect on the pipeline response. Radial pressure induces an axial strain via the Poisson's ratio effect:

$$\varepsilon_{xx} = -\frac{\nu}{E}(\sigma_h + \sigma_r) \qquad\qquad [33.10]$$

where:

ε_{xx} = axial strain
ν = Poisson's ratio
σ_h = hoop stress
σ_r = radial stress
E = Young's modulus
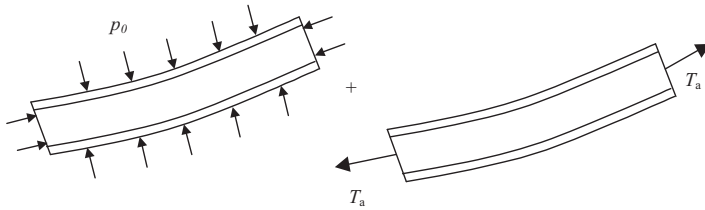
Figure 33.14 Effective axial tension.

The hoop and radial stresses are given by Lame's equation. If the pipe ends are free, the strain introduces no stress. However, if the ends are constrained, axial force develops. This effect is similar to thermal loads.

When the pipe ends are capped, a force is induced:

$$T_p = p_o A_o - p_i A_i \qquad\qquad [33.11]$$

where

p_o = external pressure
p_i = internal pressure
A_o = outside cross-sectional area
A_i = inside cross-sectional area

The distributed pressure on a deflected pipeline alters the tension-stiffening effect and indirectly affect the curvature of pipeline.

As shown in Figure 33.14, the effective axial tension, T_e, in the pipeline is defined as

$$T_e = T_a + T_p \qquad\qquad [33.12]$$

The definition of effective axial tension was already discussed in Chapter 9. The true tension is an integration of stress over the cross section of the steel wall. In deep water, T_p usually is greater than T_a. The result of this is that T_e becomes negative and the pipe section, as a beam, is in state of compression instead of tension. The force T_p is a function of the water depth, so T_e always is positive at the sea surface and positive or negative at the seabed, depending on the relationship between T_a and T_p.

Strain Concentration and Residual Strain

Offshore pipelines are usually coated with concrete to counteract buoyancy and guarantee on-bottom stability. The pipeline is also covered with anticorrosion coating. The effect of the coating weight may be easily accounted for in analysis. The concrete coating also has an effect on the pipe stiffness, this is because the concrete has high compressive strength and low tensile strength; however, this effect can be neglected for FE model analysis. Due to the discontinuity of concrete coating, a strain concentration may occur at field joints during bending of the pipeline.
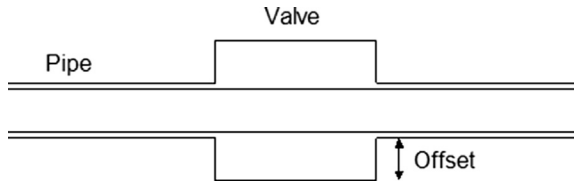
Figure 33.15 Offset of pipeline when valve is located at the support.

During installation, the pipeline is exposed to plastic strains when the pipeline passes over the stinger with a relative big curvature. This means that the pipeline leaves the stinger with a residual strain. When passing the inflection point, the bending of the pipeline is reversed; that is, the residual strain has to be overcome. This phenomenon occurs partially through bending and partially twisting. The pipeline has residual strain when it is installed at the seabed, because it has been exposed to plastic strains (Endal et al., 1995) [5].

Rigid Section in Pipeline

A valve usually has a larger outer diameter and is more rigid than the adjacent pipeline, which can cause a higher bending moment. The increase in bending moment can trigger higher strains in the adjacent pipeline. Therefore, to reduce the bending moment in the sagbend, a higher laying tension should be applied to the pipeline. The laying tension then is higher than normal value as long as the valve is located in the sagbend.

Reducing the bending moment in overbending can be more complicated. When the valve is located at a support, the pipeline are lifted locally, because the valve has a larger outer radius than the pipeline, which can cause a great extra bending moment in the pipeline. The lifted distance is named *offset*, see Figure 33.15.

One way to reduce the bending moment in overbending is to increase the stinger radius. The laying tension for the entire pipeline is higher if the stinger radius is increased to reduce the bending moment. In addition, increasing the stinger radius may not reduce the moment much in overbending. Keeping the strain in the adjacent pipeline at an acceptable level may require strapping wood timber (or something similar) onto the adjacent pipeline sections. This strapping of wood timber is called *tapering*; the timber can be strapped to the underside of the pipeline on each side of the valve, as shown in Figure 33.16. This tapering can have different shapes, such as linear or parabolic.

The positive effect from this tapering is a reduction of the bending moment in the pipeline caused by an offset. The tapering has to be able to withstand the loads between the pipeline and the support. If the pipeline is not tapered, the reaction force normal to the valve is overstressed locally. However, by tapering the pipeline, the reaction force is evenly distributed to the adjacent supports. Furthermore, the local change in pipe curvature is less as a result of tapering.
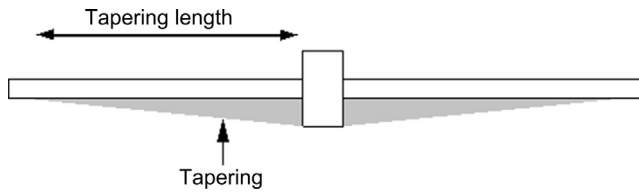
Figure 33.16 **Principle of tapering for a pipeline with a valve.**

Dry Weight and Submerged Weight

In "real life," the steel pipe is covered with anticorrosion coating and concrete coating, which have different mass of density with respect to steel. What is worth mentioning is that, in the analysis, the total weight of the pipeline has to be represented only by the steel pipe, because just the bare steel pipe is modeled in the analyses. Therefore, equivalent density has to be used for the steel (material) in the analysis rather than the actual steel density from the design data.

During installation, a part of the pipeline is above the sea surface and the rest is under the sea surface. From a point at the stinger, the pipeline is submerged into the water. The pipeline then is exposed to a buoyancy force and hydrostatic pressure. This is applied to the pipeline in ABAQUS by using the command PB. This command can apply a distributed pressure load and a distributed buoyancy load to the submerged part of the pipeline.

When computing the distributed buoyancy loads, ABAQUS assumes closed-end conditions. The pressure field varies with the vertical coordinate z. For hydrostatic pressure, the dependence on the vertical coordinate is linear in z:

$$p = \rho g(z_0 - z) \tag{33.13}$$

Here z_0 is the vertical location of the free surface of the fluid, ρ is the density of the water, and g is the acceleration due to gravity.

Pipe Rotation

Severe pipe rotation has been experienced during deepwater pipe laying, but the reasons causing this phenomenon are still not understood in the industry. While analytical models have demonstrated the influence of residual curvature on pipe rotation, 3D FE simulations of the pipe-laying process are needed to predict rotation.

Damsleth et al. (1999) deals with the consequences of the plastic strain that can occur in the outer fibers of the pipe wall as it passes over the stinger during laying [6]. Endal et al. (1995) shows that the pipe twists, that is, rotates around its axis [5]. They also show that, provided the plastic strain is small, the on-bottom configuration is straight and flat as for an entirely elastic process. Thus, the main consequence is the rotation during pipe laying. They also state that pipeline twist acts only in the elastic

sagbending (or underbending) section and can be characterized as a typical instability phenomenon.

During installation, the pipe extends from the horizontal tension machine, bends over the stinger, and while sloping downward through the water, bends gradually in the opposite direction onto the horizontal seabed. The tensioner provides the upper support for the pipe while the seabed provides the lower support, where residual tension is balanced by friction. Customary terms used to describe this S-lay pipe configuration are *overbending, inflection point* and *sagbending*.

How does the residual strain in the overbending change the value of the potential energy? An example illustrates this point: Consider first that the suspended pipe is entirely in the vertical plane. Assume two pipe laying scenarios that differ only because one material remains completely elastic whereas the other experiences plastic strains in the overbending section on the stinger. In the sagbending section, the pipe with plastic strain hangs higher than the elastic one, because its natural (unloaded) shape has become convex. This means that the potential energy is higher for the plastically deformed pipe than for the elastic one. Allowing for a 3D deformation, the bent pipe can reduce its potential energy through twisting. The elastic pipe is already at its lowest potential energy, and so it is stable.

It is reasonable to conclude from this argument that the reduction of potential energy is the mechanism that underlies pipeline rotation during pipe laying. The theory of large deflection of beams is found in classic texts, such as Landau or Love. A nonlinear 3D finite element program can solve the virtual work equation with very few approximations. Three simple models illustrate the main point of interest. All represent a pipe of length 1218 m and with $D/t = 36$. All are fixed at one end and pinned at the other end, where a sliding condition is specified. Both ends are at the same elevation, and the body force is equal to the submerged weight. To produce elastic strains below 0.035%, an appropriate horizontal force is applied in the pinned end to represent the laying tension.

A 3D load case is created by means of a horizontal force corresponding to a sea current of 0.5 m/s applied normal to the plane of the equilibrium configuration. First, the horizontal force is applied, then the submerged weight. Before the application of the horizontal force, the pinned end is locked in all translational degrees of freedom at their current values. The models are

1. Straight pipe.
2. Precurved "overbending" pipe, $R = 571$ m.
3. Precurved "sagbending" pipe, $R = 571$ m.

The displacement and rotation of a point in the middle of the span is studied for each of the models. The equilibrium configurations shown are similar to that of the sagbending during pipe laying, where the pipe is subject to its submerged weight and axial tension. The precurved overbending pipe represents a pipe that has been plastically deformed on the stinger to give 0.1% residual strain, while the precurved sagbending pipe illustrates a naturally stable case from the gravitational viewpoint. The reference system has its *x*-axis origin at the fixed point with positive direction toward right in the figures that follow and positive *z* upward.
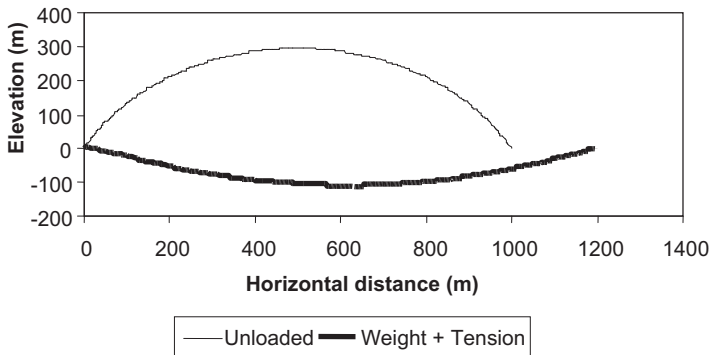
Figure 33.17 Precurved "overbending" model in its free and loaded conditions.

Figures 33.17 and 33.18 show the installed pipeline configurations in both unloaded shapes and equilibrium configurations under tension and weight. One important observation can be made from the equilibrium of the overbending curve: Since the midpoint is below the horizontal plane, this pipe would have ended up flat if laid on the seabed, as found by Endal et al. (1995) [5].

Figure 33.19 shows the lateral deflections under horizontal loading. All three curves show practically the same deflections, as expected. The twist of the midpoint is exhibited in Figure 33.20. The horizontal axis represents the evolution of the rotation as the applied horizontal force raises from zero to full value. First, consider the straight model. It has negligible twist around the x-axis. The sagbending curve rotates at maximum $1°$ in the direction of a pendulum. However, the overbending curve shows a rotation of $17°$ in the negative direction. When it rotates, it tries to tip over from the overbending shape into the sagbending shape to reduce its potential energy. At the same time, twist energy starts to increase, reaching equilibrium when the two energy changes are equally large.
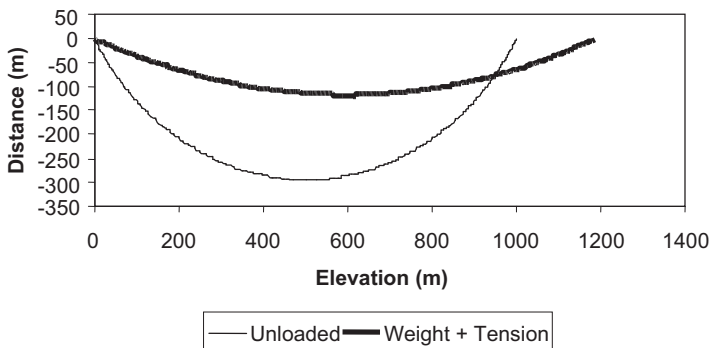
Figure 33.18 Precurved "sagbending" model in its free and loaded conditions.

Lateral deflection at mid-span
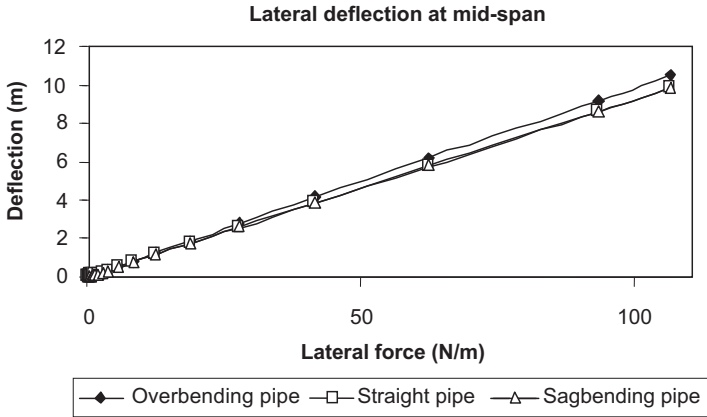
Figure 33.19 Displacement at mid-span subject to a lateral force.

While twist cannot occur in the 2D case, the simple models demonstrate that 3D is a necessary, but not sufficient, condition for twist. Endal et al. (1995) [5] characterize the twist as instability. We repeat their analysis with a stiff pipe ($D/t = 36$), where the twist emerges much more slowly. In a model of the pipe laying process, the initiation of the laying with plastic strain over the stinger shows that the twist occurs even more slowly. After a few kilometers of pipe laying, the twist in one joint has a constant angular velocity as the joint leaves the stinger and descends toward the seabed. The nature of the twist phenomenon is, thus, in general, not instability.

Pipe rotation at mid-span
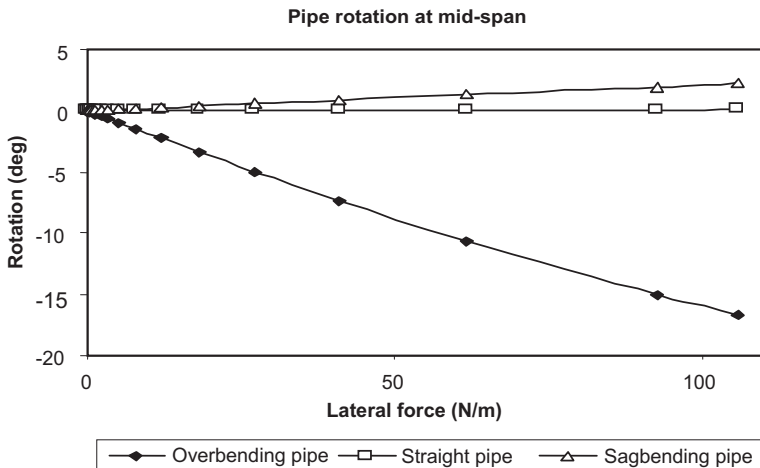
Figure 33.20 Rotation at mid-span subject to a lateral force.

Installation Behavior of Pipe with Residual Curvature

Pipe laying vessels have gradually adapted to the technical challenges of deepwater projects by increasing their tension capacity and stinger length. The larger laying vessels have reached physical limitations, where further increase in their capacity would, in principle, be too costly for a low–price oil scenario. Increasing the utilization of the pipe strength capacity by curving the stinger more sharply to obtain steeper departure angles is a cost-effective alternative. Since the tension required to install the pipe is lower, it brings the added benefit of reducing the seabed intervention needed for free span support [6, 7]. See Damsleth et al. (1999) [6].

Today's larger S-lay vessels are fitted with total tension capacity of 300 to 600 tonnes. The stingers are 60 to 100 m long to cope with installing pipelines in 300 m to 700 m water depths. But the present 45° to 55° stinger departure angles result in about half the laying tension remaining with the pipe on the seabed. In areas where the seabed is uneven, the high residual tension develops both larger and more frequent free spans. To obtain the lowest residual tension, the stinger must provide a departure angle as steep as possible.

The stingers of most of the larger pipe laying vessels have already been extended to install increasing pipe sizes in deeper water. Extending them further would make them more vulnerable to environmental loads and increased weather downtime. To install large-diameter pipe in very deep water (1500 m to 2500 m) with the present tension capacity requires stingers with up to 90° departure angles. The present stinger arc lengths can be maintained while the curvature is increased. Depending on the D/t of a given pipe size, a permanent curvature in the overbending may develop, causing eventual pipe rotation.

While the controlled curvature of the stinger permits the use of strain criteria, deeper water installation demands stinger curvature leading to greater plastic deformation of the pipe in the overbending. Detailed structural analysis can be used to develop project-specific strain criteria for installation (Bai et al. 1999) [7] that allows plastic strain in the overbending. However, it has been demonstrated that permanent curvature of the pipe can lead to unacceptable rotation, where Tees and other fixtures are to be installed in the line. This phenomenon need not become an installation problem, provided the rotation can be predicted and controlled.

It is difficult to quantify pipeline twist for the construction phase, since the behavior of the pipeline during installation is specific to the pipe's characteristics and the installation configuration. While design codes provide criteria for maximum overbending strain to avoid pipeline twist, the resulting laying configuration may be too costly. Or, strain concentrations due to coatings, undermatched welds, buckle arrestors, and other in-line components may produce permanent overbending curvature that could cause pipe rotation.

Therefore, nonlinear 3D FE models using elastoplastic beam and friction or contact elements are used to analyze the load history of the pipeline during the pipe laying process, which accounts for the complex interaction between constant as well as time and position varying loads involving all six degrees of freedom. The FE model can simulate pipeline rotation to determine whether control measures are necessary, as well as demonstrate the effectiveness of correction measures.
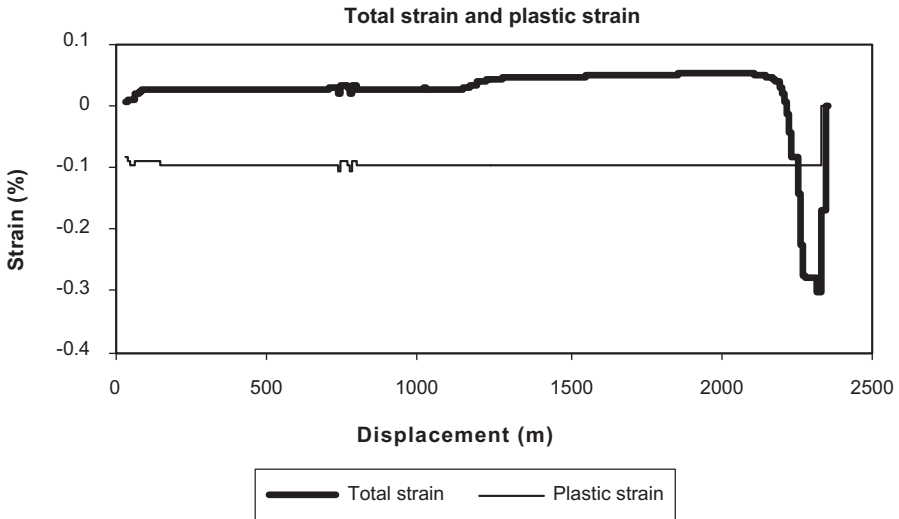
Figure 33.21 Total axial strain and plastic strain in an elastoplastic pipe from free end on seabed to tensioner.

Figures 33.21 to 33.23 illustrate the twist phenomenon during laying of a 2.4 km section of deepwater pipeline with a 0.5 m/s lateral current. Pipe laying initiation was by deadman anchor so that the end was free to rotate. Rotational friction on the seabed is ignored in this case.

Figure 33.21 shows the situation after 2.4 km of pipe laying, indicating total strain and permanent strain in the vertical plane after the pipe has been subject to elastoplastic bending over the stinger during laying. Figure 33.22 shows a net rotation of 60° of the free end due to the twist effect for an elastoplastic pipe material and 0° for a completely elastic pipe. Figure 33.23 shows the resulting rotational moment along the elastoplastic pipe that compares to the near-zero moment of the elastic pipe. The only difference between the curves is due to the 0.1% residual strain of the elastoplastic pipe material, demonstrating that plastic strain, combined with a lateral disturbing force, is the source of the pipe rotation.

With 0.1% residual strain, this pipe lays flat on the seabed. The 60° rotation along the free span, and seabed poses no problem unless in-line components requiring access are present. In this case, the most cost-effective solution is to design the big launcher for multiple point access, because the pipe may continue rotating as the laying vessel moves forward until friction builds up.

6.   Analytical Method for S-Lay Installation

According to different mechanic characteristics, the pipeline analytical model from the tensioner to the seabed is divided into four sections [8, 9]: the first section is from the tensioner to the separation point of the stinger; the second section is from the
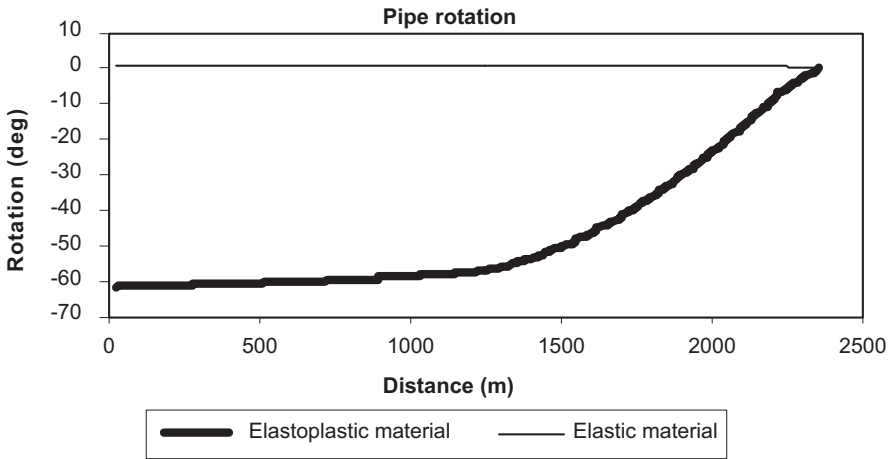
Pipe rotation

Figure 33.22 Axial rotation of the pipeline from the free end.

separation point to the inflection point; the third section is from the inflection point to the touchdown point; the fourth section is from the touchdown point to the pipeline section contacting with the seabed. In this section, a numerical iteration model for deepwater pipeline S-lay laying process is proposed and the continuity between the neighboring sections is well guaranteed. Figure 33.24 illustrates the S-lay pipeline configuration.

The First Section

The first part is laid on the stinger, where the curvature is the same as the stinger. The coordinate system is created and the origin is located at the tensioner, which is shown in Figure 33.25.

Torsional moment
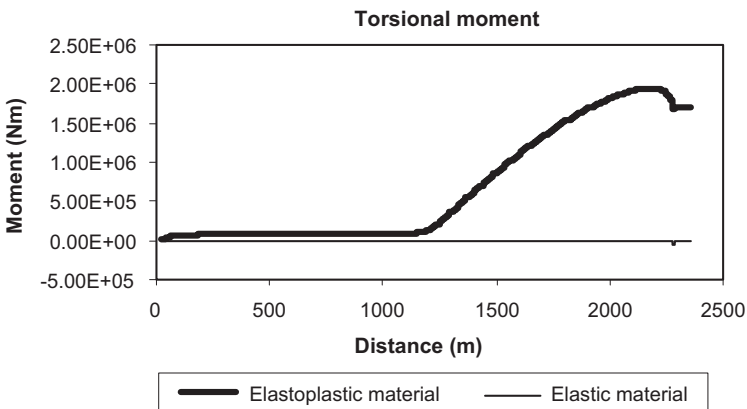
Figure 33.23 Torsion moment in pipeline from free end on seabed to tensioner.
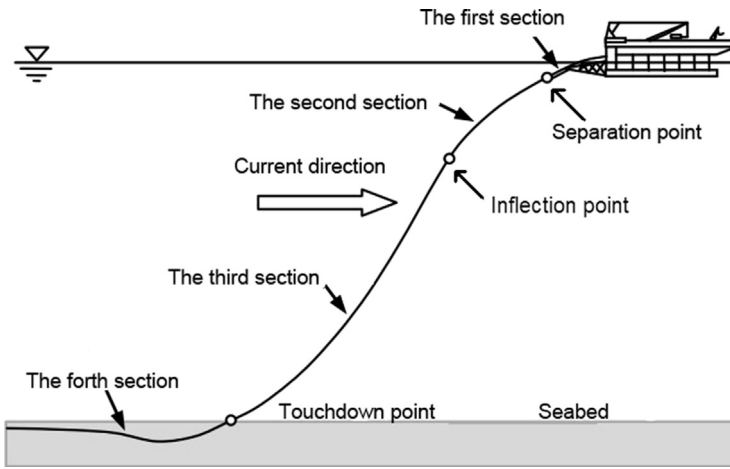
Figure 33.24 Configuration of pipeline by the S-lay method.

The pipeline of this section comprises two parts: part A in the air and part B in water. For a differential segment of part A, the forces acting on this segment contain self-weight, stinger resistance, and tensioner tension; while the segment of part B contains extra hydrodynamic forces. The force diagrams of the differential segments in the air and in water are shown in Figure 33.26.

To the section in the air, w_a is the unit weight of pipe in air; therefore, the equilibrium equation is

$$T\cos\frac{d\phi}{2} - w_a ds \cdot \sin\left(\phi + \frac{d\phi}{2}\right) - (T + dT)\cos\frac{d\phi}{2} = 0 \qquad [33.14]$$
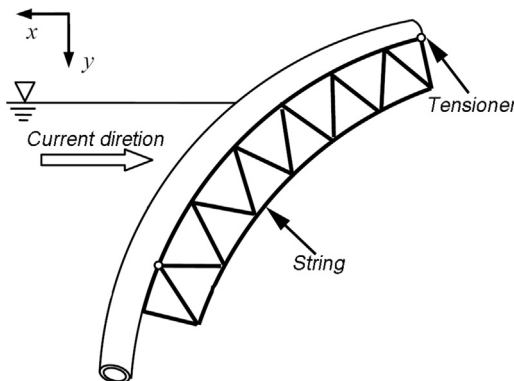
Figure 33.25 Scheme of the first section.

(a) **Part A**   (b) **Part B**
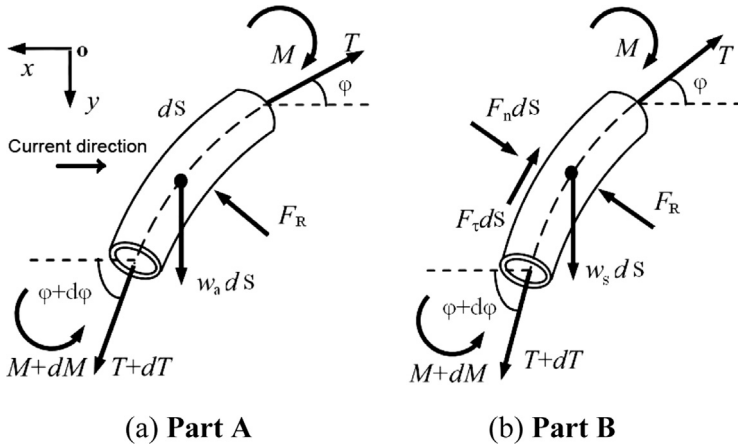
Figure 33.26 Force equilibrium for the first section.

Equation [33.14] is revised to

$$dT = -w_a ds \cdot \sin\phi \qquad [33.15]$$

The section in seawater, where w_s is the unit weight of pipe in water, takes into account the force from ocean current, so the equilibrium equation is

$$T\cos\frac{d\phi}{2} + F_\tau ds - w_s ds \cdot \sin\left(\phi + \frac{d\phi}{2}\right) + (T + dT)\cos\frac{d\phi}{2} = 0 \qquad [33.16]$$

After deductions, Eq. [33.15] turns out to be

$$dT = -w_a ds \cdot \sin\phi + F_\tau ds \qquad [33.17]$$

where the ocean current force can be calculate by using Morison equation. In the interaction of axial force and moment, the axial stress and strain can be calculated according to knowledge of material mechanics:

$$\varepsilon = \frac{T}{EA} + \frac{\phi(R_s \pm r) - \phi R_s}{\phi R_s} = \frac{T}{EA} \pm \frac{r}{R_s} \qquad [33.18]$$

$$\sigma = E\varepsilon = \frac{T}{A} \pm \frac{Er}{R_s} \qquad [33.19]$$

where the sign $\pm$ means that when the pipeline is stretched under the bending moment, the sign $+$ is adopted; while the pipeline is compressed, the sign $-$ should be used.

The Second Section

The second section (Figure 33.27) is from the separation point to the inflection point, so the curvature of this part is not only affected by hydrodynamic forces and self-weight but also greatly influenced by the bending moment at separation point. Thus, the curvature of the pipeline can be expressed as

$$\frac{1}{R(s)} = \frac{1}{R_{\mathrm{m}}(s)} - \frac{1}{R_{\mathrm{w}}(s)} - \frac{1}{R_{\mathrm{c}}} \qquad [33.20]$$

where

s = arc length beginning from the separation point
$1/R(s)$ = pipeline curvature at arc length of s
$1/R_{\mathrm{m}}(s)$ = curvature caused by moment at the separation point
$1/R_{\mathrm{w}}(s)$ = curvature by pipeline's gravity
$1/R_{\mathrm{c}}$ = curvature by the current

According to beam theory, the expressions are shown as follows:

$$\frac{1}{R_{\mathrm{m}}(s)} = \frac{1}{R_{\mathrm{st}}}\left[ch\sqrt{\frac{T}{EI}}\,s - sh\sqrt{\frac{T}{EI}}\,s\right] \qquad [33.21]$$

$$\frac{1}{R_{\mathrm{w}}(s)} = \frac{w_{\mathrm{s}}\cdot\cos\phi}{T} \qquad [33.22]$$

$$\frac{1}{R_{\mathrm{c}}} = \frac{F_{\mathrm{n}}ds}{2EI} \qquad [33.23]$$
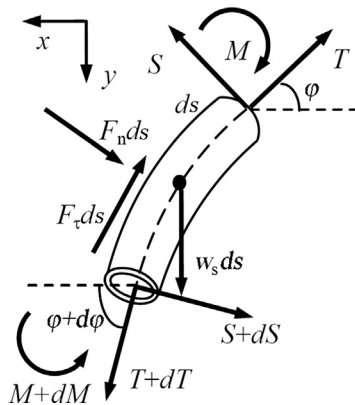
Figure 33.27 Force equilibrium for the second section.

By taking the force equilibrium, the governing equation in the tangential direction can be expressed

$$dT = -w_s ds \cdot \sin\phi + F_\tau ds \qquad [33.24]$$

The Third Section

The curvature is mainly affected by the tension from top pipelines in the sagbending region (Figure 33.28). Considering mechanic properties of this section, the catenary method can be used to well simulate pipeline's spacial configuration.

In the vertical direction for the force balance, the equation can be derived as follows:

$$w_s ds + T_v + dT_v - F_\tau ds \cdot \sin\phi + F_n ds \cdot \cos\phi = 0 \qquad [33.25]$$

After deduction, Eq. [33.25] turns out to be

$$dT_v = F_\tau ds \cdot \sin\phi - F_n ds \cdot \cos\phi - w_s ds \qquad [33.26]$$

Similarly available in the horizontal direction,

$$dT_h = F_n ds \sin\phi + F_\tau ds \cos\phi \qquad [33.27]$$

The moment in the pipeline can be approximately calculated with the moment equation in material mechanics:

$$M = -\frac{EI}{R(s)} \qquad [33.28]$$
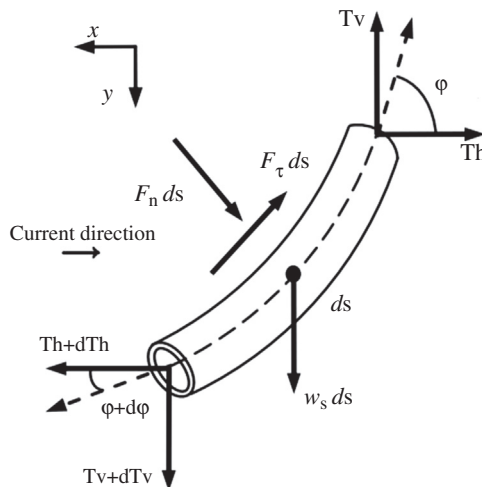
Figure 33.28 Force equilibrium for the third section.
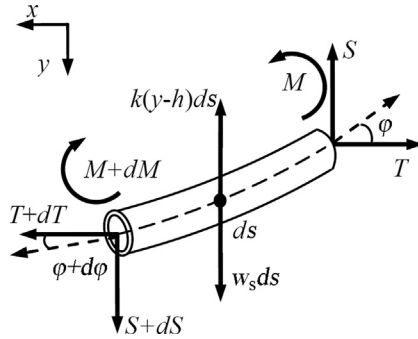
Figure 33.29 Force equilibrium for the fourth section.

The Fourth Section

In this section, the subsea soil could not be totally rigid, especially in the actual laying process (Figure 33.29). Therefore, it is assumed that the seabed is an elastic base and analysis requires a differential equation based on beam theory, as follows:

$$EI\frac{d^4y}{dx^4} - T\frac{d^2y}{dx^2} + k(y - h_1 - h_2) = w_s \qquad [33.29]$$

where T is a constant. For $T > 2\sqrt{EIk}$, no real solution can be obtained, but for $T \leq 2\sqrt{EIk}$, the general solution can be obtained as

$$y = h_1 + h_2 + \frac{w_s}{k} + c_1 e^{-\alpha x}\cos(\beta x) + c_2 e^{-\alpha x}\sin(\beta x)$$
$$+ c_3 e^{\alpha x}\cos(\beta x) + c_4 e^{\alpha x}\sin(\beta x) \qquad [33.30]$$

where

k = seabed stiffness
h_1 = height from the deck to water surface (free board)
h_2 = water depth
$\alpha = \frac{1}{2}\sqrt{2\sqrt{\frac{k}{EI}} + \frac{T}{EI}}$
$\beta = \frac{1}{2}\sqrt{2\sqrt{\frac{k}{EI}} - \frac{T}{EI}}$

Considering the boundary condition for infinite distance, especially when $x \to \infty$, $y \approx h_1 + h_2 + w_2/k$, so $c_3 = c_4 = 0$, thus, the differential equation can be simplified as

$$y = h_1 + h_2 + \frac{w_s}{k} + c_1 e^{-\alpha x}\cos(\beta x) + c_2 e^{-\alpha x}\sin(\beta x) \qquad [33.31]$$

Then, the associated moment in pipeline can be expressed as

$$M = -EI\frac{d^2y}{dx^2} \tag{33.32}$$

7. FEA of Pipeline Installation with an In-line Valve

Pipeline Static Configuration

Martinsen [10] gives an FEA for installation analysis of a pipeline with in-line valve in his Master's thesis, supervised by the author. The FE analysis procedure using ABAQUS software for the installation is detailed in this section.

- **Load step 1:** The initial configuration for the pipeline is a straight line when starting to find the static configuration for the pipeline. In step 1, a horizontal concentrated force is applied at the pipeline end, as shown in Figure 33.30. An estimate of the necessary force can be calculated with Eq. [33.9].
- **Load step 2:** A prescribed displacement in the vertical direction is applied at the pipeline end, as shown in Figure 33.31. The prescribed displacement induces a displacement of the node in the *x*-direction and rotation about the *z*-axis. The concentrated force is a follower force. This means that the direction of the force rotates with the rotation of the node. During this step, a part of the pipeline encounters the stinger. This part of the pipe is bending. The rest of the pipe is still almost straight.
- **Load step 3:** The dry weight, buoyancy, pressure, and the distributed load specified in the user subroutine are applied. The node where the concentrated force is applied moves left until the pipeline has found static equilibrium, as shown in Figure 33.32. The pipeline has to be long enough in its initial configuration that a part of the pipeline lies horizontal and slides on the seabed when the static configuration is computed.

The required tension at the laying barge for installation of the pipeline is the reaction force at the fixed node. The load effect on the pipeline for the applied tension has to be checked against the design criteria. The result of this check may be that the applied

Figure 33.30 Pipeline initial configuration and load step 1.
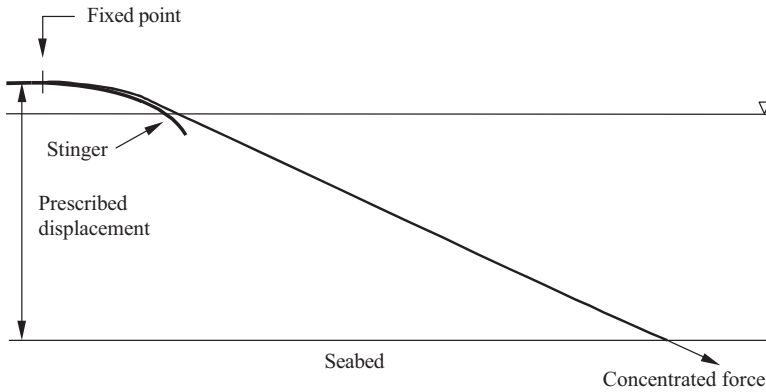
Figure 33.31 Pipeline configuration after load step 2.

tension has to be changed. The pipeline has found its static configuration, but the design criteria tell us that the tension has to be increased or that it can be decreased This procedure can be done repeatedly until a load that satisfies the design criteria has been applied. For each new try, there is enough to change the concentrated load in the restart file and read from the original results file.

Pipeline Sliding on a Stinger

A pipeline with a length equal to the length that is going to be installed on the seabed has to be specified in front of the first tensioner (fixed point). A horizontal surface is also specified in front of the first tensioner to support this part of the pipeline. The pipeline is fixed at two nodes on the laying ramp. These nodes are the one located at the same place as the first tensioner and the end node of the pipeline, located at the "vessel". The initial configuration of the pipeline is then as in Figure 33.33.
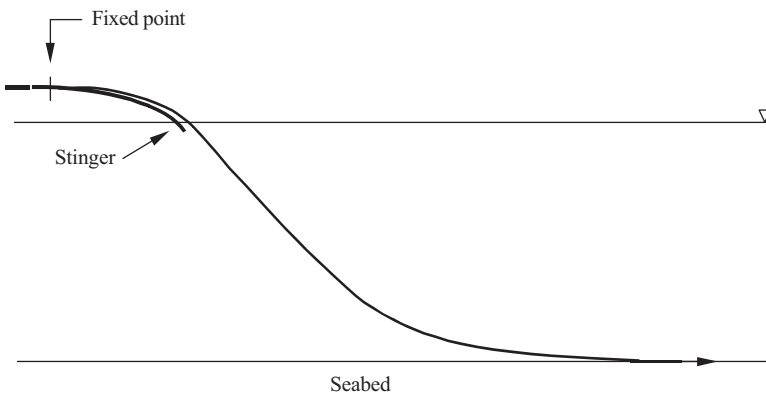
Figure 33.32 Pipeline configuration after load step 3.
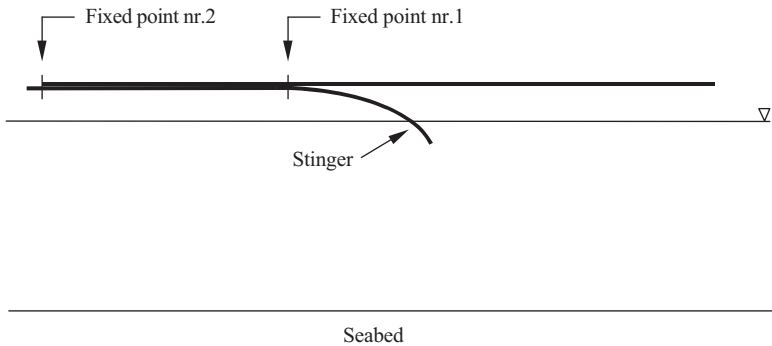
Figure 33.33 Initial configuration.

The first three load steps are the same as used for finding the static pipeline configuration explained in last section. Weight, buoyancy, and pressure are applied to the entire pipeline in load step 3. This means that weight is applied to the entire pipeline and pressure and buoyancy to the submerged part of the pipeline. In load step 4, the boundary conditions in fixed point nr.1 (No. 1) are changed. The pipeline separates 0.01–0.1 m from the stinger at this point when the node is released. The result is a small change in the static configuration for the pipeline and the contact forces between the pipeline and the stinger.

The next and last step is to move the surface representing the laying vessel/stinger to the left. The whole laying vessel/stinger has one single reference node. The laying vessel/stinger is then moved through moving the reference node in Figure 33.34. Point nr.2 (No. 2) remains fixed. A pipeline cross section then moves from the vessel, over the stinger, and through the sagbending to the seabed.

Convergence problems often occur when the node in fixed point nr.1 is released. The longer the distance between fixed point nr.2 and fixed point nr.1 is, the more difficult it is to make the model converge.
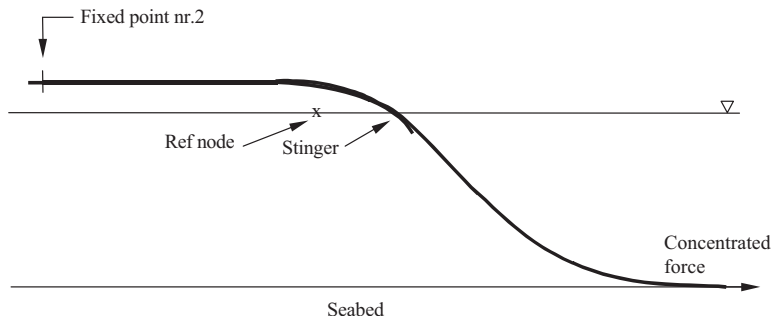
Figure 33.34 Pipeline configuration before the pipeline slides on the stinger.

Installation of the In-line Valve

The purpose of this design example is to illustrate the effect an in-line valve has on the strain level in the pipeline. Analyses are performed for a valve located in sagbending and a valve located at a support on the stinger. The results also is compared with the design criteria regarding the allowable strain level in sagbending and overbending, as defined in Statoil specification F-SD-101:

- Pipeline overbending (stinger) 0.23%.
- Pipeline sagbending (suspended part) 0.15%.
- No contact between pipeline and last support.

The problem with installation of an in-line valve is the increase in bending moment and strain locally, because the valve's stiffness is larger than the adjacent pipeline. The increase in bending moment because of valve's a larger stiffness occurs both in overbending and in the sagbending. The increase in bending moment induces higher strains in the adjacent pipeline. If the strain in the adjacent pipeline in the sagbending exceeds the design criteria, a higher laying tension can be applied to the pipeline to reduce the strain.

When a valve is placed at a support, the adjacent pipeline is lifted as a result of the contact between the valve and the support. This also leads to an increased bending moment locally. The result of these two effects is that the strain in the adjacent pipeline increases. To reduce the increased bending moment, because the pipeline is lifted, the pipeline can be tapered.

8.   Two-Medium Pipeline Design Concept

Introduction

The design and construction of pipelines is one of the key issues for the development of deepwater production and transportation facilities. The installation of large-diameter trunk lines has been limited to around 600 m (Rivett et al., 1997 [11]). Smaller-diameter pipelines have been installed in as much as 3000 m depth. New challenges presented by projects currently undertaken in even deeper water confront the present pipeline technology and stimulate the development of new concepts (Dretvik and Damsleth, 1998 [12]; Walker and Tam, 1998 [13]).

It is known that line pipe material cost takes a large portion of the CAPEX of pipeline projects. Using present technology, installation design for external pressure govern wall thickness selection for deepwater pipelines. There is a need to develop design concepts to avoid this situation (Palmer, 1997 [14]) and make deepwater pipelines as commercially competitive as their shallow water counterparts.

Until a few years ago, pipeline design was based on simplified capacity equations and some special purpose computer programs for installation and on-bottom stability design. Recently, use of nonlinear finite element simulations and limit state design has become acceptable practice (Bai and Damsleth, 1997 [15], 1998 [16]) in situations where design criteria have a significant cost impact. The technological advances in

finite element simulation have permitted project-specific optimizations that have saved up to 16% of the pipeline CAPEX development (Holme et al., 1999 [17]) for pipelines in water depths of 350 m. The potential for optimization can be even greater for deeper water pipelines.

Wall Thickness Design for Three-Medium and Two-Medium Pipelines

Subsea pipelines have historically been designed for three different mediums: air (during installation), water (during precommissioning), and the product (gas or oil). In shallow water, air-filled pipelines at near atmosphere pressure cause no particular difficulty, because the wall thickness is sized for the internal pressure of the product or the pressure test. In deep water, provided the same installation and operation approach is adopted, the pipeline is sized for external pressure for the installation phase. This phenomenon is clearly illustrated in Figures 33.35 and 33.36, which show how the operation, testing, and installation phases dictate the pipeline wall thickness requirements for increasing water depths. This section presents a new design concept for deepwater installation, which is called *two-medium pipeline* (Bai et al., 1999 [7]).

If the pipeline is designed to carry two mediums, water (during installation and testing) and product (gas or oil during operation), then the wall thickness requirements can be drastically reduced for the deepwater pipeline. This approach (Figure 33.35) is not limited by collapse resistance until a significantly deeper water depth is reached (Figure 33.36). Hence, the wall thickness requirements should be less for dense oil than for gas.

Installing Free Flooding Pipelines

Installing pipelines dry has been logically adopted as the laying tensions can be kept relatively low and a large margin is gained with the increased submerged weight
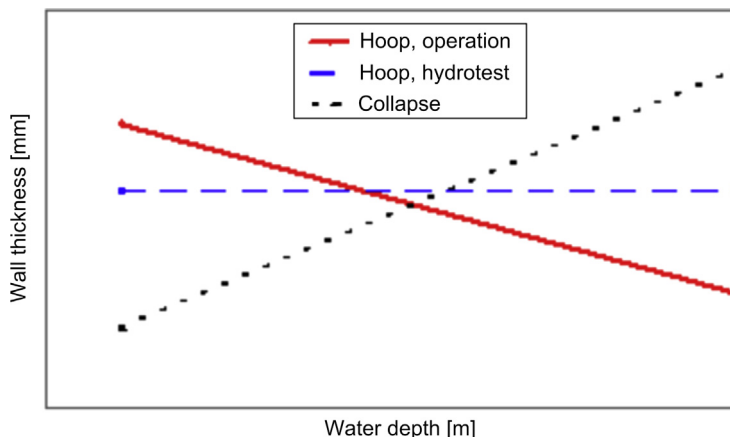
Figure 33.35 Wall thickness selection as a function of water depth (three mediums). (For color version of this figure, the reader is referred to the online version of this book.)
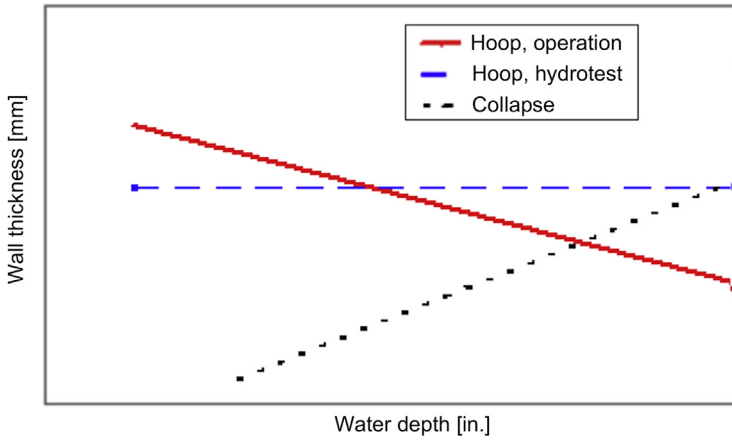
Figure 33.36 Wall thickness selection as as function of water depth (two mediums). (For color version of this figure, the reader is referred to the online version of this book.)

during operation (for stability purposes). This logic is sound in shallow water but cannot be extrapolated to depths in excess of 1000 m. The required wall thickness of an air-filled pipeline becomes so large that the associated submerged weight requires laying tensions significantly greater than present laying barge capacity.

To illustrate this phenomenon, Figures 33.37 and 33.38 show the required pipeline wall thickness for a range of pipeline diameters. For the purposes of comparison, it is assumed the pipeline is carrying oil at a density of 800 kg/m^3 at a pressure of 200 barg. Figure 33.37 illustrates the wall thickness for a pipeline installed while empty, and Figure 33.38 illustrates the associated wall thickness when the pipeline is installed flooded.

When the line is installed empty, a direct consequence of the wall-thickness required in deep water is the large submerged weight. This becomes significant
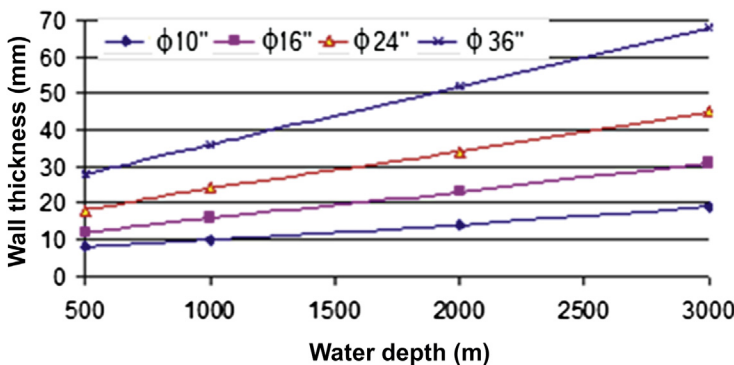
Figure 33.37 Pipeline wall-thickness for installed empty pipeline. (For color version of this figure, the reader is referred to the online version of this book.)
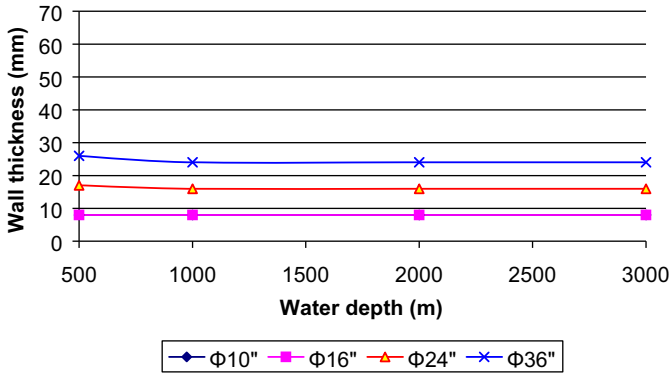
Figure 33.38 Pipeline wall-thickness for installed flooded pipeline. (For color version of this figure, the reader is referred to the online version of this book.)

when water depth is deeper than 1000 m, where the submerged weight doubles every 1000 m (Figure 33.39). As would be expected, the submerged weights are still lower than having a flooded line, until water depths of circa 2000 m are reached. At 2000 m, the submerged weight of a flooded line can be less than an empty line, because hydrostatic collapse is not a failure mode.

Figure 33.40 illustrates the associated pipeline submerged weights for a range of pipeline diameters when installed wet. The on-bottom stability requirements benefit from the increase in the submerged weight due to the heavier wall thickness. This example has not accounted for thermal insulation coating, which would reduce the submerged weights while still satisfying stability requirements.

S-lay versus J-lay

The offshore pipeline industry is familiar with installing air-filled pipelines by the S-lay method. An indication of the absolute minimum laying tensions is illustrated in
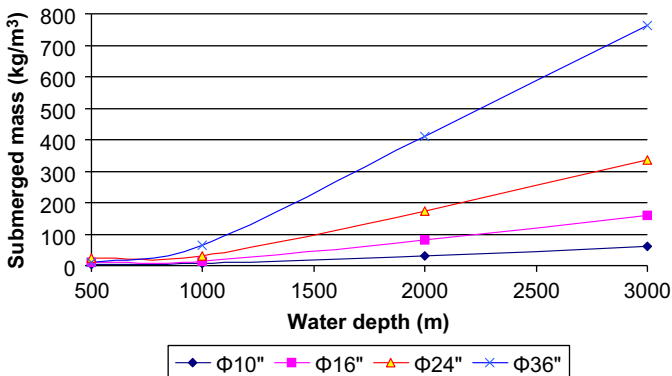
Figure 33.39 Installed submerged weight for installed empty pipeline. (For color version of this figure, the reader is referred to the online version of this book.)
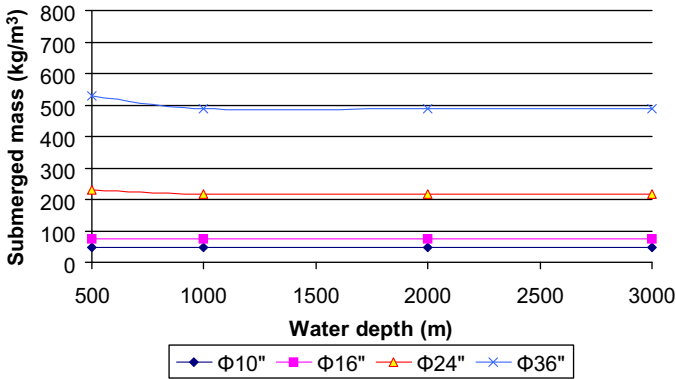
Figure 33.40 Installed submerged weight for flooded pipeline. (For color version of this figure, the reader is referred to the online version of this book.)

Figure 33.41, which is generated on the basis that no additional weight coatings are required for stability purposes. On the basis that existing spreads have a maximum laying tension capacity of between 400 and 500 tonnes, then the deepest water depth can be installed for an 16 in. pipeline is 2000 m (Figure 33.41).

It is interesting to note that the laying tension in 2000 m water depth would be the same (or less) to install the 16 in. pipeline flooded as opposed to dry (Figure 33.42), but the associated cost would be less, as the required pipe steel would be approximately half of that installing the line dry. The difference is even more dramatic for a 10 in. line, which can be installed in over 3000 m of water with existing spreads (when flooded) compared to 2500 m when dry.

The difference becomes even more noted when comparing J-lay capabilities. To install the same 16 in. pipeline in 2000 m by J-lay requires a tension of 200 tonnes, whether installed wet or dry (Figures 33.43 and 33.44). The big benefit from the wet installation, apart from requiring only half the material, is that existing equipment can install an 16 in. pipeline in over 4000 m compared to over 2000 m in the dry state. An observation from this study is that installation of an 24 in. pipeline still requires very large laying tensions, even with J-lay. There is scope to reduce the submerged weight of the line by the addition of buoyant insulation, with this and flooding the line, there
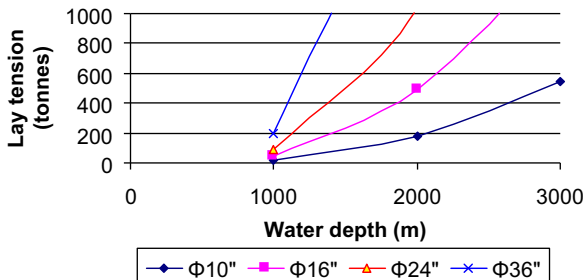
Figure 33.41 S-lay of dry pipeline. (For color version of this figure, the reader is referred to the online version of this book.)
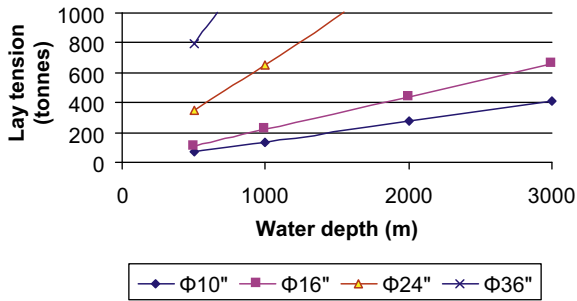
Figure 33.42 S-lay of wet pipeline. (For color version of this figure, the reader is referred to the online version of this book.)
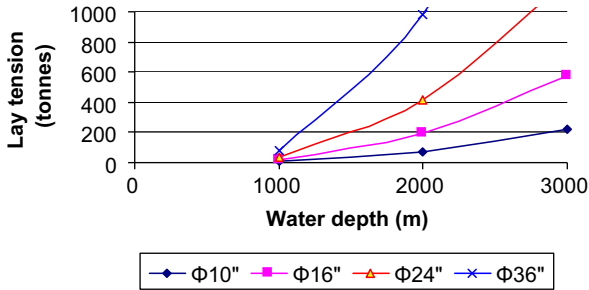
Figure 33.43 J-lay of dry pipeline. (For color version of this figure, the reader is referred to the online version of this book.)
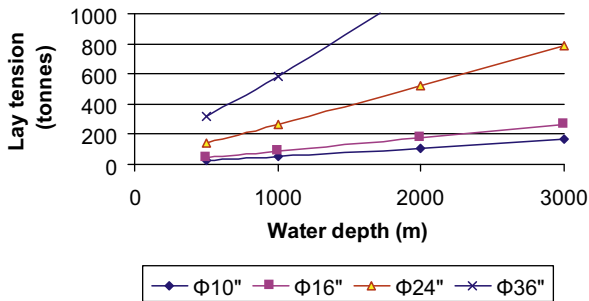
Figure 33.44 J-lay of wet pipeline. (For color version of this figure, the reader is referred to the online version of this book.)

is the potential to reduce laying tensions in 3000 m to more achievable laying tensions.

S-lay installation tension is limited by a more horizontal departure angle at the stinger tip. The present stingers on the larger vessels have already been extended for 400 to 600m and are designed to provide departure angels of up to about 60 degrees. The required angle for ultra deep water would be the equivalent of J-Lay, or virtually 90 degrees. To keep stinger lengths within the present size (max 100 m arc length), it is necessary to increase the curvature which will plastically deform the pipeline in the overbend providing a permanent residual strain in the pipe on the seabed. The effect of residual strain is not well documented but two phenomena are identified. The first one is the tendency of the pipe to twist due to instability in the sag-bend introduced by the reverse plastic strain. The second one is that the pipe may adopt a "corkscrew" configuration on the seabed. If the plastic strain is not severe then these effects can be avoided or be used to benefit the pipeline installation operation.

Economic Implication

Pipeline project CAPEX can be broken down into the following main areas:

> Management and design, 5%.
> Materials and fabrication, 55%.
> Installation, 29%.
> Commissioning, 1%.
> Insurance and miscellaneous, 2%.

- **Management and design:** The approach has no direct commercial impact on the management and design process. However, the design should address all the potential limitations of a two-medium pipeline to ensure that they are acceptable to the operations phase. One point that must be addressed is a system of assuring that pressure in the line never drops below a prescribed minimum. One approach is to have isolation valves at the ends of the pipeline, which are activated on detection of pressure drops as a HIPPS is applied to HP lines.
- **Materials and fabrication:** The required wall thickness is significantly reduced. Some reduction in wall thickness is achieved for water depths less than 1000 m. But in water depths of 2000 m or more, the reduction is at least 50%.
- **Installation:** As addressed already, for pipelines in excess of 2000 m, there is a significant reduction in laying tension requirements. An additional benefit is that laying rates should be faster as the wall thickness of the pipeline is significantly reduced. It can be envisaged that no adverse commercial impact will come of this phase. If conventional installation methods can be used, the cost will be reduced further.
- **Commissioning:** Although the conventional approach of dewatering and drying the pipeline may not be possible, precommissioning techniques, using liquids (methanol) at the required pressure, could be implemented. The approach may have a good commercial impact.
- **Insurance and miscellaneous:** Although this is not a well-proven technique, it is technically feasible. It has been used where the pipeline is too light to be stable on the seabed, but not in ultra deep water. Insurance would be related to repair costs rather than risk of damage.

In summary, installation of a wet pipeline in 1000–3000 m water depths is technically feasible, and it could reduce the pipeline CAPEX (due to material savings) by up to

27%. There is greater emphasis on the design aspects, but with modern analysis methods and tools, the engineering can be performed reliably and efficiently.

References

[1]   Li N. Retrospect and prospect of oil and gas pipelines in China. Oil Gas Storage Transportation; 2002.

[2]   Zhou J. Research on deepwater submarine pipeline S-lay and construction technology. Hangzhou, China: Zhejiang University; 2008.

[3]   Baker B, Mcclure L. Reel method speeds lay of pipe-in-pipe. Offshore; 2002.

[4]   Li JR. Submarine pipeline reliability design method and construction programming. Hangzhou, China: Zhejiang University; 2004.

[5]   Endal G, Ness OB, Verley R, Holthe K, Remseth S. Behaviour of offshore pipelines subjected to residual curvature during laying. Denmark: Copenhagen. Proc. of OMAE'95; 1995.

[6]   Damsleth PA, Bai Y, Nystrøm PR, Gustafsson C. Deepwater pipeline installation with plastic strain. Canada: St. John's; 1999. Proc. of OMAE'99.

[7]   Bai Y, Damsleth PA, Langford G. Strength design of deepwater pipelines. In: Proc. of Second International Conference on Deepwater Pipeline Technology. DPT-99; 1999.

[8]   Zhu LY Bai Y. S-lay installation analysis for deepwater pipeline. Harbin, China: Harbin Engineering University; 2011.

[9]   Wang LZ, Yuan F, Guo Z. Numerical analysis for pipeline installation by S-lay method. Shanghai, China: Proc. of OMAE 2010-20552; 2010.

[10] Martinsen M. A finite element model for pipeline installation analysis. Stavanger, Norway: Master's thesis. Stavanger University; 1998.

[11] Rivett SM, Raven PWJ, Baker DW. Pipeline design and construction in deep and ultra deep water—An overview. Deep Water Drilling and Production Technology Symposium, Black Sea; 1997.

[12] Damsleth PA, Dretvik S. The Åsgard Flowlines—Phase 1 design and installation challenges. OPT'98; 1998.

[13] Walker A, Tam CKW. Deepwater pipeline design, Deepwater Pipeline Technology (DPT) Conference; March 1998.

[14] Palmer A. Pipelines in deep water, interaction between design and construction. In: Estefen SE, et al., editors. Proceedings of Workshop on Subsea Pipelines. Rio de Janeiro, Brazil: Federal University of Rio de Janeiro; 1997.

[15] Bai Y, Damsleth PA. Limit state design of offshore pipelines. Yokohama, Japan; 1997. Proc. of OMAE'97.

[16] Bai Y, Damsleth PA. Design through analysis applying limit state concepts and reliability methods. Montreal, Canada; 1998. Proc. of Eighth International Offshore and Polar Engineering Conference. ISOPE-98.

[17] Holme R, Levold E, Langford G, Slettebø H. Åsgard transport—The design challenges for the longest gas trunkline in Norway. OPT'99; 1999.

34 Pipeline Commissioning, Operations, and Maintenance

Chapter Outline

1. Introduction

The commissioning of a pipeline involves the activities after installation required to put the pipeline system into service, which the activities include hydrostatic testing, cleaning and drying, and the introduction of the product to be transported into the pipeline system.

Pipeline operations are generally carried out by the pipeline operating company (operator). Detailed operation and maintenance procedures for the pipeline system should be prepared for use before the pipeline is commissioned and handed over to the operator.

Manuals for operations and maintenance should be prepared, including the schedules, procedures, and instructions to which the activities are to be carried out [1].

2. Precommissioning Activities

All pipelines should be thoroughly cleaned internally before the products are introduced into them. The cleaning procedure starts in the pipe fabrication yard, where the

pipe is often placed outside for long durations, causing rust to occur. External rust is easily removed prior to pipe coating, though internal rust can create a problem if consideration is not given to its mitigation. Normally, the internal rust and loose mill-scale are removed by internal brush cleaning, performed a few weeks ahead of pipe shipment. However, when the degree of precleaning is even more critical, the pipe is grit blasted internally and a vapor phase inhibitor (for example, an inert gas with an inhibitor for internal protection) is inserted into each pipe joint and the ends are capped.

If these precautions are taken, the pipeline still needs cleaning to remove construction debris and small quantities of rust. If the pipeline is installed unclean, then more extensive cleaning may be required. Apart from debris removal, cleaning improves the production quality and reduces flow resistance because of a smooth internal surface. It also enables more complete dewatering, because less residual water is left on pipe wall interstices. Internally coating each pipe joint with a suitable anticorrosion or flow enhancing coating system immediately after grit blasting has similar effects, such as aid in dewatering and less internal cleaning, although at a higher cost. Internal coating also has more benefits, such as improving flow and requiring less cleaning during operation.

Flooding, Cleaning, and Gauging

Cleaning and gauging may be combined with the initial flooding of the pipeline system, be run as a separate procedure, or be combined with the weld sphere removal after the installation of pipeline system is completed.

The flooding procedures generally take into consideration the following issues:

- Appropriate measures should be taken to ensure that any suspended and dissolved substances in the fluid used for this procedure are compatible with the pipe material and internal coating (if applied) and that deposits are not formed in the pipeline system.
- Addition of corrosion inhibitor, oxygen scavenger, biocide, and dye chemicals to the filling water requires consideration of water residence time in the line, leak detection methods, and eventual discharge of line contents. If the pipelines are in arctic areas, antifreeze chemicals may also be used.
- Water to be used for flooding should have a minimum quality corresponding to filtration to remove suspended particles (in general, 50 micron filters). For a long pipeline or heavily contaminated fill water, it is advisable to provide a double filtration unit.
- If water is to remain in the pipeline for an extended period, measures to control bacterial growth and internal corrosion by chemical treatment should be considered.
- A bi-directional pig is often the first pig to traverse the pipeline, the bypass ports fitted to the pig should be considered that help keep the accumulated debris in suspension and reduce the chance of a stuck pig.
- Isolation from other existing facilities.

The pipeline should be gauged internally by a gauging pig to ensure that the pipeline system is free of all buckles, kinks, weld over-penetration, and dents. The gauging pig can either be run within the trailing end of the pig cleaning train or separately. The gauging plate diameter is normally sized 95–98% of the internal diameter of pipeline and is made either of steel or aluminum.

Before the pipeline is gauged, it is necessary to clean the pipeline to collect all the loose debris that could affect the gauge plate. The pipeline cleaning should consider

- Protecting of pipeline components and facilities (e.g., valves) from damage by cleaning fluids and pigs.
- Using testing devices, such as isolation spheres.
- Removing substances that may contaminate the product to be transported.
- Removing particles and residue from testing and mill scale.
- Avoiding organisms and residue resulting from test fluids.
- Removing chemical residue and gels.
- Removing metallic particles that may affect future inspection activities.

The procedures covering pipeline cleaning and gauging should include the following items:

- Applicable safety and environmental regulations.
- Minimum equipment and instrumentation requirements.
- Gauge dimensions and acceptance criteria.
- Fill water quality and chemical additives.
- Basic filling and gauging procedure.
- Pig tracking requirements.
- Minimum and maximum pig speeds.
- Operation monitoring and control requirements.

Pressure Testing

A hydrostatic pressure test is normally performed on a pipeline to prove its structural integrity and leak tightness to the satisfaction of both the pipeline operator and the regulatory authorities. No pipeline operator in the United States may operate a pipeline or a new segment of pipeline without the pressure testing in accordance with CFR Title 49, Part 195 [2] for liquid pipelines and CFR Title 49, Part 192 [3] for gas pipelines and without leakage. The required hydrostatic pressure is different for the location class of the pipeline, a pressure equal to at least 125% of the maximum allowable operating pressure (MAOP) for subsea pipeline is required [4], [5].

A pipeline system pressure test should be performed from pig trap to pig trap, including all components and connections within the pipeline system. The system may be tested as separate sections, provided that the tie-in welds between sections have been subject to 100% radiographic, ultrasonic, and magnetic particle testing or by other methods that provide the verification of acceptable weld quality.

There is no restriction to using seawater or freshwater, although using seawater is a more practical consideration for subsea pipelines. The pressure test procedures using seawater and freshwater are essentially the same, but there are more considerations with using seawater, such as filtering and chemical treatment.

The pipeline section under test should be isolated from other pipelines and facilities. Pressure testing should not be performed against in-line valves, unless possible leakage and damage to the valve is considered and the valve is designed and tested for the pressure test condition in its manufacture. Blocking off or removing

small-bore branches and instrument tapings should be considered to avoid possible contamination.

End closures, manifolds, and other temporary testing equipment in the pipeline system should be designed and fabricated according to recognized codes and with the design pressure equal to the pipeline's design pressure, such items should be individually pressure tested to at least the same test pressure as the pipeline.

Pressure Test Procedures

The correlations of the effect of temperature changes on the test pressure should be developed and accepted prior to the pressure test. Temperature measuring devices should be positioned close to the pipeline, and the difference between the devices should be based on temperature readings along the pipeline route. The relationship between pressure and temperature can be calculated, for example, from the method given in BS 8010 Part 2 [6]. The normal pressure test procedures are as follows:

1. **Pressurization:** The pressure is slowly increased, holding at 35% of the test pressure for approximately 30 minutes to check for air content. There are various ways for calculating the air content, one such method is given by BS 8010 Part 2 [6].
2. **Stabilization:** The pressure is increased to 70% and held until visual checks are carried out on all flanges, including subsea flanges, if possible. Once accomplished, the pressure is raised to 80% of test pressure and held for approximately 2–4 hours to allow pressure stabilization.
3. **Holding period:** Once the preceding step is satisfied, pressurization continues to 95% test pressure, at which stage another hold is made for stabilization. This holding period should be for a minimum of 1 hour and is intended to allow any pressure surges to dissipate. So far, all pressurization should have been at a rate of 1 bar per minute; however, from this step to full test pressure, the pressurization rate should be reduced to 0.5 bar or less per minute.
4. **Acceptance:** When the pressure is at full test pressure, the stabilization period depends on the length of the line and the relative temperatures of the line filling, ambient sea, and pressurizing water. Full stabilization can be accomplished in 4–6 hours but increases with pipeline length. For example, 24 and even 48 hours have been experienced, especially for a very long pipeline. Throughout this period, the rate of pressure increases and the volume of water introduced into the line is constantly monitored and recorded. The common practice is for the test holding period to be monitored by chart recorder and hand recorded every 15 minutes. The pressure test is acceptable if the pipeline is free from leaks and the pressure variation is within ±0.2% of the test pressure.
5. **Depressurization:** Except in special circumstances, the pipeline is typically depressurized at double the pressurizing rate.

Determination of Residual Air Volume in Pipeline

The presence of residual air in the pipeline test section influences the behavior of the test section during the leak test holding period and tends to disguise the presence of small leaks. It is necessary to demonstrate that the quantity of residual air that may be present in a pipeline is below a minimum acceptable value prior to commencing the leak test holding period. Figure 34.1 demonstrate the method for calculating the
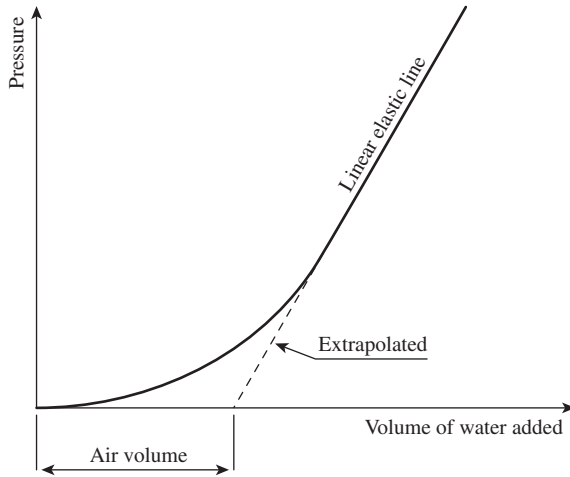
Figure 34.1 Determination of residual volume of air.

residual air volume. The air content of the test water should be assessed by constructing a plot of the pressure against volume during the initial filling and pressurization, until a definite linear relationship is apparent. The assessed air content should not normally exceed 0.2% of the calculated total volume of the pipeline or pipeline section under test. The maximum air content value of 0.2% is given by the DNV [7], and this is also common practice.

Hydrostatic Leak Test Evaluation

Prior to commencing the leak test holding period, sufficient time should have been allowed for the pipeline and its contents to stabilize to the prevailing surrounding temperature. Once stabilized and the leak test commences, provided the pipeline does not contain a leak or excessive quantities of air, any variations in the test pressure over the holding period should be as a result of minor temperature fluctuations.

To determine whether any pressure variations are a result of temperature fluctuation or a leak is present, the pressure/volume and temperature/volume relationships for the particular pipeline test section must be considered. For an infinitely long, fully restrained pipeline, this relationship is governed by the following equations:

$$\frac{\Delta V}{\Delta p} = V\left[\frac{D}{Et}\left(1 - v^2\right) + C\right] \tag{34.1}$$

$$\frac{\Delta V}{\Delta T} = V[\gamma - 2\alpha] \tag{34.2}$$

where

V = fill volume of pipeline
D = outside diameter of pipe
E = Young's elastic modulus of steel
t = wall thickness of pipe
ν = Poisson's ratio of steel
C = compressibility of water (3.20×10^{-6} in^3/in^3/psi)
γ = volumetric expansion of water
α = linear expansion of steel

By comparison of the incremental volume changes due to pressure and temperature fluctuations over the leak test holding period, the acceptability of the test can be established. In the event of any doubt after evaluation of the holding period, the test should be extended until such time as the acceptability is adequately demonstrated or, alternatively, the presence of a leak is confirmed. In the latter event, the leak has to be located and removed from the pipeline prior to testing.

Location of Leaks during Hydrostatic Testing

While the incidence of leakages and failures during hydrostatic testing is relatively low, its occurrence can cause considerable delays and additional costs. A variety of techniques are available for locating leaks, in both onshore and subsea pipelines. To minimize the potential delay and cost, at an early stage of the project, it is prudent to formulate a contingency plan that can be swiftly put into action if required. Such a contingency plan could, for example, include the addition of a dye to the test water in a subsea pipeline so that, in the event of a leak, it would not become necessary to refill the pipeline with water containing dye.

Dewatering and Drying

Dewatering is required before introducing the production fluid into the pipeline system. Drying may be required to prevent an increase in the corrosion potential or hydrate formation for a gas pipeline, The drying process is to be preceded by thorough cleaning and dewatering to ensure that no debris and no water are left in the pipeline. Under certain conditions, it may be possible that deficiencies in dryness can be compensated for by inhibition [8].

Dewatering and Drying Methods

Selection of dewatering and drying methods and chemicals should consider any effect on valve and seal materials, any internal coating, and trapping of fluids in valve cavities, branch piping, instruments, and the like. The following methods are commonly used in the practice:

- **Air or gas drying:** This method relies on the absorption of the remaining water film into dry air or dry gas, which is commonly achieved by passing dried air or dry gas through the pipeline in conjunction with foam pigs until the desired degree of dryness is achieved.

- **<u>Liquid swabbing:</u>** In this method, the remaining water film is diluted by a solvent, such as methanol or glycol. If the propellant is air, then a nitrogen slug is required between the air and methanol to ensure that a potentially explosive mixture of air and methanol does not occur. If methanol or glycol batches are used, the composition of the methanol or glycol may be analyzed at the end of the pigging run, which indicates the amount of water remaining in the pipeline.
- **<u>Vacuum drying:</u>** This method relies on the vaporization of the remaining water film in the pipeline at lower pressure and the evacuation of the water vapor from the pipeline. The vaporization is effected by lowering the pressure in the pipeline to a vacuum level, at which the water boils at the ambient temperature.
- **<u>Pigging:</u>** Disc pigs are commonly used for dewatering due to their superior sealing with the pipe wall, minimizing bypass. Foam pigs can be used subsequently to absorb residual water. However, in very long pipelines, numerous foam pigs would be required. Typically, regardless of the type of pigs chosen, several passes of pigs are required to achieve satisfactory dewatering.

3.   Commissioning

The commissioning of a pipeline system starts when the pipeline is connected to the upstream and downstream production facilities and considered ready for its operational duty, which means

- Construction of pipeline system completed and checked in accordance with the design requirements.
- Pipeline system preconditioned to a specified degree of cleanliness and dryness to prevent unacceptable corrosion or hydrate formation during commissioning.
- Pipeline system filled with a suitable medium, which can be safely displaced by the transport medium.
- Pipeline operating control system tested for its operability.

4.   Operations

Operating Philosophy

A pipeline operations philosophy needs to be developed and incorporated into the operations manual. The philosophy should address the overall issues that dictate gas operation, such as [1]

- Maximum and minimum design and operating limits on gas flow rate, pressure, and temperature,
- Sales contract requirements,
- Utilization of line pack to satisfy fluctuations in demand,
- Gas delivery requirements at third party tie-ins,
- Actions to be taken in the event of planned or unplanned shutdowns of the compressor station; for example, allow gas delivery to continue via line pack inventory until minimum delivery pressure limits are reached.
- Actions to be taken in the event of planned or unplanned shutdowns of the delivery station; for example, continue gas pumping until maximum pipeline pressure limits are reached.

Pipeline Security

Certain control systems must be provided so that the pipeline may be operated safely. The following functions are the minimum to be provided [9].

Emergency Shutdown

A means of shutting down the pipeline must be provided at each of its initial and terminal points. The emergency shutdown systems must be equipped so that any shutdown registers at the control center and a positive alarm system draws the attention of the persons in charge of the control center to the event. The response time of an emergency shutdown valve should be appropriate to the fluid in the pipeline and the operating conditions.

Pressure, Temperature, and Flow Control

Instrumentation must be provided at the control center to register the pressure, temperature, and rate of flow in the pipeline. Any variation outside the allowable transients must activate an alarm in the control center.

To ensure protection to the pipeline against over (and under, for example, when there is leakage) pressurization and excessively high temperatures, automatic primary and secondary trips should be installed at the compressor station. Details as to their location and their high and low pressure and high temperature settings are required as input into the operations manual.

Relief Systems

Relief systems, such as relief valves, are typically required to ensure the maximum pressure of the pipeline does not exceed a certain value. Relief valves must be correctly sized, redundancy provided, and must discharge in a manner that will not cause fire, health risk, or environmental pollution.

High-integrity protective systems (HIPS) may be considered when the conventional relief methods are unsuitable for ultimate plant protection. However, the application of the HIPS must be justified and its design must be agreed on by the relevant regulatory authority. The following main principles apply:

- A clear economic advantage must be demonstrated over the conventional approach to justify the increased complexity and dependence on rigorously controlled maintenance associated with HIPSs.
- The HIPS must be designed with appropriate redundancy and testing frequency to ensure higher reliability than conventional protection systems.
- Economic comparisons should take into account the life cycle maintenance and testing costs.
- The HIPS must respond quickly enough to prevent overpressure if downstream systems can be suddenly blocked in. This is one reason why HIPSs lend themselves to protection of large-volume systems, including pipelines, rather than small sections of plant.
- The HIPS isolation valves must have a tight shutoff. Otherwise, partial capacity relief valves are needed after the HIPS isolation valves to accommodate leakage rates, should the HIPS isolation valves fail.

Leak Detection

The pipeline must have an integrity monitoring system capable of detecting leaks. A leak detection system in itself has no effect on the leak expectancy of a pipeline and only makes the operator aware of the occurrence of a leak, enabling him or her to take remedial actions to limit the consequences of the release. The leak detection system requirements vary, depending on the pipeline system in question (e.g., offshore or onshore, length, etc.); however, the following should be considered at the design stage or implemented during operation.

For online leak detection,

- Continuous mass balance of the pipeline.
- Continuous volumetric balance corrected for temperature and pressure of the pipeline.
- Continuous monitoring of rate of pressure change.
- Continuous monitoring of rate of flow change.
- Low-pressure alarms.
- High-pressure alarms.
- High-flow alarms.

For offline leak detection,

- Visual inspection of the pipeline route.
- Running of a leak detection pig.
- Methane in water sensing by a remotely operated vehicle.

Several other methods of online leak detection are available, some of which also indicate the location of a suspected leak. However, in general, a good deal of intermediate pressure, temperature, and flow information is required with attendant telemetry; and for this reason, such methods are not generally suitable for offshore use.

Operational Pigging

The conflicting balance of sensitivity to leaks and false alarms determine the sensitivity of an online leak detection system. Large leaks can normally be detected more rapidly than small ones. To maintain the user's confidence in the system, avoiding false alarm should have a higher priority than attempting to shorten the leak detection time or reduce the minimum detectable leak rate.

In the field, a device that travels inside a pipeline to clean or inspect it is typically known as a *pig*. Operational pigging is performed to maintain pipeline integrity. With regular operational pigging, the pipeline should be maintained at its optimum throughput capacity and a higher efficiency be achieved. Typically, the following purposes are served by regular pigging:

- Prevention of scale buildup.
- Cleaning of the pipe wall.
- Removal of internal debris.
- Removal of liquids (condensate and water).
- Enhancement of the performance of corrosion inhibitors.
- Provision of a means to verify the occurrence of corrosion.

Pig Type and Frequency

Operational pig runs are performed in pipelines using cup or bidirectional pigs to remove water dropout, soft wax, sand deposits, scale, and other debris buildup. The operational pigging frequency is different for each pipeline and varies with changes in flow conditions, gas composition, and corrosion condition in the pipeline. Depending on the results of the pigging evaluation and the corrosion monitoring assessment, the pigging frequencies are reviewed and updated regularly. As an example, for the Balingian gas trunk line network operated by Sarawak Shell Berhad in Malaysia, the cleaning pigging frequency shown in Table 34.1 is required

Several types of pigs can be used, as shown in Figure 34.2. The selection of pig type depends on the purpose of the pigging run. The following gives a brief description of some of the main types of pig used in normal operation:

- **Cleaning pigs:** Cleaning pigs are available fitted with a number of sealing cups (omnidirectional) or sealing discs (bidirectional). The cleaning devices attached to the pig body range from carbon or stainless steel wire brushes, which are spring loaded to the pipe wall, to oversized circular wire brushes interfering on the pipe wall. For internally lined pipelines, nylon bristle brushes can be used. There are also scrapers molded to resemble plough blades in polyurethane, or for nonlined pipes, hardened steel blades profiled to suit the pipeline inner diameter. All pigs are designed for the brushes or blades to cover the circumference of the pipe surface.
- **Foam pigs:** Pipeline cleaning foam pigs are made of hard polyurethane and covered with abrasive coating or wire brush bands. Pigs manufactured of soft open-cell polyurethane foam are used for water absorption in swabbing and drying service.
- **Spheres:** Spherical molded tools are made of polyurethane or neoprene, of which the larger sizes are inflatable. The larger diameter spheres have facilities (inlets) whereby the spheres may be inflated to slightly greater diameters. The main application is in pipelines that have not been designed to accept standard pigs or in two-phase pipelines to remove liquid holdup and product separation.

Pigging Operations

The detailed procedures required for carrying out a routine pigging run should be contained or referenced within the pipeline operating manual. Typically, the pipeline operations department should carry out the following activities:

1. Check whether the pig trap isolation valves have been leak tested in the previous 6 months. The 6-month duration is a good common practice. If not, then leak testing is recommended prior to commencing a pig run.

Table 34.1 Cleaning Pigging Frequency of Balingian gas Trunk Line Network

Pipeline	Pigging Frequency
Balingian oil (12, 16, and 18 inch)	1 in 3 months
Temana oil (8 and 12 inch)	1 in 3 months
Samarang oil (8, 12, and 18 inch)	1 in 2 weeks
Balingian gas (12 and 18 inch)	1 in 6 months
Loconia gas (30, 32 , and 36 inch)	1 in 6 months

Figure 34.2 Pipeline operational pigs.
Source: Girard Industries [10]. (For color version of this figure, the reader is referred to the online version of this book.)

2. Ensure that the launcher has been correctly isolated, depressurized, vented, and purged and is safe to open and ready to receive pigs.
3. Ensure that all valves on the pig route are or will be fully open.
4. Ensure that all pig indicators are correctly set and operational.
5. Inform the receiving station of the following items:
   - Pig type.
   - Bypass setting (that is, the pig has a bypass facility in the case that the pressure buildup behind the pig is too great).
   - Time of launch.
   - Estimated time of pig arrival.
   - Inlet and outlet flow conditions at time of launch.
6. Keep track of the pig run by continuously monitoring the pressure and flow conditions at the inlet and outlet. Remain in regular contact with the receiving station and exchange updates on estimated time of pig arrival.
7. Receiver station to notify launcher station when pig arrives in receiver then isolate, depressurize, vent, and purge receiver prior to removal of pig and inspection for damage and wear.

Data Monitoring

Each pig run should be evaluated to determine the effectiveness of the operation. This information is used to enable a proper decision for future pigging runs and any other action to be taken. Typically, the following are evaluated:

- The actual pig arrival time is compared with the estimated arrival time. In conjunction with known flow rates and associated flow conditions throughout the pigging run, an estimate of pig bypass and pig slippage can reasonably be made.
- The wear on the pigs is determined and classified.
- The total weight of the debris received in the pig trap is measured. A sample also is taken for subsequent analysis.
- An estimation of the water volume swept ahead of the pig should be made, if suitable equipment is available at the receiver station.

Pipeline Shutdown

A pipeline shutdown can be initiated in the following three circumstances:

- An emergency.
- Major maintenance.
- Production shutdown.

An emergency shutdown of the pipeline is achieved by closing the appropriate emergency shutdown (ESD) valves. The ESD valves are closed automatically by one of the following:

- Fusible plug loops, which can be tripped in case of fire.
- Low-pressure trips in case of a pipeline leak.
- High-pressure trips in case of high pressure in the pipeline.
- Low-instrument air supply.
- Terminal ESD valve as per the shutdown sequence.

A pipeline ESD valve should also be able to be closed manually at the control room and locally at the valve itself. The closing of the ESD valve should be linked to the prime mover shutdown.

Pipeline Depressurization

For most pipelines, in the event of pipeline rupture, depressurization of the line must be carried out immediately to reduce the amount of escaped gas. For onshore pipelines, closure of line sectioning valves, each side of the rupture, may further limit the amount of product inventory escaping.

The time taken to fully depressure a pipeline to atmospheric pressure depends on several factors, not least of which includes the size and type of pipeline inventory, the operating pressure at time of rupture, the rate of flow escaping, and the maximum vent rate at the end station.

For long, large diameter gas trunk lines, the time taken to fully depressure a line can easily be on the order of several days.

The procedures for emergency depressurization are an essential part of the pipeline operating manual and should state, along with the actions required, the maximum achievable depressurization rate during emergency blowdown.

5. Maintenance

Introduction

The principle function of maintenance is to ensure that physical assets continue to fulfill their intended purpose. The maintenance objectives with respect to any item of equipment should be defined by its functions and its associated standards of performance [1].

Prior to setting out to analyze the maintenance requirements of equipment, it is essential to develop a comprehensive equipment register. In general terms, the equipment included relate only to onshore pipelines (or onshore sections), since

maintenance work on subsea pipelines is not foreseen; that is, all subsea equipment should be designed to be maintenance free throughout the design life expectancy of the pipeline. This is not to say that remedial work on a subsea pipeline will never occur, only that it should not be a planned occurrence. However, in the case of subsea pipeline repairs, it is prudent for most operators to keep a set (or to share a set) of emergency pipeline repair equipment on standby. This may include repair equipment such as pipeline repair clamps and full hyperbaric welding spreads. This equipment should be maintained along with onshore pipeline equipment.

Generally, preventive maintenance is carried out on onshore pipeline equipment with dominant failure modes (e.g., wear out of pump impellers) at predetermined intervals or to prescribed criteria, with the intent to reduce the probability of failure or the performance degradation of the item. It should go without saying that all maintenance work should attempt to minimize the effect to normal production operations. (e.g., schedule critical activities to coincide with a planned pipeline shutdown).

Maintenance should be carried out on all pipeline-associated equipment (e.g., pipeline valves and actuators, pig traps, pig signalers, and other pipeline attachments). Maintenance procedures and routines should be developed with account taken of previous equipment history and performance.

Pipeline Valves

Pipeline valves should be lubricated and functionally operated at least once annually and in accordance with the valve manufacturer's recommendations. Functional operation of subsea valves should also be carried out annually. However, where valves are located in unfavorable conditions (e.g., valve pits subject to flooding or general dampness), it may be advisable to increase the maintenance frequencies to account for these conditions.

All valve actuators, whether they be manual, pneumatic, hydraulic, or electrical, should be functionally tested at least once per year and in accordance with the actuator manufacturer's recommendations.

In developing maintenance routines, account should be taken, where applicable, of the requirement to test the equipment by remote operation or by simulating line-break conditions. Operations involving the closure of block valves should be a coordinated exercise with all the relevant parties.

Pig Traps

Pig trap maintenance should be carried out strictly in accordance with the manufacturer's guidelines for the type of pig launcher and receiver facilities used and these guidelines incorporated in the maintenance routine. However, at a minimum, a full inspection and survey of the condition of the pig traps should be conducted annually and should include

- Condition of launcher and receiver barrel.
- End closure seals.
- Bleed locks and electrical bond.

- Locking rings.
- Pig signalers.
- Associated valves and pipework.

Pipeline Location Markers

Aerial markers and pipeline markers should be maintained on an ongoing basis with the information contained on the marker posts verified and updated annually.

Above-ground crossing points should be examined at least once per year for condition of supports and associated structures, including paintwork and protective wrap, and refurbished where necessary.

References

[1] Bai Y, Bai Q. Subsea Pipelines and risers. 2nd ed. New York: Elsevier Science Ltd.; 2005.
[2] 49 CFR Part 195. Transportation of hazardous liquids by pipeline. Code of Federal Regulations; 2005.
[3] 49 CFR Part 192. Transportation of natural and other gas by pipeline: Minimum federal safety standards. Code of Federal Regulations; 2005.
[4] ASME 31.4. Pipeline transportation systems for liquid hydrocarbons and other liquids. New York: American Society of Mechanical Engineers; 2006.
[5] ASME B31.8. Gas transmission and distribution piping systems. New York: American Society of Mechanical Engineers; 2007.
[6] BS 8010. Code of practice for pipeline. Part 2. Pipeline subsea. London: British Standards Institute; 2004.
[7] DNV. Offshore Standard OS-F101. Submarine pipeline systems. Oslo: Det Norke Veritas; 2010.
[8] Langford GL, et al. Dewatering and commissioning the UK Central Area Transmission System (CATS) pipeline. OTC 7576, Houston, TX; 1994.
[9] Jackson L, Wilkins R. The development and exploitation of British gas pipeline inspection technology. Institution of Gas Engineers 55th Autumn Meeting; 1989.
[10] Girard Industries. Pipeline cleaning pig for every application. Available at www.girardind.com/.

Index

Note: Page numbers followed by "f" denote figures; "t" tables.